TR 2987

3162156
TR 2987

Modelling of Long-Stroke Hydraulic Servo-Systems for Flight Simulator Motion Control and System Design

Gert van Schothorst

'Godloosheid is een bewijs van denkkracht, maar slechts tot op zekere hoogte.'
Uit: 'Gedachten', Blaise Pascal.

Aan Caroline

Dit proefschrift is goed gekeurd door de promotoren:
Prof.ir. O.H. Bosgra
Prof.dr.ir. J.A. Mulder

Toegevoegd promotor:
Dr.ir. A.J.J. van der Weiden

Samenstelling promotiecommissie:

Rector Magnificus	voorzitter
Prof.ir. O.H. Bosgra	Technische Universiteit Delft, eerste promotor
Prof.dr.ir. J.A. Mulder	Technische Universiteit Delft, tweede promotor
Dr.ir. A.J.J. van der Weiden	Technische Universiteit Delft, toegevoegd promotor
Prof.dr.ir. P.T.L.M. van Woerkom	Technische Universiteit Delft
Prof.dr.ir. K. van der Werff	Technische Universiteit Delft
Prof.dr.ir. J.B. Jonker	Universiteit Twente
Prof.dr.ir. J.J. Kok	Technische Universiteit Eindhoven

Ir. P.C. Teerhuis heeft als begeleider in belangrijke mate aan het totstandkomen van het proefschrift bijgedragen.

ISBN: 90-370-0161-0
©1997, G. van Schothorst, The Netherlands

Modelling of Long-Stroke Hydraulic Servo-Systems for Flight Simulator Motion Control and System Design

PROEFSCHRIFT

ter verkrijging van de graad van doctor
aan de Technische Universiteit Delft,
op gezag van de Rector Magnificus Prof.dr.ir. J. Blaauwendraad,
in het openbaar te verdedigen ten overstaan van een commissie,
door het College van Dekanen aangewezen,
op dinsdag 9 september 1997 te 13.30 uur
door

Gerard VAN SCHOTHORST

werktuigkundig ingenieur

geboren te Ede

AFDELING TECHNISCHE UNIVERSITEIT DELFT

Summary

Modelling of Long-Stroke Hydraulic Servo-Systems for Flight Simulator Motion Control and System Design

G. van Schothorst

In many applications, the use of hydraulic drives is still preferable to alternative drive technologies. For instance, in flight simulator motion systems, hydraulic actuators are still widely applied, because the technology of electrical actuators does not (yet) provide the superior performance of hydraulic actuators in generating high-power long-stroke linear motions. However, with increasing demands on the performance of complex motion systems, the limits of performance of hydraulic servo-systems come into the picture. The application of long-stroke hydraulic actuators in a flight simulator motion system, considered in this thesis, shows that the dynamics and non-linearities of the servo-valve and of the transmission lines, located between the servo-valve and the actuator compartments, basically constitute the limits of the performance of the controlled servo-system. Especially in case of conventional, proportional feedback control strategies, the combination of valve dynamics and transmission line dynamics appears to be easily destabilizing the pressure difference control loop.

In order to obtain structural insight in the way that the performance is limited by the properties of (the subsystems of) the hydraulic servo-system, the modelling of this system has been treated thorougly in this thesis. At the one hand, this has opened the way to model-based control design, so that unavoidable limits of performance can be narrowly approached. At the other hand, the obtained insight appears to be useful in the system design stage, such that potential control problems may be avoided by proper system design.

Because of the twofold purpose of the modelling, with control design requiring quantitatively accurate models and system design requiring qualitative insight in the system behaviour, the so-called grey-box modelling approach has been applied. This approach comprises physical modelling including model analysis by means of simulation, and subsequent identification and validation of the obtained physical models, using experimental data.

In the physical modelling stage, extensive non-linear dynamic models have been derived for the three subsystems of the hydraulic servo-system: the electro-hydraulic servo-valve (of the flapper-nozzle type), the hydraulic actuator (of the double-concentric type), and the transmission lines between the actuator and the valve. By means of linearization of the theoretical models, the dynamic properties of the subsystems have been analysed. The considered three-stage valve shows a 5^{th} order low-pass characteristic, where the main spool behaves as a pure integrator, and the flapper-nozzle pilot-valve as a 4^{th} order low-pass system. The actuator is well described by the well-known 3^{rd} order dynamics, a pure integrator in series with badly damped second order low-pass dynamics. Finally, the behaviour of the transmission lines in the hydraulic servo-system is characterized by a series of badly damped resonances in the high-frequency region of the pressure difference

transfer function, of which the first modes may lie within the servo-valve bandwidth.

Besides the dynamic properties of the system, the non-linearities have been investigated by means of simulation of the physical model. This led to the insight, that only some of the modelled non-linear effects are really relevant, such as the non-linear flow characteristic of the servo-valve spool due to non-ideal port geometries and non-zero load pressure, and the position dependence of the actuator dynamics.

The result of the physical modelling consists of physically structured non-linear dynamic models, describing the relevant dynamics and non-linearities of the subsystems of the hydraulic servo-system, in a qualitative sense. Quantitative accuracy has been given to these models, by means of experimental identification of the model parameters and the dominant non-linearities of the system. This identification has been performed in the frequency domain, using the Sinusoidal Input Describing Function (SIDF) as a tool to explicitly characterize the non-linearities of the system. Besides the implicit validation by the satisfactory identification results, the validity of the obtained models has been shown by means of some cross-validation results.

Experiments with a hydraulic actuator in a single degree-of-freedom setup have shown the validity of a model-based approach for control design. An analysis of different control strategies for this setup led to the conclusion, that high-gain pressure difference feedback leads to a good performance, provided that a good reference signal for the pressure difference is available. Thereby, the model-based design of a robust dynamic pressure difference feedback loop appeared to be necessary and sufficient to avoid stability problems due to the combination of valve dynamics and transmission line dynamics. For a good performance in the low-frequency region, the feedforward of the desired velocity appeared to be essential. Alternatively, positive feedback of the (estimated) velocity can be applied, where some possibilities to obtain such an estimated velocity signal have been experimentally evaluated.

The combination of high-gain pressure difference feedback and positive velocity feedback is called the cascade ΔP control strategy; it realizes a decoupling between the control of the pressure dynamics of the hydraulic servo-system and the control of the mechanics of the load. For this reason, this hydraulic actuator control strategy is well-suited for the control of multi degree-of-freedom motion systems; it fits well in a two-level strategy, where the high-level control copes with the non-linear multivariable control of the load dynamics, and the low-level control takes care of the (pressure) dynamics of the hydraulic actuators.

Whenever possible, preliminary model analysis should be performed to avoid serious performance limitations due to improper system design. It may help in making decisions concerning servo-valve choice, placement of the pressure difference transducer, and transmission line design.

A system design topic which is of special importance for flight simulator motion systems, is the design of safety cushionings at the end of the actuator stroke. A model-based design procedure has been developed and applied in practice, which directly leads to well-performing safety cushionings. In this way, costly iterations in the design cycle (due to repetitive experimental verification) could be avoided.

Voorwoord

De mogelijkheid om diep in de materie van de hydraulische servo techniek te duiken, in de vorm van uitgebreide modelvorming en regelaarontwerp; de uitdaging om in een interfacultair samenwerkingsverband mee te werken aan de realisatie van een compleet nieuwe vluchtsimulator met zes graden van vrijheid; de relatief grote vrijheid van een AIO-er; een goede kans om mijn blik te verruimen op niet-technisch gebied. Dat waren globaal de redenen om mijn studieperiode in Delft te verlengen met nog eens vier jaar AIO-schap, hoewel het vooruitzicht een dissertatie te moeten schrijven niet aantrekkelijk was. En het was inderdaad niet gemakkelijk. Desondanks, en gedeeltelijk ook gedreven door het ideaal, om het gedane werk over te dragen aan andere mensen, die met hydraulische servo-systemen werken, is dit proefschrift geworden wat het nu is.

Op dit moment, na afronding van het werk, kan ik zeggen dat deze periode als AIO-er mij zelfs meer gegeven heeft dan ik had kunnen verwachten. Ongetwijfeld is dit ook voor een belangrijk deel het resultaat van de bijdrage van veel mensen in mijn omgeving, gedurende deze tijd. Het is niet mogelijk een ieder met name te noemen; daarom wil ik op voorhand een ieder bedanken, die mijn werk met belangstelling gevolgd heeft, op welke wijze dan ook.

Toch zijn er mensen, die ik in het bijzonder zou willen bedanken. Allereerst zijn dat mijn promotoren. Prof. Bosgra, die mij kon confronteren met de zwakke punten van mijn werk, en vanuit een enorme schat aan kennis en overzicht van het vakgebied richting gaf om die punten te versterken. Zijn overtuigende, maar ook stimulerende begeleiding heeft ongetwijfeld een grote bijgedrage geleverd aan de kwaliteit van het onderzoek. Prof. Mulder, die met een haast grenzeloos enthousiasme stimulerende impulsen gaf, zowel in het begin als aan het einde van het promotiewerk. Verder mijn directe begeleiders, Ton van der Weiden en Piet Teerhuis. Was er een probleempje, iets te overleggen, dan kon ik bij hen terecht. Als het iets meer theoretisch of organisatorisch (of 'politiek') was, bij Ton; als het meer praktisch was op het gebied van hydrauliek of in het kader van het SIMONA-project, bij Piet.

Het meedraaien in het SIMONA-project heeft voor mij veel kleur aan het onderzoek gegeven, en dan niet alleen technisch-inhoudelijk. Ik heb er veel geleerd, o.a. door de samenwerking met verschillende mensen. Ik denk met name aan Sunjoo Advani, maar ook aan andere L&R-medewerkers: Max Baarspul, Paul van Gool, Henk Kluiters, Henk Lindenburg, Adri Tak, Ruud van Olden, en anderen.

Naast deze projectmatige contacten, waren er de dagelijkse contacten met de collega's van de vakgroep Meet- en Regeltechniek. Dan denk ik in de eerste plaats aan hen, die voor de technische ondersteuning zorgden. Zoals Rens de Keyzer, die altijd wel wilde helpen bij het (om)bouwen van de opstelling. In de loop van het onderzoek ben ik zijn kritische verhalen (niet alleen op het gebied van de hydrauliek) en opmerkingen steeds meer gaan waarderen. Maar ook Fred den Hoedt, Henk Huisman, Rolf van Overbeek, Kees Slinkman en Peter Valk hebben altijd met hun diensten klaar gestaan.

De contacten met de collega-AIO's van de vakgroep heb ik ook als heel vruchtbaar ervaren. Met name de besprekingen met de 'vakbroeders' Hans Heintze en Gert-Wim van der Linden. Hoewel we potentieel met ons onderzoek in elkaars vaarwater zaten, is dit eerder bevorderend geweest dan dat het problemen opleverde. Het doet me ook goed, dat

ik hen (zeker Hans als mijn afstudeerbegeleider), als succesvolle promovendi vóór zag gaan. Van de andere AIO's wil ik Sjirk Koekebakker nog noemen, die met het onderzoek in het kader van het SIMONA-project verder gaat. Dankzij de overlap in tijd was er een goede mogelijkheid om mijn resultaten over te dragen, wat ik als heel plezierig heb ervaren. Ik zal de uitkomsten van dit vervolgonderzoek met belangstelling volgen.

Zoals in veel gevallen, nam ook in mijn promotieonderzoek het werk van afstudeerders een bijzondere plaats in. Zeer zeker hebben Eddy van Oosterhout en Oscar van Wel met hun werk de basis gelegd voor het stuk theoretische modelvorming, dat ik heb uitgewerkt in dit proefschrift. Mede dankzij hun ijver en nauwgezetheid, kon ik in dit opzicht een 'vliegende start' maken. Later heeft Paul Kok met zijn creatieve ideeën mij de gereedschappen aangereikt, om op een goede manier de niet-lineaire dynamica van het systeem te identificeren en valideren. Ik heb ieders persoonlijke bijdrage erg gewaardeerd.

Tenslotte wil ik familie en vrienden bedanken voor hun belangstelling gedurende mijn Delftse tijd; in het bijzonder mijn ouders, die mij in deze tijd op de achtergrond voortdurend ondersteund hebben. Ook denk ik aan mijn huisgenoten in 'Huize Henaleger', die een sociale sfeer hebben geschapen, die mijn werk indirect ten goede kwam, met name in de tijd dat ik thuis zat te schrijven aan m'n boekje. Verder was het Caroline, nu mijn vrouw, die indirect een belangrijke bijdrage leverde aan de voltooiïng van het promotiewerk, met name door steeds mee te leven, en constructief mee te denken over de niet-technische aspecten van het werk, ook als het einddoel mij minder helder voor ogen stond.

Hoewel al deze dankwoorden zeker op hun plaats zijn, komt uiteindelijk God de HEERE de meeste dank toe, omdat Hij in alles voorzien heeft, wat voor dit werk nodig was.

Gert van Schothorst Hedel, juli 1997.

Contents

Summary vii

Voorwoord ix

1 Introduction 1
- 1.1 Hydraulic servo technique . . . 1
  - 1.1.1 History and motivation for hydraulic drives . . . 1
  - 1.1.2 Characterization of hydraulic servo-systems . . . 2
- 1.2 Flight simulator motion control . . . 5
  - 1.2.1 The SIMONA project . . . 5
  - 1.2.2 Motion control for flight simulator systems . . . 6
  - 1.2.3 Hydraulic actuator control problems and system requirements . . . 8
- 1.3 Problem statement . . . 9
  - 1.3.1 General problem statement . . . 9
  - 1.3.2 Elaboration of the problem statement . . . 9
- 1.4 Approach for research . . . 15
- 1.5 Outline of the thesis . . . 16
  - 1.5.1 Overview of contents . . . 16
  - 1.5.2 Structure of the thesis . . . 17

2 Physical modelling of hydraulic servo-systems 19
- 2.1 Introduction . . . 19
  - 2.1.1 System description and system boundary . . . 19
  - 2.1.2 Approach to modelling . . . 22
  - 2.1.3 Outline of the Chapter . . . 26
- 2.2 Modelling and simulation of an electro-hydraulic servo-valve . . . 26
  - 2.2.1 Introduction . . . 26
  - 2.2.2 Modelling of the flapper-nozzle system . . . 30
  - 2.2.3 Modelling of a two-stage flapper-nozzle valve . . . 33
  - 2.2.4 Modelling of a three-stage servo-valve . . . 36
  - 2.2.5 Simulation of the non-linear servo-valve model . . . 38
- 2.3 Modelling and simulation of a hydraulic actuator . . . 51
  - 2.3.1 Introduction . . . 51
  - 2.3.2 Basic actuator model . . . 52
  - 2.3.3 Leakage and friction of hydrostatic bearings . . . 54
  - 2.3.4 Actuator modelling example . . . 55
  - 2.3.5 Simulation of the non-linear actuator model . . . 58
- 2.4 Modelling and analysis of transmission line effects . . . 65
  - 2.4.1 Introduction . . . 65
  - 2.4.2 Theoretical modelling of a single transmission line . . . 69
  - 2.4.3 Approximation of transmission line dynamics . . . 78

2.4.4 Integration of subsystem models for inclusion of transmission line effects . . . 82
2.4.5 Analysis of the effect of transmission line dynamics . . . 86
2.4.6 Conclusion . . . 90
2.5 Analysis of servo-valve dynamics . . . 91
2.5.1 Linearization of the theoretical model . . . 91
2.5.2 Physically argued reduction and simplification of the model of the flapper-nozzle valve . . . 93
2.5.3 Simplified servo-valve model . . . 97
2.6 Analysis of actuator and transmission line dynamics . . . 99
2.6.1 Linearization of the theoretical actuator model . . . 99
2.6.2 Physically argued simplification and reduction of the actuator model 100
2.6.3 Inclusion of transmission line dynamics . . . 102
2.6.4 Summary . . . 105
2.7 Inclusion of relevant non-linearities in the hydraulic servo-system model . . 105
2.7.1 Introduction . . . 105
2.7.2 Non-linearities of the flapper-nozzle servo-valve . . . 106
2.7.3 Non-linearities of the hydraulic servo-system . . . 111
2.8 Conclusion . . . 116

3 Experimental identification and validation of the model 119
3.1 Introduction . . . 119
3.1.1 Starting point for identification and validation . . . 119
3.1.2 Identification and validation of non-linear systems . . . 121
3.1.3 Approach to identification and validation . . . 126
3.1.4 Outline of the Chapter . . . 128
3.2 Elaboration of approach to identification and validation . . . 128
3.2.1 Sinusoidal Input Describing Functions . . . 128
3.2.2 Input amplitude filter design . . . 133
3.2.3 Identification and validation of linear dynamics . . . 137
3.2.4 Identification of static non-linearities . . . 140
3.2.5 Validation of non-linear dynamic model . . . 143
3.2.6 Estimate-based reconstruction of physical parameters . . . 144
3.2.7 Conclusion . . . 145
3.3 Experimental setup . . . 145
3.3.1 General setup . . . 146
3.3.2 Three-stage servo-valve . . . 149
3.3.3 Measurement and control devices . . . 150
3.4 Indentification and validation of the flapper-nozzle valve model . . . 152
3.4.1 Introduction . . . 152
3.4.2 Identification of linear dynamics . . . 153
3.4.3 Identification and validation of non-linearities . . . 153
3.4.4 Cross-validation . . . 156
3.4.5 Estimate-based reconstruction of physical parameters . . . 157
3.5 Indentification and validation of three-stage servo-valve model . . . 158
3.5.1 Introduction . . . 158
3.5.2 Identification of linear dynamics . . . 159

3.5.3 Identification and validation of non-linearities . . . 162
3.5.4 Cross-validation . . . 164
3.5.5 Estimate-based reconstruction of physical parameters . . . 168
3.5.6 Conclusion . . . 169
3.6 Identification and validation of hydraulic actuator model . . . 169
3.6.1 Introduction . . . 169
3.6.2 Identification of linear dynamics . . . 170
3.6.3 Identification of actuator non-linearities . . . 174
3.6.4 Cross-validation . . . 177
3.6.5 Estimate-based reconstruction of physical parameters . . . 180
3.6.6 Conclusion . . . 183
3.7 Indentification and validation of actuator including transmission lines . . . 184
3.7.1 Introduction . . . 184
3.7.2 Identification of transmission line dynamics . . . 185
3.7.3 Cross-validation . . . 188
3.7.4 Estimate-based reconstruction of physical parameters . . . 191
3.7.5 Conclusion . . . 197
3.8 Conclusion . . . 197

4 Design and application of hydraulic actuator control 201
4.1 Introduction . . . 201
4.2 Task specification . . . 204
4.2.1 Control setting for single hydraulic actuator . . . 204
4.2.2 Choice of reference generator for single DOF hydraulic actuator control 205
4.2.3 Task specification for single DOF hydraulic actuator control . . . 207
4.3 Control strategies for hydraulic servo-systems . . . 207
4.3.1 Introduction and literature survey . . . 207
4.3.2 Position servo including pressure feedback . . . 209
4.3.3 State feedback . . . 212
4.3.4 Cascade ΔP control . . . 215
4.3.5 Velocity feedforward . . . 218
4.3.6 Non-linear control . . . 219
4.3.7 Effect of position dependence on control . . . 222
4.3.8 Conclusion . . . 223
4.4 Implications of servo-valve and transmission line dynamics . . . 224
4.4.1 Performance limitation due to valve dynamics . . . 224
4.4.2 Implication of transmission line dynamics . . . 226
4.4.3 Open control design issues . . . 231
4.4.4 System design issues for hydraulic servo-systems . . . 233
4.4.5 Conclusion . . . 236
4.5 Velocity estimation . . . 237
4.5.1 Direct velocity estimation . . . 237
4.5.2 Standard estimator design . . . 238
4.5.3 Experimental evaluation of velocity estimation . . . 243
4.5.4 Conclusion . . . 250
4.6 Experimental evaluation of control strategies . . . 251
4.6.1 Experimental conditions for controller evaluation . . . 252

4.6.2 Performance dynamic pressure difference control loop 253
4.6.3 Experimental comparison of control strategies 254
4.6.4 Improved performance by velocity feedforward 255
4.6.5 Load sensitivity of actuator control performance 256
4.6.6 Effect of non-linear control 258
4.6.7 Evaluation time domain performance and conclusions 260
4.7 Conclusions 263

5 Model-based cushioning design **267**
5.1 Introduction 267
5.2 Modelling of cushionings 268
5.2.1 Description of the cushionings 268
5.2.2 Modelling of peg-in-hole (PIH) cushioning 269
5.2.3 Modelling of closing-drain-holes (CDH) cushioning 275
5.2.4 Choice of model parameters and intermediate model validation . . . 282
5.3 Cushioning design 284
5.3.1 Introduction; design objective 284
5.3.2 Desired motion profile 285
5.3.3 Design procedure for PIH cushioning 289
5.3.4 Design procedure for CDH cushioning 295
5.4 Experimental evaluation of the cushioning design 299
5.4.1 Final model validation 299
5.4.2 Experimental evaluation of the PIH cushioning 301
5.4.3 Experimental evaluation of the CDH cushioning 304
5.5 Conclusions 308

6 Conclusions and recommendations **311**
6.1 Conclusions 311
6.1.1 Modelling of the hydraulic actuator 312
6.1.2 Modelling of the servo-valve 312
6.1.3 Modelling of transmission line dynamics 313
6.1.4 Control design for hydraulic servo-systems 315
6.1.5 System design and cushioning design 316
6.2 Recommendations for future work 317

A Overview of properties of the model of a hydraulic servo-system **319**
A.1 Overview of dynamics of a hydraulic servo-system 319
A.1.1 Dynamics of a flapper-nozzle valve 319
A.1.2 Dynamics of a three-stage valve 320
A.1.3 Dynamics of a hydraulic actuator 321
A.1.4 Dynamics of a transmission line 322
A.1.5 Dynamics of complete hydraulic servo-system; rules for modelling . 322
A.2 Overview of non-linearities of a hydraulic servo-system 323
A.2.1 Torque motor non-linearity 324
A.2.2 Flapper-nozzle non-linearity 324
A.2.3 Non-linear flow forces on flapper 324
A.2.4 Coulomb friction on the spool 325

A.2.5 Ball clearance of feedback spring 325
A.2.6 Non-linear flow through spool ports 325
A.2.7 Non-linear flow forces on spool 326
A.2.8 Leakage of hydrostatic bearing 326
A.2.9 Coulomb friction in the actuator 327
A.2.10 Position dependence of actuator dynamics 327

B Algebraic loops in the simulation model **329**
B.1 Algebraic loops in three-stage valve model 329
B.2 Algebraic loops due to manifold losses 330

C Leakage and axial forces of hydrostatic bearing **333**
C.1 Leakage flow 334
C.2 Axial bearing force 336

D Modal approximation of pressure dynamics in actuator chamber **339**
D.1 Modal representations of the terms $Z_c \cosh(\Gamma)/\sinh(\Gamma)$ and $Z_c/\sinh(\Gamma)$ . . 339
D.2 Modal approximation and state space form 342

E Steady state behaviour of modal approximations **345**

F Parameter values for simulation theoretical model **349**

G Technical specifications of transducers **353**

Bibliography **355**

Index **365**

Glossary of symbols **371**

Samenvatting **381**

Curriculum Vitae **384**

Chapter 1

Introduction

Although electrical drives become more and more popular for high-performance motion control, hydraulic servo-systems still find a wide variety of applications in present-day industrial motion systems, for instance in flight simulator motion systems. With increased possibilities in applying advanced control methods, among others due to increased computer power and ongoing developments in control theory, higher demands are made on the modelling of the non-linear dynamic behaviour of hydraulic servo-systems. More detailed descriptions of dominant non-linear characteristics and relevant dynamics over wider frequency ranges have to be taken into account.

Against the background of a specific application, a flight simulator motion system, an integrated approach to the modelling of a hydraulic servo-system is presented in this thesis. On the one hand, this involves a consistent integration of the non-linear dynamic modelling of the different subsystems of the hydraulic servo-system, namely servo-valve, transmission lines and actuator. On the other hand, it comprises a systematic approach of theoretical modelling, model simplification and identification, and experimental validation. In this approach, the link between the physical and the system theoretic interpretation of the properties of the hydraulic servo-system is strongly emphasized. This makes, that the presented models are not only useful for flight simulator motion control design, but also for the design of the hydraulic servo-system.

After an introduction into the hydraulic servo technique in Section 1.1, the role of hydraulic servo technique in flight simulator motion control is high-lighted in Section 1.2. This discussion basically motivates the research on the modelling of hydraulic servo-systems, leading to the problem statement of Section 1.3. A rather extensive elaboration of the problem statement is also included in this latter Section. After that, the approach for research is given in Section 1.4, while an outline of the thesis in Section 1.5 completes this Chapter.

1.1 Hydraulic servo technique

1.1.1 History and motivation for hydraulic drives

The fluid power technology has developed mainly from the beginning of this century, where the first generation of hydraulic drives consisted of some flow control device, driving the hydraulic actuator in an open loop manner. Thereby, one could think of applications as hydraulic presses, jacks and winches. The main advantage of fluid power, which made it so widely used, is the good ratio between delivered force or torque on the one hand and the

actuator weight and size on the other hand. In many applications, this allows the so-called direct drive construction, so that wear-sensitive gear-boxes can be avoided. Examples are different types of hydraulic drives and transmissions in mobile systems.

Whereas hydraulic drives were initially used for open loop actuation, servo control techniques became widely applied later on, particularly since World War II, allowing accurate closed loop motion control. This opened a wide range of applications, still to be found in industry, such as machine tools, robotics, motion simulators, excitation systems, fatigue testing systems and so on. Although some of these applications also allow the use electrical drives in some cases, hydraulic actuators are often in favour for a number of reasons, as mentioned by Merrit [98]:

- High power to weight ratios can be achieved, because generated heat due to internal losses is carried away by the fluid and easily exchanged in a cooler outside the system.
- The hydraulic fluid acts as a lubricant and avoids wear.
- Force and torque levels are extremely high as compared to electrical drives; limits are imposed by safe stress levels, and not by saturation effects as in electrical motors.

An additional argument for the use of hydraulic actuators holds in cases where long-stroke linear actuators are required, allowing operation both at high speeds and high force levels. A typical example of such an application is a flight simulator motion system; till now, these systems are hardly equipped with electrical actuators.

Besides the advantages of fluid power, there are obviously some disadvantages, some of which are [98]:

- There is always a need for hydraulic power generation; electrical power is generally more readily available.
- Components of hydraulic systems are relatively expensive because of the small allowable tolerances.
- A hydraulic system is relatively difficult to maintain; it should be free from leaks, the fluid should be free of dirt and contamination, and breaks with complete loss of fluid should be prevented as much as possible.

Despite these disadvantages, there are various applications, where their advantages make hydraulic drives the best alternative. In most of these present applications, accurate motion control is required. This means, that hydraulic systems generally operate in closed loop, i.e. as a servo-system. A characterization of such hydraulic servo-systems is given in the next Section.

1.1.2 Characterization of hydraulic servo-systems

A hydraulic servo-system is characterized by a number of subsystems, to be described subsequently: the supply unit providing pressurized fluid, the servo-valve controlling the fluid flow to and from the actuator, the actuator itself, and the measurement and control devices.

Supply unit

Although there is a lot of technology involved in modern power units for the oil supply of a hydraulic servo-system, the functionality of this subsystem is simple, at least from the point of view of hydraulic servo control. The supply unit should provide fluid power to

the servo-system, in the form of a constant supply pressure, independent of the demanded flow as much as possible. Generally, this fluid power is generated by an electrical motor, driving a hydraulic pump. By means of a pressure control mechanism, for instance a pressure relief valve, a constant supply pressure level is maintained. Short term pressure variations due to pump flow pulsations and peak flow demands are mostly equalized by a hydraulic accumulator, which should be mounted at a short distance from the servo-valve. A cooling system with a temperature control loop maintains an operational temperature, generally in between 30 and 40 °C.

Servo-valve

The servo-valve in a hydraulic servo-system is generally a flow control valve of the electro-hydraulic type. Different types of flow control valves have been developed for hydraulic control systems, as described by Merrit [98]. For double-acting hydraulic actuators the four-way spool valve of the flapper-nozzle type is most widely applied, so that the attention in this thesis will be restricted to this type of servo-valves, with a possible extension to a three-stage configuration. The working principle of this type of servo-valve is described in more detail in Subsection 2.2.1; the functionality is, that an electrical control signal is converted into a high-power oil flow, driving the actuator. Thereby, the relation between control input and delivered flow is generally aimed to be linear, which can be achieved by applying critical-centre valves [98, 139], allowing proper closed loop servo control of the actuator.

Actuator

In the complete range of hydraulic actuators, a major classification can be given by distinguishing actuators with a limited and with a continuous travel. The latter ones are always of the rotary type, and can generally be used either as pump or as motor. Although these motors are mostly servo controlled and show resemblance with other servo-actuators, they are left out of consideration here.

The limited travel actuators can be classified as either rotary actuators of the vane type or as linear actuators of the piston type. From servo control point of view, vane actuators are completely equivalent to piston actuators, with the restriction that vane actuators are by definition symmetric, i.e. the displacement flow during motion is equal for both actuator chambers. So, without loss of generality at this point, the attention can be restricted to linear hydraulic actuators.

In the class of linear actuators, there are different basic configurations, as shown in Fig. 1.1, suitable for different applications. Most well-known are the symmetric (double-rod) and the asymmetric (single-rod) actuator. The main advantage of the symmetric actuator is its stiffness and its symmetric load capability, which makes the actuator useful for high-performance applications with dynamic loads. The asymmetric actuator to the contrary, is less stiff, but is well-suited to counteract large asymmetric (static) loads, e.g. gravity forces.

An advantage of the single-rod actuator with respect to the double-rod type is its compact size; there are even applications, like flight simulator motion systems, where it is simply impossible to apply double-rod actuators for geometrical reasons. A construction which combines the advantages of the asymmetric and the symmetric actuator is the

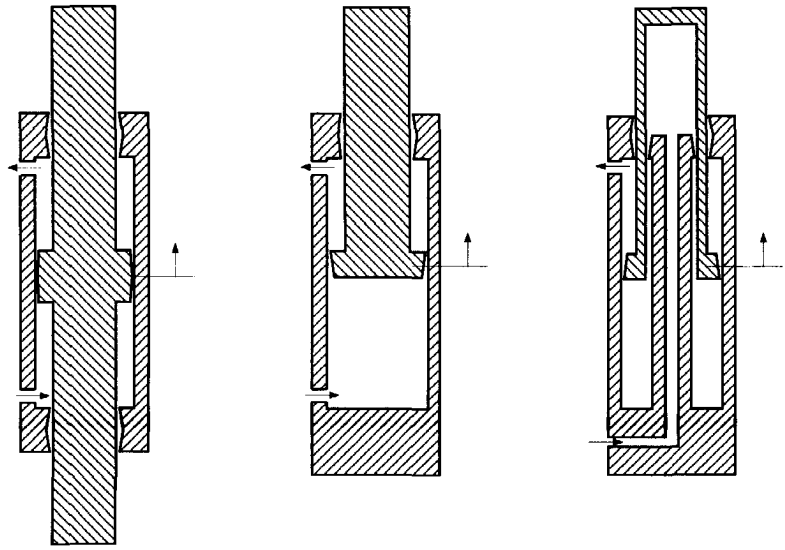


Fig. 1.1: Different configurations of linear hydraulic actuators of the piston type; double-rod (left), single-rod (middle) and double-concentric (right)

double-concentric actuator shown in the right plot of Fig. 1.1. This actuator has only a single rod end, while it has the dynamic (stiffness) properties of a symmetric actuator; by proper dimensioning, the area at the inside end of the piston rod can be chosen equal to the area at the up-side of the piston head, resulting in equal displacement flows for both actuator chambers. Obviously, the construction is more complicated and costly than the traditional configurations, but for high-performance applications like a motion simulator this solution may well be attractive.

So, it is clear that the type of actuator to be used is highly dependent on the application, where aspects as sort of load, available construction space, required performance and allowed costs play a role in the choice. In the trade-off between the latter two aspects, the possible choice for the hydrostatic bearing technique also comes into the picture. With the work of Blok [16] and Viersma [139] on the development of conical bearings (also schematically depicted in Fig. 1.1), a generation of high-performance frictionless hydraulic actuators came available, with worldwide use in various applications, especially flight simulator motion systems, where smooth and highly accurate motions are required.

From the viewpoint of servo control, it may be emphasized here, that a good system design should be seen as a prerequisite to achieve a good performance by means of closed loop control. In other words, closed loop control should not be used to compensate for the shortcomings in the system design, but to obtain an optimal performance given a well-designed system. Actually, the measurement and control hardware, necessary to close the loop of the servo-system, form an important part of this system design.

Measurement and control hardware

In early days of hydraulic position servo control, the actuator position was fed back mechanically to the valve spool, for instance in power steering systems. Nowadays, the actuator is provided with one or more transducers and an electronic control device.

The basic feedback in a hydraulic servo-system is generally obtained from a position transducer, measuring the piston displacement, and allowing the control of it. Besides that, a pressure difference transducer is widely applied, to obtain damping of the natural oscillation of the hydraulic system, or even to allow the control of exerted forces. In applications where explicit force control is the primary goal, such as fatigue testing machines, it is usual to mount a force transducer instead of a pressure difference transducer. In cases, where high-bandwidth position control is required, a velocity transducer may be added, although this is a rather expensive solution. Moreover, for long-stroke actuators velocity transducers are hardly available.

So, for feedback control purposes, transducers for position, pressure difference and possibly the exerted force, are most usual. Additionally, absolute pressure transducers and accelerometers are sometimes used for testing purposes, for instance in experimental setups and prototype systems.

In the past decades the control hardware generally consisted of an analog device, in which the (linear) control algorithm was implemented. Nowadays, most hydraulic servo-systems are controlled by more powerful digital control systems. For instance, the combination of high-resolution AD- and DA-conversion with a Digital Signal Processor (DSP) is a powerful means to achieve a high closed loop performance, by implementing complex dynamic and possibly non-linear control algorithms. Therewith, the hydraulic servo technique has evolved to a high level of technology, where new limits on system requirements and control performance can now be reached.

1.2 Flight simulator motion control

An illustrative example, posing new limits in the hydraulic servo technique, is the development of a new flight simulator at Delft University of Technology. After a brief description of the SIMONA project in Subsection 1.2.1, some developments in motion control for flight simulator systems are outlined in Subsection 1.2.2. Within the scope of these developments, strong requirements are imposed on the hydraulic servo-system to be applied, as discussed in Subsection 1.2.3.

1.2.1 The SIMONA project

Within the International Centre for Research in Simulation, Motion and Navigation Technologies, SIMONA, three faculties of Delft University of Technology are cooperating on the development of a full scale 6 degree-of-freedom (DOF) flight simulator, the SIMONA Research Simulator [2]. Not only in the development phase, but also in the future, when the simulator will be operational, each of the faculties delivers a specific contribution to the research programme:

- The Faculty of Aerospace Engineering is primarily involved in the development of the simulation software and the realization of the interior and the vision system of the simulator. In the operational phase, the research of the Section Stability and

Control of this faculty will focus on flight control, the interaction between the human pilot and the aircraft, and on further improvement of the simulation models, e.g. for helicopters.

- The Systems and Control Group of the Faculty of Mechanical Engineering and Marine Technology is responsible for the development of the 6 DOF hydraulic motion system, including the motion control. After the realization of a first operational version of the motion system, ongoing research will be performed to improve the performance of the motion system, by means of application of advanced motion control concepts.
- The research of the Faculty of Electrical Engineering, Section Telecommunications and Traffic-Control Systems and Services, is concerned with the simulation of existing, and the development of new navigation technologies. In this research programme, the SIMONA Research Simulator can serve as a test-bed for newly developed technologies.

From a mechanical engineering point of view, it is understood that the design of the motion system including the motion control is crucial to the quality of the generated motion cues, and hence the simulation fidelity. This viewpoint has led to the design of an integrated platform/cockpit-structure, made of the light-weight material TWARON/carbon, in order to minimize the weight and also the height of the centre of gravity. In this way, the construction design has been optimized with respect to the dynamic performance of the motion system [2]. An artist's impression of the resulting motion system design is given in Fig. 1.2.

Besides the design of the moving platform, special attention has been paid to the design of the frictionless, long-stroke, double-concentric hydraulic actuators (see also Fig. 1.1) of the motion system. The actuators have been developed and manufactured under supervision of the Mechanical Engineering Systems and Control Group, and actually form the subject of the research reported in this thesis. Thus, the research on hydraulic servo-systems, described in this thesis, forms part of the contribution of the Mechanical Engineering Systems and Control Group to the SIMONA project. In other words, the development of a motion control system for a flight simulator system has been a direct motivation for the work of this thesis on hydraulic servo technique, as will be further explained below.

1.2.2 Motion control for flight simulator systems

The function of the motion control system within the complete flight simulation concept is depicted in Fig. 1.3. A computer program that simulates the vehicle dynamics provides the motion system with the vehicle motions. Because of the finite stroke of the actuators, these vehicle motions have to be transformed to desired platform motions by the motion drive laws, using feedback of the motion system state. The task of the motion control system is then, to compute the actuator control inputs, based on feedback from the actuators, in order to realize the desired motions. The actual hardware to be controlled consists of two parts: the six hydraulic actuators and the inertial motion platform. Through a mechanical coupling, the actuators drive the platform by exerting forces on the platform, while the resulting platform motions prescribe the actuator displacements.

Within this setting, the task specification for the motion control system is to achieve an accurate and high-bandwidth (up to 15 [Hz]) control of specific forces and angular accelerations at some point of the motion platform. The major contribution to these motion quantities is due to the actual accelerations of the inertial platform. In traditional

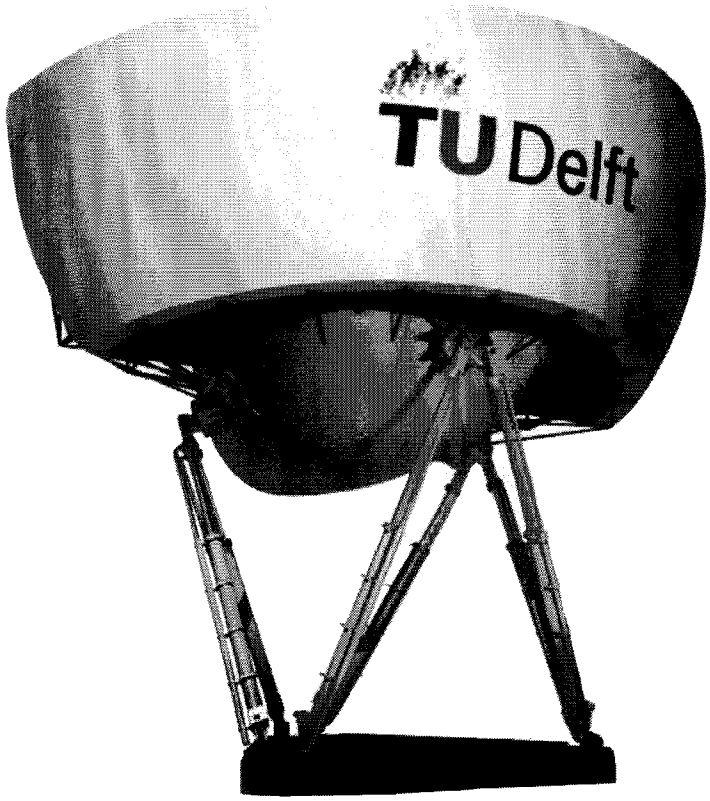


Fig. 1.2: Artist's impression of SIMONA flight simulator motion system

motion control concepts for flight simulation [11], the desired platform accelerations are translated to commanded actuator positions, which are tracked by Single Input Single Output (SISO) actuator position control loops. For low-bandwidth systems (<5 [Hz]) this works well, but for increasing bandwidths of the actuator control loops, stability problems are encountered due to the coupling between the inertial effects of the platform and the dynamics of the hydraulic actuators. Moreover, this coupling is highly non-linear: the simulator motion response is dependent on the position and orientation of the platform, at least for higher frequencies.

So, to meet high performance demands, required for simulation fidelity, the traditional strategy of control design, manual tuning of the SISO actuator position control loops, no longer suffices. What is required, is a model-based approach to control design, in order to cope with the non-linear, multivariable character of the flight simulator motion system. This means, that non-linear, multivariable, robust control techniques as developed and applied in robotic systems [3, 7, 132], are now to be applied also to the 6 DOF flight simulator motion system. Thanks to developments in digital control hardware (see Sub-

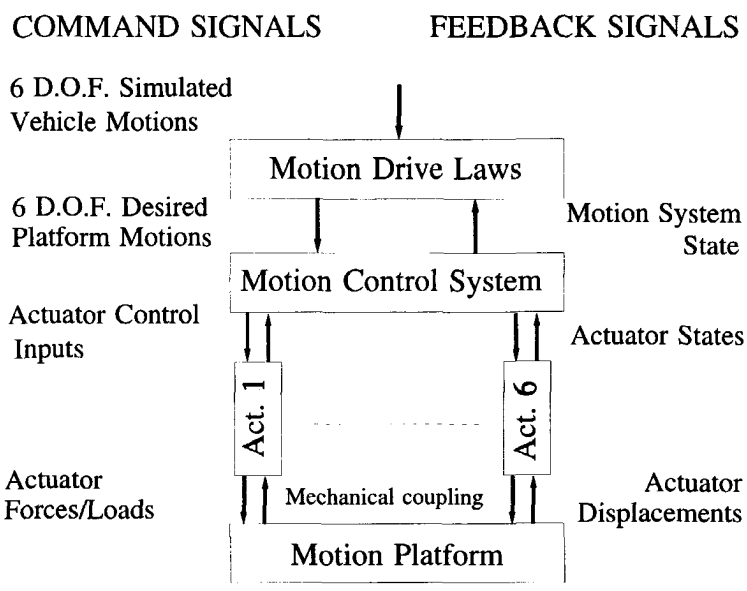


Fig. 1.3: Schematic representation of flight simulator motion system

section 1.1.2), this is now possible; the motion control no longer needs to be implemented as analog control loops, as in the past [11].

With the developments in flight simulator motion control, sketched here, higher demands are posed on the hydraulic servo-systems of the motion system than before, involving new actuator control problems, as discussed next.

1.2.3 Hydraulic actuator control problems and system requirements

When applying non-linear, multivariable control techniques to hydraulically driven motion systems in order to achieve a high performance, a high-gain pressure difference feedback loop is generally involved [51, 54, 83, 124]. Although a proportional feedback loop, which is easily tuned by hand, may be sufficient in some cases [51, 54, 124], another approach will be required in case extreme performance demands are posed on the hydraulic actuator control loops, because high-frequency dynamics of the servo-system can no longer be neglected.

For instance, the dynamics of the servo-valve may have to be taken into account explicitly. This especially holds for the long-stroke actuators of the flight simulator motion system. Due to the long stroke, relatively long transmission lines are present between the valve and the actuator chambers, inducing badly damped resonances in the high-frequency range. These resonances, together with the servo-valve dynamics, should definitely be taken into account in the actuator control design. In other words, the hydraulic actuator control design problem asks for a model-based approach, requiring more extensive modelling of the hydraulic servo-system than before.

Besides these typically control-related arguments for modelling, the requirement of good

system design, mentioned earlier, based on insight in the system behaviour, is also a strong argument for accurate modelling of the hydraulic servo-system.

Given the flight simulator application, an additional system requirement on the hydraulic actuator plays a role, which is related to performance in the sense of safe operation, rather than closed loop control. What is meant here, is the presence of proper hydraulic safety buffers at both ends of the actuator. These so-called cushionings should be designed such, that they dissipate the kinetic energy of the system, when an actuator moves with full speed to the end of its stroke in case of failing control, without excessive acceleration peaks. As no direct design rules are available, the design of these cushionings also asks for a model-based approach, in order to avoid a costly design process based on experimental research.

Summarizing, the system requirements for the hydraulic servo-system to be considered here, ask for a model-based approach to both control design and system design. Thereby, in the scope of this thesis, the attention will be restricted to linear long-stroke hydraulic actuators with two- or three-stage electro-hydraulic servo-valves.

1.3 Problem statement

1.3.1 General problem statement

Motivated by the application of long-stroke hydraulic actuators in a flight simulator motion system, in which extreme performance demands are posed on the hydraulic servo-system, extensive and accurate modelling of this system is to be performed. Therefore, the problem statement for this thesis is formulated as follows:

> IMPROVE THE QUALITY OF THE MODELS OF HYDRAULIC SERVO-SYSTEMS WITH RESPECT TO THEIR INTENDED USE:
>
> - TO OBTAIN INSIGHT IN THE SYSTEM BEHAVIOUR,
> - TO PERFORM MODEL-BASED CONTROL DESIGN, AND
> - TO PERFORM MODEL-BASED SYSTEM / CUSHIONING DESIGN.

1.3.2 Elaboration of the problem statement

Because of the three-fold intended use of the models, a rather general approach to the modelling of hydraulic servo-systems is required, covering the whole range of theoretical modelling (for insight), identification and validation (for reliable use in control design), and the application of the model-knowledge in control design and system design. Given the scope of the research, described in the previous Sections, with increased performance requirements on long-stroke hydraulic servo-systems, it seems to be especially important to include the properties of the servo-valve and the transmission lines in the investigations. Against this background, the general problem statement is worked out in five main topics for the research:

1. Modelling of the hydraulic actuator
2. Modelling of the servo-valve
3. Modelling of transmission line dynamics
4. Control design for hydraulic servo-systems
5. System design and cushioning design

Each of these topics will be worked out below, as a motivation for the approach for research, to be given in Section 1.4.

1. Modelling of the hydraulic actuator

The theoretical modelling of hydraulic actuators is well-developed in the past decades. Standard text-books on hydraulic servo-systems, as for instance those by Merrit [98] and by Viersma [139], provide a thorough analysis of the basics of the hydraulic servo technique. Among others, this analysis comprises the theoretical modelling of the dynamical and non-linear effects in various hydraulic components, among which hydraulic actuators. Besides these basic contributions of Merrit and Viersma, there are numerous other contributions [1, 19, 35, 52, 66, 73, 91, 94, 124, 125, 148], in which the basic modelling of hydraulic actuators is reported. Although there are some differences in the presented models, generally related to the kind of application at hand, the basic model of the hydraulic actuator is similar in all cases.

Despite the fact that the modelling of hydraulic actuators is well-established in literature, it is highly important to include it in this research, for several reasons:

- Like in other modelling examples in literature, the specific application at hand requires a dedicated model. In this case, this means that the behaviour of hydrostatic bearings is to be taken into account, while the effects of Coulomb friction will be given few attention.
- The model of the hydraulic actuator forms the basis of this research; all four remaining research topics will have to be adressed in relation to the basic behaviour of the hydraulic actuator.
- In literature, the experimental identification of the theoretical model of the actuator is often not adressed. In this work, a general approach is to be presented, starting with theoretical model relations and ending with an experimentally identified and validated model, that can be used directly for control design.

So, the modelling of the hydraulic actuator is a necessary and important part of this research. However, the main contribution of this thesis lies in the fact that servo-valve dynamics and transmission line dynamics are explicitly included in the approach to hydraulic servo control design and system design. For that purpose, the other four research topics are considered.

2. Modelling of the servo-valve

In the field of servo-valve modelling, extensive theoretical modelling work has been presented with emphasis on different subjects. Basic work has been performed again by Merrit [98], where he mainly takes the viewpoint of system design, and comes up with very useful design rules for spool valves, flapper-nozzle elements, etcetera. Furthermore, the effect of turbulent flow through small orifices has been extensively studied in literature [39, 44, 99],

as well as flow forces on a flapper element [15, 31, 79, 97, 98, 127] and leakage flows along a valve spool [72]. There are also studies considering the complete non-linear dynamic behaviour of a flapper-nozzle valve, among others by Lin and Akers [80, 81], Lebrun and Scavarda [74], Vilenius and Vivaldo [140] and Wang et.al. [144].

Although these references are quite valuable from a theoretical point of view, especially because they often include an experimental validation of the studied phenomena, they do not provide the link to the practice of hydraulic servo control design, because it is generally not clear, how the model parameters have been chosen. A serious complication is here, that manufacturers are not willing to provide the necessary information on geometrical parameters, and even may not be able to provide some of the model parameters because they are not (easily) measurable. This implies, that the model parameters have to be identified from input-output behaviour. Generally, this identification issue is not adressed in literature on servo-valve modelling, although Handroos and Vilenius [49] form an exception. Another problem with available literature is, that the discussions mainly remain restricted to the servo-valve behaviour on its own, without considering the implications for closed loop servo control.

Contrary to the theoretical modelling approach for hydraulic servo-valves found in literature, there is a tendency in contributions on hydraulic servo control design, to approximate servo-valve dynamics by simple linear low-order models [36, 62, 105, 150, 146]. Also in these cases, the identification issue is mostly not adressed, while moreover the adopted models do not properly reflect the underlying physical behaviour of the valve. This also holds for the third order linear model proposed by Thayer [135], which does not generally represent the dynamics of a flapper-nozzle valve, as shown by Wang et.al. [144].

In short, a general approach to the physical modelling and experimental identification of the non-linear dynamic behaviour of servo-valves, including the link to closed loop control design, is not available, and needs to be developed. This motivates the modelling of the servo-valve as a main research topic, where some constraints are imposed on the approach, and some choices are made, according to the following considerations:

- In order to obtain insight in the dynamics and non-linearities of the servo-valve, extensive theoretical modelling is to be performed. The desired insight not only concerns the character of the dynamics of the servo-valve, but also the relevance of different non-linearities, related to certain physical effects, that may be present in the servo-valve. Thus, the obtained insight can be used in system design, i.e. to determine the requirements on the servo-valve.
- For control design purposes, experimentally validated dynamic models of the servo-valve are required. Thereby, the relevant non-linearities are to be included, in order to use the models for robustness analysis and possibly for non-linear control design. So, non-linear identification of the servo-valve models is to be performed, such that the obtained insight from the theoretical modelling is preserved. This requires special attention for the experiment design and the identification method.
- Related to the previous item, black-box identification is left out of consideration in this research, as it can not handle the physical structure of the model. On the other hand, white-box modelling is not possible either, because there is insufficient a-priori knowledge on the theoretical model parameters. For these reasons, a grey-box model for the servo-valve will be derived.
- Although the experimental part of the servo-valve modelling is necessarily applied to a certain type of servo-valve (related to the hydraulic servo-system for the flight

simulator application), the approach to the modelling of the servo-valve should be general, so that it also applies to other valves of the flapper-nozzle type.
- The previous requirement implies, that it should also be possible to omit, for instance, the dynamic part of the model, depending on the application at hand. In other words, in relation to the complete model of the hydraulic servo-system, the model of the servo-valve should be included in a modular way.

With this discussion, a line of thinking is developed for the modelling of servo-valves, which actually also applies roughly to the modelling of transmission line dynamics, as explained next.

3. Modelling of transmission line dynamics

The direct reason to take transmission line dynamics explicitly into account, is that they were found to play a dominant role in the given application with long-stroke hydraulic actuators, causing stability problems under weak proportional pressure feedback [119]. So, in order to obtain insight in this phenomenon and to know whether transmission line dynamics are relevant for control design, the modelling of transmission line dynamics is included in the research.

The phenomenon of transmission line dynamics in hydraulic systems has been extensively studied in the past. Main contributions are due to Iberall [61], Nichols [106] and d'Souza and Oldenburger [33]. Goodson and Leonard [42] give a clear overview of different representations of the transmission line models. In the field of hydraulic servo-systems, the phenomenon has been studied as far as supply lines are concerned by Ham and Viersma [47, 139], while the effect of transmission line dynamics between valve and actuator has been adressed, among others, by Watton et.al. [146, 150, 151].

However, what is lacking in these contributions, is a clear relation between the theoretical modelling of transmission line dynamics and the system theoretic interpretation of the modelled effects on the behaviour of the servo-system, including the implications for control design. The problem is thereby, that theoretical transmission line models, as the ones presented by Goodson and Leonard [42], consist of complex transfer functions, which do not allow direct inclusion in simulation models of a complete hydraulic servo-system. Moreover, identification of the model parameters from experiments is difficult due to the complexity of the model. So, it is difficult to obtain reliable models, that can be used for control design, via theoretical modelling of the transmission line dynamics.

The solution to these problems is found in the use of approximations of the theoretical models of the transmission line dynamics. Thereby, numerous possibilities are available. For instance, the method of characteristics [158, 163] allows time domain simulations, the method using causal (delay) operators [34, 69] allows both time domain and frequency domain analysis, and modal approximation techniques [59, 60, 92, 155, 160] allow a clear system theoretic interpretation in terms of linear low-order dynamic models.

Thus, the research on the modelling of transmission line dynamics will have to focus on the inclusion of approximations of the theoretical models of transmission lines in the complete model of the hydraulic servo-system. Thereby, the following aspects have to be considered:

- As the models are not only to be used for control design, but also to derive the implications of transmission line dynamics for system design, the approximations

will have to allow a clear physical interpretation. In other words, the parameters of the approximate models of the transmission lines will have to be stated in terms of physical quantities, for instance geometrical parameters.

- In order to be useful for control design and analysis of the dynamic behaviour of the hydraulic servo-system including transmission line dynamics, both in the frequency and in the time domain, the approximations will have to be of sufficiently low order. Moreover, experimental identification of the parameters will have to be performed again in the sense of grey-box modelling, in order not to loose the physical interpretation of the models.
- In fact, the grey-box modelling approach is strongly related to the requirement, that the model of the complete hydraulic servo-system has to be modular, in the sense that the (approximate) models of the transmission lines can easily be included or omitted, depending on the application. Special attention is required here for the proper integration of the basic actuator model and the approximate models of the transmission lines.

With the first three research topics directly dedicated to the modelling of hydraulic servo-systems, the remaining two focus on the use of the model-knowledge in control design and system design respectively.

4. Control design for hydraulic servo-systems

As mentioned earlier, high-performance motion control asks for model-based control. As far as position control for hydraulic actuators is concerned, basic principles have been discussed thouroughly by Merrit [98] and Viersma [139]. Besides that, applications of more modern control techniques to hydraulic servo-systems have been reported extensively in literature. Examples are state feedback control [36, 66, 104, 105, 147, 153], robust control [70, 83, 159] and adaptive techniques [57, 65, 66, 113, 111, 161], to mention only some. Another interesting development in hydraulic servo control is the so-called cascade ΔP control strategy, presented by Sepheri et.al. [124] and worked out and formalized by Heintze et.al. [54]. This method actually emphasises high-frequency pressure difference control by high-gain pressure difference feedback, rather than position control.

Although the different applications reported in literature are quite valuable, in the sense that they prove the validity of a certain control design approach for a certain application, a general relation between the application dependent control requirements and the applied control strategy can hardly be recognized. What is desirable in fact, is a general approach for model-based control design for hydraulic servo-systems, based on task specifications of the application and on available model knowledge of the system at hand. This actually constitutes the fourth research topic of this thesis, including the following aspects to be considered:

- Against the background of the flight simulator application, it is to be taken into account, that the control design for hydraulic servo-systems forms part of the multivariable motion control of multi DOF systems. This does not mean, that the topic of multivariable control of multi DOF systems itself is included in the research, but that the task specifications for hydraulic servo control are to be considered in a setting of multivariable motion control.
- Given the task specification for the control loop of the hydraulic servo-system, a survey of basic actuator control strategies will be given, where the design is obviously

model-based. This will have to include a discussion of the benefits of certain control strategies with respect to the given task specification, possibly in relation to the type of application.

- Highly important is the explicit inclusion of the implications of the properties of the servo-valve and the transmission lines on the closed loop performance, when discussing the control design for hydraulic servo-systems. In fact, this is the point, where the benefits of model-based control design should really become clear.
- For the flight simulator application with long-stroke actuators, for which velocity transducers are hardly available, velocity estimation requires attention, as a velocity signal may be required in certain control strategies.
- A last but not least important aspect concerns the experimental evaluation of model-based control design. This means, that only control design and testing at simulation level is not sufficient, but that experimental implementation by means of digital controllers is required. Therewith, it is not only possible to evaluate the model-based control design strategy, but also to validate the obtained models of the system in view of control design.

Besides that the model knowledge is to be used for control design, there are some issues in system design and cushioning design, that deserve a model-based approach.

5. System design and cushioning design

The basics of hydraulic servo-system design are well-known, and can be found in the books of Merrit [98], Viersma [139], and Walters [143]. What is hardly mentioned in these books however, or at least not enough emphasized, is the important role of the properties of the servo-valve and transmission lines in hydraulic servo control, especially for long-stroke actuators. It is therefore necessary, that the model knowledge concerning the servo-valve and the behaviour of the transmission lines is utilized in system design. This issue will be adressed in this thesis.

An aspect of system design, which is not at all found in literature, neither in the books of Merrit and Viersma, nor in other references, is the model-based design of safety cushionings. Especially for applications like flight simulator motion systems, where safe operation is a prerequisite, this is a highly important issue. Therefore, in line with the work on the modelling of the hydraulic actuator, and motivated by the SIMONA project (see Subsection 1.2.1), the cushioning design issue is included in the research. In the approach to this research topic, the following considerations play a role:

- The type of cushioning that is applied at the top-side and the bottom-side of the hydraulic actuator respectively, is determined by the construction. This implies, that the model-based cushioning design to be developed is constrained to the optimization of the cushioning geometry, given the type of cushioning. The optimization is to be performed with respect to some desirable cushioning performance, which guarantees a smooth and safe stop of the actuator in case of control failure.
- The model-based cushioning design requires an extension of the actuator models with models for the cushionings, with the type of the cushionings being given. The modelling of the cushionings is necessarily based on basic physical laws, as no experimental data are available beforehand. Moreover, the design requires physical insight in the cushioning process, which is only to be obtained by theoretical, physical modelling.

- The quality of the cushioning models is only to be evaluated with respect to the experimental performance of the cushionings, that are designed on the basis of the models. So, no accurate quantitative validity of the cushioning models is required.
- An experimental evaluation of the performance of designed cushionings is possible in the scope of the SIMONA project, and shall complete the research on cushioning design.

Based on the elaboration of the problem statement in five main research topics, as given in this Subsection, the approach for the research, reported in this thesis, has been chosen.

1.4 Approach for research

In the description of the approach for research in this Section, the five main research topics are (to some extent) taken together. Actually, it is a functional description of the approach for research, rather than a detailed overview of the research programme.

In order to obtain structural insight in the behaviour of the hydraulic servo-system, with respect to relevant dynamics as well as relevant non-linearities, the starting point is the theoretical, physical modelling of the complete servo-system. That means, that a theoretical model is constructed from basic physical laws, using and combining available contributions on theoretical modelling of hydraulic systems in literature. The result is a non-linear dynamic (simulation) model of the hydraulic servo-system, including actuator, servo-valve and transmission lines. This model is used to perform various simulations, with realistic physical parameters for the given flight simulator application, so that structural insight in the relevant dynamics and non-linearities of the system can be obtained.

The obtained insight can be used to simplify and reduce the model where possible, and to neglect irrelevant non-linearities. In this phase, linearization of the model plays an important role, as it provides much insight in the dynamic characteristics of the system. For instance, it allows a judgement, whether dynamics due to the servo-valve and/or the transmission lines may be expected to play an important role or not. Another reason for linearizing and reducing the theoretical model is the fact that the original complex non-linear model is not identifiable: the model parameters can not be identified uniquely from experimental data. Simplification and reduction to an identifiable form facilitates the identification of model parameters in a later stage.

An important issue in the linearization and simplification step is the physical structure of the dynamic model. This structure is always preserved in the chosen approach, in order to allow the inclusion of the relevant physical non-linearities in the model. The judgement whether non-linearities are relevant or not is primarily based on non-linear simulation results.

After the model has been linearized, reduced and relevant non-linearities have been included again, the model parameters are identified from experimental data. Thereby, the dominant non-linearities of the system are explicitly taken into account by proper experiment design and by applying the well-known Describing Function Method in an appropriate way. Experimental validation of the identified non-linear dynamic models of the servo-system is performed by comparing non-linear simulations with corresponding measurements.

With an experimentally validated model of the complete hydraulic servo-system available, a survey of basic (model-based) control strategies can be given. Thereby, aspects

like application dependent task specifications, implications of servo-valve dynamics and/or transmission line dynamics, absence of velocity measurement, and experimental conditions are considered.

As a final part of the research, the possibilities of improved system design, using the available model knowledge, are investigated. On the one hand, this concerns the avoidance of potential control problems due to non-linear valve dynamics and/or transmission line dynamics. On the other hand, the model knowledge is utilized for the optimization of the geometry of two types of cushioning. This involves the inclusion of cushioning models in the models of the hydraulic actuator, the development of a model-based design procedure and the experimental evaluation of the cushioning performance, that can be achieved with the model-based approach.

1.5 Outline of the thesis

After a sketch of the general approach for research in the previous Section, an overview of the contents of the thesis follows in Subsection 1.5.1, by discussing the subdivision in Chapters. In order to further elucidate the structure of the thesis, a rather detailed overview of the research topics is given in Subsection 1.5.2.

1.5.1 Overview of contents

The first two main Chapters of the thesis deal with the complete modelling approach for hydraulic servo-systems, i.e. the first three main research topics discussed in Subsection 1.3.2. Thereby, a subdivision is made with respect to the two main phases in this modelling approach: Chapter 2 treats the physical modelling of the different subsystems, while the identification and experimental validation of the models is discussed in Chapter 3. After that, Chapter 4 and 5 treat the other two main research topics, the application of the obtained models to control design and to system design respectively.

Chapter 2: Physical modelling

Starting with a description of the system and definition of the system boundaries, this Chapter gives the theoretical model relations, that constitute the non-linear dynamic model of the complete hydraulic servo-system. This involves models for the servo-valve, the actuator and the transmission lines in between. Thereby, an extensive analysis of the non-linear models is given, by means of the discussion of simulation results obtained with the physical models.

After that, an analysis is given of the servo-valve dynamics and the actuator dynamics (including transmission lines) respectively, by means of linearization and physically argued reduction of the models. In a next step, the relevant non-linearities of the physical model are included in the linearized models, such that relatively simple, non-linear, identifiable models are obtained. A summary of the results of Chapter 2 is given in Appendix A, in the sense that it provides an overview of the relevant modelling aspects of a hydraulic servo-system.

Chapter 3: Identification and experimental validation

Chapter 3 starts with the discussion of the experiment design and the method of identification and validation, to be applied to the hydraulic servo-system. After that, a description is given of the real hydraulic servo-system, that is to be applied in a flight simulator motion system, and which is used for an experimental verification of the different results of this thesis.

In the remainder of Chapter 3, the identification and validation techniques, discussed before, are applied to the described servo-system, involving the servo-valve, the actuator, and the actuator including transmission lines, respectively. So, the different subsystem models of Chapter 2 are identified, both with respect to the dynamics and the dominant non-linearities. Furthermore, an experimental validation is provided, by comparing simulation results to experimental data, in order to prove the validity of followed approach of theoretical modelling and subsequent simplification and identification.

Chapter 4: Control design

The purpose of Chapter 4 is to give a survey of basic strategies in model-based control design for hydraulic servo-systems, including a discussion of experimental issues. Therefore, possible task specifications for this type of systems are briefly discussed, after which a number of basic control strategies for hydraulic actuators is considered. Thereby, the implications of the experimentally validated model knowledge of the system, especially with regard to servo-valve and transmission lines, are emphasized. Furthermore, the role of proper system design in view of control performance, utilizing the obtained insight in the system behaviour, is touched upon. The practically very important issue of velocity estimation for hydraulic servo-systems is also adressed. Finally, an experimental evaluation of the different basic control strategies completes the discussion on model-based control design for hydraulic servo-systems.

Chapter 5: Cushioning design

Using the available knowledge of the dynamic behaviour of the hydraulic actuator, a model-based cushioning design procedure can be developed, by slightly extending the available models. An experimental evaluation of the validity of this procedure is also provided, by showing the experimental performance of two types of cushionings, that have been designed with the procedure. With the discussion of these issues, Chapter 5 ends the main part of this thesis.

Chapter 6: Conclusions and recommendations

The final Chapter of this thesis gives the conclusions that can be drawn on the presented results, as well as a number of recommendations for future work.

1.5.2 Structure of the thesis

To some extent, a sort of matrix-structure is present in the research described in this thesis. On the one hand, there is a subdivision related to the different subsystems of the hydraulic servo-system, namely servo-valve, actuator, and transmission lines. Actually, the

first three main research topics of Subsection 1.3.2 are directly related to this subdivision. On the other hand, there is a subdivision related to the different phases in the approach for research. It is this subdivision, which is reflected in the subdivision in Chapters of Subsection 1.5.1.

The matrix-structure becomes more clear, when the subdivision of the Chapters in Sections is considered. In order to provide more insight at this point, an abstract representation of this structure is given in Table 1.1. The columns represent the three subsystems, where the transmission lines are basically taken together with the actuator; the rows represent the various phases in the approach for research. Obviously, the double horizontal lines indicate the subdivision in Chapters.

	Servo-valve	Actuator	Actuator with transm. lines
Theoretical modelling and simulation	Sect. 2.2	Sect. 2.3	Sect. 2.4
Analysis of dynamics	Sect. 2.5	Sect. 2.6	
Inclusion of main non-linearities	Sect. 2.7		
Approach to identif. & validation	Sect. 3.2		
Experimental results identif. & validation	Sect. 3.4 & 3.5	Sect. 3.6	Sect. 3.7
Control design strategies	–	Sect. 4.2 & 4.3	–
Robust control design & system design issues	Sect. 4.4		
Velocity estimation	–	Sect. 4.5	–
Experimental results control design	Sect. 4.6		
Cushioning design	–	Sect. 5.2, 5.3 & 5.4	–

Table 1.1: Abstract representation of the structure of the thesis

With this overview of the contents, together with the index, it should be easy to find a way through this thesis.

Chapter 2

Physical modelling of hydraulic servo-systems

In this Chapter, a physical model of a hydraulic servo-system is presented, which includes the most relevant dynamic and non-linear effects that are involved in hydraulic servo-systems. Although the presented model has to be identified and validated experimentally, as discussed in the next Chapter, it forms a good basis both for contol design and for system design.

2.1 Introduction

The introduction of this Chapter starts with a brief description of the system to be modelled, the hydraulic servo-system, and the system boundary, in Subsection 2.1.1. After that, the modelling approach is discussed in some detail in Subsection 2.1.2, while Subsection 2.1.3 provides an outline of this Chapter.

2.1.1 System description and system boundary

A general characterization of a hydraulic servo-system has been given in the previous Chapter, in Subsection 1.1.2. However, in view of the mathematical modelling of this system, a more precise description is to be given, including the system boundary.

From a modelling point of view, almost any flow-controlled hydraulic servo-system can be reduced to the basic configuration shown in Fig. 2.1. The control input u of the servo-valve is used to control the oil flow through the ports of the solenoid. Oil is supplied by a power supply unit under a presumably constant supply pressure P_s, while the return flow is fed to a tank under the (small) return pressure P_t.

The resulting oil flow Φ_p into and from the lower and upper actuator compartments respectively, drives the piston, thereby generating the required the pressure difference ΔP_p to move the load of the actuator. In this way, the piston motion (expressed in terms of piston velocity $\dot{q}$) depends on the load of the actuator. Actually, for motion systems with free moving bodies, this load can be seen as an inertia M_p plus some external force F_{ext}, which might include gravity forces for example.

Drawing the system boundary around the hydraulic servo-system, described above, there are a number of interfaces with the environment of the system, where energy exchange may take place. Basically, these interfaces can be seen as bilateral couplings, with energy

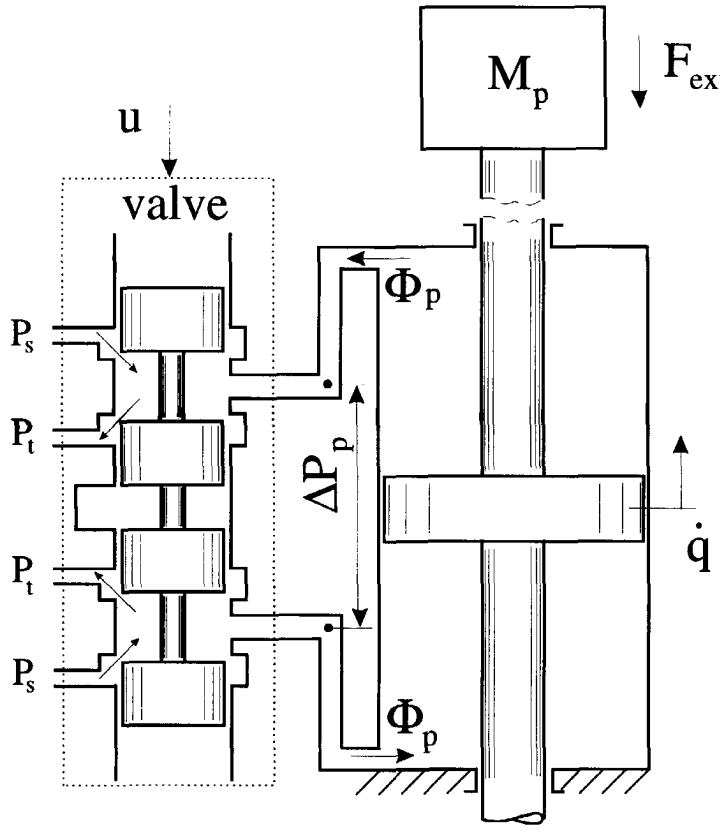


Fig. 2.1: Schematic drawing of hydraulic servo-system

exchange by means of a flow variable and a potential variable. This bilateral coupling is easily taken into account in the model by proper definition of impedance and admittance relations, both for the system and the environment. However, in many cases, simplifying assumptions are quite realistic, for instance when the interface is meant for informantion exchange rather than energy exchange. This especially holds for the first two of the total of five interfaces of the system with the environment:

1. **Control input.** For the control input u, generally a voltage, it is quite realistic to consider it as an ideal input signal; the input impedance for the electrical signal is infinitely large.
2. **Measured outputs.** Depending on the application or the experimental setup, a number of system states can be measured by means of sensors (transducers). The sensors are designed to be ideal in the sense that their output impedance is zero, while they do not affect the measured states.
3. **Actuator load.** This is the most important interface, because there is a significant energy exchange. The type of energy exchange depends on the the load characte-

ristics, i.e. the load impedance $\frac{F_{ext}}{\dot{q}}$, and determines the total dynamic behaviour of the servo-system.

4. **Actuator base.** The actuator base should always be designed to be as stiff as possible, with an impedance (say: inertia) which is large enough to avoid parasitic energy exchange. In other words, no parasitic motions of the base should occur. Whenever (unexpected) parasitic motions occur in an application, one should be aware of the fact, that the system dynamics are affected by the impedance of the base. In that case, the actuator can not be assumed to be rigidly connected to a base with infinite impedance.
5. **Power supply.** In most hydraulic servo applications, the power supply unit is designed in such a way, that the system maintains a constant supply pressure for a certain range of operation, i.e. oil flow demand. An effective way to do this, is the application of hydraulic accumulators [139], in combination with a pressure controlled flow pump. Especially for high performance demands on the hydraulic servo-system with respect to piston-velocity, one should be aware that the limits of the range of operation may be reached, resulting in pressure drops. This may be taken into account in the model, by modelling the supply pressure P_s, as well as the return pressure P_t, to be dependent on the delivered flow Φ_p. For ideal oil supply, the pressures P_s and P_t are constant.

In order to reduce the complexity of the modelling of the system inside the defined system boundary, it is useful to distinguish a number of (causal) subsystems.

First, there is the electro-hydraulic servo-valve, which transfers the control input into an oil flow Φ_p, dependent on the actuator pressure difference ΔP_p. Although this device is designed to be fast and to show linear input-output behaviour, its actual behaviour is generally not ideal. Because the servo-valve flow drives the actuator, any non-ideal behaviour of the valve propagates through the complete servo-system, for which reason the servo-valve is explicitly considered in the modelling as a separate subsystem.

Second, there is the hydraulic actuator including load mass, with the driving oil flow Φ_p and the external force F_{ext} as inputs, and correspondingly the actuator pressure difference ΔP_p and velocity $\dot{q}$ as outputs. The hydraulic actuator as subsystem forms the kernel of the comlete hydraulic servo-system; the servo-valve and possibly transmission lines leave the basic behaviour of the system unaffected, although in many cases, they may not be neglected, as will be shown in the remainder of this thesis.

The set of transmission lines between the servo-valve and the actuator is to be considered as a third subsystem, which is especially important when the actuator has a long stroke. Because of the compressibility and the inertia of the oil, the relatively long transmission lines cannot be seen as static devices; pressure waves travel with a finite velocity through the line and are almost ideally reflected at the end of the line. Due to the small amount of damping of the fluid, badly damped resonances can occur in the system, which are relevant for actuator control. Therefore, a dynamic relation between the states at the upstream side and those at the downstream side of the line should be taken into account. This is indicated in Fig. 2.2, where the pressures P and the flows Φ have been given indices, depending on whether the upstream states or the downstream states are concerned; the index $_{i1}$ denotes the inlet or valve-side of transmission line 1, while the index $_{o1}$ denotes the outlet or actuator-side; the indices $_{i2}$ and $_{o2}$ denote the inlet and outlet side of transmission line 2 respectively.

Thus, taking transmission line dynamics into account, the complete hydraulic servo-

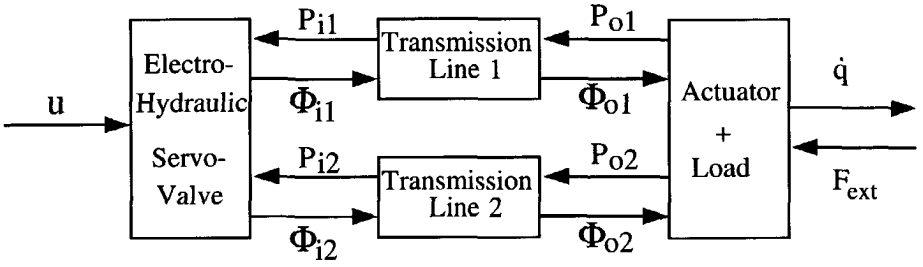


Fig. 2.2: Subsystems of hydraulic servo-system with interconnections

system can be represented by its three subsystems, with interconnections as shown in Fig. 2.2. The physical modelling of these subsystems is the subject of this Chapter. In order to obtain the desired modelling results, a certain approach has been chosen, as explained in the next Subsection.

2.1.2 Approach to modelling

For the approach to modelling, the intended use of the models is of importance. On the one hand, the resulting models should provide physical insight in the system behaviour and in the different physical phenomena that play a role in this behaviour, in order to allow their use for system design. On the other hand, model-based control design requires an accurate mathematical description of the real system, both with respect to dynamics and with respect to relevant non-linearities. In order to cope with this requirements on the modelling, a general modelling approach is chosen, which is worked out below, for the different subsystems respectively.

General approach to modelling

In order to obtain insight in the various physical phenomena, that play a role in the behaviour of the hydraulic servo-system, the modelling approach starts with extensive theoretical modelling of the complete system. Thereby, the models are based on basic physical laws, such as mass balances for oil volumes, equations of motion for moving parts, equations for turbulent flow through small restrictions, and so on. In the theoretical modelling, all effects are included that are expected to play a role in the (dynamic) behaviour of the system, based on earlier work in the area of hydraulic servo technique.

The actual insight in the system behaviour is obtained by performing lots of simulations with the non-linear theoretical model. These simulation results are used to judge, whether certain physical effects deliver a relevant contribution to the over-all system behaviour or not. This may be in the sense of dynamics, or in the sense of non-linearity. It should be noted here, that this insight is mainly of *qualitative* value; because it is difficult to find a realistic set of physical parameters for the theoretical model, this model does not have a high predictive value in the *quantitative* sense.

Whereas the model of the hydraulic servo-system is also to be used for control design, the model should not only be qualitatively correct, but should also have predictive value in

a quantitative sense. This means, that the model should accurately represent the dynamic and non-linear behaviour of a real system. This is possible, if there is a clear relation between the input-output behaviour of the model and the parameters of the model, so that the parameters can be chosen or adjusted such that the model fits the behaviour of some real servo-system. In other words, it should be possible to identify the model from experimental input/ouput data.

For this purpose, it is at least required, that the model is of the same order as the relevant dynamics of the real system, and that only the dominant non-linearities of the real system are included in the model. So, the model should not include irrelevant dynamics and/or non-linearities. Actually, the theoretical model, including 'all' physical phenomena that possibly play a role in the system behaviour, does not fulfil these requirements on the model; it is too complex to be used directly for identification and control design purposes. It should therefore be simplified.

However, in order not to disregard the advantages of the theoretical model, the simplification should be such, that:

- the (dominant) dynamic behaviour described by the theoretical model is preserved, and
- the physical structure of the model is preserved, so that (dominant) non-linear effects related to certain physical phenomena can be taken into account.

Related to these requirements, a simplified model of the hydraulic servo-system is obtained in two stages.

In the first stage, the dynamic behaviour of the system is abstracted from the theoretical model by means of linearization. Based on physical insight, partially obtained from the simulations with the theoretical model, the linearized model can be reduced (while preserving the physical structure of the model) such as to obtain minimal order models, describing the dominant dynamic behaviour of the system.

In the second stage, the obtained models are extended with the non-linearities of the theoretical model that seem to be relevant, again based on the results of the simulations with the theoretical model. Thereby, the non-linear effects described by non-linear equations in the theoretical model are rewritten in a simplified form, with a minimum number of parameters, like proposed by Handroos and Vilenius [49]. In this way, there is a clear relation between the model parameters and the resulting non-linearity in the system, while physical interpretation is still possible. So, the effects of non-linearities, related to certain physical phenomena, on the system behaviour, can be analyzed easily, in a quantitative sense, by means of simulations with the simplified non-linear dynamic model.

With this two-stage approach to the simplification of the theoretical model, a physically structured non-linear dynamic model of the hydraulic servo-system is obtained, which forms the basis for experimental identification and validation, as discussed in Chapter 3.

Given the general approach to modelling, outlined here, the approach to the modelling of the different subsystems can be further elaborated as follows.

Approach to servo-valve modelling

Because the flapper-nozzle servo-valve is a rather complicated device, the theoretical modelling is rather involved. In line with other research on this topic, reported in the literature [98, 80, 81, 74, 140, 144], a lot of dynamic and non-linear effects are included, resulting in a rather complex non-linear model, just for the servo-valve.

A problem with this model is, that it is difficult to choose the large number of physical parameters in the model such that quantitatively valid simulation results are obtained. Although a lot of parameters may be known rather exactly a priori, many parameters are only known within some (wide) range, and some are even completely unknown. This may be due to manufacturing tolerances, or due to the fact that manufacturers do not provide parameter values, because they consider it as proprietary information [144].

The consequence of this problem is, that the theoretical model is not useful for quantitative analysis of the servo-valve behaviour. Nevertheless, a lot of qualitative insight can be obtained from simulations, which can be utilized to reduce the (linearized) servo-valve model such, that only relevant dynamics are taken into account. Furthermore, the simulation results provide the necessary insight to decide, which non-linearities of the servo-valve are (possibly) relevant. Thus, a relatively simple model for the servo-valve can be derived, which includes relevant non-linearities and dynamics, and which forms a good basis for experimental identification of the servo-valve properties, as explained in Chapter 3.

Approach to actuator modelling

The theoretical modelling of the hydraulic actuator is less involved than that of the servo-valve. Basically, the principal model relations have been given earlier, among others, by Merrit [98] and by Viersma [139]. Other aspects of the basic actuator model have also been adressed in literature before, like Coulomb friction [6, 52, 131], and hydrostatic bearings [16]. So in fact, the theoretical modelling of the actuator is not a new development. Yet, it forms a necessary and important part of the modelling of the complete servo-system, since it provides basic insight in the system behaviour by means of simulations with the non-linear model.

Although most parameters of the theoretical actuator model are rather accurately known a priori, the quantitative validity of the model can generally be improved by experimental identification of the parameters. For this purpose, the theoretical model is slightly simplified, neglecting irrelevant dynamics and non-linearities, resulting in a compact model for the actuator, which is easily identified from experiments.

Approach to transmission line modelling

In the approach to transmission line modelling, insight in the physical backgrounds of the transmission line behaviour is an important issue. This especially holds for the implications of the presence of transmission lines in a hydraulic servo-system. It should be easy to investigate these implications, preferably by a modular setup of the model, in which the transmission line models are easily included or omitted. For this reason, the basis for transmission line modelling lies in the theoretical, physical modelling of a single transmission line, extensively reported in literature [33, 42, 61, 106].

As already indicated in Fig. 2.2, the transmission line models typically have the form of a four-port with two inputs and two outputs. Given the character of the transmission line dynamics, involving badly damped resonances as a result of (partial) reflection of transients at the line ends, it is highly important to account for the bilateral coupling of this subsystem with the other subsystems properly. Although the theoretical models of the different subsystems principally allow to do this, just by interconnecting them as shown in Fig. 2.2, a practical problem is involved because the theoretical transmission line models

are of infinite order. The result is, that an approximation step is required, in order to obtain a model of the complete system, which is well-suited for analysis, both in the time domain and in the frequency domain. In other words, an approximation step is required to obtain insight in the coupled system behaviour.

In the approximation step, a principal choice is to be made, closely related to the difference between open loop and closed loop model reduction, a topic investigated extensively by Wortelboer [156]. In terms of the modelling of a hydraulic servo-system with transmission lines, open loop approximation refers to the approximation of a single transmission line model and subsequent integration of the approximate transmission line models with the other subsystem models. Closed loop approximation, to the contrary, involves the approximation of the total coupled system model by a low-order model.

In literature on hydraulic servo-systems with transmission lines, the open loop type of approximation is commonly applied [34, 59, 60, 69, 92, 155, 160]. The disadvantage of this approach is, that some modelling accuracy is lost. The reason is, that high-frequency errors in the approximation of a single transmission line model may affect the accuracy of the model of the complete coupled system at lower frequencies. This effect is typical for open loop model reduction [156]. Despite this disadvantage, the open loop approach to the approximation of the theoretical transmission lines is chosen, for the following reasons:

- The coupling of the infinite order transmission line models with the other subsystem models is not attractive; it is mathematically quite complicated, especially when system non-linearities are to be included in the analysis. A solution might be, first to approximate the transmission line models by accurate models of (very) high order, second to couple these models, and finally to approximate the complete system model by a model of sufficiently low order. However, this approach is not chosen either, because of the next reason.
- A severe disadvantage of 'closed loop' model reduction, i.e. approximation of the coupled system, is the fact, that the physical structure of the model is generally not preserved. Thus, it is impossible to include non-linearities, related to certain physical phenomena, in the approximate model. Moreover, the desirable modularity of the model, such that the transmission line models can be easily included or omitted, is lost. This disadvantage is considered to be much more important than the advantage of quantitative accuracy, as explained by the final reason to choose the open loop approach.
- Quantitative accuracy of the coupled system model is not that important, because this accuracy is to be obtained by means of experimental identification, as a next part of the general approach to modelling.

So, the main requirement on the approximate model of the hydraulic servo-system including transmission line dynamics is, that it provides the right model structure, with the possibility to include non-linearities. For this purpose, the approach of open loop approximation of the transmission line models and successive coupling of the subsystem models according to Fig. 2.2 is most suited.

It might be noted here, that the servo-valve dynamics are actually not involved in this coupling, because the spool position of the servo-valve is basically not affected by the pressures P_{i1} and P_{i2} in Fig. 2.2. So, except for a non-linearity in the expression for the servo-valve flow which is explicitly to be taken into account, the servo-valve can be considered as an ideal flow source. This means, from a modelling point of view, that the

investigation of the effect of transmission line dynamics actually involves the inclusion of transmission line dynamics in the basic model of the hydraulic actuator. This explains, why the procedure of modelling the complete servo-system has been subdivided into three parts: the modelling of the servo-valve, of the actuator, and of the actuator including transmission lines, respectively. As described in the next Subsection, this subdivision partially determines the outline of this Chapter.

2.1.3 Outline of the Chapter

The first part of this Chapter comprises the description of the theoretical modelling of the complete servo-system, including the discussion of a considerable number of simulation results, obtained with the presented models. First, the results concerning the electro-hydraulic servo-valve are presented in Section 2.2. Then, in Section 2.3, the modelling and simulation of the hydraulic actuator is discussed, while the modelling and simulation of transmission line effects are considered in Section 2.4.

In the second part of the Chapter, the obtained insight in the system behaviour is utilized to abstract the relevant dynamics and non-linearities from the theoretical model. This starts with an extensive analysis of the (relevant) dynamics of the system; Section 2.5 treats the servo-valve dynamics, and Section 2.6 the actuator dynamics, including transmission line effects. This leads to relatively simple, linear models, describing the relevant dynamics of the system. After that, a number of non-linearities is included again, namely those that appeared to be important from earlier simulation results. This inclusion of non-linearities in the linear dynamic models is the topic of Section 2.7. Finally, Section 2.8 gives some conclusions.

As a result of the extensive analysis of the dynamics and non-linearities of the model in this Chapter, it is possible to give an overview of modelling aspects concerning hydraulic servo-systems with flow control valves, which is done in Appendix A. In order to get an impression of which modelling aspects are important for a specific hydraulic servo-system, the reader may first read Appendix A roughly, before continuing with the detailed discussion of all modelling aspects in the Sections below. Besides that, Appendix A may serve as a quick reference, after reading this Chapter.

2.2 Modelling and simulation of an electro-hydraulic servo-valve

2.2.1 Introduction

The objective of the modelling and simulation of the electro-hydraulic servo-valve is to obtain insight in its dynamic and non-linear behaviour. It is desirable to know, which physical phenomena do cause severe non-linearity in the (dynamic) behaviour of the servo-valve, and how they affect the performance of the complete hydraulic servo-system, in order to be able to come up with proper specifications for the servo-valve. For instance, manufacturers provide frequency responses in their catalogs, which show considerable amplitude dependence [89]. By means of extensive theoretical modelling and simulation, the backgrounds of the non-linear servo-valve behaviour may be understood, and implications on the servo-system performance may be investigated.

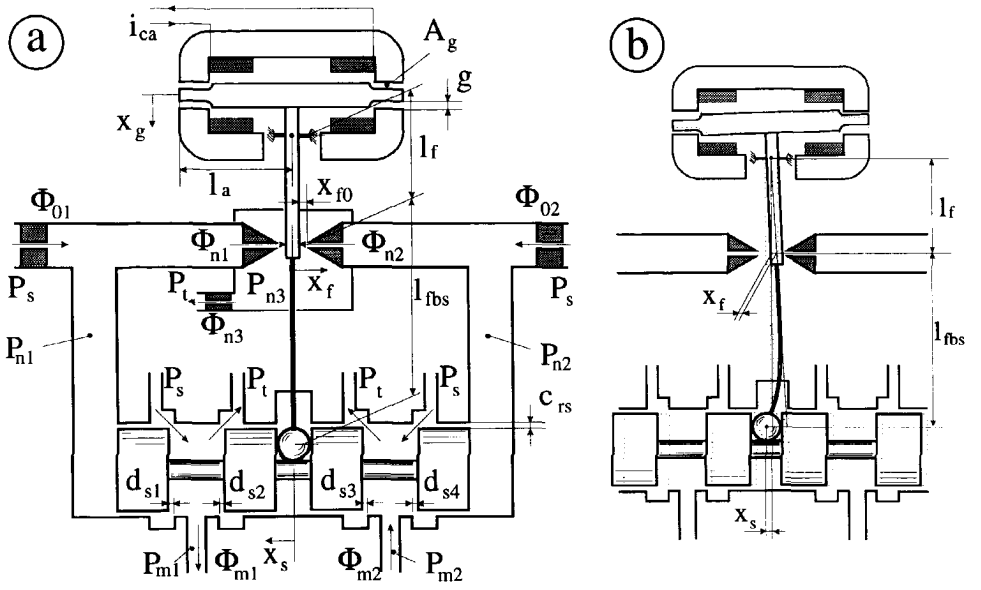


Fig. 2.3: Schematic drawing of two-stage flapper-nozzle valve; overview with valve in null position (a); flapper deflection and spool displacement for positive input (b)

After a description of the servo-valve, an explanation of the model structure is given, including a discussion of the non-linear effects to be taken into account, followed by a description of the subdivision of this rather extensive Section.

Description of the servo-valve

The basic function of an electro-hydraulic servo-valve is to control a high power output, the oil flow, with a low-power input, the electrical control signal. Thereby, the input-output relation should be linear over some defined input range, independent of the power demand at the output. As already depicted in Fig. 2.1, the control of the oil flow takes place by the control of a number of port openings via the positioning of a spool in its bushing. Because the spool position may be affected by the delivered oil flow due to flow forces, especially if a large power amplification (large flow) is required, flow-control valves are often of the servo-valve type with multiple stages.

One of the most common servo-valve types is the two-stage flapper-nozzle valve, as depicted in Fig. 2.3. Actually, there are two stages of power amplification. First, the flapper-nozzle system converts the flapper motion, driven by a low-power electrical torque motor, into a hydraulically powered motion of the spool. Second, the small spool motions control relatively large oil flows through the spool ports, which is the second power amplification.

Referring to Fig. 2.3, the principle of operation of this type of servo-valves can be explained as follows. The electro-magnetic torque motor drives the flapper, which is connected

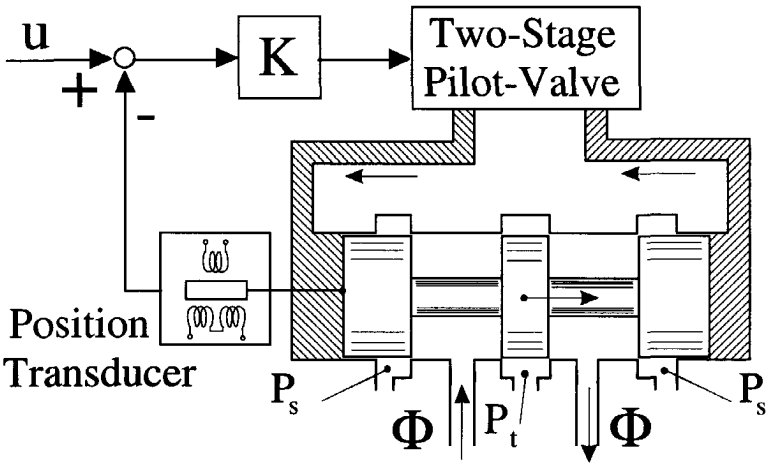


Fig. 2.4: Schematic drawing of three-stage servo-valve

to the housing by a spring-like element, the flexure tube; viscous damping is provided because the flapper is surrounded by oil. The generated flapper deflection x_f (see Fig. 2.3 (b)) controls the oil flows through the nozzles; the flow through the right nozzle reduces, while the flow throught the left nozzle increases. Thus, the pressures at both sides of the spool are controlled, while the spool moves leftward. The resulting deformation of the feedback spring provides a force feedback: in the steady state situation, the torque from the torque motor is in equilibrium with the feedback spring deformation, which is proportional to the spool position. In a number of cases, especially when a high performance is required, the feedback spring as scetched in Fig. 2.3 is replaced by an electrical feedback loop, feeding the measured spool position back to the torque motor input.

In case very large oil flows are required, say > 100 [l/min], it may even be necessary to have an additional stage in the servo-valve. In that case, a two-stage servo-valve may serve as a pilot-valve for the third stage, so that the configuration of Fig. 2.4 is obtained. Because the modelling of the third stage is rather straightforward, most attention will be given to the modelling of the flapper-nozzle valve.

Structure of the flapper-nozzle valve model

There are different contributions in the literature, in which (parts of) non-linear dynamic models of a flapper-nozzle valve are presented [98, 80, 81, 74, 140, 144]. Like all these theoretical models, the model to be presented in this Section reflects the physical structure of the system. Thereby, a large number of (non-linear) effects is included, leading to a model structure as depicted in Fig. 2.5.

The background behind this model structure, and the motivation to include the indicated (non-linear) effects is as follows:

- **Non-linear Torque Motor.** Although for small flapper deflections the torque motor behaves linear [98], the underlying physics involve a non-linearity, which may affect the static and even the dynamic input-output behaviour [98, 144].

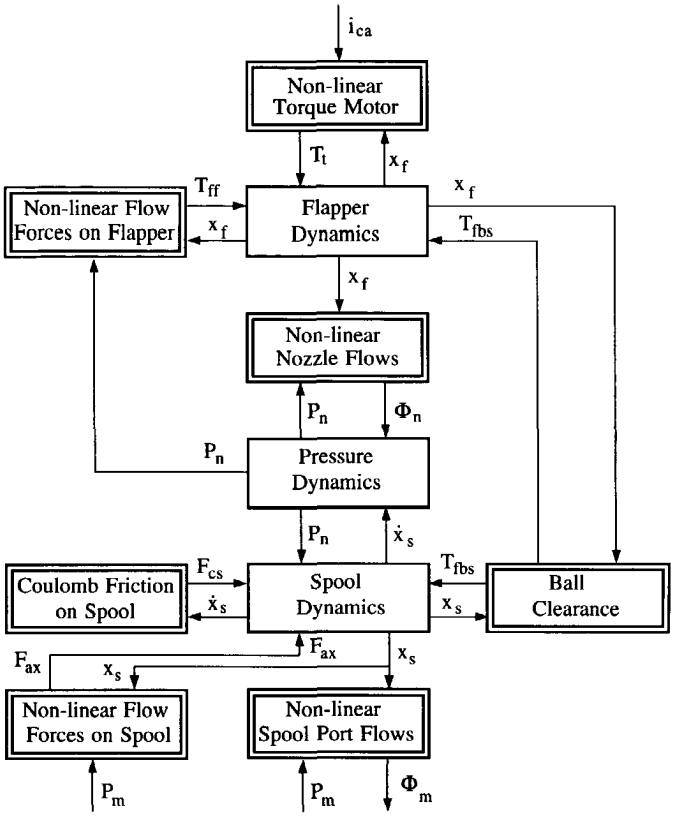


Fig. 2.5: Block scheme representation of non-linear flapper-nozzle valve model

- **Flapper Dynamics.** Due to the significant inertia of the flapper, together with the spring-like behaviour of the flexure tube, flapper dynamics are involved. The model of these dynamics is constituted by an equation of motion, including interaction forces due to the nozzle flows and the feedback spring.
- **Non-linear Nozzle Flows.** The flapper position x_f controls the nozzle flows Φ_n, depending on the nozzle pressures P_n. The non-linear model for these nozzle flows forms a key-stone of the flapper-nozzle valve model; in fact, the principle of operation of this type of valve is based on this flapper-nozzle element.
- **Non-linear Flow Forces on Flapper.** Directly related to the nozzle flows, and therefore also dependent on the flapper position x_f and the nozzle pressures P_n, are the flow forces on the flapper. These forces effectively result in a non-linear torque T_{ff} on the flapper, which may affect the dynamic behaviour of the valve [74, 81, 97, 98].
- **Pressure Dynamics.** As the model structure of Fig. 2.5 clearly indicates, the motion of the spool is actually driven by the pressure dynamics, for which the nozzle flows form a direct input. So these pressure dynamics, a result of the compressibility of the oil, also form an important link in the model.
- **Spool Dynamics.** The inertia of the spool introduces spool dynamics, to be descri-

bed by an equation of motion. Different non-linear effects contribute to this motion, as explained next.

- **Ball clearance.** There may be some clearance of the ball at the end of the feedback spring in the slot of the spool. The result is a non-linearity in the feedback spring torque T_{fbs} as a result of the flapper position x_f and the spool position x_s, which may have serious implications for the input-output behaviour of the valve.
- **Coulomb Friction on Spool.** The motion of the spool may be disturbed by the effect of Coulomb friction on the spool; this effect is also to be considered in the model.
- **Non-linear Spool Port Flows.** The actual flow to be controlled by the servo-valve is determined by the spool port configuration, and depends not only on the spool position x_s, but also on the pressures P_m at the spool ports. Considerable non-linearity may be involved here [98, 139], requiring special attention in the modelling and simulation of the servo-valve model.
- **Non-linear Flow Forces on Spool.** Comparable to the flow forces on the flapper, the flows through the spool ports induce non-lineari forces on the spool, which may have some effect on the input-output behaviour of the valve [5, 15, 96, 97, 99].

Given the model structure of Fig. 2.5, the model equations are to be given in the remainder of this Section, including a discussion of simulation results.

Subdivision of the Section

In the subsequent Subsections, theoretical model relations for the different stages of the servo-valve are presented respectively: for the flapper-nozzle system in Subsection 2.2.2, for the two-stage valve in Subsection 2.2.3 and for the three-stage valve in Subsection 2.2.4. The sign-definitions of the variables in the equations, are indicated in Fig. 2.3 (page 27) and Fig. 2.7 (page 37) respectively. The Section is completed with the extensive Subsection 2.2.5, in which a number of simulation results with respect to the various modelled (non-linear) phenomena is discussed.

2.2.2 Modelling of the flapper-nozzle system

Torque motor

The electro-magnetic torque motor, which drives the flapper, is controlled by an electical current i_{ca}. This current is generated by a current amplifier, which converts the valve control input u (a voltage) into a current, with a current amplifier gain K_{ca}:

$$i_{ca} = K_{ca} u \tag{2.1}$$

Because the dynamics of the electric circuitry of the current amplifier and of the electro-magnetic circuitry of the torque motor are relatively fast, they are neglected. Often the torque T_t generated by the torque motor is assumed to be linearly dependent of the input current for the small rotations of the armature occurring in the servo-valve [98]. However, theoretically the following non-linear relation describes the input-output behaviour of the torque motor [98, 144]:

$$T_t = \frac{\mu_0 A_g l_a}{4} \left[\left(\frac{M_0 + i_{ca} N}{g - x_g} \right)^2 - \left(\frac{M_0 - i_{ca} N}{g + x_g} \right)^2 \right] \tag{2.2}$$

with μ_0 the magnetic permeability of air, A_g the area of the gap normal to the magnetic flux direction, l_a the length of the armature, M_0 the magnetomotive force of the permanent magnets, N the number of coil windings and g the gap distance at neutral position of the armature.

The variation of the gap distance due to armature rotations is expressed in the displacement of the armature tip x_g, which is related to the deflection of the flapper between the nozzles, x_f, by the armature rotation and the flapper length l_f, as follows:

$$x_g = \frac{l_a}{l_f} x_f \tag{2.3}$$

Actually both displacements are described by the equation of motion of the flapper-armature combination, which constitutes the flapper dynamics.

Flapper dynamics

The equation of motion of the flapper has the torque T_t as driving torque. As the flapper rotates only over small angles (≈ 0.01 [rad]), the equation of motion can be expressed in terms of the flapper deflection [74, 80, 81]:

$$\frac{J_a}{l_f}\ddot{x}_f = T_t - B_a\dot{x}_f - K_a x_f + T_{ff} - T_{fbs} \tag{2.4}$$

with J_a the inertia of the flapper-armature, B_a the viscous friction coefficient of the flapper, and K_a the spring constant of the flexure tube that connects the flapper to the housing. The fourth term in the right-hand side of (2.4) represents the (non-linear) contribution due to flow forces on the flapper. The last term in (2.4) is the feedback spring torque T_{fbs}, which only applies in case of mechanical spool position feedback, see Subsection 2.2.3.

Nozzle flows

The flow forces on the flapper are determined by the pressures in the nozzles and the actual flow through the nozzles. With the nozzle pressures $P_{ni}, i = 1, 2$ being determined by the second stage, Subsection 2.2.3, the nozzle flows $\Phi_{ni}, i = 1, 2$ are modelled as turbulent flows through small restrictions [97, 98]. Because the ratio of the flapper-nozzle distance $x_{f0} \pm x_f$ (with x_{f0} the flapper-nozzle distance in neutral position, and x_f the flapper displacement, see Fig. 2.3) with respect to the nozzle diameter D_n is small ($< .1$), it is assumed that the nozzle flows are determined by the curtain area between nozzle and flapper [98]. This results in:

$$\Phi_{n1} = C_d \pi D_n (x_{f0} + x_f)\sqrt{2\tfrac{P_{n1}-P_{n3}}{\rho}} \qquad \Phi_{n2} = C_d \pi D_n (x_{f0} - x_f)\sqrt{2\tfrac{P_{n2}-P_{n3}}{\rho}} \tag{2.5}$$

Hereby, C_d is the discharge coefficient for turbulent flows, and ρ is the density of the fluid (oil). The pressure P_{n3} is the common nozzle outlet pressure.

The value of the pressure P_{n3} is determined by a leakage restriction, which is present in most flapper-nozzle valves. The collective nozzle flows return to tank through this outlet restriction, so that the common nozzle output pressure P_{n3} is considerably higher than the small return pressure P_t. This not only reduces the sum of the (leakage) flows through the nozzles (2.5), but also avoids cavitation effects in the flapper-nozzle system.

The outlet restriction introduces a dynamic equation for the common nozzle output pressure in the theoretical model. This equation is obtained by writing the mass balance for the volume between the nozzles and the outlet orifice as follows, assuming turbulent flow through the outlet orifice [74]:

$$\dot{P}_{n3} = \frac{E}{V_{n3}} \left(\Phi_{n1} + \Phi_{n2} - C_d A_{n3} \sqrt{2 \frac{P_{n3} - P_t}{\rho}} \right) \tag{2.6}$$

with E the bulk modulus of oil, V_{n3} the volume of oil between the nozzles and the outlet orifice, and A_{n3} the orifice area.

Flow forces on flapper

With the nozzle pressures determined by the second stage, and the flows by (2.5) and (2.6), it is possible to describe the flow forces on the flapper in (2.4) in more detail. Several researchers have been investigating these flow forces and reported their results in literature [15, 31, 79, 97, 98, 127]. In general form, the force $F_{fi}, i = 1, 2$, due to a nozzle flow on the flapper can be expressed as [79]:

$$F_{fi} = \frac{\pi}{4} D_n^2 F R_i(x_f) \left(P_{ni} - P_t \right) \qquad i = 1, 2 \tag{2.7}$$

where $FR_i(x_f), i = 1, 2$ is the so-called Force Ratio, depending on the flapper position. A Force Ratio $FR = 1$ corresponds to the situation, that the flapper-nozzle distance is zero: the flow force then equals the static nozzle-pressure times the nozzle area.

An expression for the Force Ratio, which is mostly used to model flow forces in literature [74, 81, 97, 98], can be obtained by a simple momentum analysis [79], and reads as follows:

$$FR_1(x_f) = 1 + \left[\frac{4 C_d (x_{f0} + x_f)}{D_n} \right]^2 \qquad FR_2(x_f) = 1 + \left[\frac{4 C_d (x_{f0} - x_f)}{D_n} \right]^2 \tag{2.8}$$

With this expression, and l_f the length of the flapper, the resulting torque in equation (2.4) due to flow forces on the flapper becomes:

$$\begin{aligned} T_{ff} &= l_f \left[F_{f1} - F_{f2} \right] \\ &= \tfrac{\pi}{4} D_n^2 l_f \left\{ \left[1 + \left(\tfrac{4 C_d (x_{f0} + x_f)}{D_n} \right)^2 \right] (P_{n1} - P_{n3}) - \left[1 + \left(\tfrac{4 C_d (x_{f0} - x_f)}{D_n} \right)^2 \right] (P_{n2} - P_{n3}) \right\} \\ &= \tfrac{\pi}{4} D_n^2 l_f \left\{ \left[1 + \tfrac{16 C_d^2}{D_n^2} \left(x_{f0}^2 + x_f^2 \right) \right] (P_{n1} - P_{n2}) + \left[\tfrac{16 C_d^2}{D_n^2} 2 x_{f0} x_f \right] (P_{n1} + P_{n2} - 2 P_{n3}) \right\} \end{aligned} \tag{2.9}$$

It might be noted from equation (2.9), that there is a major contribution to the torque due to flow-forces from the difference of the two nozzle pressures, which only slightly depends on the flapper position x_f in a quadratic way. On the other hand, there is a contribution which is linear in x_f, in which the average of pressure difference between the nozzle pressures and the outlet pressure is involved.

Note hereby, that the torque T_{ff} depends on the flapper position x_f with a positive sign, as the nozzle pressures P_{n1} and P_{n2} are always larger than the outlet pressure P_{n3}. Physically, this positive sign corresponds to a negative 'stiffness': the flow forces tend to *destabilize* the flapper position, contrary to what is reported by Wang et al. [144].

Anyhow, given the theoretical expression for the torque due to flow forces on the flapper (2.9), it can be stated that the contribution of these forces, modelled this way, is almost linear. However, depending on the geometry of the flapper-nozzle system, the Force Ratio occurring in practice may be completely different from (2.8). For instance, Lichtarowicz [79] reports experimental results, that show highly non-linear variations of the Force Ratio with respect to the flapper posisition. In order to simulate the non-linear dynamics of a flapper-nozzle valve sufficiently, it may well be necessary to adopt one of the non-linear Force Ratio characteristics of [79], instead of (2.8), as discussed Subsection 2.7.2.

2.2.3 Modelling of a two-stage flapper-nozzle valve

Pressure and spool dynamics

In the two-stage flapper-nozzle valve, the flapper-nozzle system may be seen as a flow controller, according to equation (2.5). Together with the flows through the inlet restrictions:

$$\Phi_{01} = C_d A_0 \sqrt{2\frac{P_s - P_{n1}}{\rho}} \qquad \Phi_{02} = C_d A_0 \sqrt{2\frac{P_s - P_{n2}}{\rho}} \tag{2.10}$$

where A_0 is the orifice area of the inlet restrictions, the nozzle flows determine the nozzle pressures, as the following mass balances for the valve chambers must hold [74, 80, 81, 98]:

$$\dot{P}_{n1} = \frac{E}{V_{n1}} \left(\Phi_{01} - \Phi_{n1} + A_s \dot{x}_s \right) \qquad \dot{P}_{n2} = \frac{E}{V_{n2}} \left(\Phi_{02} - \Phi_{n2} - A_s \dot{x}_s \right) \tag{2.11}$$

Herein, $V_{ni}, i = 1, 2$ are the valve chamber volumes, and A_s and $\dot{x}_s$ the spool side area and the spool velocity respectively. Although theoretically the valve chamber volumes change with spool position, this effect is not taken into account, because this variation is relatively small ($< 5\%$) in general.

The spool velocity, and also the spool position, is described by the equation of motion of the spool [74, 80, 81]:

$$M_s \ddot{x}_s = A_s \left(P_{n2} - P_{n1} \right) - w_s \dot{x}_s - \frac{T_{fbs}}{(l_f + l_{fbs})} - F_{cs} - F_{ax} \tag{2.12}$$

where M_s is the mass of the spool, w_s the viscous friction coefficient, l_{fbs} the length of the feedback spring (if present), and F_{cs} and F_{ax} the Coulomb friction force and the axial flow force on the spool respectively. The axial flow force on the spool will be described in more detail later in this Section.

Concerning the Coulomb friction force on the spool, it can be modelled in many different ways [6]. In this case, a model is adopted where the friction force F_{cs} is constant during movement (acting in opposite direction of the velocity), and varying during standstill (representing 'stiction'), similar as described in [131].

If a mechanical feedback of the spool position to the flapper position is present, the corresponding feedback spring torque acting on the flapper can be related to virtual deformations at the end of the spring, using the feedback spring constant K_{fbs}, as follows (see also Fig. 2.3 (b)):

$$T_{fbs} = K_{fbs} \left[\frac{l_f + l_{fbs}}{l_f} x_f + x_s \right] \tag{2.13}$$

In case there is some clearance of the ball fitting in the slot in the spool, to be denoted by c_b, the above equation is modified such that the feedback spring torque equals zero for:

$$-c_b \leq \left(\frac{l_f + l_{fbs}}{l_f}\right) x_f + x_s \leq c_b \tag{2.14}$$

Outside these bounds the spool displacement x_s in equation (2.13) is replaced by $x'_s = x_s + c_b$ if the bound (2.14) is exceeded on the right hand side, and by $x'_s = x_s - c_b$ if the bound (2.14) is exceeded on the left hand side.

Obviously, the feedback spring torque T_{fbs} introduces a reaction force on the spool in equation (2.12). Therewith, the feedback spring constitutes a strong coupling between the dynamics of the flapper motion 2.4 and those of the spool motion (2.12). In case the spool position feedback is not mechanical, but electrical, this coupling is not present, and the contributions of the feedback spring torque T_{fbs} in (2.4) and (2.12) have to be set to zero. In the same time, the equation for the torque motor input (2.1) has to be modified to:

$$i_{ca} = K_{ca}\,(u - K_{sp} x_s) \tag{2.15}$$

with K_{sp} the feedback gain, including the spool position transducer gain.

With the equations so far, the closed loop dynamics of the flapper-nozzle system and the spool have been modelled. The actual model of the two-stage valve is now completed by describing the resulting flows through the spool ports.

Spool port flows and corresponding forces

A lot of fundamental research has been performed on flows through small restrictions [39, 44, 99]. A more practical treatment for the case of flow through the ports of a servo-valve spool is given by Merrit and Viersma [98, 139]. They state, that the flows can in general be assumed to be turbulent, possibly with constant discharge coefficient C_d. In that case, for given spool position x_s and pressures at the spool ports P_{m1} and P_{m2}, the valve flows are determined by a static relation, which reflects the geometry of the ports. For the configuration, shown in Fig. 2.3, the equations for the servo-valve flows Φ_{m1} and Φ_{m2} read:

$$\begin{aligned} \Phi_{m1} &= C_d A_{s1}\sqrt{2\tfrac{P_s - P_{m1}}{\rho}} - C_d A_{s2}\sqrt{2\tfrac{P_{m1} - P_t}{\rho}} + \Phi_{l,s1} - \Phi_{l,s2} \\ \Phi_{m2} &= C_d A_{s3}\sqrt{2\tfrac{P_{m2} - P_t}{\rho}} - C_d A_{s4}\sqrt{2\tfrac{P_s - P_{m2}}{\rho}} + \Phi_{l,s1} - \Phi_{l,s4} \end{aligned} \tag{2.16}$$

Assuming sharp edges, the spool port opening areas A_{si}, $i = 1, 2, 3, 4$ can be written as:

$$\begin{aligned} A_{si} &= \begin{cases} h_s\sqrt{(x_s + d_{si})^2 + c_{rs}^2} & x_s \geq -d_{si} \\ 0 & x_s < -d_{si} \end{cases} \quad i = 1, 3 \\ A_{si} &= \begin{cases} h_s\sqrt{(d_{si} - x_s)^2 + c_{rs}^2} & x_s \leq d_{si} \\ 0 & x_s > d_{si} \end{cases} \quad i = 2, 4 \end{aligned} \tag{2.17}$$

where h_s is the width of the spool port openings, c_{rs} the radial clearance between the spool and its bushing, and d_{si} the underlap of port i in the neutral spool position.

For the leakage flows $\Phi_{l,si}$, $i = 1, 2, 3, 4$, that occur when the ports are overlapped (closed) as depicted in the left drawing of Fig. 2.6, it is mostly assumed that they are dominated by viscosity effects [72]. Thereby, the laminar resistance depends linearly on

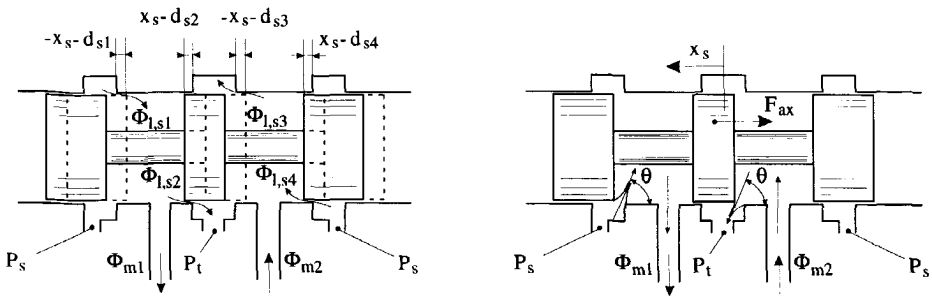


Fig. 2.6: Leakage flows through overlapped ports (left); Axial flow force on spool due to unequal jet angles (right)

the overlap distance, which varies with spool position. However, assuming only laminar resistance for the leakage flow would result in infinite leakage flow for zero overlap.

In order to avoid this, and to have continuity in the flow equations (2.16), it is assumed that the resistance for the leakage flows consists of two parts. The laminar part is related to the viscous flow through the clearance between spool and bushing, and the turbulent part is related to the inflow or outflow along the edge of the spool. This results in a set of quadratic equations for the leakage flows in case of spool overlap, which can easily be solved explicitly for the leakage flows $\Phi_{l,si}$, $i = 1, 2, 3, 4$:

$$\begin{aligned}
\tfrac{\rho}{2C_d^2 h_s^2 c_{rs}^2}\Phi_{l,s1}^2 - \tfrac{12\eta(x_s+d_{s1})}{h_s c_{rs}^3}\Phi_{l,s1} &= P_s - P_{m1}, \quad x_s < -d_{s1} \\
\tfrac{\rho}{2C_d^2 h_s^2 c_{rs}^2}\Phi_{l,s2}^2 + \tfrac{12\eta(x_s-d_{s2})}{h_s c_{rs}^3}\Phi_{l,s2} &= P_{m1} - P_t, \quad x_s > d_{s2} \\
\tfrac{\rho}{2C_d^2 h_s^2 c_{rs}^2}\Phi_{l,s3}^2 - \tfrac{12\eta(x_s+d_{s3})}{h_s c_{rs}^3}\Phi_{l,s3} &= P_{m2} - P_t, \quad x_s < -d_{s3} \\
\tfrac{\rho}{2C_d^2 h_s^2 c_{rs}^2}\Phi_{l,s4}^2 + \tfrac{12\eta(x_s-d_{s4})}{h_s c_{rs}^3}\Phi_{l,s4} &= P_s - P_{m2}, \quad x_s > d_{s4} \\
\Phi_{l,si} &= 0, \quad x_s \geq -d_{si} \quad i = 1,3 \\
\Phi_{l,si} &= 0, \quad x_s \leq d_{si} \quad i = 2,4
\end{aligned} \tag{2.18}$$

With the above equations, (2.16), (2.17) and (2.18), the flows through non-overlapped ports are assumed to be turbulent, with constant discharge coefficient. More accurate models take into account, that rounded edges and radial clearance cause laminar flows for small port openings [72, 97, 139]. However, simulations show, that the above model is sufficient to describe the main non-linearity in the servo-valve flow, Subsection 2.2.5.

Closely related to the flows through the spool ports is the axial flow force on the spool. This flow force originates from the change of momentum of the flow, due to a difference in jet angles for inlet flows and outlet flows. As depicted in the right part of Fig. 2.6, the servo-valve flows Φ_{m1} and Φ_{m2} enter or leave the spool chambers with a jet angle of 90°, while, due to the port geometry, the jet angle θ of the spool port flows (from supply and to tank) is much smaller. This requires a change of momentum of the oil flows in axial direction, which causes an axial reaction force F_{ax} on the spool, that tends to close the ports.

Applying Newton's third law and using Bernoulli's law for the occurring spool port flows, the following expression for the axial flow force can be derived, according to Merrit [98]:

$$F_{ax} = 2\cos\theta C_d \left[A_{s1}\left(P_s - P_{m1}\right) - A_{s2}\left(P_{m1} - P_t\right) + A_{s3}\left(P_{m2} - P_t\right) - A_{s4}\left(P_s - P_{m2}\right)\right] \tag{2.19}$$

where the spool port opening areas are given by (2.17). Note that a non-ideal port-geometry (underlaps and radial clearance) cause the axial flow force to be non-linearly dependent of the spool position due to (2.17).

Although the jet angle θ basically varies with the spool position in case of rounded edges and radial clearance, this variation is relatively small for small radial clearances [15, 96, 97, 99]. Therefore, the expression for the flow force can be simplified, assuming that θ is constant [5]. As far as the jet angle is concerned, this corresponds to the assumption that the edges are sharp and that the clearance is zero. Von Mises [99] derived a theoretical value of θ for this case, namely $\approx 69°$, leading to $\cos\theta = 0.358$.

As a final remark, it is noted that despite the assumption of constant jet angle, the axial flow force is not linear in the spool position, like in [15], but non-linear, depending on the spool port configuration.

Given the equations of Subsection 2.2.2 and Subsection 2.2.3, a theoretical model of the two-stage flapper-nozzle valve is available. In case such a valve serves as a pilot-valve for a three-stage valve, this model can be included as a subsystem model for the complete three-stage servo-valve model.

2.2.4 Modelling of a three-stage servo-valve

The modelling of a three-stage valve actually consists of the extension of the pilot-valve model with a model for the third stage, including the feedback. As depicted in Fig. 2.4, the third stage, which will be called the main spool, is driven by the oil flows of the pilot-valve.

In general, the side areas of the main spool are relatively large with respect to the chamber volumes at both sides of the main spool. Moreover, the acceleration and friction forces are generally very small related to the maximum driving force on the spool, namely $P_s A_m$, with A_m the spool side area. Therefore, the natural frequency related to the spool mass on the compressible oil is in general very large (> 2.5 [kHz]). For the frequency range of interest (< 1 [kHz]) this means, that the pressure dynamics of the third stage can be neglected. This implies, that the main spool pressures P_{mi}, $i = 1, 2$ are algebraically related to other model variables.

This requires two static model relations, being the (static) mass balances for the main spool chambers on the one hand, and the static force balance for the main spool on the other hand. Referring to Fig. 2.7 for the sign-definitions, this gives:

$$\Phi_{m1} = A_m \dot{x}_m = \Phi_{m2} \tag{2.20}$$

$$A_m\left(P_{m1} - P_{m2}\right) = 0 \tag{2.21}$$

In fact, these equations, together with the port flow equations (2.16) and (2.17), give the main spool the character of a non-linear integrator. Depending on the port geometry (2.17), the the main spool velocity $\dot{x}_m$ is related non-linearly to the spool position x_s. It should be noted here, that the modelling of the main spool by (2.20) and (2.21) introduces algebraic

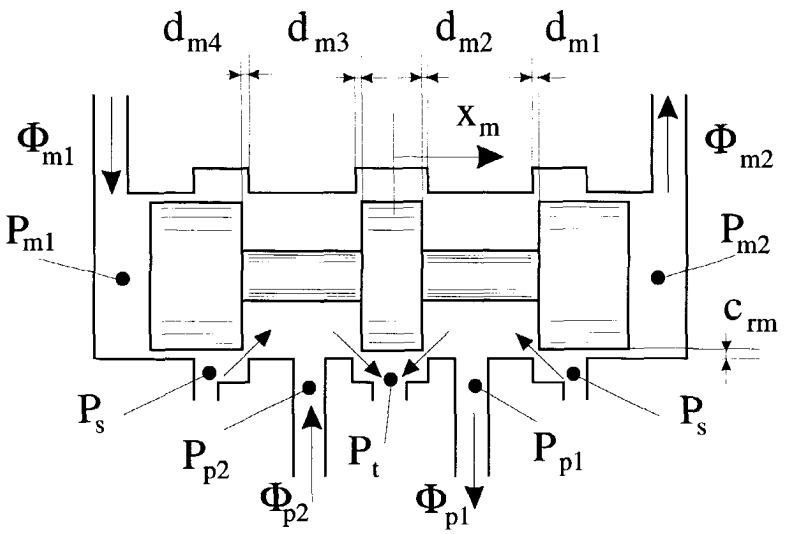


Fig. 2.7: Schematic drawing of main spool of three-stage servo-valve

loops in the non-linear simulation model, which may give rise to simulation problems. For a discussion of this topic, the reader is referred to Appendix B.

In order to stabilize the integrator, the position of the main spool x_m is fed back to the pilot stage by an electrical (mostly proportional) feedback loop, where K_{pm} is the feedback gain and K_{ms} the main spool position sensor gain:

$$u = K_{pm}\left(u_r - K_{ms}x_m\right) \tag{2.22}$$

Thus, the three-stage valve can be seen as a servo-system, with the measured main spool position following the reference signal u_r. Like in the case of the two-stage flapper-nozzle valve, the main spool position controls the actuator oil flows. With the sign-definitions of Fig. 2.7, the following static relations describe the actuator flows Φ_{p1} and Φ_{p2}, given the main spool position x_m and the actuator pressures P_{p1} and P_{p2}:

$$\begin{aligned}
\Phi_{p1} &= C_d A_{m1}\sqrt{2\tfrac{P_s - P_{p1}}{\rho}} - C_d A_{m2}\sqrt{2\tfrac{P_{p1} - P_t}{\rho}} + \Phi_{l,m1} - \Phi_{l,m2} \\
\Phi_{p2} &= C_d A_{m3}\sqrt{2\tfrac{P_{p2} - P_t}{\rho}} - C_d A_{m4}\sqrt{2\tfrac{P_s - P_{p2}}{\rho}} + \Phi_{l,m1} - \Phi_{l,m4}
\end{aligned} \tag{2.23}$$

Assuming sharp edges again, the main spool port opening areas A_{mi}, $i = 1,2,3,4$ are written as:

$$\begin{aligned}
A_{mi} &= \begin{cases} h_m\sqrt{\left(x_m + d_{mi}\right)^2 + c_{rm}^2} & x_m \geq -d_{mi} \\ 0 & x_m < -d_{mi} \end{cases} \qquad i = 1,3 \\
A_{mi} &= \begin{cases} h_m\sqrt{\left(d_{mi} - x_m\right)^2 + c_{rm}^2} & x_m \leq d_{mi} \\ 0 & x_m > d_{mi} \end{cases} \qquad i = 2,4
\end{aligned} \tag{2.24}$$

where h_m is the width of the main spool port openings, c_{rm} the radial clearance between the main spool and its bushing, and d_{mi} the underlap of port i in the neutral position of the main spool.

Combining laminar and turbulent resistance again for the leakage flows throug the overlapped spool ports, the following expressions provide the leakage flows $\Phi_{l,mi}$, $i = 1, 2, 3, 4$:

$$\begin{aligned}
\frac{\rho}{2C_d h_m^2 c_{rm}^2}\Phi_{l,m1}^2 - \frac{12\eta(x_m+d_{m1})}{h_m c_{rm}^3}\Phi_{l,m1} &= P_s - P_{p1}, \quad x_m < -d_{m1} \\
\frac{\rho}{2C_d h_m^2 c_{rm}^2}\Phi_{l,m2}^2 + \frac{12\eta(x_m-d_{m2})}{h_m c_{rm}^3}\Phi_{l,m2}8 &= P_{p1} - P_t, \quad x_m > d_{m2} \\
\frac{\rho}{2C_d h_m^2 c_{rm}^2}\Phi_{l,m3}^2 - \frac{12\eta(x_m+d_{m3})}{h_m c_{rm}^3}\Phi_{l,m3} &= P_{p2} - P_t, \quad x_m < -d_{m3} \\
\frac{\rho}{2C_d h_m^2 c_{rm}^2}\Phi_{l,m4}^2 + \frac{12\eta(x_m-d_{m4})}{h_m c_{rm}^3}\Phi_{l,m4} &= P_s - P_{p2}, \quad x_m > d_{m4} \\
\Phi_{l,mi} &= 0, \quad x_m \geq -d_{mi} \quad i = 1,3 \\
\Phi_{l,mi} &= 0, \quad x_m \leq d_{mi} \quad i = 2,4
\end{aligned} \tag{2.25}$$

With the equations for the third stage of the three-stage valve, given in this Subsection, the description of the complete non-linear servo-valve model is completed. An extensive analysis of the modelled effects is given in the next Subsection, by discussing a number of simulation results, obtained with the given servo-valve model.

2.2.5 Simulation of the non-linear servo-valve model

The aim of the simulations to be presented in this Subsection is primarily to obtain qualitative insight in the modelled phenomena of the servo-valve. Based on this insight, irrelevant effects may be dropped out of the model in a later stage of the modelling process, while important phenomena are to be preserved in the model. In that way, a somewhat simplified model can be obtained (see Section 2.5), which forms the basis for experimental identification and validation in Chapter 3. So in fact, the objective is not to describe the input-output behaviour of a certain valve *exactly* by means of simulations with the non-linear theoretical model, but only to distinguish between relevant and irrelevant dynamics and non-linearities. An accurate quantitative description is to be obtained later, by means of experimental identification and validation.

After a description of the parameterset that was used in the simulations, a series of simulation results of the non-linear servo-valve model is discussed below. When going through all these simulation results, the reader may refer to Fig. 2.5 on page 29, in order to keep the right overview of the different modelled phenomena, that are discussed.

Parameters to be used in the simulation model

As it appeared not to be possible to obtain a complete set of physical parameters related to a certain flapper-nozzle valve, some parameterset has been constructed, reflecting characteristics that may be expected for a small sized servo-valve (nominal flow 5 [l/min] at 70 [bar]).

Thereby, some parameters were indicated by the manufacturer [100, 89], others were reported in literature [74, 81, 140], and a few were estimated by inspection of a destructed MOOG series 77 servo-valve [152]. The set obtained from these information sources actually served as an initial guess, and did not reflect very realistic (dynamic) behaviour. Therefore, some heuristic optimization of the parameterset was performed, such that the frequency response of the linearized model (see Section 2.5) reflected some desired dynamic behaviour,

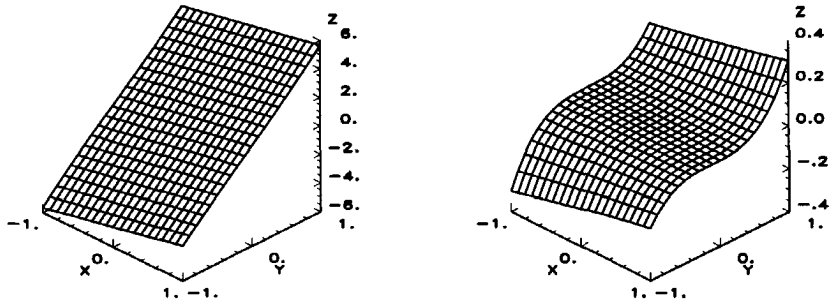


Fig. 2.8: Three-dimensional representation of torque motor non-linearity; $x = \bar{i}_{ca}$, $y = \bar{x}_f$, $z = \bar{T}_t$; including linear contribution $\bar{T}_t = T_t/T_{max}$ (left) and excluding linear contribution $\bar{T}_t = (T_t - T_{t,lin})/T_{max}$ (right)

for instance as reported by Thayer [134]. Also some manual changes were made in the parameterset, looking at the resulting input-output behaviour, and thus gaining insight in the model. The parameterset, that was finally used to produce the simulation results of this Subsection is given in Table F.1, Appendix F.

Non-linear torque motor

The character of the non-linearity in the torque motor equation (2.2) is best understood by observing that the generated torque is a non-linear function of the input i_{ca} at the one hand, and of the flapper position x_f (via (2.3)) at the other hand. Thereby, the flapper position is a dynamic state, so there is a *dynamic* relation between the two variables in the non-linear equation.

To illustrate the character of the non-linearity, a three-dimensional representation of (2.2) is given in the left plot of Fig. 2.8. In this Figure, the two input variables i_{ca} and x_f have been scaled with respect to their physical maxima, being the maximum input current i_{max} and the maximum flapper deflection x_{f0} respectively. The torque motor output T_t has also been scaled, namely with respect to the maximum torque T_{max}, which is generated for $i_{ca} = i_{max} \wedge x_f = 0$. The numerical values of the respective scaling factors are given in Table F.2 in Appendix F.

Note, that due to the parameter settings of Table F.1 in Appendix F, the maximum flapper deflection x_{f0} corresponds to a maximum armature tip deflection which is only 15 % of its physical maximum, namely g. This explains why the left plot of Fig. 2.8 is rather flat; within this range the torque motor behaves almost linear.

This is further illustrated by the right plot of Fig. 2.8. This plot represents the same non-linearity, but now without the linear contributions of the inputs. Actually, the torque shown in this plot equals $\frac{(T_t - T_{t,lin})}{T_{max}}$, where $T_{t,lin}$ is obtained by linearization of the non-linear equation (2.2), substituting (2.3), leading to the simple expression:

$$T_{t,lin} = K_t i_{ca} + K_b x_f \tag{2.26}$$

Hereby K_t is the torque motor gain, and K_b the magnetic stiffness of the torque motor. The values of these constants, corresponding to the parameter values used for simulation,

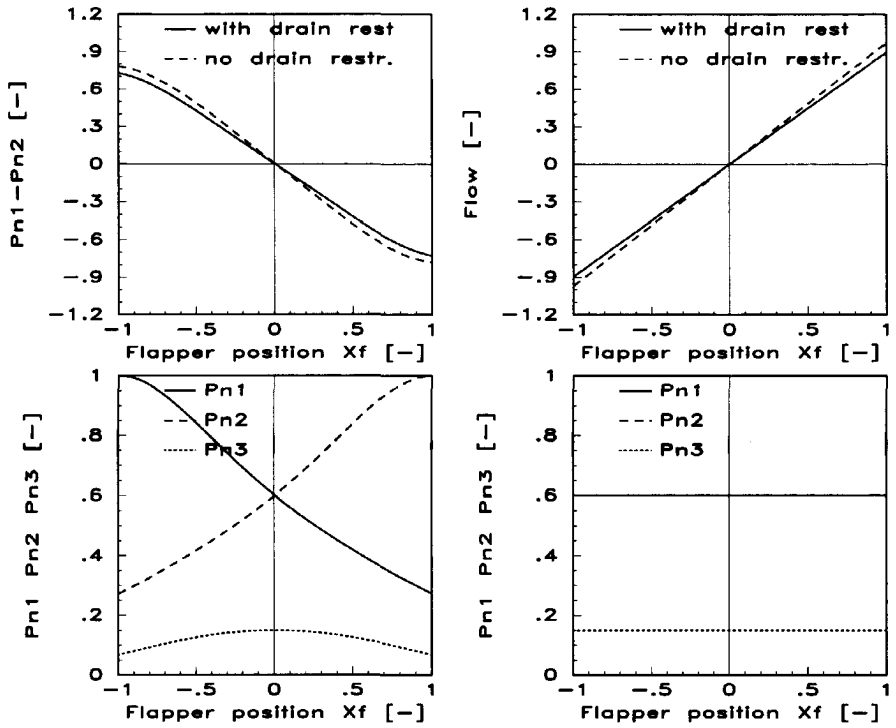


Fig. 2.9: Steady state characteristics flapper-nozzle system. Pressure difference gain (upper left) and corresponding pressures (lower left); flow gain (upper right) and corresponding pressures (lower right)

are listed in Table F.1. It is remarkable, that the magnetic stiffness of the torque motor is in the same order of magnitude as the spring stiffnes of the flexure tube. Apparently, the flexure tube has to be stiff enough to stabilize the flapper, where the (negative) magnetic stiffness of the torque motor tries to destabilize it.

Given the choice of physical parameters, with $x_g \ll g$ (which can be seen from (2.3) and Table F.1), it can be concluded from the plots of Fig. 2.8, that the torque is not very non-linear and can well be approximated by (2.26).

Non-linear nozzle flows

The non-linearity of the flapper-nozzle system is also best understood by analyzing the steady state characteristics corresponding to the equations for the nozzle flows and pressures (2.5), (2.6), (2.10) and (2.11). Thereby, two special cases are considered:

1. *The flapper-nozzle system acts as pressure control system.*
   This corresponds to the situation that the spool is blocked by some counteracting force, so that the spool velocity $\dot{x}_s = 0$ in (2.11). The nozzle pressures reach an equilibrium such that the inlet flows (2.10) equal the nozzle flows (2.5). The resulting pressures are plotted as a function of the flapper displacement in the left plots of Fig. 2.9, with pressures scaled by the supply pressure P_s and flapper position by x_{f0}.

In the upper left plot of this Figure, two simulation results are given. One result has been obtained with the outlet restriction according to (2.6) included in the model; the other result has been obtained by assuming that no outlet restriction is present, so that the pressure P_{n3} equals the return pressure P_t. The pressures in the lower left plot correspond to the first case with outlet restriction.
The conclusion from this simulation is, that the pressure gain of the flapper-nozzle system is reasonably linear, especially for small flapper deflections. The presence of the outlet restriction does not make that much difference; the pressure gain is slightly decreased and slightly more linear.

2. *The flapper-nozzle system acts as flow control system.*
In this situation it is assumed that the spool is moving freely, which is the same as short-circuiting the valve chambers at both spool sides. This means that the nozzle pressures P_{n1} and P_{n2} are equal, and such that $\Phi_{n1} - \Phi_{01} = A_s\dot{x}_s = \Phi_{02} - \Phi_{n2}$, because of (2.11). Simulation results corresponding to this situation are given in the right plots of Fig. 2.9, where the flows have been scaled with respect to the nominal nozzle flow $\Phi_{n,nom}$. This nominal nozzle flow is defined as $\Phi_{n,nom} = C_d\pi D_n x_{f0}\sqrt{P_s/\rho}$ (compare (2.5)). For the numerical value, see Table F.2.
In the upper right plot of Fig. 2.9, the effective flow driving the spool is given as function of the flapper displacement for the cases with and without outlet restriction, as before. In the lower right plot, the pressures are given, that correspond to the flow characteristic with outlet restriction.
The conclusion from this simulation is, that the flapper-nozzle system as flow controller behaves quite linear. The presence of the outlet restriction only makes difference in the sense that the flow gain is slightly smaller with outlet restriction.

For the above two special cases, the flapper-nozzle system behaves almost linear. However, in the operation of the two-stage flapper-nozzle valve, the flapper-nozzle system acts as a flow controller which is loaded by the impedance of the spool dynamics (including the feedbackspring). So in fact, a complete characterization of the flapper-nozzle non-linearity consists of a surface, representing the flow driving the spool as a function of both the flapper position x_f and the nozzle pressure difference ΔP_n. A simulation of this characteristic is given in the left plot of Fig. 2.10, while the right plot shows the same characteristic but with the linear contribution of the inputs subtracted, similar to Fig. 2.8.

This Figure shows that the characteristic is indeed linear for small flapper deflections and nozzle pressure differences (flatness of the surface in the middle region). However, for the more extreme cases that the flapper position is small and the pressure difference is large, the surface shows considerable deviations from the linear (flat) characteristic, up to 20 %, meaning non-linear behaviour. To which extent this non-linearity is propagated to the behaviour of the complete valve is to be investigated by dynamic simulations of the complete valve model.

Non-linear flow forces on flapper

It has already been argued in Subsection 2.2.2, that the torque due to the flow forces on the flapper, as theoretically modelled by (2.9), is almost linear as a function of the flapper displacement x_f and the nozzle pressure difference ΔP_n. It is easily seen, that in case one of the inputs equals zero, the flow force torque T_{ff} is exactly linear in the other input.

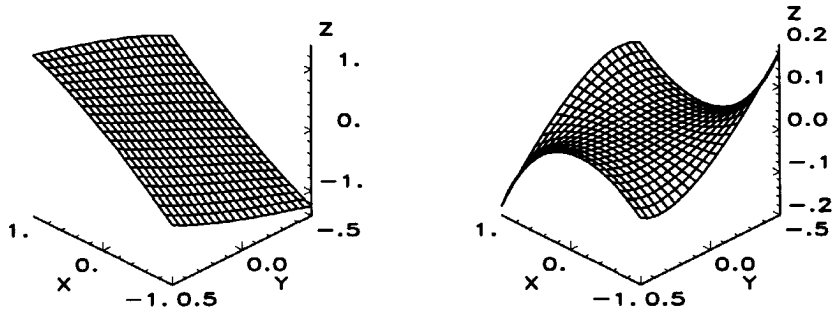


Fig. 2.10: Three-dimensional representation of flapper-nozzle non-linearity; x = $\bar{x}_f$, y = $\overline{\Delta P}_n$, z = $\bar{\Phi}_{n1} - \bar{\Phi}_{01} = \bar{\Phi}_{02} - \bar{\Phi}_{n2}$; actual non-linear characteristic (left) and non-linear characteristic excluding linear contribution (right)

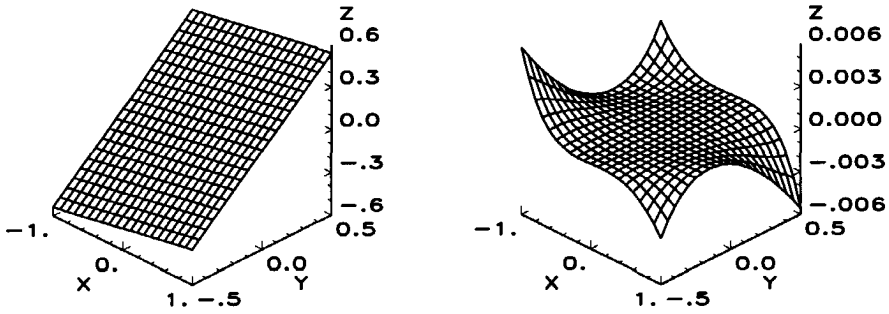


Fig. 2.11: Three-dimensional representation of non-linear torque due to nozzle flows; x = $\bar{x}_f$, y = $\overline{\Delta P}_n$, z = $\bar{T}_{ff}$; actual non-linear characteristic (left) and non-linear characteristic excluding linear contribution (right)

As for previous non-linearities, the characteristic of the non-linear torque due to nozzle flow forces can be further clarified by simulations presented in Fig. 2.11. Again the left plot shows the actual non-linear characteristic with scaled variables, while the right plot shows the same result, but with linear contribution of the inputs subtracted. From this Figure it is clear that, even in the areas where both input variables x_f and ΔP_n are unequal to zero, the flow force torque T_{ff} according to the theoretical expression (2.9) can be considered to be linear.

Coulomb friction on spool

The occurance of Coulomb friction is inherent to mechanical control systems [6]. Unlike ball clearance, Coulomb friction of the spool in a flow control valve is unavoidable. The effect on the input-output behaviour is again a severe non-linearity, namely a hysteresis loop in the steady state characteristic. This is shown by the simulation result in the left plot of Fig. 2.12, where the static and dynamic friction force were chosen to be 0 and 1 % respectively of the maximum spool force $F_{s,max} = P_s A_s$; for numerical value of $F_{s,max}$ see

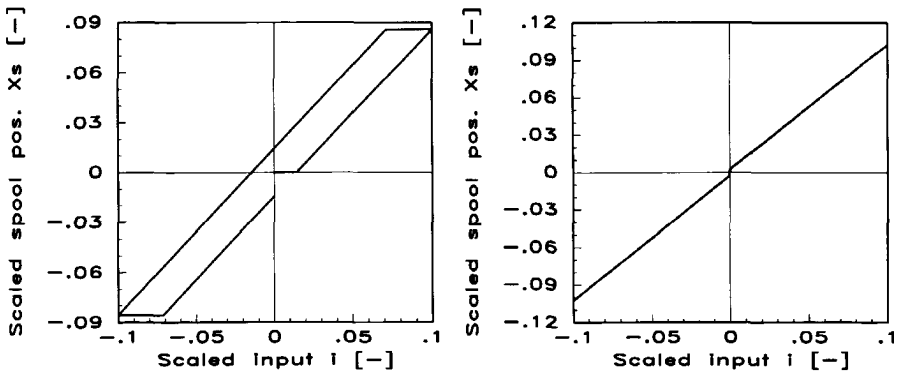


Fig. 2.12: Effect of Coulomb friction on spool (left) and ball clearance (right) on steady state characteristic of flapper-nozzle valve

Table F.2 in Appendix F.

Fortunately, in practice it is rather well possible to diminish the effect of Coulomb friction by applying a dither signal. So, referring to Subsection 3.3.2 for some practical issues related to the adjustment of the dither signal, it will be assumed in the remainder, that the effect of Coulomb friction has been eliminated this by means of dither.

Ball clearance

Ball clearance causes a dead band in the mechanical feedback path, which together with the integrating behaviour of the valve causes a discontinuity in the steady state characteristic of the servo-valve. For a clearance of $c_b = 1\ 10^{-6}$ [m], the result is shown in the right plot of Fig. 2.12. Besides the jump in the steady state characteristic, ball clearance may also lead to limit cycling behaviour [139]. Actually, this behaviour is quite undesirable, and servo-valves showing this behaviour due to ball clearance can be considered to be worn and should not be used for control purposes.

Non-linear spool port flows

Because an electro-hydraulic servo-valve is a flow control device, it is important to understand its basic steady state behaviour, constituted by the relation between the controlled oil flow and the valve spool position. Because of the similarity of this relation for the spool flows of the flapper-nozzle valve (2.16) and for those of the three-stage valve (2.23), only the two-stage valve flows will be considered; the results are also valid for the three-stage valve.

From the equations that describe the spool flows, namely (2.16), (2.17) and (2.18), it is clear that these flows Φ_{m1} and Φ_{m2} are basically dependent on the spool position, but also on the pressures P_{m1} and P_{m2} of the controlled device. Considering the steady state behaviour, the pressures P_{m1} and P_{m2} have reached equilibria, such that the spool flows Φ_{m1} and Φ_{m2} (driving some controlled device with some resistance) are constant and equal, and that the pressure difference $\Delta P_m = P_{m1} - P_{m2}$ agrees with the flow and the impedance of the controlled device.

This steady state behaviour can again be characterized by a 3D-plot, for instance as

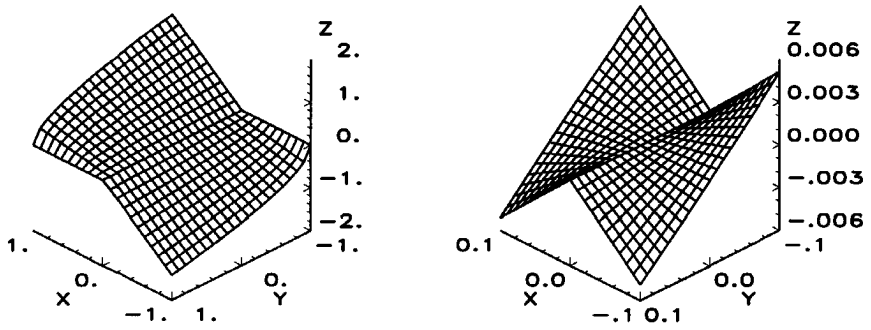


Fig. 2.13: Three-dimensional representation of ideal spool flow characteristic; x = $\bar{x}_s$, y = $\overline{\Delta P}_m$, z = $\bar{\Phi}_m = \bar{\Phi}_{m1} = \bar{\Phi}_{m2}$; non-linear characteristic on full scale (left) and non-linear characteristic excluding linear contribution on 10 % scale (right)

shown in Fig. 2.13, where the left plot gives the actual non-linearity on full input scales, and the right plot shows the residue of the non-linearity if the linear contribution is subtracted, on 10 % input scales. The inputs are the (scaled) spool position $\bar{x}_s = \frac{x_s}{x_{s,max}}$ and the (scaled) pressure difference $\overline{\Delta P}_m = \frac{\Delta P_m}{P_s}$ related to the spool position and some impedance of the controlled device. The output is the resulting steady state flow (scaled) $\bar{\Phi}_m = \frac{\Phi_m}{\Phi_{m,nom}}$, where the nominal spool flow is defined as (compare (2.16) and (2.17)):

$$\Phi_{m,nom} = C_d h_s x_{s,max} \sqrt{P_s/\rho}$$

For numerical values of the scalings, see Table F.2.

Actually, the results of Fig. 2.13 represent the ideal characteristic (though non-linear) of the spool flow, whereas the underlaps $d_{si}, i = 1, 2, 3, 4$ and the radial spool clearance c_{rs} in (2.17) were all set to zero in the simulation model. This situation is often referred to, as the use of a critical-centred valve [139]. The basic non-linearity obtained this way, and shown in the left plot of Fig. 2.13, is inherent to hydraulic servo-systems with flow control valves, and can be characterized by the following properties:

- For zero load pressure ΔP_m the flow Φ_m is linear in the spool displacement x_s.
- For zero spool displacement, the flow is independent of the load pressure.
- For zero load pressure, the load dependence $\frac{\partial \Phi_m}{\partial \Delta P_m}$ varies linearly with the absolute value of the spool displacement $|x_s|$.
- For non-zero load pressure, the flow gain $\frac{\partial \Phi_m}{\partial x_s}$ depends on the load pressure at the one hand, and on the sign of the spool displacement on the other hand. It even becomes zero for maximum load pressure and opposite spool displacement.

For small inputs and load pressures, these properties are once more illustrated by the right plot of Fig. 2.13, where the linear contribution of the spool displacement to the flow is subtracted. It shows, that for these input ranges, which are often the most important ranges for servo control, the effects of the load pressure are not so large; the flows due to non-linearity are smaller than 5 % (relatively).

However, due to manufacturing tolerances, the underlaps and clearances as modelled by (2.17) are non-zero in practice. Normalizing these parameters[1] with respect to the

[1]Normalization is denoted by a bar.

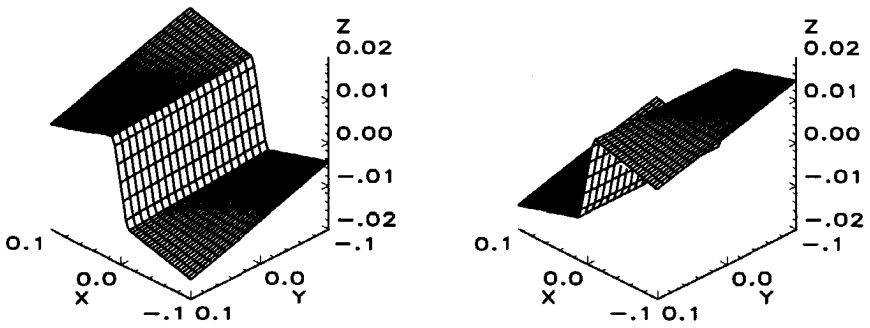


Fig. 2.14: Three-dimensional representation of spool flow characteristic with linear contribution subtracted; x = $\bar{x}_s$, y = $\overline{\Delta P}_m$, z = $\bar{\Phi}_m = \bar{\Phi}_{m1} = \bar{\Phi}_{m2}$; equal underlaps 1 % (left) and equal overlaps 1 % (right)

maximum spool displacement $x_{s,max}$, it is often found that underlaps or overlaps (negative underlaps) are in the order of magnitude of 1 %. The radial clearance may be in the order of magnitude of 2 μm, which is about .2 % of $x_{s,max}$ given in Table F.2. Although there are many configurations of different underlaps and clearances possible, it is tried to gain some insight by analyzing the effect of some characteristic configurations.

To start with, it is assumed that all spool ports have equal underlaps or equal overlaps of 1 %, so $\bar{d}_{s1} = \bar{d}_{s2} = \bar{d}_{s3} = \bar{d}_{s4} = 0.01$ and -0.01 respectively. The radial clearance $\bar{c}_{rs}$ is still assumed to be zero. The results for underlaps and overlaps are shown in the left and right plot respectively of Fig. 2.14.

Comparing these plots with the right plot of Fig. 2.13, it is clear that the deviations in the spool port configuration cause a severe non-linearity in the flow characteristics for small spool displacements. Actually, the underlaps cause a doubled flow gain $\frac{\partial \Phi_m}{\partial x_s}$ in the underlap region, while the overlaps result in zero flow gain in the overlap region. Outside these regions, there is a constant deviation in the absolute flow of 1 % (the amount of underlap/overlap) of the nominal flow.

Concerning the load dependence $\frac{\partial \Phi_m}{\partial \Delta P_m}$, which can be recognized as the slope of the 3D-surface in y-direction, comparison of Fig. 2.14 and Fig. 2.13 shows hardly any influence of spool port underlaps and overlaps. So deviations in the geometry of the spool manifest themselves mainly in a strong non-linearity of the flow gain for small spool displacements, while the load dependence remains characterized by the non-linear characteristics of Fig. 2.13. For this reason, further analysis of the effect of spool port configurations on the flow characteristics will be performed using 2D-plots of the flow with respect to the spool displacement.

Where in previous results the radial clearance was neglected, the effect of this clearance is shown in Fig. 2.15. Clearly, the clearance and the accompanying leakage flows are smoothing the characteristic, and result in a slightly decreased gain in the underlap region and in non-zero gain in the overlap region, contrary to the case of no clearance. In fact, the characteristics with radial clearance are more realistic.

Even more realistic is the situation, that the port configuration is not symmetric. As many valves have underlaps rather than overlaps in order to avoid dead-band behaviour like in the right plot of Fig. 2.15, only some asymmetric underlap configurations are considered.

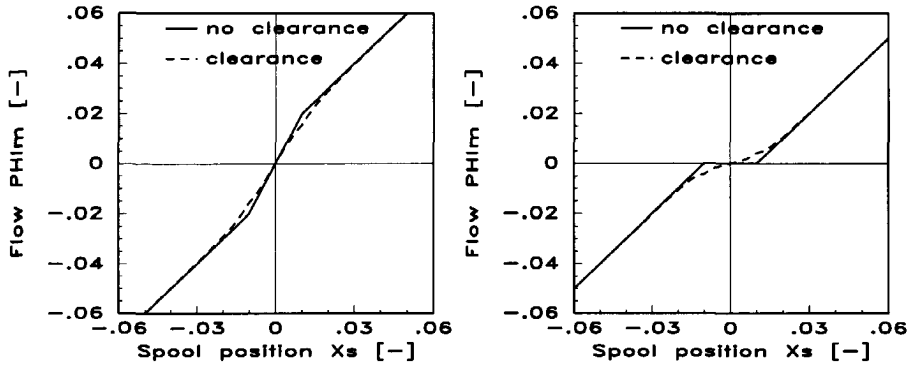


Fig. 2.15: Effect radial spool clearance $\bar{c}_{rs} = 0.005$ in combination with underlaps of 1 % (left) and overlaps of 1 % (right) on steady state flow characteristic for zero load pressure $\overline{\Delta P}_m$

The resulting flow characteristics are shown in the upper plots of Fig. 2.16. The lower plots of this Figure show the spool port pressure $\bar{P}_m = \bar{P}_{m1} = \bar{P}_{m2}$ (equality because the load pressure is zero), that is required to have steady state flow. These results give rise to the following remarks:

- For the given variations in spool port configurations, the flow characteristics hardly depend on the configuration. This is partially due to the regularity in the chosen underlaps.
- Asymmetric underlap configurations can result in offsets of the flow characteristic.
- Different underlap configurations can result in identical flow characteristics, with different spool port pressure characteristics and vice versa. This is due to the symmetry in the flow equations.
- Related to the previous item: the characteristic of the spool port pressures isn't a measure for the linearity of the flow characteristic, and is therefore not relevant for the input-output behaviour of the spool flow equations. However, if underlap configurations of the spool are to be identified, the pressure characteristics are relevant.

Although many other configurations might be analyzed, the Figures 2.13 up to and including 2.16 summarize the basic characteristics of the spool flows, and effects related to the geometry of the spool on this flow characteristics.

Non-linear flow forces on spool

Comparing the equation for the axial flow force on the spool (2.19) with the equation for the spool flows (2.16), there is great similarity. In fact, the only structural difference is, that the flows depend on the square root of the pressure difference across a port, whereas the axial flow forces depend linearly on this pressure difference. The result is, that the shape of the flow force characteristic is comparable to Fig. 2.13, the only difference being that the lines in y-direction (load dependence) are straight, instead of curved according to the square root expression.

Effectively, this means that axial flow force on the spool may be interpreted as an imaginary non-linear spring, driving the spool back to its neutral position. Thereby, the non-linearity is similar to the steady state output non-linearity of the flapper-nozzle valve,

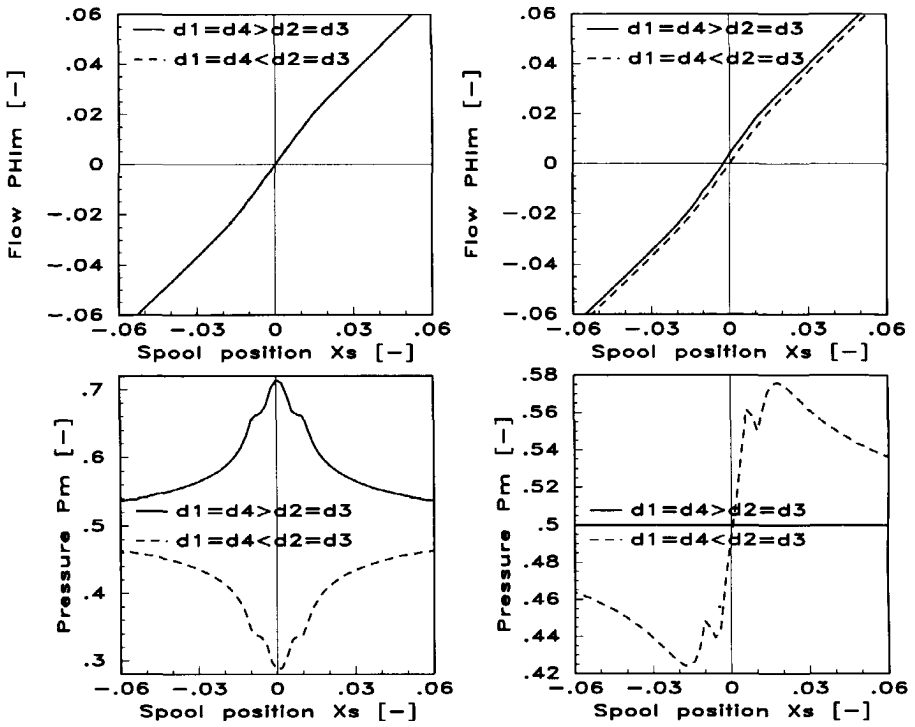


Fig. 2.16: Effect unequal underlaps on flow $\bar{\Phi}_m$ (upper) and spool port pressure $\bar{P}_m$ (lower) for zero load pressure. Radial spool clearance .5 %; $\bar{d}_{s1} = \bar{d}_{s4} = 2\bar{d}_{s2} = 2\bar{d}_{s3} = 0.01$ & $2\bar{d}_{s1} = 2\bar{d}_{s4} = \bar{d}_{s2} = \bar{d}_{s3} = 0.01$ (left) and $\bar{d}_{s1} = \bar{d}_{s3} = 2\bar{d}_{s2} = 2\bar{d}_{s4} = 0.01$ & $\bar{d}_{s1} = \bar{d}_{s2} = 2\bar{d}_{s3} = 2\bar{d}_{s4} = 0.01$ (right)

namely the (load dependent) flow characteristic. How this non-linearity affects the final input-output behaviour of the valve, is to be analyzed by simulations with the complete servo-valve model.

Step responses of the flapper-nozzle valve model

With the different non-linear parts of the model of the flapper-nozzle servo-valve being analyzed, the question arises, to what extent the different phenomena do affect the (dynamic) input-output behaviour. For this purpose, a number of step responses has been simulated, with one or more of the non-linear effects included in the model.

The first result to be shown here, given in Fig. 2.17, is obtained with all non-linear effects included, except ball clearance and Coulomb friction, for reasons mentioned earlier. The numerical values, used for this simulation, are listed in Table F.1. In order to provide insight in the dynamic behaviour of the model, the response of different variables is shown for a step input of 25 % of full scale.

For this input, the flapper position responds quickly and oscillatory, with shortly a maximum deflection. This means, that the non-linear region of the torque motor equations, visualized in Fig. 2.8 is entered during this response. The oscillation corresponds to the

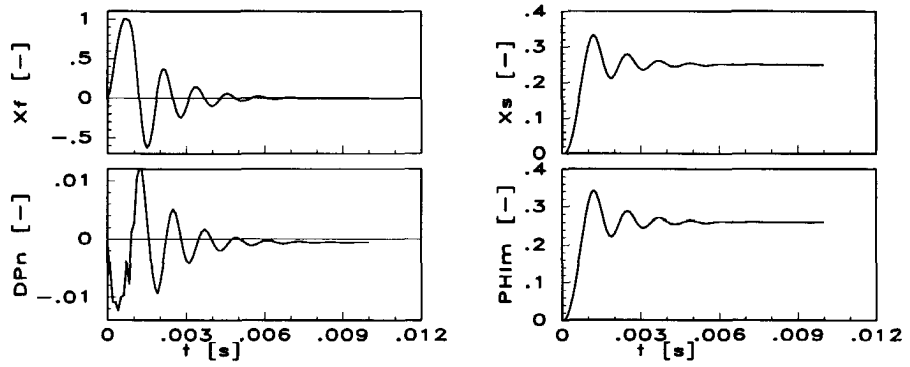


Fig. 2.17: Step response of flapper-nozzle valve model with 25 % step input; zero load pressure ΔP_m. Flapper position $\bar{x}_f$ and nozzle pressure difference $\overline{\Delta P}_n$ (left); spool position $\bar{x}_s$ and resulting spool flow $\bar{\Phi}_m$ (right)

natural frequency of the flapper-armature in combination with the different stiffness-effects in (2.4).

By means of the nozzle flows, the flapper position controls the nozzle pressure difference, which shows a similar dynamic response. Note that the pressure difference is in magnitude, meaning that the dynamic response only covers the 'linear' region of the flapper-nozzle equations, as visualized in Fig. 2.10.

The spool is quickly accelerated by the nozzle pressure difference, where the flapper oscillation comes through in the spool position response, to reach its final position in steady state. Clearly, the spool flow is directly related to the spool position.

In steady state, an equilibrium is reached, as well for the torques on the flapper due to torque motor input, feedback spring force, and flow forces on the flapper, as for forces on the spool due to nozzle pressure difference, feedback spring force and axial flow force. It might be noted, that the nozzle pressure difference in this equilibrium corresponds to the (very small and invisible in Fig. 2.17) steady state flapper deflection.

Now that the dynamic behaviour is somewhat clarified, the influence of different phenomena is illustrated by the responses shown in Fig. 2.18, obtained with different effects included in the model. Each strip shows four normalized responses of the resulting spool flow $\bar{\Phi}_m$ on a step wise input of the steering current $\bar{i}_{ca}$ of .1 %, 1 %, 10 % and 25 % respectively; the responses are normalized with respect to the input step size, clearly showing the effective non-linearity.

The results of Fig. 2.18 make clear that, given the theoretical model structure, presented in this Section, and the parameter settings of Table F.1:

- The non-linear flapper-nozzle flow equations (2.5), (2.6), (2.10) and (2.11) do not result in non-linearity in the dynamic input-output behaviour.
- The flow forces on the flapper according to (2.8) and (2.9) do slightly increase the speed of response or, in other words, destabilize the flapper dynamics, but do not cause non-linearity.
- The non-linearity of the torque motor gives considerable deviations of the dynamic behaviour for large input amplitudes; this non-linearity seems to be serious.
- Non-ideal port geometry of the spool causes non-linearity in the sense of steady state

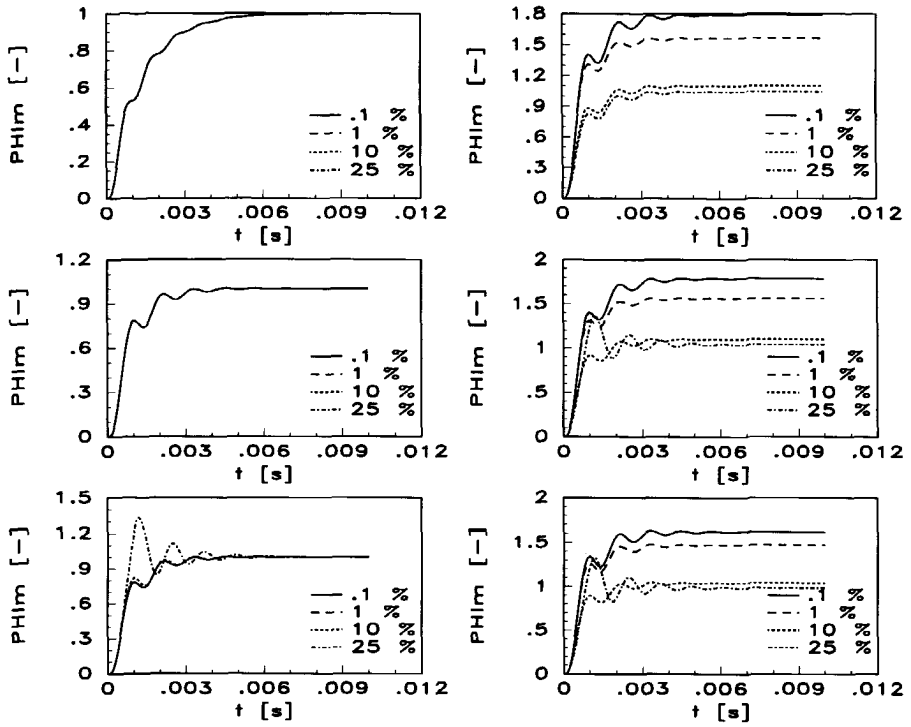


Fig. 2.18: Normalized step responses of flapper-nozzle valve flow $\bar{\Phi}_m$ for varying step amplitudes of $\bar{i}_{ca}$; zero load pressure ΔP_m. Only NL flapper-nozzle flow (upper left); NL flapper-nozzle flow plus -forces (middle left); idem plus NL torque motor (lower left); NL flapper-nozzle flow plus underlaps and radial clearance (upper right); idem plus NL torque motor (middle right); idem plus axial spool flow forces (lower right)

gain, especially for small amplitudes.

- A combination of the torque motor non-linearity and the spool flow non-linearity gives non-linear behaviour over the complete input range.
- The axial flow forces on the spool effectively decrease the steady state gain of the valve, but do not affect the linearity.

The given results have been restricted to simulations with inputs until 25 % of full scale. The reason is, that with the same parameter settings, a larger step input would cause the flapper to hit the nozzles during the response. Although this strong non-linearity might be included in the model, it is not done, because it is not very likely that the flapper hits the nozzles regularly in reality (this would cause serious wear). It is more likely, that the parameterset, that is used here, is not quite realistic. Nevertheless, a qualitative interpretation of the results provides a lot of insight in the model.

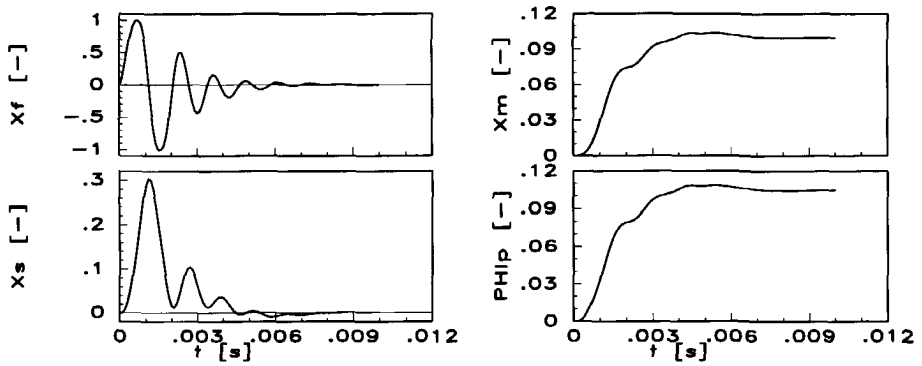


Fig. 2.19: Step response of three-stage valve model with 10 % step input; zero load pressure ΔP_p. Flapper position $\bar{x}_f$ and pilot-valve spool position $\bar{x}_s$ (left); main spool position $\bar{x}_m$ and resulting main spool flow $\bar{\Phi}_p$ (right)

Step responses of the three-stage valve model

In case the two-stage flapper-nozzle valve is used as a pilot-valve in a three-stage valve, its non-linear dynamic behaviour will be crucial for the (non-linear) dynamic behaviour of the complete three-stage servo-valve. This is briefly illustrated by a series of simulated step responses, using exactly the same model for the flapper-nozzle valve as before, and using the equations of Subsection 2.2.4 for the third stage in the simulation model. The parameter values can be found again in Table F.1.

For the given parameters, with small underlaps and radial clearance of the main spool, and the feedback gain K_{pm} adjusted such that a reasonable closed loop response is obtained, the simulated closed loop response on a step input of 10 % of full scale is given in Fig. 2.19. The response has been obtained with zero load pressure $\Delta P_p = P_{p1} - P_{p2}$ for the main spool flow, and the pressures P_{p1} and P_{p2} such that the main spool flows are equal: $\Phi_p = \Phi_{p1} = \Phi_{p2}$. The main spool flow shown in the Figure is scaled like before: $\bar{\Phi}_p = \frac{\Phi_p}{\Phi_{p,nom}}$, where the nominal main spool flow is defined as:

$$\Phi_{p,nom} = C_d h_m x_{m,max} \sqrt{P_s/\rho}$$

The left plots of Fig. 2.19 show two state variables of the pilot-valve; the flapper position and the spool position. Obviously, the closed loop configuration with the integrator of the main spool causes the pilot-valve to respond in a high-pass manner, while also the original dynamics of the flapper-nozzle valve are recognized.

The response of the third stage is a nice closed loop response, as shown in the right plots of Fig. 2.19. The main spool position is clearly the integral of the pilot-valve spool position, including the flow non-linearity due to non-ideal port geometry of the pilot-valve. The resulting main spool flow is statically related to the main spool position, where the non-linearity of (2.23) and (2.24) plays a role.

In order to elucidate the non-linearity in the step responses somewhat more, Fig. 2.20 shows normalized step responses of the main spool position $\bar{x}_m$ and the resulting flow $\bar{\Phi}_p$ for different step amplitudes, namely .1 %, 1 % and 10 %. Whereas the responses of the main spool position show a unity steady state gain, the resulting flows vary with input amplitude. This is typical for the non-linearity of the flow characteristic of the main spool.

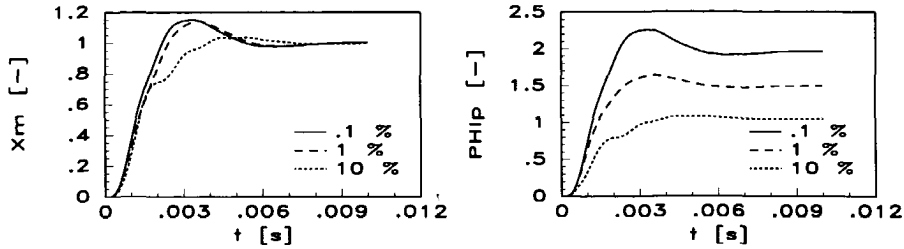


Fig. 2.20: Step response of three-stage valve model with .1 %, 1 % and 10 % step input respectively; zero load pressure ΔP_p. Main spool position $\bar{x}_m$ (left) and resulting main spool flow $\bar{\Phi}_p$ (right)

However, the difference in the transients of the main spool position can only be the result of non-linearity of the pilot-valve. Using the insight obtained before, it can be stated that the response with large input amplitude (10 %) is affected by the torque motor non-linearity, resulting in more oscillatory behaviour. On the other hand, the response with small input (.1 %) is influenced by the non-linearity due to the port geometry of the pilot-valve spool, because the pilot-valve operates in this non-linear region during the response. This means, that the *static* non-linearity of the pilot-valve causes non-linearity in the *dynamic* behaviour of the three-stage valve.

Conclusion

Although it is problematic to find a reasonable set of physical parameters for the theoretical servo-valve model of this Section, a preliminary simulation analysis of the model, as performed in this Subsection, provides a lot of insight in the non-linear dynamic behaviour of the servo-valve. Dominant dynamic effects are the second order behaviour of the flapper, combined with the pressure dynamics of the spool. For the three-stage valve, the dynamics are dominated by the pilot-valve dynamics at the one hand, and the integrating behaviour with the feedback of the third stage at the other hand. Most important non-linearities are to be sought in the torque motor and in the flow characteristics of the pilot-valve spool and the main spool respectively.

With this conclusion on the simulation results of the non-linear servo-valve model, the discussion of the modelling and simulation of an electro-hydraulic servo-valve is completed, and a starting point for further analysis of the servo-valve model is given. However, before doing this in Section 2.5, a similar discussion of the modelling and simulation of the other subsystems of the hydraulic servo-system is given. In the next Section, this is done for the basic subsystem, namely the hydraulic actuator.

2.3 Modelling and simulation of a hydraulic actuator

2.3.1 Introduction

Whereas the servo-valve is used to control a high power oil flow, the hydraulic actuator transforms this hydraulic energy in terms of flow and pressure into mechanical energy in terms of velocity and force. In many cases, this results in large motions of an inertial load; in other cases it results in large exerted forces to a stiff environment under small

actuator displacements. Thus, the hydraulic actuator is the basic functional element of the hydraulic servo-system, and so is the model of the actuator the basic element of the complete servo-system model. In this Section, the theoretical model of the actuator is presented, and an analysis of the dynamics and non-linearities of the actuator is given.

As outlined in Chapter 1, the configuration of the actuator will depend on the application. Nevertheless, it is possible to cover most hydraulic servo actuators in a theoretical model by representing them by two actuator chambers, separated by a moving piston, like depicted in Fig. 2.21. This leads to the basic actuator model, given in Subsection 2.3.2.

In the basic actuator model, internal leakage and friction of the actuator have to be taken into account. Many hydraulic actuators in servo applications are provided with hydrostatic bearings, and for this type of bearings theoretical relations for the leakage and friction are available, which will be presented in Subsection 2.3.3.

For the special double-concentric actuator configuration, which is also used in the experimental investigations of Chapters 3, 4 and 5, the complete theoretical model of the hydraulic actuator is given in Subsection 2.3.4, as a 'modelling example'. An analysis of the modelled dynamics and non-linearities of the hydraulic actuator is given in Subsection 2.3.5, where a number of simulation results is discussed, which are obtained with the model of Subsection 2.3.4.

2.3.2 Basic actuator model

The physical modelling of a hydraulic actuator is well-known from books as [98, 139] and is very often described in literature, for instance in [1, 19, 35, 52, 66, 73, 91, 94, 124, 125, 148]. The actuator model consists of mass balances for each actuator chamber, and an equation of motion for the piston.

With the sign-definitions of the actuator variables given in Fig. 2.21, the mass balances of the respective actuator chambers give state equations for the actuator pressures at both sides of the piston, by taking into account the oil compressibility with bulk modulus E:

$$\begin{aligned} \dot{P}_{p1} &= \frac{E}{A_{p1}(q_{max}+q)+V_{l1}} \left(\Phi_{p1} - \Phi_{lp} - \Phi_{l1} - A_{p1}\dot{q}\right) \\ \dot{P}_{p2} &= \frac{E}{A_{p2}(q_{max}-q)+V_{l2}} \left(-\Phi_{p2} + \Phi_{lp} - \Phi_{l2} + A_{p2}\dot{q}\right) \end{aligned} \tag{2.27}$$

Hereby, q_{max} is half the actuator stroke and A_{p1} and A_{p2} are the respective piston areas, which are not necessarily equal in the general case. The latter also holds for V_{l1} and V_{l2}, the volumes of the respective actuator chambers that do not belong to the stroke of the actuator, and therefore often called ineffective volumes. For instance, channels in the manifold and transmission lines contribute to these ineffective volumes.

For the leakage flows across the piston Φ_{lp} and the leakage flows Φ_{l1} and Φ_{l2} out of the respective actuator chambers, it is often assumed that they can be described as small laminar flows through a narrow gap, see for instance [19, 52, 93, 145]. Defining some laminar leakage coefficients LP_p, LP_1, LP_2, the respective leakage flows in Fig. 2.21 can be described by:

$$\begin{aligned} \Phi_{lp} &= LP_p \left(P_{p1} - P_{p2}\right) \\ \Phi_{li} &= LP_i P_{pi}, \qquad\qquad i = 1, 2 \end{aligned} \tag{2.28}$$

In case that the actuator is provided with hydrostatic bearings, theoretical expressions for the leakage flows are given in Subsection 2.3.3 and Subsection 2.3.4.

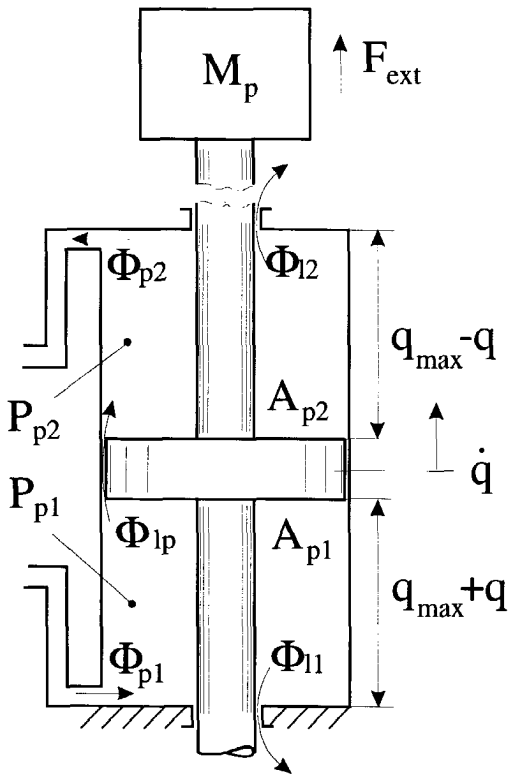


Fig. 2.21: Schematic drawing of symmetric hydraulic actuator

The piston position q and velocity $\dot{q}$ in (2.27) are obtained from the equation of motion of the piston:

$$M_p\ddot{q} = A_{p1}P_{p1} - A_{p2}P_{p2} - F_{vp} - F_{cp} + F_{ext} \tag{2.29}$$

where M_p is the inertia of the piston including the inertia of the load. F_{vp} is the viscous friction force on the piston due to viscosity effects of oil films in the actuator bearings, and can in general be characterized by a viscous friction coefficient w_p as follows:

$$F_{vp} = w_p\dot{q} \tag{2.30}$$

Like for the leakage flows, theoretical expressions for the viscous friction are given in Subsection 2.3.3 and Subsection 2.3.4, for the case that the actuator is provided with hydrostatic bearings.

The Coulomb friction force on the piston F_{cp}, which will mostly be present due to the presence of seals in the actuator, is modelled in the same way as the Coulomb friction on the spool of the flapper-nozzle valve in Subsection 2.2.2. The external force F_{ext} finally, may consist of different contributions, e.g. gravity forces, and is defined as follows:

Definition 2.3.1 *The external force F_{ext} is the sum of the forces acting on the piston, that are not algebraically related to the actuator pressures or the velocity or the acceleration of the piston.*

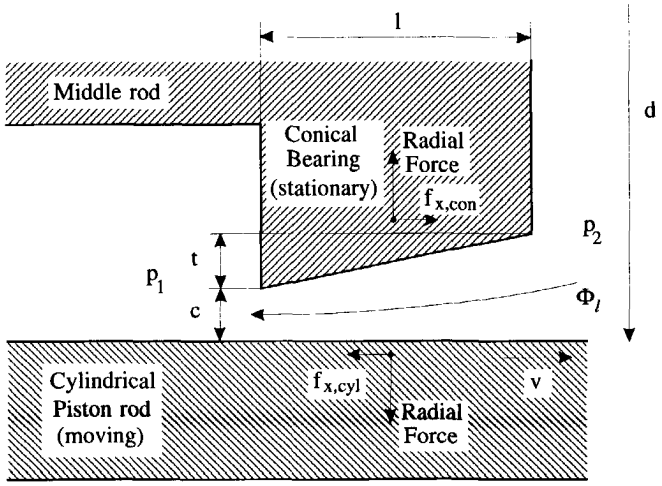


Fig. 2.22: The principle of a conical hydrostatic bearing

With the differential equations (2.27) and (2.29) the basic actuator dynamics are modelled, including leakage and friction effects. A more detailed description of these latter phenomena in the case that the actuator has hydrostatic bearings, is given in the next Subsections.

2.3.3 Leakage and friction of hydrostatic bearings

The use of hydrostatic bearings in hydraulic actuators, mostly in applications where smooth operation is required, has proven to be a good means to minimize Coulomb friction [139]. The idea behind the technique is, that a static pressure difference across the bearing maintains an oil film between the moving parts, avoiding dry friction due to metal-to-metal contact. Using a slightly conical bearing, like depicted in Fig. 2.22, the pressure distribution in the gap will generate radial bearing forces, which increase with decreasing clearance. This effect causes a centering force on the cylinder in the bearing. Obviously, this bearing technique introduces leakage flows, and besides radial bearing forces also axial forces are present.

In the development of the conical bearing technique by Blok [16] and Viersma [139], they focussed their attention mainly on the effect of the design parameters on the performance of the bearing, in the sense of allowable radial bearing force and resulting leakage flows. They give a lot of theoretical, approximate and experimental results, including possible cavitation effects. Based on these investigations, they present design rules and design examples for conical hydrostatic bearings.

For design purposes, the description of radial bearing forces and of leakage flows, depending on the excentricity of the cylinder in the bearing, is most important; Blok [16] and Viersma [139] have given this description in detail. On the other hand, for the purpose of the dynamic modelling of a hydraulic actuator, it is important to investigate those effects

of the hydrostatic bearing, that play a role in the actuator model, Subsection 2.3.2. This means, that especially the *axial* bearing forces have to be taken into account, because they contribute to the actuator dynamics via the equation of motion of the piston (2.29). As the derivation of expressions for these axial forces is not described in [16, 139], it is given in Appendix C, Section C.2. Besides the derivation of the axial bearing forces, a recapitulation of the derivation of the leakage flows, which also affect the actuator dynamics, is given in Appendix C, Section C.1.

Thereby, it is assumed that the cylinder is centered in the bearing. Although excentricity was taken into account initially, a preliminary analysis by means of simulations of the actuator dynamics showed hardly any effect of lateral forces (acting in radial direction on the actuator bearings) on the longitudinal motions of the actuator. For this reason, and because no lateral motions were observed in practice, only longitudinal effects have been taken into account in the actuator model, corresponding to the assumption that the excentricity of the hydrostatic bearings is zero.

With this assumption, the leakage flow Φ_l through a single hydrostatic bearing as shown in Fig. 2.22 is (see equation (C.7) and Fig. C.1):

$$\Phi_l = -\phi_x = \frac{\pi d c^3}{6\,\eta l} \frac{\left(1+\frac{t}{c}\right)^2}{\left(2+\frac{t}{c}\right)} (p_2 - p_1) - \pi d c \frac{\left(1+\frac{t}{c}\right)}{\left(2+\frac{t}{c}\right)} v \tag{2.31}$$

In this equation, the dimensions are like depicted in Fig. 2.22: d is the diameter of the bearing, c the clearance between the bearing and the cylindrical part, l the length of the bearing, and t the tapering of the conical part. The velocity of the moving part is v, while the local pressures at the left and the right side of the bearing are denoted as p_1 and p_2 respectively.

For the axial bearing forces $f_{x,cyl}$ and $f_{x,con}$ on the cylindrical part and the conical part of the bearing respectively, given the same configuration of Fig. 2.22, the following expressions can be used (see (C.8) and (C.9)):

$$f_{x,cyl} = \pi d c \frac{\left(1+\frac{t}{c}\right)}{\left(2+\frac{t}{c}\right)} (p_2 - p_1) + \left[-\frac{\pi d}{c} \frac{6\,\eta l}{\left(2+\frac{t}{c}\right)} + \frac{\pi d}{t} 4\,\eta l \ln\left(1+\frac{t}{c}\right) \right] v \tag{2.32}$$

$$f_{x,con} = -\pi d c \frac{\left(1+\frac{t}{c}\right)}{\left(2+\frac{t}{c}\right)} (p_2 - p_1) + \left[\frac{\pi d}{c} \frac{6\,\eta l}{\left(2+\frac{t}{c}\right)} - \frac{\pi d}{t} 2\,\eta l \ln\left(1+\frac{t}{c}\right) \right] v \tag{2.33}$$

Given these expressions, the leakage flows in the mass balances (2.27), and the viscous friction force in the equation of motion (2.29) can be described as the resultants of the leakage flows and axial friction forces of the different hydrostatic bearings of the actuator. Obviously, the resulting leakage and friction models are strongly dependent on the construction of the actuator, i.e. where and how the bearings are applied. This is illustrated in the modelling example, given in the next Subsection.

2.3.4 Actuator modelling example

Although the model relations of the previous Subsections do not yet constitute a complete model for one specific hydraulic actuator, they form the ingredients for the theoretical

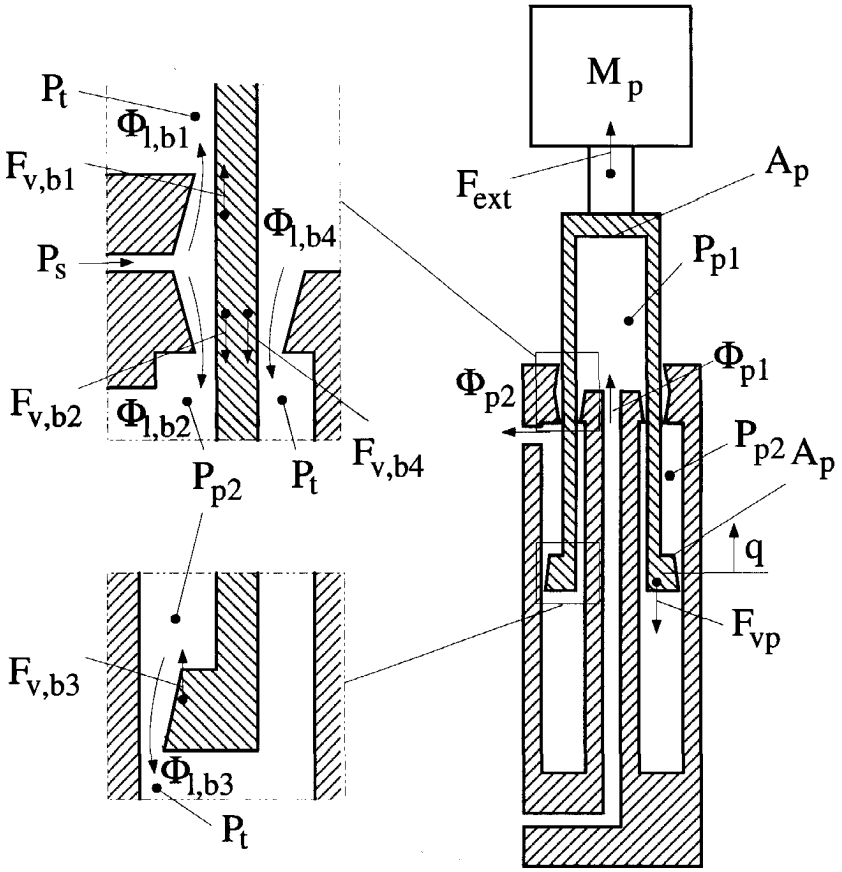


Fig. 2.23: Schematic drawing double-concentric symmetric hydraulic actuator

models of different types of hydraulic actuators, as mentioned in Chapter 1, and depicted in Fig. 1.1.

As an example, the complete dynamic actuator model will be given here for the double-concentric hydraulic actuator, which is also used for experimental validation of the models, Chapter 3. For a drawing of the construction including the sign-definitions of the variables, see Fig. 2.23.

Because of the special symmetric design, the piston areas are equal, so $A_{p1} = A_{p2} = A_p$. Furthermore the construction implies, that there is no leakage across the piston, as described by Φ_{lp} in (2.28): there is no direct flow possible from the one actuator chamber to the other. So, for this example, the differential equations for the cylinder pressures read:

$$\begin{aligned} \dot{P}_{p1} &= \frac{E}{A_p(q_{max}+q)+V_{l1}} (\Phi_{p1} - \Phi_{l1} - A_p\dot{q}) \\ \dot{P}_{p2} &= \frac{E}{A_p(q_{max}-q)+V_{l2}} (-\Phi_{p2} - \Phi_{l2} + A_p\dot{q}) \end{aligned} \tag{2.34}$$

The leakage terms in these equations are determined by the leakage flows of the four

hydrostatic bearings (two single and one double bearing) of the actuator, as depicted in Fig. 2.23:

$$\begin{aligned} \Phi_{l1} &= \Phi_{l,b4} \\ \Phi_{l2} &= -\Phi_{l,b2} + \Phi_{l,b3} \end{aligned} \tag{2.35}$$

Hereby, the leakage flows of bearing i, $i = 1, 2, 3, 4$ (indicated with subscript bi), are given as:

$$\begin{aligned} \Phi_{l,b1} &= LP_{b1}\,(P_s - P_t) + A_{p,b1}\dot{q} \\ \Phi_{l,b2} &= LP_{b2}\,(P_s - P_{p2}) - A_{p,b2}\dot{q} \\ \Phi_{l,b3} &= LP_{b3}\,(P_{p2} - P_t) + A_{p,b3}\dot{q} \\ \Phi_{l,b4} &= LP_{b4}\,(P_{p1} - P_t) - A_{p,b4}\dot{q} \end{aligned} \tag{2.36}$$

where for bearing i, $i = 1, 2, 3, 4$, the following parameters are defined, according to (2.31):

$$LP_{bi} = \frac{\pi d_{bi} c_{bi}^3}{6\,\eta l_{bi}} \frac{\left(1 + \frac{t_{bi}}{c_{bi}}\right)^2}{\left(2 + \frac{t_{bi}}{c_{bi}}\right)}; \quad A_{p,bi} = \pi d_{bi} c_{bi} \frac{\left(1 + \frac{t_{bi}}{c_{bi}}\right)}{\left(2 + \frac{t_{bi}}{c_{bi}}\right)}; \quad i = 1, 2, 3, 4 \tag{2.37}$$

Actually, the parameter LP_{bi} is the leakage parameter for bearing i, while the parameter $A_{p,bi}$ can be seen as a virtual piston area, resulting in an extra displacement flow due to bearing i.

The equation of motion for the actuator considered here, is almost equal to the general form (2.29):

$$M_p \ddot{q} = A_p\,(P_{p1} - P_{p2}) - F_{vp} - F_{cp} + F_{ext} \tag{2.38}$$

Given the actuator configuration with hydrostatic bearings according to Fig. 2.23, the viscous friction force on the piston can be written as the sum of the contributions of each bearing:

$$F_{vp} = -F_{v,b1} + F_{v,b2} - F_{v,b3} + F_{v,b4} \tag{2.39}$$

Taking into account, that the moving part (the piston) forms the cylindrical part of the bearing for $i = 1, 2, 4$ and the conical part of the bearing for $i = 3$, the axial bearing forces are given by:

$$\begin{aligned} F_{v,b1} &= A_{p,b1}\,(P_s - P_t) - w_{p,b1}\dot{q} \\ F_{v,b2} &= A_{p,b2}\,(P_s - P_{p2}) + w_{p,b2}\dot{q} \\ F_{v,b3} &= A_{p,b3}\,(P_t - P_{p2}) - w_{p,b3}\dot{q} \\ F_{v,b4} &= A_{p,b4}\,(P_{p1} - P_t) + w_{p,b4}\dot{q} \end{aligned} \tag{2.40}$$

where the virtual piston areas $A_{p,bi}$ are defined as before, and the viscous friction coefficent $w_{p,bi}$ for bearing i, $i = 1, 2, 3, 4$ defined as follows, using (2.32) and (2.33):

$$\begin{aligned} w_{p,bi} &= \left[-\frac{\pi d_{bi}}{c_{bi}} \frac{6\,\eta l_{bi}}{\left(2 + \frac{t_{bi}}{c_{bi}}\right)} + \frac{\pi d_{bi}}{t_{bi}} 4\,\eta l_{bi} \ln\left(1 + \frac{t_{bi}}{c_{bi}}\right) \right], i = 1, 2, 4 \\ w_{p,bi} &= \left[\frac{\pi d_{bi}}{c_{bi}} \frac{6\,\eta l_{bi}}{\left(2 + \frac{t_{bi}}{c_{bi}}\right)} - \frac{\pi d_{bi}}{t_{bi}} 2\,\eta l_{bi} \ln\left(1 + \frac{t_{bi}}{c_{bi}}\right) \right], i = 3 \end{aligned} \tag{2.41}$$

With these equations, the complete theoretical dynamic model of the double-concentric hydraulic actuator is given. In order to obtain insight in the basic dynamic and non-linear behaviour of this hydraulic actuator, a simulation analysis of the presented model is given in the next Subsection.

2.3.5 Simulation of the non-linear actuator model

Like in the case of the servo-valve, the aim of the simulations to be presented in this Subsection is primarily to obtain qualitative insight in the basic behaviour of the hydraulic actuator. The obtained insight is then to be used to simplify the model if possible, such that only relevant dynamics and non-linearities are taken into account. This leads to a simplified dynamic model, to be given later in Section 2.6, in which the dominant non-linearities can be included as described in Section 2.7. The resulting model then serves as a basis for the identification and validation of an accurate experimental non-linear dynamic model of the hydraulic actuator, as described in Chapter 3.

The organization of the Subsection is as follows. First, the parameterset that has been used in the simulations is discussed. Then, the possible non-linearity of the static system behaviour due to the leakage and the axial forces of the hydrostatic bearings is investigated, by discussing some simulation results. After that, the dynamic behaviour of the actuator is discussed, including the effects of the hydrostatic bearings, showing simulated step responses of the actuator model. Finally, some simulation results are discussed, which illustrate the non-linearity in the dynamic actuator behaviour due to position dependence and Coulomb friction respectively.

Parameters to be used in the simulation model

Contrary to the case of the servo-valve, it is not difficult to find a set of realistic physical parameters for the hydraulic actuator. Especially for the case that will be described here as an example, with model equations as described in Subsection 2.3.4, the physical parameters are known a-priori, because the design drawings of the actuator are available[2]. For instance, the design parameters of the hydrostatic bearings, such as length and clearance, are known exactly; they are listed in Table F.3 in Appendix F. Using the expressions (2.37), (2.41), the parameters for the model equations (2.36), (2.40) can be calculated. A complete list of parameters used for the simulations to be discussed below, is given in Table F.4 in Appendix F.

When simulating the actuator model, some assumption has to be made concerning the servo-valve, controlling the actuator flows. For this purpose, it is assumed that the (normalized) position of the main spool $\bar{x}_m$ of a three-stage valve can be seen as input of the actuator model; the dimensions of the main spool are chosen identical to those in the previous Section.

Leakage of hydrostatic bearing

One of the basic properties of a hydraulic actuator is, that in steady state the velocity of the actuator is directly related to the servo-valve flows. This results from the mass balances of the actuator chambers. However, when considering these balances in the actuator modelling example, (2.34), it is clear that the leakage flows also contribute to this steady state relation.

Without leakage, the steady state velocity $\dot{q}$ corresponding to some valve spool position x_m equals the servo-valve flow $\Phi_p = \Phi_{p1} = \Phi_{p2}$ divided by the piston area A_p. Hereby, the cylinder pressures P_{p1} and P_{p2} are such that the equality of flows Φ_{p1} and Φ_{p2} (see

[2]The actuator design has been part of the SIMONA-project, see Subsection 1.2.1.

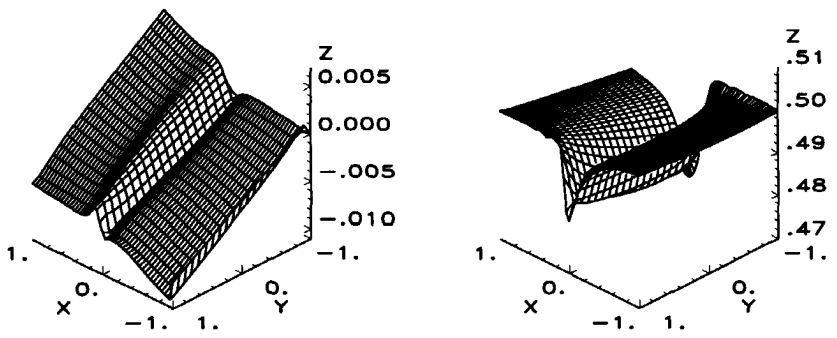


Fig. 2.24: Three-dimensional representation of the effect of leakage flows on actuator velocity (left) and actuator pressure level (right); $\mathsf{x} = \bar{x}_m$, $\mathsf{y} = \overline{\Delta P}_p$, $\mathsf{z} = \overline{\Delta q}$ (left), $\mathsf{z} = \bar{P}_p = (\bar{P}_{p1} + \bar{P}_{p2})/2$ (right)

(2.23), (2.24)) holds, under the condition that the difference of the pressures $P_{p1} - P_{p2}$ equals the load pressure ΔP_p. The latter results from equilibrium of forces for the piston during steady motion. Actually, this is just what is visualized in Fig. 2.13; the steady state velocity depends non-linearly on spool position and load pressure.

However, when leakage is present, the same spool position and load pressure will lead to a different steady state velocity; it now equals the net flow $\Phi_{p1} - \Phi_{l1} = \Phi_{p2} + \Phi_{l2}$ divided by A_p, with similar conditions for the cylinder pressures P_{p1} and P_{p2}. In other words, the effect of leakage can be represented by a deviation of the steady state velocity, $\Delta\dot{q}$, which depends on the valve spool position x_m and the load pressure ΔP_p.

For the actuator modelling example of Subsection 2.3.4, with parameters given in Table F.4, the steady state velocity deviation due to the leakage is given in the left plot of Fig. 2.24. Thereby, the velocity deviation has been normalized with respect to the maximum actuator velocity $\dot{q}_{max} = \Phi_{p,nom}/A_p$. The right plot of the same Figure shows the steady state pressure level in the actuator chambers, represented by the mean pressure P_p, corresponding to the considered leakage configuration.

Because the spool geometry is symmetric in the simulation, the steady state pressure level would equal 0.5, if no leakage was present. The right plot of Fig. 2.24 shows, that the leakage causes a deviation of this value of about 4 %. This illustrates, that the leakage flows do affect the mass balances of the actuator chambers in a non-linear way. Actually, this is the reason why the velocity deviation is rather non-linear for small spool displacements, as shown by the left plot of Fig. 2.24.

More specifically, the following conclusions can be drawn concerning the effect of leakage of hydrostatic bearings:

- The order of magnitude of velocity deviations due to leakage is 1 % of full scale, which is relatively large for low-velocity motions.
- Due to the configuration of the bearings, see Fig. 2.23, the velocity deviation due to leakage is negative in the normal area of operation (spool displacement and load pressure).
- The main contribution of leakage is a velocity deviation, which is linearly dependent on the load pressure ΔP_p; the gain $\frac{\partial \Delta\dot{q}}{\partial \Delta P_p}$ varies with spool position, thereby depending on the spool port configuration.

- The linear contribution of the spool position to the velocity deviation due to leakage is relatively small; this contribution is constituted by the velocity dependence of the leakage flows in (2.36), where the virtual piston areas $A_{p,bi}$, $i = 1, 2, 3, 4$ of the respective bearings are in the order of magnitude of only .2 % of the piston area A_p (see Table F.4).
- Given the combination of spool port configurations and bearing leakages, the non-linear effect of the leakage flows appears to be most severe for small spool displacements (low velocities). This holds with respect to the dependence on the spool position as well as the load pressure.

In short, the leakages of the hydrostatic bearings have similar effects as spool port underlaps: they change the velocity characteristic of the valve-actuator combination with serious non-linearity at small spool displacements, i.e. at low velocities. Moreover, they cause the actuator flow (velocity) to be dependent on load pressure for zero and small spool displacements. The consequence of these effects on the dynamic actuator behaviour is discussed later on.

Axial (friction) forces of hydrostatic bearing

In the equation of motion for the piston (2.38), the viscous damping term is constituted by the axial bearing forces according to (2.39) and (2.40). Without using simulation results, the effect of these forces is easily analyzed by looking at the numerical values of the different coefficients, as the equations are linear.

In fact, there are two contributions to the axial bearing forces:

1. *Pressure forces.*
   These forces are related to the static supply pressure P_s and return pressure P_t at the one hand, and the cylinder pressures P_{p1} and P_{p2} at the other hand. Due to symmetry, the effect of the supply pressure is eliminated. The return pressure is small (assumed to be zero), so that only the cylinder pressures contribute to the axial bearing force.
   With the virtual piston areas $A_{p,bi}$, $i = 1, 2, 3, 4$ given in Table F.4, a mean cylinder pressure $\bar{P}_p = \frac{1}{2}$ results in a static axial bearing force of .16 % of the maximum actuator force $F_{p,max} = P_s A_p$, which is relatively small. The additional bearing force due to a load pressure $\overline{\Delta P}_p = \pm 1$ is $\pm$ .33 % of the maximum actuator force, and also very small in relation to the force generated by the piston area times the pressure difference.
   Although these forces may not be neglegible in the sense of equilibrium of forces for free moving pistons, they are generally negligible in situations of (dynamically) loaded actuators.
2. *Viscous friction force.*
   This force is linearly related to the actuator velocity $\dot{q}$; the effective viscous friction coefficient equals the sum of the friction coefficients $w_{p,bi}$, $i = 1, 2, 3, 4$. With the numerical values of Table F.4, this means for the modelling example, that the viscous friction force at maximum actuator velocity $\dot{q}_{max}$ is about .15 % of the maximum actuator force $F_{p,max}$. So, theoretically the viscous friction of the hydrostatic bearings has minor effect on the force balance.

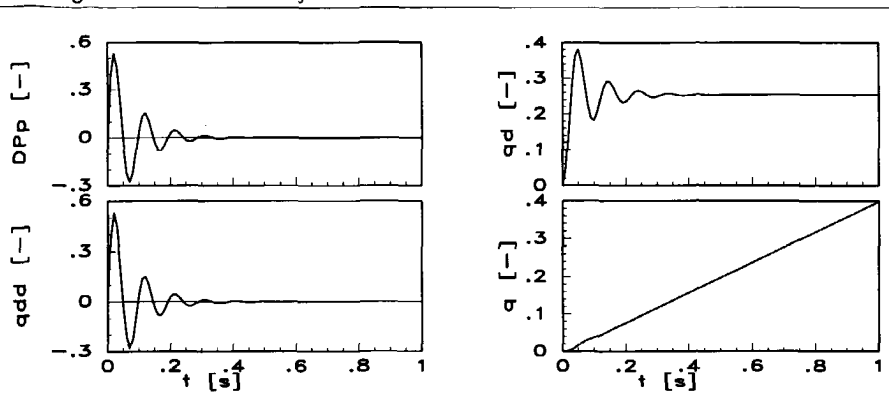


Fig. 2.25: Simulated open loop step response of non-linear dynamic actuator model; step size 25 % of full scale. Actuator pressure difference $\overline{\Delta P}_p$ (upper left); acceleration $\bar{\ddot{q}}$ (lower left); velocity $\bar{\dot{q}}$ (upper right) and position $\bar{q}$ (lower right)

The given numerical analysis of the theoretical model of the axial bearing forces leads to the intermediate conclusion, that these forces are so small, that they may well be neglected. This conclusion is supported by simulations of the complete dynamic actuator model.

Step responses of the actuator model

To investigate the different dynamic and non-linear phenomena of the hydraulic actuator, some open loop step responses of the complete actuator model of Subsection 2.3.4 have been simulated. The first simulation result, with a step input of 25 % of full scale, is given in Fig. 2.25, and gives some insight in the physics of the model.

The upper left plot shows the actuator pressure difference, responding on the step wise valve spool displacement. Due to the compressibility of oil, the initial flow through the valve spool is integrated to some pressure difference (2.34). Because the external force F_{ext} has been kept to zero, and the friction forces are small, the pressure difference is closely related to the acceleration $\ddot{q}$ of the load (2.38). This acceleration is given in the lower left plot, where it has been normalized with respect to its maximum, which is $\ddot{q}_{max} = P_s A_p / M_p$. The reasonably damped oscillatory transient is the result of the coupling of the inertial load dynamics (2.38) and the pressure dynamics (2.34) via the actuator velocity $\dot{q}$.

This velocity is shown in the upper right plot of Fig. 2.25. After the transient, the actuator reaches a steady state velocity, which corresponds to the steady state valve flow related to the open loop input value. The actuator velocity is integrated to the actuator position q, which is shown in the lower right plot. This position is scaled with the maximum actuator excursion q_{max}, which equals half the actuator stroke.

For the given actuator configuration, according to the parameterset of Table F.4, the 25 % input excites the actuator dynamics such, that the actuator pressure difference (and therewith the acceleration) reaches half the maximum pressure difference P_s during the transient. For the valve spool flow, this means that the load pressure becomes 0.5 during the transient, so that considerable non-linearity may be expected from Fig. 2.13.

The non-linearity of the open-loop actuator model, depending on the modelled phenomena, is further investigated by comparing the normalized responses on different step sizes, while including different phenomena. The results are presented in Fig. 2.26.

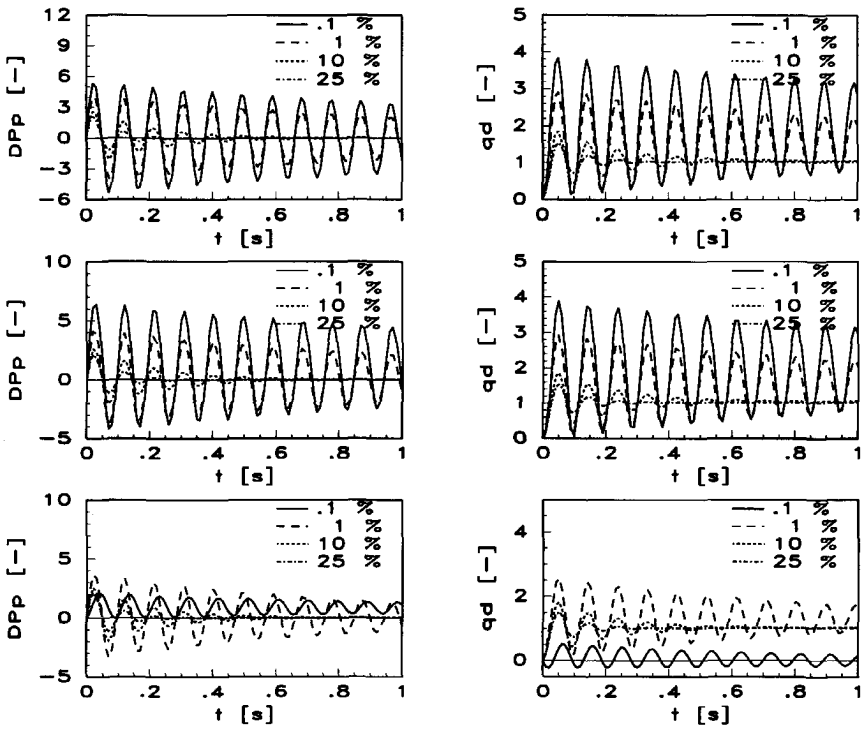


Fig. 2.26: Normalized step responses of actuator pressure difference $\overline{\Delta P}_p$ (left) and actuator velocity $\bar{\dot{q}}$ (right) for varying step amplitudes of $\bar{x}_m$; zero external force F_{ext}. Only NL valve spool flow (upper); NL valve spool flow plus axial bearing forces (middle); idem plus leakage flows bearings (lower)

The most striking fact in this Figure is the amplitude dependent damping of the transient response: the larger the input amplitude, the larger the damping. As explained by Viersma [139], this can be ascribed to the opening of the servo-valve ports, which makes the servo-valve flow dependent on the load pressure (see Fig. 2.13). This can be interpreted as 'leakage' which provides damping of the oscillation. Besides the damping, the steady state velocity gain varies with input amplitude, which is caused by the non-linear spool flow characteristic due to the port geometry (underlaps and clearance).

Comparing the middle plots of Fig. 2.26 to the upper plots, it is clear that the axial bearing forces hardly influence the dynamic response of the actuator model. Only for the very small input amplitude of .1 %, there is a small offset in the pressure difference, which can be ascribed to the pressure forces. However, the actuator motion is not affected by these forces, so that the axial bearing forces may well be neglected.

The effect of the leakage flows is clearly visualized in the lower plots of Fig. 2.26. Besides a considerable increase of the amount of damping for small input amplitudes, the leakage flows cause a deviation in the steady state velocity, which is relatively large for small input amplitudes. So leakage flows play an important role in the non-linearity of the open loop dynamics of the hydraulic actuator.

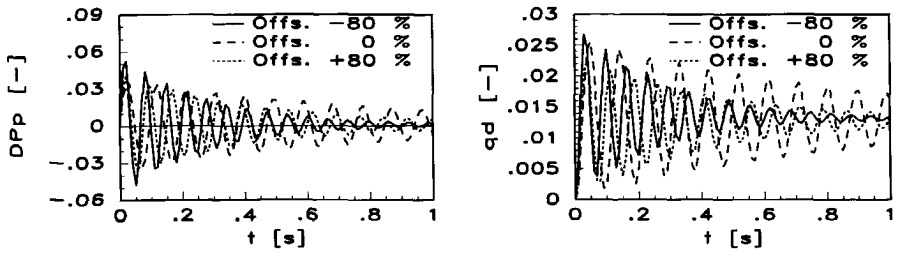


Fig. 2.27: Effect of actuator position on open loop response of dynamic actuator model on 1 % step input. Actuator pressure difference $\overline{\Delta P_p}$ (left) and velocity $\bar{q}$ (right)

Position dependence

So far, the analysis of the actuator model has taken place with the piston in the middle position, so for $q = 0$. This is of importance for the pressure dynamics described by (2.34). In fact, these pressure dynamics are position dependent, because the 'stiffness of the oil column' varies with actuator position q, according to (2.34). The result is, that the open loop dynamic actuator response depends on the actuator position, as shown in Fig. 2.27.

Clearly, the effect of the position dependent 'actuator stiffness' is, that the natural frequency and therewith the damping coefficient of the transient dynamics varies with actuator position. Note that the middle position (lowest stiffness) results in the smallest natural frequency and damping. Actually, this phenomenon constitutes a substantial non-linearity of the hydraulic actuator dynamics.

Coulomb friction in the actuator

It was mentioned earlier, that friction due to hydrostatic bearings is negligible. However, this does not mean, that viscous friction is entirely negligible; for instance, an actuator with hydrostatic bearings will also have sealings to prevent external leakage. This sealing often gives a considerable amount of friction, which is difficult to quantify theoretically, and often is a combination of viscous friction and Coulomb friction. For this reason, it can be stated that, to some extent, every hydraulic actuator has Coulomb friction.

Generally, the amount of friction is expressed in relation to the maximum actuator force $F_{p,max}$. For hydraulic actuators without hydrostatic bearings, the Coulomb friction may be as large as 5 % of $F_{p,max}$, whereas the hydrostatic bearing technique may reduce this to less than .5 %.

In order to give an impression of the effect of Coulomb friction, the open loop responses on a 0.5 [Hz] sine-wave with 10 % input amplitude have been simulated with the dynamic actuator model, without and with Coulomb friction included in the model. The results are shown in Fig. 2.28. The left plot shows the resulting actuator pressure difference, and the right plot the actuator velocity.

Note, that the amount of friction in the simulation was chosen relatively large, in order to emphasize its effect, namely 5 % of the maximum actuator force. It is clear from the plots of Fig. 2.28, that the pressure difference has to counteract the Coulomb friction force; the change of moving direction causes a large jump in the pressure difference. Actually, for this low-frequency motion the pressure difference is dominated by the Coulomb friction, and not by the acceleration forces as in the case without Coulomb friction.

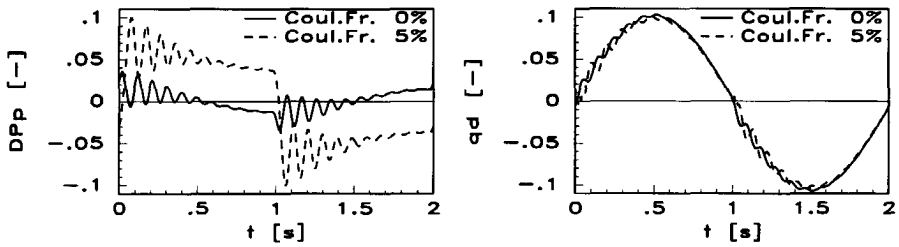


Fig. 2.28: Effect of 5 % Coulomb friction on open loop actuator response on 10 % 0.5 [Hz] sine-wave input. Actuator pressure difference $\overline{\Delta P}_p$ (left) and actuator velocity $\bar{\dot{q}}$ (right)

In the case that no Coulomb friction is present, the change of moving direction excites the actuator dynamics; a lightly damped oscillation occurs. This is caused by the non-linearity of the spool flow: during the transition from positive to negative spool displacement and vice versa, there is locally an increased velocity gain due to the underlaps. This can be interpreted as a small acceleration peak during the transition, which excites the actuator dynamics.

The same kind of effect is seen, in the case that Coulomb friction is present. The situation is slightly different, because the Coulomb friction with the modelled stiction force tries to keep the actuator at zero velocity during the change of moving direction. This can be seen in the plot of the actuator velocity in Fig. 2.28: there is a small delay between reaching zero velocity and the start of motion. The irregularity in the acceleration due to this effect makes, that the actuator dynamics is now even more excited than without Coulomb friction.

The given result shows, that Coulomb friction can be a severe non-linearity for a hydraulic actuator. It results in excitation of the actuator dynamics during change of moving direction, and it strongly affects the pressure difference, which can be serious for feedback control.

Conclusion

For the hydraulic actuator model, it is reasonably easy to find a set of realistic parameters in order to investigate the dominant dynamics and non-linearities of the actuator. The dominant dynamics are constituted by an integrator, integrating the steady state valve flow to an actuator position, and by the second order behaviour due to the coupling of the pressure dynamics to the motion dynamics of the inertial load on the piston. The most important non-linearity affecting these dynamics is the non-linear steady state velocity characteristic (as function of spool position and load pressure), which depends on the spool port configuration and on the leakage due to the bearing configuration. Other important non-linearities, which are generally not negligible, are the position dependence of the actuator dynamics due to varying actuator stiffness as a result of varying actuator chamber volumes, and Coulomb friction due to sealings or due to the absence of hydrostatic bearings.

In fact, this conclusion summarizes the basic dynamic and non-linear behaviour of the hydraulic actuator. It might be noted here, that the servo-valve model of the previous Section is easily coupled to the actuator model, since the valve spool position x_m, which

is the output of the dynamic servo-valve model, is just the input of the actuator model. Thus, the model of the hydraulic servo-system is easily obtained as a series connection of the servo-valve model of Section 2.2 and the actuator model of this Section.

However, as already mentioned in Section 2.1, the situation may be more complicated, because transmission line effects may have to be taken into account. In that case, which most frequently occurs with long-stroke actuators, the actuator model of this Section is only part of an interconnection of subsystem models, as shown in Fig. 2.2 on page 22. The extension of the model of the hydraulic servo-system with subsystem models for the transmission lines is the subject of the next Section.

2.4 Modelling and analysis of transmission line effects

2.4.1 Introduction

As already indicated in Chapter 1, relatively long transmission lines may introduce high-frequency dynamics, which should be taken into account in the modelling of and control design for hydraulic servo-systems. In general, this situation applies for long-stroke hydraulic servo-systems, for which relatively long transmission lines between the valve and the actuator compartments are required. For instance, taking the standard actuator configuration of Fig. 2.21, minimum length of the (longest) transmission line is obtained by placing the servo-valve half-way the actuator. This means, that the minimum line length is at least half the actuator stroke.

In the case of the double-concentric configuration of Fig. 2.23, which is considered in this work, the situation is even worse. Because of the construction, a transmission line inside the actuator is required, which is at least as long as the complete stroke of the actuator. In order to minimize the length of the transmission line for this inside actuator chamber, the servo-valve should be placed at the bottom of the actuator. This means, that the length of the transmission line for the other actuator chamber will also be approximately equal to the stroke of the actuator.

Because severe implications for the control of this type of long-stroke actuators are encountered, as described in [119] and later in Section 4.4, transmission line dynamics in hydraulic servo-systems are considered in this Section in more detail. Before giving the subdivision of this Section at the end of this Subsection, the character of transmission line dynamics in hydraulic control systems will be briefly discussed next, as well as the system configuration and the modelling approach.

Transmission line effects in hydraulic control systems

In literature, dynamic effects such as oscillations, related to relatively long lines in hydraulic systems, are often referred to as 'water-hammer' [12]. Basically, these effects are caused by a combination of compressibility and inertia of the fluid in a transmission line: a sudden change in pressure or flow at one end of the line travels with a finite velocity (the sound velocity of the fluid) along the line, and is reflected (partially) at the other end of the line. Thus, related to the time domain behaviour of the transmission line, these effects can be interpreted as the presence of time delays between cause and effect. Related to the frequency domain behaviour, transmission line effects can be interpreted as the occurrence

of standing wave forms along the line for certain (resonance) frequencies, related to the geometry of the pipeline.

The analysis of transient effects in fluid lines stems already from the end of the 19th century. Since then, numerous researchers have contributed to the insight in these effects with theoretical and experimental results. A good overview of these results, reported in literature, is given by Goodson and Leonard [42]. In a more recent publication, Yang and Tobler [160] also summarize some important results in the analysis of transmission line dynamics.

As far as hydraulic control systems are concerned, there are mainly two ways in which transmission line effects may play an important role in the system behaviour.

First, there are many applications, in which the oil supply unit is separated from the hydraulic servo-system, often requiring long supply lines. The dynamics due to these long lines may in practice lead to undesired oscillations, possibly excited by the pump-flow-pulsations. Research performed by Ham [47] and Viersma [139] has provided a lot of insight in these dynamics, and has also led to practical means to suppress ripples in the supply pressure due to these dynamics.

Second, in some applications transmission line dynamics are important because it is not possible to place the servo-valve directly on the actuator chambers, so that relatively long transmission lines between the valve and the actuator chambers are required. As explained before, this typically holds for long-stroke linear actuators, but there are also some (heavy duty) rotary drive applications, where it is practically impossible to place the servo-valve on the actuator. Relevant work on the modelling of this kind of systems has been performed by Watton et. al., where they consider the behaviour of transmission lines coupled to underlapped servo-valves [150, 151]. Watton also includes the behaviour of a hydraulic drive in the analysis in [146].

In fact, this second type of applications involving transmission line dynamics is of interest here, because it relates to the application of the long-stroke double-concentric actuator, considered in this thesis. However, as already explained in the Introduction of this thesis, Chapter 1, Subsection 1.3.2, a satisfactory treatment of the problems involved in transmission line modelling is not found in the references of Watton et. al. [150, 146, 151]. What is actually lacking, is the clear relation between the theoretical modelling and the system theoretic interpretation of the dynamic effects of fluid transmission lines as part of the hydraulic servo-system. Therefore, an analysis of transmission line effects in hydraulic servo-systems is given in this Section, where the system configuration to be considered is given next.

System configuration

When considering the effect of transmission lines between valve and actuator, the system configuration can be schematically depicted as in Fig. 2.29. Note, that a clear distinction is made between the states (pressures P and flows Φ) at the inlet side and at the oulet side of the transmission lines, like earlier indicated in Fig. 2.2 on page 22. Note further from Fig. 2.29, that the sign definitions of the flows of the two transmission lines are different; this choice is made for reasons of consistency with the model equations for the servo-valve flow (2.23) and the actuator mass balances (2.34).

Although in the configuration of Fig. 2.29 the effect of finite wave propagation velocity is considered for the relatively long transmission lines, the actuator chambers are still

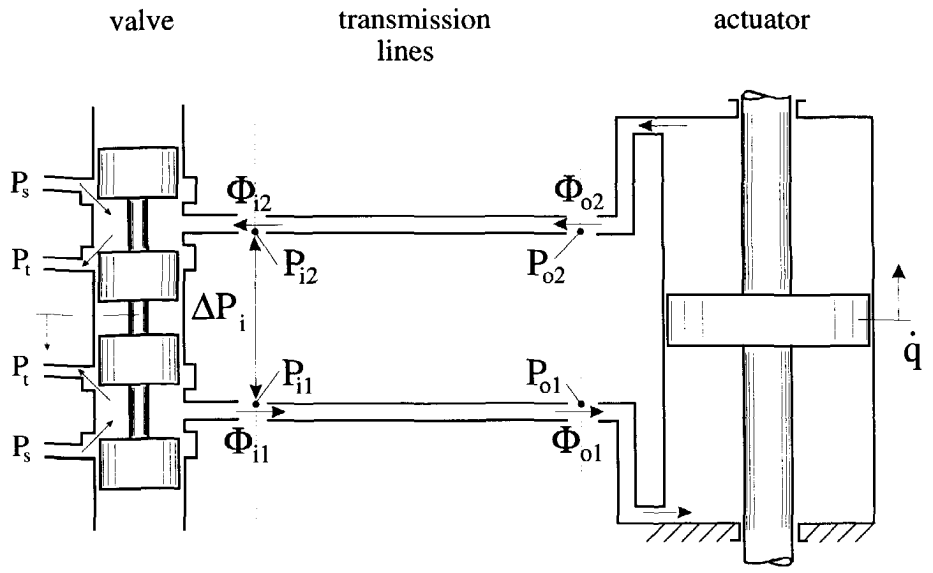


Fig. 2.29: Setup with long transmission lines between valve and actuator, assuming uniform pressure distribution in actuator chambers

considered as compartments with a certain capacity, with a uniform pressure distribution, simply described by mass balances. However, for long-stroke actuators, the finite wave propagation time in the (relatively long) actuator chambers may also be of importance. To investigate this effect, the configuration of Fig. 2.30 is to be considered, where a distinction is made between the states at the inlet sides of the actuator chambers P_{o1}, P_{o2}, Φ_{o1} and Φ_{o2}, and those at the piston sides P_{p1}, P_{p2}, Φ_{p1} and Φ_{p2}.

As indicated in Fig. 2.30, it is thereby considered that the lengths of the transmission lines, L_{tl1} and L_{tl2} respectively, are not necessarily equal. The lines may also have a different radius, r_{tl1} and r_{tl2} respectively. Note furthermore from Fig. 2.30, that the lengths of the actuator chambers, L_{ac1} and L_{ac2} respectively, are unequal and even not constant, but a function of the actuator position. A final remark on the configuration of Fig. 2.30 concerns the radius of the actuator chambers. Because the actuator chamber is generally not circular, but a hollow cylinder, the so-called hydraulic radius should be used in the transmission line models. This hydraulic radius is defined as $r_h = 2\frac{A}{O}$, with A the surface and O the circumference of the cross-section of the actuator chamber. Again, the hydraulic radius may be different for the two actuator chambers, namely $r_{h,ac1}$ and $r_{h,ac2}$ respectively.

In fact, the configuration of Fig. 2.30 is taken as a starting point for the modelling of transmission line effects in the hydraulic servo-system. Thereby, the following modelling approach is chosen.

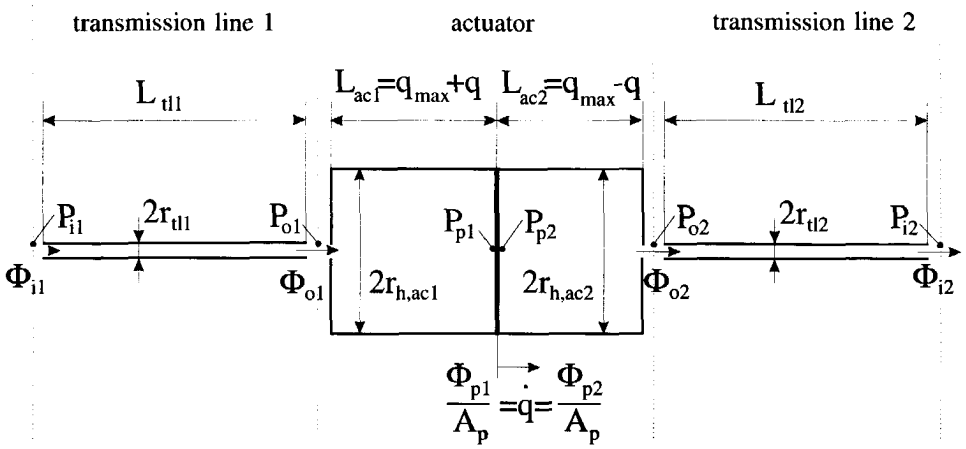


Fig. 2.30: Configuration for modelling of transmission line effects, both in transmission lines and actuator chambers

Modelling approach

The approach to the modelling of transmission line effects is already outlined in a rather general setting in Subsection 2.1.2. It is briefly recapitulated and reformulated here for the system configuration of Fig. 2.30.

Basically, the modelling approach comprises the extension and modification of the basic actuator model, as presented in Section 2.3, to include transmission line effects. Thereby, for reasons of physical insight in the model, it is required that the resulting model is modular, so that transmission line effects are easily included or omitted, be it for the lines between valve and actuator, or for the actuator chambers. In fact, this requirement has already been formulated in the Introduction, Subsection 1.3.2.

The basis for the modular inclusion of transmission line effects lies in the theoretical modelling of a single transmission line; via proper bilateral coupling, the transmission line models for the different parts of the configuration of Fig. 2.30 can be joined together, to constitute a complete dynamic model of the hydraulic actuator. However, using theoretical transmission line models as modules of the complete model, infinite order models result, which do not allow proper analysis in both time domain and frequency domain. Moreover, they are not suitable for experimental identification and validation. Therefore, the transmission line models are to be approximated by low-order models.

As motivated and explained on page 25 in Subsection 2.1.2, an open loop approximation technique, which preserves the physical interpretation of the model parameters is most suited here, and will be applied. Because the physical structure of the model is preserved, it is easy to analyze the effect of including transmission line models, be it for the lines between valve and actuator, or for the actuator chambers. Thus, the relevance of the effects of a finite wave propagation velocity in hydraulic servo-systems can be evaluated. Based on this evaluation, it may be decided whether these effects have to be taken into account, and if so, whether both transmission lines and actuator chambers should be modelled this way, as in Fig. 2.30, or only the transmission lines, according to Fig. 2.29.

Besides that this approach provides insight in the relevance of transmission line effects

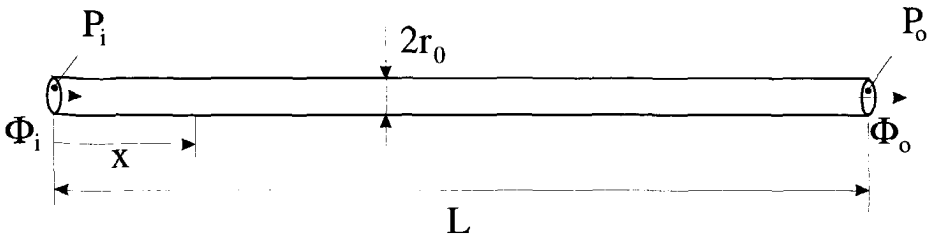


Fig. 2.31: Flow through a single transmission line

in hydraulic servo-systems, it also results in a physically structured model of this type of systems, which forms a basis for a model that is suitable for experimental identification and validation. This model will be presented in a later Section, in Subsection 2.6.3.

Subdivision of the Section

Given the approach to transmission line modelling, sketched previously, the Section is subdivided as follows. First, the theoretical modelling of a single fluid transmission line, as it is found in literature, is discussed in Subsection 2.4.2. Thereby, different model representations are investigated, while some attention is given to the interpretation of the results, in order to provide some insight in the special character of the transmission line dynamics. To some extent, this insight can be used in the treatment of approximation techniques for transmission line models; this treatment is given in Subsection 2.4.3, including the discussion of a modal approximation technique, which is to be applied here. Using the modal approximations of the transmission line elements as subsystem models, a complete model of the hydraulic servo-system, including transmission line effects, is obtained by proper integration of the subsystem models, as explained in Subsection 2.4.4. With the use of this model, an analysis of the transmission line effects in the hydraulic servo-system is performed, of which the results are discussed in Subsection 2.4.5.

2.4.2 Theoretical modelling of a single transmission line

In the theoretical modelling, a single transmission line with length L and radius r_0, as depicted in Fig. 2.31, is considered. Under a number of assumptions, relatively simple forms of the partial differential equations (PDE's), the basic equations describing the distributed parameter behaviour of the transmission line, can be obtained. These PDE's have analytical solutions in the frequency domain, where the boundary conditions determine the form of the solution; the causality issue is involved here, and will be adressed. Finally, given the purpose of the transmission model, certain representations of the model are most suitable; they are given at the end of this Subsection.

Modelling assumptions and basic equations

For the modelling of the dynamics of the transmission line shown in Fig. 2.31, a number of assumptions are made, similar to the work of Yang and Tobler [160].

Assumption 2.4.1 *For transmission line modelling, it is assumed that:*

- *The wall of the transmission line is rigid. Finite wall stiffness can be taken into account by a correction of the oil bulk modulus [42, 47].*
- *The flow through the line is laminar (Re < 2000); transmission lines are generally designed such, that this assumption holds under normal operating conditions.*
- *The temperature is constant, and therewith the fluid properties; most hydraulic servo-systems operate with temperature controlled oil supply systems, justifying this assumption. Moreover, for liquid fluids, heat transfer effects in the transmission line can be neglected [42].*
- *The flow is one-dimensional. This means that radial and rotational flows in the transmission line are neglected. This assumption is justified by the work of D'Souza and Oldenburger [33].*

With this Assumption, damping effects due to the viscosity of the fluid are not neglected in the modelling, but it is not yet specified how these viscosity effects are to be included. As described by Goodson and Leonard [42], the developments of transmission line modelling in this century initially started with lossless models, in which viscosity effects were neglected, and evolved to the derivation of accurate models, including dissipative effects due to the viscosity of the fluid. Basically, all these models are constituted by a set of two PDE's, which describe the state (pressure and velocity) of the fluid as a function of both the time t and the place x in Fig. 2.31. Thus, the work on transmission line modelling up to the year 1962 can be summarized by three basic models, as follows [42]:

- `Model A`: The Lossless Fluid Line model.

  This model describes the basic behaviour of transmission line dynamics, but no viscosity effects are included. The PDE's constituting this model are obtained by writing down the mass balance and the momentum balance respectively, for an element of the line at the location x, with length Δx, $\Delta x \to 0$, and can be written as follows:

$$\frac{\partial P(x,t)}{\partial t} + \frac{c_0^2 \rho}{\pi r_0^2} \frac{\partial \Phi(x,t)}{\partial x} = 0 \tag{2.42}$$

$$\frac{\partial \Phi(x,t)}{\partial t} + \frac{\pi r_0^2}{\rho} \frac{\partial P(x,t)}{\partial x} = 0 \tag{2.43}$$

  Hereby, use is made of the relation between local variations in the density ρ and the pressure P; this relation is constituted by the sound velocity c_0 in the fluid, which is defined by:

$$c_0^2 = \frac{E}{\rho} \Leftrightarrow c_0 = \sqrt{\frac{E}{\rho}} \tag{2.44}$$

  It might be noted here, that the mass balance (2.42) and the momentum balance (2.43) are easily combined to the following second order partial differential equation of the hyperbolic type, which is well-known as the wave equation:

$$\frac{\partial^2 P(x,t)}{\partial t^2} = c_0^2 \frac{\partial^2 P(x,t)}{\partial x^2} \tag{2.45}$$

  This means, that the Lossless Fluid Line model can be interpreted as the model that describes the undamped oscillations (standing wave forms), that may occur in

the line due to the combination of the elastic and inertial properties of the fluid, characterized by the wave propagation velocity c_0.

- `Model B`: The Linear Friction Model.

  In this model, viscous friction is included by adding a linear friction term to the momentum balance, using the kinematic viscosity constant μ of the fluid, resulting in the following set of PDE's:

$$\frac{\partial P(x,t)}{\partial t} + \frac{c_0^2 \rho}{\pi r_0^2} \frac{\partial \Phi(x,t)}{\partial x} = 0 \tag{2.46}$$

$$\frac{\partial \Phi(x,t)}{\partial t} + \frac{8\mu}{r_0^2} \Phi(x,t) + \frac{\pi r_0^2}{\rho} \frac{\partial P(x,t)}{\partial x} = 0 \tag{2.47}$$

  In this model, the pressure losses are linear to the mean velocity in the line, and the shape of the velocity profile over a cross-section of the line is not considered. This type of flow is often referred to as the Hagen-Poiseuille flow through a circular line.

- `Model C`: The Dissipative Model.

  The Dissipative Model is the most accurate model, and may even include heat transfer effects. However, with Assumption 2.4.1, heat transfer effects can be neglected, so that only a dissipative friction model is included here. This model takes into account that the velocity profile over a cross-section of the line changes with time t and place x. This means, that the radial fluid velocity v is taken into account, and that both the radial fluid velocity v and the axial fluid velocity u are expressed as functions of the time t, the place x and the radial coordinate r, so $u = u(x,r,t)$ and $v = v(x,r,t)$. Herewith, the PDE's corresponding to the mass balance and the momentum balance respectively, become:

$$\frac{\partial P(x,t)}{\partial t} + c_0^2 \rho \left[\frac{\partial u(x,r,t)}{\partial x} + \frac{\partial v(x,r,t)}{\partial r} + \frac{v(x,r,t)}{r} \right] = 0 \tag{2.48}$$

$$\frac{\partial u(x,r,t)}{\partial t} + \frac{1}{\rho} \frac{\partial P(x,r,t)}{\partial x} = \mu \left[\frac{\partial^2 u(x,r,t)}{\partial r^2} + \frac{1}{r} \frac{\partial u(x,r,t)}{\partial r} \right] \tag{2.49}$$

  For comparison with the other sets of PDE's, note that the flow $\Phi(x,t)$ may be seen as the integral of the velocity profile over the whole cross-section, i.e. (using the mean velocity $\bar{u}(x,t)$):

$$\Phi(x,t) = \pi r_0^2 \, \bar{u}(x,t) = \int_0^{r_0} u(x,r,t) \, 2\pi r \, dr$$

Obviously, the basic character of these sets of PDE's is similar for all three models, and so are their solutions. Actually, these solutions can only be formulated analytically in the frequency domain, and can be found by applying the Laplace transform to the PDE's. To illustrate the basic ideas behind this method, it will be worked out for the second model, `Model B`. This case is easily simplified to that of `Model A`, and has strong analogy with that of `Model C`, but the elaboration of the solution for the latter case is much more involved.

Frequency domain solutions and causality issues

Important work on the development of analytic solutions in the frequency domain for the PDE's of the transmission line model has been performed in the fifties and sixties, by Iberall [61] and Nichols [106]. Goodson and Leonard [42] give a good overview of this and other work in the field, and discuss different forms of the available solutions in the frequency domain. Obviously, the choice of representation depends on the purpose of the model. Especially for simulation purposes, a primary requirement on the model representation is causality.

Although in many publications causality or physical realizability is mentioned [34, 42, 92, 128, 160], a clear discussion of the causality issue is mostly lacking. In some cases, non-causal representations (of the so-called matrix form [42]) are even given [69, 139, 151], be it for purposes of mathematical analysis rather than for simulation purposes. So, what is desirable in fact, is some more insight in the causality issue of the representations of the frequency domain solution of the transmission line model. For this reason, the derivation of the frequency domain solution for `Model B` is discussed here in more detail, and an interpretation of the results is given.

Starting with the two PDE's of `Model B`, (2.46) and (2.47), and writing them in vector form, gives:

$$\frac{\partial}{\partial t}\begin{bmatrix} P(x,t) \\ \Phi(x,t) \end{bmatrix} + \begin{bmatrix} 0 & \frac{c_0^2\rho}{\pi r_0^2} \\ \frac{\pi r_0^2}{\rho} & 0 \end{bmatrix} \frac{\partial}{\partial x}\begin{bmatrix} P(x,t) \\ \Phi(x,t) \end{bmatrix} + \begin{bmatrix} 0 & 0 \\ 0 & \frac{8\mu}{r_0^2} \end{bmatrix} \begin{bmatrix} P(x,t) \\ \Phi(x,t) \end{bmatrix} = 0 \qquad (2.50)$$

In order to obtain a set of ordinary differential equations instead of partial differential equations, the Laplace transform is applied, assuming zero initial conditions:

$$s\begin{bmatrix} P(x,s) \\ \Phi(x,s) \end{bmatrix} + \begin{bmatrix} 0 & \frac{c_0^2\rho}{\pi r_0^2} \\ \frac{\pi r_0^2}{\rho} & 0 \end{bmatrix} \frac{\partial}{\partial x}\begin{bmatrix} P(x,s) \\ \Phi(x,s) \end{bmatrix} + \begin{bmatrix} 0 & 0 \\ 0 & \frac{8\mu}{r_0^2} \end{bmatrix} \begin{bmatrix} P(x,s) \\ \Phi(x,s) \end{bmatrix} = 0 \qquad (2.51)$$

Or, after rearranging and dividing the second row by $\left(1+\frac{8\mu}{sr_0^2}\right)$:

$$s\begin{bmatrix} P(x,s) \\ \Phi(x,s) \end{bmatrix} + \begin{bmatrix} 0 & \frac{c_0^2\rho}{\pi r_0^2} \\ \frac{\pi r_0^2}{\rho\left(1+\frac{8\mu}{sr_0^2}\right)} & 0 \end{bmatrix} \frac{\partial}{\partial x}\begin{bmatrix} P(x,s) \\ \Phi(x,s) \end{bmatrix} = 0 \qquad (2.52)$$

Although this equation may be solved for certain boundary conditions, the solution is not easily interpreted in terms of causality, because of the strong coupling between the pressure P and the flow Φ. Therefore, the vector equation (2.52) is diagonalized by applying a transformation of the variables, as follows. First, the eigenvalues of the matrix

$$\begin{bmatrix} 0 & \frac{c_0^2\rho}{\pi r_0^2} \\ \frac{\pi r_0^2}{\rho\left(1+\frac{8\mu}{sr_0^2}\right)} & 0 \end{bmatrix}$$

are determined from its characteristic polynomial:

$$\lambda^2 - \frac{c_0^2}{\left(1+\frac{8\mu}{sr_0^2}\right)} = 0 \quad \Leftrightarrow \quad \lambda_{1,2} = \pm\frac{c_0}{\sqrt{1+\frac{8\mu}{sr_0^2}}}$$

Corresponding to these eigenvalues, a set of two eigenvectors is easily found as:

$$m_1 = \begin{bmatrix} \frac{c_0\rho}{\pi r_0^2}\sqrt{1+\frac{8\mu}{sr_0^2}} \\ 1 \end{bmatrix}, \quad m_2 = \begin{bmatrix} -\frac{c_0\rho}{\pi r_0^2}\sqrt{1+\frac{8\mu}{sr_0^2}} \\ 1 \end{bmatrix}$$

The transformation of the variables, that diagonalizes the vector equation (2.52) is then given, using the matrix $[m_1\ m_2]^{-1}$, as:

$$\begin{bmatrix} z_1(x,s) \\ z_2(x,s) \end{bmatrix} = \begin{bmatrix} \frac{\pi r_0^2}{2\rho c_0\sqrt{1+\frac{8\mu}{sr_0^2}}} & \frac{1}{2} \\ -\frac{\pi r_0^2}{2\rho c_0\sqrt{1+\frac{8\mu}{sr_0^2}}} & \frac{1}{2} \end{bmatrix} \begin{bmatrix} P(x,s) \\ \Phi(x,s) \end{bmatrix} \tag{2.53}$$

while the corresponding inverse transformation reads:

$$\begin{bmatrix} P(x,s) \\ \Phi(x,s) \end{bmatrix} = \begin{bmatrix} \frac{c_0\rho}{\pi r_0^2}\sqrt{1+\frac{8\mu}{sr_0^2}} & -\frac{c_0\rho}{\pi r_0^2}\sqrt{1+\frac{8\mu}{sr_0^2}} \\ 1 & 1 \end{bmatrix} \begin{bmatrix} z_1(x,s) \\ z_2(x,s) \end{bmatrix} \tag{2.54}$$

With the transformation of variables (2.53), the set of PDE's (2.52) becomes:

$$s\begin{bmatrix} z_1(x,s) \\ z_2(x,s) \end{bmatrix} + \begin{bmatrix} \frac{c_0}{\sqrt{1+\frac{8\mu}{sr_0^2}}} & 0 \\ 0 & -\frac{c_0}{\sqrt{1+\frac{8\mu}{sr_0^2}}} \end{bmatrix} \frac{\partial}{\partial x}\begin{bmatrix} z_1(x,s) \\ z_2(x,s) \end{bmatrix} = 0 \tag{2.55}$$

Supposing now, that the solution at $x = 0$ can be given as boundary condition for this equation, the solution at $x = L$ can be obtained by analytically integrating the equation (2.55) with respect to x. The result is:

$$\begin{bmatrix} z_1(L,s) \\ z_2(L,s) \end{bmatrix} = \begin{bmatrix} e^{-\frac{sL}{c_0}\sqrt{1+\frac{8\mu}{sr_0^2}}} & 0 \\ 0 & e^{\frac{sL}{c_0}\sqrt{1+\frac{8\mu}{sr_0^2}}} \end{bmatrix} \begin{bmatrix} z_1(0,s) \\ z_2(0,s) \end{bmatrix} \tag{2.56}$$

Obviously, with the chosen boundary conditions, the solution is non-causal; the second transfer function in (2.56) has the character of an inverse time delay. Apparently, it is not possible to choose the boundary conditions for both z_1 and z_2 at $x = 0$; the boundary condition for z_2 should be chosen at $x = L$, in order to reverse the non-causal relationship into a causal one. Thus, defining the well-known propagation operator $\Gamma(s)$, which represents the travelling time of a pressure wave along the line, for the case of `Model B` as [42]:

$$\Gamma(s) = \frac{Ls}{c_0}\sqrt{1+\frac{8\mu}{r_0^2 s}} \tag{2.57}$$

the solution (2.56) reads in causal form (a slightly more detailed discussion of the causality of this form follows later):

$$\begin{bmatrix} z_1(L,s) \\ z_2(0,s) \end{bmatrix} = \begin{bmatrix} e^{-\Gamma(s)} & 0 \\ 0 & e^{-\Gamma(s)} \end{bmatrix} \begin{bmatrix} z_1(0,s) \\ z_2(L,s) \end{bmatrix} \tag{2.58}$$

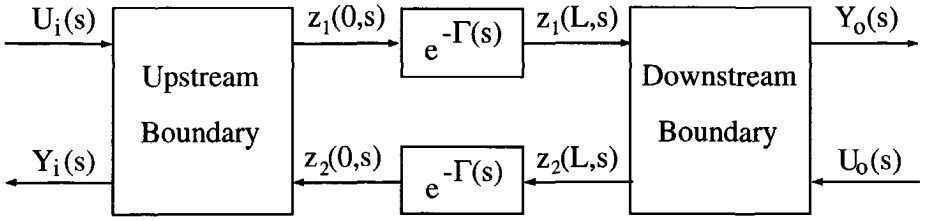


Fig. 2.32: Physically realizable form of transmission line model

So, as this form of the solution makes clear, the transmission line dynamics are constituted by a combination of propagation effects, one in forward direction and one in backward direction. The implication of this character of the dynamics is, that it is principally required to choose one boundary condition at the upstream line end, $z_1(0,s)$, and one at the downstream line end, $z_2(L,s)$, as depicted in Fig. 2.32. This means, with the (inverse) transformations given by (2.53) and (2.54), that in terms of the physical variables P and Φ, one of them can be chosen as input variable U_i at the upstream end, so P_i *or* Φ_i, and one of them can be chosen as input variable U_o at the downstream end, so P_o *or* Φ_o. Obviously, the remaining variables are the outputs Y_i and Y_o at the upstream line end and the downstream line end, respectively.

In other words, there are four possible sets of boundary conditions, corresponding to four input-output configurations, that lead to a causal transmission line model (see also Ezekiel and Paynter [34], Goodson and Leonard [42] and Sidell and Wormley [128]). These input-output configurations are given in Table 2.1. Note from this Table, that all configurations are constituted by a bilateral coupling, at both line ends, of the transmission line model with its environment. Due to this character of the model, the transmission line model according to Fig. 2.32 is often called a four-port model.

	Config.1	Config.2	Config.3	Config.4
$U_i \rightarrow Y_i$	$\Phi_i(s) \rightarrow P_i(s)$	$\Phi_i(s) \rightarrow P_i(s)$	$P_i(s) \rightarrow \Phi_i(s)$	$P_i(s) \rightarrow \Phi_i(s)$
$U_o \rightarrow Y_o$	$\Phi_o(s) \rightarrow P_o(s)$	$P_o(s) \rightarrow \Phi_o(s)$	$\Phi_o(s) \rightarrow P_o(s)$	$P_o(s) \rightarrow \Phi_o(s)$

Table 2.1: Input-output definitions at upstream boundary ($U_i \rightarrow Y_i$) and at downstream boundary ($U_o \rightarrow Y_o$) for different configurations corresponding to causal forms of transmission line model

Now, defining the well-known characteristic impedance $Z_c(s)$, which represents the relation between pressure and flow at a certain cross-section of the line, for the case of `Model B` as [42]:

$$Z_c(s) = \frac{\rho c_0}{\pi r_0^2}\sqrt{1+\frac{8\mu}{r_0^2 s}} \tag{2.59}$$

the boundary expressions for the four possible input-output configurations of Table 2.1

are obtained by rewriting the (inverse) transformations of the variables, (2.53) and (2.54) respectively, in bilaterally coupled forms:

$$\Phi_i(s) \rightarrow P_i(s) \; : \; \begin{bmatrix} z_1(0,s) \\ P_i(s) \end{bmatrix} = \begin{bmatrix} 1 & -1 \\ Z_c(s) & -2Z_c(s) \end{bmatrix} \begin{bmatrix} \Phi_i(s) \\ z_2(0,s) \end{bmatrix} \tag{2.60}$$

$$P_i(s) \rightarrow \Phi_i(s) \; : \; \begin{bmatrix} z_1(0,s) \\ \Phi_i(s) \end{bmatrix} = \begin{bmatrix} \frac{1}{Z_c(s)} & 1 \\ \frac{1}{Z_c(s)} & 2 \end{bmatrix} \begin{bmatrix} P_i(s) \\ z_2(0,s) \end{bmatrix} \tag{2.61}$$

$$\Phi_o(s) \rightarrow P_o(s) \; : \; \begin{bmatrix} P_o(s) \\ z_2(L,s) \end{bmatrix} = \begin{bmatrix} 2Z_c(s) & -Z_c(s) \\ -1 & 1 \end{bmatrix} \begin{bmatrix} z_1(L,s) \\ \Phi_o(s) \end{bmatrix} \tag{2.62}$$

$$P_o(s) \rightarrow \Phi_o(s) \; : \; \begin{bmatrix} \Phi_o(s) \\ z_2(L,s) \end{bmatrix} = \begin{bmatrix} 2 & -\frac{1}{Z_c(s)} \\ 1 & -\frac{1}{Z_c(s)} \end{bmatrix} \begin{bmatrix} z_1(L,s) \\ P_o(s) \end{bmatrix} \tag{2.63}$$

With these boundary expressions and with the equation for the dynamics (2.58), causal representations according to Fig. 2.32 are available for the different input-output configurations of Table 2.1. Although the derivations have been given for the Linear Friction Model, `Model B`, the results are similar for the other models. In fact, the equations in terms of the propagation operator $\Gamma(s)$ and the characteristic impedance $Z_c(s)$ hold for all three transmission line models `Model A`, `Model B` and `Model C`.

The only difference is the definition of these operators; referring to Goodson and Leonard [42] again, these definitions are given in Table 2.2. In this Table, j is the imaginary number, defined as $j = \sqrt{-1}$, while J_0 and J_1 are Bessel functions of the first kind, of order zero and one respectively. For a detailed description of the inclusion of dissipative effects due to viscosity (`Model C`) in the frequency domain description by means of the given Bessel function ratio, the reader is referred to the work of d'Souza and Oldenburger [33].

	Model A	Model B	Model C
$\Gamma(s)$	$\frac{Ls}{c_0}$	$\frac{Ls}{c_0}\sqrt{1+\frac{8\mu}{r_0^2 s}}$	$\frac{Ls}{c_0}\frac{1}{\sqrt{1-\frac{2J_1\left(jr_0\sqrt{s/\mu}\right)}{jr_0\sqrt{s/\mu}J_1\left(jr_0\sqrt{s/\mu}\right)}}}$
$Z_c(s)$	$\frac{\rho c_0}{\pi r_0^2}$	$\frac{\rho c_0}{\pi r_0^2}\sqrt{1+\frac{8\mu}{r_0^2 s}}$	$\frac{\rho c_0}{\pi r_0^2}\frac{1}{\sqrt{1-\frac{2J_1\left(jr_0\sqrt{s/\mu}\right)}{jr_0\sqrt{s/\mu}J_1\left(jr_0\sqrt{s/\mu}\right)}}}$

Table 2.2: Propagation operator Γ and characteristic impedance Z_c for different transmission line models

From Table 2.2 it is clear, that the Lossless Fluid Line model, `Model A`, is directly obtained from the Linear Friction Model, `Model B`, by setting the viscosity factor μ zero. Note, that for this simple case, the characteristic impedance, Z_c, and therewith the boundary expressions (2.60) – (2.63), contain no dynamics, while the propagation operator, Γ,

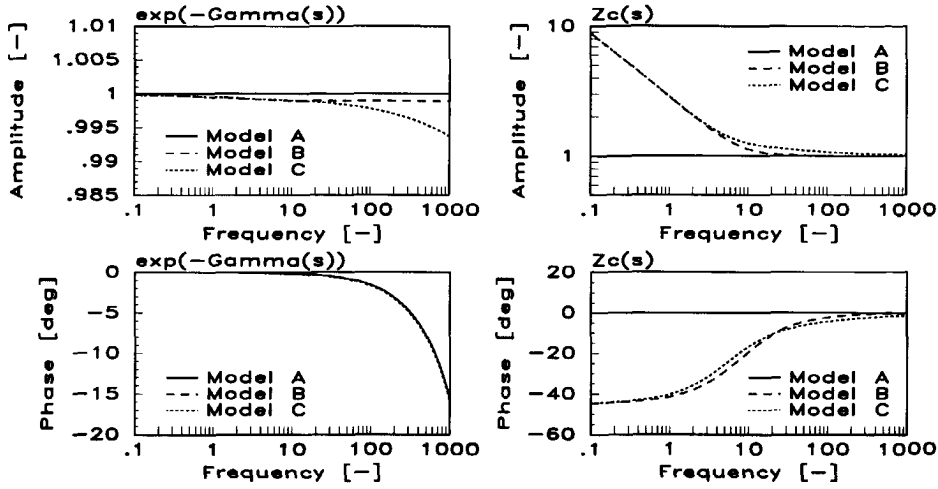


Fig. 2.33: Bode plots of delay operator $e^{-\Gamma(j\bar{\omega})}$ (left) and characteristic impedance $Z_c(j\bar{\omega})$ (right); `Model A`: Lossless Fluid Line (solid), `Model B`: Linear Friction Model (dashed) and `Model C`: Dissipative Model (dotted)

deduces to a simple time delay. So, it is obvious, that the representation according to Fig. 2.32 of `Model A` is causal.

In order to illustrate that this representation, in the form of (2.58), with boundary expressions (2.60) – (2.63), is still causal for the more complex models, `Model B` and `Model C`, the effect of the frequency dependent behaviour of $\Gamma(s)$ and $Z_c(s)$ is investigated. For that purpose, the delay operator $e^{-\Gamma(s)}$ and the characteristic impedance $Z_c(s)$ are evaluated in the frequency domain, using the expressions of Table 2.2. The results are given in Fig. 2.33, where the frequency axis is normalized with respect to the so-called viscosity frequency $\omega_c = \mu/r_0^2$, while the characteristic impedance $Z_c(s)$ is normalized with respect to its nominal value, which is its constant value for `Model A` given in Table 2.2.

Whereas the representation (2.58) is causal for `Model A`, the left plots of Fig. 2.33 show that this representation is also causal for `Model B` and `Model C`, as the frequency dependence of the delay operator only introduces a little extra phase lag. Furthermore, the boundary expressions (2.60) – (2.63) also remain causal for the viscous transmission line models, as the right plots of Fig. 2.33 show. Actually, both the impedance Z_c in (2.60) and (2.62), and the inverse impedance $1/Z_c$ in (2.61) and (2.63) represent causal behaviour. Only in the low- and the mid-frequency region, the friction models introduce dynamics with phase lag (impedance) or lead (inverse impedance). But in the high-frequency region, both the impedance Z_c and the inverse impedance $1/Z_c$ tend to a constant gain, with zero phase lag or lead, as if the impedance Z_c were a proper (not: strictly proper) system.

With these results, a causal representation of the theoretical transmission line model is available for the three different friction models, where four input-output configurations according to Fig. 2.32 and Table 2.1 are allowable. Herewith, the final representations of the theoretical transmission line model can be given, so that they can be included as subsystem models of the hydraulic servo-system model.

Final representations of the theoretical transmission line model

The purpose of the transmission line modelling is to include the effects of finite wave propagation velocity in the hydraulic servo-system, as indicated in Fig. 2.30 on page 68. Thereby, the (theoretical) model of a single transmission line or actuator chamber is to be included in a modular way, as a subsystem model. With the previous discussion of the causality issue, this requires proper bilateral coupling of the different subsystem models, i.e. a proper choice of input-output configurations. As will be explained later, in Subsection 2.4.4, this implies that the application of the theoretical model of a single transmission line according to Fig. 2.32, requires that:

- for the transmission lines between valve and actuator, `Config.2` from Table 2.1 is applied, with corresponding boundary expressions (2.60) and (2.63).
- for the modelling of the distributed pressure dynamics in the actuator chambers, `Config.1` from Table 2.1 is chosen, with corresponding boundary expressions (2.60) and (2.62).

Although the model representation according to Fig. 2.32 is well-suited to address the causality issue as it is done before, it is less suited to investigate the dynamic input-output behaviour of the transmission line, given the input-output configuration. The reason is, that the boundary expressions (2.60) – (2.63) constitute a coupling between the internal variables $z_1(s)$ and $z_2(s)$, resulting in a certain 'feedback configuration' according to Fig. 2.32, with corresponding dynamic input-output behaviour. Actually, in order to explicitly represent this input-output behaviour, the transmission line model of Fig. 2.32 should be written in a transfer function matrix form. It might be noted here, that every input-output configuration of Table 2.1 leads to a specific transfer function matrix representation.

Because `Config.1` and `Config.2` are to be applied here, the corresponding transfer function matrix representations are given here. These are easily found from (2.58) and the boundary expressions (2.60), (2.62) (for `Config.1`) or (2.60), (2.63) (for `Config.2`), by eliminating $z_1(s)$ and $z_2(s)$. This leads to the following results (see also [42]):

$$\texttt{Config.1}: \quad \begin{bmatrix} P_i(s) \\ P_o(s) \end{bmatrix} = \begin{bmatrix} \frac{Z_c(s)\left(1+e^{-2\Gamma(s)}\right)}{\left(1-e^{-2\Gamma(s)}\right)} & -\frac{2Z_c(s)e^{-\Gamma(s)}}{\left(1-e^{-2\Gamma(s)}\right)} \\ \frac{2Z_c(s)e^{-\Gamma(s)}}{\left(1-e^{-2\Gamma(s)}\right)} & -\frac{Z_c(s)\left(1+e^{-2\Gamma(s)}\right)}{\left(1-e^{-2\Gamma(s)}\right)} \end{bmatrix} \begin{bmatrix} \Phi_i(s) \\ \Phi_o(s) \end{bmatrix} \tag{2.64}$$

$$\texttt{Config.2}: \quad \begin{bmatrix} P_i(s) \\ \Phi_o(s) \end{bmatrix} = \begin{bmatrix} \frac{2e^{-\Gamma(s)}}{\left(1+e^{-2\Gamma(s)}\right)} & \frac{Z_c(s)\left(1-e^{-2\Gamma(s)}\right)}{\left(1+e^{-2\Gamma(s)}\right)} \\ -\frac{Z_c(s)\left(1-e^{-2\Gamma(s)}\right)}{\left(1+e^{-2\Gamma(s)}\right)} & \frac{2e^{-\Gamma(s)}}{\left(1+e^{-2\Gamma(s)}\right)}2 \end{bmatrix} \begin{bmatrix} P_o(s) \\ \Phi_i(s) \end{bmatrix} \tag{2.65}$$

Instead of using these representations, it is usual in literature to express the transfer function matrix in terms of cosine hyperbolic and the sine hyperbolic functions, which are defined as:

$$\cosh x = \frac{e^x + e^{-x}}{2} = \frac{1 + e^{-2x}}{2e^{-x}}, \quad \sinh x = \frac{e^x - e^{-x}}{2} = \frac{1 - e^{-2x}}{2e^{-x}}$$

With these definitions, the matrix representation of the dynamics of the transmission line depicted in Fig. 2.31, for `Config.1` and `Config.2` respectively, becomes [42]:

$$\texttt{Config.1}: \quad \begin{bmatrix} P_i(s) \\ P_o(s) \end{bmatrix} = \begin{bmatrix} \frac{Z_c(s)\cosh\Gamma(s)}{\sinh\Gamma(s)} & -\frac{Z_c(s)}{\sinh\Gamma(s)} \\ \frac{Z_c(s)}{\sinh\Gamma(s)} & -\frac{Z_c(s)\cosh\Gamma(s)}{\sinh\Gamma(s)} \end{bmatrix} \begin{bmatrix} \Phi_i(s) \\ \Phi_o(s) \end{bmatrix} \tag{2.66}$$

$$\texttt{Config.2}: \quad \begin{bmatrix} P_i(s) \\ \Phi_o(s) \end{bmatrix} = \begin{bmatrix} \frac{1}{\cosh\Gamma(s)} & \frac{Z_c(s)\sinh\Gamma(s)}{\cosh\Gamma(s)} \\ -\frac{\sinh\Gamma(s)}{Z_c(s)\cosh\Gamma(s)} & \frac{1}{\cosh\Gamma(s)} \end{bmatrix} \begin{bmatrix} P_o(s) \\ \Phi_i(s) \end{bmatrix} \tag{2.67}$$

Actually, these equations, together with the definitions of Γ and Z_c in Table 2.2, constitute the final representations of the theoretical model of a transmission line as subsystem of the hydraulic servo-system. Note, that this description of the transmission line dynamics is given in terms of physical parameters, as was desired. The problem with this description is, however, that it is an infinite order model, corresponding to the distributed parameter character of the system. This makes the theoretical frequency domain model less suitable for system analysis, especially in the time domain. In order to overcome this problem, approximation of the theoretical models (2.66) and (2.67) is required.

2.4.3 Approximation of transmission line dynamics

In Subsection 2.1.2, page 25, a rather extensive motivation has been given for the choice for open loop approximation of the transmission line models. This means, that the theoretical models (2.66) and (2.67) are replaced by approximated models with the same input-output configuration, which serve as new subsystem models to be integrated to a complete servo-system model, as will be discussed in Subsection 2.4.4.

In literature, some approximation techniques of transmission line dynamics are given, as discussed below. Because of its good applicability in the modelling approach of this thesis, specific attention will be given to a modal approximation technique. Using this technique, low-order subsystem models, describing the transmission line effects in the hydraulic servo-system, will be given.

Some approximation techniques

Whereas the frequency domain approach appears to be suitable to analyze the transmission line dynamics and to give analytic solutions for the partial differential equations in the form of equations (2.67) and (2.66), time domain analysis requires some simplifications and approximations. Important work in the field of the analysis of transient responses has been performed by Brown [22, 23]. As a numerical method to solve the PDE's, the method of characteristics appeared to be well suited for the investigation of fluid transients, including different friction models, as described by Zielke [163] and by Wylie and Streeter [158].

Another approach to transmission line modelling is directly based on the representation of the transmission line dynamics in terms of causal (delay) operators, as in Fig. 2.32. This representation has mainly been utilized to perform time domain simulations, see for instance Ezekiel and Paynter [34] and Sidell and Wormley [128]. In a more recent developement, Krus et al. [69] included an approximation of frequency dependent friction in this setting, resulting in a rather accurate simulation model, as compared to experimental results.

Despite good modelling results, there are some disadvantages with the modelling techniques mentioned before: the frequency domain techniques do not easily allow time domain interpretations, and vice versa. Therefore people have been looking for model descriptions in terms of linear systems theory, which are suited for both time and frequency domain analysis, and moreover accurately approximate the exact theoretical transmission line models. The key was found in the infinite product representations of hyperbolic functions (of which type the frequency domain solutions are, see (2.66) and (2.67)), as described by Oldenburger and Goodson [108]. This resulted in the development of modal approximation techniques [59, 60, 155], which utilize the fact, that the transmission line dynamics can be characterized as a series of badly damped resonance modes, which are reasonably distinct from each other. Thus, it is possible, to approximate each mode of the transmission line dynamics by a second order linear model.

Especially for the modelling of complex fluid networks, this modal approximation technique is useful, as shown by Margolis and Yang [92]. They use a dissipative modal approximation for each transmission line element. A disadvantage of their method is, that there is no clear relation between the modal coefficients and the physical parameters of the line; the modal coefficients are derived from tables. However, it appears also to be possible, to preserve the physical parameters in the approximating linear models, as described by Yang and Tobler [160]. Therefore, in order to allow a direct physical interpretation of the dynamic effects of the approximate transmission line model, the modal approximation according to Yang and Tobler [160] will be adopted here, rather than the method of Margolis and Yang [92].

Modal approximations of the theoretical models

Adopting the modal approximation technique of Yang and Tobler [160] for the modelling of the transmissin line effects of the long-stroke hydraulic actuator in the configuration of Fig. 2.30, the modal approximations of the theoretical transmission line models (2.66) and (2.67) are to be presented here.

The input-output behaviour of the theoretical models can be represented by infinite product series of second order models [108]. Each of these models (which may be state space models) then represents a single resonance mode of the transmission line dynamics. Within this setting, the modal approximation of a transmission line model can be seen as a finite dimensional state-space model, which has been obtained by taking into account a finite number of modes only.

For the investigation of the transmission line effects in the long-stroke hydraulic actuator, two modes are taken into account for each subsystem, as well for the transmission lines between the valve and the actuator as for the actuator chambers. As far as the transmission lines are concerned, it is argued in [119] that these first two modes of each transmission line may be expected to be relevant. Concerning the actuator chambers, the choice for approximation by the first two modes is somewhat arbitrary; in fact, the primary objective of the investigation of distributed pressure dynamics in the actuator chambers is to see, whether these dynamics are relevant or not. For this purpose, two resonance modes are expected to be at least sufficient.

So, with two modes being taken into account for all transmission line models, the modal approximations of the theoretical models (2.66) and (2.67) become fourth order linear models. For `Config.2`, i.e. for the models of the transmission lines between valve

and actuator (2.67), the modal approximation in state space form is given by Yang and Tobler [160], with the viscosity frequency $\omega_c = \mu/r_0^2$, as:

$$\begin{aligned} \tfrac{1}{\omega_c}\dot{X}_{tl} &= A_{tl}X_{tl} + B_{tl}U_{tl} \\ Y_{tl} &= C_{tl}X_{tl} \end{aligned} \tag{2.68}$$

with:

$$\begin{aligned} X_{tl} &= \left[\, P_{i_1} \;\; \Phi_{o_1} \;\; P_{i_2} \;\; \Phi_{o_2} \,\right]^T \\ U_{tl} &= \left[\, P_o \;\; \Phi_i \,\right]^T \\ Y_{tl} &= \left[\, P_i \;\; \Phi_o \,\right]^T \\ A_{tl} &= \operatorname{diag}\left[\, A_{tl_1} \;\; A_{tl_2} \,\right] \qquad A_{tl_i} = \begin{bmatrix} 0 & (-1)^i Z_0 \lambda_{ci} \\ \frac{(-1)^{i+1}\lambda_{ci}}{Z_0 \alpha_{ci}^2} & -\frac{8\beta_{ci}}{\alpha_{ci}} \end{bmatrix} \quad i = 1,2 \\ B_{tl} &= \left[\, B_{tl_1}^T \;\; B_{tl_2}^T \,\right]^T \\ C_{tl} &= \begin{bmatrix} 1 & 0 & 1 & 0 \\ 0 & 1 & 0 & 1 \end{bmatrix} \qquad B_{tl_i} = \begin{bmatrix} 0 & \frac{2Z_0}{D_n} \\ -\frac{2}{Z_0 D_n \alpha_{ci}^2} & 0 \end{bmatrix} \quad i = 1,2 \end{aligned}$$

The modal approximations for `Config.1`, i.e. for the models of the distributed pressure dynamics in the actuator chambers (2.66), are slightly different; they are not given by Yang and Tobler [160], but they are derived in Appendix D, using the techniques from [160]. The resulting state space form is:

$$\begin{aligned} \tfrac{1}{\omega_c}\dot{X}_{ac} &= A_{ac}X_{ac} + B_{ac}U_{ac} \\ Y_{ac} &= C_{ac}X_{ac} \end{aligned} \tag{2.69}$$

with:

$$\begin{aligned} X_{ac} &= \left[\, x_0 \;\; x_{1_1} \;\; x_{2_1} \;\; x_{1_2} \;\; x_{2_2} \,\right]^T \\ U_{ac} &= \left[\, \Phi_i \;\; \Phi_o \,\right]^T \\ Y_{ac} &= \left[\, P_i \;\; P_o \,\right]^T \\ A_{ac} &= \operatorname{diag}\left[\, A_{ac_0} \;\; A_{ac_1} \;\; A_{ac_2} \,\right] \\ B_{ac} &= \left[\, B_{ac_0}^T \;\; B_{ac_1}^T \;\; B_{ac_2}^T \,\right]^T \\ C_{ac} &= \left[\, C_{ac_0} \;\; C_{ac_1} \;\; C_{ac_2} \,\right] \end{aligned} \qquad \begin{aligned} A_{ac_0} &= 0 \\ A_{ac_i} &= \begin{bmatrix} 0 & -\frac{\lambda_{si}^2}{\alpha_{si}^2} \\ 1 & -\frac{8\beta_{si}}{\alpha_{si}} \end{bmatrix} \quad i = 1,2 \\ B_{ac_0} &= \begin{bmatrix} \frac{Z_0}{D_n} & -\frac{Z_0}{D_n} \end{bmatrix} \\ B_{ac_i} &= \begin{bmatrix} \frac{2Z_0}{D_n}\frac{8\beta_{si}}{\alpha_{si}} & (-1)^{i+1}\frac{2Z_0}{D_n}\frac{8\beta_{si}}{\alpha_{si}} \\ \frac{2Z_0}{D_n} & (-1)^{i+1}\frac{2Z_0}{D_n} \end{bmatrix} \quad i = 1,2 \\ C_{ac_0} &= \begin{bmatrix} 1 & 1 \end{bmatrix}^T \\ C_{ac_i} &= \begin{bmatrix} 0 & 1 \\ 0 & (-1)^i \end{bmatrix} \quad i = 1,2 \end{aligned}$$

The two most important line parameters in the expressions above, the dissipation number D_n, and the line impedance constant Z_0, are calculated as follows:

$$D_n = \frac{L\mu}{c_0 r_0^2}; \qquad Z_0 = \frac{\rho c_0}{\pi r_0^2} \tag{2.70}$$

Clearly, these parameters are related to the propagation operator $\Gamma(s)$ and line characteristic impedance $Z_c(s)$ in the theoretical transmission line model, see Table 2.2, and actually refer to the Lossless Fluid Line model, `Model A`. Obviously, the line length L and radius r_0 in (2.70) should be taken different for each subsystem, according to the definitions of Fig. 2.30. Note, that this implies, that the modal approximations for the actuator chambers (2.69) become highly position dependent, as $L = q_{max} \pm q$. In some sense, this effect is similar to the position dependence of the uniformly distributed pressure dynamics (2.34).

Besides the dissipation number D_n and the impedance constant Z_0, the state-space models (2.68) and (2.69) are mainly determined by the parameters λ_{ci} and λ_{si} respectively. These are the normalized (by ω_c) modal undamped natural frequencies of a blocked line and of an open line respectively (see Yang and Tobler [160] and also Appendix D):

$$\lambda_{ci} = \frac{\pi(2i-1)}{2D_n} \qquad i = 1, 2 \tag{2.71}$$

$$\lambda_{si} = \frac{\pi i}{D_n} \qquad i = 1, 2 \tag{2.72}$$

The final parameters to be determined in the state space models (2.68) and (2.69) are the frequency modification factors α_{ci} and α_{si}, and the damping modification factors β_{ci} and β_{si}, introduced by Yang and Tobler [160]. These factors actually represent the type of friction model that is used, as follows:

- For the Lossless Fluid Line, `Model A`, $\alpha_{ci} = \alpha_{si} = 1$ and $\beta_{ci} = \beta_{si} = 0$.
- For the Linear Friction Model, `Model B`, $\alpha_{ci} = \alpha_{si} = 1$ and $\beta_{ci} = \beta_{si} = 1$.
- For the Dissipative Model, `Model C`, the factors α_{ci}, α_{si}, β_{ci} and β_{si} are frequency dependent. They can be determined from Figures given in [160], where α_{ci} and β_{ci} have to be evaluated at the frequencies λ_{ci} given by (2.71), while α_{si} and β_{si} have to be evaluated at the frequencies λ_{si} given by (2.71).

Thus, with the dissipation number D_n, the impedance constant Z_0, the natural frequencies λ_{ci} and λ_{si}, and the frequency dependent modification factors α and β, the state space forms of the modal approximations (2.68) and (2.69) of the theoretical transmission line models (2.67) and (2.66) are properly defined. However, there is still one issue to be discussed, namely the steady state behaviour of the modal approximations. Although the dominant dynamic modes, and therewith the transient properties, are accurately approximated, steady state accuracy is lost in general by modal approximations.

For the primary purpose of the modal approximations, namely the inclusion of transmission line effects in the actuator model as described in Subsection 2.6.3, such that they can be experimentally identified and validated (see Chapter 3), the steady state accuracy is not relevant. The reason is, that the actuator model including the modal approximations for the transmission line effects only needs to have the correct physical structure, while the parameters of the model are to be identified from experiments. However, if the modal approximations are to be used for the purpose of time domain simulations of the theoretical actuator model, including transmission line effects, steady state accuracy is required. This is because of the fact that integrating behaviour is involved; a steady state error in the flow balance of a certain (transmission line) element may well cause the pressure to drift away from the nominal value.

Although time domain simulations including transmission line effects are not discussed in this thesis, the modal approximations have been used for this type of simulations,

requiring proper steady state behaviour. For completeness, a discussion of this steady state behaviour of the modal approximations is given in Appendix E.

With the state space models (2.68) and (2.69), useful low-order approximate models for the transmission line effects in the hydraulic servo-system are available, in which the physical structure and the physical parameters are clearly preserved. Actually, these approximate representations form a good basis for an integrated model of the hydraulic servo-system, including transmission line effects with frequency dependent friction, both for the transmission lines between valve and actuator and for the actuator chambers (see Fig. 2.30).

2.4.4 Integration of subsystem models for inclusion of transmission line effects

Considering the obtained transmission line models as subsystems models of the model of the hydraulic servo-system, the model of the complete system is obtained by proper integration of the different subsystem models. In the following the reasoning behind the chosen input-output configurations of the transmission line models is given. After that, three alternative integrated models of the hydraulic servo-system are summarized, depending on which transmission line effects from Fig. 2.30 are to be taken into account.

Input-output configuration of transmission line models

It has already been mentioned, that different input-output configurations of the transmission line model are to be applied in the model of the hydraulic servo-system. The reason is, that the transmission line models, as subsystem models, should be properly integrated with the other subsystem models via bilateral coupling, as explained next.

The subsystem models for the transmission lines between valve and actuator (see also Fig. 2.29) should have the input-output configuration denoted by `Config.2` (see Table 2.1), for the following reason. From the valve flow equations (2.23) in Subsection 2.2.4, it is clear that the flows Φ_{i1}, Φ_{i2} at the valve side have to be defined as inputs U_i of the transmission line models, and correspondingly the pressures P_{i1}, P_{i2} as outputs Y_i. On the other hand, the equations (2.27) or (2.34) describing the pressure dynamics in the actuator model of Section 2.3, require the pressures P_{o1}, P_{o2} at the actuator side to be defined as inputs U_o of the transmission line models, and the actuator flows Φ_{o1}, Φ_{o2} as outputs Y_o.

For the subsystem models for the actuator chambers (see Fig. 2.30), the situation is different. In fact, the four-port models for the actuator chambers should replace their lumped parameter counterparts, the mass balances (2.27) or (2.34). In order to allow a proper coupling with the remaining model equations, they should have the input-output configuration denoted by `Config.1` in Table 2.1. This can be explained by noting that the actuator flows Φ_{o1}, Φ_{o2} have been defined as outputs of the models for the transmission lines just before, implying that they serve as inputs U_i for the models of the actuator chambers. Bilateral coupling then requires the pressures P_{o1}, P_{o2} to be the outputs Y_i of the actuator chamber models. For the piston side of the actuator chambers, it is noted, that the four-port models for the actuator chambers are coupled to the equation of motion of the piston (2.38) via force and velocity. Actually, the displacement flows Φ_{p1}, Φ_{p2} due to the actuator velocity $\dot{q}$ can be seen as inputs U_o, while the piston forces in the form of

pressures P_{p1}, P_{p2} at the piston side of the actuator chambers can be seen as the outputs Y_o of the four-port models.

Alternative integrated models for the hydraulic servo-system

Depending on which transmission line effects are taken into account, three alternative integrated models for the hydraulic servo-system are summarized below, denoted as `Model 1`, `Model 2` and `Model 3` respectively.

- `Model 1`: No transmission line dynamics taken into account; only the servo-valve flow and actuator dynamics are described.

  The servo-valve flow is given by (2.23):

$$\begin{aligned} \Phi_{p1} &= C_d A_{m1}\sqrt{2\tfrac{P_s-P_{p1}}{\rho}} - C_d A_{m2}\sqrt{2\tfrac{P_{p1}-P_t}{\rho}} + \Phi_{l,m1} - \Phi_{l,m2} \\ \Phi_{p2} &= C_d A_{m3}\sqrt{2\tfrac{P_{p2}-P_t}{\rho}} - C_d A_{m4}\sqrt{2\tfrac{P_s-P_{p2}}{\rho}} + \Phi_{l,m1} - \Phi_{l,m4} \end{aligned} \tag{2.73}$$

  with corresponding leakage flows $\Phi_{l,m}$ as in (2.25).

  The mass balances describing the uniformly distributed pressure dynamics in the actuator chambers are written as (see (2.34)):

$$\begin{aligned} \dot{P}_{p1} &= \tfrac{E}{A_p(q_{max}+q)+V_{l1}}\left(\Phi_{p1} - \Phi_{l1} - A_p\dot{q}\right) \\ \dot{P}_{p2} &= \tfrac{E}{A_p(q_{max}-q)+V_{l2}}\left(-\Phi_{p2} - \Phi_{l2} + A_p\dot{q}\right) \end{aligned} \tag{2.74}$$

  with corresponding leakage flows Φ_{l1} and Φ_{l2} according to (2.35) and (2.36).

  The equation of motion of the piston (2.38) completes the model:

$$M_p\ddot{q} = A_p\left(P_{p1} - P_{p2}\right) - F_{vp} - F_{cp} + F_{ext} \tag{2.75}$$

- `Model 2`: Transmission line dynamics between valve and actuator chambers *are* taken into account, and integrated with the valve flow equations and the actuator model, according to Fig. 2.29.

  The valve flow is taken again from (2.23) to be:

$$\begin{aligned} \Phi_{i1} &= C_d A_{m1}\sqrt{2\tfrac{P_s-P_{i1}}{\rho}} - C_d A_{m2}\sqrt{2\tfrac{P_{i1}-P_t}{\rho}} + \Phi_{l,m1} - \Phi_{l,m2} \\ \Phi_{i2} &= C_d A_{m3}\sqrt{2\tfrac{P_{i2}-P_t}{\rho}} - C_d A_{m4}\sqrt{2\tfrac{P_s-P_{i2}}{\rho}} + \Phi_{l,m1} - \Phi_{l,m4} \end{aligned} \tag{2.76}$$

  with corresponding leakage flows $\Phi_{l,m}$ as in (2.25).

  With `Config.2` as input-output configuration, the transmission line models are given in the form of (2.68):

$$\begin{aligned} \tfrac{1}{\omega_{c,tl1}}\dot{X}_{tl1} &= A_{tl1}X_{tl1} + B_{tl1}U_{tl1} & \tfrac{1}{\omega_{c,tl2}}\dot{X}_{tl2} &= A_{tl2}X_{tl2} + B_{tl2}U_{tl2} \\ Y_{tl1} &= C_{tl1}X_{tl1} & Y_{tl2} &= C_{tl2}X_{tl2} \end{aligned} \tag{2.77}$$

  with:

$$\begin{aligned} U_{tl1} &= \begin{bmatrix} P_{o1} & \Phi_{i1} \end{bmatrix}^T & U_{tl2} &= \begin{bmatrix} P_{o2} & -\Phi_{i2} \end{bmatrix}^T \\ Y_{tl1} &= \begin{bmatrix} P_{i1} & \Phi_{o1} \end{bmatrix}^T & Y_{tl2} &= \begin{bmatrix} P_{i2} & -\Phi_{o2} \end{bmatrix}^T \end{aligned}$$

with corresponding matrices A_{tl1}, A_{tl2}, B_{tl1}, B_{tl2}, C_{tl1}, C_{tl2}, state vectors X_{tl1} and X_{tl2}, and viscosity frequencies $\omega_{c,tl1}$ and $\omega_{c,tl2}$ as in (2.68). Note the minus sign for the flows of the second transmission line, resulting from the sign definition in Fig. 2.29.

Similar mass balances describing the uniformly distributed pressure dynamics in the actuator chambers hold as before (2.34):

$$\begin{aligned} \dot{P}_{o1} &= \frac{E}{A_p(q_{max}+q)+V_{l1}}\left(\Phi_{o1} - \Phi_{l1} - A_p\dot{q}\right) \\ \dot{P}_{o2} &= \frac{E}{A_p(q_{max}-q)+V_{l2}}\left(-\Phi_{o2} - \Phi_{l2} + A_p\dot{q}\right) \end{aligned} \tag{2.78}$$

with leakage flows Φ_{l1} and Φ_{l2} as in (2.35) and (2.36).

The equation of motion of the piston (2.38) again completes the model:

$$M_p\ddot{q} = A_p\left(P_{o1} - P_{o2}\right) - F_{vp} - F_{cp} + F_{ext} \tag{2.79}$$

- `Model 3`: Transmission line effects are taken into account, both for the transmission lines between valve and actuator chambers, and for the distributed pressure dynamics in the actuator chambers; corresponding dynamic models are integrated with the valve flow equations and the equation of motion of the piston. This model refers to the situation, depicted in Fig. 2.30.

The valve flow is still given by (2.23):

$$\begin{aligned} \Phi_{i1} &= C_d A_{m1}\sqrt{2\tfrac{P_s - P_{i1}}{\rho}} - C_d A_{m2}\sqrt{2\tfrac{P_{i1} - P_t}{\rho}} + \Phi_{l,m1} - \Phi_{l,m2} \\ \Phi_{i2} &= C_d A_{m3}\sqrt{2\tfrac{P_{i2} - P_t}{\rho}} - C_d A_{m4}\sqrt{2\tfrac{P_s - P_{i2}}{\rho}} + \Phi_{l,m1} - \Phi_{l,m4} \end{aligned} \tag{2.80}$$

with corresponding leakage flows $\Phi_{l,m}$ as in (2.25).

The transmission lines between valve and actuator chambers again have the form of (2.68):

$$\begin{aligned} \tfrac{1}{\omega_{c,tl1}}\dot{X}_{tl1} &= A_{tl1}X_{tl1} + B_{tl1}U_{tl1} & \tfrac{1}{\omega_{c,tl2}}\dot{X}_{tl2} &= A_{tl2}X_{tl2} + B_{tl2}U_{tl2} \\ Y_{tl1} &= C_{tl1}X_{tl1} & Y_{tl2} &= C_{tl2}X_{tl2} \end{aligned} \tag{2.81}$$

with:

$$\begin{aligned} U_{tl1} &= \begin{bmatrix} P_{o1} & \Phi_{i1} \end{bmatrix}^T & U_{tl2} &= \begin{bmatrix} P_{o2} & -\Phi_{i2} \end{bmatrix}^T \\ Y_{tl1} &= \begin{bmatrix} P_{i1} & \Phi_{o1} \end{bmatrix}^T & Y_{tl2} &= \begin{bmatrix} P_{i2} & -\Phi_{o2} \end{bmatrix}^T \end{aligned}$$

with corresponding matrices A_{tl1}, A_{tl2}, B_{tl1}, B_{tl2}, C_{tl1}, C_{tl2}, state vectors X_{tl1} and X_{tl2}, and viscosity frequencies $\omega_{c,tl1}$ and $\omega_{c,tl2}$ as in (2.68).

For the distributed pressure dynamics in the actuator chambers, the input-output configuration `Config.1` applies, with corresponding state space models according to (2.69):

$$\begin{aligned} \tfrac{1}{\omega_{c,ac1}}\dot{X}_{ac1} &= A_{ac1}X_{ac1} + B_{ac1}U_{ac1} & \tfrac{1}{\omega_{c,ac2}}\dot{X}_{ac2} &= A_{ac2}X_{ac2} + B_{ac2}U_{ac2} \\ Y_{ac1} &= C_{ac1}X_{ac1} & Y_{ac2} &= C_{ac2}X_{ac2} \end{aligned} \tag{2.82}$$

with:

$$U_{ac1} = \left[(\Phi_{o1} - \Phi_{l,b4}) \;\; A_p\dot{q} \right]^T \quad U_{ac2} = \left[-(\Phi_{o2} - \Phi_{l,b2}) \;\; -(A_p\dot{q} - \Phi_{l,b3}) \right]^T$$
$$Y_{ac1} = \left[P_{o1} \;\; P_{p1} \right]^T \quad Y_{ac2} = \left[P_{o2} \;\; P_{p2} \right]^T$$

and corresponding matrices A_{ac1}, A_{ac2}, B_{ac1}, B_{ac2}, C_{ac1}, C_{ac2}, state vectors X_{ac1} and X_{ac2}, and viscosity frequencies $\omega_{c,ac1}$ and $\omega_{c,ac2}$ as in (2.69).

Note, that corresponding to the definitions in Fig. 2.23 on page 56, the different leakage flows are combined either with the flow at the manifold side, or with the displacement flow at the piston side of the actuator chamber. For completeness, the corresponding leak flow equations are repeated here from (2.36), using the correct indices for the pressures:

$$\begin{aligned} \Phi_{l,b1} &= LP_{b1}(P_s - P_t) + A_{p,b1}\dot{q} \\ \Phi_{l,b2} &= LP_{b2}(P_s - P_{o2}) - A_{p,b2}\dot{q} \\ \Phi_{l,b3} &= LP_{b3}(P_{p2} - P_t) + A_{p,b3}\dot{q} \\ \Phi_{l,b4} &= LP_{b4}(P_{o1} - P_t) - A_{p,b4}\dot{q} \end{aligned} \tag{2.83}$$

Again, the equation of motion (2.38) completes the model:

$$M_p\ddot{q} = A_p(P_{p1} - P_{p2}) - F_{vp} - F_{cp} + F_{ext} \tag{2.84}$$

It should be noted at this point, that the connections at both sides of the transmission lines between the servo-valve and the actuator chambers have been assumed to be lossless (`Model 2` and `Model 3`). In other words, ideal energy exchange at both sides of the transmission lines is assumed. However, in reality there will be some energy loss in the hydraulic manifolds, connecting the transmission lines to the servo-valve at the one side and to the actuator chambers at the other side, dependent on the construction of the manifolds (diameter of channels, number of direction changes of the fluid flow). Especially for high-speed motions, i.e. large oil flows, the losses in a manifold may be considerable due to turbulence of the flow.

In order to take this non-linearity into account, the manifold may be modelled by a turbulent flow restriction, generating a manifold pressure loss which modifies the pressures P_{i1}, P_{i2}, P_{o1} and P_{o2} into:

$$\begin{aligned} P'_{i1} &= P_{i1} + \mathrm{sign}(\Phi_{i1})\frac{\rho\Phi_{i1}^2}{2C_d^2A_{man,i1}^2} \quad P'_{o1} = P_{o1} + \mathrm{sign}(\Phi_{o1})\frac{\rho\Phi_{o1}^2}{2C_d^2A_{man,o1}^2} \\ P'_{i2} &= P_{i2} - \mathrm{sign}(\Phi_{i2})\frac{\rho\Phi_{i2}^2}{2C_d^2A_{man,i2}^2} \quad P'_{o2} = P_{o2} - \mathrm{sign}(\Phi_{o2})\frac{\rho\Phi_{o2}^2}{2C_d^2A_{man,o2}^2} \end{aligned} \tag{2.85}$$

where A_{man} is the representative area of the turbulent restriction in the manifold. Although with the expressions (2.85) algebraic loops are introduced in the simulation model, the model is still properly stated. The possible simulation problems related to the algebraic loops are easily solved as discussed in Appendix B.

For clarity, a graphical representation of the resulting interconnection of the subsystem models for `Model 2`, including the manifold losses (2.85), is given in Fig. 2.34.

In conclusion of this Subsection, it can be stated that three alternative integrated models for the hydraulic servo-system can be distinguished, depending on which transmission line effects are taken into account. Because of the physical background of the models, they are well-suited for analysis and for getting insight in the relevance of the dynamic effects, related to the transmission line effects, as discussed next.

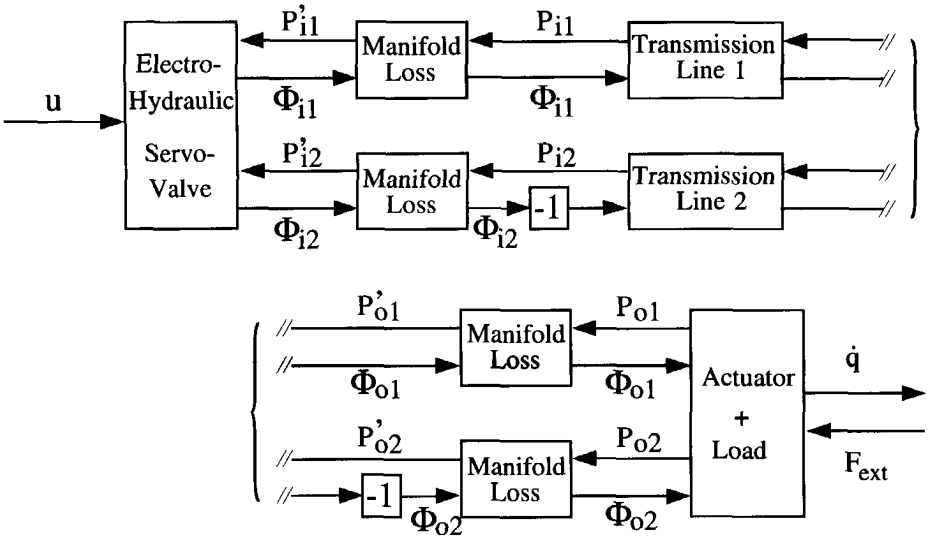


Fig. 2.34: Subsystems of hydraulic servo-system with interconnections, including manifold losses

2.4.5 Analysis of the effect of transmission line dynamics

In order to obtain insight in the relevance of the modelled transmission line effects, the three models `Model 1`, `Model 2` and `Model 3` of the previous Subsection have been analysed at simulation level. Contrary to the non-linear dynamics of the servo-valve model and of the basic actuator model (Subsection 2.2.5 and 2.3.5), the models including transmission line effects are not analyzed in the time domain, but in the frequency domain, using Bode plots of the simulation model. The reason is, that the transmission line models do not introduce non-linearities to be considered in the time domain, while their main contribution is a dynamic effect in the high-frequency range, which is best analyzed in the frequency domain.

The outline of this Subsection is as follows. First, some remarks are made concerning the model parameters that have been used in the theoretical model. After that, some representative Bode plots of the three alternative dynamic models of the hydraulic actuator are presented and discussed. Special attention is given then to the position dependence of the actuator dynamics, in relation to the transmission line effects. Finally, the Section is concluded with some remarks on the relevance of the modelled transmission line effects.

Model parameters

The effect of transmission line dynamics is investigated for the same actuator configuration as in Subsection 2.3.5, with parameters as given in Table F.4, except that the Coulomb friction parameters are set to zero. For the transmission line models, as given in Subsection 2.4.3, the parameters of Table F.5 of Appendix F are used, which correspond to the actual geometry of the actuator modelled in Subsection 2.3.4. The frequency dependent

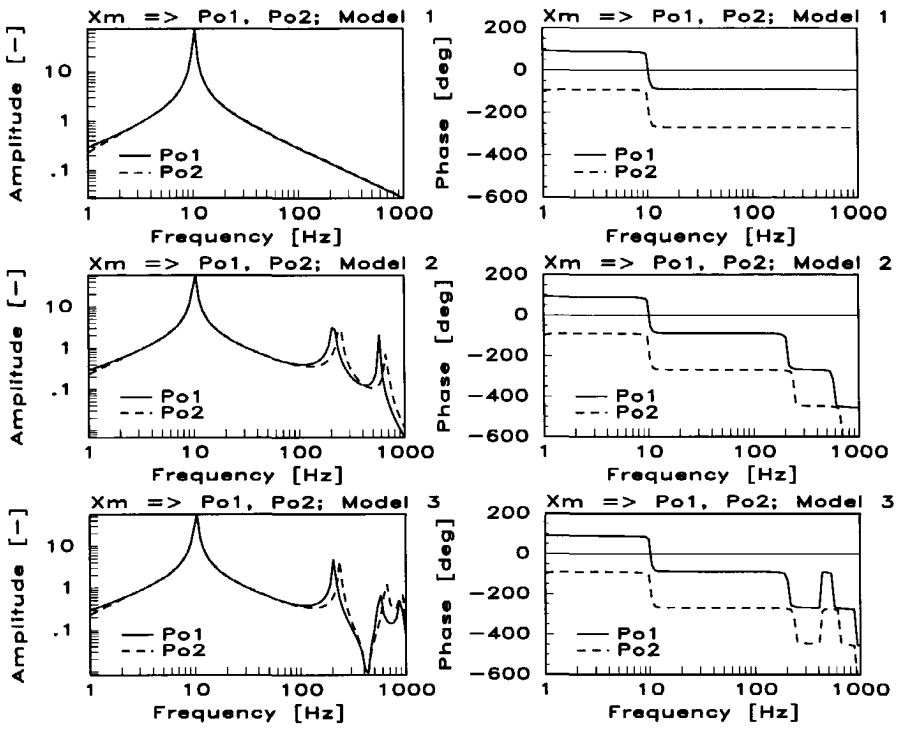


Fig. 2.35: Bode plots of simulation model from $\bar{x}_m(s)$ to $\bar{P}_{o1}(s)$ and $\bar{P}_{o2}(s)$ respectively. `Model 1`: Basic actuator model (upper); `Model 2`: dynamics of transmission lines between valve and actuator included (middle); `Model 3`: actuator chambers as transmission lines (lower)

factors α and β are derived from Figures given by Yang and Tobler [160].

It should be noted here, that if the dynamics due to the transmission lines between valve and actuator chambers are taken into account, the ineffective volumes V_{l1} and V_{l2} in (2.34) are set to zero. The reason is, that the ineffective volumes are used to model the capacity (stiffness) of the oil in the transmission lines in the basic actuator model, while the extended model, including transmission line dynamics, inherently includes this capacity in the transmission line model.

Effect of transmission line modelling on Bode plots

With models `Model 1`, `Model 2` and `Model 3` being defined in the previous Subsection, Bode plots of these three alternative models are given in Fig. 2.35. Hereby, the main spool position x_m is taken as the input and the pressures in the actuator chambers (at the manifold side) $P_{o1}(s)$ and $P_{o2}(s)$ are taken as the outputs of the transfer functions. A physical interpretation of the results gives rise to the following remarks:

- `Model 1` shows the basic dynamics of the hydraulic actuator: a badly damped resonance due to the coupling of the load dynamics and the pressure dynamics.

- For `Model 1` the dynamic behaviour of the two actuator pressures is hardly distinguishable; the only difference is the phase (sign). Actually, the sum of the actuator pressures (the pressure level) is uncontrollable; only the pressure difference is controllable.
- The low-frequency dynamics are unaffected by a proper inclusion of transmission line dynamics.
- `Model 2` clearly shows the effect of the dynamics of the transmission lines between valve and actuator: badly damped resonance peaks in the high-frequency region are the result. The location of these peaks is different for the different actuator pressures; this is caused by the different geometry of the two transmission lines.
- Because each transmission line introduces its own resonance peaks, the actuator pressures can now be seen as independent state variables of the actuator model; the mean pressure is no longer uncontrollable, at least not for high frequencies.
- The responses of `Model 3` show an anti-resonance in between the resonance frequencies of the transmission lines. Besides that, additional resonance peaks are introduced, which are not shown because they are beyond the frequency range of Fig. 2.35.
- The modelling of distributed pressure dynamics in the actuator chambers (`Model 3`) does not affect the location of the resonance peaks due the transmission lines (compare `Model 2`). In fact, there is only minor difference between the models for the frequency region of interest (< 1 [kHz]).

Although the above remarks explain some basic phenomena related to transmission line modelling, some more insight can be obtained by considering the state variable that is most relevant for control: the pressure difference. Thereby three pressure differences can be distinguished, depending on the location where the actuator pressures are considered. This can be at the valve side of the transmission lines (ΔP_i) or at the actuator side (ΔP_o), or at the piston side of the actuator chambers (ΔP_p). The Bode plots of these transfer functions, with x_m as input, for the three different models, are given in Fig. 2.36. The results lead to some additional remarks on transmission line dynamics:

- The low-frequency behaviour of the actuator pressures neither depends on whether transmission line effects are taken into account, nor on which pressure (difference) is considered.
- If the pressure difference at the valve side ΔP_i is considered and transmission line dynamics are taken into account, different anti-resonances are found in the transfer function. The result is, that the actuator model does not show high-frequence roll-off, and that the phase lag remains smaller than 90°.
- There is only little difference in whether the pressure difference ΔP_o or ΔP_p is considered. In other words, there is little difference between the pressure differences at both sides of the actuator chambers, which is equivalent to saying that the pressures in the actuator chambers do not need to be modelled by distributed parameter models.

Position dependence

As already concluded from the time domain simulations of the non-linear actuator model, the dynamics of the hydraulic actuator are highly position dependent, because of the varying 'stiffness' of the oil volumes in the actuator chambers. This effect also propagates to the dynamics related to transmission line effects, as illustrated in Fig. 2.37, showing

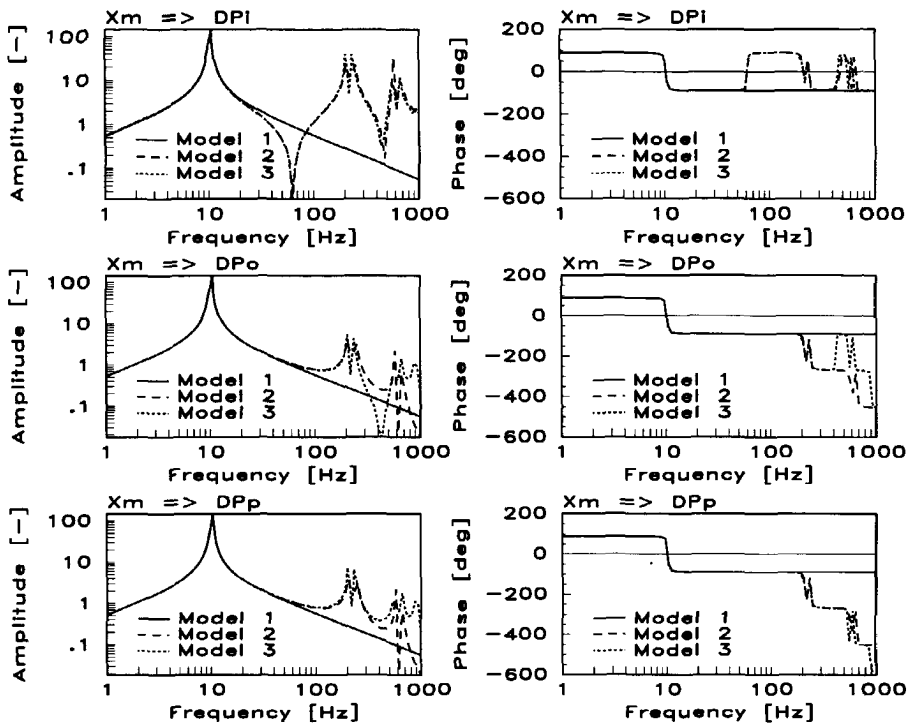


Fig. 2.36: Bode plots of pressure difference transfer functions for different simulation models: `Model 1`, `Model 2` and `Model 3` respectively. Input: $\bar{x}_m(s)$. Outputs: $\overline{\Delta P}_i(s)$ (upper); $\overline{\Delta P}_o(s)$ (middle); $\overline{\Delta P}_p(s)$ (lower)

Bode plots of the actuator model for $q = -0.5$ [m], $q = 0$ [m] and $q = 0.5$ [m] respectively. In this Figure, the pressure difference near the valve ΔP_i has been chosen as an example; similar results are obtained for the other pressure differences.

The upper Bode plots clearly show the variation of the basic natural frequency of the actuator due to varying actuator position. As expected, this effect is also present in `Model 2` and `Model 3`. However, not only the first resonance peak varies with actuator position, but also the resonance peaks due to the dynamics of the transmission lines. This is physically interpretable, as follows.

The actuator position determines the volume of the actuator chamber. If the chamber volume becomes large, the transmission line acts more or less as open line, and its resonance frequency will tend to the value represented by (2.72). On the other hand, if the chamber volume becomes small, the transmission line acts more or less as a blocked line, and its resonance frequency will tend to the value represented by (2.71). Note hereby, that for monotonously varying actuator position, the resonance frequency of one transmission line increases, while the other decreases. Actually, the phenomenon discussed here, clearly illustrates the effect of the bilateral coupling of the subsystems: the transmission line resonance frequencies are directly affected by the boundary conditions of the transmission line model, which are determined by the coupled models of the actuator chambers.

Comparison of the Bode plots of `Model 2` and `Model 3` in Fig. 2.37 once more confirms

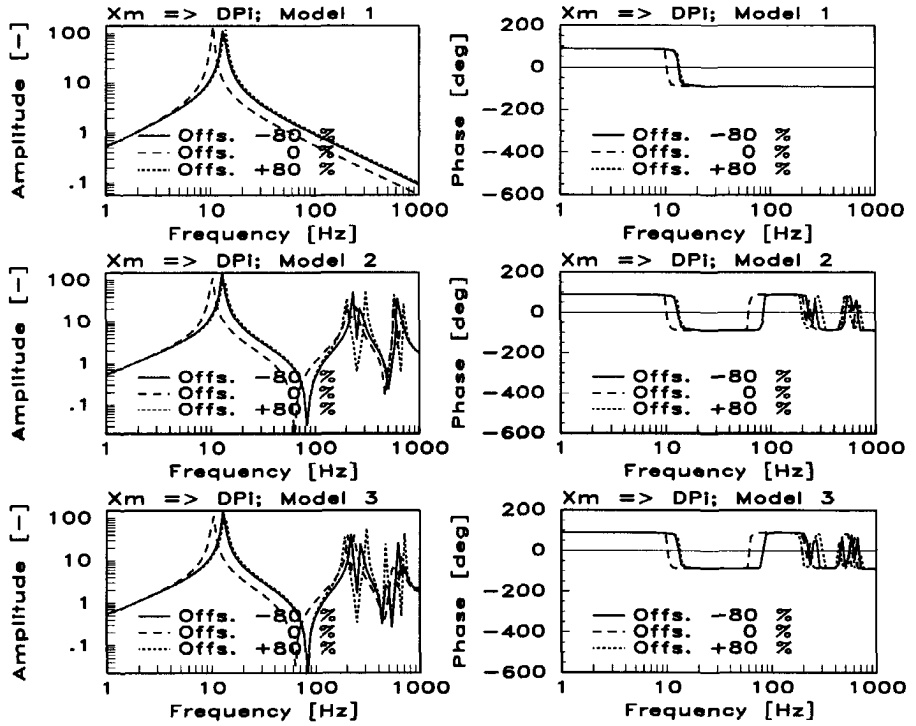


Fig. 2.37: Bode plots of pressure difference transfer functions from $\bar{x}_m(s)$ to $\overline{\Delta P}_i(s)$ for different actuator positions. `Model 1` (upper); `Model 2` (middle); `Model 3` (lower)

the conclusion, that the modelling of the actuator chambers as distributed parameter systems is not relevant. But the position dependence of the transmission line dynamics is not negligible.

2.4.6 Conclusion

If relatively long transmission lines are present between the servo-valve and the actuator chambers, transmission line dynamics may have to be taken into account. In this Section, the theoretical background of transmission line modelling has been discussed, providing insight in the underlying dynamic behaviour of the transmission lines. Thereby, different assumptions on damping due to (viscous) friction effects lead to different models of different complexity. Furthermore, it has been illustrated, that causality issues play a basic role in transmission line modelling, and impose restrictions on the input-output configurations of transmission line models.

For the inclusion of transmission line effects in the model of the hydraulic servo-system, a modular setup has been chosen, in which a single transmisson line is seen as a subsystem. The theoretical model of such a single transmisson line, which is of infinite order, is approximated by a modal approximation technique, adopted from Yang and Tobler [160], in which the physical structure of the model is preserved. The integrated model of the hydraulic

servo-system is obtained by proper bilateral coupling of the different subsystems.

Analysis of the resulting model for a modelling example, that reflects the servo-system considered in this thesis, shows that transmission lines between valve and actuator chambers introduce badly damped resonances in the high-frequency behaviour of the actuator. Especially when the pressure difference at the valve side of the transmission lines is considered, these dynamics are relevant, because the system shows no roll-off for high frequencies. Moreover, the location of the resonance peaks varies with the actuator position, implying non-linear behaviour.

Although it is theoretically plausible and possible to use a distributed parameter model for the actuator chambers of a long-stroke actuator, Bode plots of the considered simulation model show, that this is not necessary. The modelled dynamics are not relevant in the frequency range of interest.

With this conclusion, the first part of the Chapter, comprising the description of the theoretical modelling and the discussion of some simulation results, is completed. In the next part of the Chapter, the (relevant) dynamics of the hydraulic servo-system are analysed rather extensively, in order to be able to abstract the relevant dynamics and non-linearities of the system from the theoretical models. As discussed in Subsection 2.1.2, this is to be done in such a way, that the input-output behaviour of the model is directly related to the parameters in the physically structured model. In the next Section, the analysis of the dynamics of the system starts with considering the servo-valve dynamics.

2.5 Analysis of servo-valve dynamics

By means of linearization of the theoretical model of Section 2.2, a characterization of the *dynamic* behaviour of the servo-valve is obtained in the form of a linear state space model, Subsection 2.5.1. So the non-linearities are left out of consideration for a while; they will be considered again in Section 2.7.

The problem with the obtained linearized model is, that it is of high order and contains a lot of parameters, which makes it difficult to relate the dynamic input-output behaviour to the model parameters. This especially holds for the two-stage flapper-nozzle pilot-valve. Using physical insight, the linear model of the pilot-valve can be reduced and simplified, as described in Subsection 2.5.2. The simplified model of the pilot-valve can then be used to obtain a more condense characterization of the dynamics of the three-stage valve, as shown in Subsection 2.5.3.

2.5.1 Linearization of the theoretical model

Under a number of assumptions and for some point of operation, a linearized model of the servo-valve can be derived.

Linearization point and assumptions

As the servo-valve mainly operates in the null-region when it is controlling a hydraulic actuator, the linearization point is chosen to be the steady state equilibrium for zero reference input u_r. Because of the integrating character of the main spool, this corresponds to zero input $u = i_{ca}$ for the flapper-nozzle pilot-valve model, according to (2.22). Further

analysis of the theoretical model shows, that this input corresponds to an equilibrium, where $x_f = x_s = 0$, $P_{n1} = P_{n2} = 0.6$ and $P_{n3} = 0.15$ (compare Fig. 2.9).

Because the linearization is meant to abstract the dominant dynamics from the theoretical model, it is not desirable to take hard non-linearities into account, that strongly affect the steady state behaviour around the linearization point. Therefore, the following assumption is used.

Assumption 2.5.1 *For the derivation of a linearized model for the servo-valve it is assumed that:*

- *There is no ball clearance in the pilot-valve.*
- *The pilot-valve spool has no Coulomb friction.*
- *The pilot-valve spool is critically centred and has no radial clearance.*
- *The main spool is critically centred and has no radial clearance.*

Linearized model of the servo-valve

Linearization of the theoretical model equations of Section 2.2 is performed by writing them as Taylor expansions and neglecting the higher order terms. Referring to [152] for a detailed description of the linearization, the resulting linear dynamic model of the flapper-nozzle valve is given here in state space form:

$$\begin{bmatrix} \ddot{x}_f \\ \dot{x}_f \\ \ddot{x}_s \\ \dot{x}_s \\ \dot{P}_{n1} \\ \dot{P}_{n2} \\ \dot{P}_{n3} \end{bmatrix} = \begin{bmatrix} -\theta_1 & -\theta_2 & 0 & -\theta_3 & \theta_4 & -\theta_4 & 0 \\ 1 & 0 & 0 & 0 & 0 & 0 & 0 \\ 0 & -\theta_6 & -\theta_7 & -\theta_8 & -\theta_9 & \theta_9 & 0 \\ 0 & 0 & 1 & 0 & 0 & 0 & 0 \\ 0 & -\theta_{12} & \theta_{10} & 0 & -\theta_{11} & 0 & \theta_{13} \\ 0 & \theta_{12} & -\theta_{10} & 0 & 0 & -\theta_{11} & \theta_{13} \\ 0 & 0 & 0 & 0 & \theta_{14} & \theta_{14} & -\theta_{15} \end{bmatrix} \begin{bmatrix} \dot{x}_f \\ x_f \\ \dot{x}_s \\ x_s \\ P_{n1} \\ P_{n2} \\ P_{n3} \end{bmatrix} + \begin{bmatrix} \theta_5 \\ 0 \\ 0 \\ 0 \\ 0 \\ 0 \\ 0 \end{bmatrix} i_{ca} \tag{2.86}$$

$$x_s = \begin{bmatrix} 0 & 0 & 0 & 1 & 0 & 0 & 0 \end{bmatrix} \begin{bmatrix} \dot{x}_f & x_f & \dot{x}_s & x_s & P_{n1} & P_{n2} & P_{n3} \end{bmatrix}^T$$

Obviously, the model (2.86) is physically structured, with 7 physical quantities as states. The parameters $\theta_1, \ldots, \theta_{15}$ have a known physical interpretation, such that they are all positive.

As output of the linearized flapper-nozzle valve model, the spool position x_s has been chosen. The reason is, that due to Assumption 2.5.1, the linearization of the pilot-valve flow equations (2.16) and (2.17) just leads to a linear algebraic relation between Φ_m and the spool position x_s. So the output of the pilot-valve model is easily related to the main spool velocity by rewriting (2.20) as:

$$\dot{x}_m = \theta_{16} x_s \tag{2.87}$$

With the feedback law (2.22) being rewritten as:

$$i_{ca} = \theta_{17} u_r - \theta_{18} x_m$$

and linearizing (2.23) and (2.24) to $\Phi_p = \theta_{19} x_m$, the linearized model of the three-stage valve becomes:

$$\begin{bmatrix} \ddot{x}_f \\ \dot{x}_f \\ \ddot{x}_s \\ \dot{x}_s \\ \dot{P}_{n1} \\ \dot{P}_{n2} \\ \dot{P}_{n3} \\ \dot{x}_m \end{bmatrix} = \begin{bmatrix} -\theta_1 & -\theta_2 & 0 & -\theta_3 & \theta_4 & -\theta_4 & 0 & -\theta_5\theta_{18} \\ 1 & 0 & 0 & 0 & 0 & 0 & 0 & 0 \\ 0 & -\theta_6 & -\theta_7 & -\theta_8 & -\theta_9 & \theta_9 & 0 & 0 \\ 0 & 0 & 1 & 0 & 0 & 0 & 0 & 0 \\ 0 & -\theta_{12} & \theta_{10} & 0 & -\theta_{11} & 0 & \theta_{13} & 0 \\ 0 & \theta_{12} & -\theta_{10} & 0 & 0 & -\theta_{11} & \theta_{13} & 0 \\ 0 & 0 & 0 & 0 & \theta_{14} & \theta_{14} & -\theta_{15} & 0 \\ 0 & 0 & 0 & \theta_{16} & 0 & 0 & 0 & 0 \end{bmatrix} \begin{bmatrix} \dot{x}_f \\ x_f \\ \dot{x}_s \\ x_s \\ P_{n1} \\ P_{n2} \\ P_{n3} \\ x_m \end{bmatrix} + \begin{bmatrix} \theta_5\theta_{17} \\ 0 \\ 0 \\ 0 \\ 0 \\ 0 \\ 0 \\ 0 \end{bmatrix} u_r$$

$$\Phi_p = \begin{bmatrix} 0 & 0 & 0 & 0 & 0 & 0 & 0 & \theta_{19} \end{bmatrix} \begin{bmatrix} \dot{x}_f & x_f & \dot{x}_s & x_s & P_{n1} & P_{n2} & P_{n3} & x_m \end{bmatrix}^T \tag{2.88}$$

Although this model allows systematic analysis, the number of parameters is large, and the relation between model parameters and dominant dynamics is not easily found. Therefore, the model is further simplified in the subsequent Sections.

2.5.2 Physically argued reduction and simplification of the model of the flapper-nozzle valve

In practice, the dynamics of a flapper-nozzle valve can be described with models of lower order than (2.86). For instance, the simulations presented in Subsection 2.2.5, Fig. 2.17 and 2.18, show a badly damped oscillation superponed to a first or second order response. Thayer even proposes a very simple third order linear model for the flapper-nozzle valve [135]. So, appearantly the same dominant dynamics can be modelled by a reduced order model with less parameters. In order to be able to include non-linearities again later on, the model reduction is performed on a physical basis, such that the physical interpretation of the model (2.86) is preserved.

Controllability of the pressures

It can be noted from the model structure of (2.86), that regarding the nozzle pressures P_{n1}, P_{n2} and the outlet pressure P_{n3}, only the nozzle pressure difference $\Delta P_n = P_{n1} - P_{n2}$ can be controlled. Because of the symmetry in the fifth and the sixth state equations of (2.86), the mean nozzle pressure $P_n = (P_{n1} + P_{n2})/2$ and the outlet pressure P_{n3} are uncontrollable (compare Fig. 2.9). Therefore, the last three rows of the state equation of (2.86) can be replaced by a single dynamic equation for ΔP_n, namely:

$$\dot{\Delta P_n} = -2\,\theta_{12} x_f + 2\,\theta_{10} \dot{x}_s - \theta_{11} \Delta P_n \tag{2.89}$$

This simplification reduces the model with two orders to the following fifth order model:

$$\begin{bmatrix} \ddot{x}_f \\ \dot{x}_f \\ \ddot{x}_s \\ \dot{x}_s \\ \Delta\dot{P}_n \end{bmatrix} = \begin{bmatrix} -\theta_1 & -\theta_2 & 0 & -\theta_3 & \theta_4 \\ 1 & 0 & 0 & 0 & 0 \\ 0 & -\theta_6 & -\theta_7 & -\theta_8 & -\theta_9 \\ 0 & 0 & 1 & 0 & 0 \\ 0 & -2\,\theta_{12} & 2\,\theta_{10} & 0 & -\theta_{11} \end{bmatrix} \begin{bmatrix} \dot{x}_f \\ x_f \\ \dot{x}_s \\ x_s \\ \Delta P_n \end{bmatrix} + \begin{bmatrix} \theta_5 \\ 0 \\ 0 \\ 0 \\ 0 \end{bmatrix} i_{ca} \qquad (2.90)$$

$$x_s = \begin{bmatrix} 0 & 0 & 0 & 1 & 0 \end{bmatrix} \begin{bmatrix} \dot{x}_f & x_f & \dot{x}_s & x_s & \Delta P_n \end{bmatrix}^T$$

The model can be further reduced by doing some physical assumptions. Depending on the assumptions, three alternative low-order models for the flapper-nozzle valve are obtained.

Three alternative models for the flapper-nozzle valve

For three alternative assumptions, the correspondingly resulting simplified models are derived below.

Assumption 2.5.2 *The spool mass M_s is negligible (zero).*

Although in literature [74, 81] the acceleration forces are taken into account in the force balance of the spool (2.12), analysis of the model (2.90) using the parameters of Table F.1 shows, that the pole related to these forces lies far beyond 1 [kHz]. Thus, the first order differential equation described by the third row of (2.90) can be reduced to an algebraic equation, from which the spool velocity can be solved:

$$\dot{x}_s = -\frac{\theta_6}{\theta_7} x_f - \frac{\theta_8}{\theta_7} x_s - \frac{\theta_9}{\theta_7} \Delta P_n \qquad (2.91)$$

With this expression for $\dot{x}_s$, the equation for ΔP_n (2.89) can be written as:

$$\Delta\dot{P}_n = \left(-2\,\theta_{12} - 2\,\theta_{10}\,\frac{\theta_6}{\theta_7}\right) x_f + \left(-2\,\theta_{10}\,\frac{\theta_8}{\theta_7}\right) x_s + \left(-\theta_{11} - 2\,\theta_{10}\,\frac{\theta_9}{\theta_7}\right) \Delta P_n \qquad (2.92)$$

Using these equations, the reduced model of the flapper-nozzle valve becomes:

$$\begin{bmatrix} \ddot{x}_f \\ \dot{x}_f \\ \dot{x}_s \\ \Delta\dot{P}_n \end{bmatrix} = \begin{bmatrix} -\theta_1 & -\theta_2 & -\theta_3 & \theta_4 \\ 1 & 0 & 0 & 0 \\ 0 & -\frac{\theta_6}{\theta_7} & -\frac{\theta_8}{\theta_7} & -\frac{\theta_9}{\theta_7} \\ 0 & -2\,\frac{(\theta_7\theta_{12}+\theta_6\theta_{10})}{\theta_7} & -2\,\frac{\theta_{10}\theta_8}{\theta_7} & -\frac{(\theta_7\theta_{11}+2\,\theta_9\theta_{10})}{\theta_7} \end{bmatrix} \begin{bmatrix} \dot{x}_f \\ x_f \\ x_s \\ \Delta P_n \end{bmatrix} + \begin{bmatrix} \theta_5 \\ 0 \\ 0 \\ 0 \end{bmatrix} i_{ca}$$

$$x_s = \begin{bmatrix} 0 & 0 & 1 & 0 \end{bmatrix} \begin{bmatrix} \dot{x}_f & x_f & x_s & \Delta P_n \end{bmatrix}^T \qquad (2.93)$$

Given the fact that the parameters θ_i, $i = 1, \ldots, 15$ are positive because of their physical background, the transfer function $\frac{x_s(s)}{i_{ca}(s)}$ of this model has one transmission zero in the right half plane and four stable poles.

Depending on the type of flapper-nozzle valve, this fourth order model may even be to complex to describe the dominant dynamics. In that case, a stronger assumption may be done.

Assumption 2.5.3 *The spool mass M_s and viscous friction w_s are negligible (zero).*

As can be seen from (2.90), the assumption that the viscous friction can be neglected corresponds to assuming that θ_7 is zero. Thus, the force balance, leading to (2.91) when neglecting the spool mass, now leads to an algebraic expression, which relates the pressure difference directly to a linear combination of spool and flapper displacement:

$$\Delta P_n = -\frac{\theta_6}{\theta_9} x_f - \frac{\theta_8}{\theta_9} x_s \tag{2.94}$$

Differentiating (2.94) and successively substituting the obtained expressions for ΔP_n and $\dot{\Delta P}_n$ in (2.89) gives a new equation for the spool velocity:

$$\dot{x}_s = -\frac{\theta_6}{(2\,\theta_9\theta_{10} + \theta_8)} \dot{x}_f + \frac{(2\,\theta_9\theta_{12} - \theta_6\theta_{11})}{(2\,\theta_9\theta_{10} + \theta_8)} x_f - \frac{\theta_8\theta_{11}}{(2\,\theta_9\theta_{10} + \theta_8)} x_s \tag{2.95}$$

Furthermore substituting (2.94) in the equation of motion of the flapper (the first row of the state equation in (2.90)), the pressure difference is completely eleminated from the model, and the following third order model is obtained:

$$\begin{aligned} \begin{bmatrix} \ddot{x}_f \\ \dot{x}_f \\ \dot{x}_s \end{bmatrix} &= \begin{bmatrix} -\theta_1 & -\frac{(\theta_2\theta_9 + \theta_4\theta_6)}{\theta_9} & -\frac{(\theta_3\theta_9 + \theta_4\theta_8)}{\theta_9} \\ 1 & 0 & 0 \\ -\frac{\theta_6}{(2\,\theta_9\theta_{10} + \theta_8)} & \frac{(2\,\theta_9\theta_{12} - \theta_6\theta_{11})}{(2\,\theta_9\theta_{10} + \theta_8)} & -\frac{\theta_8\theta_{11}}{(2\,\theta_9\theta_{10} + \theta_8)} \end{bmatrix} \begin{bmatrix} \dot{x}_f \\ x_f \\ x_s \end{bmatrix} + \begin{bmatrix} \theta_5 \\ 0 \\ 0 \end{bmatrix} i_{ca} \\ x_s &= \begin{bmatrix} 0 & 0 & 1 \end{bmatrix} \begin{bmatrix} \dot{x}_f & x_f & x_s \end{bmatrix}^T \end{aligned} \tag{2.96}$$

Like the fourth order model corresponding to Assumption 2.5.2, the transfer function $\frac{x_s(s)}{i_{ca}(s)}$ of this third order model corresponding to Assumption 2.5.3 has a transmission zero in the right half plane. In fact, this rhp-zero is typical for the assumption that the inertial forces of the spool can be neglected, while the oil is assumed to be compressible. The physical interpretation is, that due to the stiffness of the feedback spring the spool initially moves in the same direction as the flapper, which means a negative spool displacement for a positive flapper displacement, see Fig. 2.3. This is possible, because the pressure difference is not instantaneously counteracting the feedback spring force; the pressure difference only responds on the flapper displacement with first order dynamics due to the compressibility of the oil.

For clarity, it should be noted here, that elimination of the pressure difference ΔP_n as state variable from the model, does not mean that the compressibility of the oil is neglected. Actually, the model (2.96) could have been written with the pressure difference ΔP_n as a state variable instead of x_s, and then using (2.94) to write the output x_s as linear combination of the state variables.

Although the compressibility of the oil is principal in the dynamic behaviour of hydraulic servo-systems, it might be argued for the servo-valve, that the volumes are so small, that the compressibility effect can be neglected. So, if the desired model order is three, one might think of assuming the oil to be incompressible instead of assuming the viscous friction to be zero.

Assumption 2.5.4 *The spool mass M_s is negligible (zero), and the oil is incompressible ($E = \infty$).*

Neglecting the oil compressibility is equal to changing the dynamic expression (2.89) into the static (flow) balance, which relates the pressure difference to the flapper displacement and the spool velocity as:

$$\Delta P_n = -2\frac{\theta_{12}}{\theta_{11}}x_f + 2\frac{\theta_{10}}{\theta_{11}}\dot{x}_s \tag{2.97}$$

Combining this equation with the force balance for the spool (2.91), eliminating the spool velocity x_s, ΔP_n can also be written as a linear combination of the flapper and the spool position:

$$\Delta P_n = -2\frac{(\theta_7\theta_{12} + \theta_6\theta_{10})}{(2\,\theta_9\theta_{10} + \theta_7\theta_{11})}x_f - \frac{2\,\theta_8\theta_{10}}{(2\,\theta_9\theta_{10} + \theta_7\theta_{11})}x_s \tag{2.98}$$

Similarly combining (2.97) and (2.91) and solving for the spool velocity $\dot{x}_s$, while eliminating ΔP_n, gives:

$$\dot{x}_s = \frac{(2\,\theta_9\theta_{12} - \theta_6\theta_{11})}{(2\,\theta_9\theta_{10} + \theta_7\theta_{11})}x_f - \frac{\theta_8\theta_{11}}{(2\,\theta_9\theta_{10} + \theta_7\theta_{11})}x_s \tag{2.99}$$

Finally substituting (2.98) in the equation of motion of the flapper (the first row of the state equation in (2.90)) and using (2.99) as dynamic equation for the spool position, the following third order model is obtained:

$$\begin{bmatrix} \ddot{x}_f \\ \dot{x}_f \\ \dot{x}_s \end{bmatrix} = \begin{bmatrix} -\theta_1 & -\left(\theta_2 + \theta_4\frac{2(\theta_7\theta_{12}+\theta_6\theta_{10})}{(2\,\theta_9\theta_{10}+\theta_7\theta_{11})}\right) & -\left(\theta_3 + \theta_4\frac{2\,\theta_8\theta_{10}}{(2\,\theta_9\theta_{10}+\theta_7\theta_{11})}\right) \\ 1 & 0 & 0 \\ 0 & \frac{(2\,\theta_9\theta_{12}-\theta_6\theta_{11})}{(2\,\theta_9\theta_{10}+\theta_7\theta_{11})} & -\frac{\theta_8\theta_{11}}{(2\,\theta_9\theta_{10}+\theta_7\theta_{11})} \end{bmatrix} \begin{bmatrix} \dot{x}_f \\ x_f \\ x_s \end{bmatrix} + \begin{bmatrix} \theta_5 \\ 0 \\ 0 \end{bmatrix} i_{ca}$$

$$x_s = \begin{bmatrix} 0 & 0 & 1 \end{bmatrix} \begin{bmatrix} \dot{x}_f & x_f & x_s \end{bmatrix}^T \tag{2.100}$$

Analysis of this model shows, that the input-output transfer function $\frac{x_s(s)}{i_{ca}(s)}$ has no transmission zeros. The model just describes coupling of the second order flapper dynamics with the first order spool dynamics via the static flow balance and the feedback spring force. This confirms the earlier interpretation of the rhp-zero being introduced by the compressibility of oil.

For all three reduced order linear models of the flapper-nozzle valve, given in equations (2.93), (2.96) and (2.100) respectively, the number of physical parameters $\theta_1, \ldots, \theta_{12}$ is much larger than the number of parameters actually required to describe the dynamics of the model: the number of poles plus the number of zeros plus one parameter for the static gain. Furthermore, the parameter combinations are very complex; although the relation between the physical interpretation of the parameters and the dynamics of the model is present, the insight in this relation is more or less lost.

For practical use of the models, for instance for parameter identification (see Subsection 3.2.3 and Subsection 3.4.2), it is desirable to describe the same dynamics with a **minimum number of parameters**[3]. For each of the three alternative models for the flapper-nozzle valve, this can be done by means of a scaling of the state vector and a replacement of the comlex parameter combinations by simple parameters. As the procedure is similar for all three models, it is only worked out for one model below; the model given in (2.93) according to Assumption 2.5.2 is chosen as an example because it is used later on.

[3]This refers to the concept of identifiability of the parameters, a topic which is discussed in more detail in Subsection 3.2.3 on page 137.

Scaling of the state

Any state space model can be written with a minimum number of parameters by transforming it to a canonical form by means of a state transformation [26]. However, because some physical non-linearities of the theoretical model are to be included in the model (see Subsection 2.7.2), the physical interpretation of the states has to be preserved. Therefore, the transformation is restricted to a *diagonal* state transformation, i.e. a scaling of the state vector. This scaling is chosen such, that it normalizes the lower diagonal elements of the A-matrix of (2.93). Together with an input-output scaling normalizing the steady state gain,

$$\bar{x}_s = \frac{x_s}{x_{s,max}} \qquad \bar{i}_{ca} = \frac{i_{ca}}{i_{max}}$$

the following scaling of the state:

$$\begin{bmatrix} \dot{\tilde{x}}_f \\ \tilde{x}_f \\ \tilde{x}_s \\ \widetilde{\Delta P}_n \end{bmatrix} = \text{diag}\left[-\frac{\theta_7}{\theta_6 x_{s,max}} \quad -\frac{\theta_7}{\theta_6 x_{s,max}} \quad \frac{1}{x_{s,max}} \quad -\frac{2\,\theta_8\theta_{10}}{\theta_7 x_{s,max}} \right] \begin{bmatrix} \dot{x}_f \\ x_f \\ x_s \\ \Delta P_n \end{bmatrix}$$

results in the final reduced order linear model for the flapper-nozzle valve under Assumption 2.5.2:

$$\begin{bmatrix} \ddot{\tilde{x}}_f \\ \dot{\tilde{x}}_f \\ \dot{\tilde{x}}_s \\ \widetilde{\Delta P}_n \end{bmatrix} = \begin{bmatrix} -c_1 & -c_2 & c_3 & c_4 \\ 1 & 0 & 0 & 0 \\ 0 & 1 & -c_5 & c_6 \\ 0 & -c_7 & 1 & -c_8 \end{bmatrix} \begin{bmatrix} \dot{\tilde{x}}_f \\ \tilde{x}_f \\ \tilde{x}_s \\ \widetilde{\Delta P}_n \end{bmatrix} + \begin{bmatrix} -c_9 \\ 0 \\ 0 \\ 0 \end{bmatrix} \bar{i}_{ca} \qquad (2.101)$$

$$\bar{x}_s = \begin{bmatrix} 0 & 0 & 1 & 0 \end{bmatrix} \begin{bmatrix} \dot{\tilde{x}}_f & \tilde{x}_f & \tilde{x}_s & \widetilde{\Delta P}_n \end{bmatrix}^T$$

Note, that the parameters $c_1, \ldots, c_9$ still have a physical interpretation, such that they are all positive. A graphical representation of the model structure is given in Fig. 2.38.

Using physical insight and physically argued assumptions, the linearized flapper-nozzle model (2.90) has been simplified and reduced to a fourth order model (2.101). As such, the model is suitable to use as pilot-valve model in a simplified model for the three-stage servo-valve.

2.5.3 Simplified servo-valve model

Looking at the linearized model of the three-stage valve (2.88), it is clear that the model complexity mainly originates from the pilot-valve model. With this latter model being simplified in the previous Section, a simplified model with a minimum number of parameters for the three-stage valve is easily derived. Thereby, some parameters are combined, while normalization of the inputs and outputs also reduces the number of parameters.

Normalization of the main spool position x_m with respect to its maximum $x_{m,max}$, like in Subsection 2.2.5, and using it as a new scaled state variable, leads to a new expression for (2.87), the main spool integrator equation:

$$\dot{\tilde{x}}_m = \dot{\bar{x}}_m = c_{10}\,\bar{x}_s = c_{10}\,\tilde{x}_s \qquad (2.102)$$

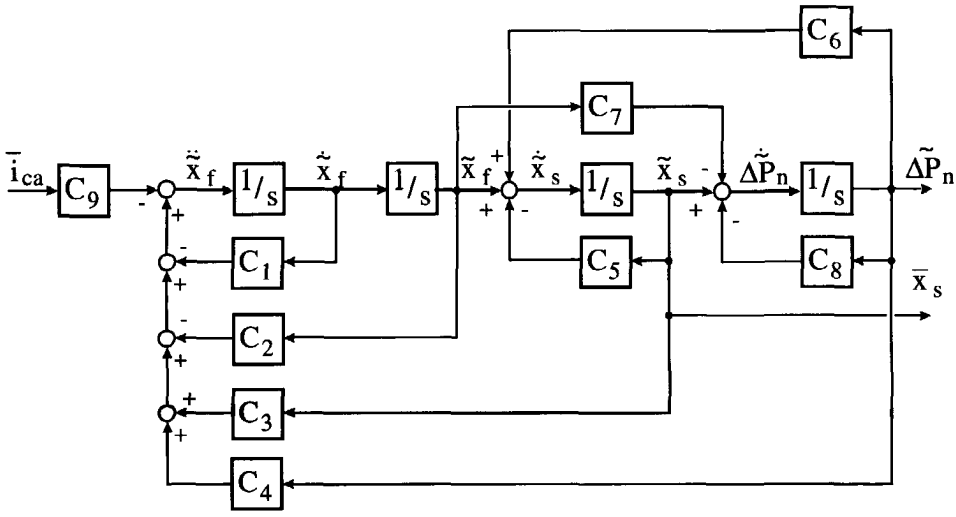


Fig. 2.38: Block scheme linear model flapper-nozzle valve

Also normalizing the flow Φ_p with respect to its maximum $\Phi_{p,nom}$, the parameter θ_{19} in the output equation of (2.88) is eliminated, because $\bar{\Phi}_p = \bar{x}_m$. Finally normalizing the input u_r and scaling the feedback gain K_{pm} correspondingly, the feedback law (2.22) can be rewritten once more as:

$$\bar{i}_{ca} = \bar{K}_{pm}\,(\bar{u}_r - \bar{x}_m) \tag{2.103}$$

In this way, using (2.101), the following simplified three-stage valve model results:

$$\begin{bmatrix} \dddot{\tilde{x}}_f \\ \ddot{\tilde{x}}_f \\ \dot{\tilde{x}}_s \\ \dot{\widetilde{\Delta P}}_n \\ \dot{\tilde{x}}_m \end{bmatrix} = \begin{bmatrix} -c_1 & -c_2 & c_3 & c_4 & c_9\bar{K}_{pm} \\ 1 & 0 & 0 & 0 & 0 \\ 0 & 1 & -c_5 & c_6 & 0 \\ 0 & -c_7 & 1 & -c_8 & 0 \\ 0 & 0 & c_{10} & 0 & 0 \end{bmatrix} \begin{bmatrix} \ddot{\tilde{x}}_f \\ \dot{\tilde{x}}_f \\ \tilde{x}_s \\ \widetilde{\Delta P}_n \\ \tilde{x}_m \end{bmatrix} + \begin{bmatrix} -c_9\bar{K}_{pm} \\ 0 \\ 0 \\ 0 \\ 0 \end{bmatrix} \bar{i}_{ca}$$

$$\bar{\Phi}_p = \bar{x}_m = \begin{bmatrix} 0 & 0 & 0 & 0 & 1 \end{bmatrix} \begin{bmatrix} \ddot{\tilde{x}}_f & \dot{\tilde{x}}_f & \tilde{x}_s & \widetilde{\Delta P}_n & \tilde{x}_m \end{bmatrix}^T \tag{2.104}$$

Analyzing this fifth order model, it becomes clear that it contains the same rhp-zero as the pilot-valve model. This means, that the input-output transfer function $\frac{\bar{x}_m(s)}{\bar{u}_r(s)}$ shows non-minimum-phase behaviour.

Comparing the servo-valve model to the initial linearized model (2.88), the number of parameters has been drastically reduced; only 10 parameters $c_1, \ldots, c_{10}$ need to be determined, for instance by means of identification. Nevertheless, the states of the model still have a direct physical interpretation, which provides the possibility to include non-linearities of the theoretical model within the linear model structure, that describes the dynamic behaviour of the valve.

In order to obtain insight in the dynamics of the complete hydraulic servo-system, the procedure of deriving a simple linear model describing the relevant dynamics of the theoretical model will also have to be applied to the hydraulic actuator.

2.6 Analysis of actuator and transmission line dynamics

The dynamic behaviour of a hydraulic actuator can be abstracted from the theoretical model by means of linearization of the basic actuator model, as described in Subsection 2.6.1. Further reduction and simplification in Subsection 2.6.2 clearly illustrates the basic dynamic properties of the actuator. How the transmission line dynamics can be included in the linear actuator model, such that a compact linear dynamic model of the actuator with transmission lines is obtained, is discussed in Subsection 2.6.3.

2.6.1 Linearization of the theoretical actuator model

Under some assumptions and for some point of operation, a linearized model of the hydraulic actuator can be derived.

Linearization point and assumptions

The linearization point for the actuator is commonly chosen as the equilibrium state for zero valve spool position $x_m = 0$ and some initial actuator position $q = q_0$ [139]. The reason is, that in many applications the hydraulic actuator serves as position servo-system, where the valve operates in its null-region. Although the dynamic effect of external forces on the actuator behaviour is to be taken into account, the linearization is performed for zero external force $F_{ext} = 0$.

In Subsection 2.3.5, the effects of the non-linearities of the actuator model have been investigated rather extensively. Based on the insight obtained that way, and taking into account that the linearization is meant to abstract the dominant dynamics from the theoretical model, the following set of assumptions is justified.

Assumption 2.6.1 *For the derivation of a linearized actuator model it is assumed that:*

- *The actuator flows are equal, so $\Phi_{p1} = \Phi_{p2} = \Phi_p$. The actuator flow Φ_p is taken as input, and is assumed to be just linearly dependent on the main spool position x_m (compare Assumption 2.5.1).*
- *The actuator leakages can be described by:*

$$\Phi_{l1} = -\Phi_{l2} = \Phi_{lp} = LP_p\,(P_{p1} - P_{p2})$$

This means that the leakage flows (due to hydrostatic bearings) do not affect the steady state velocity for zero load pressure ΔP_p, and that they do not affect the steady state cylinder pressures. In other words, the left plot of Fig. 2.24 is flat, but inclined in y-direction; the right plot is flat and horizontal.

- *The actuator piston has no Coulomb friction, and the friction forces can be described by:*

$$F_{vp} = w_p \dot{q}$$

Linearized model of the hydraulic actuator

Because the linearized dynamic model of the actuator will be used for control design (Chapter 4), which also includes disturbance rejection, not only the controlled input Φ_p is chosen as input, but also the disturbance input F_{ext}. Furthermore, it is common that besides the piston position q, also the actuator pressure difference ΔP_p is measured, so they are chosen as model outputs. Herewith, linearization of the theoretical model of the actuator given in Subsection 2.3.4, under Assumption 2.6.1, results in the following state space description:

$$\begin{bmatrix} \ddot{q} \\ \dot{q} \\ \dot{P}_{p1} \\ \dot{P}_{p2} \end{bmatrix} = \begin{bmatrix} -\frac{w_p}{M_p} & 0 & \frac{A_p}{M_p} & -\frac{A_p}{M_p} \\ 1 & 0 & 0 & 0 \\ -\frac{EA_p}{V_{ac1}} & 0 & -\frac{ELP_p}{V_{ac1}} & \frac{ELP_p}{V_{ac1}} \\ \frac{EA_p}{V_{ac2}} & 0 & \frac{ELP_p}{V_{ac2}} & -\frac{ELP_p}{V_{ac2}} \end{bmatrix} \begin{bmatrix} \dot{q} \\ q \\ P_{p1} \\ P_{p2} \end{bmatrix} + \begin{bmatrix} 0 & \frac{1}{M_p} \\ 0 & 0 \\ \frac{E}{V_{ac1}} & 0 \\ -\frac{E}{V_{ac2}} & 0 \end{bmatrix} \begin{bmatrix} \Phi_p \\ F_{ext} \end{bmatrix}$$
$$\begin{bmatrix} q \\ \Delta P_p \end{bmatrix} = \begin{bmatrix} 0 & 1 & 0 & 0 \\ 0 & 0 & 1 & -1 \end{bmatrix} \begin{bmatrix} \dot{q} & q & P_{p1} & P_{p2} \end{bmatrix}^T \tag{2.105}$$

with:

$$\begin{aligned} V_{ac1} &= A_p(q_{max} + q_0) + V_{ls1} \\ V_{ac2} &= A_p(q_{max} - q_0) + V_{ls2} \end{aligned} \tag{2.106}$$

Clearly, the resulting model depends on the linearization position q_0. This explains why the natural frequency of the actuator depends on the actuator position.

Although the linearized model has a transparant structure, there are still 8 physical parameters required to describe the dynamics. In order to obtain a more direct relation between the parameters and the dynamics of the model, among others for identification purposes, the actuator model is further simplified.

2.6.2 Physically argued simplification and reduction of the actuator model

The number of parameters of the linearized actuator model can be reduced by a proper scaling of the model variables. Further analysis of the model structure and physical insight suggest a reduction of the model to third order, which is in most cases sufficient to describe the dominant dynamics of the actuator [1, 19, 52, 124, 139].

Scaling of the state variables

Using the normalizations of the pressures, the input flow and the external force with respect to the supply pressure P_s, the maximum flow $\Phi_{p,nom}$ and the maximum actuator

force $F_{p,max}$ respectively, the linearized model reads:

$$\begin{bmatrix} \ddot{q} \\ \dot{q} \\ \dot{\bar{P}}_{p1} \\ \dot{\bar{P}}_{p2} \end{bmatrix} = \begin{bmatrix} -\zeta_1 & 0 & \zeta_2 & -\zeta_2 \\ 1 & 0 & 0 & 0 \\ -\zeta_3\zeta_5 & 0 & -\zeta_4\zeta_5 & \zeta_4\zeta_5 \\ \zeta_3\zeta_6 & 0 & \zeta_4\zeta_6 & -\zeta_4\zeta_6 \end{bmatrix} \begin{bmatrix} \dot{q} \\ q \\ \bar{P}_{p1} \\ \bar{P}_{p2} \end{bmatrix} + \begin{bmatrix} 0 & \zeta_2 \\ 0 & 0 \\ \zeta_5 & 0 \\ -\zeta_6 & 0 \end{bmatrix} \begin{bmatrix} \bar{\Phi}_p \\ \bar{F}_{ext} \end{bmatrix}$$
$$\begin{bmatrix} q \\ \overline{\Delta P}_p \end{bmatrix} = \begin{bmatrix} 0 & 1 & 0 & 0 \\ 0 & 0 & 1 & -1 \end{bmatrix} \begin{bmatrix} \dot{q} & q & \bar{P}_{p1} & \bar{P}_{p2} \end{bmatrix}^T \tag{2.107}$$

Note that the parameters ζ_5, ζ_6 in this model are position dependent. In general, they will be different, but for certain position q_0 they will be equal, namely if $V_{ac1} = V_{ac2}$ in (2.106). In that special case, the state equations for the actuator pressures are completely symmetric.

Controllability of the pressures

Like for the nozzle pressures of the flapper-nozzle valve, the symmetry in the state equations for the actuator pressures $\bar{P}_{p1}$, $\bar{P}_{p2}$ in the actuator model shows, that only the actuator pressure difference $\overline{\Delta P}_p = \bar{P}_{p1} - \bar{P}_{p2}$ can be controlled. The mean actuator pressure $\bar{P}_p = (\bar{P}_{p1} + \bar{P}_{p2})/2$ is uncontrollable. This is also physically interpretable: for symmetric servo-valve flows, the flow into the one actuator chamber equals the flow out of the other chamber. With (almost) symmetric stiffness of the oil in the actuator chambers, this means that the pressure rise in the one chamber equals the pressure drop in the other, so that the mean pressure remains unchanged.

Theoretically, the pole related to the dynamics of the mean pressure in the actuator model (2.107) is only uncontrollable if $\zeta_5 = \zeta_6$. However, if ζ_5 and ζ_6 are close to each other, which is often the case in the normal working range of a (symmetric) actuator, the mean pressure $\bar{P}_p$ is hardly controllable, and at least unobservable with the output matrix of (2.107). This generally justifies the reduction of the model to the following third order actuator model:

$$\begin{bmatrix} \ddot{q} \\ \dot{q} \\ \dot{\overline{\Delta P}}_p \end{bmatrix} = \begin{bmatrix} -\zeta_1 & 0 & \zeta_2 \\ 1 & 0 & 0 \\ -\zeta_3(\zeta_5+\zeta_6) & 0 & -\zeta_4(\zeta_5+\zeta_6) \end{bmatrix} \begin{bmatrix} \dot{q} \\ q \\ \overline{\Delta P}_p \end{bmatrix} + \begin{bmatrix} 0 & \zeta_2 \\ 0 & 0 \\ (\zeta_5+\zeta_6) & 0 \end{bmatrix} \begin{bmatrix} \bar{\Phi}_p \\ \bar{F}_{ext} \end{bmatrix}$$
$$\begin{bmatrix} q \\ \overline{\Delta P}_p \end{bmatrix} = \begin{bmatrix} 0 & 1 & 0 \\ 0 & 0 & 1 \end{bmatrix} \begin{bmatrix} \dot{q} & q & \overline{\Delta P}_p \end{bmatrix}^T \tag{2.108}$$

This model structure is the most compact state space description of the dominant actuator dynamics, with physical quantities constituting the model state. The model has three poles, of which one lies in 0, representing the integrating behaviour of the actuator. The steady state gain of this integrator is determined by the velocity gain (ζ_3). The two other poles form a complex pair. The corresponding natural frequency is determined by the load mass (ζ_2) and the stiffnes of the oil compartments, which is position dependent ($\zeta_5 + \zeta_6$). The damping of the resonance frequency is determined by the viscous friction (ζ_1) and the leakage (ζ_4).

With (2.108) the desired simplified model for the hydraulic actuator is available, which directly relates its parameters to the dominant dynamics of the system. In most cases, this model will be sufficient to describe the dynamics of a hydraulic actuator driving a stiff inertial load. If the load is not stiff, but constituted by some flexible mechanical system, the model will have to be extended with some states, describing the dynamics of the load. This is rather straight-forward, and falls beyond the scope of this thesis.

Another reason why the model (2.108) may be too simple, is the presence of transmission line dynamics, constituting part of the dominant actuator dynamics. In that case, inclusion of transmission line models in the (linearized) actuator model is required.

2.6.3 Inclusion of transmission line dynamics

In order to have a minimum number of parameters describing the dynamics introduced by the transmission lines, it is useful to analyse and rewrite the modal approximation of the transmission line dynamics first. After that, a complete linear dynamic model of the hydraulic actuator is easily obtained by integrating the transmission line models and the actuator model.

Simplified dynamic model of one transmission line

In order to obtain insight in the actuator dynamics when including transmission line dynamics, especially with respect to the position dependence, it is important to preserve the physical structure of the model. This makes the modal approximation of the dynamics of one transmission line, as described in Subsection 2.4.3 and given by (2.68), (2.70) and (2.71), quite useful for inclusion in the complete dynamic actuator model, because this modal approximation is physically structured.

Although it is easy to calculate the (theoretical) values of the coefficients of the transmission line model, it is not exactly clear how the model parameters can be related to the input-output behaviour of the model. Especially for identification purposes (Chapter 3), the latter is important. Analysis of the transmission line model (2.68) shows, that its input-output behaviour is principally characterized by six independent parameters:

- *A steady state gain.* Because the model (2.68) is not corrected for its steady state gain, there is one independent parameter which determines the steady state gain of the diagonal elements of the transfer function matrix.
- *A characteristic impedance parameter.* This parameter represents the static gain which relates flow to pressure and vice versa. It actually determines the gain of the non-diagonal elements of the transfer function matrix with respect to the gain of the diagonal elements.
- *Two resonance frequencies.* Although these frequencies are theoretically coupled as integer multiples of the base harmonic frequency, they may be modelled as independent parameters, because of the frequency dependency, which is brought into account by the frequency modification factors α_{ci} in (2.68).
- *Two damping coefficients.* These damping coefficients correspond to the resonance frequencies, and may also be modelled indepently because of the frequency dependency, which is brought into account by the damping modification factors β_{ci} in (2.68).

While applying a normalization of the pressures and flows as before, and using the above characteristics of the transmission line behaviour, the modal approximation of the transmission line model can be rewritten as:

$$\begin{bmatrix} \dot{\bar{P}}_{i_1} \\ \dot{\bar{\Phi}}_{o_1} \\ \dot{\bar{P}}_{i_2} \\ \dot{\bar{\Phi}}_{o_2} \end{bmatrix} = \begin{bmatrix} 0 & -\xi_1 & 0 & 0 \\ \xi_2 & -\xi_3 & 0 & 0 \\ 0 & 0 & 0 & 3\xi_1 \\ 0 & 0 & -3\xi_2\xi_4 & -\xi_5 \end{bmatrix} \begin{bmatrix} \bar{P}_{i_1} \\ \bar{\Phi}_{o_1} \\ \bar{P}_{i_2} \\ \bar{\Phi}_{o_2} \end{bmatrix} + \begin{bmatrix} 0 & \xi_6 \\ -\frac{\xi_2}{\xi_1}\xi_6 & 0 \\ 0 & \xi_6 \\ -\frac{\xi_2\xi_4}{\xi_1}\xi_6 & 0 \end{bmatrix} \begin{bmatrix} \bar{P}_o \\ \bar{\Phi}_i \end{bmatrix}$$
$$\begin{bmatrix} \bar{P}_i \\ \bar{\Phi}_o \end{bmatrix} = \begin{bmatrix} 1 & 0 & 1 & 0 \\ 0 & 1 & 0 & 1 \end{bmatrix} \begin{bmatrix} \bar{P}_{i_1} & \bar{\Phi}_{o_1} & \bar{P}_{i_2} & \bar{\Phi}_{o_2} \end{bmatrix}^T \tag{2.109}$$

Hereby, the physical interpretation of the parameters, according to the original modal approximation (2.68), is as follows:

ξ_6	$\sim$	$\frac{2Z_0}{D_n}$	steady state gain
$\frac{\xi_2}{\xi_1}$	$\sim$	$\frac{1}{Z_0^2\alpha_{c1}^2}$	inverse of characteristic impedance squared
$\xi_1\xi_2$	$\sim$	$\frac{\lambda_{c1}^2}{\alpha_{c1}^2}$	first resonance frequency
ξ_3	$\sim$	$\frac{8\beta_{c1}}{\alpha_{c1}}$	damping first resonance
ξ_4	$\sim$	$\frac{\alpha_{c1}^2}{\alpha_{c2}^2}$	modification factor for second resonance frequency
ξ_5	$\sim$	$\frac{8\beta_{c2}}{\alpha_{c2}}$	damping second resonance

It is noted here, that one might only be interested in the first harmonic resonance of the transmission line dynamics, for instance when designing controllers (Chapter 4). In that case the transmission line model may even be reduced from fourth order to second order, by simply truncating the second mode. In that way, two parameters (ξ_4, ξ_5) drop out of the model, and only four parameters are required to describe the dynamics of a single transmission line.

Integration of transmission line and actuator dynamics

If no transmission line dynamics were taken into account, the basic actuator dynamics could be represented by the third order model (2.108); due to symmetry the two actuator pressures are not independently controllable. However, when considering transmission line dynamics in the actuator, *simulation of the theoretical model in* Subsection 2.4.5 already showed, that each transmission line separately affects the dynamics of the pressure in actuator chamber that is connected by that transmission line, Fig. 2.35. Because of the position dependent volume of the two actuator chambers, these dynamics (transmission line coupled to actuator chamber) are also position dependent. This implies that, if transmission line dynamics are to be included in a linear actuator model, while correctly describing the position dependence of the pressure dynamics, the fourth order linearized actuator model should be used, and not the third order model.

Because the simplified transmission line model (2.109) is just linear, a complete linear dynamic model of the actuator including two transmission lines is simply obtained by interconnection of the subsystem models. One should only take care of the flow as (controlled)

input and the pressure difference as (measured) output signal; due to the transmission line dynamics, pressures and flows at the actuator side have to be distinguished from those at the valve side. Actually, it is the valve flow Φ_i that is controlled, so that it becomes the input instead of Φ_p, while generally the pressure difference is measured at the valve side of the transmission lines, so that ΔP_i is the measured output.

Thus, composing a single state space model from the actuator model (2.107) and from two transmission line models (2.109), with sign definitions of flows given in Fig. 2.29, results in:

$$\begin{aligned} \dot{X} &= \begin{bmatrix} A_{11} & A_{12} & A_{13} \\ A_{21} & A_{22} & A_{23} \\ A_{31} & A_{32} & A_{33} \end{bmatrix} X + \begin{bmatrix} B_1 \\ B_2 \\ B_3 \end{bmatrix} U \\ Y &= \begin{bmatrix} C_1 & C_2 & C_3 \end{bmatrix} X \end{aligned} \tag{2.110}$$

with:

$$\begin{aligned} X &= \begin{bmatrix} \dot{q} & q & \bar{P}_{o1} & \bar{P}_{o2} & \bar{P}_{i1_1} & \bar{\Phi}_{o1_1} & \bar{P}_{i1_2} & \bar{\Phi}_{o1_2} & \bar{P}_{i2_1} & \bar{\Phi}_{o2_1} & \bar{P}_{i2_2} & \bar{\Phi}_{o2_2} \end{bmatrix}^T \\ U &= \begin{bmatrix} \bar{\Phi}_i & \bar{F}_{ext} \end{bmatrix}^T \\ Y &= \begin{bmatrix} q & \overline{\Delta P_i} \end{bmatrix}^T \end{aligned}$$

and:

$$A_{11} = \begin{bmatrix} -\zeta_1 & 0 & \zeta_2 & -\zeta_2 \\ 1 & 0 & 0 & 0 \\ -\zeta_3\zeta_5 & 0 & -\zeta_4\zeta_5 & \zeta_4\zeta_5 \\ \zeta_3\zeta_6 & 0 & \zeta_4\zeta_6 & -\zeta_4\zeta_6 \end{bmatrix} \quad A_{12} = \begin{bmatrix} 0 & 0 & 0 & 0 \\ 0 & 0 & 0 & 0 \\ 0 & \zeta_5 & 0 & \zeta_5 \\ 0 & 0 & 0 & 0 \end{bmatrix} \quad A_{13} = \begin{bmatrix} 0 & 0 & 0 & 0 \\ 0 & 0 & 0 & 0 \\ 0 & 0 & 0 & 0 \\ 0 & \zeta_6 & 0 & \zeta_6 \end{bmatrix}$$

$$A_{21} = \begin{bmatrix} 0 & 0 & 0 & 0 \\ 0 & 0 & -\frac{\xi_2}{\xi_1}\xi_6 & 0 \\ 0 & 0 & 0 & 0 \\ 0 & 0 & -\frac{\xi_2\xi_4}{\xi_1}\xi_6 & 0 \end{bmatrix} \quad A_{22} = \begin{bmatrix} 0 & -\xi_1 & 0 & 0 \\ \xi_2 & -\xi_3 & 0 & 0 \\ 0 & 0 & 0 & 3\xi_1 \\ 0 & 0 & -3\xi_2\xi_4 & -\xi_5 \end{bmatrix} \quad A_{23} = \begin{bmatrix} 0 & 0 & 0 & 0 \\ 0 & 0 & 0 & 0 \\ 0 & 0 & 0 & 0 \\ 0 & 0 & 0 & 0 \end{bmatrix}$$

$$A_{31} = \begin{bmatrix} 0 & 0 & 0 & 0 \\ 0 & 0 & 0 & -\frac{\xi_8}{\xi_7}\xi_{12} \\ 0 & 0 & 0 & 0 \\ 0 & 0 & 0 & -\frac{\xi_8\xi_{10}}{\xi_7}\xi_{12} \end{bmatrix} \quad A_{32} = \begin{bmatrix} 0 & 0 & 0 & 0 \\ 0 & 0 & 0 & 0 \\ 0 & 0 & 0 & 0 \\ 0 & 0 & 0 & 0 \end{bmatrix} \quad A_{33} = \begin{bmatrix} 0 & -\xi_7 & 0 & 0 \\ \xi_8 & -\xi_9 & 0 & 0 \\ 0 & 0 & 0 & 3\xi_7 \\ 0 & 0 & -3\xi_8\xi_{10} & -\xi_{11} \end{bmatrix}$$

$$B_1 = \begin{bmatrix} 0 & 0 & 0 & 0 \\ \zeta_2 & 0 & 0 & 0 \end{bmatrix}^T \quad B_2 = \begin{bmatrix} \xi_6 & 0 & \xi_6 & 0 \\ 0 & 0 & 0 & 0 \end{bmatrix}^T \quad B_3 = \begin{bmatrix} -\xi_{12} & 0 & -\xi_{12} & 0 \\ 0 & 0 & 0 & 0 \end{bmatrix}^T$$

$$C_1 = \begin{bmatrix} 0 & 1 & 0 & 0 \\ 0 & 0 & 0 & 0 \end{bmatrix} \quad C_2 = \begin{bmatrix} 0 & 0 & 0 & 0 \\ 1 & 0 & 1 & 0 \end{bmatrix} \quad C_3 = \begin{bmatrix} 0 & 0 & 0 & 0 \\ -1 & 0 & -1 & 0 \end{bmatrix}$$

The advantage of this model structure is its physical background. For instance, it is easy to reduce the transmission line models to second order if desired, while maintaining the same model structure. Furthermore, the position dependence of the pressure dynamics is very transparant in this structure: like before, only the parameters ζ_5, ζ_6 are position dependent. It is also clear from the model structure, that the poles of the interconnected

system are dominated by the poles of the separate subsystems, although there is a direct coupling via the non-zero elements in the non-diagonal blocks of the state matrix.

The physical background of the model has allowed to represent the rather complex (high order) dynamic behaviour of the actuator with transmission lines by a relatively small number of parameters. Analysis of the input-output behaviour of the model (2.110) shows namely, that besides the 12 poles of the system, there are a large number of zeros in the different transfer functions. Just only the transfer function $\frac{\Delta P_1}{\Phi_i}$ already has 9 zeros plus a steady state gain, where the reader is referred to the upper plots of Fig. 2.36 for an impression of this transfer function. So, with the model structure (2.110), with only 18 parameters necessary to describe the input-output behaviour, a very compact dynamic model is available.

2.6.4 Summary

For the low-frequency behaviour, where transmission line effects do not play a role in the input-output behaviour, the basic dynamics of the hydraulic actuator can be found by linearization of the theoretical model. Based on physical insight, it can in general be justified to adopt a third order model for a hydraulic actuator driving a stiff inertial load.

In case the dynamics of transmission lines between valve and actuator play an important role, for instance with long-stroke actuators, simplified transmission line models can easily be integrated with the fourth order linearized model of the actuator. This results in a compact model, with few parameters, which allows clear physical interpretation of the dynamics, because the state variables are physical quantities.

Within both linear model structures (without and with transmission lines), there is the possibility to consider one or two parameters to be position dependent, therewith introducing an important non-linear effect in the simple linear model structure. In fact, both the simplified servo-valve model of Section 2.5, (2.104), and the linear actuator models of this Section have a physical structure which allows the inclusion of different non-linear effects of the theoretical model. Which non-linearities are to be included in the obtained linear model, and how this can be done, is the topic of the next Section.

2.7 Inclusion of relevant non-linearities in the hydraulic servo-system model

2.7.1 Introduction

As described in the introduction of this Chapter, in Subsection 2.1.2, the second stage of obtaining simplified models of the hydraulic servo-system consists of extending the linear dynamic models with the dominant non-linearities of the theoretical model. This inclusion is to be performed such, that only a few parameters are required to represent a specific non-linearity, while the dynamic properties of the model remain unaffected, at least in the linearization point.

The basic idea behind the way of doing this is as follows. The theoretical equations describing the investigated non-linearity are scaled, such that the structure and physical interpretation of the non-linear equation is preserved. Furthermore, the physical parameters are grouped, such that a minimum number of independent parameters remain, that

can be adjusted to describe certain non-linear input-output behaviour. The non-linearity is included in the (linear) dynamic model, by replacing a linear dynamic equation in the state space model by the obtained (simplified) non-linear equation. In order to guarantee that the linearization of the newly obtained non-linear model equals the original linear model, the independent parameters of the non-linear equation are subjected to some conditions, which are easily derived.

Concerning the different non-linearities in the complete servo-system, the same division can be made as for the dynamics. One part of the non-linearities is related to the dynamic behaviour of the servo-valve, Subsection 2.7.2. This includes the non-linearities of the flapper-nozzle valve that influence its dynamics, and if the flapper-nozzle valve serves as pilot-valve for a third stage, also the non-linear steady state characteristic of the pilot-valve. The other part of the non-linearities consists of the non-linearities related to the combination of servo-valve spool and actuator, Subsection 2.7.3.

2.7.2 Non-linearities of the flapper-nozzle servo-valve

Based on the insight obtained by the simulations of the non-linear theoretical model in Subsection 2.2.5, a decision is made on which non-linearities should be included in the model. For each non-linearity, the procedure of including it in the linear dynamic model is subsequently presented.

Selection of non-linearities to be included

The first non-linearity of the flapper-nozzle valve analyzed in Subsection 2.2.5, the torque motor non-linearity, seemed not to be so serious, given the chosen parameters, see Fig. 2.8. However, dynamic simulations showed considerable influence for large input amplitudes, see Fig. 2.18. Moreover, the exact physical parameters are generally unknown, so that the negligibility of this non-linearity can not be concluded beforehand. Therefore, this non-linearity is included in the analyses below.

The second non-linearity, that of the flapper-nozzle system, shows serious non-linear behaviour, Fig. 2.9, 2.10. In order to be able to investigate the effect of this fundamental non-linearity on the dynamic behaviour of the valve in more detail, it is included in the model.

The third non-linearity that might be included, is that of the non-linear flow forces on the flapper. As mentioned in Subsection 2.2.2, many researchers have investigated this complex non-linear phenomenon. Although theoretical modelling appears to be difficult, there are some experimental results, showing severe non-linearity of the flow forces (the flow force ratio FR) as function of the flapper position [31, 79]. Inclusion of these experimental non-linear characteristics in the linear dynamic model of the flapper-nozzle valve can explain severe non-linear dynamic behaviour, as described by Schothorst et al. in [120]. However, the phenomenon has not been experimentally verified (compare Section 3.4).

Because of the lack of experimental evidence for the non-linear effect of the nozzle flow forces on the valve dynamics, and because the generally adopted theoretical model of Subsection 2.2.2 shows only minor non-linearity, see Fig. 2.11, this non-linear effect is not taken into account any further.

Two hard non-linearities that may occur in the flapper-nozzle valve, Coulomb friction of the spool and ball clearance, are not considered in the analysis below, for reasons given

earlier in Subsection 2.2.5: the effect of Coulomb friction can be minimized by applying a dither signal, while ball clearance is to be avoided for any application.

The final and possibly major non-linearity of the flapper-nozzle servo-valve actually does not influence its dynamics, but is only concerned with the steady state output gain: the non-linear flow through the spool ports. How to include this effeciently in the simplified servo-valve model is the final subject of this Subsection.

Non-linear torque motor model

The theoretical non-linear equation for the torque motor torque reads as follows (see equations (2.2) and (2.3)):

$$T_t = \frac{\mu_0 A_g l_a}{4}\left[\left(\frac{M_0 + Ni_{ca}}{g - \frac{l_a}{l_f}x_f}\right)^2 - \left(\frac{M_0 - Ni_{ca}}{g + \frac{l_a}{l_f}x_f}\right)^2\right]$$

In order to obtain a flexible description of this non-linearity, which fits easily in the linear model structure of the flapper-nozzle valve (2.101), this non-linear equation has to be rewritten. Thereby, the variables are chosen as in the linear model (2.101), so $\tilde{x}_f$ for the flapper position and $\bar{i}_{ca}$ for the input current. Note that the sign definition of $\tilde{x}_f$ is the reverse of x_f due to the scaling of the state vector in (2.101). Furthermore grouping the (redundant) physical parameters in the above equation to three independent parameters, the following non-linear equation is obtained:

$$\tilde{T}_t = k_1\left[\left(\frac{1 + k_2\bar{i}_{ca}}{1 + k_3\tilde{x}_f}\right)^2 - \left(\frac{1 - k_2\bar{i}_{ca}}{1 - k_3\tilde{x}_f}\right)^2\right] \tag{2.111}$$

This non-linear equation is simply integrated with the linear flapper-nozzle valve model (2.101) by replacing the first row (state equation) of that model by:

$$\ddot{\tilde{x}}_f = -c_1\dot{\tilde{x}}_f - c_2'\tilde{x}_f + c_3\tilde{x}_s + c_4\widetilde{\Delta P}_n - \tilde{T}_t \tag{2.112}$$

The minus sign for the torque again originates from the sign definition of the states of the linear model.

The parameters k_1, k_2, k_3 can be seen as tuning knobs, which can be used to investigate the character and influence of the torque motor non-linearity for different parameter combinations. However, there are restrictions in choosing them: they need to be positive because of their physical interpretation, and moreover, the dynamic properties of the model (2.101) should be preserved, at least in the linearization point. This means, that the linearization of (2.112) has to be equal to the first state equation of the linear model (2.101). Using $\frac{\partial \tilde{T}_t}{\partial \bar{i}_{ca}} = 4k_1k_2$; $\frac{\partial \tilde{T}_t}{\partial \tilde{x}_f} = 4k_1k_3$, this leads to the following conditions:

$$\begin{aligned} -\tfrac{\partial \tilde{T}_t}{\partial \bar{i}_{ca}} = -c_9 \quad &\Rightarrow \quad k_1 = \tfrac{c_9}{4k_2} \\ -c_2' - \tfrac{\partial \tilde{T}_t}{\partial \tilde{x}_f} = -c_2 \ &\Rightarrow \ c_2' = c_2 + \tfrac{k_3}{k_2}c_9 \end{aligned}$$

Thus, given a linear dynamic model (2.101) with parameters $c_1, \ldots, c_9$, for instance obtained by means of identification, the effect of the torque motor non-linearity can be investigated by including this non-linearity in the way described here. Effectively, there are

two tuning knobs for this non-linearity: k_2 and k_3. In fact, k_2 determines the measure of non-linearity in the input $\bar{i}_{ca}$, and k_3 the measure of non-linearity in the flapper-position $\tilde{x}_f$. The constant k_1 is dependent on k_2 and c_9, in order to preserve the steady state gain of the model, while the coefficient c_2 has to be adjusted in order to preserve the dynamic properties of the model in the linearization point.

The same procedure of including a non-linearity in the linear model while preserving the dynamic properties is applied to the non-linearity of the flapper-nozzle system.

Non-linear pressure dynamics of the flapper-nozzle valve

In Subsection 2.2.2 and 2.2.3, the theoretical model describing the flapper-nozzle non-linearity has been given (equations (2.5), (2.6), (2.10) and (2.11))). In this model, the effect of an outlet restriction in the flapper-nozzle system has been included. However, simulations with this model, with results discussed in Subsection 2.2.5, showed that the outlet restriction hardly contributes to the non-linearity of the system (see Fig. 2.9). For this reason, when including the flapper-nozzle non-linearity in the simplified dynamic model, it is assumed that no outlet restriction is present. With this assumption, and assuming that the return pressure $P_t = 0$, the theoretical model for the flapper-nozzle non-linearity is represented by the following set of equations:

$$\begin{aligned}
\Phi_{01} &= C_d A_0 \sqrt{2\tfrac{P_s - P_{n1}}{\rho}} & \Phi_{02} &= C_d A_0 \sqrt{2\tfrac{P_s - P_{n2}}{\rho}} \\
\Phi_{n1} &= C_d \pi D_n (x_{f0} + x_f) \sqrt{2\tfrac{P_{n1}}{\rho}} & \Phi_{n2} &= C_d \pi D_n (x_{f0} - x_f) \sqrt{2\tfrac{P_{n2}}{\rho}} \\
\dot{P}_{n1} &= \tfrac{E}{V_{n1}} (\Phi_{01} - \Phi_{n1} + A_s \dot{x}_s) & \dot{P}_{n2} &= \tfrac{E}{V_{n2}} (\Phi_{02} - \Phi_{n2} - A_s \dot{x}_s)
\end{aligned} \tag{2.113}$$

After linearization of the theoretical model of the flapper-nozzle valve, it appeared that only the nozzle pressure difference ΔP_n is controllable, while the mean nozzle pressure P_n is uncontrollable, leading to a reduction of the pressure dynamics to (2.89), see Subsection 2.5.2. For the non-linear model, this is not directly clear. However, in order to fit the non-linear pressure dynamics (2.113) into the linear model structure (2.101), it is useful to rewrite these dynamics into a controllable part and an almost uncontrollable part. Applying the well known scalings for pressures and flapper position, this results in:

$$\begin{aligned}
\dot{\overline{\Delta P}}_n &= c_{11} \left[\sqrt{1 - \bar{P}_n - \tfrac{1}{2}\overline{\Delta P}_n} - \sqrt{1 - \bar{P}_n + \tfrac{1}{2}\overline{\Delta P}_n} \right] \\
&\quad - c_{12} \left[(1+\bar{x}_f) \sqrt{\bar{P}_n + \tfrac{1}{2}\overline{\Delta P}_n} - (1-\bar{x}_f) \sqrt{\bar{P}_n - \tfrac{1}{2}\overline{\Delta P}_n} \right] + 2c_{13} \dot{\bar{x}}_s \\
\dot{\bar{P}}_n &= \tfrac{c_{11}}{2} \left[\sqrt{1 - \bar{P}_n - \tfrac{1}{2}\overline{\Delta P}_n} + \sqrt{1 - \bar{P}_n + \tfrac{1}{2}\overline{\Delta P}_n} \right] \\
&\quad - \tfrac{c_{12}}{2} \left[(1+\bar{x}_f) \sqrt{\bar{P}_n + \tfrac{1}{2}\overline{\Delta P}_n} + (1-\bar{x}_f) \sqrt{\bar{P}_n - \tfrac{1}{2}\overline{\Delta P}_n} \right]
\end{aligned} \tag{2.114}$$

The exact physical interpretation of the constants c_{11}, c_{12}, c_{13} can be derived from (2.113). However, instead of using a-priori knowledge, which is often not available, the values of these constants, and therewith the character of the non-linearity, are determined by relating the non-linear equations (2.114) to the fourth state equation of the linear model (2.101). In fact, the character of the non-linearity is a matter of scaling of the variables in (2.114); if $\bar{x}_f$ and/or $\overline{\Delta P}_n$ approach ± 1 in dynamic simulations, there may be serious non-linearity. Therefore, in order to tune the measure of non-linearity, the non-linear nozzle

pressure dynamics (2.114) are related to the linear flapper-nozzle valve dynamics (2.101) by means of the following scalings:

$$\bar{x}_f = -k_4\tilde{x}_f; \qquad \overline{\Delta P}_n = -k_5\widetilde{\Delta P}_n; \qquad \dot{\bar{x}}_s = \dot{\tilde{x}}_s \tag{2.115}$$

Note, that the minus signs in these scalings correspond to the scaling of the state vector of the linear model in Subsection 2.5.2, such that a correct physical interpretation is possible for $k_4, k_5 > 0$.

Because simulations with the non-linear model equations (2.114) showed little influence of the steady state value of $\bar{P}_n$ on the character of the non-linearity, the steady state level of the nozzle pressures is assumed to be half the supply pressure P_s. In other words, it is assumed that $\bar{P}_n = \frac{1}{2}$ in steady state, which is quite reasonable [98]. Applying this for $\bar{x}_f = 0$, $\overline{\Delta P}_n = 0$, the second equation of (2.114) imposes a restriction on the parameters of the non-linearity, namely $c_{11} = c_{12}$.

As said before, the values of the parameters c_{11}, c_{12}, c_{13} are found by relating the non-linear pressure dynamics to its linear counterpart in the dynamic servo-valve model, by means of scalings k_4, k_5. Actually, the requirement is, that the linearization of (2.114), using (2.115), equals the fourth state equation of (2.101). Using the assumption on the steady state nozzle pressures, this linearization with equilibrium point $\bar{x}_f = 0$, $\overline{\Delta P}_n = 0$ reads:

$$\begin{aligned} \dot{\widetilde{\Delta P}}_n &= -\tfrac{1}{k_5}\left[\tfrac{1}{2}\sqrt{2}\,(c_{11}+c_{12})\,k_5\widetilde{\Delta P}_n + \sqrt{2}c_{12}k_4\tilde{x}_f + 2c_{13}\dot{\tilde{x}}_s\right] \\ \dot{\bar{P}}_n &= 0 \end{aligned} \tag{2.116}$$

As expected, the linearized mean pressure $\bar{P}_n$ is uncontrollable and can be neglected. Using the third state equation of (2.101) to substitute $\dot{\tilde{x}}_s$ in the above equation, and equalling the expression for $\dot{\widetilde{\Delta P}}_n$ to the fourth state equation of (2.101) gives:

$$\begin{aligned} \dot{\widetilde{\Delta P}}_n &= -\left[\tfrac{1}{2}\sqrt{2}\,(c_{11}+c_{12}) + 2\tfrac{c_{13}c_6}{k_5}\right]\widetilde{\Delta P}_n - \left[\sqrt{2}c_{12}\tfrac{k_4}{k_5} + 2\tfrac{c_{13}}{k_5}\right]\tilde{x}_f + 2\tfrac{c_5c_{13}}{k_5}\tilde{x}_s \\ &= -c_8\widetilde{\Delta P}_n - c_7\tilde{x}_f + \tilde{x}_s \end{aligned} \tag{2.117}$$

From this equation, the parameters of the non-linear model relations (2.114) are easily expressed in terms of the parameters of the linear model and the scaling factors k_4 and k_5:

$$c_{11} = -\tfrac{2k_4(c_6-c_5c_8)+k_5(c_5c_7-1)}{\sqrt{2}k_4c_5}; \quad c_{12} = \tfrac{k_5(c_5c_7-1)}{\sqrt{2}k_4c_5}; \quad c_{13} = \tfrac{k_5}{2c_5} \tag{2.118}$$

These expressions suggest that, given the parameters $c_5, \ldots, c_8$, k_4 and k_5 can be chosen independently. However, due to the assumption on the steady state pressure level above, c_{11} should equal c_{12}, so that k_4 and k_5 are related to each other as:

$$k_5 = -\frac{(c_6 - c_5c_8)}{(c_5c_7 - 1)}k_4 \tag{2.119}$$

Summarizing, the procedure of including the non-linear flows through the flapper-nozzle system is as follows. The linear equation for the pressure dynamics of the flapper-nozzle valve (the fourth state equation of the linear model (2.101)) is replaced by a pair of equations describing the non-linear pressure dynamics, namely (2.114). The interconnection with the linear model takes place via scalings (2.115). Hereby, k_4 can be used as tuning parameter to adjust the measure of non-linearity, while k_5 is related to k_4 by (2.119). The parameters in the equations of the non-linear dynamics finally, are given by (2.118).

The advantage of this procedure is, that given a linear dynamic model according to (2.101), there is only one additional parameter required to tune the measure of non-linearity due to the flapper-nozzle system, while the linearization of the non-linear model is guaranteed to be equal to the original linear model.

Because the non-linearities of the torque motor and of the flapper-nozzle system enter the dynamic model equations, they had to be included such, that the dynamic properties of the original linear model were preserved. The last non-linearity to be considered is of a different type: the non-linear flow through the spool ports is only an output non-linearity.

Non-linear flow through spool ports

In Subsection 2.2.5, a rather extensive discussion of the non-linear character of the spool port flows has been given. In short, there are two major contributions to this non-linearity: the load dependence of the flow and the non-linearity due to non-ideal port geometry.

The first of these two only plays a role if a load pressure ΔP_m is present across the spool ports, corresponding to the case that the spool flow is driving a (loaded) actuator. In fact, this non-linearity is inherent to the combination of servo-valve and actuator, and is seen as a non-linearity of the hydraulic servo-system. As such, it is discussed in the next Subsection.

In case the load pressure ΔP_m across the spool ports is negligible, for instance when the spool flow is driving another spool as third stage of a three-stage valve, like modelled in Subsection 2.2.4, only the non-linearity due to the spool port configuration plays a role. The reason is, that the spool port pressures P_{m1} and P_{m2} are equal in that case, and instantaneously adjust themselves such that the spool port flows Φ_{m1} and Φ_{m2} are equal. Recalling the equations describing these flows, namely (2.16), (2.17) and (2.18), it is clear that in the resulting spool flow Φ_m is just a non-linear function of the spool displacement x_s.

The theoretical model shows, that the non-linear function between the no-load spool flow Φ_m and the spool position x_s depends on a number of geometrical parameters, such as the individual spool port underlaps or overlaps, the radial clearance of the spool and the spool port width, while also the discharge coefficient C_d is involved. In general, most of these parameters are not known a-priori; especially the value of C_d is rather uncertain. Moreover, the large number of parameters complicates a systematic analysis of the influence of these parameters on the resulting (static) non-linearity. This especially holds because the flow Φ_m can not be calculated explicitly as function of the spool displacement x_s; the flow Φ_m and the pressure P_m have to be solved simultaneously from equations (2.16), as discussed more extensively in Section B.1 of Appendix B.

When analyzing the effect of non-ideal spool port configurations on the resulting spool flows in Subsection 2.2.5, the above problem was already mentioned. Although much insight can be obtained by analyzing the theoretical model, it is hardly possible to analyze all possible configurations systematically. It is even impossible, to characterize the non-linear flow characteristic uniquely by means of the spool port configuration, as different configurations can result in similar flow characteristics. Moreover, due to the assumptions in the theoretical model, such as constant discharge coefficient C_d, it may be impossible to characterize some flow characteristics by any configuration of spool ports within the given model structure.

For these reasons, the non-linear flow characteristic for zero load pressure ΔP_m is

represented by a very general, non-parametric function. Applying the usual normalizations for flow and spool position like in Subsection 2.2.5, this non-parametric model of the flow non-linearity is written as:

$$\bar{\Phi}_m = f_1(\bar{x}_s) \tag{2.120}$$

In here, f_1 may be some analytical function representing or approximating the theoretical non-linearity, but it may also be a lookup-table. Due to the normalization, for the theoretical model of a critical-centred spool the expression (2.120) reduces to the following equality: $\bar{\Phi}_m = \bar{x}_s$. This means, that in case the spool flow Φ_m drives the main spool of a three-stage valve, the static non-linearity (2.120) is easily included in the dynamic model of the three-stage valve (2.104). This can be deduced from equation (2.102); the last state equation of the state space model (2.104) of the servo-valve can directly be replaced by:

$$\dot{\bar{x}}_m = c_{10} f_1(\bar{x}_s) \tag{2.121}$$

Thus, the inclusion of the static non-linearity of the pilot-valve in the simplified servo-valve model allows the description of non-linearity in the dynamics of the three-stage valve. This is just what was shown in the simulation results with the theoretical model in Fig. 2.20.

Summary

For three important non-linearities of the flapper-nozzle valve, compact representations have been given, that allow the inclusion of these non-linearities within the structure of the simplified, linear models of the servo-valve. At the one hand the non-linearities of the torque motor and the flapper-nozzle system are taken into account by replacing state equations of the linear flapper-nozzle valve model (2.101) by non-linear equations. On the other hand, the static flow non-linearity of the flapper-nozzle valve is taken into account by adding a non-parametric non-linearity to the output of the model.

In this way, a non-linear dynamic model for the flapper-nozzle valve is obtained, which can be represented in a block scheme as in Fig. 2.39. Note the resemblance with the linear model structure in Fig. 2.38. If the non-linear model of the flapper-nozzle valve is combined with the main spool dynamics and feedback of a three-stage valve, a non-linear dynamic model for the three-stage valve is obtained, as given in Fig. 2.40.

The non-linearities included in the simplified models so far, are restricted to those that affect the servo-valve dynamics. Although the inclusion of (non-linear) servo-valve dynamics is essential for high-performance control of a hydraulic servo-system Chapter 4, there may be applications where servo-valve dynamics are not of major importance. In that case, it is more important to include the basic non-linearities of the hydraulic servo-system in the model analysis; these non-linearities are related to the combination of servo-valve spool and actuator.

2.7.3 Non-linearities of the hydraulic servo-system

Using the insight obtained from the simulation results of the non-linear theoretical model of the spool-actuator combination, discussed in Subsection 2.3.5, it is argued below which actuator non-linearities are so basic and important, that they should be included in the actuator model. After that, it is described how to do this, without increasing model complexity too much, while preserving dynamic properties described by the linearized actuator model.

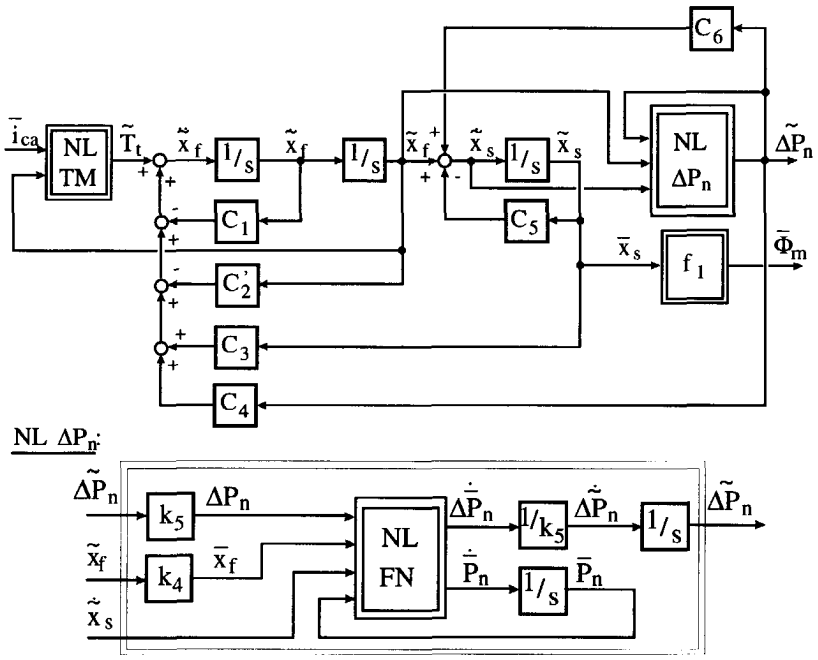


Fig. 2.39: Block scheme non-linear pilot-valve model

Selection of non-linearities to be included

The analysis of the non-linearities of the servo-system starts with an investigation of the flows through the spool, driving the actuator. Contrary to the case in the previous Subsection, the spool flow is now dependent on the load pressure; due to the dynamics of the (possibly loaded) actuator, ΔP_p may be considerably large during normal operation of the servo-system. As illustrated by the simulated spool flow characteristics of Fig. 2.13, discussed in Subsection 2.2.5, this load dependence causes severe non-linearity, which needs to be taken into account, besides the effects of non-ideal spool port geometry.

The non-linearity of the actuator that is most related to the non-linear spool flows, is the effect of leakage flows. Whereas the linear contribution of these leakage flows is already taken into account in the linear actuator model by the leakage parameter LP_p (see Assumption 2.6.1), only the non-linear effects need attention. As explained in Subsection 2.3.5, leakage and spool flows are so closely related, that the non-linear effect of leakage can just be interpreted as a modification of the steady state spool flow characteristic. Therefore, non-linear leakage effects are not included separately in the simplified actuator model, but they are taken into account by a rather general description of the spool flow non-linearity.

Concerning the axial (bearing) forces on the piston, it was concluded in Subsection 2.3.5, that the forces related to the presence of hydrostatic bearings are negligible. Nevertheless, there may be considerable friction forces, for instance due to sealings. On the one hand, these forces are included in the simplified actuator model by means of the viscous friction coefficient w_p (see Assumption 2.6.1). On the other hand, if necessary, the non-linear part

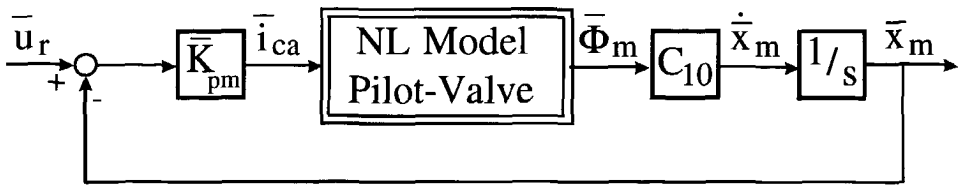


Fig. 2.40: Block scheme non-linear servo-valve model

of these friction forces, such as Coulomb friction effects, may be included in the simplified actuator model as described in the sequel.

When including the main non-linearities of the servo-system in the simplified actuator model, transmission line dynamics are not considered. This is allowed, because the non-linearities mainly affect the steady state and low-frequency behaviour of the servo-system. If transmission line dynamics are to be taken into account, the non-linearities can be included in the model in exactly the same way as described below, except that care should be taken in choosing the pressures: the pressures in the actuator chambers should be distinguished from the pressures at the valve ports.

Finally, because the position dependent dynamics of the pressures in the actuator chambers is explicitly taken into account in the analysis of the (linear) actuator dynamics, Section 2.6, it is not necessary to consider this non-linearity here.

Non-linear load dependent valve flow

In the previous Subsection, the inclusion of non-linear flow due to non-ideal spool port geometry is discussed. It was proposed to take this into account by a general non-parametric model, namely (2.120). As shown by the results of the simulation of actuator leakage, Fig. 2.24, the combination of spool port geometry and bearing leakage causes a sort of modification of the non-linear relation between valve flow Φ_p and valve spool position x_m. Therefore, following the same reasoning as in the previous Subsection, it is useful to combine the effects of non-linearity due to actuator leakage and (main) spool port configuration, for zero load pressure, into a single non-parametric model:

$$\left[\bar{\Phi}_p\right]_{\overline{\Delta P}_p=0} = f_2(\bar{x}_m) \tag{2.122}$$

With this non-linear expression describing the non-linearity of the spool flow with respect to the (main) spool position, only the load dependence of this flow remains to be taken into account. Concerning the load dependence of the flow due to leakage, it is concluded from Fig. 2.24, Subsection 2.3.5, that this effect can rather well be approximated by a linear relationship, characterized by the leakage parameter LP_p (see Assumption 2.6.1).

Thus, the attention can be restricted to the load dependence of the flow through the valve spool. The analysis of this effect actually refers to the theoretical model of Subsection 2.2.4, equations (2.23), (2.24) and (2.25), and to the simulated flow characteristics corresponding to these equations, shown in Fig. 2.13 to 2.16, Subsection 2.2.5. It was already concluded in the latter Section, that the load dependence of the spool flow is hardly

influenced by the spool port configuration, and is actually characterized by the 3D-surfaces shown in Fig. 2.13, which correspond to a critical-centre valve.

For this reason, the load dependence for the critical-centre valve is worked out, in order to include this basic non-linearity in the actuator model. Applying normalizations for flow, pressure and spool position, and assuming zero return pressure P_t, the flow equations (2.23) for a critical-centre valve can be rewritten as:

$$\bar{\Phi}_{p1} = \begin{cases} \bar{x}_m\sqrt{2\left(1-\bar{P}_{p1}\right)} & \bar{x}_m \geq 0 \\ \bar{x}_m\sqrt{2\bar{P}_{p1}} & \bar{x}_m < 0 \end{cases} \qquad \bar{\Phi}_{p2} = \begin{cases} \bar{x}_m\sqrt{2\bar{P}_{p2}} & \bar{x}_m \geq 0 \\ \bar{x}_m\sqrt{2\left(1-\bar{P}_{p2}\right)} & \bar{x}_m < 0 \end{cases}$$

In order to describe the load dependence of the servo-valve flow in terms of the load pressure ΔP_p, the separate pressures P_{p1} and P_{p2} can be expressed in combinations of the **load pressure ΔP_p and the mean actuator pressure P_p. Recalling from Subsection 2.6.2,** that P_p is uncontrollable, it can be assumed to be constant, and equal to the value that is required for equality of the servo-valve flows Φ_{p1}, Φ_{p2}, namely $P_p = \frac{1}{2}P_s$. Herewith, the following compact description of the load dependent flow through a critical-centre valve is obtained:

$$\bar{\Phi}_p = \begin{cases} \bar{x}_m\sqrt{1-\overline{\Delta P}_p} & \bar{x}_m \geq 0 \\ \bar{x}_m\sqrt{1+\overline{\Delta P}_p} & \bar{x}_m < 0 \end{cases} \tag{2.123}$$

In fact, this equation describes one of the very basic non-linearities of the hydraulic servo-system. The two major implications of this non-linearity were encountered earlier when discussing simulations of the theoretical model:

- For non-zero load pressure, the flow gain $\frac{\partial \Phi_p}{\partial x_m}$ depends on the load pressure itself, and on the sign of the spool displacement, see also Fig. 2.13 in Subsection 2.2.5. So for zero crossings of the spool displacement, the flow gain suddenly changes. This is a severe non-linearity.
- The load dependence of the flow $\frac{\partial \Phi_p}{\partial \Delta P_p}$ depends on the spool position. This can be interpreted as a 'leakage' across the spool ports, which depends on the spool port openings. Actually, this effect was found back earlier in the amplitude dependent damping of the actuator step responses in Subsection 2.3.5.

Combining the basic non-linearity of the load dependence of the flow (2.123) with the non-linear effects of spool port geometry and leakage described by (2.122), the final non-linear expression for the servo-valve flow is obtained as:

$$\bar{\Phi}_p = \begin{cases} f_2(\bar{x}_m)\sqrt{1-\overline{\Delta P}_p} & f_2(\bar{x}_m) \geq 0 \\ f_2(\bar{x}_m)\sqrt{1+\overline{\Delta P}_p} & f_2(\bar{x}_m) < 0 \end{cases} \tag{2.124}$$

Because in Section 2.6 the servo-valve flow $\bar{\Phi}_p$ is chosen as the control input of the linearized actuator models (2.107) and (2.108), the non-linear valve flow equation (2.124) is easily included in these respective model structures. It is just a matter of adding an input non-linearity, where the actuator pressure difference, one of the model state variables, to some extent determines the input gain via the square root.

This fact has brought some researchers to the viewpoint, that a hydraulic servo-system can be treated as a bilinear system [45, 103, 123], with a bilinear system being defined as

a system with a state equation of the form:

$$\dot{X} = AX + [NX + B]U$$

In here, X is the state vector, U the input vector, and A, B and N constant matrices with appropriate dimensions [45]. Applying this model structure to a hydraulic servo-system, the bilinear term NXU is used to approximate the pressure dependent input gain according to the square root expression in (2.124).

Although the work of Schwarz et al. [45, 123] provides a theoretical background and possible benifits of this approach, there is a fundamental shortcoming in the presented bilinear approximation of a hydraulic servo-system. It is not taken into account, that the pressure dependence of the input gain depends on the sign of the input according to (2.124), so that the matrix N should not be taken constant, but should depend on the sign of U. Naujoks and Wurmthaler [103] to the contrary, have taken this property into account, and come up with more convincing results, be it that they do not provide any experimental validation.

Despite the possible advantages of a bilinear description over a linear description, the analytic description of the input non-linearity (2.124) is preferred because of its physical background, providing more fundamental insight in the non-linear system behaviour. Another advantage of the physically structured input non-linearity is, that apart from the non-parametric model f_2, no parameters need to be chosen to describe the non-linearity.

Coulomb friction

The other actuator non-linearity that may be relevant to include in the simplified actuator model is non-linear friction. Depending on the application, especially Coulomb friction and stiction effects may influence the actuator behaviour so seriously, that they have to be taken into account. As mentioned in Subsection 2.2.3, there are many different ways of modelling Coulomb friction and related effects [6]. In the most general case, the non-linear friction force on the piston depends not only on the actuator velocity $\dot{q}$, but also on the pressure difference across the piston ΔP_p (when the piston is sticking), and possibly on the piston position q. Thus, applying the normalizations for pressures and forces as earlier, the general non-linear friction model reads:

$$\bar{F}_{cp} = f_{cp}(\dot{q}, q, \overline{\Delta P}_p) \tag{2.125}$$

In many applications, the friction model need not to be that complicated, for instance when no stiction is observed and the Coulomb friction force is rather constant over the complete actuator stroke. In that case the following simplified Coulomb friction model will be sufficient, where the tuning parameter k_6 represents the amount of Coulomb friction as a fraction of the maximum actuator force $F_{p,max}$:

$$\bar{F}_{cp} = -k_6 \operatorname{sign}(\dot{q}) \tag{2.126}$$

Whatever friction model is used, due to the normalizations of the equations (2.125) and (2.126), it is easy to include this non-linearity in the linearized actuator model, e.g. (2.108). The normalized friction force $\bar{F}_{cp}$ is just plugged in in the first state equation with the same input gain (ζ_2) as the external force $\bar{F}_{ext}$.

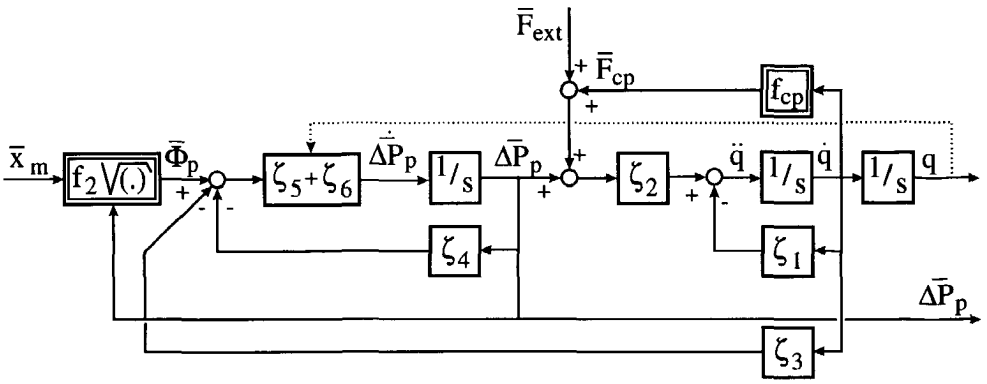


Fig. 2.41: Block scheme non-linear actuator model

Because Coulomb friction is a hard non-linearity (according to the definition given by Slotine and Li [130]), linearization of a dynamic model including this non-linearity is only possible by neglecting the phenomenon. From this viewpoint, it can be stated, that the inclusion of this non-linearity in the simplified actuator model in the way described above, does not affect the linear dynamics of the model. So, again the basic idea behind including the most important non-linearities in the servo-system models has been followed.

Summary

The two basic non-linear properties of a hydraulic servo-system that are not included in the position dependent linearized models of the hydraulic actuator, given in Section 2.6, are the load dependent valve flow and the non-linear (Coulomb) friction force. The load dependent valve flow, which includes non-linear effects due to leakage, is represented by a non-parametric model for the non-linearity due to the spool port configuration, plus a square root expression for the non-linear load dependence. The non-linear friction force is described by some friction model; in case only Coulomb friction is taken into account, this model contains only one parameter: the magnitude of the Coulomb friction.

Because of the simplified representation of the two basic non-linearities of the combination of valve spool and actuator, mainly due to normalization, it is straightforward to include them in the linear actuator model structure. The resulting non-linear dynamic model is shown in the form of a block scheme in Fig. 2.41. Note that a series connection of the servo-valve model of Fig. 2.40 and the actuator model of Fig. 2.41 results in a compact non-linear dynamic model for the complete hydraulic servo-system.

2.8 Conclusion

The approach of physical modelling appears to be well-suited to obtain insight in the relevant dynamic and non-linear effects of a hydraulic servo-system.

In the modelling approach, the distinction of different subsystems plays an important

role; it simplifies the modelling process, and it provides insight in the (dynamic) behaviour of the system, caused by interaction of the subsystems. For the hydraulic servo-system this means, that a distinction is made between the servo-valve, the hydraulic actuator, and the transmission lines between the servo-valve and the actuator. In order to investigate both the dynamic properties and the non-linearities of the system, the modelling approach starts with the theoretical modelling of the subsequent subsystems.

In the theoretical model, which is highly detailed, any dynamic and non-linear effect that might play a role in the hydraulic servo-system, is included. By means of simulations with this model, the relevance of those effects is investigated, at least qualitatively. Subsequent analysis of the dynamic properties of the subsystem models by means of linearization leads to basic insight in the dynamic behaviour of the hydraulic servo-system. It appears, that the dynamics of the complete system can be seen as a series connection of the servo-valve dynamics and the actuator dynamics. Furthermore, in case the actuator has a long stroke, the transmission lines between the valve and the actuator compartments should explicitly be taken into account; a proper connection of the transmission line models with the basic model of the hydraulic actuator typically leads to an extended actuator model with badly damped resonances at high frequencies.

As a result of the analysis of the dynamics, a reasonably simple linear model is obtained, describing the relevant dynamic behaviour of the servo-system with few model parameters, while the physical structure of the model is preserved. The latter allows to include the most important non-linearities of the system in the linearized model, which have shown to be relevant by the abovementioned simulations. Thereby, only a few parameters are used to quantify the underlying non-linear physical effects, such that the simple structure of the linearized models is preserved again. In short, the most relevant non-linearities are: the torque motor non-linearity (flapper-nozzle valve dynamics), the non-linear spool port flows (the *basic* non-linearity of any hydraulic servo-system), Coulomb friction (if no hydrostatic bearings are applied), and position dependence of the actuator dynamics.

For a complete overview of the modelling aspects of hydraulic servo-systems, with a summary of modelled dynamics and non-linearities, the reader is referred to Appendix A. In fact, Appendix A just summarizes the results of this Chapter, being physically structured non-linear dynamic models of the hydraulic servo-system, which are sufficiently simplified to allow identification of the model parameters from experimental data, as well as experimental validation of the quality of the models. These topics, identification and experimental validation, form the subject of the next Chapter.

Chapter 3

Experimental identification and validation of the model

In the previous Chapter, the theoretical model of the hydraulic servo-system has been presented, simulated, and analyzed. This finally led to a relatively simple non-linear dynamic model, describing the relevant dynamics and non-linearities of the system, which forms the basis for experimental identification and validation. The identification of the model parameters from experiments and the validation of the resulting simulation model for a real hydraulic servo-system is the topic of this Chapter.

3.1 Introduction

In the introduction of this Chapter, a motivation is given for the chosen approach to the identification and validation of the model of a hydraulic servo-system. First, the starting point for the identification and validation of the model is outlined in Subsection 3.1.1. After that, a number of issues concerning the identification and validation of non-linear systems is discussed in Subsection 3.1.2. As a result of this discussion, given the starting point, the approach for the identification and validation of the models is presented in Subsection 3.1.3. Finally, the outline of the Chapter is given in Subsection 3.1.4.

3.1.1 Starting point for identification and validation

In Chapter 2, the subsystem models of the hydraulic servo-system have been brought into such a form, that:

- The dynamic properties of the system are described by a linear (state space) model with a direct physical interpretation of the model structure.
- The non-linearities of the system are characterized:
  - either by a single static non-linearity on a known location in the model structure, possibly parametrized as a piece-wise-linear function,
  - or by a non-linear expression in one of the state equations, being parametrized simply by some tuning parameters, which determine the influence of the non-linearity on the system behaviour in a transparant way.

- The linearization of the non-linear model, in the zero input equilibrium state, leads to a linear model with exactly the same dynamic properties as the original linear model, i.e. the non-linearities in the model do not affect the linear dynamics in the chosen operating point.

In the last item, the term *linear dynamics* is used. Actually, this notion plays a key role in the identification approach, so that it needs to be defined more precisely[1]:

Definition 3.1.1 *The linear dynamics of a non-linear system (for some operating point) are the dynamics of that system after linearization (in that operating point).*

In fact, in the analysis of the previous Chapter, the physical structure of the model has been exploited to distinguish between linear parts of the system and non-linearities. Especially the static non-linearities f_1 and f_2, corresponding to the flow characteristics of the pilot-valve and the three-stage servo-valve respectively, have been clearly isolated from the linear dynamic blocks. This has been depicted in the block scheme representations of the different subsystem models, for which the reader is referred to Fig. 2.39 on page 112 (flapper-nozzle pilot-valve), Fig. 3.13 on page 158 (three-stage servo-valve) and Fig. 2.41 on page 116 (basic actuator model) respectively. Note, that the parametrization of the linear dynamic blocks, shown in these Figures, stems from the corresponding state space models of the linear dynamics, (2.101), (2.104) and (2.108) respectively, and that this parametrization needs to be preserved, in order to include the modelled non-linearities in the model.

The aim of the identification and validation is, to use experimental data from the different subsystems, to determine the parameters in linear dynamic blocks and to validate the adopted model structure (number of poles and zeros). Besides that, the modelled non-linearities are to be identified and validated, both the (expectedly dominant) static non-linearities f_1 and f_2, and the other modelled non-linearities. Actually, the non-linear identification problem posed here, is a typical example of what is often referred to in identification literature as grey-box modelling, see for instance Ljung [85].

Because the resulting identified and validated models are primarily to be used for control design, which in many cases takes place in the frequency domain, the frequency domain interpretation of the system behaviour is highly important. Moreover, the accuracy of the identified model is most relevant, in view of control design, in frequency regions where stability of the closed loop is concerned, mostly the cross-over region [46, 122]. In order to be able to emphasize these frequency regions explicitly during the identification of the model, e.g. by frequency-weighting, it makes sense to perform the identification in the frequency domain. So, the identification and validation of the non-linear model of the hydraulic servo-system primarily takes place in the frequency domain, based on measured (non-linear) frequency responses.

Because of the frequency domain approach, and because the identification can be performed off-line, it is not necessary to use sampled time domain data for the identification procedures, as is usually done (see Ljung [85] and references therein). Moreover, the grey-box models to be identified are stated in the continuous time domain. This is not only a result of their origin, namely the theoretical model of the system, but it is also useful because the physical interpretation of non-linear models is more clear in continuous time.

[1] In certain operating points, linearization may be impossible because the model is not differentiable due to hard non-linearities. A definition of the linear dynamics for that case is given later, on page 124.

Consequently, continuous time representation of the system models will be part of the identification and validation approach.

Summarizing, the starting point for the identification and validation of the hydraulic servo-system is grey-box identification of non-linear continuous time state space models in the frequency domain. Obviously, this approach differs considerably from the non-linear black-box modelling approach, applied to a hydraulic servo-system by Van der Linden [82]. Although his work clearly shows the feasibility of that approach to obtain accurate non-linear models of a hydraulic servo-system for control design, the resulting models do not easily allow a physical interpretation of the identified dynamic and non-linear effects.

Given the posed problem of grey-box identification, the question is, what techniques are available in the field of identification and validation of non-linear systems, to deal with this problem. Therefore, a brief survey of some literature on this topic is given in the next Subsection.

3.1.2 Identification and validation of non-linear systems

For the identification of non-linear systems, it is important to properly define the type of system to be identified. Some characterizations, found in literature, are reviewed. Besides the adopted system strucure, the characterization of the input-output behaviour is highly important. Because the identification is to be performed in the frequency domain, the interpretation of non-linear frequency responses is briefly adressed, including the relation to the linear dynamics of the system. Thereby, the type of signals to be used during experiments plays a role. Therefore, the excitation of non-linear system dynamics is also discussed. Finally, given the tools available in the field of identification of non-linear systems, it is to be considered, how the identified models can be validated.

Characterization of non-linear systems

As outlined by Stoica and Söderström [133], two principal tendencies can be recognized in the field of identification of non-linear systems. The first is to use a very general description to represent the non-linear system, while the second shows the use of some particular characterizations for certain classes of non-linear systems.

Examples of the general type of descriptions are functional series expansions and state space models [133]. In the functional series expansions, descriptions with Volterra kernels and with Wiener kernels can be distinguished, as mentioned by Billings [13] and Wigren [154]. The problem of using these general descriptions in system identification is, that it leads to quite complicated numerical problems of large dimensions [133]. Moreover, the descriptions do not allow a direct physical interpretation of the model. The latter problem does not hold for methods based on (discrete time) state space representations, such as the extended Kalman filter [78] and non-linear Maximum Likelihood estimators[2] [88]. Although these methods primarily apply to discrete time descriptions, the estimation of parameters in continuous time is also possible. However, the problem with these methods is, that the frequency domain interpretation is not directly clear; the methods typically comprise (recursive) time domain identification.

[2]These Maximum Likelihood estimators have found their application, for example, in non-linear aircraft flight-path reconstruction [28, 101].

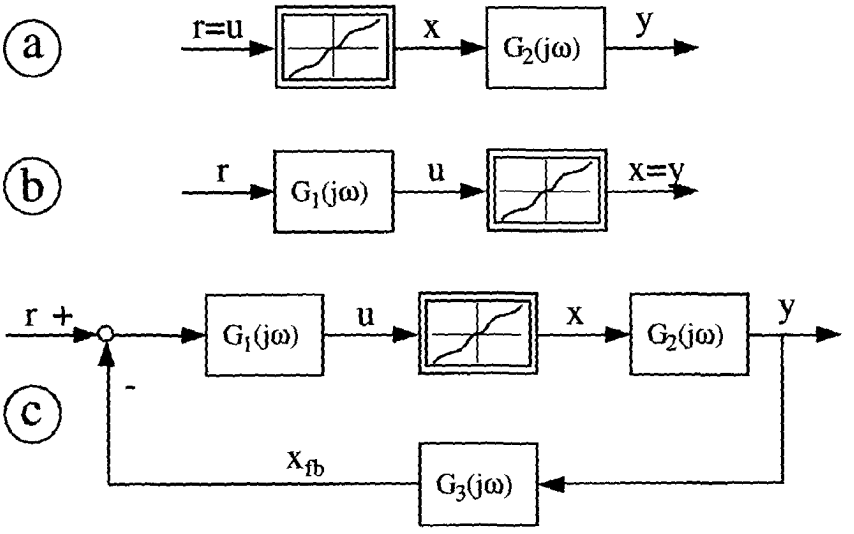


Fig. 3.1: Block scheme representations of three basic structures of non-linear systems; Hammerstein model (a); Wiener model (b); general model (c)

Considering the non-linear models of some particular type, Stoica and Söderström state that they lead to more feasible estimation methods [133]. In general, these models represent the non-linear system by some combination of linear dynamic blocks and one or more static non-linear block(s). Some of these particular models are well-known and widely used in non-linear system identification [13]; they are depicted in Fig. 3.1. In this Figure, r denotes the system input, y is the system output, u is the input of the static non-linearity; x is the output of the static non-linearity, and x_{fb} denotes an internal feedback signal.

Actually, the system models of Fig. 3.1 cover a wide class of non-linear control systems found in practice, since it often occurs, that the non-linear behaviour of a control system is dominated by a single static non-linearity [9, 38]. Obviously, the Hammerstein model represents a dynamic system with a static non-linearity at the input, while the Wiener model (actually originating from the Wiener kernel representation [154]) characterizes a dynamic system with a static output non-linearity. In fact, these models are just specifial forms of the general model, depicted in Fig. 3.1 (c), which represents a feedback control system, with a single static non-linearity in the control loop.

The Hammerstein model is the most attractive, from a system identification point of view. Especially when the input non-linearity can be approximated by a (fixed order) polynomial expansion, it is easy to use standard identification schemes, by considering the system as a multi input single output (MISO) linear system [85, 154]. Thus, the identification of Hammerstein systems is extensively treated in literature, with different identification methods and refinements applied. To mention only some, Instrumental Variable methods have been applied by Stoica and Söderström [133], more general regression methods by Greblicki and Pawlak [43], and a new polynomial method by Lang [71].

The identification of Wiener models is more difficult, because the input of the non-

linearity is not measurable and therefore unknown, because the linear dynamics are still to be identified. A clear survey of topics and problems related to the identification of Wiener models is given by Wigren [154], be it that he restricts the attention to recursive estimation methods.

As compared to the Hammerstein and Wiener models, the approach to the identification of the general model of a non-linear system, depicted in Fig. 3.1 (c), is much more complicated. Billings and Fakhouri [14] have considered this case, and come up with a unified theory for the identification of this class of processes, using the theory of Volterra kernels and correlation analysis techniques. The problem with this theory is, however, that it is primarily developed in a discrete time setting, and that it does not allow the required grey-box modelling approach.

In fact, the non-linear system identification techniques referred to so far, do not fit well in the setting for the identification and validation of the hydraulic servo-system, presented in Subsection 3.1.1. Nevertheless, the characterization of non-linear systems by some particularly structured models, as in Fig. 3.1, does apply to the hydraulic servo-system. Restricting attention for a while to the dominant static non-linearities, it is easily seen, that the pilot-valve model is of the Wiener type and the actuator model of the Hammerstein type, while the three-stage valve model is a typical example of the general model structure of Fig. 3.1 (c).

So what is required in the approach to identification and validation, is a characterization of the non-linear system by the general model structure of Fig. 3.1 (c) (which includes the simpler Hammerstein and Wiener models), and which moreover allows a continuous time state space representation of the linear dynamic blocks, and also a frequency domain interpretation of the dynamic behaviour of the non-linear system. Although in a setting, completely different from the standard system identification approach sketched before, this way of describing non-linear systems can be found in the field of Describing Function (DF) theory. It is remarkable, that Atherton, who provides an extensive treatment of DF theory in his book [9], takes the general model of Fig. 3.1 (c) as a basis for the analysis of non-linear system dynamics. In fact, the same approach is found by Föllinger [38].

Although the Describing Function method is to be discussed in more detail in Subsection 3.2.1, a rough characterization is given here to indicate how this method fits in the desired approach to identification. Basically, the DF method has been developed and applied, in order to allow a frequency domain approach to the control design for non-linear systems [9, 38, 130, 137]. Roughly speaking, the DF of a system can be seen as its 'frequency response', which depends on the amplitude of the input signal. In case of a memoryless non-linearity, the DF reduces to a gain, which depends on the amplitude of the non-linearity input signal.

The properties of the DF make it especially useful for the analysis of the dynamic behaviour of non-linear systems, especially those characterized by the general model of Fig. 3.1 (c). Atherton [9] and Föllinger [38] give numerous examples of this, among others the analysis of limit cycling behaviour. Furthermore, Atherton briefly describes, how a measured DF of a static non-linearity can be used to identify the underlying non-linear function, for instance in the form of a piece-wise-linear function [9].

So, the Describing Function method allows a proper characterization of the general model of Fig. 3.1 (c) in the frequency domain, and also allows the identification of static non-linearities. What is not found in literature, however, is a combination and extension of these possibilities of the DF method, in order to identify both the linear dynamics and

the static non-linearity of the system. Actually, this is an important topic to be considered in this Chapter. It might be noted here, that the DF method allows any representation of the linear dynamic blocks in Fig. 3.1, so that the method fits well in the desirable grey-box modelling approach.

Obviously, when applying the Describing Function method to non-linear system identification in the frequency domain, it is highly important to understand how the DF method is to be interpreted in terms of input-output behaviour. In other words, it is important to know, what interpretation is to be given to the frequency response of a non-linear system. This subject is discussed next.

Interpretation of non-linear frequency responses; linear dynamics

Although the Volterra kernel representation is not suitable for identification purposes, Peyton Jones and Billings have used this description of non-linear systems to give an interpretation of the frequency response of a non-linear system [114]. Without going into details, some of their main ideas are briefly mentioned here.

Related to the so-called higher order kernels of the Volterra series expansion, higher order (i.e. multidimensional) frequency responses are defined, which describe the dynamic input-output behaviour of a non-linear system. As described by Peyton Jones and Billings, typically non-linear phenomena in the input-output behaviour of the system in the frequency domain, that can not be explained by the unidimensional linear frequency response, may be resolved into two basic interference effects [114]:

- *Intra-kernel interference.* This occurs within any of the Volterra kernels. This effect is primarily non-linear in frequency and describes the transfer of energy between spectral components in the frequency domain, i.e. the output spectrum at certain frequency is determined by the input spectrum of several (possibly all) frequencies.
- *Inter-kernel interference.* This occurs between each of the Volterra kernels. This interference effect determines the non-linear input amplitude dependence of the gain and the phase at a certain frequency.

Obviously, these interference effects are not found in linear systems, where input frequencies pass independently through the system, while the gain and phase at each frequency is independent of the amplitude of the input signal.

With the interpretation of non-linear frequency responses in terms of higher order interference effects, described above, Peyton Jones and Billings show the close links to Describing Function theory [114]. They recall, that the DF is a quasi-linear (but amplitude dependent) transfer function relating input and output components at the same frequency, and show that the DF is given by the linear frequency response of the system, whose gain and phase are modified by the inter-kernel interference terms of higher order. They also illustrate, that these interference terms vanish, if the input amplitude goes to zero (apart from a steady state or d.c. input). With this interpretation, it is possible to come up with a new definition of the linear dynamics of a non-linear system [114], which may also be applied to systems with hard non-linearities, because DF theory also applies to this type of systems [9, 130]:

Definition 3.1.2 *The linear dynamics of a non-linear system (for some operating point) are the dynamics of that system, represented by the first order frequency response of the system, being the Describing Function of the system as the amplitude approaches zero.*

Although this definition clearly illustrates the relation between the non-linear frequency response, the Describing Function and the linear dynamics of a non-linear system, the question remains how the linear dynamics are to be identified from measured frequency responses. The reason is, that the frequency response is necessarily obtained by applying an input signal of non-zero amplitude. In other words, the question remains, how the non-linear system dynamics are to be excited. This is discussed next.

Excitation of non-linear system dynamics

In the field of (non-)linear system identification, the use of Pseudo Random Binary Signals (PRBS) is widespread [76, 85]. However, Leontaritis and Billings show [76], that for non-linear systems identifiability can be lost with this type of excitation signal. Therefore, they recommend other types of random excitation signals, such as an independent sequence with a gaussian distribution for a system with power constraints, and an independent sequence with a uniform distribution for a system with an amplitude constraint on the input. Although these signals are optimal in some sense for open loop configurations, the situation for the closed loop configuration of Fig. 3.1 (c) is more complicated.

This case is treated by Billings and Fakhouri [14]. They show, that for proper identification of the general model, separable (random) processes are required as inputs. Without treating this property in detail here, it can be stated that gaussian processes (so with normal distribution) and sinewave processes belong to this class [14]. This is also shown by Atherton [9], who uses this property to show that the Describing Function leads to the best linear approximation of the system for that class of input signals. It is therefore not surprising, that Atherton treats two types of DF's, namely the Sinusoidal Input Describing Function (SIDF) and the Random Input Describing Function (RIDF).

So, when applying DF theory to characterize the dynamics of a non-linear system, a choice has to be made between sinusoidal input signals and normally distributed random signals. In this work, sinusoidal inputs have been used, for two reasons:

- Sinusoidal signals have a deterministic and periodic character, so that they excite the non-linearities of a system in a deterministic and reproducable way. Given the periodic character of the input signal, time averaging may be used to get rid of noise effects, without affecting the deterministic (non-linear) input-output behaviour [141]. This does not hold for input signals with a random character; they excite the non-linearities of the system in a random way, and time averaging will also reduce the effects of the non-linearity on the input-output behaviour. The result is, that the random signal causes the input-output behaviour to be 'linearized'.
  In case a linear characteristic of the system is required, while no structural information on the non-linearity of the system is available, this linearizing effect of random excitation signals may be utilized. However, when structural insight in the non-linear character of the system is available, which is the case here, this information should be utilized to distinguish between linear dynamics and non-linearity, meaning that random excitation signals are not appropriate.
- An important reason to apply sinusoidal signals is to avoid the effect of intra-kernel interference [114]. Because the DF method might be interpreted as that input frequencies pass independently through the system, it is important to obtain experimental DF's under conditions that avoid intra-kernel interference. This is possible by

applying a sinusoidal input of a single input frequency, which guarantees that the output at that frequency component is just the result of the applied input signal at that frequency, and not related to other spectral components of the input.

With the arguments given so far in this Subsection, the method of Sinusoidal Input Describing Functions (SIDF's), that will be discussed in more detail in Subsection 3.2.1, has been chosen as a keystone in the approach to the identification of the non-linear models of the hydraulic servo-system. Actually, the same arguments also play a role in the validation of the identified models, as is discussed next.

Validation of non-linear system models

The problem of model validation is to determine whether the identified model does agree sufficiently well with the behaviour of the real system, as it is described by available data [85]. Thereby, two types of model validation can be distinguished:

- Validation of the identified model with respect to the data that were used for the identification.
- Validation of the model with respect to 'fresh' data, which were not used for the identification step. This is called cross-validation [85]. The fresh data may be just another measurement, i.e. obtained with another realization of the stochastic input and/or noise processes. However, it is also possible to validate the model with data, obtained from other types of input signals.

In the field of system identification, different techniques of (non-linear) model validation are found [77, 85, 154], such as statistical tests on residuals (correlation tests), evaluation of the loss function as a function of the model order, and simulation of the identified model. Because the identification is performed using frequency domain data, correlation tests are not directly applicable. Furthermore, it might be noted that the effect of the model order on the loss function is especially useful for black-box identification, where the required model order is completely unknown a-priori. In the chosen grey-box modelling approach however, this method is not quite useful. So, what remains as most practical method of model validation, is simulation of the identified non-linear model. Besides that, physical insight in the system behaviour will be used interprete and evaluate the outcomes of the identification.

In this Subsection, some techniques for the identification and validation of non-linear systems have been discussed. In fact, the discussion already contains some choices in the approach to the identification and validation of the hydraulic servo-system models, given the starting point of Subsection 3.1.1. The outline of this approach is desribed further in the next Subsection.

3.1.3 Approach to identification and validation

The chosen approach to identification and validation may be briefly characterized as the identification of a grey-box (state space) model in the frequency domain, based on measured Sinusoidal Input Describing Functions (SIDF's), and subsequent validation by means of model simulation. What is actually new in this approach, and needs special attention,

is the fact that the SIDF method will be used for the identification of both the linear dynamics and the static non-linearity in the general model structure of Fig. 3.1 (c).

As will be worked out later, in Subsection 3.2.2, the location of the static non-linearity in the closed loop configuration causes non-linearity of the frequency response due to inter-kernel interference effects. These effects can be avoided by proper input amplitude filtering (see Subsection 3.2.2), allowing the identification of the linear dynamics of the system, based on measured frequency responses. This identification comprises the fit of the frequency response of a linear model, of fixed order, and subsequent reconstruction of the state space model parameters. Thereby, the identifiability issue is to be considered (see Subsection 3.2.3). It might be noted, that the identification of the linear dynamics implies the validation of the chosen model structure, which resulted from the physical modelling of Chapter 2; the model structure is seen to be valid if the identification leads to satisfactory frequency response fits.

Once the linear dynamics have been identified and validated, the amplitude dependence of the system behaviour can be utilized to identify the (dominant) static non-linearity of the system, as will be explained in Subsection 3.2.4. The idea behind this technique is, to use the basic principles of DF theory [9, 38] to reconstruct the SIDF of the static non-linearity in Fig. 3.1 (c) from the measured SIDF of the whole system. After that, the static non-linearity can be identified from its DF, using the method of Atherton [9].

Applying the approach to identification and validation to the (subsystems of the) hydraulic servo-system, the linear dynamics and the dominant static non-linearities can be identified. Yet, there are some additional non-linearities in the hydraulic servo-system model to be identified and validated. Because these non-linearities are not easily characterized by a standard non-linear system structure like depicted in Fig. 3.1, no general approach to the identification and validation of these non-linearities is available. Therefore, these non-linearities will be identified and validated at an ad-hoc manner, using physical insight in the system behaviour. Thereby, emphasis is most on (qualitative) validation of the modelled effects, rather than on identification. As part of this ad-hoc approach, some dedicated measurements are to be performed with the system, such as to obtain data that clearly represent the non-linear behaviour to be validated.

A final issue to be mentioned here, is the reconstruction of physical parameters. In the grey-box modelling approach, the identified parameters have a physical interpretation. In some cases, it is desirable for insight in the system behaviour, to reconstruct the underlying physical quantities from the identified parameters. When applying the identification and validation approach to the real hydraulic servo-system, this issue will be adressed briefly.

Summarizing, the approach to the identification and validation of the hydraulic servo-system model, using experimental data of the real system, consists of three or four steps:

1. Identification and validation of linear dynamics.
2. Identification and validation of system non-linearities.
3. (Cross-)validation of the complete non-linear dynamic model.
4. If possible and desired, estimate-based reconstruction of physical parameters.

A more extensive elaboration of this approach, and the application of the approach to the real system, forms the contents of this Chapter.

3.1.4 Outline of the Chapter

The outline of the Chapter is as follows. First, the approach to the identification and validation of the system is elaborated in more detail in Section 3.2. After that, the experimental setup is described in Section 3.3. This description concerns the actual system, the servo-valve and the actuator, and the measurement and control devices that were used to obtain the experimental data. Then, the subsequent Sections treat the application of the identification procedure to the different subsystems of the hydraulic servo-system, respectively.

In Section 3.4, the results obtained with a flapper-nozzle valve are presented; it actually concerns the flapper-nozzle valve that acts as a pilot-valve for the three-stage valve. The latter is the system to be identified and validated in Section 3.5. The identification and validation of the hydraulic actuator is performed in two stages. The first stage is restricted to the basic actuator dynamics and non-linearities, and is discussed in Section 3.6. In the second stage, the identified basic properties of the actuator are preserved, while transmission line dynamics are included in the identification procedure. With the different subsystem-models being identified, some conclusions can be drawn on the obtained results, which will be done in Section 3.8.

3.2 Elaboration of approach to identification and validation

As a result of the discussion in the previous Section, an approach to identification and validation has been chosen, as presented in Subsection 3.1.3. This approach will be elaborated below, where two parts may be distinguished.

In the first part, consisting of two Subsections, the tools that are used in the presented approach are treated. This primarily concerns the method of Sinusoidal Input Describing Functions, which is treated in some detail in Subsection 3.2.1. Furthermore, the application of an input amplitude filter plays an important role in distinguishing between linear dynamics and static non-linearities, as explained in Subsection 3.2.2.

In the second part, comprising the remaining Subsections, the four steps in the procedure of identifying and validating the non-linear system models are treated. The identification of the linear dynamics can be performed as discussed in Subsection 3.2.3. In the next step, piece-wise-linear models of static non-linearities can be identified by a technique, presented in Subsection 3.2.4. The resulting model can be further validated as described in Subsection 3.2.5, while physical parameters may be deduced from identification results or from additional experimental data, as pointed out in Subsection 3.2.6. Finally, the Section is concluded in Subsection 3.2.7.

3.2.1 Sinusoidal Input Describing Functions

Background and basic principle

As mentioned earlier, it is often desirable to represent non-linear system behaviour in the frequency domain. The reason is, that linear system theory is well-established, and many tools are available to treat linear dynamic systems, especially frequency domain techniques like Nyquist stability analysis and frequency domain control design techniques. However,

direct application of these techniques to non-linear systems is not possible, because the well-known frequency response function cannot be defined for non-linear systems. Yet, for some non-linear systems, and under certain conditions, the *Describing Function* (DF) method, which can be seen as an extended version of the frequency response method, can be used to approximately characterize non-linear system behaviour [9, 130].

The basic idea behind the Describing Function method is, that the input-output behaviour of the system is represented by the steady state gain and phase relation between the base harmonics of the periodic input signal and the resulting periodic output signal. It should be noted, that this input-output relation not only depends on the frequency of the input signal, but also on its amplitude. For the most common case that the input is sinusoidal, for reasons described in Subsection 3.1.2, the resulting system representation is called a Sinusoidal Input Describing Function (SIDF) [102].

Although the Describing Function method is also called Harmonic Linearization Method, and can be seen as a quasi-linearization method [9], it differs considerably from the normal linearization method. The major difference is, that the Describing Function describes the input-output behaviour dependent on the amplitude of the input signal (like quasi-linearization). This allows the use of the method for robust control design [102]. Another difference is, that the Describing Function method is capable of characterizing systems with hard non-linearities [9, 130, 137]. Actually, both these properties make, that the Describing Function method is most frequently used for limit cycle analysis.

Before explaining how the SIDF method can be used for the identification and validation of non-linear physical models, the basic assumptions, the definition and the advantages of the method are discussed in the sequel.

Basic assumptions

In general, the SIDF method is applied to systems of the general type of Fig. 3.1 (c) [9]. However, the method is not restricted to this class of systems; it is also possible to use SIDF's for series connections of linear systems and non-linear blocks [38]; non-linear multivariable systems can be handled, and even non-linearities with multiple inputs can be considered instead of single input static non-linearities [9]. In fact, the application of the SIDF method is only subject to a very basic assumption, which is often referred to as the filter hypothesis [9]:

Assumption 3.2.1 *The non-linear system has low-pass characteristics, such that:*

1. *The fundamental component of the periodic output signal y of the non-linear system is large with respect to the higher harmonics, given a sinusoidal system input r, i.e.* $|H_{ry}(j\omega)| \gg |H_{ry}(jn\omega)|$, $n = 3, 5, 7, \ldots$.
2. *The fundamental component of the periodic input signal of the non-linearity u is large with respect to the higher harmonics, despite the feedback of non-sinusoidal signals from the non-linearity output signal x, i.e.* $|H_{xu}(j\omega)| \gg |H_{xu}(jn\omega)|$, $n = 3, 5, 7, \ldots$.

In this Assumption, $H_{ry}(j\omega)$ denotes the closed loop transfer function of the system, while $H_{xu}(j\omega)$ denotes the transfer function of the open loop of the system, including the feedback path, opened at the location of the non-linearity. For instance, considering Fig. 3.1 (c), $H_{xu}(j\omega) = G_1(j\omega)G_2(j\omega)G_3(j\omega)$.

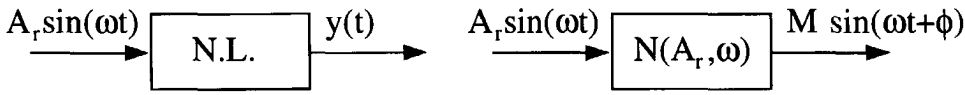


Fig. 3.2: Non-linear system and SIDF representation

For many systems, Assumption 3.2.1 is valid, especially for mechanical systems. Due to the inertial nature of this type of systems, they have a natural high-frequency roll-off, providing the necessary low-pass characteristics.

Although Assumption 3.2.1 forms the only inherent assumption for the SIDF method, a lot of systems allow somewhat more restrictive assumptions, which facilitate the analysis. So, just for reasons of simplicity of the analysis, the following assumptions are used in the remainder.

Assumption 3.2.2 *For the application of the Sinusoidal Input Describing Function method it is assumed, that:*

1. *The system contains only odd non-linearities.*
2. *The system is of the Single Input Single Output type (SISO).*

Note that this Assumption holds for the general model of Fig. 3.1 (c), if the static non-linearity is odd. For the hydraulic servo-system, this is a reasonable assumption, since the dominant static non-linearities of the system represent non-linear flow characteristics, which are generally odd and (approximately) symmetric.

Definition of the SIDF

Although different definitions of the SIDF are possible [9], it is most common to base the definition of the SIDF on a Fourier analysis of the output waveform, as follows [9, 38, 130]. Let a non-linear system be given, satisfying Assumption 3.2.1 and 3.2.2, with a sinusoidal input signal of amplitude A_r and frequency ω, i.e. $r(t) = A_r \sin(\omega t)$, as depicted in Fig. 3.2. The output $y(t)$ of this system will also be a periodic signal, though non-sinusoidal. Using Fourier series expansion, this output signal can be written as:

$$y(t) = \frac{a_0}{2} + \sum_{n=1}^{\infty} [a_n \cos(n\omega t) + b_n \sin(n\omega t)] \tag{3.1}$$

with the Fourier coefficients given by:

$$\begin{aligned} a_0 &= \tfrac{1}{\pi} \textstyle\int_{-\pi}^{\pi} y(t) \mathrm{d}(\omega t) \\ a_n &= \tfrac{1}{\pi} \textstyle\int_{-\pi}^{\pi} y(t) \cos(n\omega t) \mathrm{d}(\omega t) \\ b_n &= \tfrac{1}{\pi} \textstyle\int_{-\pi}^{\pi} y(t) \sin(n\omega t) \mathrm{d}(\omega t) \end{aligned} \tag{3.2}$$

In these equations, the coefficient a_0 represents the mean value of the output signal. Because the non-linearity is odd, Assumption 3.2.2, the sinusoidal input results in a zero-mean output signal, so $a_0 = 0$. It should be noted, that for a given system, the other

coefficients in (3.2) depend on both the amplitude A_r and the frequency ω of the input signal.

As stated earlier, the basic idea behind SIDF is now, that the output signal $y(t)$ of (3.1) is approximated by its base harmonic:

$$\hat{y}(t) = a_1 \cos(\omega t) + b_1 \sin(\omega t) = (b_1 + j a_1) e^{j\omega t} = M e^{j(\omega t + \phi)} = M \sin(\omega t + \phi) \qquad (3.3)$$

where the amplitude of the approximate output signal M and its phase ϕ are given by:

$$M(A_r, \omega) = \sqrt{a_1^2 + b_1^2}; \qquad \phi(A_r, \omega) = \arctan \frac{a_1}{b_1}$$

Using this approximation of the output of the non-linear system, the Sinusoidal Input Describing Function is defined as follows (see also Fig. 3.2):

Definition 3.2.3 *The Sinusoidal Input Describing Function (SIDF) of a non-linear system is the complex ratio of the fundamental component of the output signal and the sinusoidal input signal, i.e.*

$$N(A_r, \omega) = \frac{M e^{j(\omega t + \phi)}}{A_r e^{j\omega t}} = \frac{M}{A_r} e^{j\phi} = \frac{1}{A_r}(b_1 + j a_1) \qquad (3.4)$$

Advantages of the SIDF-method

From the definition of the SIDF, the relation between the SIDF and the frequency response is clear: for a linear system, the SIDF is independent of the input amplitude and equals the frequency response $G(j\omega)$ of the system. This is actually one of the major advantages of the method. A more specific overview of the advantages of the use of SIDF's to characterize non-linear systems is given in the following list:

- The SIDF can be interpreted as the frequency response (for certain input amplitude) of a non-linear system, and therewith allows application of available analysis and control design tools for linear systems to non-linear systems [9, 130].
- For small input amplitudes, the SIDF converges to the frequency response of the linear dynamics of the system, as defined by Definition 3.1.1 for the case that no hard non-linearities are present (normal linearization), and defined by Definition 3.1.2 for the case that hard non-linearities are present [114].
- The SIDF method gives a good quasi-linear approximation of the input-output behaviour for large input amplitudes, contrary to normal linearization methods [9]. This makes the SIDF-method valuable for:
  - identification and validation purposes: the system can be excited with large input signals, yielding good signal to noise ratios. Applying the SIDF-method to both system and model, identification and validation of non-linear dynamics is possible.
  - control design purposes: the SIDF describes amplitude dependent dynamics, which have to be controlled robustly. Modern control design techniques can be used to find robust controllers that reduce the amplitude sensitivity of the system [102].

- The SIDF-method allows approximation of systems with hard non-linearities, like Coulomb friction [9, 38, 130].
- With dedicated measurement devices, Subsection 3.3.3, it is easy to determine an experimental SIDF of a non-linear system. What is mostly called the frequency response of a real system is actually a SIDF, as discussed below.

Determination of a SIDF of a non-linear system

In order to use the SIDF method properly for identification and validation purposes, it is important that the determination of the SIDF of the non-linear model corresponds to the experimental determination of the SIDF of the real non-linear system. For a non-linear model, there are some different ways to determine the SIDF, depending on the model structure.

For static non-linearities such as a saturation, possibly in series connection with linear dynamics, it is possible to calculate the SIDF analytically by solving (3.2). Examples are given in [9, 130]. Alternatively, the integrals of (3.2) can be computed by numerical integration. For more complex models however, for instance with non-linearities in a feedback loop as in Fig. 3.1 (c), direct calculation of the SIDF from the non-linearity is not possible. In that case, the SIDF can be determined by simulating the non-linear model with a sinusoidal input, and determining the fundamental harmonic (3.3) of the steady state output signal.

Although the fundamental harmonic may be determined by numerically integrating the integrals of (3.2), it is faster to make use of the fact that (3.3) is just the sinusoidal signal that minimizes the error between the real output y and the approximate output $\hat{y}$ in the sense of a mean squares criterion, as explained by Towill [137] and also by Atherton [9]. Suppose, that one period of the output signal (for sinusoidal input at frequency ω and input amplitude A_r) is available as a simulated time series y_N, with N the number of data points. Then the signal that approximates this simulated output is written as:

$$\hat{y}_N = \hat{a}_1 u_{cos,N} + \hat{b}_1 u_{sin,N} = \Phi_N \hat{\theta}_N \tag{3.5}$$

with the regression vector Φ_N being composed of discrete time series $u_{cos,N}$ and $u_{sin,N}$ of the cosine and the sine function respectively, and $\hat{\theta}_N$ the parameter vector containing the Fourier coefficients of the fundamental harmonic to be determined. The values of these coefficients are found by minimizing the following least squares criterion:

$$V_N(\theta) = \frac{1}{N}(y_N - \Phi_N\theta)^T(y_N - \Phi_N\theta) \tag{3.6}$$

This quadratic optimization has an analytical solution in the desired parameter vector θ, namely [85]:

$$\hat{\theta}_N = \begin{bmatrix} \hat{a}_1 \\ \hat{b}_1 \end{bmatrix} = \left[\Phi_N^T \Phi_N\right]^{-1} \Phi_N^T y_N \tag{3.7}$$

Thus, substituting the coefficients $\hat{a}_1$ and $\hat{b}_1$ that minimize (3.6) in the definition of the SIDF (3.4), the SIDF of the simulation model is determined for the concerning input frequency ω and amplitude A_r. Obviously, this operation can be repeated for a whole range of discrete input frequencies and amplitudes.

For practical use of the SIDF-method, it is not useful to cover the whole two-dimensional space of varying input frequencies and amplitudes. Therefore, only two types of SIDF's will be used in the remainder, namely the *frequency response* and the *amplitude response.* To avoid confusion, they are defined more specifically.

Definition 3.2.4 *The frequency response $H_{ry}^{A_r}(j\omega)$ of a non-linear system or model with input r and output y, is a SIDF according to Definition 3.2.3, for certain fixed input amplitude A_r, and for certain continuous or discrete frequency interval $[\omega_1, \omega_2]$.*

Definition 3.2.5 *The amplitude response $N_{ry}^{\omega}(A_r)$ of a non-linear system or model with input r and output y, is a SIDF according to Definition 3.2.3, for certain fixed input frequency ω, and for certain continuous or discrete input amplitude interval $[A_{r1}, A_{r2}]$.*

Besides that these input-output characteristics of non-linear systems can easily be determined with software tools for simulation models [67], there are also hardware tools to determine these characteristics experimentally for real systems. For instance, the well-known frequency response measurements using a sinusoidal source signal, also known as swept-sine measurements, are easily performed (automatically) with a dynamic signal analyzer or with a harmonic analyzer. Strictly spoken, these measurements, which are generally performed for certain input amplitude, exactly constitute the measured frequency response of a non-linear system according to Definition 3.2.4. Basically, the hardware tools also allow the measurement of amplitude responses according to Definition 3.2.5, though not fully automized.

As already indicated in Subsection 3.1.3, the use of SIDF's for the identification and validation of the hydraulic servo-system is based on the distinction between the non-linearity of the system and its linear dynamics. Whereas the amplitude responses are used to characterize and validate the non-linearities of the system, the frequency responses play an important role in the identification of the dynamics of the system. Clearly, from this viewpoint it is necessary, that the measured frequency response represents the linear dynamics of the system according to Definition 3.1.1 or Definition 3.1.2. In that case namely, it is possible to identify linear models for the dynamics from measured frequency response data, see Subsection 3.2.3. As explained in the next Subsection, a measured frequency response does not describe the linear dynamics in the general case, but it does if proper filtering of the input amplitude is applied.

3.2.2 Input amplitude filter design

In general, the frequency response of a non-linear system is inherently non-linear. However, for a somewhat restricted class of non-linear systems, it is possible to represent the linear dynamics of the system by frequency response measurements using an input amplitude filter.

Non-linearity of frequency response (SIDF)

As argued in Subsection 3.1.2, sinusoidal inputs have been chosen to measure the frequency response of the system, in order to avoid non-linearity due to intra-kernel interference. Nevertheless, in the general setting of Fig. 3.1 (c), the measured frequency response (SIDF)

from input to output is non-linear. This non-linearity of the frequency response is actually caused by inter-kernel interference (amplitude dependent behaviour), and can be interpreted as follows.

The frequency response is taken for some constant input amplitude A_r at some frequency interval, Definition 3.2.4. Due to the dynamics $G_1(j\omega)$, the amplitude A_u of the periodic input signal of the non-linearity will not only depend on the input amplitude A_r, but also on the frequency ω. This implies, that for constant A_r, the amplitude A_u varies for the different frequencies of the frequency response measurement. Because the gain (DF) of the non-linear block depends on its input amplitude A_u, it is clear that the (closed loop) gain of the system varies with frequency. In other words, different points of the frequency response correspond to different dynamic behaviour. So the frequency response is inherently non-linear.

The result is, that it is not possible to fit the frequency response by a linear dynamic model. Actually, the well-known gain-phase relationship for linear systems, shown by Bode [18] and discussed by Maciejowski [87], is violated. As described by Tomlinson et. al. [129, 136], it is possible to detect this kind of non-linearity in the frequency response by applying the Hilbert Transform. Using the properties of causal linear systems, it can be shown that the Hilbert Transform of a frequency response equals the original frequency response if and only if the frequency response is linear. So the Hilbert Transform of a non-linear frequency response results in a new, different frequency response. The deviation is a measure for the non-linearity [129, 136].

Although the Hilbert Transform seems valuable to detect non-linearity from a theoretical point of view, its practical use is quite restrictive. For frequency responses on a finite frequency interval, which is the practical situation, it is actually necessary to extend the data-set in order to obtain reliable results [67]. This extension requires a-priori knowledge on the model order and structure. Although this knowledge is assumed to be available, Subsection 3.1.1, the method of Hilbert Transform is still rather complicated. Therefore, it is better to use the a-priori knowledge to find linear models of correct order and structure that approximate the frequency responses, Subsection 3.2.3, and consider the misfit as a measure of non-linearity.

In the approach to identification and validation of the hydraulics servo-system models, Subsection 3.1.3, it is not primarily important to detect non-linearity of the system, but the linear dynamics should be explicitly distinguished from the non-linearity. In other words, a linear frequency response measurement should be obtained from the system. Under certain conditions, this is possible for the systems of Fig. 3.1, by applying an input amplitude filter, manipulating the input amplitude A_u of the non-linearity such, that the non-linearity behaves like a constant gain during the frequency response measurement.

Iterative input amplitude filter design

The basic idea behind input amplitude filtering is, that the amplitude of the sinusoidal input A_r is not constant over frequency, but depends on frequency such that the amplitude A_u of the periodic input of the non-linearity is constant over frequency. In that case, the static non-linearity behaves like a constant gain for all frequencies, and the resulting frequency response reflects linear dynamic behaviour.

Denoting the input amplitude filter by its frequency response function $F(j\omega)$, and applying it to the general model of Fig. 3.1 (c), the configuration of Fig. 3.3 is obtained.

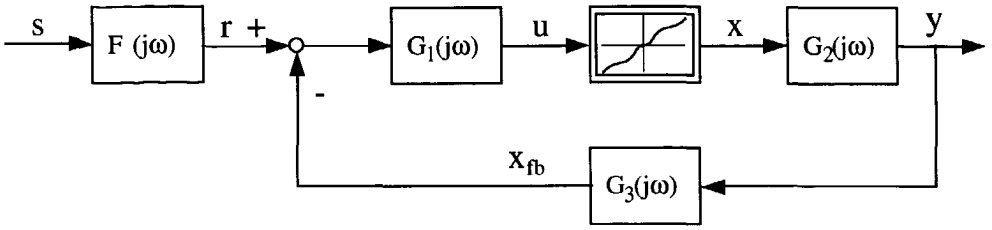


Fig. 3.3: Block scheme representation of non-linear system (general model) with input amplitude filtering

In this setting, the technique of applying an input amplitude filter $F(j\omega)$ such that the resulting frequency response $\tilde{H}_{ry}$[3] of the system is linear, is formalized by the following Theorem:

Theorem 3.2.6 *Given a non-linear system according to Fig. 3.3, satisfying Assumption 3.2.1 and 3.2.2, the input-output frequency response $\tilde{H}_{ry}^{\alpha_s}(j\omega)$ of the system with source input amplitude $A_s = \alpha_s$ is linear if the applied amplitude filter $F(j\omega)$ satisfies:*

$$|F(j\omega)| = \left|\tilde{H}_{ry}^{\alpha_s}(j\omega)\right|^{-1} |G_2(j\omega)| \tag{3.8}$$

where the input-output frequency response can be written as:

$$\tilde{H}_{ry}^{\alpha_s}(j\omega) = \frac{G_2(j\omega)\beta G_1(j\omega)}{1 + G_3(j\omega)G_2(j\omega)\beta G_1(j\omega)} \tag{3.9}$$

and $\beta = N_{ux}(\alpha_u)$ is the real gain of the static non-linearity for input amplitude $A_u = \alpha_u$. The input amplitudes of the signals s and u are related to each other as:

$$\alpha_u = \alpha_s \frac{1}{\beta} \tag{3.10}$$

Proof: For some constant source amplitude $A_s = \alpha_s$ and some filter $F(j\omega)$ that satisfies:

$$|F(j\omega)| = \left|\frac{G_2(j\omega)\tilde{H}_{ux}(A_u, j\omega)G_1(j\omega)}{1 + G_3(j\omega)G_2(j\omega)\tilde{H}_{ux}(A_u, j\omega)G_1(j\omega)}\right|^{-1} |G_2(j\omega)|$$

the frequency response of the system can be written as (see Atherton [9], page 140):

$$\tilde{H}_{ry}^{\alpha_s}(j\omega) = \frac{G_2(j\omega)\tilde{H}_{ux}(A_u, j\omega)G_1(j\omega)}{1 + G_3(j\omega)G_2(j\omega)\tilde{H}_{ux}(A_u, j\omega)G_1(j\omega)} \tag{3.11}$$

with $\tilde{H}_{ux}(A_u, j\omega)$ the SIDF of the static non-linearity, corresponding to the given source signal and filtering. This frequency response is linear, if the SIDF of the static non-linearity is a constant, so if $\tilde{H}_{ux}(A_u, j\omega) = \beta$, $\forall\omega$.

[3]The tilde denotes that the frequency response has been obtained using an input amplitude filter.

It is easily proved, that the SIDF of a static non-linearity is a constant if and only if the input amplitude of the non-linearity A_u is constant, so $A_u(j\omega) = \alpha_u$, $\forall\omega$. Hereby, $\beta = N_{ux}(\alpha_u)$.

In order to prove that appropriate filtering gives $A_u(j\omega) = \alpha_u$, $\forall\omega$, the amplitude of the input signal u is written as:

$$\begin{aligned} A_u(j\omega) &= \left|\frac{G_1(j\omega)}{1+G_3(j\omega)G_2(j\omega)\tilde{H}_{ux}(j\omega)G_1(j\omega)}\right| |F(j\omega)|\, A_s \\ &= \left|\frac{G_1(j\omega)}{1+G_3(j\omega)G_2(j\omega)\tilde{H}_{ux}(j\omega)G_1(j\omega)}\right| \left|\frac{1+G_3(j\omega)G_2(j\omega)\tilde{H}_{ux}(j\omega)G_1(j\omega)}{G_2(j\omega)\tilde{H}_{ux}(j\omega)G_1(j\omega)}\right| |G_2(j\omega)|\ \alpha_s \end{aligned}$$

using the basic principles of the DF method [9, 38]. Obviously, $A_u(j\omega) = \alpha_u$, $\forall\omega$, if the filter $F(j\omega)$ is such that $\tilde{H}_{ux}(j\omega) = \beta$, $\forall\omega$, which is satisfied by (3.8),(3.9) and (3.10). □

From the above Theorem, it is clear that for any system according to Fig. 3.3, there is a filter $F(j\omega)$ **that results in a linear frequency response** $\tilde{H}_{ry}^{\alpha_s}(j\omega)$ **of the system. The problem** is however, that Theorem 3.2.6 formulated in an implicit form. For the filter design, the linear frequency response of the system, $\tilde{H}_{ry}^{\alpha_s}(j\omega)$, is required. On the other hand, the filter is necessary to obtain the linear frequency response. This problem is effectively solved by adopting an iterative design procedure.

Starting with a frequency response measurement without filter, a first approximate filter is designed based on the measured (non-linear) frequency response. Because the non-linear frequency response roughly reflects the linear dynamics, the first filter design is already a good approximation of the final design. Applying the designed filter, a next frequency response is measured, which is used for the design of the filter in the next iteration step, and so on.

Besides the implicit character, there are two other complications in the filter design. First, $G_2(j\omega)$ has to be known a-priori. Second, the input amplitude level α_s has to be chosen such that $\beta = N_{ux}(\alpha_u)$ (with α_u by (3.10)) corresponds to β in the frequency response $\tilde{H}_{ry}^{\alpha_s}(j\omega)$, (3.9). The seriousness of these problems depends on the smoothness of the non-linearity.

If the non-linearity is smooth, the amplitude response $N_{ux}(A_u)$ is rather flat, at least in some amplitude range, which means that the gain β is not very sensitive to the input amplitude level α_s in the corresponding input amplitude range. Using some (physical) insight in the system behaviour, possibly obtained during the iterative filter design process, one could probably choose an input amplitude level α_s in the desired range, leading to reasonable results.

From this viewpoint, the requirement that $G_2(j\omega)$ has to be known can be somewhat relaxed: its steady state gain needs not to be known exactly, because it can be accounted for by the choice of the input amplitude α_s. The result is, that only the *dynamics* of $G_2(j\omega)$ need to be known.

Given the setting of the identification problem in Section 3.1, where the general model structure of Fig. 3.1 (c) applies to the three-stage servo-valve, with f_1 as dominant non-linearity, the dynamics of $G_2(j\omega)$ are known, because $G_2(j\omega)$ represents the main spool as an integrator, of which the gain is unknown. Actually, the input amplitude filter design for the other subsystems to be identified is much simpler; for the flapper-nozzle pilot-valve, with output non-linearity f_1, only $G_2(j\omega) = 1$ and $G_3(j\omega) = 0$, while for the actuator model, with input non-linearity f_2, $G_1(j\omega) = 1$ and $G_3(j\omega) = 0$. In the latter case, the input amplitude filter even reduces to a unity gain, as might be expected.

So, in short, using some insight in the system behaviour, it is possible to iteratively design an input amplitude filter $F(j\omega)$ in the setting of Fig. 3.3, according to Theorem 3.2.6, such that the measured frequency response $\tilde{H}_{ry}^{\alpha_r}$ is linear, i.e. reflects the linear dynamics of the system. As such, the filter design is to be performed as a first step prior to the actual four-step identification and validation procedure, presented in Subsection 3.1.3. As the first of these four steps, the identification and validation of the linear dynamics of the system is discussed in the next Subsection.

3.2.3 Identification and validation of linear dynamics

Given the setting described in Section 3.1, the identification problem for the linear dynamics can be formulated as is done below. Further, the solution to the identification problem is discussed, including the identifiability issue. Finally, the validation of the adopted model structure is briefly adressed in the end of this Subsection.

The identification problem

The identification problem concerns the identification of a structured linear state space model:

$$M(\theta): \begin{cases} \dot{X} &= A(\theta)X + B(\theta)U \\ Y &= C(\theta)X \end{cases} \tag{3.12}$$

with matrices A, B, C parametrized by the m-dimensional parameter vector $\theta = [\theta_1 \cdots \theta_m]^T$, and U, X, Y the input-, state- and output vector respectively. Note, that this system is not necessarily of the SISO type, so U and/or Y may be vector-valued.

Now suppose, that measured frequency response data $H_{UY}(j\omega_i)$, $i = 1, \ldots, N$ are available[4], corresponding to the transfer function matrix $G_{UY}(j\omega, \theta)$ of the system (3.12). The identification problem is then, to find an optimal parameter vector $\hat{\theta}$ such that the corrresponding frequency response $\hat{G}_{UY}(j\omega_i, \hat{\theta})$, $i = 1, \ldots, N$ of the model (3.12) matches the experimental data.

Identifiability of parameters

When identifying parameters in a certain pre-specified model structure $M(\theta)$, one should take care of the identifiability of the parameters. Hereby, identifiability means that the identification of the parameter vector θ from experimental data leads to a unique result. This identifiability issue has been adressed rather extensively in literature in the field of system identification, for instance in Walter (Ed.) [142] and Ljung [85]. Without extensively discussing issues like local and global structural identifiability, the identifiability of the model structure $M(\theta)$, given by (3.12), is defined as follows [25, 40, 75, 85]:

Definition 3.2.7 *A linear state space model $M(\theta)$ according to (3.12) is identifiable from a transfer function matrix of proper dimensions, in a certain frequency interval $[\omega_1, \omega_2]$, if:*

$$G_{UY}(j\omega, \theta) = G_{UY}(j\omega, \theta') \Rightarrow \theta = \theta', \quad \omega \in [\omega_1, \omega_2]$$

where $G_{UY}(j\omega, \theta) = C(\theta)\left[j\omega I - A(\theta)\right]^{-1} B(\theta)$.

[4]The superscript A_U denoting the input amplitude is omitted for ease of notation.

With this Definition, identifiability can be seen as a structural property of the model structure $M(\theta)$, which is determined by the parametrization of the state space model (3.12). Obviously, this parametrization is the result of the physical modelling process, and can not be changed as long as the physical structure of the model is to be preserved. Thus, identifiability is a property of the model, which can be tested, and for which conditions on the parametrization may be derived, but which can not be changed without changing the model structure.

In Walter (Ed.) [142], Godfrey and DiStefano [40] give a clear overview of some basic methods to test the identifiability of linear (continous time) state space models, and show with examples that they lead to similar results. One of these methods is the Transfer Function Approach, and is well-applicable to low-order SISO models. The method involves the elaboration of the transfer function $G_{uy}(j\omega, \theta)$ of (3.12) in terms of the m elements of the parameter vector θ, possibly using software tools for symbolic computation [75]. Thus, each of the n coefficients in the transfer function is expressed in terms of the m parameters of the state space model. Hereby, $n = 1 + p + z$ is the number of parameters that can be identified from the input-output transfer function, with p the number of poles and z the number of zeros; one parameter corresponds to the gain of the system.

Given the n coefficients of the transfer function of the model $M(\theta)$, expressed in the m state space parameters, identifiability according to Definition 3.2.7 is checked by analyzing whether the m parameters in θ can be solved explicitly from the n coefficients. Obviously, this is not the case if $m > n$, and the model is not identifiable. In this case, $m - n$ parameters have to be chosen a-priori, for instance based on physical arguments. Hereby, the symbolic expressions for the n coefficients will indicate which parameters have to be chosen beforehand, in order to arrive at an identifiable model structure.

Although the Transfer Function Approach for testing identifiability may work for low-order SISO models, the method has some disadvantages [40], especially for higher order models. For these models namely, the (symbolic) expressions of the coefficients in the transfer function $G_{uy}(j\omega, \theta)$ can become extremely complicated and unsolvable for the elements of the parameter vector θ. In that case, other methods might be preferable, for instance the Markov Parameter Approach or the Similarity Transform Approach [40, 75]. For a discussion of these methods, the reader is referred to the given references.

Once the model (3.12) is found to be identifiable, possibly using additional a-priori information, the remaining problem is to estimate a parameter vector $\hat{\theta}$, by identifying a transfer function model $\hat{G}_{UY}(j\omega_i)$, $i = 1, \ldots, N$ with a pre-specified number of poles and zeros from experimental data $H_{UY}(j\omega_i)$, $i = 1, \ldots, N$. The technique(s) to be used for this parameter estimation problem will be discussed next.

Parameter estimation

For the general problem of identifying linear models in the frequency domain, different techniques are available, for instance curve-fitting techniques as described by Hakvoort [46]. Application of these techniques, or more specifically using the software tools that are based on these techniques, requires some experience. From a practical point of view, in order to obtain good frequency domain fits, experience in choosing model orders and frequency domain weightings is more important than knowledge of the theoretical background of the identification method. From this point of view, the parameter estimation problem is solved by just using standard available software tools, in this case within the software package

Matrix$_X$. Thereby, the estimation of a SISO transfer function model is distinguished from the more general case involving the estimation of multiple transfer functions, as in a MIMO model.

The identification of a SISO transfer function $\hat{G}_{uy}(j\omega_i)$, $i=1,\ldots,N$ with pre-specified numbers of poles p and zeros z, is simply performed using a standard tool, in this case the TFID-command (Transfer Function IDentification) of Matrix$_X$. With this tool, a continuous SISO transfer function is identified, using Chebyshev polynomials as basis functions [63]. With this tool, it is easy to emphasize the accuracy of the fit in certain frequency regions, by applying a frequency dependent real, positive weighting vector $W_{uy}(\omega_i)$, $i=1,\ldots,N$. By means of visual inspection of the resulting fit, the weightings may be adjusted somewhat, and reasonable fits are readily found, as shown later in Subsection 3.5.2.

For the more general case, a non-linear optimization routine is applied to solve the stated identification problem. This method was developed by De Boer [19] and earlier applied by Heintze et.al. [52]. The method does not directly identify a SISO transfer function model $\hat{G}_{uy}(j\omega_i)$, $i=1,\ldots,N$ like the TFID-command, but optimizes the parameter vector θ with respect to a user-defined cost function, which quantifies the mismatch between the K frequency response(s) of the model and the corresponding measured frequency response(s), at N frequency points ω_i as follows:

$$\hat{\theta} = \arg\min_{\theta} \sum_{k=1}^{K} \sum_{i=1}^{N} W_k(\omega_i) \left\{ \frac{|G_k(j\omega_i,\theta)| - |H_k(j\omega_i)|}{|H_k(j\omega_i)|} \right\}^2 \tag{3.13}$$

The real positive weighting vector $W_k(\omega_i)$, $i=1,\ldots,N$ can be used to emphasize the mismatch of certain frequency response k for certain frequency regions. Note, that the cost criterion in (3.13) actually sums the quadratic relative errors in the amplitude of the frequency response. Relative errors have been used instead of absolute differences, in order to avoid heavy weight of resonance peaks and light weight of anti-resonance dips.

The big advantage of solving the identification problem by the optimization (3.13) is, that the method is not restricted to (low order) SISO systems. Provided that a good routine is available to solve the non-linear optimization problem, for instance OPTIMIZE of Matrix$_X$, this method is quite tractable. The only point that needs attention, is the issue of convergence to the global optimum, which is mainly a matter of providing the optimization routine with a good initial estimate θ_0.

If a reasonably accurate theoretical model is available, it is obvious to use the linearization of this model as the initial estimate. If the subsequent optimization leads to an optimum with satisfactory fits of the frequency responses, this can be seen as an inherent validation of the adopted (theoretical) model structure. Might the initial estimate not lead to satisfactory results, an alternative is to use the experimental data to find an initial estimate, as described by De Boer [19]. He proposes to first identify a model that minimizes an equation-error criterion. Because this optimization problem is linear in the parameters, it has an analytical solution. The resulting model can then be used as the initial estimate for the non-linear optimization, which now should lead to a satisfactory identification result, if the model structure is valid.

Validation of model structure

Although the model order and even the structure are assumed to be given as a result of physical modelling, there is always the possibility that model order and/or structure appear to be invalid during the identification step. The model may appear to be either too simple or too complex.

In the first case, it will be impossible to find parameters that give a satisfactory fit of the model frequency response on the experimental response. Typical forms of undermodelling are the presence of (anti-)resonance peaks and phase lag due to high-frequency dynamics in the experimental frequency response, which can not be represented by the model. Obviously, this requires a review of the physical modelling of the system, leading to the inclusion of the unmodelled dynamic phenomena in the model. An extended (higher order) physically structured linear model will be the result, which should lead to a satisfactory match by identifying its parameters.

Another reason for mismatch during the identification might be the non-linearity of the frequency response. If possible, an imput amplitude filter $F(j\omega)$ should be applied, such as to avoid the excitation of the non-linearity, as described in Subsection 3.2.2. Otherwise, the mismatch will have to be accepted, provided that it is sure that the mismatch is not due to dynamic undermodelling.

The second case, namely that the model is too complex, occurs if too many dynamic effects have been included in the physical model. This may lead to identifiability problems, given experimental data for a certain frequency range, which do not reflect these dynamics. Note, that this is not a matter of identifiability of parameters within a given (correct) structure in the sense of Definition 3.2.7, but that the model structure is too wide. The result may be, that the identification leads to a model with pole/zero cancellations or with dynamics outside the relevant frequency range.

This effect might be denoted as overmodelling, just the reverse of undermodelling. As indicated by Ljung [85], overmodelling can be readily recognized, if the chosen model structure is compeared with the (anti-)resonances and high-frequency roll-off and phase lag of the experimental frequency response. Like in the case of undermodelling, a review of the physical modelling of the system is required in case of overmodelling; the model order should be reduced, preferably based on reasonable physical assumptions.

With the identification of the parameters and the validation of the model structure, discussed in this Subsection, the linear dynamics of the system are estimated. The next step in the procedure is then to identify the static non-linearities.

3.2.4 Identification of static non-linearities

The setting for the identification of the static non-linearity of the system has already been outlined in Section 3.1, where the starting point is the general model structure of Fig. 3.1 (c), given on page 122. Making Assumptions 3.2.1 and 3.2.2, the non-linearity of this system is supposed to be characterized by an experimental amplitude response $N^{\omega}_{ry}(A_{r,i})$, $i=1,\ldots,N$, of the system, according to Definition 3.2.5. The problem is now, to identify the static non-linearity $x = f(u)$ of this system from the given experimental amplitude response, provided that the linear dynamics have been identified.

To solve this problem, a rather strong Assumption is required, which is partially related to the required information on the system structure for the input amplitude filter design

in Subsection 3.2.2.

Assumption 3.2.8 *The a-priori knowledge of the system in Fig. 3.1 (c) is rich enough to calculate the transfer functions $\hat{G}_1(j\omega)$, $\hat{G}_2(j\omega)$ and $\hat{G}_3(j\omega)$ from the estimated closed loop transfer function:*

$$\hat{G}_{ry}(j\omega) = \frac{\hat{G}_2(j\omega)\hat{\beta}\hat{G}_1(j\omega)}{1 + \hat{G}_3(j\omega)\hat{G}_2(j\omega)\hat{\beta}\hat{G}_1(j\omega)}$$

with the real number $\hat{\beta}$ the gain of the non-linearity for the experiment used for identification, according to Theorem 3.2.6.

Although this Assumption is rather restrictive, many systems satisfy it. Note for instance, that the Hammerstein and the Wiener systems, as depicted in Fig. 3.1 (a) and (b) respectively, automatically satisfy this Assumption, because $G_3(j\omega) = 0$ is zero, and either $G_1(j\omega) = 1$ or $G_2(j\omega) = 1$.

Given Assumption 3.2.8, the idea behind the identification of the static non-linearity $x = f(u)$ from the measured closed loop amplitude response $N^{\omega}_{ry}(A_{r,i})$, $i = 1, \ldots, N$, is as follows. First, the knowledge of the linear system dynamics is utilized to calculate an estimated 'open loop' amplitude response $\hat{N}^{\omega}_{ux}(A_{u,i})$, $i = 1, \ldots, N$ of the static non-linearity from the closed loop amplitude response $N^{\omega}_{ry}(A_{r,i})$, $i = 1, \ldots, N$. In a second step, an approximate non-linear function $x = \hat{f}(u)$ is reconstructed from the estimated 'open loop' amplitude response. Although this two-step procedure has not been found in literature, it just utilizes basic principles from DF theory [9, 38], as explained below.

Referring to (3.11) on page 135 for the closed loop frequency response, the closed loop amplitude response of the system in Fig. 3.1 (c) for certain frequency ω can be written as:

$$N^{\omega}_{ry}(A_r) = \frac{G_2(j\omega)N^{\omega}_{ux}(A_u)G_1(j\omega)}{1 + G_3(j\omega)G_2(j\omega)N^{\omega}_{ux}(A_u)G_1(j\omega)} \tag{3.14}$$

In this equation, the amplitudes A_r and A_u of the signals r and u respectively, are related to each other as:

$$A_u = A_r \left| G_1(j\omega) \left[1 - G_3(j\omega)N^{\omega}_{ry}(A_r) \right] \right| \tag{3.15}$$

which is easily seen by writing down the signal balance for the system of Fig. 3.1 (c) in the frequency domain [38]:

$$\begin{aligned} u(j\omega) &= G_1(j\omega)\left[r(j\omega) - G_3(j\omega)y(j\omega)\right] \\ &= G_1(j\omega)\left[1 - G_3(j\omega)N^{\omega}_{ry}(A_r)\right] r(j\omega) \end{aligned}$$

With (3.14) and (3.15), an estimation for the 'open loop' amplitude response can be calculated from an experimental closed loop amplitude response, for certain frequency ω, as:

$$\hat{N}^{\omega}_{ux}(\hat{A}_{u,i}) = \frac{N^{\omega}_{ry}(A_{r,i})}{\hat{G}_1(j\omega)\hat{G}_2(j\omega)\left[1 - \hat{G}_3(j\omega)N^{\omega}_{ry}(A_{r,i})\right]}, \; i=1, \ldots, N \tag{3.16}$$

where the input amplitudes of the non-linearity, $\hat{A}_u$, and of the system, A_r, are related to each other as:

$$\hat{A}_{u,i} = \left| \hat{G}_1(j\omega)[1 - \hat{G}_3(j\omega)N^{\omega}_{ry}(A_{r,i})] \right| A_{r,i}, \; i=1, \ldots, N \tag{3.17}$$

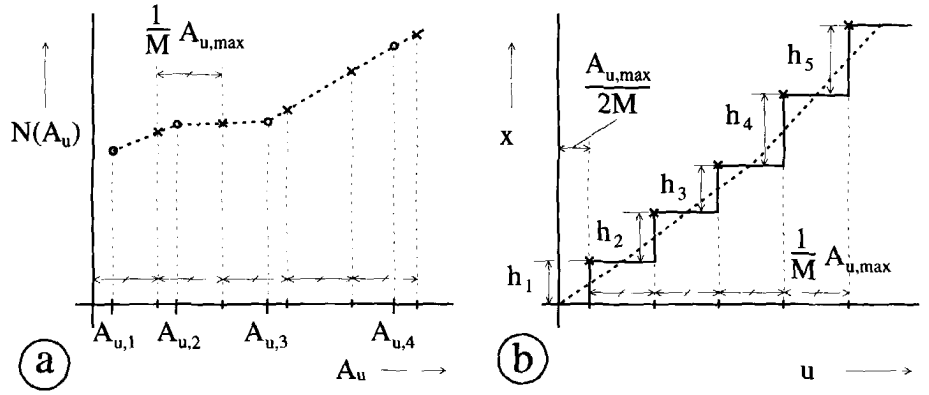


Fig. 3.4: Reconstruction of static non-linearity from amplitude response (DF); measured amplitude response (**o**) and interpolated points for equidistant grid (**x**) (a); reconstructed quantized non-linearity (solid) and piece-wise-linear function $x = \hat{f}(u)$ (dashed) (b)

With $\hat{N}_{ux}(\hat{A}_{u,i})$, $i = 1, \ldots, N$ available, an approximate non-linear function $x = \hat{f}(u)$ can be reconstructed, because there is a unique relation between the odd, , static non-linearity and its amplitude response (DF) [9]. This is denoted by Atherton ([9], page 104ff) as the identification of a static non-linearity from its DF. Several methods to do this are mentioned by Atherton; here, the approximate method of reconstructing a quantized non-linearity will be discussed, because it is most easily implemented in simulation software [9], like Matrix$_X$.

The starting point is the estimated amplitude response $\hat{N}_{ux}(\hat{A}_{u,i})$, $i = 1, \ldots, N$, indicated by the circles (**o**) in Fig. 3.4 (a). In order to obtain a quantized non-linearity like depicted in Fig. 3.4 (b), the amplitude range $[0, A_{u,max}]$ is divided into M equal intervals. By means of linear interpolation, the estimated amplitude response is evaluated at the M new equidistant grid points, as indicated by the crosses (**x**) in Fig. 3.4 (a). The interpolated amplitude response is denoted by the pair of $(M*1)$-dimensional vectors $(\tilde{A}_u, \tilde{N}_{ux})$.

The quantized non-linearity of Fig. 3.4 (b) (solid line) can now be reconstructed, using the analytic expression for the amplitude response (DF) of such a quantized non-linearity, given by Atherton [9] as:

$$N_{ux}(\frac{k}{M}A_{u,max}) = \frac{4M}{k\pi A_{u,max}} \sum_{m=1}^{k} h_m \sqrt{1 - \left(\frac{2m-1}{2k}\right)^2}, \quad k = 1, \ldots, M \tag{3.18}$$

Hereby, the non-linearity is quantized by steps of height h_m at the points $u = \frac{(2m-1)}{2M}A_{u,max}$, $m = 1, \ldots, M$, like depicted in Fig. 3.4 (b), the solid line.

Now, the quantized non-linearity is reconstructed from the interpolated amplitude response, by successively solving the quantization steps h_m from (3.18) as follows:

$$h_k = \begin{cases} \frac{\pi A_{u,max}}{2\sqrt{3}M} \tilde{N}_{ux}(\frac{A_{u,max}}{M}), & k = 1 \\ \frac{\left[\tilde{N}_{ux}(\frac{kA_{u,max}}{M}) - \frac{4M}{k\pi A_{u,max}} \sum_{m=1}^{k-1} h_m \sqrt{1-\left(\frac{2m-1}{2k}\right)^2}\right]}{\frac{4M}{k\pi A_{u,max}} \sqrt{1-\left(\frac{2k-1}{2k}\right)^2}} & k=2,\ldots,M \end{cases} \tag{3.19}$$

Obviously, once the quantized non-linearity is obtained using this equation, it is straightforward to construct a piece-wise-linear function $x = \hat{f}(u)$, as shown by the dashed line in Fig. 3.4 (b). It might be noted, that the approximation involved here, due to quantization and piece-wise-linear approximation, can be kept small by choosing a sufficiently fine grid.

With the piece-wise-linear function $x = \hat{f}(u)$ available as approximation of the static non-linearity, it is easily integrated with the identified linear dynamics. For instance, the non-linearity can be implemented as a look-up table in a simulation model, with model structure according to Fig. 3.1. Comparing simulations of the resulting model with experimental data leads to a validation of the identification results, the next topic to be discussed.

3.2.5 Validation of non-linear dynamic model

The third step in the identification and validation of a physical model is the validation of the model after the linear dynamics and the static non-linearities have been identified, as outlined in Subsection 3.1.3. Of course this validation partially takes place during the identification step: the match of the identified models on the experimental data, used for the identification, is a measure for the validity of the obtained model. In two respects, further validation of the physical model is possible: validation of additional non-linearities that are not described by simple static non-linearities, and cross-validation of the resulting model with data that were not used during the identification. As already argued in Subsection 3.1.2, this validation of the non-linear system model will take place by means of a comparison of simulations of the non-linear model and experimental data.

Validation of additional non-linearities

As mentioned in Subsection 3.1.1, some non-linearities of the physical model may have been characterized by some additional parameters. These parameters will be called tuning knobs. They determine the character of the non-linearity in a transparant way.

The validation of this kind of non-linearities is based on the insight of the engineer in the effect of the non-linearity on the input-output behaviour of the model. This insight is to be obtained by performing simulations of frequency responses and/or amplitude responses for different values of the tuning knobs. If the match between the simulation results and available experimental data can be improved by adjusting the tuning knobs, the modelled non-linearity is validated. If this improvement of match can not be achieved by reasonable values for the tuning parameters, the modelled non-linearity is invalidated and can be dropped out of the physical model.

Cross-validation

In the preceding discussion on identification and validation, experimental data were used to identify or to adjust parameters, such that the match between model response and data is as good as possible. The validity of the identified model was judged with respect to the match that was achieved. However, there is some risc in concluding validity of the model this way. The reason is, that the identification procedure may have resulted in a model, that explains the used data rather than the actual system behaviour. Therefore, it makes sense to perform the so-called cross-validation, using fresh data that were not used for identification (see also Subsection 3.1.2).

In the setting of the identification of linear systems, cross-validation is mainly meant to check, that the identified model did not match the specific realization of the random noise contribution [85]. For non-linear systems, the situation is more complex. As discussed in Subsection 3.1.2 and in Subsection 3.2.2, the system response depends on the experiment design due to the non-linearity of the system. So in order to check the validity of the identified non-linear model of the system, it is important to use a fresh data-set, obtained with different input signals. For instance, if the linear dynamics have been estimated from an experimental frequency response, obtained with input amplitude filtering (see Subsection 3.2.2), a measured frequency response obtained *without* input amplitude filtering may be used for cross-validation. Another possibility is, to perform measurements with the system and simulations with the identified model, using non-sinusoidal inputs, and evaluate the match between measured and simulated outputs in the time domain.

In the end, it depends on the intentional use of the identified models, to which extent the models should be validated. If the models are to be used for control design, Chapter 4, it is mainly important to validate the models with respect to:

- the range of input signals that may be expected during operation of the closed loop system,
- the dynamics that are relevant in the control design,
- the non-linearities that are relevant for the robustness of the control design, and those that can be used explicitly in non-linear control design.

If, on the other hand, the models are to be used for system design, it is often important to validate the models with respect to system properties, that are directly related to physical parameters, which in turn are related to design parameters. This is the subject of the next Subsection.

3.2.6 Estimate-based reconstruction of physical parameters

In Subsection 3.2.3, the identifiability of the parameters of the physically structured linear dynamic model (3.12) has been discussed. Actually, for the hydraulic servo-system under consideration, the model structures (3.12) of the subsystem models have been derived in Section 2.5 and 2.6 in such a way, that the parameter vector θ contains as few elements as possible, given the physical structure of the state space model. This means, that the elements of θ consist of combinations of physical parameters, so that the number of parameters in θ are generally (much) less than the number of underlying physical parameters. For this reason, it is impossible to reconstruct all physical parameters of the theoretical model from the identified parameters.

In some cases, reconstruction of the physical parameters is desirable, for instance for system design purposes. The idea is then, to use a-priori knowledge for part of the physical parameters, such as geometrical parameters, and to reconstruct the uncertain remaining parameters from the identified parameters. Clearly, this procedure is highly dependent on the system at hand, and requires insight in the system behaviour, obtained by theoretical modelling.

Besides reconstruction of physical parameters from identified parameters, it is sometimes possible to estimate certain physical parameters from *additional experiments*. These experiments, possibly just with a subsystem of the complete system, are often aimed at isolating a certain physical phenomenon. For instance, performing measurements on required forces for constant velocity motions, provides information on the friction properties of the (sub)system.

Thus, a combination of theoretical knowledge and experimental data, results in a model of the true system, that not only provides qualitative insight in the system behaviour, but that is also quantitatively valid.

3.2.7 Conclusion

In this Section, the approach to the identification and validation of the non-linear (subsystem) models of the hydraulic servo-system has been rather extensively elaborated. Thereby, special attention has been given to the distinction between the linear dynamics and the (static) non-linearity of the system, along with the use of Sinusoidal Input Describing Functions (SIDF's) to characterize the non-linear input-output behaviour of the system.

The method of input amplitude filtering has been proposed, to avoid non-linearity in the frequency response, so that the linear dynamics can be directly identified from measured frequency response data. Furthermore, a technique is presented to use the closed loop amplitude response of the non-linear system according to Fig. 3.1 (c), to identify an approximate characteristic for the static non-linearity in the system. Finally, it is argued, how the obtained models can be further validated, and that physical parameters may in some cases be reconstructed from the identification results.

The techniques presented in this Section, clearly have been worked out against the background of the specific application, namely the hydraulic servo-system. Before discussing the experimental results, obtained by applying the proposed techniques to a real hydraulic servo-system, a description of the experimental setup will be given in the next Section.

3.3 Experimental setup

Although the results presented so far have been formulated such that they apply generally for hydraulic servo-systems, the experimental verification has taken place with just one specific setup. As mentioned in Chapter 1, Subsection 1.2.1, this concerns a long-stroke linear actuator of the double-concentric type, to be used in a flight simulator motion system.

After the description of the general setup in Subsection 3.3.1, the applied servo-valve will be described in some more detail in Subsection 3.3.2, and the measurement and control devices in Subsection 3.3.3.

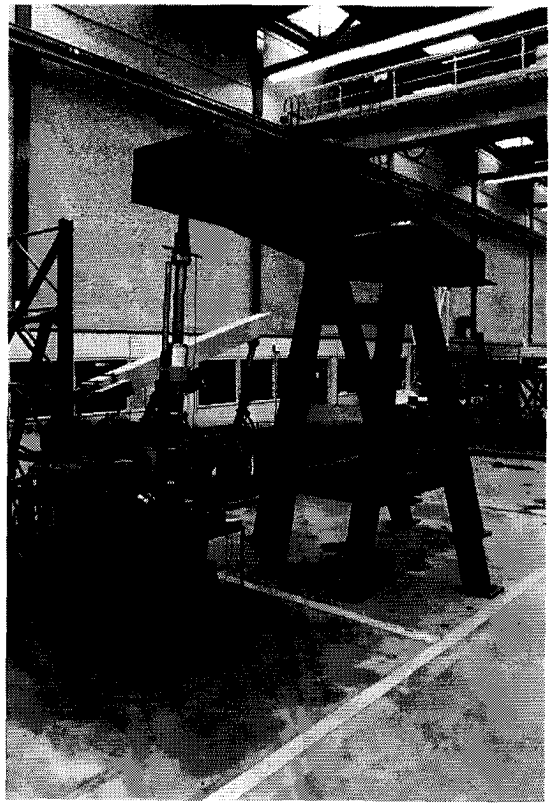


Fig. 3.5: Experimental test rig for hydraulic actuator

3.3.1 General setup

As mentioned in Chapter 1, the double-concentric actuator under consideration has been developed at the Mechanical Engineering Systems and Control Group of Delft University of Technology. One of the design topics was the development of a model-based cushioning design, as described in Chapter 5. For the purpose of extensive testing of the actuator including the cushioning, a test rig has been built; a picture of the setup is given in Fig. 3.5. This test rig has also been used for extensive experiments for identification, model validation and control design.

A schematic drawing of the setup is given in Fig. 3.6. The test rig consists of a horizontal lever, which is connected in the middle with a hinge joint to a standing frame. Extension and retraction of the actuator results in rotational motions of the horizontal lever. The rotational inertia of this lever can be seen as an inertial load or reflected mass for the actuator. By means of removable loads, different load conditions can be created, such as to simulate different load conditions for the hydraulic actuators occurring in a flight simulator motion system. In case all loads are removed, the reflected mass at the actuator end-point is about 750 [kg]. Placing the loads on the lever, a maximum reflected mass at the actuator end-point of about 3000 [kg] can be achieved.

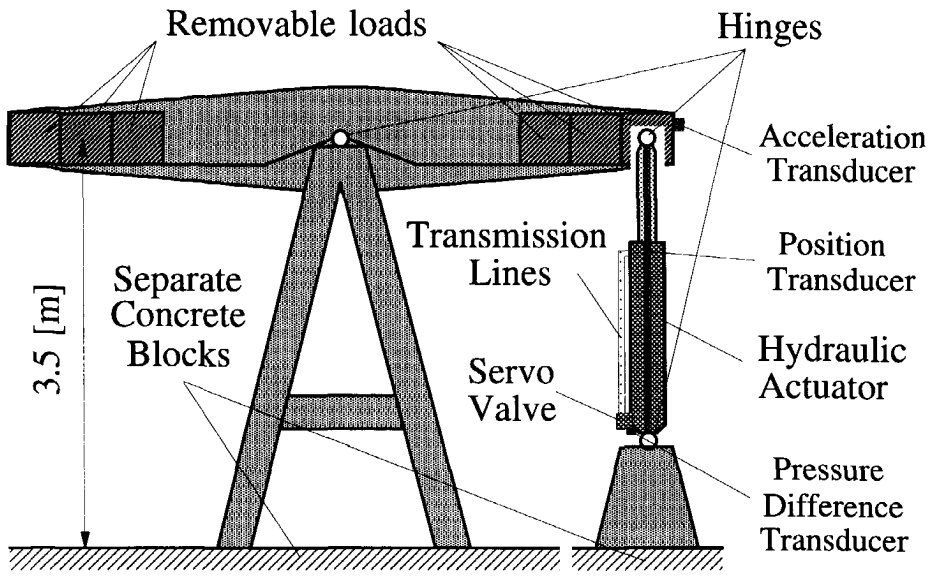


Fig. 3.6: Schematic drawing of experimental test rig for hydraulic actuator

Besides variations in the inertial load, the removable loads also allow adjustment of the static load on the actuator. With loads placed at the left hand side only or at the right hand side only, this static load corresponds to about -1500 [kg] and about 1500 [kg] at the actuator end-point respectively. Obviously, for certain load condition, the static and inertial load on the actuator varies slightly with actuator position due to geometric non-linearity. However, the dimensions are such, that these variations are minor in the normal working range of the actuator. Only for extreme positions, occurring in cushioning tests (Chapter 5), these variations have to be taken into account.

Of course, the test rig has been designed to constitute a stiff inertial load for the actuator. Due to the stiff construction, the first bending mode of the lever lies at about 50 [Hz], which is well beyond the natural frequency of the open loop actuator. So for the basic actuator dynamics, the load can be considered to be stiff; for higher frequencies, parasitic effects are present due to the bending modes of the lever.

Besides flexibility in the test rig itself, there is also flexibility in the base. In order to avoid excitation of the dynamics of the building, the test rig has been based on a large block of concrete, isolated from the building. Unfortunately, the actuator and the bearing frame were based on different blocks, as indicated in Fig. 3.6. Under some load conditions, this caused considerable parasitic motions in the system, in the frequency range of 20 - 30 [Hz].

The actuator that was used for the experiments, is a symmetric actuator of the double-concentric type, and has already been discussed as the actuator modelling example in Subsection 2.3.4. A schematic drawing of the actuator, including the measurement and

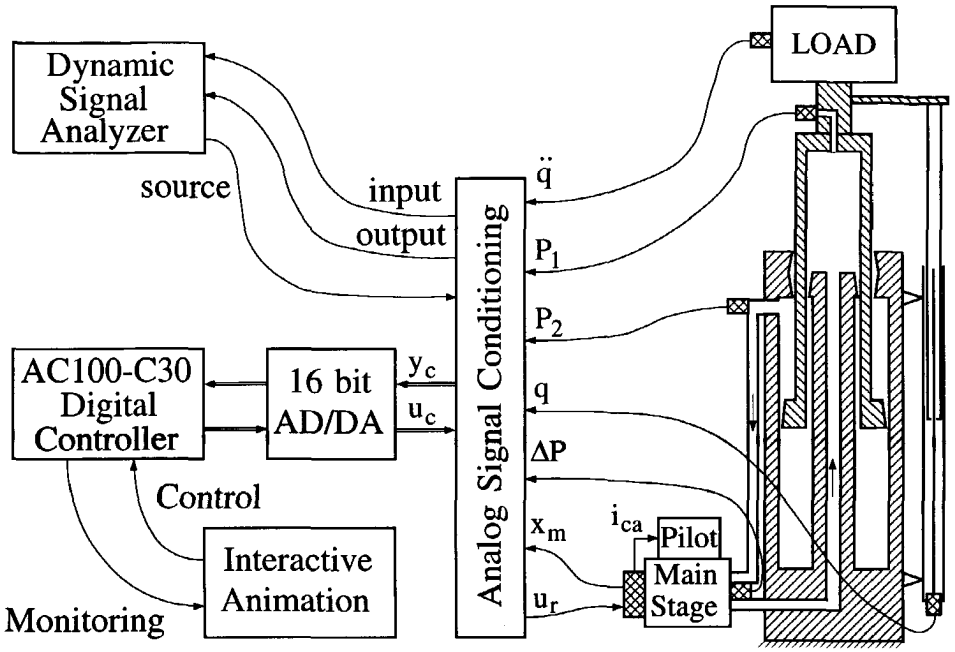


Fig. 3.7: Schematic drawing of experimental setup including measurement and control devices

control devices to be discussed later, is given in Fig. 3.7.

The characteristics of the actuator are briefly summarized here. Using a pressure controlled flow pump and some hydraulic accumulators, the servo-valve is supplied with a constant supply pressure $P_s = 160$ [bar]. Herewith, the delivered flow of the three-stage valve is about $\Phi_{p,nom} = 150$ [l/min]. With a piston area $A_p = 25\ 10^{-4}$ [m^2], this results in a maximum actuator velocity $\dot{q}_{max} = 1$ [m/s]. The maximum force exerted by the actuator equals the supply pressure times the piston area, which makes $F_{p,max} = 40$ [kN]. Finally, the maximum displacement of the actuator from mid-position is $q_{max} = 0.625$ [m]. With safety buffers of about 0.065 [m] and 0.1 [m] respectively on each end, this results in an effective stroke of 1.085 [m].

Due to the double-concentric construction of the actuator, the transmission lines between valve and actuator chambers are at least as long as the stroke of the actuator, see Fig. 3.7. For the given actuator, these lengths are $L_{tl1} = 1.4$ [m] and $L_{tl2} = 1.2$ [m] respectively. For other transmission line parameters, see Table F.5 in Appendix F. The parameters for the geometry of the hydrostatic bearings are given in Table F.3.

Whereas the actuator under consideration has been developed for application in a flight simulator motion system, seven of them have been manufactured; six for the simulator, and one spare. This allowed experimental comparison of the (dynamic) properties of the identical actuators; the resulting figures will be discussed later, in Subsection 3.7.4. For the seven actuators, seven three-stage servo-valves have been purchased; their characteristics will be discussed in more detail next.

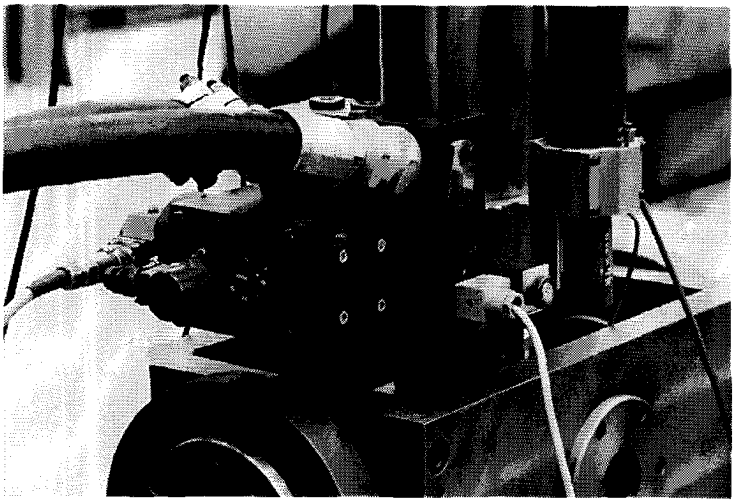


Fig. 3.8: Three-stage valve on supply manifold at the bottom of the actuator

3.3.2 Three-stage servo-valve

Originally, one three-stage valve has been purchased for testing purposes; a close-up of the valve, mounted on the supply manifold at the bottom of the actuator, is given in Fig. 3.8. The dynamic behaviour of this valve[5], with flow capacity mentioned above, has been extensively investigated. Actually, the development of the approach to the identification of non-linear systems, discussed in Section 3.2, has been an important part of these investigations. The results of the experimental application of the developed identification procedure will be discussed in later in this Chapter, in Section 3.5.

During experiments with the original three-stage valve, it was concluded that the original pilot-valve, with a flow capacity of 3.3 [l/min] at 70 [bar], was a bit under-sized; for high-bandwidth performance of the closed loop three-stage valve, the pilot-valve saturated. Therefore, the six servo-valves purchased eventually for the flight simulator motion system were of the same type, but with larger pilot-valves, namely with a flow capacity of 6.6 [l/min] at 70 [bar].

Based on simulation results, discussed in Subsection 2.2.5, it was argued that the spool port configuration of the servo-valve is important for the non-linearity of the system. In this respect, it is useful to note that the manufacturer has provided the pilot-valve with small overlaps, be it smaller than 0.5 % according to the catalogue [89]. The main spool port configuration is aimed to be critical-centre, but may have small underlaps, again smaller than 0.5 % according to the catalogue [89].

The analog main spool position feedback loop that is required for the three-stage valve, is realized in a piece of built-in electronics by the manufacturer. Instead of the simple proportional feedback law (2.103), that was assumed in the model on page 98, the following feedback loop was implemented for the considered three-stage valve:

$$\bar{i}_{ca} = \bar{K}_{pm}\left(\bar{u}_r - (1 + \bar{K}_{dm}s)\bar{x}_m\right) \tag{3.20}$$

[5]Type no.: Rexroth 4WSE3EE16-11/100B9ET210Z9EM

The proportional and differential feedback gains $\bar{K}_{pm}$ and $\bar{K}_{dm}$ respectively, are set by the manufacturer. In the experimental work presented here, the original gain settings were bypassed, and $\bar{K}_{pm}$ and $\bar{K}_{dm}$ were set to known values.

Obviously, a main spool position measurement is required for this feedback loop. A LVDT-sensor and 10 [kHz] modulator/demodulator device provides this signal $\bar{x}_m$; the signal is also available for external measurement.

Besides the feedback loop, a 400 [Hz] oscillator is implemented in the analog built-in electronics of the valve, which generates a dither signal. As explained by Atherton, using DF theory [9], the application of a dither signal may modify the non-linear behaviour of a system in a desirable way. In practice, when applied to the three-stage valve, this dither signal appears to be necessary and sufficient to eliminate hysteresis effects due to Coulomb friction of the pilot-valve spool. In fact, the pilot-valve dynamics are continuously excited at the dither frequency, resulting in a sustained oscillation of the spool. Because 400 [Hz] is well beyond the bandwidth of the three-stage valve, the amplitude of the dither is significantly attenuated, so that it does not excite the system dynamics too much.

The amplitude of the dither signal is to be adjusted by the user, and depends among others on the supply pressure. In practice, the dither adjustment was found to be rather sensitive. If the amplitude was chosen too small, the pilot-valve spool sticked, resulting in very bad low-frequency behaviour of the three-stage valve. On the other hand, if the dither amplitude was chosen too large, the system dynamics were audibly excited. After some fine-tuning, a good adjustment could be found.

Besides the actual hardware under investigation, the servo-valve and the hydraulic actuator, the measurement and control devices form an important part of the experimental setup. They will be described in the next Subsection.

3.3.3 Measurement and control devices

Referring to Fig. 3.7 for an overview of the configuration of the measurement and control devices for the experimental setup, the different devices will be described subsequently. Finally, some dedicated devices for the measurement of servo-valve characteristics will be described.

Sensors and signal conditioning

In Fig. 3.7 an overview is given of the signals that could be measured in the experimental setup. For a detailed overview of the purpose and the technical specifications of the available transducers, the reader is referred to Appendix G. Although many signals are available in the given setup, it should be noted here, that in the general case, only the position and pressure difference transducer will be available for control purposes. So, the remaining sensors applied here, are mainly used for identification and validation purposes.

The analog signal conditioning in Fig. 3.7 is used to subtract offsets and amplify, attenuate or filter signals if necessary. For instance, the position signal is filtered to avoid aliasing effects in digital control. Furthermore, the analog devices are used to make the desired connections between measurement devices, the actuator hardware and the digital control system.

Digital control system

The digital control system, as it is schematically represented in Fig. 3.7, is used to implement algorithms for the control of the hydraulic actuator. With the use of the control design and simulation software package Matrix_X / System-Build [63], the digital controllers are designed. Via automatic code-generation and compilation, the controller software code is downloaded in a C30-DSP processor. This processor, together with IO-cards for AD- and DA-conversion, is embedded in a 486-Industrial PC. Via an Ethernet-connection, the process is controlled and monitored on a VAX-Workstation, using the Interactive-Animation software. With an update rate of 50 [Hz], the measured signals are recorded on a terminal, while controller parameters can be changed on-line from the same terminal.

Besides for the implementation of control algorithms, the control system is also used for signal generation (sinusoids, square waves, saw-tooth), for the implementation of safety algorithms, and for the implementation of digital filters. These digital filters are used as an input amplitude filter during frequency response measurements, for reasons given in Subsection 3.2.2.

With the AC100-C30 system, it is quite easy to implement multi-rate algorithms; digital filters and feedback control algorithms are implemented at a sample rate of 5 [kHz], which is high enough to cope with the high-frequency dynamics of the system, such as the transmission line dynamics and the valve dynamics. Other tasks, as signal generation and safety, are implemented at a lower sample rate, 1 [kHz].

A final important feature of the AC100-C30 system is, that it is easily used for time domain data acquisition. While the control system is running, data acquisition can be performed on any of the input or output signals, at any sample rate. After automatic conversion, the time-domain data can be evaluated in Matrix_X. Thus, time domain validation of developed simulation models can be performed.

Dynamic Signal Analyzer

For measurements in the frequency domain, a dedicated apparatus is used, namely the HP 3562-A Dynamic Signal Analyzer. It generates a source signal, which is supplied to the system. Under this excitation, two signals are measured by the signal analyzer, and transformed into the frequency domain by Discrete Fourier Transform techniques. Considering the measured signals as the input and the output of the system respectively, the input-output behaviour of the system is characterized. Using sinusoidal source signals with prespecified amplitude, which are possibly led through an input amplitude filter implemented in the AC100-C30 system, SIDF's are measured, as discussed in Subsection 3.2.1.

Concerning the frequency response measurements, it is remarked that the frequency range of these measurements depends on the purpose of the measurement. For the identification and validation of the actuator model including the transmission line dynamics, the actuator dynamics have been measured over a range of 1 - 1000 [Hz]. Because the valve shows no relevant dynamics up to 10 [Hz], the servo-valve measurements were restricted to a range of 10 - 1000 [Hz].

Servo-valve test facilities

For modelling purposes, it is desirable to perform measurements, in which the servo-valve behaviour is isolated from the actuator behaviour. Whereas it is impossible to perform

actuator measurements without a servo-valve, it is possible to obtain measurements that purely reflect servo-valve properties. Three practical examples, which have been applied, are given.

1. *Steady state test facility*
   Mounting the servo-valve on a special manifold, the steady state characteristics can be measured. Using a flow meter, the steady state flow characteristic is measured according to *Specification Standards for Electro-Hydraulic Flow Control Valves*, [134]. Using pressure transducers, the absolute pressures during this measurement are recorded; these pressures are an indication of the spool port geometry (see Subsection 2.2.5).
2. *Dynamic test facility*
   In the laboratory, a small scale unloaded actuator is available, with a natural frequency of about 3000 [Hz]. For frequencies up to 1000 [Hz], this actuator behaves as a pure integrator. Using a velocity sensor, and mounting the servo-valve to this special purpose actuator, the dynamic characteristics of the servo-valve can easily be measured, as the actuator velocity is a direct measure for the servo-valve flow. Due to the small scale, this facility is only suitable for valves with flow capacity less than 20 [l/min]. Therefore, it is only used for the pilot-valves, and not for the three-stage valves.
3. *On the actuator with large offset in spool position*
   If the (main) spool position feedback is purely electrical, the servo-valve dynamics can be assumed to be independent of the (main) spool position. In this case, dynamic measurements can be performed with the servo-valve mounted on the actuator. Giving the valve a large offset, the actuator will take an extreme position, with supply pressure in the one chamber, and return pressure in the other. Exciting the servo-valve dynamics with (small) AC-signals, and measuring the servo-valve spool position, the dynamic characteristics of the valve can be measured, without exciting actuator dynamics. This method has been applied to the three-stage valve.

With the measurement and control devices described here, the experimental setup allows extensive experimentation for modelling and control purposes. Many measurements in frequency domain and time domain have been performed, both of the servo-valve and of the complete hydraulic servo-system. How these experiments are used for the identification and validation of the developed models, is discussed in the remaining Sections of this Chapter.

3.4 Indentification and validation of the flapper-nozzle valve model

3.4.1 Introduction

The pilot-valve of the three-stage valve is just a two-stage flapper-nozzle valve. For this system, the model to be identified is given in Fig. 2.39 on page 112. Its linear dynamics is represented by (2.101), page 97. This fourth order model is chosen beforehand from the alternatives (see Appendix A), because this model will appear to fit the experimental data

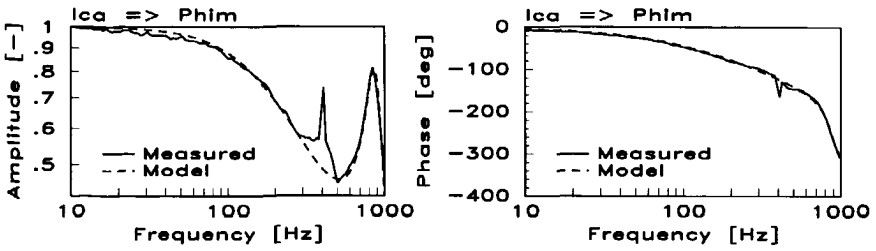


Fig. 3.9: Fit of linear frequency response $\hat{G}_1(j\omega)$ (dashed) on measurement $\tilde{H}^{0.5\,\%}_{\tilde{i}\tilde{\Phi}_m}(j\omega)$ (solid) of pilot-valve dynamics

very well. In general, an iterative procedure of identification and validation of linear model structure is necessary to find the correct model structure, as described in Subsection 3.2.3.

The character of the non-linearities of the torque motor and of the flapper-nozzle system is such, that they can be considered linear for small input amplitudes, see Subsection 2.2.5 and 2.7.2. So, if an experimental frequency response is available, obtained with small input amplitude, only the output non-linearity (2.120) has to be taken into account. So, the flapper-nozzle valve model can be represented by the model of Fig. 3.3 with $G_2(j\omega) = 1$ and $G_3(j\omega) = 0$.

Thus, taking the adopted model structure as a starting point, the different steps in the identification approach can be taken, as discussed in the subsequent Subsections below.

3.4.2 Identification of linear dynamics

Applying Theorem 3.2.6, a linear frequency response of the flapper-nozzle valve can be obtained by iteratively designing and applying an input amplitude filter $F(j\omega)$, such that[6]:

$$|F(j\omega)| = \left|\tilde{H}^{\alpha_s}_{\tilde{i}\tilde{\Phi}_m}(j\omega)\right|^{-1} = \left[\beta\left|\hat{G}_1(j\omega)\right|\right]^{-1}$$

The resulting linear experimental frequency response $\tilde{H}^{\alpha_s}_{\tilde{i}\tilde{\Phi}_m}(j\omega)$ can be used to fit the frequency response $\hat{G}_1(j\omega)$ of a linear SISO model with the TFID-command of Matrix$_X$, as described in Subsection 3.2.3. The resulting fit for a fourth order model with one rhp-zero, corresponding to the adopted model structure (2.101), is given in Fig. 3.9. The good fit illustrates the validity of the model structure; there is only a significant difference around 400 [Hz], which can be ascribed to the presence of the dither signal.

Whereas the transfer function $G(j\omega)$ of (2.101) has $p = 4$ poles and $z = 1$ zero, $n = 6$ parameters can be identified. So from the $m = 9$ parameters $c_1, \ldots, c_9$ in the state space model, three have to be chosen a-priori, Subsection 3.2.3. Using physical insight, c_5, c_6 and c_8 have been chosen, and the remaining parameters could be calculated from the identification result. The resulting set of model parameters is given in Table 3.1.

3.4.3 Identification and validation of non-linearities

After the identification of the linear dynamics, the static non-linearity (2.120) can be identified as described in Subsection 3.2.4. For this purpose, an amplitude response $N^{10\,\mathrm{Hz}}_{\tilde{i}\tilde{\Phi}_m}(A_{\tilde{i}})$

[6] In the remainder, the subscript ca in i_{ca} is mostly omitted for ease of notation.

Parameter	Id. Value	Parameter	Id. Value	Parameter	Id. Value
c_1	$3.64\ 10^3$	c_2	$2.98\ 10^7$	c_3	$2.70\ 10^{10}$
c_4	$1.12\ 10^{11}$	c_5	$1.00\ 10^2$	c_6	$1.00\ 10^4$
c_7	$9.86\ 10^{-1}$	c_8	$4.00\ 10^3$	c_9	$3.09\ 10^{10}$

Table 3.1: Identified parameter values pilot-valve model

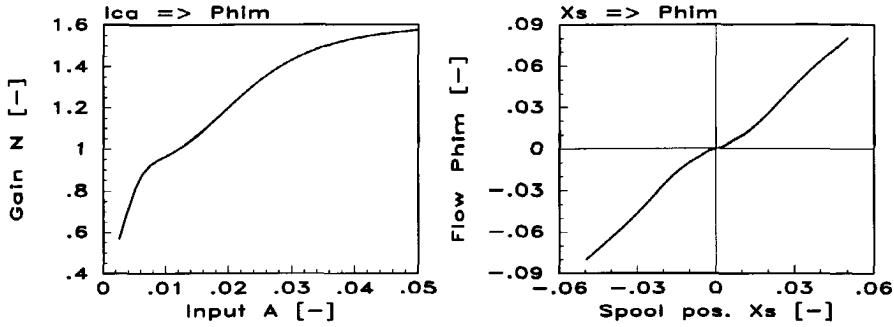


Fig. 3.10: Measured amplitude response $N^{10\,\mathrm{Hz}}_{\tilde{i}\bar{\Phi}_m}(A_{\tilde{i}})$ (left) and reconstructed static non-linearity $\bar{\Phi}_m = \hat{f}_1(\bar{x}_s)$ (right) of pilot-valve

of the pilot-valve has been measured. The result is given in the left plot of Fig. 3.10; because the phase was hardly dependent on the input amplitude, only the gain is shown.

Using the physical insight obtained from the simulation model, Subsection 2.2.5, it can be stated that the flapper deflections at the chosen frequency of 10 [Hz] are (very) small, so that the torque motor and the flapper-nozzle system can be assumed to behave linear. This means, that the non-linearity can be completely ascribed to the output non-linearity (2.120). Because the dynamic transfer function $\hat{G}_1(j\omega)$ has been normalized, the amplitude response of this non-linearity, $\hat{N}^{10\,\mathrm{Hz}}_{\bar{x}_s\bar{\Phi}_m}(\hat{A}_{\bar{x}_s})$, equals the measured amplitude response $N^{10\,\mathrm{Hz}}_{\tilde{i}\bar{\Phi}_m}(A_{\tilde{i}})$, according to (3.16) and (3.17).

As described in Subsection 3.2.4, an approximate non-linear function $\bar{\Phi}_m = \hat{f}_1(\bar{x}_s)$ can be reconstructed from the amplitude response of the non-linearity. The result is given in the right plot of Fig. 3.10. The physical interpretation of this plot is, that the flow gain of the pilot-valve is smaller than unity for small spool displacements. This agrees with the information that the spool has small overlaps (see Subsection 3.3.2), while there is probably some radial clearance, as explained by the non-linear simulations in Subsection 2.2.5.

Having reconstructed the static non-linearity (2.120), further validation of the non-linearities of the flapper-nozzle valve consists of the validation of the non-linearity of the torque motor and of the flapper-nozzle system, as depicted in Fig. 2.39. In Subsection 2.7.2, page 106, these non-linearities have been rewritten into a simple form, such that only some tuning parameters need to be specified to determine the character of the non-linearity. For the non-linearity of the torque motor, to be denoted by "NL-TM", these parameters are k_2 and k_3 in (2.111). For the non-linearity of the flapper-nozzle system, to be denoted by

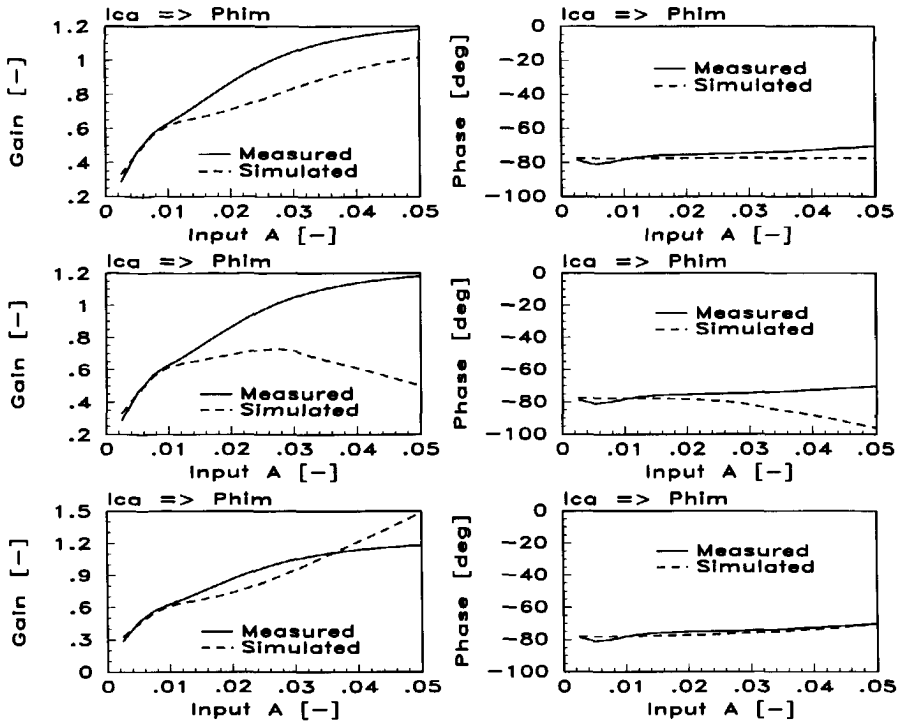


Fig. 3.11: Measured (solid) and simulated (dashed) amplitude response $N_{i\Phi_m}^{200\,\mathrm{Hz}}(A_i)$ of pilot-valve; simulations with $\hat{f}_1$ (upper), $\hat{f}_1$ + NL-ΔP_n (middle) and $\hat{f}_1$ + NL-TM (lower)

"NL-ΔP_n", the parameter k_4 can be tuned.

Again referring to the non-linear simulations of Subsection 2.2.5, it is clear that the influence of the two non-linearities NL-TM and NL-ΔP_n is only observed in the high-frequency range, where the flapper deflections are relatively large. From this viewpoint, the amplitude response of the system at 200 [Hz] is used to characterize the non-linearity. So, the validation of these two non-linearities takes place by comparing measured and simulated amplitude responses at that frequency.

In Fig. 3.11 some validation results are given. The simulation results have been obtained using the identified linear model with the parameters of Table 3.1 and the reconstructed static non-linearity $\hat{f}_1$ according to Fig. 3.10. The tuning parameter values were set respectively to $k_2 = 0.01$, $k_3 = 0.01$, $k_4 = 1$ (upper), $k_2 = 0.01$, $k_3 = 0.01$, $k_4 = 50$ (middle) and $k_2 = 20$, $k_3 = 0.5$, $k_4 = 1$ (lower). With these tuning parameter values, the remaining model parameters can be calculated with expressions given in Subsection 2.7.2. Some comments on the results:

- The identified static output non-linearity $\hat{f}_1$ explains the major part of the non-linearity, although it does not explain the input amplitude dependence of the phase.
- The choice of tuning parameters for the upper plot corresponds to linear behaviour of torque motor and flapper-nozzle system; the magnitude of the signals and their am-

plification in the non-linear equations is such, that the non-linearity is approximately linear.

- For the middle plot, the tuning parameter for the flapper-nozzle non-linearity k_4 has been increased until non-linearity in the simulated amplitude response was observed. The resulting response shown in the middle plot Fig. 3.11 is typical for the flapper-nozzle non-linearity: until certain input amplitude (in this case $A_{\tilde{i}} = 0.025$), the effect of the non-linearity is hardly observable; the response is similar to that without flapper-nozzle non-linearity. For larger input amplitudes, a considerable drop of the amplitude and the phase occurs, which is not observed in the experimental response. Further analysis of the simulation result made clear, that this behaviour is caused by the phenomenon that the flapper hits the nozzles in the simulation model. This is not realistic and not observed in practice, so that it can be concluded that the non-linear model of the flapper-nozzle system, which is based on non-linear equations for the turbulent nozzle flows, is not valid. It does not explain the non-linearity in the dynamics of a flapper-nozzle valve.
- The choice of tuning parameters for the lower plot introduces severe non-linearity due to the torque motor; the settings were found by performing simulations and gaining insight in the effect of the tuning parameters.
  With the given parameters, this non-linearity roughly explains the amplitude dependence of the phase for larger input amplitudes, and clearly represents non-linearity in the dynamics of the valve. To some extent, the inclusion of this non-linearity also improves the fit of the gain. The non-linearity is therewith validated, in the sense that the non-linear torque motor model explains non-linear experimental behaviour.

Summarizing, the identification and validation of non-linearities of the flapper-nozzle valve has led to an approximation of the static output non-linearity, a validation of the torque motor non-linearity in the sense that it improves the fit of simulated amplitude response data on experimental data, and an invalidation of the flapper-nozzle non-linearity as explanation for non-linearity in the pilot-valve dynamics.

3.4.4 Cross-validation

Besides the frequency response data used for identification in Subsection 3.4.2 and the amplitude response data used to characterize non-linearity in Subsection 3.4.3, a number of frequency responses $H_{\tilde{i}\Phi_m}^{A_{\tilde{i}}}(j\omega)$ were measured at different input amplitude levels, without input amplitude filtering. For three input amplitudes, $A_{\tilde{i}} = 0.5$ %, 1 % and 2.5 % respectively, these responses are plotted in the upper plots of Fig. 3.12.

In the middle and lower plots of this Figure, the actual cross-validation is presented in the form of differences in the amplitudes and phases respectively of the measured and simulated frequency responses. Related to the actual magnitude of the frequency response amplitudes and phases, the differences are reasonably small (in the order of magnitude of 10 %) if both the static non-linearity and the torque motor non-linearity are taken into account (lower plot). Given the strong non-linearity of the system (upper plot), this means, that a rather accurate, valid non-linear dynamic model of the pilot-valve has been obtained.

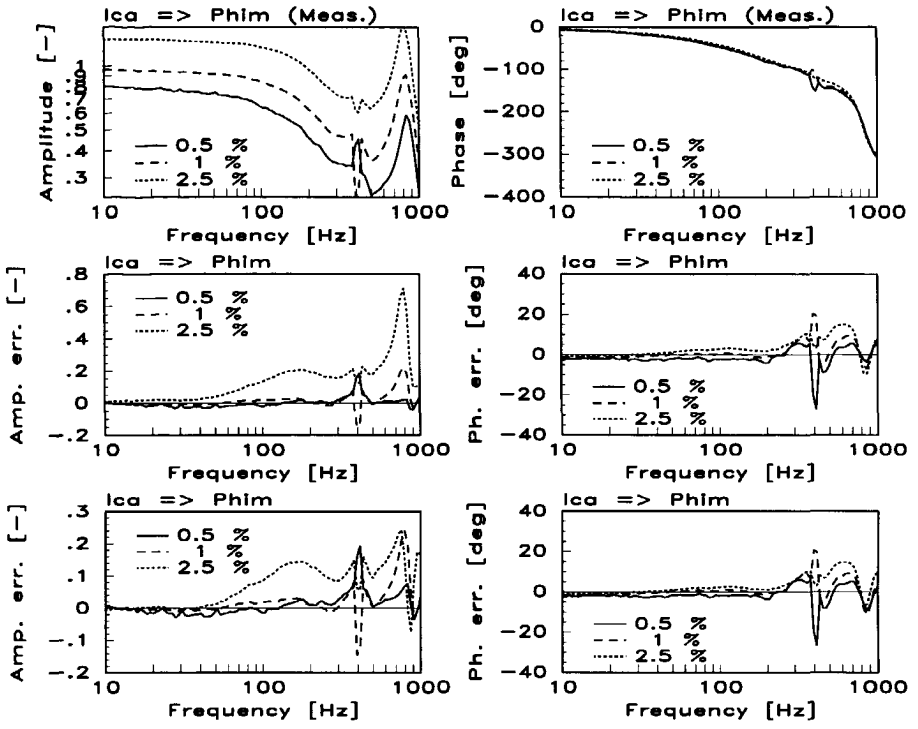


Fig. 3.12: Measured frequency responses $H_{i\bar{\Phi}_m}^{A_i}(j\omega)$ of pilot-valve (upper); difference of amplitudes $|H(j\omega)| - |\hat{H}(j\omega)|$ (left) and phases $\angle H(j\omega) - \angle \hat{H}(j\omega)$ (right) of measured and simulated responses (middle & lower): only $\hat{f}_1$ as non-linearity in model (middle); $\hat{f}_1$ + NL-TM as non-linearities in model (lower)

3.4.5 Estimate-based reconstruction of physical parameters

The identification of the flapper-nozzle valve dynamics in the form of a physically structured linear model (2.101) allowed the (in)validation of some structural non-linearities in the model. Theoretically, a further validation of physical properties might be possible, because the identified parameters of Table 3.1 have physical background. This background lies in the derivation of the linear model in Section 2.5.

However, as it is already mentioned in Subsection 2.1.2, there is a lack of a-priori knowledge of physical parameters of the servo-valve model. This knowledge is at least insufficient to determine the physical parameters in the theoretical model uniquely from the identified parameters. This means that concerning the flapper-nozzle valve, there remains a kind of gap between the theoretical model and the identified model in the following sense.

The theoretical model is very detailed and allows detailed qualitative analysis of physical phenomena in the system, providing insight that might be used for the design of the valve. However, the phenomena can not be quantitatively validated. The identified model on the other hand, can be quantitatively validated, including some structural non-linearities. It provides a rather accurate, reliable model of the non-linear dynamics of the flapper-nozzle valve, which can very well be used for (robust) control design.

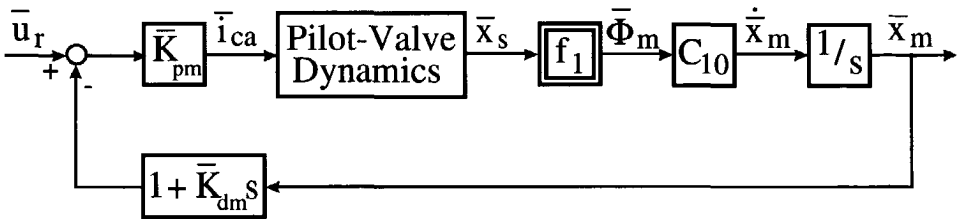


Fig. 3.13: Block scheme experimental three-stage servo-valve model

From system design point of view, the use of the identified model for the (in)validation of some main non-linearities is of importance. It shows that the torque motor is a possible source of non-linearity in the valve dynamics. The flapper-nozzle system on the other hand, behaves linear, as long as the nozzle flows can be assumed to be turbulent. The most important non-linearity however, which is clearly validated with the identified model, is the static output non-linearity due to the spool port geometry. This non-linearity causes the flow gain of the valve to be highly dependent of the input signal amplitude.

Besides the use of the SIDF (amplitude response) for the identification of the static flow non-linearity, it is common practice to use a flowmeter to measure this non-linearity, where it is often represented graphically in an xy-graph, see Subsection 3.3.3. This method has also been applied to the pilot-valve under consideration; without showing the result it is concluded that this measurement agrees with the right plot of Fig. 3.10. Actually, this can be seen as a cross-validation of the physical property of the non-linearity of the flow characteristic.

The statement that the static non-linearity of the flapper-nozzle valve is quite important is justified by investigating the behaviour of this valve as a pilot-valve for a three-stage servo-valve. This is the topic of the next Section.

3.5 Indentification and validation of three-stage servo-valve model

3.5.1 Introduction

In Subsection 2.7.2, the non-linear model structure for the three-stage servo-valve has been presented in Fig. 2.40 on page 113, where the pilot-valve model is represented by the preceding blockscheme, Fig. 2.39. Based on the results of the previous Section, it is assumed that only the static output non-linearity of the pilot-valve is relevant. Combined with the experimentally implemented feedback law (3.20) for the three-stage valve, Subsection 3.3.2, the non-linear model for the three-stage valve becomes as shown in Fig. 3.13. Note that the main spool position $\bar{x}_m$ is the output of the dynamic servo-valve model; the non-linear flow characteristic of the main spool is taken into account during the identification of the actuator model in the next Section.

For the pilot-valve dynamics, the fourth order model structure (2.101) is adopted again, and the corresponding transfer function is denoted as $G_{pv}(j\omega)$. Herewith, the three-stage valve model can be represented by the non-linear model structure of Fig. 3.3, where:

$$\begin{aligned} G_1(j\omega) &= G_{pv}(j\omega)\bar{K}_{pm} \\ G_2(j\omega) &= \tfrac{c_{10}}{j\omega} \\ G_3(j\omega) &= (1 + \bar{K}_{dm} j\omega) \end{aligned} \tag{3.21}$$

With this characterization of the model structure, there are two options for the identification and validation of the three-stage valve:

1. In a first step the pilot-valve dynamics $G_{pv}(j\omega)$ and the static non-linearity f_1 are identified and validated as discussed in Section 3.4. In a second step, the integrator gain is estimated from proper closed loop measurements, using the identified model and the knowledge of the controller gains $\bar{K}_{pm}$ and $\bar{K}_{dm}$.
2. Using the knowledge of the model structure and of the controller gains $\bar{K}_{pm}$ and $\bar{K}_{dm}$, the linear dynamics of the pilot-valve $G_{pv}(j\omega)$ and the integrator gain c_{10} of the third stage are identified from closed loop measurements, obtained using an input amplitude filter. Thereafter, the static non-linearity f_1 is identified, also from closed loop measurements, and the resulting model is validated.

In both methods the application of the procedure of Section 3.2 plays a key role. The difference is, that the first method treats the non-linearity of the system in an 'open-loop' setting, while the second method takes the 'closed loop' configuration as a starting point. Without showing the results of the first method, it is stated that the second method leads to better results. Two reasons can be given for it:

- In the first method, the estimation of the pilot-valve dynamics may be slightly biased due to dynamic properties of the test facility, despite the efforts to avoid this.
- Accordingly, in the second method, the estimation of the pilot-valve dynamics may be biased due to some unmodelled non-linearities of the servo-valve. Although this causes the estimated pilot-valve dynamics not to be the 'true' linear dynamics, the identified model is the best approximation of the pilot-valve dynamics in this specific closed loop configuration. This actually refers to some advantages of closed loop identification, as discussed extensively by Schrama [122].

Besides that the second method provides better results, there is a practical advantage, which may be important: the method can be applied with the three-stage valve on the actuator, so that a dynamic valve test facility is not required (see Chapter 3.3.3). So, the application of the second method will be the topic of the sequel of this Section. Thereby, special attention will be paid to the effect of the application of an input amplitude filter $F(j\omega)$, according to Theorem 3.2.6, on the identification result.

3.5.2 Identification of linear dynamics

Iterative filter design

Because the non-linearity f_1 is now present in a dynamic closed loop configuration, the iterative filter design is less straightforward than in the case of the pilot-valve. Actually, some complications discussed in Subsection 3.2.2 have to be dealt with, such as the choice of input signal level $A_{\bar{u}_s}$ and the a-priori knowledge of $G_2(j\omega)$.

Fortunately, the physical insight in the model allows a subdivision of the model according to Fig. 3.3 with subsystems given by (3.21). Apart from the gain, $G_2(j\omega)$ is therewith

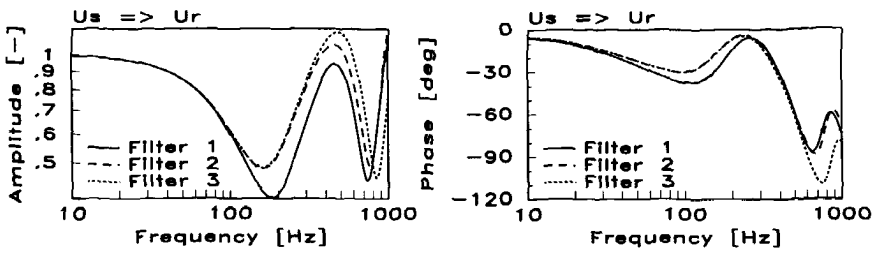


Fig. 3.14: Measured frequency responses $H^{1\%}_{\bar{u}_s\bar{u}_r}(j\omega)$ of implemented input amplitude filters. Three respective designs `Filter 1` (solid); `Filter 2` (dashed); `Filter 3` (dotted)

known; it is just an integrator. Using this in applying Theorem 3.2.6, each step in the iterative filter design is the determination of a filter $F(j\omega)$ that satisfies:

$$|F(j\omega)| \;=\; \left|\tilde{H}^{A_{\bar{u}_s}}_{\bar{u}_r\bar{x}_m}(j\omega)\right|^{-1}\left|\tfrac{1}{j\omega}\right| \tag{3.22}$$

Hereby, $\tilde{H}^{A_{\bar{u}_s}}_{\bar{u}_r\bar{x}_m}(j\omega)$ is the frequency response of the three-stage valve, measured with the previously designed input amplitude filter. In the first iteration step, this filter is a unity gain. Concerning the amplitude $A_{\bar{u}_s}$ of the source signal, a reasonable value has been chosen for it, such that the system is not excited too heavily: $A_{\bar{u}_s} = 0.5$ % has been used.

For practical reasons, namely to avoid saturation for low frequencies, the pure integrator that occurs in the filter (3.22) is fed back such that the filter has unity gain for low frequencies. After digital implementation of the subsequent filter designs, frequency responses of the filters have been measured. They are given in Fig. 3.14, and denoted as `Filter 1`, `Filter 2`, and `Filter 3` respectively. Note from the discussion of Subsection 3.2.2 that the phase lag of the filter is not 8involved in the measurement of the systems frequency response, so that the phase lag due to digital implementation is no problem.

It is clear from this Figure, that the first design (`Filter 1`) is still considerably biased by the influence of the non-linearity. The second design (`Filter 2`) already converges to the desired amplitude response for a frequency range up to about 300 Hz. The third design (`Filter 3`) in fact is a modification of the previous filter in order to compensate for the frequency distortion for high frequencies, caused by discretization effects [68].

With the final design `Filter 3`, the spectrum of $\left|H^{0.5\%}_{\bar{u}_s\bar{u}_r}(j\omega)\right|\left|\tilde{H}^{0.5\%}_{\bar{u}_r\bar{x}_m}(j\omega)\right||j\omega|$ appeared to be reasonably flat, meaning that the signal amplitude $A_{\bar{x}_s}$ has been almost constant over frequency. The effect of this on the identification result is discussed next.

Identification results

The experimental frequency responses $H^{0.5\%}_{\bar{u}_r\bar{x}_m}(j\omega)$ and $\tilde{H}^{0.5\%}_{\bar{u}_r\bar{x}_m}(j\omega)$ are used to fit the frequency response $\hat{G}(j\omega)$ of a linear SISO model. For this SISO model, a fifth order model with one rhp-zero is chosen, corresponding to (2.104). Although for the experimental situation, differential feedback is present according to (3.20), instead of only proportional feedback according to (2.103), the model structure (2.104) is still valid. In fact, the differential action only changes the (1,3)-element of the state matrix of (2.104) from c_3 into $(c_3 + c_9\bar{K}_{pm}\bar{K}_{dm}c_{10})$.

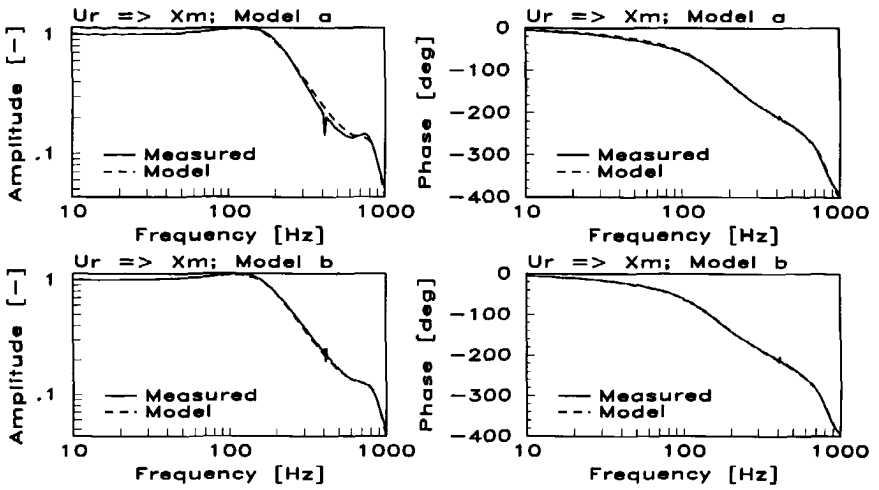


Fig. 3.15: Fits of linear frequency responses $\hat{G}(j\omega)$ (dashed) on measurements of three-stage valve dynamics (solid); measurements obtained without filtering $H^{0.5\%}_{\tilde{u}_r\tilde{x}_m}(j\omega)$ (upper) and with filtering $\tilde{H}^{0.5\%}_{\tilde{u}_r\tilde{x}_m}(j\omega)$ (lower)

The resulting fits of the SISO model are given in Fig. 3.15. Using the known controller gains, the parameters of the state space model can be reconstructed from the identified transfer function. Similar to the case of the pilot-valve in the previous Section, c_5, c_6 and c_8 are chosen a-priori, so that the remaining parameters can be calculated. The resulting parameters for the two fits are given in Table 3.2.

	Model a	Model b		Model a	Model b		Model a	Model b
c_1	$3.11\ 10^3$	$4.29\ 10^3$	c_2	$3.06\ 10^7$	$2.96\ 10^7$	c_3	$1.56\ 10^{10}$	$2.30\ 10^{10}$
c_4	$6.02\ 10^{10}$	$1.13\ 10^{11}$	c_5	$1.00\ 10^2$	$1.00\ 10^2$	c_6	$1.00\ 10^4$	$1.00\ 10^4$
c_7	1.14	$9.93\ 10^{-1}$	c_8	$4.00\ 10^3$	$4.00\ 10^3$	c_9	$1.81\ 10^{10}$	$2.68\ 10^{10}$
c_{10}	$1.45\ 10^2$	$1.27\ 10^2$	$\bar{K}_{pm}$	8.0	8.0	$\bar{K}_{dm}$	$4.9\ 10^{-4}$	$4.9\ 10^{-4}$

Table 3.2: Experimental parameter values identified three-stage valve models; without filtering (`Model a`) and with filtering (`Model b`)

Discussion of results

Considering the identified parameter values of Table 3.2, it is noted, that these parameters reflect the dynamics of an other pilot-valve than those of Table 3.1, so they can not be compared. For practical reasons, the closed loop identification of the three-stage valve was performed with a 3.3 [l/min] pilot-valve, while the data in the previous Section were obtained with a newer pilot-valve with a capacity of 6.6 [l/min], see Subsection 3.3.2. Though not shown here, closed loop identification results with this newer pilot-valve also

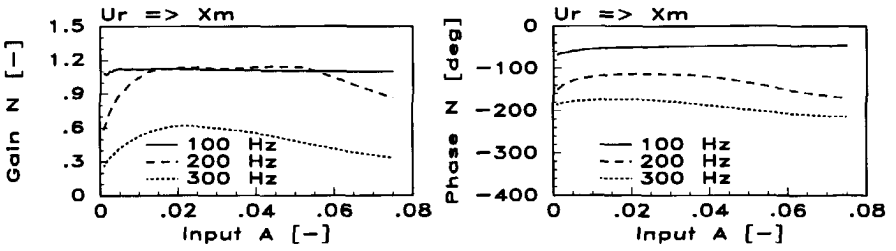


Fig. 3.16: Measured amplitude responses $N^{100\,\mathrm{Hz}}_{\bar{u}_r\bar{x}_m}(A_{\bar{u}_r})$, $N^{200\,\mathrm{Hz}}_{\bar{u}_r\bar{x}_m}(A_{\bar{u}_r})$ and $N^{300\,\mathrm{Hz}}_{\bar{u}_r\bar{x}_m}(A_{\bar{u}_r})$ of three-stage valve; gains (left) and phases (right)

result in different estimations for the linear dynamics of the pilot-valve. Reasons are given before, in Subsection 3.5.1.

Concerning the identified linear dynamics of the three-stage valve, the following conclusions are drawn from Fig. 3.15:

- For both fits, `Model a` and `Model b`, the mismatch between model and experiment is small enough to conclude that the model structure (2.104) is valid. This justifies the rather basic assumption in Subsection 2.2.4, that the main spool can be seen as an integrator.
- The measurement obtained with input amplitude filter is matched slightly better than that without filter. As reflected in the parameter values of Table 3.2 the resulting linear models are also slightly different.

3.5.3 Identification and validation of non-linearities

With identified linear dynamic models available, the static non-linearity (2.120) can be identified as described in Subsection 3.2.4. Actually, this is performed for both cases, so for the model based on data obtained without filtering as well as that based on data obtained with filtering. The results are quite similar; only the results of the case with filtering will be discussed here. In cross-validation stage in the next Subsection, both identified non-linear models will be compared.

For the purposed of the identification of the static non-linearity, closed loop amplitude responses have been measured. For clarity and extra validation, this has been done at three frequencies in a region where the influence of the non-linearity appears to be most clear, namely the bandwidth of the three-stage valve. The resulting amplitude responses at $\omega_i = 100$, 200 and 300 [Hz] for $i=1,2,3$ respectively, are shown in Fig. 3.16. Note that the amplitude responses are quite different and show significant non-linearity, especially at 200 and 300 [Hz] (around the bandwidth).

Presuming that the non-linearity can be ascribed to the static non-linearity f_1 according to Fig. 3.13, and using the identified parameters to obtain estimated transfer functions $\hat{G}_1(j\omega)$, $\hat{G}_2(j\omega)$ and $\hat{G}_3(j\omega)$ according to (3.21), the method of Subsection 3.2.4 can be applied to identify f_1. Therefore, the amplitude response $\hat{N}^{\omega_i}_{\bar{u}_r\bar{x}_m}(\hat{A}_{\bar{x}_s})$ of the static non-linearity is calculated first for the three frequencies ω_i, using (3.16) and (3.17):

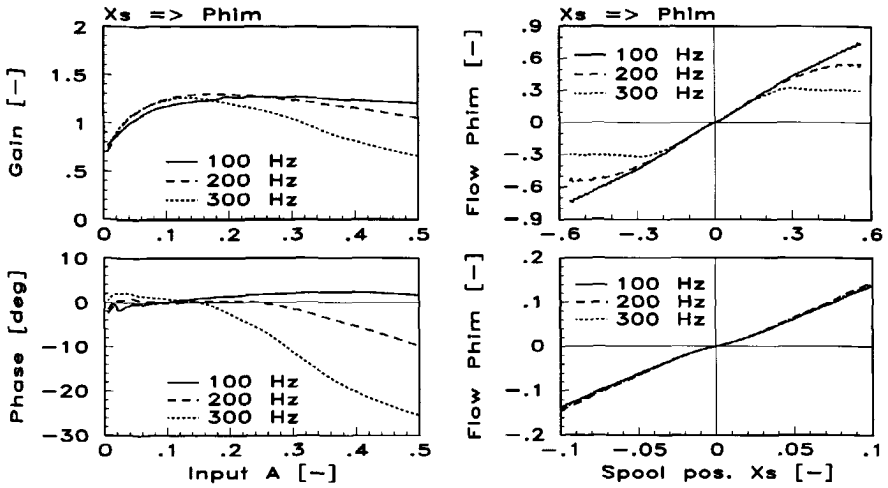


Fig. 3.17: Reconstructed amplitude responses $\hat{N}^{\omega_i}_{\bar{x}_s\bar{\Phi}_m}(\hat{A}^{\omega_i}_{\bar{x}_s})$ of static non-linearity in three-stage valve; gains (upper left) and phases (lower left); reconstructed static non-linearities $\bar{\Phi}_m = \hat{f}_1^{\omega_i}(\bar{x}_s)$ (right); $\omega_i = 100$, 200 and 300 [Hz]

$$\hat{N}^{\omega_i}_{\bar{x}_s\bar{\Phi}_m}(\hat{A}^{\omega_i}_{\bar{x}_s}) = \frac{N^{\omega_i}_{\bar{u}_r\bar{x}_m}(A_{\bar{u}_r})}{\hat{G}_1(j\omega_i)\hat{G}_2(j\omega_i)\left[1 - \hat{G}_3(j\omega_i)N^{\omega_i}_{\bar{u}_r\bar{x}_m}(A_{\bar{u}_r})\right]}, \quad i=1,2,3 \tag{3.23}$$

where the input amplitudes of the closed loop and of the non-linearity are related to each other as:

$$\hat{A}^{\omega_i}_{\bar{x}_s} = A_{\bar{u}_r}\left|\hat{G}_1(j\omega_i)[1 - \hat{G}_3(j\omega_i)N^{\omega_i}_{\bar{u}_r\bar{x}_m}(A_{\bar{u}_r})]\right|, \quad i=1,2,3 \tag{3.24}$$

The result is given in Fig. 3.17. For small amplitudes of the pilot-valve spool displacement $A_{\bar{x}_s}$, the three amplitude responses are close to each other, contrary to the measured closed loop amplitude responses. Moreover, the phase is small (< 5 [deg]). This indicates, that it is really the presumed static non-linearity at this location of the model, that causes the non-linearity of the closed loop responses. For larger input amplitudes, other (dynamic) non-linearities begin to play a role, causing the deviations between the three different responses.

Next, the approximate non-linear function $\bar{\Phi}_m = \hat{f}_1(\bar{x}_s)$ is reconstructed from the amplitude response of the non-linearity, as described in Subsection 3.2.4. Thereby, the phase of the amplitude responses is neglected. As the result in the right plot of Fig. 3.17 shows, the same type of characteristics is found as in the previous Section. Apparently, the pilot-valve here also has slightly overlapped spool ports, resulting in decreased gain for small amplitudes.

For larger amplitudes of the pilot-valve spool position, the identified non-linearities diverge for different frequencies. A kind of saturation is seen for increasing frequency. As pointed out in earlier work [121], this may be ascribed to non-linear behaviour of the flapper-nozzle system due to the fact that the flapper hits the nozzles.

In order to validate the identified static non-linearity, one of the approximate functions, namely $\bar{\Phi}_m = \hat{f}_1^{200\,\mathrm{Hz}}(\bar{x}_s)$, is integrated with the identified linear dynamics to a non-linear

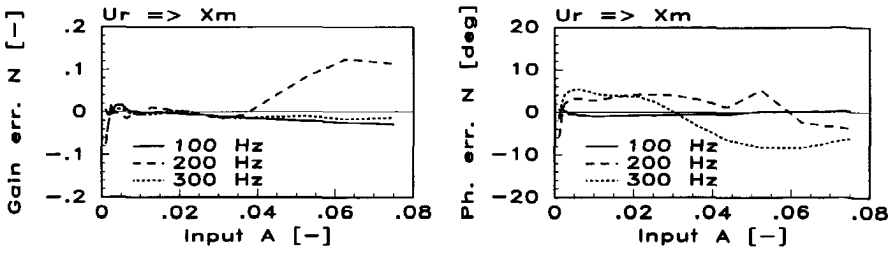


Fig. 3.18: Difference of amplitudes $|N^{\omega_i}_{\bar{u}_r\bar{x}_m}(A_{\bar{u}_r})| - |\hat{N}^{\omega_i}_{\bar{u}_r\bar{x}_m}(A_{\bar{u}_r})|$ (left) and phases $\angle N^{\omega_i}_{\bar{u}_r\bar{x}_m}(A_{\bar{u}_r}) - \angle \hat{N}^{\omega_i}_{\bar{u}_r\bar{x}_m}(A_{\bar{u}_r})$ (right) of measured and simulated amplitude responses three-stage valve

simulation model. The effect of the flapper hitting the nozzles as described in [121] is also included. The obtained model is used to reproduce the three measured amplitude responses of Fig. 3.16; the resulting errors are given in Fig. 3.18. From the close match between measurement and simulation for the different frequencies, it can be concluded that the identified non-linearity is a valid description of the basic non-linear behaviour of the three-stage valve.

3.5.4 Cross-validation

Validation results so far concerned fits on measurements that were directly used for the identification. In this Subsection, some typical results are shown, where model simulations are compared to 'fresh' measurements. First, some frequency domain results are presented to illustrate the effect of input amplitude filtering on the accuracy of the identified non-linear dynamic model. Second, the obtained model is validated with some time-domain recordings, showing the benefit of the non-linear model with respect to a linear model. And third, an evaluation of the identification procedure and the adopted model structure is given by showing validation results for six different servo-valves.

Frequency domain validation and effect of filtering

In the upper plot of Fig. 3.19, three characteristic frequency response measurements of the three-stage valve are given. It is obvious, that the dynamics are highly dependent on the input amplitude $A_{\bar{u}_r}$ due to non-linearity. It is also clear that the application of the input amplitude filter (the dotted line) has some influence on the resulting response. Compare Fig. 3.15 in this respect.

The middle and lower plots of Fig. 3.19 show the cross-validation results in the form of differences in the amplitudes and phases respectively of the measured and simulated frequency responses, with the measured responses being obtained without input amplitude filtering. In the middle plots, the results are given for `Model a`, i.e. the linear model obtained without using the filter, while the lower plots give the model mismatch on the same responses for `Model b`.

The results are quite satisfactory. Some remarks in this respect:

- The application of the filter is advantageous; the linear dynamics is apparently better estimated, such that the resulting non-linear dynamic model gives smaller errors.

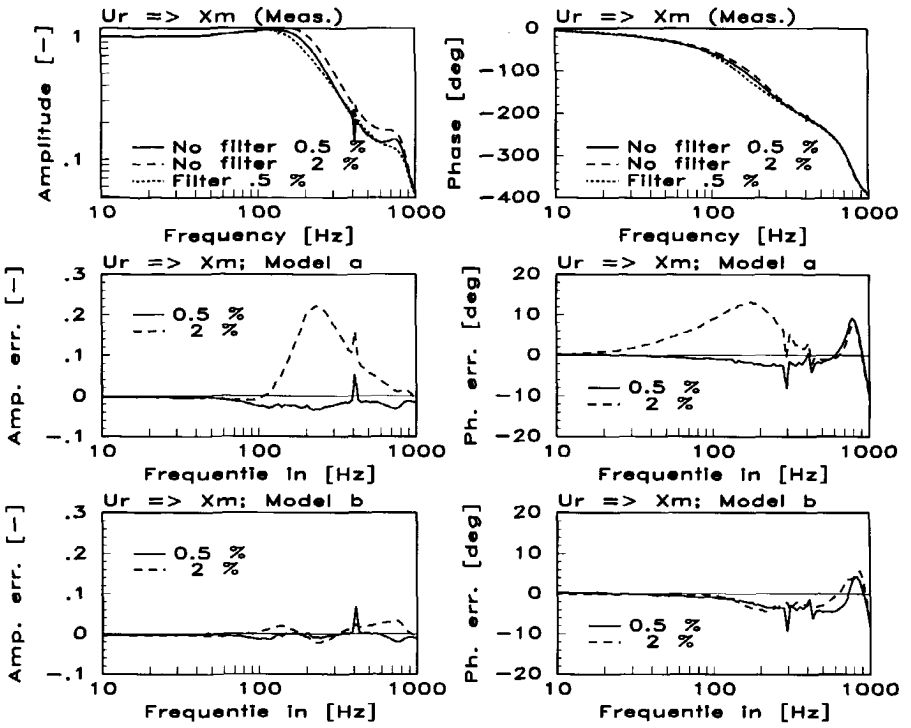


Fig. 3.19: Frequency domain validation three-stage valve. Measured frequency responses $H^{0.5\%}_{\bar{u}_r\bar{x}_m}(j\omega)$, $H^{2\%}_{\bar{u}_r\bar{x}_m}(j\omega)$ and $\tilde{H}^{0.5\%}_{\bar{u}_r\bar{x}_m}(j\omega)$ of three-stage valve (upper); difference of amplitudes $|H(j\omega)| - |\hat{H}(j\omega)|$ (left) and phases $\angle H(j\omega) - \angle \hat{H}(j\omega)$ (right) of measured and simulated responses (middle & lower): `Model a` (middle) & `Model b` (lower)

- Especially for `Model b`, the errors are relatively small. The most relevant dynamics up to 500 [Hz] are described very well for the different input amplitudes. Errors in amplitude are smaller than 5 %, and errors in phase smaller than 5 [deg], so that the models form a reliable basis for high-performance control design.

Time domain validation

For a further cross-validation, time domain recordings have been made with excitation signals that are completely different from the ones used for identification. As input for the servo-valve, white noise signals were used, with different input ranges and frequency contents.

In Fig. 3.20, an example of these time recordings is given, including some corresponding simulation results. The supplied input signal $\bar{u}_r$, with a top-top amplitude range $A_{\bar{u}_r,tt} = 2$ % and frequency contents in the range 0 - 250 [Hz] is shown in the upper plot. Actually, this input signal is typically exciting the dynamics and the non-linearity of the three-stage valve, as they have been identified in this Section. The measured output signal is given by the solid line in the lower plots. The dashed lines in these plots correspond to

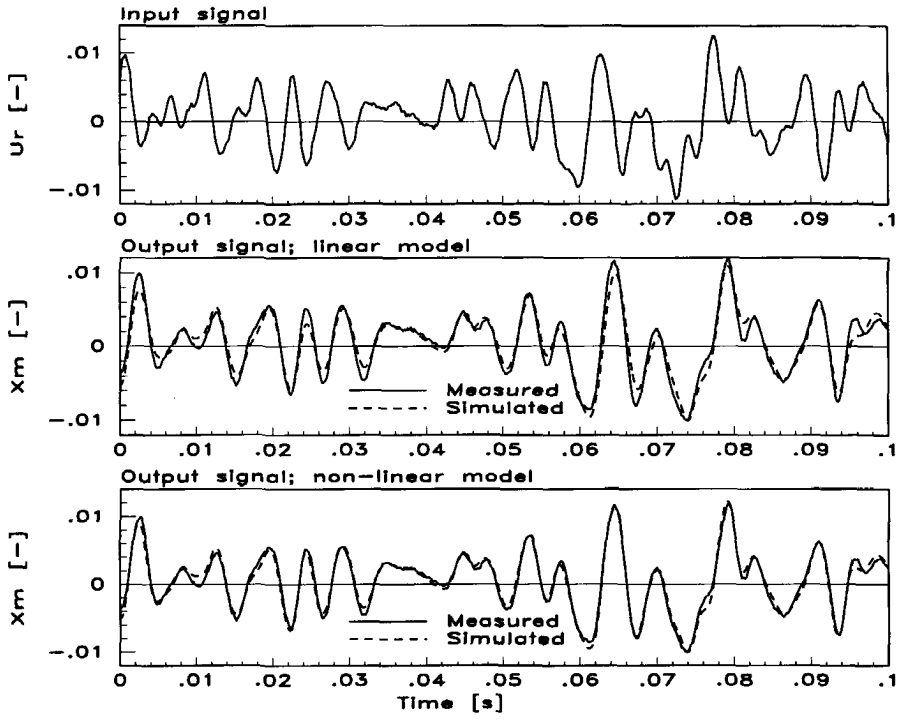


Fig. 3.20: Time domain validation three-stage valve. Measured white noise input $\bar{u}_r$ (upper); measured output $\bar{x}_m$ (solid) and simulated output $\hat{\bar{x}}_m$ (dashed) of linear model (middle) and non-linear model (lower)

the simulated outputs obtained with the linear model (middle) and the non-linear model (lower) respectively.

The results show a very good agreement between measurement and simulation, while for the given example, the non-linear model performs better than the linear model. In order to get a more complete picture of the validity of the non-linear model in the time domain, other time recordings have been evaluated as well. For this purpose, a formal distance measure is defined, instead of visually inspecting a series of plots like Fig. 3.20 [85]. Given the measured $(N*1)$-dimensional output vector $\bar{x}_m$ and the corresponding simulated output vector $\hat{\bar{x}}_m$, the mismatch between measurement and simulation is quantized by the normalized sum of squared errors:

$$V_{cv} = \frac{1}{N} \frac{1}{A^2_{\bar{u}_r,tt}} \sum_{i=1}^{N} \left[\bar{x}_{m,i} - \hat{\bar{x}}_{m,i} \right]^2 \tag{3.25}$$

For nine time recordings, this mismatch is presented in Table 3.3. Note that the result of Fig. 3.20 corresponds to the middle column of this Table.

Based on the results presented in Table 3.3 the following conclusions can be drawn:

- In the low-frequency range 0 - 25 [Hz], the model describes the time-domain behaviour very accurately, especially if the amplitude is not too small; for very small amplitudes the measurement noise contributes to the mismatch.

Freq. range	0 - 25 [Hz]			0 - 250 [Hz]			0 - 1000 [Hz]		
Input range	0.5 %	2 %	5 %	0.5 %	2 %	5 %	0.5 %	2 %	5 %
LIN-model	1.78	0.40	0.42	2.33	3.01	5.71	1.93	1.56	1.70
NL-model	1.70	0.35	0.42	2.83	1.14	1.46	2.10	1.29	0.75

Table 3.3: Normalized sum of squared errors V_{cv} (x 10^{-3}) of simulated outputs

- For the measurements where the pilot-valve operates in the null-region (either the low-frequency measurements or the high-frequency measurements with small input amplitude, < 1 %), there is no significant difference between the linear and the non-linear model.
- For the measurements with high-frequency contents and larger input amplitudes $>$ 1 %, the non-linear model performs significantly better than the linear model. During these measurements, larger pilot-valve spool displacements have occurred, such that systems response was affected by the static non-linearity. Inclusion of the identified non-linearity in the model describes this effect properly.

Different valves

As a final validation of the applied identification procedure for a three-stage valve, some results for a set of six different servo-valves are presented here. In fact, the whole procedure described in this Section has been applied to all of them, resulting in identified linear models (Subsection 3.5.2) and static non-linearities (Subsection 3.5.3). A rather condense representation of the results is given in Fig. 3.21.

The left plots show the results for valve 1, 2 and 3, the right plots for valve 4, 5 and 6. The upper plots give the identified approximate non-linear function, that represents the flow characteristic of the pilot-valve. The middle plots show the amplitude of the measured frequency responses (without amplitude filter), all with an input amplitude $A_{\bar{u}_r} = 1$ %. In the lower plots, the amplitude errors of the corresponding simulated frequency responses are given.

The results give rise to the following conclusions:

- Each pilot-valve has a different flow characteristic. The developed identification procedure is a good means to quantify this basic non-linearity using closed loop measurements on the three-stage valve.
- Each three-stage valve has different dynamic properties. Again, the developed identification procedure is well suited to find experimental non-linear dynamic models, that provide an individual description of these properties for each valve with good accuracy.
- Although difficult to see in Fig. 3.21, the differences in properties of the individual valves appear to be larger than the inaccuracy of the models.

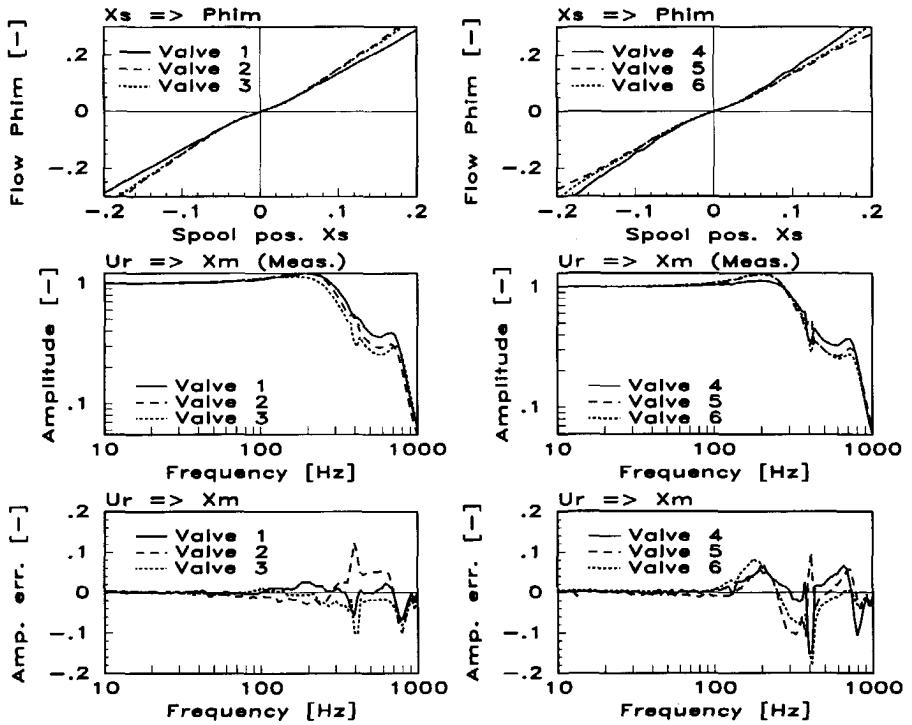


Fig. 3.21: Validation of six three-stage valves. Valve 1, 2 and 3 (left); valve 4, 5 and 6 (right). Identified static non-linearity (upper); measured frequency response $H^{1\%}_{\bar{u}_r\bar{x}_m}(j\omega)$ (middle); difference of measured and simulated amplitudes $|H(j\omega)| - |\hat{H}(j\omega)|$ (lower)

3.5.5 Estimate-based reconstruction of physical parameters

In relation to the preceding results it might be noted, that slight unknown variations in the physical dimensions of the servo-valve may cause rather large variations in the dynamic behaviour of the system. Despite the fact that the six servo-valves were of exactly the same type, different dynamic responses were observed, Fig. 3.21. Since remaining experimental conditions were identical, these differences are ascribed to manufacturing tolerances. Actually, this further illustrates that it would be impossible to arrive at accurate (in a *quantitative* sense) non-linear dynamic models by means of physical modelling alone, i.e. by just using theoretical parameters. Identification of the model parameters from experimental results of the valve under consideration, with the model structure being given by physical modelling, appears to be essential to obtain an accurate non-linear dynamic model, with small errors in the (non-linear) frequency responses. Note, that this is fully in line with the discussion in the beginning of Subsection 2.2.5, and justifies the chosen approach.

Because of the restricted value of the true underlying physical parameters in the physical model, the identification results are not used to reconstruct these parameters. The same reasoning as for the pilot-valve in Subsection 3.4.5 holds here.

3.5.6 Conclusion

By applying the identification procedure of Section 3.2, an accurate non-linear dynamic model of the three-stage valve can be identified. The use of an input amplitude filter during the frequency response measurement, in order to identify the linear dynamics, is proven to be advantageous. Thereby, the identification of the pilot-valve dynamics could best be done from closed loop measurements. The procedure also provides a quantitative representation of the non-linearity of the valve, in the form of an approximate non-linear flow characteristic of the pilot-valve.

The method is well-suited to identify an experimental model, that describes the amplitude dependent dynamics of an individual servo-valve; within the relevant amplitude and frequency range, the model errors are smaller than the variations in dynamic behaviour due to manufacturing tolerances between different valves. Besides that this makes the resulting models well-suited for (robust) control design, the obtained confidence in the model allows predictive statements based on the model. For instance, it is clear that the dynamic properties and the linearity of the flow characteristic of the pilot-valve play a crucial role in the non-linear dynamic properties of the three-stage valve.

In the discussion of this Section, the possible non-linearity of the flow characteristic of the main spool has not been considered. In accordance with the discussions in Section 2.7, this non-linearity is seen as part of the non-linear dynamics of the hydraulic actuator. As such, it is taken into account in the next Section, which discusses the identification and validation of the actuator dynamics.

3.6 Identification and validation of hydraulic actuator model

3.6.1 Introduction

In the first stage of the identification and validation of the actuator dynamics, the transmission line effects are left out of consideration, Subsection 3.1.4. Therewith, the (position dependent) linear dynamics to be identified are given by (2.108), page 101. Taking the basic non-linearities of the actuator into account, namely the valve flow non-linearity (2.124) and the Coulomb friction (2.126), the non-linear actuator dynamics are described by the model that was presented in the block scheme of Fig. 2.41 on page 116.

Because, in the first instance, the identification of the actuator dynamics is used to validate the derived model structure, and to obtain quantitative insight in the dynamics and non-linearities of the actuator, the identification is performed in open loop configuration. Or better, in quasi open-loop configuration: only a very weak position feedback loop was present just to stabilize the open loop integrator, such that a certain position is maintained during the experiment. In case that high-performance closed loop control is to be achieved, it is worth while to perform iterative control design and identification [122], but this lies beyond the scope of this thesis.

Adopting the model according to Fig. 2.41 for the hydraulic actuator, the identification procedure of Section 3.2 can be applied again. An important question thereby is, how to deal with the different non-linearities.

Fortunately, the Coulomb friction is relatively small due to the presence of hydrostatic

bearings. Actually this means, that it is only relevant to include Coulomb friction to describe the non-linear effects, that occur during velocity reversal in smooth motions. For the rest, Coulomb friction has only minor influence on the linear dynamics of the actuator. It is therefore neglected during the identification of linear dynamics; the Coulomb friction itself is identified and validated separately in a later stage.

Whereas the actuator was stabilized around certain position during the identification experiment, the obtained data describe the actuator dynamics for that position. So for one such experiment, the position dependent parameters (ζ_5 and ζ_6) in the model can be considered to be constant. Therewith, the valve flow non-linearity is the only remaining relevant non-linearity. It is clear from (2.124) and Fig. 2.41, that this non-linearity basically consists of two contributions, namely the static non-linearity f_2 and the square root expression describing the load dependence.

If the excitation signals are small, such that the load pressure $\overline{\Delta P}_p$ remains small, the square root is very well approximated by a unity gain. In that case, just a static input non-linearity f_2 remains. This is easy to deal with according to the theory of Subsection 3.2.2, where $G_1(j\omega) = 1$ and $G_3(j\omega) = 0$ in the configuration of Fig. 3.3. However, the effect of the load pressure $\overline{\Delta P}_p$ can not completely be neglected, making the identification and validation slightly more complicated. Nevertheless, the procedure described in Section 3.2 is well applicable to the non-linear actuator model as discussed in the subsequent Sections below.

3.6.2 Identification of linear dynamics

After a motivation for the applied input amplitude filtering, the identification of the linear dynamics of the actuator is discussed in this Section. First, a linear model for the middle position is identified. Subsequently, the position dependence of the linear dynamics is taken into account, by identifying models for different actuator positions.

Input amplitude filtering

Related to the input non-linearity f_2, application of the theory of Subsection 3.2.2 says, that the input amplitude $A_{\bar{x}_m}$ of the actuator should be constant over the measured frequency range, in order to obtain a measured frequency response that represents the linear actuator dynamics. Although Coulomb friction is relatively small, it is thereby necessary to choose the input amplitude large enough, for instance 2 %, in order to avoid non-linear friction effects, especially for low frequencies.

The problem is however, that the basic actuator dynamics contain a badly damped resonance frequency (see Subsection 2.3.5 and Fig. 2.35). The result is, that for constant input amplitude $A_{\bar{x}_m}$, the amplitude of the load pressure $A_{\overline{\Delta P}_p}$ becomes very large in the frequency region around this resonance. Besides that this may cause non-linearity due to the load dependence of the valve flow (2.124), this involves a heavy loading of the experimental setup.

Actually, it is mainly this practical reason, which has led to the decision to use an input amplitude filter, that tries to maintain a constant amplitude $A_{\overline{\Delta P}_p}$ of the load pressure during the frequency response measurement. The filter design was based on an initial frequency response measurement of the actuator dynamics, using a small valve input amplitude $A_{\bar{u}_r}$, over a frequency range just covering the basic actuator dynamics. Thereby, an

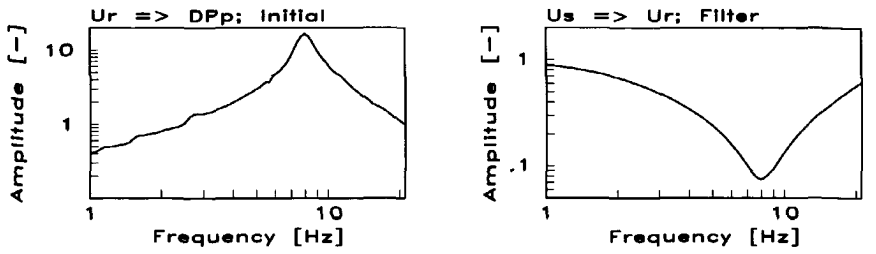


Fig. 3.22: Amplitude of initial measurement actuator dynamics $|H^{.5\%}_{\bar{u}_r\overline{\Delta P}_p}(j\omega)|$ (left) and of implemented input amplitude filter $|H^{1\%}_{\bar{u}_s\bar{u}_r}(j\omega)|$ (right)

anti-resonance was placed at the actuator resonance frequency, while the filter was given unity steady state gain and additional high-frequency dynamics to obtain high-frequency roll-off. The measured frequency responses of the basic actuator dynamics and of the correspondingly designed filter are shown in Fig. 3.22. Note from the previous Section, that for the frequency range considered here, 1 - 20 [Hz], the servo-valve has unity gain, so that the input amplitude of the servo-valve, $A_{\bar{u}_r}$, equals that of the actuator, $A_{\bar{x}_m}$.

Using the designed input filter, and taking the measured valve spool displacement signal $\bar{x}_m$ as input, a number of frequency response measurements has been performed with the experimental setup, described in Section 3.3. In the remainder of this Section, these measurements are used to identify and validate the linear dynamics of the actuator.

Linear dynamics

The identification of the linear dynamics of the hydraulic actuator corresponds to fitting the frequency responses of the model (2.108), given on page 101, on experimental frequency responses. With respect to this identification, some remarks are made preliminary to the discussion of the results:

- From the two inputs of (2.108), only the flow $\bar{\Phi}_p$ is controllable, in the sense that $\bar{x}_m$ equals the control input $\bar{u}_r$. The external force $\bar{F}_{ext}$ is not controllable; due to equal load distribution on the test rig (Fig. 3.6), the external force was almost zero and at least constant during the experiments. Because the corresponding input parameter ζ_2 is also present in the state matrix, it is still identifiable, using the controllable input.
- With the outputs q and $\overline{\Delta P}_p$ being measurable, two input-output frequency responses can be obtained, while applying the designed input amplitude filter: $\tilde{H}^{A_{\bar{u}_s}}_{\bar{x}_m q}(j\omega)$ and $\tilde{H}^{A_{\bar{u}_s}}_{\bar{x}_m\overline{\Delta P}_p}(j\omega)$.
- Because the valve spool position $\bar{x}_m$ is the measured input signal, the gain of the static non-linearity f_2 (see Fig. 2.41) is included in the frequency response measurements, and therewith in the steady state gain of the resulting identified linear model (2.108). So, the transfer functions $G_{\bar{x}_m q}(j\omega)$ and $G_{\bar{x}_m\overline{\Delta P}_p}(j\omega)$ are fitted on the experimental data, rather than $G_{\bar{\Phi}_p q}(j\omega)$ and $G_{\bar{\Phi}_p\overline{\Delta P}_p}(j\omega)$.
- In the given model structure (2.108), there are actually five parameters to be identified, namely $\zeta_1, \ldots, \zeta_4$ and the position dependent parameter combination $\zeta_{56} = \frac{1}{2}(\zeta_5 + \zeta_6)$. For the identification of these five parameters for certain position q_0, the

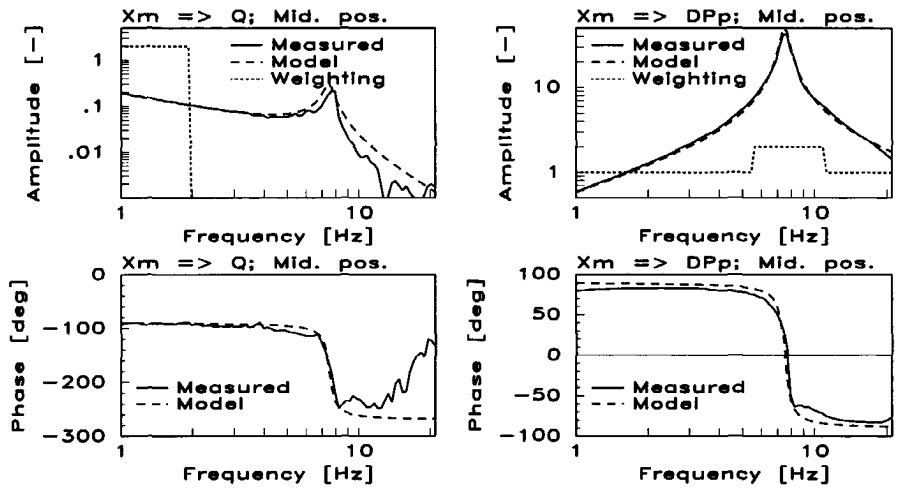


Fig. 3.23: Fits of linear frequency responses $\hat{G}_{uy}(j\omega)$ (dashed) on measurements $\tilde{H}^{2\%}_{uy}(j\omega)$ (solid) and corresponding weightings $W_{uy}(j\omega)$ (dotted) in middle position $q_0 = 0$ [m]; input $u = \bar{x}_m$; output $y = q$ (left) and $y = \overline{\Delta P}_p$ (right)

available frequency response measurements are just sufficient.

With these remarks, the setting for the identification of the linear actuator dynamics is given. Because multiple frequency responses are involved here (two outputs), the identification is performed with the OPTIMIZE-command of Matrix$_X$, minimizing the cost function (3.13), as described in Subsection 3.2.3. Starting with an initial estimate, obtained by linearization of the theoretical model, the parameters $\zeta_1, \ldots, \zeta_4$ and ζ_{56} are optimized with respect to the fit of the frequency responses of the model on the experimental data. For the measurements obtained at the middle position $q_0 = 0$ [m] of the actuator, the results are shown in Fig. 3.23, including the weightings that were applied in the cost function (3.13). In Table 3.4, the parameter values of the initial estimate and the final, optimal estimate are given.

	Initial	Final		Initial	Final		Initial	Final
ζ_1	$3.49\ 10^{-2}$	$4.47\ 10^{-2}$	ζ_2	$2.33\ 10^{1}$	$1.33\ 10^{1}$	ζ_3	1.01	$8.31\ 10^{-1}$
ζ_4	$8.98\ 10^{-3}$	$1.90\ 10^{-2}$	ζ_{56}	$1.13\ 10^{2}$	$1.01\ 10^{2}$			

Table 3.4: Experimental parameter values identified actuator model; initial estimates and final estimates for middle position $q_0 = 0$ [m]

As Fig. 3.23 shows, the weighting is such, that the mismatch of the position transfer function only contributes to the cost function for low frequencies. The reason is, that only in this region the amplitude of the measured position output signal was large enough with respect to the noise level, to provide reliable results. In fact, the fit of the position transfer function is only used to identify the steady state gain of the hydraulic actuator (represented

by ζ_3). The fit of the pressure difference transfer function is used to identify the remaining parameters, that determine the dynamics of the actuator. Thereby, the frequency region around the resonance frequency is weighted heavier, in order to obtain a good fit of this resonance frequency and its damping, i.e. the basic dynamic behaviour of the actuator.

Comparing the initial estimate with the final estimate in Table 3.4, it is clear that the initial estimate is far from optimal. Nevertheless it leads to an optimal solution that corresponds to a satisfactory match between model and experiment, Fig. 3.23. With this result, the structure of the basic actuator model (2.108) is validated, at least for one position. A further validation of the model lies in the identification of the position dependence of the actuator dynamics, which is discussed next.

Position dependence of linear dynamics

In order to identify and validate the position dependence of the linear model (2.108), the input-output frequency responses of the actuator were not only measured in the middle position $q_0^0 = 0$ [m], but also in a lower position at 75 % of half the stroke, so $q_0^- = -0.47$ [m], and in a similar upper position, so $q_0^+ = +0.47$ [m].

The position dependence of the actuator dynamics is identified from the measured data, by simultaneously fitting the frequency responses $G_{uy}^-(j\omega)$, $G_{uy}^0(j\omega)$ and $G_{uy}^+(j\omega)$ of three respective linear models (2.108) on the corresponding experimental frequency responses. Thereby, the parameters $\zeta_1, \ldots, \zeta_4$ are the same for all three models, while the position dependent parameter combination $\zeta_{56} = \frac{1}{2}(\zeta_5 + \zeta_6)$ is obviously different for the different models.

Applying similar weightings to the mismatch of the individual models as before, and summing the mismatches of the three different models to a single cost function, the parameters $\zeta_1, \ldots, \zeta_4, \zeta_{56}^-, \zeta_{56}^0$ and ζ_{56}^+ can be optimized using OPTIMIZE. The resulting fits for the amplitudes of the frequency responses are given in Fig. 3.24, while the corresponding estimates of the parameters are given in Table 3.5.

	Id. Value		Id. Value		Id. Value		Id. Value
ζ_1	$4.47\ 10^{-2}$	ζ_2	$1.27\ 10^{1}$	ζ_3	$8.31\ 10^{-1}$	ζ_4	$2.35\ 10^{-2}$
ζ_{56}^-	$1.31\ 10^{2}$	ζ_{56}^0	$1.04\ 10^{2}$	ζ_{56}^+	$1.21\ 10^{2}$		

Table 3.5: Experimental parameter values identified position dependent actuator model, based on simultaneous fit in three actuator positions

It might be noted, that the results were obtained with the same initial estimate as before, given in Table 3.4. Apparently, the requirement that the different models are fitted simultaneously, results in a slightly different optimum for $\zeta_1, \ldots, \zeta_4$. Nevertheless, the adopted model structure, with only ζ_{56} being position dependent, appears to be valid: it allows a proper characterization of the basic actuator dynamics in different actuator positions, as Fig. 3.24 illustrates. In Subsection 3.6.5, it is discussed how the underlying physical structure of the model (2.108) can be used to parametrize the parameter combination ζ_{56} in terms of the position q, so that the linear dynamics can be written explicitly as a function of the actuator position.

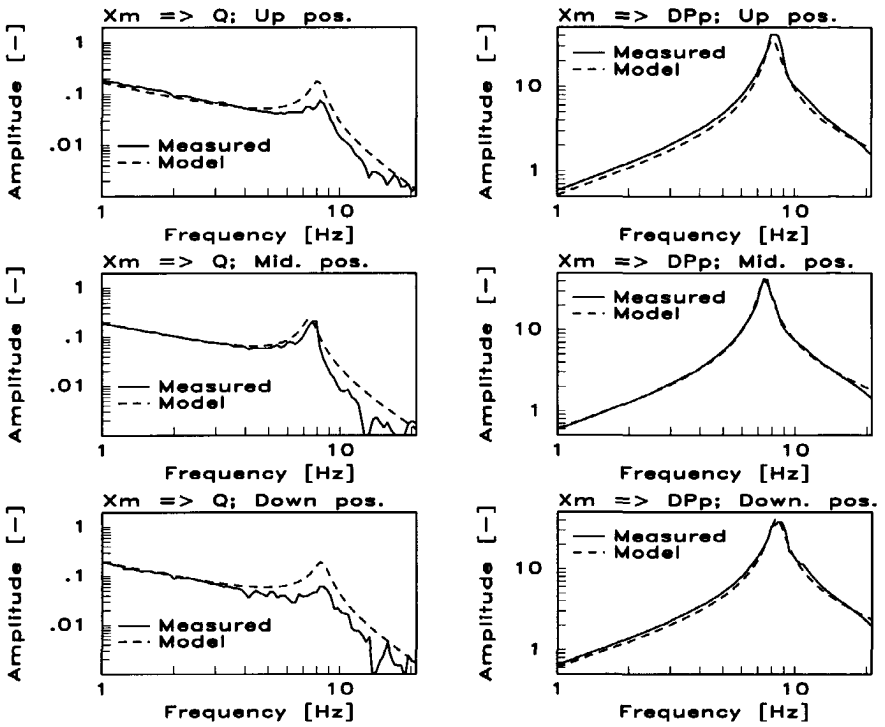


Fig. 3.24: Fits of linear frequency response amplitudes $|\hat{G}_{uy}(j\omega)|$ (dashed) on measurements $|\tilde{H}^{2\%}_{uy}(j\omega)|$ (solid) in different positions; upper position $q_0^+ = +0.47$ [m] (upper), middle position $q_0^0 = 0$ [m] (middle) and lower position $q_0^- = -0.47$ [m] (lower); input $u = \bar{x}_m$; output $y = q$ (left) and $y = \overline{\Delta P}_p$ (right)

After the identification of the basic linear dynamics of the hydraulic actuator, the identification and validation of the non-linearities in the actuator model is treated in the next Section.

3.6.3 Identification of actuator non-linearities

Referring once more to Fig. 2.41 for the basic non-linear model of the hydraulic actuator, the identification of the non-linearities focuses on the valve flow non-linearity, including the load dependence of this flow, and on the Coulomb friction.

Valve flow non-linearity

For the identification of the valve flow non-linearity, it is possible to utilize the fact that in steady state, the actuator velocity is linearly related to the valve flow by the (known) piston area A_p. Thus, the identification of the non-linear valve flow (2.124) consists of the identification of the relation between the actuator velocity $\dot{q}$ and the valve spool displacement $\bar{x}_m$, while taking into account the effect of the load pressure $\overline{\Delta P}_p$. In the usual case that the actuator velocity is not measured directly, it may be derived off-line from

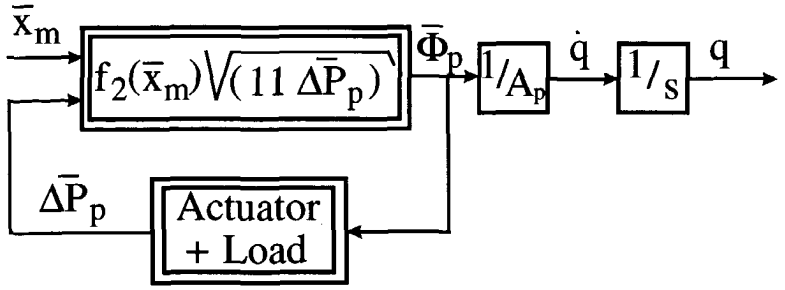


Fig. 3.25: Block scheme representation of valve flow non-linearity in identification setting

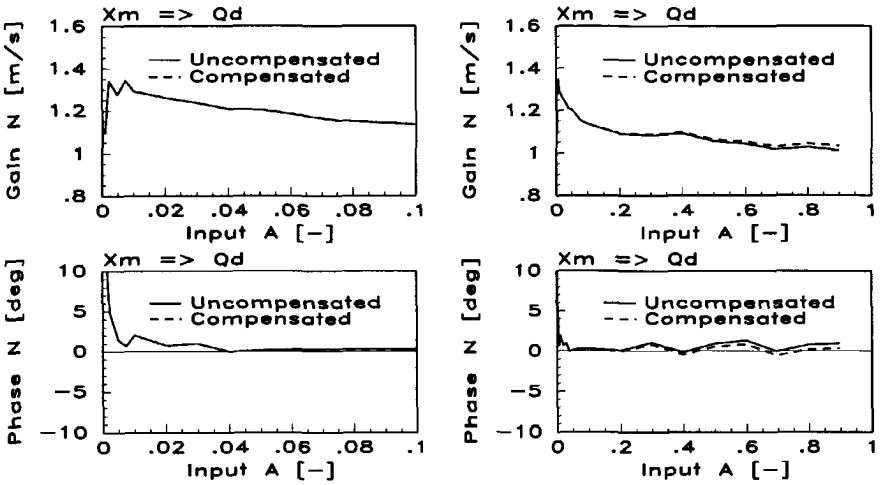


Fig. 3.26: Measured amplitude responses $N^{0.5\,\mathrm{Hz}}_{\bar{x}_m\dot{q}}(A_{\bar{x}_m})$ of hydraulic actuator; not compensated for load pressure (solid) and compensated (dashed); small input range (left) and full input range (right)

the measured position q. Therewith, the setting for the identification of the valve flow non-linearity is like shown in Fig. 3.25.

Although the configuration is slightly more complicated than in the case of the pilot-valve, Subsection 3.4.3, the static non-linearity f_2 can also be identified from a measured amplitude response of the system, obtained with sinusoidal inputs of a certain frequency. In order to have quasi steady state conditions, this frequency was chosen to be 0.5 [Hz]. An extra advantage of the application of the SIDF-method here is, that the differentiation of the measured output, a sinusoidal position signal, reduces to an amplification and a phase shift of 90 [deg]. Thus, supplying a sinusoidal input $\bar{u}_r(t)$ with different amplitudes $A_{\bar{u}_r}$ to the servo-valve, and recording the measured spool position $\bar{x}_m(t)$ and actuator position $q(t)$, the amplitude response $N^{0.5\,\mathrm{Hz}}_{\bar{x}_m\dot{q}}(A_{\bar{x}_m})$ has been determined with the techniques, described in Subsection 3.2.1. The result is shown for different input ranges by the solid curves in Fig. 3.26.

It is clear from Fig. 3.25, that the obtained amplitude response can not directly be used to determine an approximation for the static non-linearity f_2, because the effect of the load

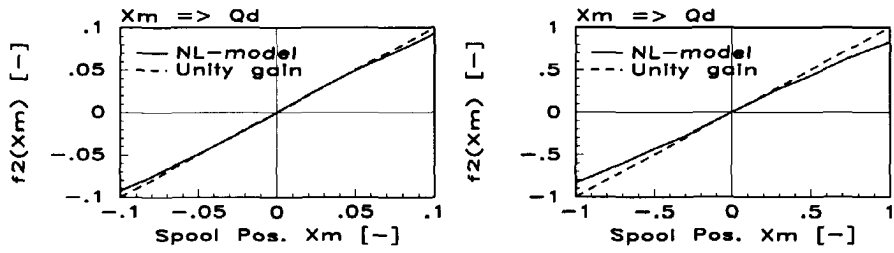


Fig. 3.27: Identified normalized static non-linearity $\hat{f}_2(\bar{x}_m)$ (solid) and unity gain as reference (dashed); small input range (left) and full input range (right)

pressure is included in the amplitude response. Actually, the amplitude response should be compensated for the influence of the non-zero load pressure $\overline{\Delta P}_p$. For that purpose, the measured time domain data have been transformed before determining the amplitude response, as follows.

First, the sinusoidal output signal $q(t)$ is transformed into an estimated velocity signal $\hat{q}(t)$ by a time shift of a quarter period and an amplification with a factor π (because of input frequency 0.5 [Hz]). This estimated velocity signal is then compensated for the load pressure, in order to obtain the velocity that would have occurred if the load pressure had been zero. For this compensation, the measured load pressure signal $\overline{\Delta P}_p(t)$ is used, as follows:

$$\hat{q}_{\overline{\Delta P}_p=0}(t) = \begin{cases} \hat{q}(t)/\sqrt{1-\overline{\Delta P}_p(t)} & \bar{x}_m(t) \geq 0 \\ \hat{q}(t)/\sqrt{1+\overline{\Delta P}_p(t)} & \bar{x}_m(t) < 0 \end{cases}$$

Using this compensated velocity signal, and the measured valve spool position, the compensated amplitude response has been determined, again using the techniques of Subsection 3.2.1. The result is shown by the dashed lines in Fig. 3.26. With this (compensated) amplitude response of the valve/actuator combination, an approximate non-linear function $\hat{f}_2(\bar{x}_m)$ can be determined, as described in Subsection 3.2.4, which characterizes the static non-linearity of the valve spool flow. Because the steady state gain of this non-linearity is already included in the identified model for the linear dynamics (Subsection 3.6.2), the approximate function $\hat{f}_2(\bar{x}_m)$ is normalized by this gain. A plot of the resulting identified static non-linearity is given by the solid line in Fig. 3.27; the dashed line is a unity gain and is given as a reference.

The Figures 3.26 and 3.27 give rise to the following conclusions concerning the valve flow non-linearity:

- According to the description of the experimental setup, Subsection 3.3.1, the maximum actuator velocity $\dot{q}_{max}$ was expected to be 1 [m/s]. This means, that the ideal amplitude response of the system would have been a unity gain. Clearly, the valve under consideration shows serious non-linearity, with a considerably larger gain for small amplitudes, and a decreasing gain for larger amplitudes.
- The phase of the amplitude response is approximately zero, confirming the steady state character of the responses. Only for very small input amplitudes, a significant non-zero phase is observed, which can be ascribed to the effect of the Coulomb friction.

- The compensation for the load pressure has only minor effect (Fig. 3.26); the load pressures were small during the experiments (< 10 %). Only for large amplitudes some difference is observed. This can be explained by the fact that at large amplitudes, the large oil flows cause pressure drops due to flow losses; these pressure drops result in load pressures $\overline{\Delta P}_p$ that decrease the actual velocity of the actuator.
- In terms of the physical model, the identified non-linearity with an increased gain in the null region indicates that the main spool has (small) underlaps, possibly with some radial clearance, as explained in Subsection 2.2.5. Whereas these quantities are closely related to manufacturing tolerances, they may well be different for different valves of the same type. This supposition is confirmed by experiments with six different valve-actuator combinations, to be presented in Subsection 3.7.4.

Combining the identified static non-linearity $\hat{f}_2(\bar{x}_m)$ with the square root expression like in (2.124), an experimental model for the non-linear valve flow is obtained, including the effect of the load dependence of the flow.

Coulomb friction

After the identification of the non-linear valve flow model, the identification of the other non-linearity, Coulomb friction, is treated briefly. Thereby, the simple friction model (2.126) is adopted. The only parameter in this model, k_6, is deduced from a very simple experiment. The actuator pressure difference $\overline{\Delta P}_p$ is recorded during two steady state motions at small velocities (1 % of $\dot{q}_{max}$): one with the actuator extending and one with the actuator retracting. The difference between the two recorded steady state pressure difference signals is a direct measure for the Coulomb friction, because:

- possible external forces are independent of the moving direction
- viscous friction effects and flow losses are negligible for these small velocities
- steady state motion implies no acceleration forces

The experiment resulted in a relative pressure difference of 0.4 [bar], which is 0.25 % with a supply pressure $P_s = 160$ [bar]. Obviously, the Coulomb friction force during motion in one direction is half this value, so that $k_6 = 1.25\ 10^{-3}$.

Having obtained this parameter, the identification of the non-linear basic actuator model according to Fig. 2.41 is completed. Without showing and discussing the validation results with respect to the experimental data that were used for the identification, the validation of the obtained model with respect to 'fresh' data is discussed in the next Section.

3.6.4 Cross-validation

In the cross-validation of the obtained actuator model, special attention is given to two aspects of the model, that were not directly involved in the identification stage. This concerns the load dependence of the valve flow and the effect of Coulomb friction on smooth motions. Additionally, the acceleration transfer function of the identified model is compared to the measured frequency response.

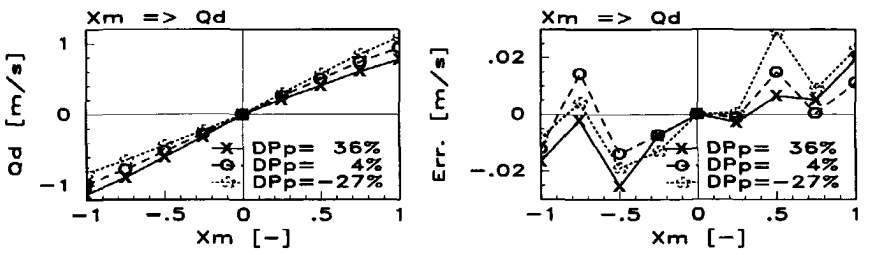


Fig. 3.28: Constant-velocity responses under different load conditions; measured velocities $\dot{q}$ (left) and velocity errors of identified model of load dependent valve flow (right)

Validation of load dependence

In the identification stage, it has been assumed, that the model for the load dependent flow through a critical-centre valve (2.123) is correct. In order to validate this assumption, a number of constant-velocity tests was performed, under different load conditions. Actually, these load conditions were created by placing and removing loads on the test rig, Subsection 3.3.1. In the left plot of Fig. 3.28, the experimental data are shown; the velocity has been obtained by off-line differentiation of the position signal. The load conditions are indicated in the plot in terms of normalized load pressures $\overline{\Delta P}_p$; the given values actually correspond to static external forces $\bar{F}_{ext}$ of the same magnitude in the actuator model Fig. 2.41.

The validation of non-linear the model (2.124) of the valve flow is given in the right plot of Fig. 3.28, which shows the difference between the measured velocities and the velocities predicted by the model. Noting the considerable variation in the actuator velocity due to the non-zero load pressure in the left plot, the small errors (independent of the load condition) in the right plot form a clear validation of the modelled non-linearity. It might be noted here, that the good results are primarily due to the modelled load dependence according to (2.123); it has brought the errors to the same order of magnitude for the different load conditions. However, the inclusion of the identified non-linearity $\hat{f}_2(\bar{x}_m)$ according to (2.124) also contributes significantly to the result; it has brought the velocity errors to the same order of magnitude for the different spool position inputs.

Coulomb friction during smooth motions

The determination of the amount of Coulomb friction has been based on steady state motions. However, the aim of the friction model is, to describe the effect of the friction during (smooth) motions, especially during velocity reversal. Obviously, the dynamics of the actuator are involved here, compare Fig. 2.28 on page 64.

In order to validate the identified non-linear actuator model of the previous Section in this respect, some time domain simulations have been performed and the match between simulated and measured outputs has been evaluated. For sinusoidal inputs $\bar{u}_r(t)$ of 0.5 [Hz] frequency, with input amplitudes $A_{\bar{u}_r} = A_{\bar{x}_m} = 0.0025$, 0.05 and 0.2 respectively, the results are given in Fig. 3.29[7]. Some remarks:

[7]Because these experimental responses were obtained with an inertial load $M_p = 815$ [kg], while the identification results were based on measurements with $M_p = 3140$ [kg], the identified parameters ζ_1 and

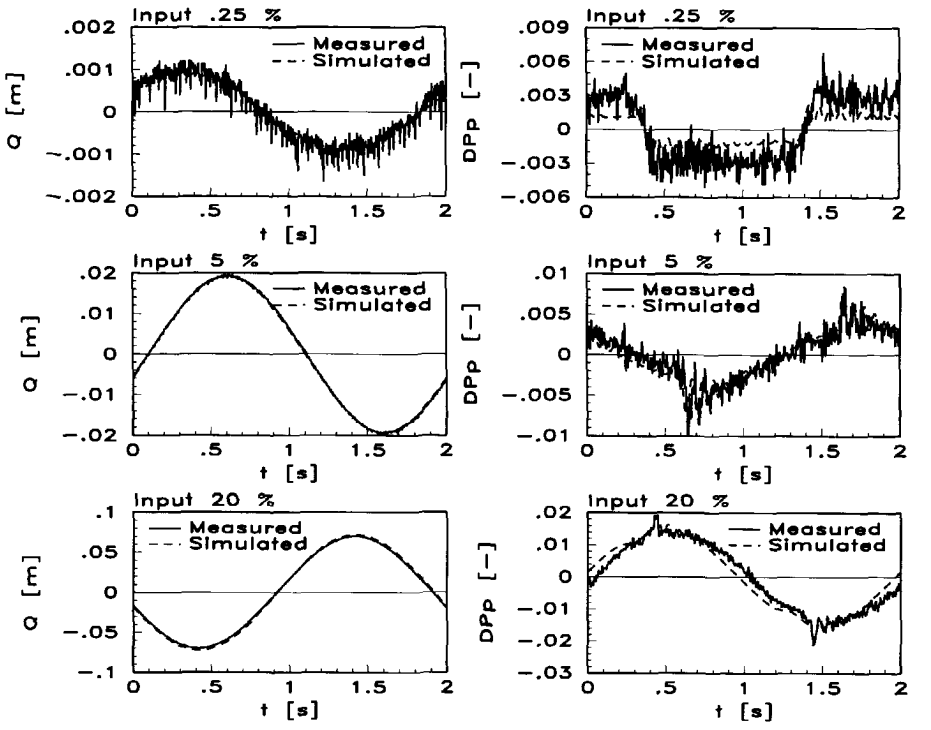


Fig. 3.29: Measured (solid) and simulated (dashed) outputs for 0.5 [Hz] sinusoidal inputs $\bar{u}_r(t)$; input amplitude $A_{\bar{u}_r} = A_{\bar{x}_m} = 0.0025$ (upper), $A_{\bar{u}_r} = A_{\bar{x}_m} = 0.05$ (middle) and $A_{\bar{u}_r} = A_{\bar{x}_m} = 0.2$ (lower); position $q(t)$ (left) and pressure difference $\overline{\Delta P}_p(t)$ (right)

- The measured pressure difference during motion with very small velocities (upper plot) is larger than simulated. Apparently, the identified value from steady state velocities of 1 % is not valid for velocities in the order of magnitude of <0.5 %. Actually, the (Coulomb) friction appears to be velocity dependent; for larger amplitude signals, the simulation of the friction level is better.
- In the middle and lower plots, it is clear that the velocity reversal causes an excitation of the actuator dynamics. This is a combined effect of the switching Coulomb friction and the crossing of the rather non-linear region of the static non-linearity; for the middle plot it is mainly the friction, while for the lower plot the non-linearity of the valve flow has considerable effect.
- The non-linearity of the open loop gain of the actuator is clear from the three responses; this can be seen as a direct validation of the identified static non-linearity of the valve flow.

Taking into account that the Coulomb friction level is relatively small, the errors between the measurements and the simulations of the identified model are small; the model provides an accurate description of the non-linear dynamic behaviour of the servo-system

ζ_2 were multiplied by $\frac{815}{3140}$ to obtain the shown simulation results

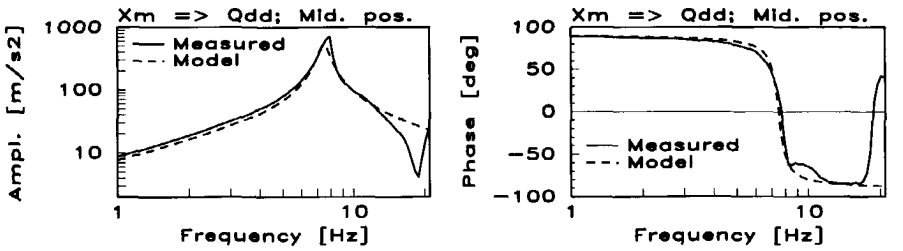


Fig. 3.30: Fit of linear frequency responses $\hat{G}_{\bar{x}_m\ddot{q}}(j\omega)$ (dashed) on measurement $\tilde{H}^{2\%}_{\bar{x}_m\ddot{q}}(j\omega)$ (solid) in middle position $q_0 = 0$ [m]

at low frequencies. Besides that the model dynamics were validated by the identification result in the frequency domain, Fig. 3.23 and 3.24, a further cross-validation is given below, using an additional frequency response measurement.

Validation of acceleration transfer function

For the purpose of validation, an additional frequency response measurement was performed, namely that of the acceleration transfer of the system, $\tilde{H}_{\bar{x}_m\ddot{q}}(j\omega)$. Obviously, the state derivative $\ddot{q}$ can easily be defined as an output of the identified model (2.108). A comparison of the transfer function $\hat{G}_{\bar{x}_m\ddot{q}}(j\omega)$ of the identified linear model and its measured counterpart is given in Fig. 3.30. The fit is good, almost comparable to the identification results of Fig. 3.23 and 3.24.

Especially around the resonance frequency, the acceleration is well predicted by the model, which means that the model gives a proper description of the ratio between actuator forces (pressure difference) and load accelerations, i.e. of the inertia of the load. In the low-frequency region, there is some mismatch; this may be ascribed to the effect of Coulomb friction. In the high frequency region, there is also a considerable difference between the predicted and the measured acceleration; this is due to parasitic dynamics of the base, as mentioned in Subsection 3.3.1.

Apart from some explainable discrepancies, the result of Fig. 3.30 validates once more the model of the basic dynamic behaviour of the hydraulic actuator. Summarizing the presented cross-validation results, it can be stated that the non-linear dynamic model of the actuator is valid in the sense that the model structure and the identified parameters provide a proper description of the non-linear dynamic input-output behaviour of the actuator. By means of reconstruction of the physical parameters of the system from identification results, further insight in the true system can be obtained.

3.6.5 Estimate-based reconstruction of physical parameters

As explained in Subsection 3.2.6, it depends on the system at hand, and its physical model, whether the underlying physical parameters of the system can be reconstructed from the identified parameters. The basic dynamic model of the hydraulic actuator is a typical example of a relatively simple model with sufficient a-priori knowledge to reconstruct unknown parameters from the identification result. Besides the reconstruction of some unknown

actuator parameters, the coupling of the identification result to the physical model allows a parametrization of the position dependence of the model, as explained below.

Reconstruction of actuator parameters

Relating the linearized physical model of the actuator, (2.105), with the position dependent term (2.106), to the simplified and normalized model (2.108), used for identification, the following expressions are obtained:

$$\begin{aligned} \zeta_1 &= \frac{w_p}{M_p} & \zeta_2 &= \frac{P_s A_p}{M_p} & \zeta_3 &= \frac{A_p}{\Phi_{p,nom}} \\ \zeta_4 &= \frac{LP_p P_s}{\Phi_{p,nom}} & \zeta_5 &= \frac{E\Phi_{p,nom}}{(A_p(q_{max}+q_0)+V_{ls1})P_s} & \zeta_6 &= \frac{E\Phi_{p,nom}}{(A_p(q_{max}-q_0)+V_{ls2})P_s} \end{aligned} \tag{3.26}$$

In these expressions, some parameters are known exactly, namely the piston area $A_p = 25\ 10^{-4}$ [m^2], half the actuator stroke $q_{max} = 0.625$ [m], and the supply pressure $P_s = 1.6\ 10^7$ [bar]. Furthermore, the ineffective volumes could be estimated from the construction drawings to be $V_{ls1} = 4.40\ 10^{-4}$ and $V_{ls2} = 3.77\ 10^{-4}$ [m^{-3}] respectively.

With this a-priori knowledge, the remaining physical parameters of the model (2.105) can be reconstructed from identified parameters, using (3.26). For the middle position $q_0 = 0$ [m], with identified parameters from Table 3.5, the results are given below, along with a discussion of the outcomes.

$\hat{E} = 1.09\ 10^9$ [N/m^2]
: This value for the oil stiffness lies in between 6.000 and 12.000 [bar], the range where it may be expected for practical situations [139].

$\hat{M}_p = 3.14\ 10^3$ [kg]
: The estimated load mass is a bit higher than expected; the loads placed on the test rig were such, that the inertia for the actuator was expected to be approximately 3.000 [kg]. However, given the good match of both the pressure difference transfer in Fig. 3.23 and the acceleration transfer in Fig. 3.30, the estimated value can be considered to be reliable.

$\hat{\Phi}_{p,nom} = 3.01\ 10^{-3}$ [m^3/s]
: The estimated value for the nominal (maximum) valve flow is a factor 1.20 larger than expected from the specifications of the manufacturer (see Subsection 3.3.1). Actually, this reflects the increased gain of the servo-valve, encountered earlier in Fig. 3.26.

$\widehat{LP}_p = 4.42\ 10^{-12}$ [m^5/Ns]
: The leakage parameter LP_p, introduced in Assumption 2.6.1, actually represents the amount of damping. So the estimated value is an estimated damping parameter rather than a theoretical leakage parameter. Nevertheless, the theoretical leakage parameters involved due to the hydrostatic bearings (see Subsection 2.3.5 and Table F.4) are in the same order of magnitude as the value estimated here. Often, the leakage is represented as a percentage of the maximum flow, for a pressure difference equal to the supply pressure. In fact, ζ_4 is exactly this number, so the estimated leakage is 2.35 %. With leakages generally ranging from 1 % to 5 %, this is a realistic value.

$\hat{w}_p = 1.41\ 10^2$ [Ns/m]

The viscous friction coefficient w_p basically reflects the low-frequency zero in the pressure difference transfer function. For frequencies below this zero, viscous friction forces dominate the pressure difference, while for frequencies higher than this zero, the acceleration forces are dominant. For the given actuator, the effect of the friction forces on the pressure difference is hardly visible in the experimental frequency responses of Fig. 3.23 and 3.24; acceleration forces are dominating. For this reason, the estimated value for w_p is quite small, which is actually not unrealistic, since the friction coefficients related to the hydrostatic bearings are also quite small (see Subsection 2.3.5 and Table F.4), and in the same order of magnitude as the estimated value.

Summarizing, the transparent structure of the physical model of the hydraulic actuator allows experimental identification of some physical parameters, that are not accurately known beforehand. The fact that the reconstructed parameters are not unrealistic, forms a further validation of the adopted (physical) model structure. This gives the physical actuator model a reliability, that motivates the use of the model not only for control design, but also for system design.

Reconstruction of position dependence parameters

In the preceding discussion, the position dependence has not been taken into account; only the middle position has been considered. In fact, with the assumed values for V_{ls1} and V_{ls2}, the position dependence of the parameter $\zeta_{56} = \frac{1}{2}(\zeta_5 + \zeta_6)$ is already determined by (3.26), as follows:

$$\zeta_{56} = \frac{1}{2}\frac{E\Phi_{p,nom}}{P_s A_p}\left[\frac{1}{q_{max} + q_0 + V_{ls1}/A_p} + \frac{1}{q_{max} - q_0 + V_{ls2}/A_p}\right] \tag{3.27}$$

However, computing ζ_{56}^- and ζ_{56}^+ this way for $q_0^- = -0.47$ [m] and $q_0^+ = +0.47$ [m] respectively, using the estimated physical parameters, values are found that differ considerably from the identified ones in Table 3.5. Therewith, the theoretical description of the position dependence of the actuator stiffness can not experimentally be validated.

Yet, an experimentally valid description of the position dependence of the actuator dynamics is to be obtained. Thereby, (q_0^-, ζ_{56}^-), (q_0^0, ζ_{56}^0) and (q_0^+, ζ_{56}^+) from Table 3.5 are available as experimental data points. Two options have been considered to come to such a parametrization of ζ_{56} with respect to q_0.

The first method concerns the replacement of the (approximately) known ineffective volumes V_{ls1} and V_{ls2} by experimental estimations. These estimations are obtained by the reconstruction of the three parameter combinations $\frac{E\Phi_{p,nom}}{P_s A_p}$, V_{ls1}/A_p and V_{ls2}/A_p, from the experimental data points, adopting the structure of (3.27). Using the known values for P_s and A_p and the previously estimated maximum flow $\hat{\Phi}_{p,nom}$, this led to the following estimations: $\hat{E} = 1.57\ 10^9$ [N/m^2], $\hat{V}_{ls1} = 1.17\ 10^{-3}$ [m^{-3}] and $\hat{V}_{ls2} = 1.37\ 10^{-3}$ [m^{-3}].

Comparing these values to the ones discussed before, they appear to be rather unrealistic. The estimated oil stiffness is very high, while the estimated ineffective volumes are almost as large as the effective volumes $q_{max} A_p = 1.56\ 10^{-3}$ [m^{-3}]. Herewith, the validity of the expression (3.27) becomes doubtful, given the experimental data points.

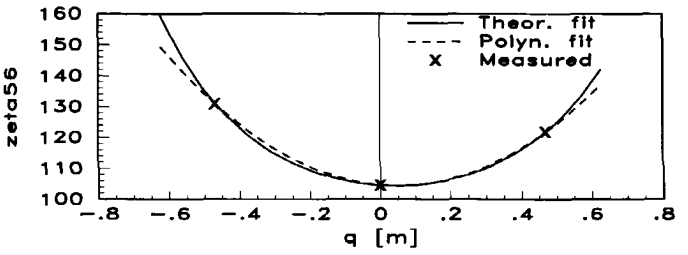


Fig. 3.31: Parametrization of position dependent actuator parameter ζ_{56} with respect to actuator position q_0; fit of theoretical model (solid), polynomial fit (dashed) and experimental data points (X)

In the second method, the physical structure of the position dependence, (3.27), is released and replaced by a second order polynomial description:

$$\zeta_{56}(q_0) = b_{56,2}q_0^2 + b_{56,1}q_0 + b_{56,0} \tag{3.28}$$

The coefficients are easily found by a least-squares fit on the data points, resulting in $b_{56,0}=104$, $b_{56,1}=-9.80$ and $b_{56,2}=99.2$.

The resulting parametrizations of $\zeta_{56}(q_0)$ related to the two methods are plotted in Fig. 3.31. Of course, both parametrizations fit the data points; the difference between the two is rather small. Therefore, and because the validity of the physically structured parametrization is not plausible, the more general and simple polynomial description (3.28) is preferred.

With the position dependence of the basic actuator model (2.108) being parametrized by (3.28), the experimental identification and validation of the actuator model is completed and the Section can be concluded.

3.6.6 Conclusion

In the experimental identification and validation of the model of the hydraulic actuator, the underlying physical structure of the model plays a key role. Actually, it allows the proper application of the tools of Section 3.2, such that an accurate experimental model is obtained, which describes both the dynamics and the dominant non-linearities of the system.

The third order linear dynamics of the actuator are easily identified from experimental frequency responses, both for the actuator position and the actuator pressure difference. For the frequency response measurements, the application of input amplitude filtering is recommendable, be it for practical reasons rather than from an identification point of view like described in Subsection 3.2.2.

Performing the frequency response measurements at three different actuator positions, the position dependence of the actuator dynamics can be identified by means of a simultaneous optimization of the fits of the position dependent linear model (2.108) on the measured responses. The position dependence of this model can effectively be parametrized by the polynomial expression (3.28).

Besides the position dependence, two basic non-linearities are included in the presented

scheme for the identification and validation of the basic model of the hydraulic actuator: the load dependent non-linear valve flow and Coulomb friction.

The static non-linearity of the valve flow causes a considerable variation in the open loop gain of the actuator, dependent on the input amplitude. An experimental quantification of this non-linearity is obtained from a measured amplitude response, applying the techniques of Subsection 3.2.4. Thereby, the load dependence of the flow can be neglected, if the frequency for this measurement is chosen small enough, for instance smaller than 0.1 times the resonance frequency of the actuator. Afterwards, the load dependence can be included according to (2.124). Cross-validation results show that the resulting model for the non-linear valve flow provides a good description of the steady state behaviour of the actuator under different load conditions.

The amount of Coulomb friction is deduced from measurements of the pressure difference during steady state motion at low velocities, and appears to be very small as a result of the presence of hydrostatic bearings. Although cross-validation results indicate that the adopted friction model (2.126) is a bit too simple to describe the complex friction phenomenon, the basic effect of Coulomb friction combined with the actuator dynamics is validated.

Reconstruction of some important physical parameters in the actuator model from the identified parameters leads to realistic estimates for those physical parameters. On the one hand, this further justifies the use of the experimental model for control design. On the other hand, it gives the the physical model a certain degree of reliability, so that the insight obtained from the physical model can be used for system design.

For reasons of generality, the discussion of this Section has been restricted to the identification and validation of the basic actuator dynamics, including the dominant non-linearities. For most hydraulic servo-systems, this is sufficient to obtain a model that describes the properties of the actuator that are relevant for either control design or system design. At least, it is sufficient in cases that transmission line dynamics can be neglected according to Rule A.1.2 (see page 322). In cases that these high-frequency dynamics can not be neglected, an extension of the identification procedure has to be made to the high-frequency region, as described in the next Section.

3.7 Indentification and validation of actuator including transmission lines

3.7.1 Introduction

After the extensive discussion of the identification and validation of the actuator model in the previous Section, the identification of the same model including transmission line dynamics is rather straightforward. It is a matter of extending the frequency range for the frequency response measurements in order to characterize the relevant resonances due to the transmission lines, and of extending the model structure in order to include these relevant resonances in the identification procedure.

For the experimental actuator under consideration, Subsection 3.3.1, transmission line dynamics are really relevant, so that the (pressure) dynamics cover a much wider frequency range than shown in the previous Section. That is why the frequency range for identification is now extended to 1 - 1000 [Hz]. Actually, the results in the previous Section have just

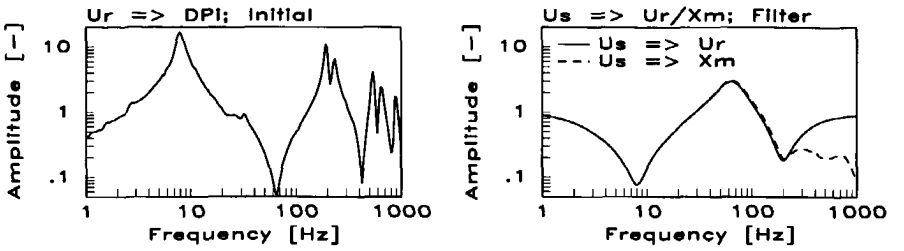


Fig. 3.32: Amplitude of initial measurement actuator dynamics $|H_{\tilde{u}_r \overline{\Delta P}_i}^{5\%}(j\omega)|$ (left) and of implemented input amplitude filter $|H_{\tilde{u}_s \tilde{u}_r}^{1\%}(j\omega)|$ (right,solid) and effective filtering including valve dynamics $|H_{\tilde{u}_s \tilde{x}_m}^{1\%}(j\omega)|$ (right,dashed)

been obtained by considering only the low-frequency part (1 - 20 [Hz]) of the measured frequency responses that are used to identify the extended actuator model.

Concerning the model structure, the identification is performed with a model, which is a simple interconnection of a fourth order actuator model and two fourth order transmission line models, as described in Subsection 2.6.3. The resulting physically structured 12^{th} order model is given by (2.110) on page 104. Note, that the part of the model that describes the actuator dynamics, is parametrized by the same parameters $\zeta_1, \ldots, \zeta_6$ as the simplified actuator model (2.108). This implies, that the identification result of the previous Section remains valid for the extended model. This also holds for the identified and validated nonlinearities, which affect mainly the steady state and low-frequency behaviour, so that they can be left out of consideration for the identification of the transmission line dynamics.

Therewith, the discussion of this Section remains restricted to the identification of the transmission line dynamics, some cross-validation results and some remarks on estimate-based reconstruction of physical parameters.

3.7.2 Identification of transmission line dynamics

Input amplitude filtering

With respect to the input amplitude filtering that was applied during the frequency response measurements, exactly the same reasoning holds as given in Subsection 3.6.2: the main reason is to avoid too heavy excitation of the experimental setup. Yet, there is one additional aspect here, because high frequencies are involved, namely the influence of valve dynamics. Obviously, the actuator dynamics cannot be excited else than with the use of the servo-valve. This means, that with respect to the transfer functions of the actuator model, with the valve spool position $\tilde{x}_m$ as input, the servo-valve acts as an input amplitude filter, additional to the implemented digital amplitude filter.

Taking these effects together, the input amplitude filtering is characterized by the plots of Fig. 3.32. The left plot gives an initial measurement of the actuator dynamics with the measured pressure difference $\overline{\Delta P}_i$ (compare Fig. 3.7 on page 148) as output, clearly showing the badly damped resonances involved. The right plot shows the frequency response of the applied input amplitude filter (solid) and the effective input amplitude filtering (dashed) due to the presence of the servo-valve dynamics. Obviously, the filter will equalize the amplitude of the measured output $\overline{\Delta P}_i$ over the complete frequency range.

Identification results

For the identification of the transmission line dynamics, it is advantageous to utilize the fact that the actuator model basically remains unchanged. Therefore, previously identified parameters can be used from Table 3.5, in order to reduce the free number of parameters to be identified. However, it is necessary to take care of the parameters ζ_5 and ζ_6 in this respect, for two reasons.

First, the identification of the actuator dynamics has only resulted in a position dependent description of the sum of these two, namely ζ_{56}, so they are not independently estimated. Second, when considering only the basic actuator dynamics, the volumes of the transmission lines are seen as ineffective volumes, which are accounted for by the position dependent parameter ζ_{56}, see (3.27). However, when including transmission line models like in (2.110), the capacity of these transmission line volumes is accounted for by the corresponding subsystem models, and not by the corresponding actuator stiffness parameters ζ_5 and ζ_6. The conclusion is, that during the identification of the transmission line dynamics as part of the complete actuator model, the parameters ζ_5 and ζ_6 have to be re-identified.

Thus, with $\zeta_1, \ldots, \zeta_4$ from Table 3.5, the parameters ζ_5, ζ_6 and $\xi_1, \ldots, \xi_{12}$ can be identified by fitting the frequency responses of the model (2.110) on experimental responses. Thereby, the setting for the identification is exactly the same as for the actuator, Subsection 3.6.2. One difference is, that the position transfer function is not included in the cost criterion (3.13), because the steady state gain (ζ_3) is already known. Moreover, the measured frequency response $\tilde{H}_{\bar{x}_m q}(j\omega)$ did not contain any reliable information above 20 [Hz].

Like before, starting with an initial estimate obtained from the linearization of the theoretical model, the parameters of the model (2.110) were identified, by a simultaneous optimization of the fit of the model responses $G_{\bar{x}_m \overline{\Delta P_i}}(j\omega)$ on measured frequency responses $\tilde{H}^{2\%}_{\bar{x}_m \overline{\Delta P_i}}(j\omega)$ in three different actuator positions, $q_0^+ = +0.47$ [m], $q_0^0 = 0$ [m] and $q_0^- = -0.47$ [m] respectively. The resulting fits are shown in Fig. 3.33, together with the weightings that were applied in the cost function (3.13), while the corresponding identified parameters are given in Table 3.6.

	Initial	Final		Initial	Final		Initial	Final
ζ_5^-	$1.90\ 10^2$	$3.05\ 10^2$	ζ_5^0	$1.08\ 10^2$	$1.61\ 10^2$	ζ_5^+	$7.57\ 10^1$	$1.10\ 10^2$
ζ_6^-	$7.19\ 10^1$	$1.55\ 10^2$	ζ_6^0	$1.01\ 10^2$	$1.50\ 10^2$	ζ_6^+	$1.68\ 10^2$	$2.82\ 10^2$
ξ_1	$6.29\ 10^2$	$6.21\ 10^2$	ξ_2	$2.22\ 10^3$	$1.77\ 10^3$	ξ_3	$2.56\ 10^1$	$4.67\ 10^1$
ξ_4	1.00	1.02	ξ_5	$2.95\ 10^1$	$8.99\ 10^1$	ξ_6	$9.43\ 10^2$	$9.28\ 10^2$
ξ_7	$7.33\ 10^2$	$8.01\ 10^2$	ξ_8	$2.59\ 10^3$	$2.05\ 10^3$	ξ_9	$2.38\ 10^1$	$1.47\ 10^2$
ξ_{10}	1.00	1.27	ξ_{11}	$2.95\ 10^1$	$2.95\ 10^1$	ξ_{12}	$1.10\ 10^3$	$1.16\ 10^3$

Table 3.6: Experimental parameter values identified position dependent actuator model including transmission lines; initial estimates and final estimates

Note from this Table, that the initial estimates, obtained from the theoretical model, are

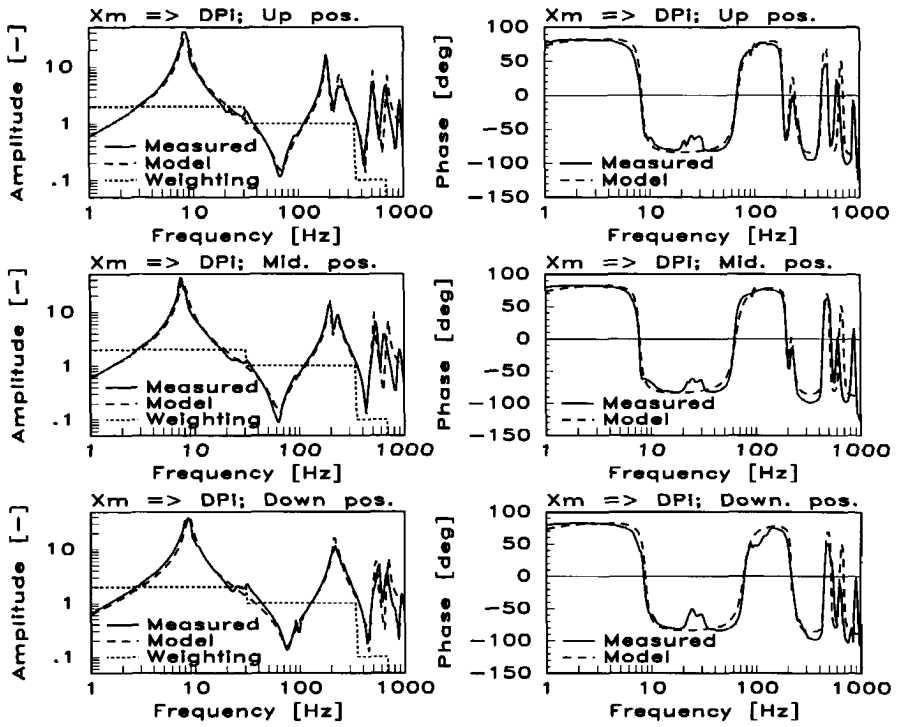


Fig. 3.33: Fits of linear frequency responses $\hat{G}_{\bar{x}_m\overline{\Delta P_i}}(j\omega)$ (dashed) of identified model on measurements $\tilde{H}^{2\%}_{\bar{x}_m\overline{\Delta P_i}}(j\omega)$ (solid) and corresponding weightings $W(j\omega)$ (dotted) in different positions; upper position $q_0^+ = +0.47$ [m] (upper), middle position $q_0^0 = 0$ [m] (middle) and lower position $q_0^- = -0.47$ [m] (lower)

rather close to the final ones. Without such a good initial guess, the non-linear optimization readily ends up in a local minimum, so that the availability of the theoretical model was almost crucial in obtaining the identification result.

The overall quality of the fits in Fig. 3.33 is very good; the results are quite satisfactory and can be provided with the following remarks:

- The quality of the low-frequency fits up to 20 [Hz] is comparable to that of Fig. 3.24; despite the inclusion of transmission line dynamics in the identification, the basic actuator dynamics are well-represented by the model.
- In the frequency region 20 - 30 [Hz], a significant misfit is observed. The experimental responses show (parasitic) dynamics , which are not covered by the model. In some sense, this is also the case at 100 [Hz]. Observations during the measurements and preliminary analysis showed, that these parasitic dynamics have to be ascribed to motions of the base in the region 20 - 30 [Hz] and to bending motions of the horizontal lever at 100 [Hz], where the reader is again referred to Subsection 3.3.1. Although these effects might be included in the model, they are left out of consideration, because they are not inherent to the dynamic behaviour of the hydraulic actuator. Another test rig or motion system would show other parasitic dynamics. For this

reason, these effects fell beyond the scope of this thesis. Moreover, the resulting mismatches are not invalidating the actuator model per sé.

- The structure of the model (2.110) concerning the presence of resonances and anti-resonances is validated in a frequency region up to about 800 [Hz].
- The identification provides a quantitatively accurate description of the dynamics up to about 500 [Hz]. Given the bandwidth of the servo-valve of about 250 [Hz] (see Section 3.5), this model is expected to be sufficiently accurate for control design purposes. Possibly, transmission line models that take only one resonance into account would also have been sufficient for these purposes, though they would not have explained the resonances in the region 500 - 800 [Hz]. On the other hand, heavier weighting in the latter region might have led to a better fit.
- The simultaneous identification of the dynamics in three actuator positions, with only ζ_5 and ζ_6 position dependent, is quite successful. Apparently, the model structure (2.110) allows a good description of the variation of the basic actuator resonance frequency as well as the variations of the resonances due to the transmission lines.

Although the good results prove the validity of the model (2.110) with respect to the measured output $\overline{\Delta P}_i$, which plays an important role in the control design, see Chapter 4, the validity with respect to the generated actuator forces, represented by the actuator pressure difference $\overline{\Delta P}_p = \overline{\Delta P}_o$, is not shown. In an indirect way, this validation is provided by the cross-validation results of the next Subsection.

3.7.3 Cross-validation

For feedback control design purposes, the identified model of the previous Subsection is expected to be sufficiently accurate in describing the dynamic behaviour of the actuator including the transmission lines. However, the derived models are not only to be used for control design, but the physical modelling has also been performed to obtain insight in the system behaviour. In this sense, it is important to validate the physical structure of the model. In other words, the predictive value of the model with respect to other output signals, than the one used for identification, is to be analysed. This can be seen as a form of cross-validation.

As indicated in the end of the previous Subsection, the pressure difference $\overline{\Delta P}_o$ is of interest, because it refers to the generated actuator force. However, the pressure difference $\overline{\Delta P}_o$ can not be measured directly by a single transducer, due to the double-concentric construction of the actuator. For that reason, two separate transducers have been applied to measure the absolute pressures $\bar{P}_{o1}$ and $\bar{P}_{o2}$, as indicated in Fig. 3.7. Using the piëzo-electric transducers, with very good dynamic properties, see Appendix G, the frequency responses of the actuator pressures $\tilde{H}^{2\%}_{\bar{x}_m \bar{P}_{o1}}(j\omega)$ and $\tilde{H}^{2\%}_{\bar{x}_m \bar{P}_{o2}}(j\omega)$ have been measured in the three well-known actuator positions, $q_0^+ = +0.47$ [m], $q_0^0 = 0$ [m] and $q_0^- = -0.47$ [m] respectively.

Because of the physical structure of the identified model (2.110), the corresponding model responses $\hat{G}_{\bar{x}_m \bar{P}_{o1}}(j\omega)$ and $\hat{G}_{\bar{x}_m \bar{P}_{o2}}(j\omega)$ are easily obtained by defining a proper output matrix; $\bar{P}_{o1}$ and $\bar{P}_{o2}$ are just the 3rd and the 4th state variable respectively. In Fig. 3.34 and 3.35 the respective validation results are given.

It is directly clear from these Figures, that the model provides a good description of the relevant dynamics (basic actuator dynamics and first resonance frequencies related to transmission lines), as well qualitatively as quantitatively. Yet, a number of remarks is

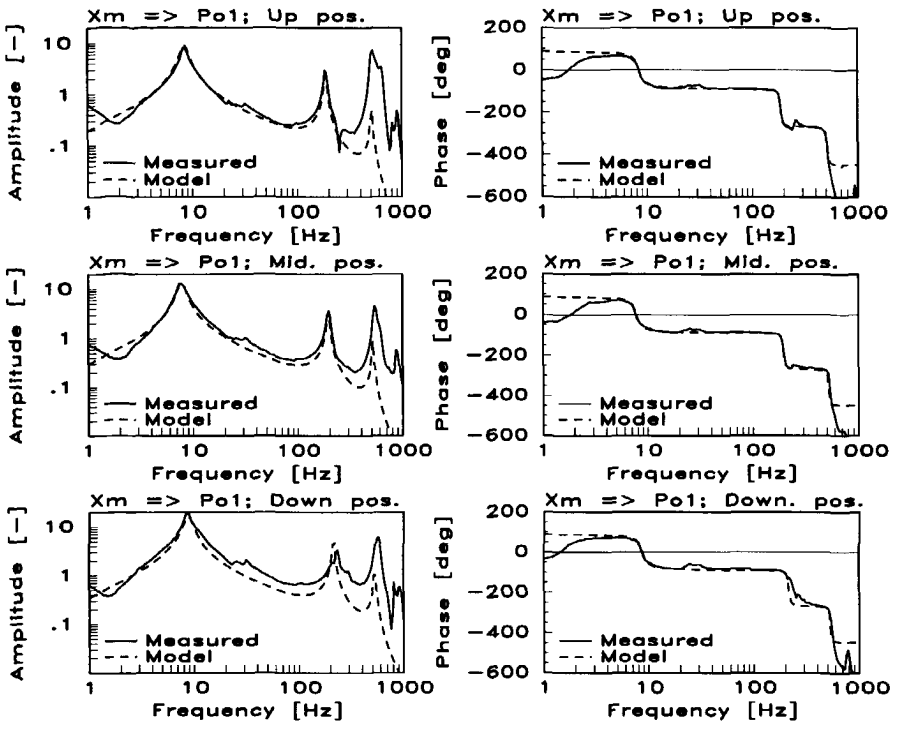


Fig. 3.34: Fits of linear frequency responses $\hat{G}_{\bar{x}_m \bar{P}_{o1}}(j\omega)$ (dashed) of identified model on measurements $\tilde{H}^{2\%}_{\bar{x}_m \bar{P}_{o1}}(j\omega)$ in different positions; upper position $q_0^+ = +0.47$ [m] (upper), middle position $q_0^0 = 0$ [m] (middle) and lower position $q_0^- = -0.47$ [m] (lower)

justified, to explain some of the observed phenomena. Thereby, the physical insight in the system behaviour obtained from simulations of the theoretical model, as described in Subsection 2.3.5 and 2.4.5, plays an important role.

- For low frequencies, < 3 [Hz], there is a considerable mismatch between model and experiment; for $\bar{P}_{o1}$ the phase even becomes negative for very low frequencies, whereas it should be positive theoretically.
  What actually happens, is that at very low frequencies the mean pressure level of both actuator compartments varies with the input signal, so that the both absolute pressures vary similarly, one in phase with the other. This effect is caused by the non-linearity of the combination of actuator and valve, where among others the actuator leakage is involved. An illustration of this effect is given by the right plot of Fig. 2.24 on page 59.
  In the sense of actuator dynamics, this phenomenon is not relevant, because the actuator forces and motions are not dependent on the absolute pressure level.
- The first resonance frequencies related to transmission line dynamics are well-predicted; they are clearly recognized in the measured responses, although in the down position some additional unmodelled effects are found.

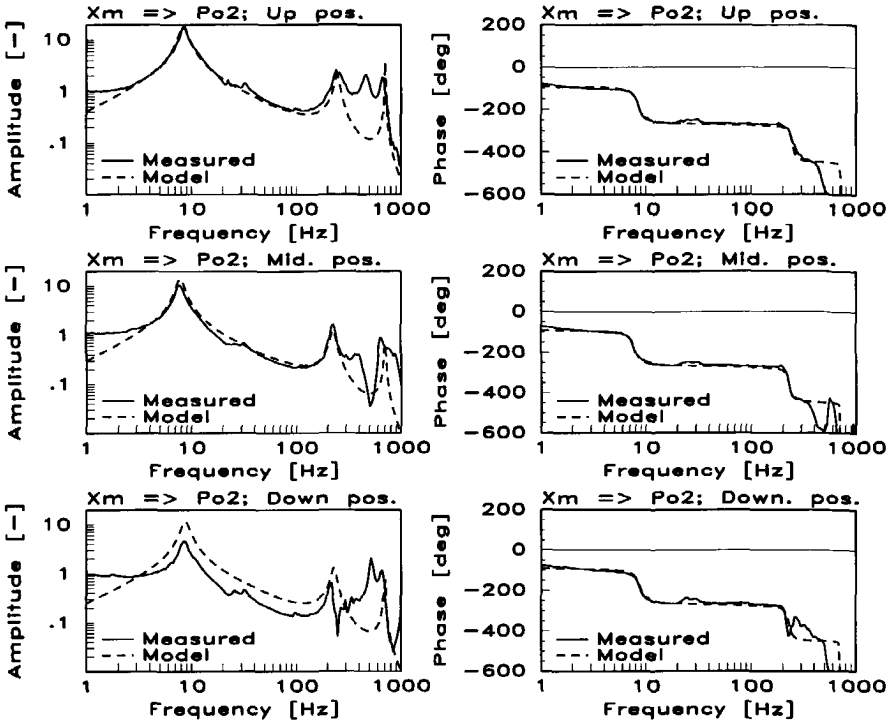


Fig. 3.35: Fits of linear frequency responses $\hat{G}_{\bar{x}_m \bar{P}_{o2}}(j\omega)$ (dashed) of identified model on measurements $\tilde{H}^{2\%}_{\bar{x}_m \bar{P}_{o2}}(j\omega)$ in different positions; upper position $q_0^+ = +0.47$ [m] (upper), middle position $q_0^0 = 0$ [m] (middle) and lower position $q_0^- = -0.47$ [m] (lower)

- The second resonance frequencies related to transmission line dynamics can also be recognized in the measured responses. However, they are not accurately predicted. For the pressure $\bar{P}_{o1}$, there is an unexplained high gain around 600 [Hz]. Furthermore, the measured responses of both pressures show additional unmodelled dynamics in the frequency region 300 - 1000 [Hz]. This may have to do with transmission line effects in the actuator compartments as described in Section 2.4, although this is not verified. The dynamic effects can also be caused by mechanical flexibilities.
- Considering the measured responses, the static gains of these responses show considerable dependence with respect to the actuator position, where the maximum amplitude at the first resonance frequency can be taken as a measure for this static gain. For $\bar{P}_{o1}$ in Fig. 3.34, the gain is small in the up position and large in the down position, while for $\bar{P}_{o2}$ in Fig. 3.35 the reverse holds.
  The explanation for this variation in gain is found in the position dependent stiffness of the 'oil-spring' in the actuator chambers, parametrized by ζ_5 and ζ_6 respectively. In the up position, the lower chamber has a relatively large volume, i.e. a small stiffness. This corresponds to a relatively small ζ_5, which makes that a flow into this actuator chamber causes a relatively small pressure variation. Therewith, the static gain of the transfer function $\hat{G}_{\bar{x}_m \bar{P}_{o1}}(j\omega)$ is relatively small. The same kind of

reasoning holds for the other actuator chamber and for the down position.

- Related to the previous remark it can be stated, that the static gain of the responses is predicted correctly by the model, apart from the down position. In this down position, the static gain for $\bar{P}_{o1}$ is predicted too small, while for $\bar{P}_{o2}$ it is predicted too large.

Summarizing, there is a satisfactory match between experiments and simulations concerning the frequency responses of the absolute pressures in the actuator chambers. Only the static gains for the down position are badly predicted.

According to the physical explanation of the variations in the static gain of the frequency responses, this static gain is related to the stiffness parameter of the corresponding actuator chamber, either ζ_5 or ζ_6. This suggests to perform a slight modification of the model for the down position, namely to enlarge ζ_5^- in order to enlarge the gain of $\hat{G}_{\bar{x}_m \bar{P}_{o1}}(j\omega)$ and to reduce ζ_6^- in order to reduce the gain of $\hat{G}_{\bar{x}_m \bar{P}_{o2}}(j\omega)$. Because the values of ζ_5^- and ζ_6^- also determine the basic resonance frequency of the actuator at about 8 [Hz], the increase of ζ_5^- should just compensate the decrease of ζ_6^- in this respect.

Thus, it was found that a modification of ζ_5^- to 1.5 ζ_5^- and of ζ_6^- to 0.5 ζ_6^- improved the quality of the model for the down position considerably. The resulting fits for the different measured frequency responses are given in Fig. 3.36; the absolute pressures are now predicted equally well as for the other positions (compare Fig. 3.34 and 3.35). The cost of the modification is negligible: there is only a slight worsening of the fit for the pressure difference $\overline{\Delta P}_i$ around the resonances of the transmission lines (compare Fig. 3.33).

Apparently, the proposed identification procedure is not very well capable of distinguishing between ζ_5 and ζ_6 in the down position. The reason is that for that position, the resonance frequencies of both transmission lines coincide, which makes the separate stiffnesses of the actuator compartments badly identifiable. Only when experimental frequency responses of the absolute actuator pressures are available (which is generally not the case), a better estimate for ζ_5 and ζ_6 can be obtained from the static gain of these frequency responses.

In conclusion, the cross-validation of the identified model with respect to the frequency responses of the absolute actuator pressures provides strong results. The physical structure of the identified model is proven to be valid; the obtained physical insight leads to a slight modification of the identified model, eliminating the only significant model error, namely the static gain of $\hat{G}_{\bar{x}_m \bar{P}_{o1}}(j\omega)$ and $\hat{G}_{\bar{x}_m \bar{P}_{o2}}(j\omega)$ in down position. Therewith, the obtained model provides an accurate description of the dynamic behaviour of the actuator including transmission lines, in different actuator positions. This holds for the measured pressure difference $\overline{\Delta P}_i$ to be used for control as well as for the absolute actuator pressures $\bar{P}_{o1}$ and $\bar{P}_{o2}$, which actually represent the generated actuator force.

3.7.4 Estimate-based reconstruction of physical parameters

As a final stage in the identification of the actuator dynamics, some aspects related to the physical parameters of the actuator model including transmission line dynamics are discussed. These aspects are the position dependence of the dynamics, the location of the transmission line resonances and the deviation in dynamic characteristics for different actuators of the same type.

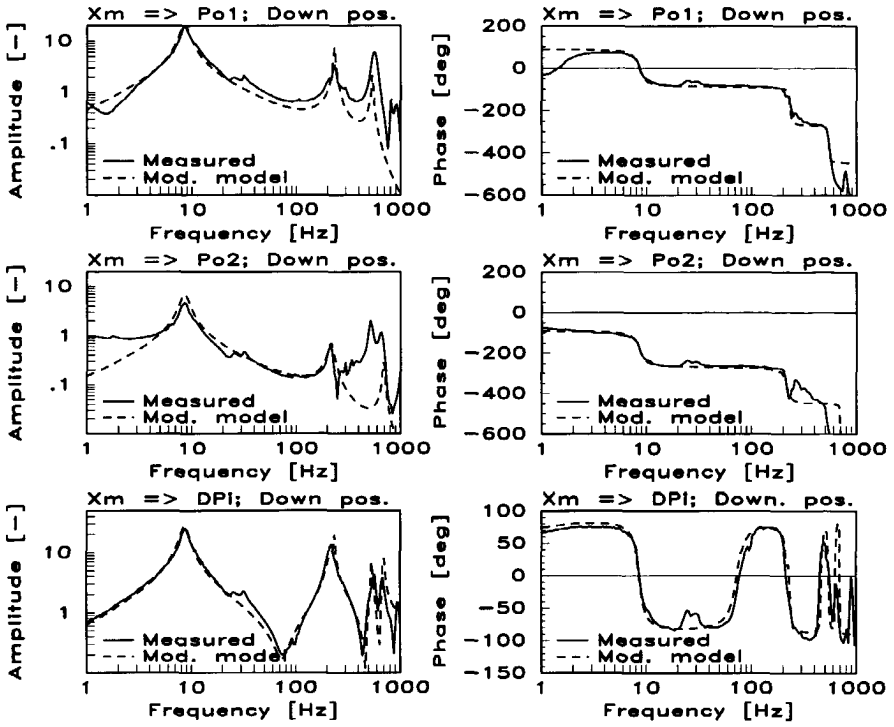


Fig. 3.36: Fits of linear frequency responses $\hat{G}_{uy}(j\omega)$ (dashed) of modified model on measurements $\tilde{H}^{2\%}_{uy}(j\omega)$ in down position $q_0^- = -0.47$ [m]; input $u = \bar{x}_m$; outputs $y = \bar{P}_{o1}$ (upper), $y = \bar{P}_{o2}$ (middle) and $y = \overline{\Delta P}_i$ (lower)

Position dependence

Contrary to the case of the previous Section, there is not one position dependent parameter ζ_{56}, but two position dependent parameters ζ_5 and ζ_6, which have to be parametrized by the actuator position q_0. Like before in Subsection 3.6.5 on page 182, there are two options for this parametrization.

The first method takes the theoretical model for the position dependence as a starting point, where ζ_5 and ζ_6 are described by:

$$\zeta_5 = \frac{E\Phi_{p,nom}}{P_s A_p} \frac{1}{q_{max} + q_0 + V_{ls1}/A_p} \qquad \zeta_6 = \frac{E\Phi_{p,nom}}{P_s A_p} \frac{1}{q_{max} - q_0 + V_{ls2}/A_p} \tag{3.29}$$

Given the identified values for ζ_5 and ζ_6 in different positions from Table 3.6 as data points, the parameter combinations $\frac{E\Phi_{p,nom}}{P_s A_p}$, V_{ls1}/A_p and V_{ls2}/A_p in (3.29) are optimized with respect to a quadratic criterion. Again using the known values for P_s and A_p and the estimated maximum flow $\hat{\Phi}_{p,nom}$ from the previous Section, estimations for $\hat{E}$, $\hat{V}_{ls1}$ and $\hat{V}_{ls2}$ are obtained.

The second method disregards any physical background in the position dependence and just fits the identified data points by second order polynomial descriptions:

$$\zeta_5(q_0) = b_{5,2}q_0^2 + b_{5,1}q_0 + b_{5,0} \qquad \zeta_6(q_0) = b_{6,2}q_0^2 + b_{6,1}q_0 + b_{6,0} \tag{3.30}$$

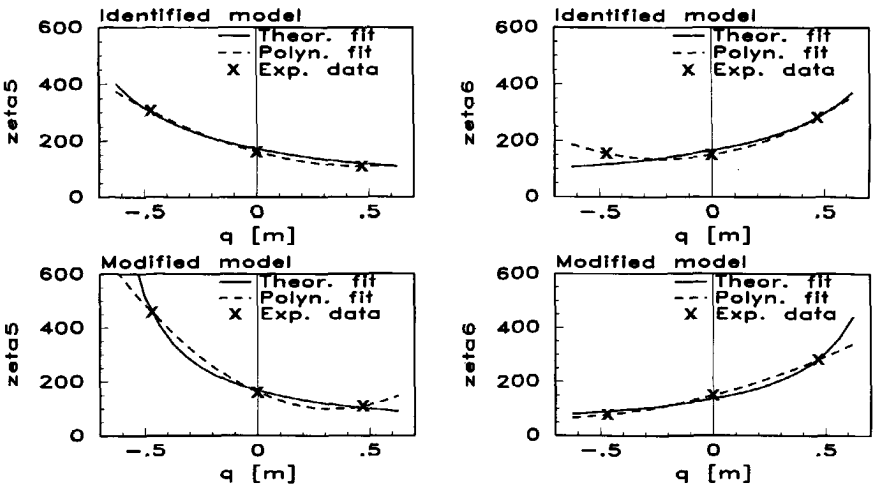


Fig. 3.37: Parametrization of position dependent actuator parameters ζ_5 and ζ_6 with respect to actuator position q_0; fit of theoretical model (solid); polynomial fit (dashed) and experimental data points (X)

The estimated parameters for the first method and the fitted coefficients for the second method are given in the first row of Table 3.7; the corresponding fits for ζ_5 and ζ_6 are given in the upper plots of Fig. 3.37.

	$\hat{E}$ [N/m^2]	$\hat{V}_{ls1}$ [m^{-3}]	$\hat{V}_{ls2}$ [m^{-3}]	$b_{5,2}$	$b_{5,1}$	$b_{5,0}$	$b_{6,2}$	$b_{6,1}$	$b_{6,0}$
Id.	$2.49\,10^9$	$1.17\,10^{-3}$	$1.26\,10^{-3}$	211	−209	161	314	136	150
Mod.	$1.65\,10^9$	$2.87\,10^{-4}$	$7.01\,10^{-4}$	558	−371	161	138	218	150

Table 3.7: Model parameters for parametrization of position dependent actuator parameters ζ_5 and ζ_6 with respect to actuator position q_0; originally identified model (first row) and modified model (second row)

The results are comparable to those of Subsection 3.6.5; the parameters according to the theoretical model (3.29) are rather unrealistic with large oil stiffness and large ineffective volumes. Moreover, the theoretical model appears not to be capable to fit both ζ_5 and ζ_6 simultaneously, as Fig. 3.37 shows. Obviously, the separate fit of the second order polynomials (3.30) provides a parametrization, exactly fitting the data points, which might be preferable because the theoretical model seems to be unrealistic.

Yet, it is remarkable that the stiffness parameter ζ_6 has a minimum. Physically, it is expectable that the stiffness of the upper compartment of the actuator decreases monotonously with the actuator position approaching its lower extremum. This actually refers to the cross-validation results of the previous Subsection 3.7.3, where this effect was already invalidated in terms of the static gain of $G_{\bar{x}_m \bar{P}_{o2}}(j\omega)$. This led to a modification of ζ_5^- and ζ_6^-. Using these modified parameters as new data points for the lower position, the

procedure of fitting (3.29) and (3.30) was repeated. The resulting parameters are given in the second row of Table 3.7, with corresponding fits in the lower plots of Fig. 3.37.

Apparently, the proposed modification of the stiffness parameters ζ_5^- and ζ_6^- leads to a rather good and realistic fit of the theoretical model (3.29) for the position dependence. Still, the oil stiffness and ineffective volumes are slightly larger than expected, but the resulting theoretical fit on ζ_5 and ζ_6 simultaneously is satisfactory. It is actually more realistic than the resulting polynomial fit (3.30), because the theoretical fit provides monotonous slopes for both stiffness parameters, as expected.

As a conclusion on the identification and parametrization of the position dependent parameters ζ_5 and ζ_6, the results are briefly summarized:

- Application of the proposed identification procedure (Subsection 3.7.2) on measured frequency responses of the pressure difference $\overline{\Delta P}_i$, leads to position dependent parameters ζ_5 and ζ_6, that explain the position dependence of the transmission line resonances in a satisfactory way. However, it is not possible to find a good and realistic theoretical parametrization of this position dependence according to (3.29). Therefore, the polynomial parametrization given by (3.30) is preferred.
- Because the resonance frequencies related to the two transmission lines coincide for the down position, the identification procedure could not distinguish between ζ_5 and ζ_6 for that position. The static gains of the transfer functions of the absolute pressures provide additional information concerning the position dependence of the stiffness parameters ζ_5 and ζ_6. With the use of this information, the theoretical model (3.29) can be validated rather than the polynomial description (3.30).

The primary objective of the reconstruction of the parameters describing the position dependence of the actuator dynamics is to find a parametrization describing this nonlinearity, which may be used for control design. Of secondary importance is the obtained insight with respect to the effect of the construction design on the actuator dynamics. This topic is discussed next, as well with respect to the position dependence as to the absolute location of the transmission line resonances.

Transmission line resonances

It is clear from Table 3.7 and Fig. 3.37, that a more flat position dependence of ζ_5 and ζ_6 corresponds to larger estimated ineffective volumes, and therewith larger estimated oil stiffness. Reversely, it is obvious that for certain physical oil stiffness, smaller ineffective volumes will lead to higher values for the stiffness parameters ζ_5 and ζ_6, together with a stronger position dependence. In order to maximize the stiffness of the actuator (and therewith the basic resonance frequency of the actuator), the ineffective volumes should be minimized in the actuator design [139]. The theoretically very strong position dependence occurring for very small ineffective volumes needs not to be feared, since position dependence appears to be much weaker in practice than theoretically expected.

Besides the two actuator stiffness parameters ζ_5 and ζ_6, the identification procedure of Subsection 3.7.2 provides 12 parameters $\xi_1, \ldots, \xi_{12}$, which are directly related to physical parameters in the transmission line models, as explained in Subsection 2.6.3 on 103. Although it is possible to reconstruct the physical quantities from the identified parameters under some assumptions, this reconstruction is not worked out for two reasons:

1. It is not possible to reconstruct the complete set of physical parameters directly from

the identified parameters, as the theoretical model (2.68) contains 9 parameters for a single transmission line, while only 6 parameters per transmission line are identified (2.109). Although this problem might be solved by using a-priori knowledge about some physical parameters, it is difficult to say which parameters can be assumed to be known.
For instance, the first resonance frequency of a transmission line with an open end equals:

$$f_0 = \frac{1}{4}\frac{\sqrt{E/\rho}}{L_{tl}} \quad [\text{Hz}]$$

With an estimation of this frequency (for the first transmission line)

$$\hat{f}_0 = \frac{1}{2\pi}\sqrt{\hat{\xi}_1\hat{\xi}_2} \quad [\text{Hz}]$$

from the identified parameters, it is not clear which of the physical parameters is to be estimated. The oil stiffness E has been estimated in an earlier stage, but possibly the effective oil stiffness in the transmission line model is different due to a finite stiffness of the wall of the transmission line. Furthermore, the oil density ρ is not exactly known, and even the effective length of the transmission lines is not exactly known, because they are not ideally straight pipes.
In other words, the a-priori knowledge does not allow to do some reasonable assumptions, such that certain unknown physical parameters can be reconstructed.

2. Because the quality of the theoretical model, including a-priori knowledge about parameter values, is quite good, the reconstruction of physical parameters from experimental data is not required to validate the adopted physical model. This statement is based on the good agreement between the simulation results of `Model 2` in Subsection 2.4.5 shown in Fig. 2.35, 2.36 and 2.37 on the one hand, and the experimental results in Fig. 3.33, 3.34 and 3.35 on the other hand.
The theoretical model, with a reasonable choice for the parameters like in Table F.5, is suitable for the investigation of the relation between physical parameters and resulting dynamic behaviour, with reasonable quantitative accuracy. For instance, the location of the first resonance frequencies of the two transmission lines was predicted by the theoretical model with an inaccuracy of about 10 %. The theoretical model predicted open end resonance frequencies f_0 at 188 and 220 [Hz] respectively, while the experimental resonances $\hat{f}_0$ were found at 167 and 203 [Hz] respectively.

So, although the theoretical model and the identified model *can* be related to each other, the models are used separately for given reasons. For control design purposes, an accurate characterization of the dynamics is required, which makes the experimental model useful. On the other hand, the theoretical model provides insight, that can be used in the construction design stage. For instance, it shows the direct relation between the length L_{tl} of the transmission line and its open end resonance frequency f_0. If possible, this relation might be used to design the transmission lines short enough, to meet Rule A.1.2 so that transmission line dynamics can be neglected.

Contrary to the theoretical model of the servo-valve, the theoretical model of the actuator including transmission lines allows a rather accurate prediction of dynamic properties based on a-priori knowledge of geometrical and other physical parameters. Whereas the

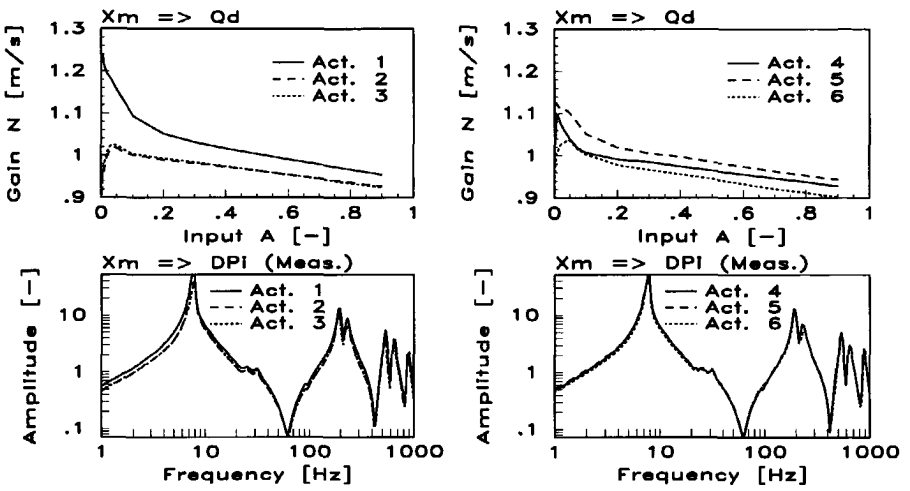


Fig. 3.38: Amplitudes of measured SIDF responses of six hydraulic actuators; actuator 1, 2 and 3 (left); actuator 4, 5 and 6 (right); amplitude responses $N^{0.5\,\mathrm{Hz}}_{\bar{x}_m\dot{q}}(A_{\bar{x}_m})$ (upper); frequency responses $\tilde{H}^{2\,\%}_{\bar{x}_m\overline{\Delta P_i}}(j\omega)$ (lower)

servo-valve dynamics appeared to be rather sensitive to slight deviations due to manufacturing tolerances, as discussed in Subsection 3.5.5, the question arises whether the actuator dynamics are less sensitive to this type of deviations.

Different hydraulic actuators

The variations in dynamic actuator behaviour due to manufacturing tolerances are investigated by comparing experimental responses of a set of six different hydraulic actuators of exactly the same type. Thereby, the basic non-linearity of the actuator due to valve flow non-linearity is also considered, as it basically determines the static gain of the hydraulic actuator. Characteristic results are given in Fig. 3.38.

The upper plots in this Figure give the measured amplitude responses $N^{0.5\,\mathrm{Hz}}_{\bar{x}_m\dot{q}}(A_{\bar{x}_m})$ of the actuators, which represent the static non-linearity $f_2(\bar{x}_m)$ of the servo-valve, as explained in Subsection 3.6.3. Clearly, there is a considerable variation in the amplitude dependent gains of this non-linearity for the different valve-actuator combinations. In fact, these variations can mainly be ascribed to variations in the spool port configuration of the different servo-valves. Similar to the case of the pilot-valves in Subsection 3.5.4, the identification procedure of Subsection 3.6.3 can be applied to each valve-actuator combination, in order to quantify the non-linearity of each system individually.

Concerning the dynamic properties of the different actuators, these are represented by the measured frequency responses $\tilde{H}^{2\,\%}_{\bar{x}_m\overline{\Delta P_i}}(j\omega)$, given in the lower plots of Fig. 3.38. Taking into account, that the different static non-linearities f_2 cause different static gains for the different responses, it can be concluded that there is an evident similarity between the responses of the different actuators. Comparing the results with the identification result in Fig. 3.33, it is clear that the variations in the actuator dynamics due to position dependence are considerably more important than the variations due to manufacturing tolerances of

different actuators.

Of course, individual dynamic models of the different actuators are easily obtained by applying the developed identification procedure for hydraulic actuators of Section 3.6 and 3.7. Instead of doing that, one might think of the identification of a single nominal model, including some uncertainty bounds, which just covers the whole bunch of measured characteristics. Although system identification literature provides some techniques in this area [46, 141], the application of these techniques falls beyond the scope of this thesis. It is not straightforward namely, how to apply these techniques within the given setting of identifying physically structured models, including certain non-linearities. Further research in this area is recommended.

3.7.5 Conclusion

After the identification and validation of the basic actuator model as described in Section 3.6, the identification and validation of an actuator model including transmission lines is a matter of extending the linear model structure and the frequency range of identification. Thereby, only the measured pressure difference $\overline{\Delta P}_i$ needs to be considered in the identification procedure.

By means of fitting frequency responses of the model on measured responses of three positions simultaneously, a position dependent actuator model including transmission line dynamics is identified. Cross-validation with measured frequency responses of the absolute actuator pressures $\bar{P}_{o1}$ and $\bar{P}_{o2}$ shows the validity of the model in different positions.

In the description of the position dependence, the two actuator stiffness parameters ζ_5 and ζ_6, related to the respective actuator chambers, play a key role. Unless the resonance frequencies of both transmission lines coincide, these parameters are well-estimated by the proposed identification method. Otherwise, dynamic measurements on the absolute pressures may help to estimate ζ_5 and ζ_6. If well-estimated, the position dependence of ζ_5 and ζ_6 can be parametrized by the underlying physical relation, involving the reconstruction of the oil stiffness E and ineffective volumes V_{ls1} and V_{ls2}.

Comparison of measured responses of a set of six actuators of the same type shows, that the main differences lie in the static non-linearity of the valve flow, related to the spool port geometry of the valves. Differences in the dynamic behaviour of the actuators due to manufacturing tolerances appear to be smaller than the identified variations per actuator due to position dependence.

With the identification of the transmission line dynamics, including a parametrization of the position dependence, an accurate experimental model is available, which is useful for (robust) control design. Besides that, the experimental results of this Section have proven the validity of the theoretical model, even in quantitative sense, so that it can be used directly for system design purposes, without adjusting it with the use of identification results.

3.8 Conclusion

Starting with the non-linear dynamic models of the subsystems of the hydraulic servo-system, as derived in Chapter 2, the aim of the experimental identification and validation, discussed in this Chapter, has been to identify the unknown model parameters and to

validate the model structure. Thereby, not only the relevant dynamics, but also the dominant non-linearities of the hydraulic servo-system have been explicitly taken into account. In fact, the grey-box modelling approach has been utilized to distinguish between linear dynamic blocks and (static) non-linearities in the system.

Because a clear interpretation of the non-linear system dynamics in the frequency domain was desired, the Sinusoidal Input Describing Function (SIDF) method has been chosen as a key tool in the approach for identification and validation of the hydraulic servo-system. Thereby, the application of an input amplitude filter has been proposed, in order to be able to identify the linear dynamics of the system correctly, despite the presence of a static non-linearity in the (closed loop) system.

The proposed approach has been applied to the hydraulic actuators of a flight simulator motion system, using a well-conditioned experimental setup, with the double-concentric hydraulic actuator placed in a test rig, provided with a three-stage servo-valve and various transducers. Based on the results of this real-life application of the non-linear identification and validation approach, it can be concluded that the proposed method properly utilizes the a-priori knowledge of the physical structure of the model to identify the non-linear dynamics of the system. More specifically:

- The linear dynamics of the system can be identified in a first step, by avoiding the excitation of the dominant non-linearity of the system during the frequency response measurement, using an input amplitude filter. This technique is especially successful for the three-stage valve with respect to the non-linearity of the pilot-valve flow. For the hydraulic actuator, the technique of input amplitude filtering is valuable to avoid too heavy excitation of the setup around the resonance frequencies of the system, while avoiding too much disturbing effect of the Coulomb friction in other frequency regions.
- The measurements of amplitude responses of the system appear to be an effective means to characterize and identify the non-linearity of the system, using the identified linear dynamics. This especially holds with respect to the static non-linearities of the hydraulic servo-system, related to the flow characteristics of the pilot-valve and the main spool of the three-stage valve respectively.

Concerning the validity of the developed models of the hydraulic servo-system, the conclusion is that for the different subsystems it appears to be possible to obtain a good fit of the modelled dynamics and non-linearities on the experimental data. Per subsystem, the identification and validation results can be summarized as follows:

- For the flapper-nozzle valve that was considered, the 4^{th} order linear dynamic model of Subsection 2.5.2 could be validated. The major non-linearity in the experimental results could be ascribed to the non-linear flow characteristic, which could be identified and validated from the measurements. Besides that, only the non-linearity of the torque motor could be qualitatively validated; the non-linearity of the flapper-nozzle flows could not be validated.
- Using the 4^{th} order model structure for the pilot-valve as part of the 5^{th} order model for the three-stage valve, Subsection 2.5.3, good identification results were obtained for the three-stage valve. Identifying both the linear dynamics and the static non-linearity of the pilot-valve flow characteristic from closed loop measurements, a valid description of the non-linear closed loop dynamics of the three-stage valve was obtained.

- The basic actuator dynamics could well be described by the position dependent linear 3^{rd} order model of Subsection 2.6.2, identified from frequency response measurements in different actuator positions. The non-linearity of the load dependent valve flow through the main spool was identified from an open loop amplitude response measurement, and cross-validated by additional steady state measurements for different load conditions. The amount of Coulomb friction could be identified and partly validated by simple time domain experiments.
- Based on frequency response measurements of the actuator pressure difference including the high-frequency range, an accurate 12^{th} order experimental model of the actuator could be obtained. Besides the basic actuator properties, this position dependent model of Subsection 2.6.3 includes the dynamic effects due to the presence of transmission lines between the valve and the actuator chambers.

Although for all subsystems the identified models are directly related to the underlying physical models, only the basic actuator model is sufficiently transparent to be able to reconstruct all physical parameters in the theoretical model from the identified parameters. Nevertheless, besides the basic actuator model with reconstructed parameters, the theoretical models for the transmission lines with a-priori chosen parameters also provide rather accurate predictions of the dynamic system behaviour. Therefore, these models are quite useful for system design, as explained further in Subsection 4.4.4.

With respect to a reliable use of the physical models for system design, the identification and validation results of this Chapter are highly important, of course. However, the main benefit of the obtained experimental models, comprising the relevant dynamic and non-linear effects of the hydraulic servo-system, is their suitability for (robust) control design. How these models play a key role in model-based control design techniques, applied to obtain optimal closed loop behaviour of the servo-system, is worked out in the next Chapter.

Chapter 4

Design and application of hydraulic actuator control

4.1 Introduction

In most applications the control problem for the hydraulic servo-system can be described as the problem of controlling the piston motion, where the hydraulic actuator should exert the forces desired for this motion. In case of multi degree-of-freedom (DOF) systems, these desired forces include interaction forces for instance. Typical examples for this kind of applications of hydraulic actuators are hydraulic robots and flight simulator motion systems.

Taking the problem of controlling a multi DOF hydraulically driven motion system, there are some options for the setup of the motion control strategy, which may all be generalized to the control structure, shown in Fig. 4.1. In this structure, three parts are recognized:

- Trajectory generation. This part, possibly fed by some external drive signal, generates the desired trajectory for the motion system. In many (industrial) applications, the trajectory generator generates just a desired position trajectory, which is to be followed by the system. More advanced trajectory generators also provide desired velocities and accelerations, which can be used in the feedforward part. For instance, in flight simulator applications, the simulation program of the vehicle dynamics and the motion drive laws (see Fig. 1.3, page 8) provide the full desired motion state of the motion system.
- Feedforward control. With the desired trajectory available, feedforward control can be used to generate signals to be supplied to the (feedback) control system, such that the controlled motion system realizes the desired trajectory as good as possible. Actually, the optimal feedforward control uses an ideal inverse model of the system, to generate just those control signals, that realize the desired trajectory. Although in that case no feedback would be necessary, the feedback part is essential, because it is impossible to implement an exact inverse model of the motion system.
- Feedback control. The feedback control can be seen as a corrective control, in order to cope with (modelling) errors in the feedforward path and with unknown disturbances. It combines the feedforward signals with the feedback of measured output signals of the system.

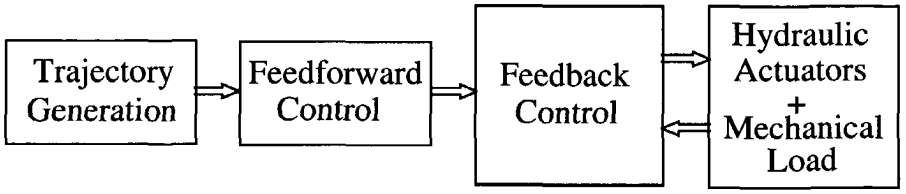


Fig. 4.1: General motion control structure for multi DOF hydraulic motion system

Considering the feedback control of hydraulic motion systems, some different strategies are available, which basically stem from control applications for electrically driven motion systems, like robot manipulators [3, 7, 132]:

- Independent joint control [19]. In this strategy, each actuator is provided with an individual reference signal (often a reference position), which is followed by a local actuator control loop. In this conventional control strategy, the actuator control loop is designed as if each actuator constitutes a one DOF motion system, for instance as if it were a position servo-system [139]. The problem of this method is, that the bandwidth of the individual loops is restricted due to the interaction of the different degrees of freedom. Moreover, the method does not take into account that geometrical non-linearities may cause highly varying system properties over the working range of the motion system, possibly resulting in robustness problems.
- Non-linear multivariable control design. The problems with independent joint control can be overcome by applying non-linear multivariable control techniques, which take into account both the interaction between the different degrees of freedom and the geometrical non-linearities of the motion system [19]. The basics of this method lie in the theory of feedback linearization [107, 130] of non-linear sytems; for robotic systems, the method is mostly referred to as Computed Torque Control [3, 7, 132]. Although this technique is successfully applied to electrically driven robots, the application to hydraulic motion systems is problematic, because the (lightly damped) dynamics of the hydraulic actuators has to be taken into account. This makes the control design rather complex. Moreover, the standard Computed Torque method involves the implementation of an inverse actuator model in the feedback controller [20], resulting in possible robustness problems because of slight model errors [19].
- Two-level motion control structure. The complexity of the control design can be reduced by distinguishing two control levels, as proposed by Heintze et.al. [53, 54, 50]. In the low-level (so-called inner loop control), independent actuator control loops give the hydraulic actuator the character of a pure force generator, independent of the resulting motion of the driven mechanical system. In the high-level (so-called outer loop control), a stabilizing, non-linear, multivariable control strategy is applied to control the motion of the mechanical system. This generally involves the feedback linearization of the geometric non-linearities and the decoupling of the different degrees of freedom, using earlier mentioned non-linear multivariable (motion) control techniques.

In the scope of this thesis, the two-level structure is taken as a starting point for the

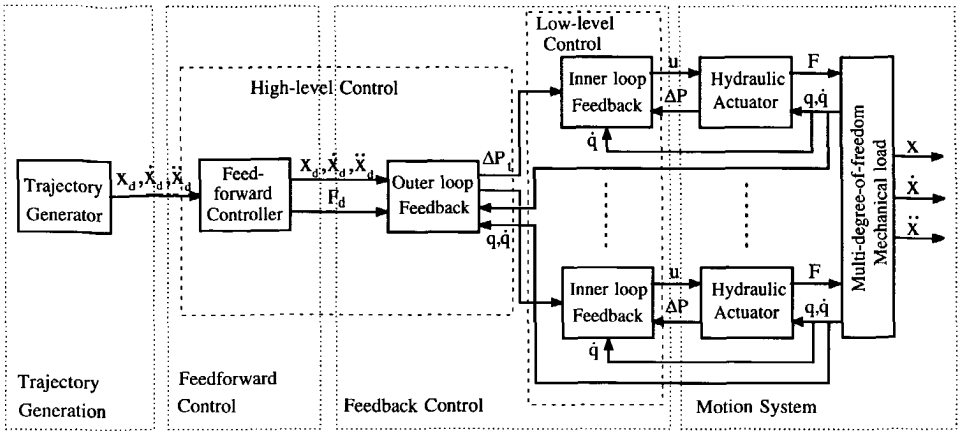


Fig. 4.2: Two-level motion control structure for multi DOF hydraulic motion system

feedback control of multi DOF hydraulic motion systems, such as flight simulator motion systems. An important reason for this choice is the fact, that the control structure reflects the mechanical configuration of the system. This can be clarified with Fig. 4.2, which schematically shows the complete motion control structure (see also Fig. 1.3 on page 8).

Besides that the configuration of Fig. 4.1 is clearly recognized, the distinction between two feedback control levels is clear. In the low-level control, inner feedback loops take care of the feedback control of the individual hydraulic actuators, coping with the inherent dynamic behaviour of these systems. For that purpose, the actuator pressure difference ΔP and the actuator velocity $\dot{q}$ are fed back. The inputs for the inner loops are the so-called 'target pressures' ΔP_t [53, 54, 50]; they can be interpreted as the required forces, that should be generated by the individual hydraulic actuators, to realize the desired motion of the mechanical load. In the high-level control, the combination of feedforward of the desired trajectory of the load, $x_d, \dot{x}_d, \ddot{x}_d$, and outer loop feedback control, using the load displacement q and velocity $\dot{q}$ as feedback signals, solves the more or less standard motion control problem of a mechanical system with multiple degrees of freedom. Note hereby, that the desired trajectory is prescribed in some workspace coordinates x, while the feedback signals are in actuator coordinates q. Obviously, proper coordinate transformations are involved here, either in the feedforward controller or in the outer loop feedback controller.

In the scope of this thesis, the general motion control structure of Fig. 4.1 is adopted as a framework for the motion control of hydraulically driven motion systems. Moreover, the more specific two-level (feedback) structure of Fig. 4.2 is supposed to be recommendable for multi DOF motion systems, because it reflects the inherent physical system structure of the system. However, because the investigations of this Chapter are actually restricted to the one DOF case, the distinction between high-level feedback control and low-level feedback control is not essential in the scope of this thesis. For this reason, the general (feedback) control design problem for hydraulic actuators will be treated.

Against this background, the Chapter is organized as follows. In Section 4.2, the specifications for the control of a single hydraulic actuator are given. Given these task specifications, a number of strategies for the design of the hydraulic actuator control loops

is outlined in Section 4.3. Thereby, as it is commonly done, the basic actuator dynamics are assumed to be of 3rd order. However, in cases that servo-valve and/or transmission line dynamics are not negligible according to the Rules of Section A.1, the 3rd order model for the actuator is not valid. As explained in Section 4.4, this has serious implications for application of the earlier discussed control design techniques.

Besides the implications of additional dynamics, the availability of a reliable estimated velocity signal is an important issue in the different actuator control strategies. This is adressed in Section 4.5, where different methods of velocity estimation are treated, including an experimental evaluation. Using the optimal velocity estimation method for the experimental setup described in Section 3.3, the different control strategies of Section 4.3 are implemented in practice. An evaluation of the experimental results for the different methods with respect to the task specifications of Section 4.2 is given in Section 4.6. After all, the results are concluded in Section 4.7.

4.2 Task specification

Focussing on the control of a single hydraulic actuator, the motion control setting of the previous Section can be somewhat simplified; as described in Subsection 4.2.1, the trajectory generation and the feedforward control can easily be integrated to a so-called reference generator for the actuator feedback control. A specific choice for this reference generator is made in Subsection 4.2.2. Given this reference generator, the task specifications of the hydraulic actuator control loops can be defined, as it is done in Subsection 4.2.3.

4.2.1 Control setting for single hydraulic actuator

Considering the control of a single hydraulic actuator, the general setting of Fig. 4.1 still holds. However, contrary to the general and more complex case of the multi DOF system, the trajectory generation and the feedforward control can always take place in the same coordinates as the feedback control, namely in actuator coordinates. This means, that the desired trajectory is generated in terms of the actuator position q, while also the feedforward is computed in terms of actuator state variables.

Yet, given this simplification, different configurations for the trajectory generation, feedforward and feedback control of a single hydraulic actuator can be considered. Actually, these configurations are related to the different control strategies for the multi DOF case, mentioned in the previous Section. This can be illustrated by the following two (extreme) cases:

- The most simple case of independent joint position control in a multi DOF system corresponds to the single DOF case of pure position control. The trajectory generator just generates a desired position q_d, while there is not really a feedforward, i.e. the feedforward block in Fig. 4.1 is a unity gain, and the feedback is a standard position control scheme for a single hydraulic actuator [98, 139].
- The rather complex two-level control structure of Fig. 4.2, to the contrary, corresponds to a more complex control setting in the single DOF case. First, the trajectory generator generates trajectory information for the full state, i.e. a desired position-velocity-acceleration trajectory q_d, $\dot{q}_d$, $\ddot{q}_d$. Second, the feedforward feeds through all this information, and additionally generates a corresponding commanded

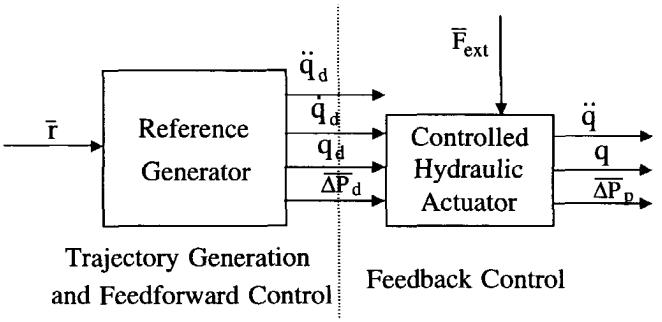


Fig. 4.3: Motion control setting for a single DOF hydraulic motion system

pressure difference $\overline{\Delta P}_d$. Thereby, a model of the load dynamics is used, such that the desired pressure difference $\overline{\Delta P}_d$ just reflects the actuator pressure difference, that is necessary to follow the desired position-velocity-acceleration trajectory under the given load conditions. This means, that besides desired acceleration (and friction) forces, it should include a contribution that compensates for the external forces, acting upon the actuator during the required motion, e.g. gravity forces. Finally, the feedback control uses the feedforward signals and feedback of the actuator state, i.e. $q, \dot{q}$ and $\overline{\Delta P}_p$, to generate a control signal for the hydraulic actuator.

In order to capture these different configurations in a single description, the motion control setting of Fig. 4.3 is adopted for the single DOF hydraulic motion system. In this setting, the trajectory generator and the feedforward control combined to the so-called reference generator, supplying references to the controlled actuator, i.e. the hydraulic actuator with its feedback loops. In fact, just one of the three reference signals, e.g. q_d, may be seen as the reference for the feedback control, while the other two signals, $\dot{q}$ and $\overline{\Delta P}_d$ can be seen as (optional) feedforward signals. Note, that the reference generator is not assumed to be autonomous; it is fed by some external source signal $\bar{r}$, which can be used to excite the system with an external source.

Given the setting of Fig. 4.3, the major aim of this Chapter is, to discuss and evaluate a number of feedback control strategies for the hydraulic servo-system. In order to be able to make a good comparison, some specific reference generator is to be chosen, as discussed next.

4.2.2 Choice of reference generator for single DOF hydraulic actuator control

The reference generator for the actuator feedback control, that will be used throughout this Chapter, is shown in Fig. 4.4. It has the general functionality of the reference generator sketched above, with a trajectory generator and a feedforward part.

The trajectory generator is just a second order low-pass filter, driven by the external input signal $\bar{r}(t)$, with adjustable cut-off frequency ω_f. By means of this frequency ω_f, the frequency contents of the desired position-velocity-acceleration trajectory can be adjusted. Note hereby, that in the high-frequency range, the desired accelerations are proportional to ω_f^2. So, in terms of physics, a high cut-off frequency ω_f implies high demands on the

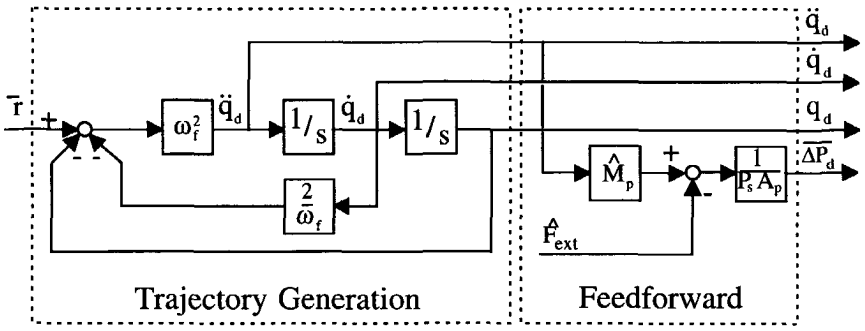


Fig. 4.4: Reference generator for actuator feedback control

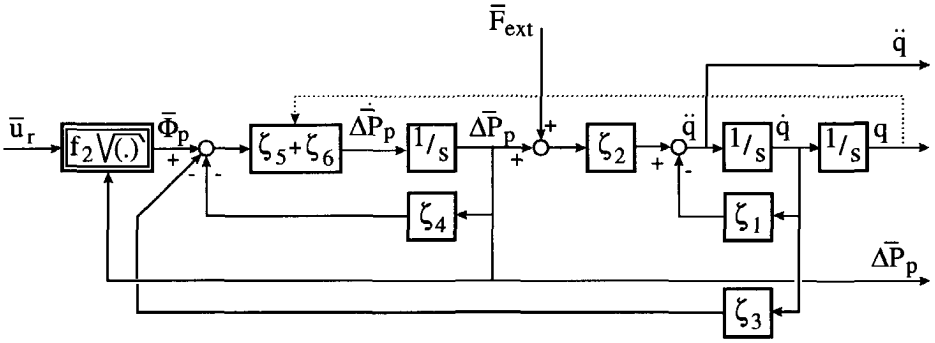


Fig. 4.5: Actuator model used for control design

system.

The feedforward part of the reference generator generates the pressure difference trajectory $\overline{\Delta P}_d(t)$, that serves as a feedforward signal for the feedback loop of the actuator pressure difference $\overline{\Delta P}_p$. For certain actuator load conditions, $\overline{\Delta P}_d(t)$ should reflect the actuator pressure difference $\overline{\Delta P}_p(t)$, that is required to achieve the desired actuator motion. Therefore, the pressure difference trajectory is based on available model knowledge concerning the load of the actuator.

Referring to the actuator model of Fig. 2.41 on page 116, which is given once more in slightly simplified form[1] in Fig. 4.5, the actuator load can be characterized by the inertia M_p of the piston including the load (encountered by ζ_2), and the external forces $\bar{F}_{ext}$. So, at the one hand, the pressure difference trajectory accounts for the desired acceleration force, where the estimated inertia $\hat{M}_p$ reflects the momentary inertial load of the actuator. At the other hand, it accounts for the external forces acting on the actuator during the motion, where $\hat{F}_{ext}$ is an on-line estimation of these forces.

[1]The Coulomb friction is omitted, because it is not explicitly taken into account in the control design discussions of this Chapter.

4.2.3 Task specification for single DOF hydraulic actuator control

If a hydraulic actuator operates in a multi DOF motion system, the load for a single hydraulic actuator may be highly varying. For instance, in the flight simulator motion system, the sum of gravity forces and acceleration forces, due to inertia, to be delivered by a single actuator, are highly dependent on the position and attitude of the motion platform. Obviously, the actuator feedback control should not be sensitive to these load variations. Therefore, when focussing on the feedback control of a single hydraulic actuator, as is done in this Chapter, it is important to incorporate different load conditions in the investigations. For that purpose, the experimental setup described in Subsection 3.3.1 is considered. With the use of the removable loads, shown in Fig. 3.6 on page 147, different load conditions for the hydraulic actuator can be created, although for certain load condition the inertia of the load M_p and the external force on the actuator $\bar{F}_{ext}$ are constant.

Within this setting, different actuator feedback control strategies are to be evaluated, including the effect of the use of (possibly available) feedforward signals. In these investigations, the reference generator of the previous Subsection is used, assuming that, if feedforward is used, a good load model is available, which properly matches the actual load conditions of the actuator. Under these conditions, the aim of the hydraulic actuator control design is, to obtain a feedback controller, that meets the following specifications:

- *The controlled hydraulic actuator tracks the desired position-velocity-acceleration trajectory $q_d(t)$, $\dot{q}_d(t)$, $\ddot{q}_d(t)$ from the reference generator as close as possible. In other words, the frequency responses $H_{q_dq}(j\omega)$, $H_{\dot{q}_d\dot{q}}(j\omega)$ and $H_{\ddot{q}_d\ddot{q}}(j\omega)$ approximate unity gain with minimum phase lag over a maximum frequency range.*
- *Different load conditions have minimum effect on the performance of the (low-level) actuator feedback control loop, while the controller structure and parameters are independent of the load condition.*

Actually these specifications are quite general, and it depends on the application, how these specifications look like in more detail. For instance, in machine-tool applications, hard requirements can be expected concerning steady state positioning accuracy and overshoot properties during transients, while tracking of the acceleration profile may be of less importance. However, taking the example of flight simulator motion control, high-bandwidth tracking of the acceleration trajectory under different load conditions is extremely important, as well as minimization of acceleration noise, while steady state positioning accuracy is not so important [118].

With a specific application of a long-stroke actuator at hand, the remainder of this Chapter is used to discuss different hydraulic actuator control design techniques with respect to the general task specification of this Section, including an experimental evaluation on the setup described in Section 3.3.

4.3 Control strategies for hydraulic servo-systems

4.3.1 Introduction and literature survey

In the field of hydraulic actuator control, a wide variety of applications is found, with different control design techniques applied to obtain the desired results. Investigating literature in this area, it is hard to find a clear relation between the task specification for the

specific application, and the applied control strategy. Nevertheless, a rough classification of control problems and control design techniques can be made.

In general, hydraulic servo control problems are treated either as position control problems [20, 29, 52, 62, 95, 98, 112, 126, 138, 139, 143, 149, 153, 161, 162], or as velocity control problems (generally for rotary drive applications) [1, 27, 64, 111] or as force control problems [65, 110, 115]. More recently, some publications are available, in which the motion control problem is treated as a force control problem at the actuator level [54, 93, 124].

Despite this clear distinction in different types of control problems, it is difficult to give a characterization in terms of control design techniques that were used to solve the posed control problems. Actually, practical reasons like available computer power, experiences and preferences of the control designer, and available transducers seem to play an important role in the choice for a certain control design strategy. Nevertheless, a brief survey of the literature on hydraulic servo control gives rise to a number of remarks:

- Linear techniques are widely applied, such as classical feedback control [98, 139] and state feedback control [36, 66, 104, 105, 147, 153] in position control problems, and frequency domain techniques [110, 115] in force control problems. Applications of modern robust control techniques, like H_∞, are also found in literature [70, 83, 159], showing a better control performance than classical model-based control design techniques.
- In order obtain a controlled servo-system that is robust against varying load conditions, a lot of different non-linear techniques have been applied. Examples are adaptive control [17, 65, 113], model reference adaptive control [57], and (adaptive) model following control [66, 111, 161]. Yet another approach is the use of fuzzy logic techniques, to select state feedback gains under varying load conditions [162].
- In case of repetitive tasks, the controller can be given learning properties. Examples are self-tuning regulators [37, 41], adaptive learning controllers [112, 116] and the non-model-based technique of neural networks [24].
- Especially when knowledge concerning the reference trajectory is available, (non-linear) feedforward techniques can significantly improve the systems performance [17, 19, 95, 149].
- Because of the bilinear character of the hydraulic servo-system (compare Subsection 2.7.3, page 114), some authors treat the hydraulic servo control problem as a bilinear control problem [45, 103]. Actually, the application of this technique seems to be driven by the search for an application of the theory, rather than by the specific requirements of the given application.
- Although most of the forementioned references treat the control design problem in the discrete time domain, increased computer power and decreased hardware costs cause a tendency towards continuous time control design combined with automized implementation of the designed controller, via discretization at a sufficiently high sample rate [84].

With these remarks it is clear, that hydraulic servo control is a rather developed research area in control; most of the available control strategies can be and have been applied to the hydraulic servo-system. Therefore, the aim of the discussion in this and following Sections is not to present new (applications of) control strategies for hydraulic servo-systems, but to give an overview of some basic actuator control strategies in relation to a given application and corresponding task specifications. Thereby, a direct model-based approach is taken

as a starting point, where in the previous Chapters extensive model knowledge has been gathered, which is now to be utilized and further validated in applied control design.

Before discussing the implications of the modelled and identified dynamics due to servo-valve and transmission lines in Section 4.4, an overview of basic actuator control strategies is given in the subsequent Subsections below. For that purpose, the 3rd order actuator model according to Fig. 4.5 is adopted, where it is assumed for the moment, that the velocity $\dot{q}$ is available for feedback, either because it can be measuremed or because it can be estimated (see Section 4.5). Furthermore, the references required for the actuator control are assumed to be generated according to Fig. 4.4.

In this setting three basic control strategies are discussed in this Section, namely position servo control (Subsection 4.3.2), state feedback control (Subsection 4.3.3) and cascade ΔP-control (Subsection 4.3.4). Besides that, the effect of direct velocity feedforward is discussed in Subsection 4.3.5, while in Subsection 4.3.6 a compensation technique for the dominant non-linearity of the hydraulic actuator, the non-linear valve flow, is presented. Finally, in Subsection 4.3.7, the effect of the position dependence of the actuator dynamics on the control performance is treated.

4.3.2 Position servo including pressure feedback

In most applications of hydraulic servo control in the past, only a position reference was available. The conventional control strategy for this type of applications is proportional feedback of the actuator position to obtain servo-behaviour, while mostly a proportional pressure difference feedback loop is included for damping purposes [98, 139]. However, if a reference for the pressure difference is available, like described in Subsection 4.2, the conventional strategy can be slightly extended to improve the performance, as explained below.

Conventional strategy

Given the model structure of the hydraulic actuator according to Fig. 4.5, a (badly damped) second order system in series with an integrator, it is clear that proportional position feedback results in tracking behaviour. Noting furthermore, that the leakage term ζ_4 provides damping, it is easily seen that a proportional pressure difference feedback loop introduces artificial leakage, and therewith damping. Thus, the control structure of Fig. 4.6 is obtained, where the dotted arrow should be left out of consideration.

According to Viersma [139], the choice of feedback gains K_q and $K_{\Delta P}$ takes place in two steps. First, the pressure difference feedback gain $K_{\Delta P}$ is tuned such that the damping ratio β of the resulting closed loop system (still with zero position feedback) is somewhere in the interval $0.3 < \beta < 0.7$. Thereafter, the position feedback gain K_q is increased to obtain position tracking, for instance until the so-called $M = 1.3$ criterion is met. The closed loop bandwidth of the system typically appoximates the basic natural frequency of the hydraulic actuator [139].

It might be noted, that the main emphasis in this control strategy is on position control, where only a position reference q_d is available. Pressure difference feedback is only used to modify the closed loop dynamics (damping), and should not be too large; a high pressure feedback gain would result in an overdamped system, with restricted bandwidth [139].

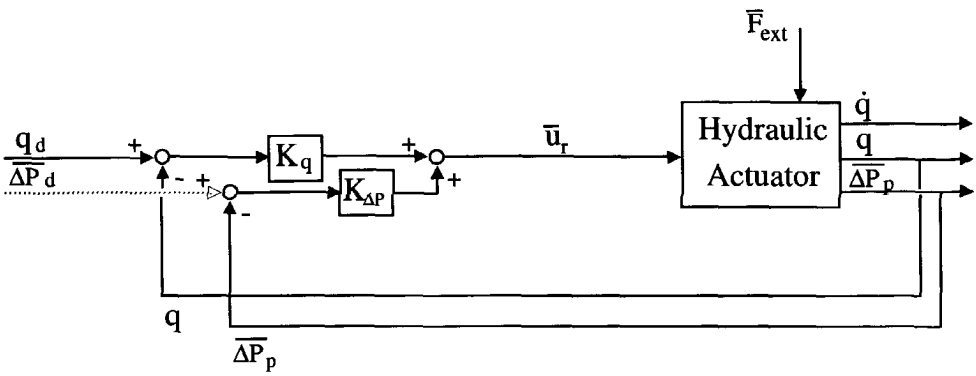


Fig. 4.6: Position servo control including pressure difference feedback and (if available) feedforward of the pressure difference reference

However, the situation is different, if a reference $\overline{\Delta P}_d$ for the pressure difference is available, for instance from a reference generator as in Fig. 4.4.

Extension with feedforward of the pressure difference reference

If a pressure difference reference (ΔP-reference) is available, it can be fed forward to the pressure difference feedback loop, as indicated by the dotted arrow in Fig. 4.6. Because the use of a pressure difference reference can be seen as a feedforward compensation, it does not affect the closed loop dynamics of the system; but in case of a correct feedforward model, i.e. a correctly estimated load $\hat{M}_p$, it contributes to a better input-output performance.

Due to the simultaneous supply of a position reference q_d and a pressure difference reference $\overline{\Delta P}_d$, the feedback control design gets the character of a trade-off between position control and pressure control. Especially when the model knowledge, used to generate the ΔP-reference, is rather accurate, pressure control can be emphasized in this trade-off. So the pressure feedback gain can be increased, at the cost of a smaller position feedback gain. Although this leads to overdamped closed loop dynamics, the input-output behaviour can be considerably improved, especially in the high-frequency region, where acceleration forces play an important role. Moreover, when the estimated $\hat{M}_p$ is correctly adapted to varying load conditions, the high-frequency input-output behaviour will be less sensitive to these varying load conditions.

An extra advantage of ΔP-reference feedforward is, that it allows compensation for external forces, provided that an estimation $\hat{F}_{ext}$ is available. Especially in the scope of two-level control of multi DOF motion systems, discussed in Section 4.1 and 4.2, this possibility can be utilized to compensate for interaction forces.

Application to simulation model

In order to illustrate the basic properties of the position control strategy, it is applied to the identified non-linear model of the basic actuator dynamics of the real system, that was described in Section 3.3. Thereby, two different load conditions are considered.

In the first load condition, denoted by `Load 1`, the actuator is loaded with an inertia $M_p = 3.14\ 10^3$ [kg] and zero static force, so $\bar{F}_{ext} = 0$. Actually, this corresponds to the basic model of Fig. 4.5 with the identified parameter values given in Table 3.5, while also

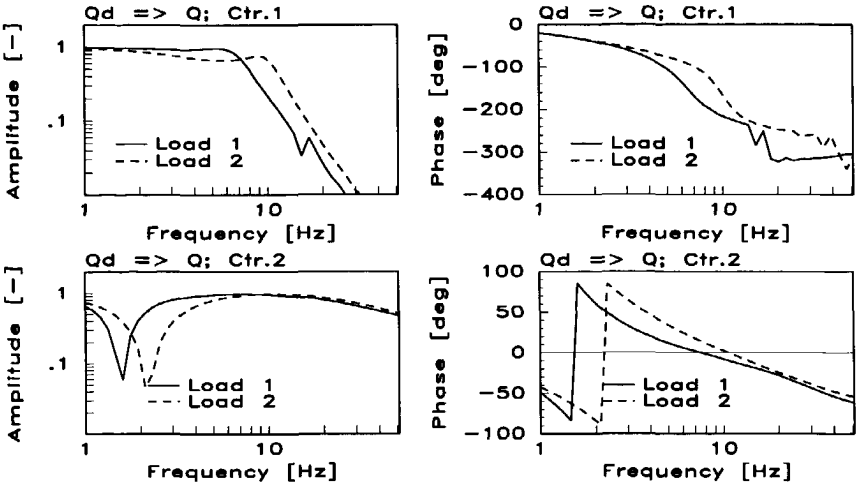


Fig. 4.7: Simulated closed loop frequency responses $\hat{H}^{0.01}_{q_d q}(j\omega)$ for position servo control `Ctr.1` (upper) and `Ctr.2` (lower); different load conditions `Load 1` (solid) and `Load 2` (dashed)

the identified valve flow non-linearity of Subsection 3.6.3 is included. In the second load condition, denoted by `Load 2`, the inertia is half as large, so $M_p = 1.57\ 10^3$ [kg], while a static force of 10 [kN] is present, so that $\bar{F}_{ext} = 0.25$. The reduced inertia for `Load 2` is accounted for in the model by taking ζ_1 and ζ_2 twice as large as for `Load 1`.

For the given system under given load conditions, two feedback controllers have been designed, with structures given by Fig. 4.6. The one without ΔP-reference is denoted as `Ctr.1`; the other is denoted as `Ctr.2`, and includes a ΔP-reference signal. Both control designs have been based on the worst load condition, i.e. `Load 1`. In Table 4.1, the resulting controller gains are given, together with the resulting closed loop poles. Note, that with the choice of controller parameters for `Ctr.2` pressure control is strongly emphasized.

	K_q [1/m]	$K_{\Delta P}$ [-]	Closed loop poles `Load 1`
`Ctr.1`	15	0.2	$-23.93 \quad -11.41 \pm 39.21j$
`Ctr.2`	7.5	1	$-203.46 \quad -5.217 \pm 8.418j$

Table 4.1: Controller gains and closed loop poles position servo control

Closing the loop of the non-linear actuator model of Fig. 4.5 with these controller settings according to Fig. 4.6, and supplying required references according to Fig. 4.4 with $\hat{M}_p = M_p$, $\hat{F}_{ext} = \bar{F}_{ext}$ and $\omega_f = 2\ \pi\ 5$ [rad/s], the closed loop performance can be judged on simulated frequency responses. For an input amplitude of $A_{\bar{r}} = 0.01$ [m], Fig. 4.7 shows the resulting closed loop frequency responses $\hat{H}^{0.01}_{q_d q}(j\omega)$.

The simulation results give rise to the following intermediate conclusions on position servo control:

- The bandwidth is basically restricted to the open loop natural frequency and is therewith dependent on the load inertia M_p in case of position control without ΔP-reference (`Ctr.1`).
- Feedforward of the ΔP-reference and emphasis on pressure control (`Ctr.2`) significantly improves input-output behaviour in the high-frequency region above 5 [Hz], both with respect to amplitude and phase lag.
- Feedforward of the ΔP-reference destroys the low-frequency tracking behaviour; a pair of complex zeros is introduced in the input-output transfer function. The location of the anti-resonance, introduced by the controller due to the simultaneous supply of the references for position and pressure difference, is strongly dependent on the load condition.
- Feedforward of inertial forces (`Ctr.2`) considerably reduces the load sensitivity of the input-output response in the high-frequency region, i.e. beyond 5 [Hz].

Although good tracking behaviour is obtained in the high-frequency region by means of supplying a good ΔP-reference, the dynamics of the closed loop servo-system are principally restricted to about the natural frequency of the open loop hydraulic actuator, i.e. the closed loop poles can not be placed arbitrarily in the complex plane [19, 139]. This restriction is avoided by applying full state feedback.

4.3.3 State feedback

It is well-known in control theory, that all poles of a system can be placed by full state feedback [26]. Thus, by adding velocity feedback to the position control scheme of the previous Subsection, the closed loop poles of the hydraulic servo-system can be placed at desired locations. This method has been succesfull in different applications [36, 66, 153, 147]. In an extended version of the method, references of all state variables are injected in the feedback loops [104, 105].

Conventional strategy

The conventional state feedback strategy for hydraulic servo-systems comprises a position control scheme like in the previous Subsection, but including velocity feedback. It is shown in the block scheme of Fig. 4.8, where the dotted arrows should be left out of consideration. Relating the velocity feedback term to the physical model structure of the hydraulic actuator in Fig. 4.5, it can be seen that it artificially increases the gain (ζ_3) of the loop that constitutes the second order dynamics. In other words, velocity feedback enlarges the system stiffness, and therewith the attainable bandwidth.

The design of the feedback gains usually takes place by standard design methods, for instance pole-placement [26]. Thereby, the poles can be placed in arbitrary patterns, e.g. corresponding to Bessel- or Butterworth characteristics. Thus, the closed loop dynamics can be shaped, where the main emphasis is on fast tracking of the position reference signal q_d. Like for the simple position control scheme of the previous Subsection, the input-output performance can be improved by supplying references of the other states as well, if they are available.

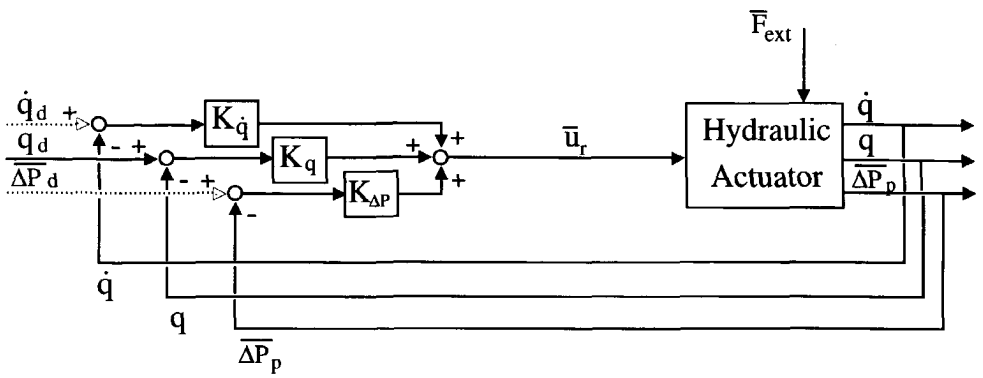


Fig. 4.8: State feedback control and (if available) feedforward of velocity and pressure difference references

Extension with state references

The extension of the state feedback control strategy with the injection of all state references is indicated in Fig. 4.8 by the dotted arrows. The situation is completely similar to that of the previous Subsection; supplying references for the velocity and the pressure difference feedback loop can be seen as feedforward of the reference signal. Therewith, the feedback design again gets the character of a trade-off between tracking of the position/velocity reference at the one hand and pressure difference control at the other hand. In this trade-off, an increase of the pressure difference feedback gain requires a reduction of the position feedback gain, while maintaining the velocity feedback gain, for well-damped closed loop dynamics.

Application to simulation model

The state feedback method is applied to exactly the same model of Fig. 4.5 as before in Subsection 4.3.2, in the same configuration with the reference generator of Fig. 4.4, and under the earlier given load conditions denoted by `Load 1` and `Load 2` respectively.

Starting with the linear 3rd order actuator model, a set of state feedback gains was determined, using a pole-placement algorithm. The poles were placed in an (approximate) Bessel-pattern with the gains shown in Table 4.2, denoted by `Ctr.3`. For the given pole locations, the closed loop servo-system shows fast position tracking, with small lag and small overshoot in the time domain, and a bandwidth of about 1.1 times the open loop natural frequency of the system. The second state feedback controller, denoted by `Ctr.4`, was designed for the case that all state references are available, and emphasizes pressure difference control. The chosen feedback gains for this controller and the resulting closed loop poles of the linear model are also given in Table 4.2.

Theoretically, given the third order actuator model, the poles can be placed arbitrarily by full state feedback, so performance is 'unlimited'. However, a rule of thumb for practical applications of state feedback on hydraulic servo-systems is, that the bandwidth cannot be chosen larger than twice the open loop natural frequency of the actuator. Besides non-linear (saturation) effects, especially concerning the control input, this restriction is caused by additional dynamics of the system, as explained in Section 4.4. Note, that the controller `Ctr.3` proposed above results in a bandwidth which is considerably smaller than

	K_q [1/m]	$K_{\dot{q}}$ [s/m]	$K_{\Delta P}$ [-]	Closed loop poles Load 1
Ctr.3	150	4	0.85	-87.59 $-47.07 \pm 48.04j$
Ctr.4	50	4	2.5	-499.89 $-12.52 \pm 10.36j$

Table 4.2: Controller gains and closed loop poles state feedback control

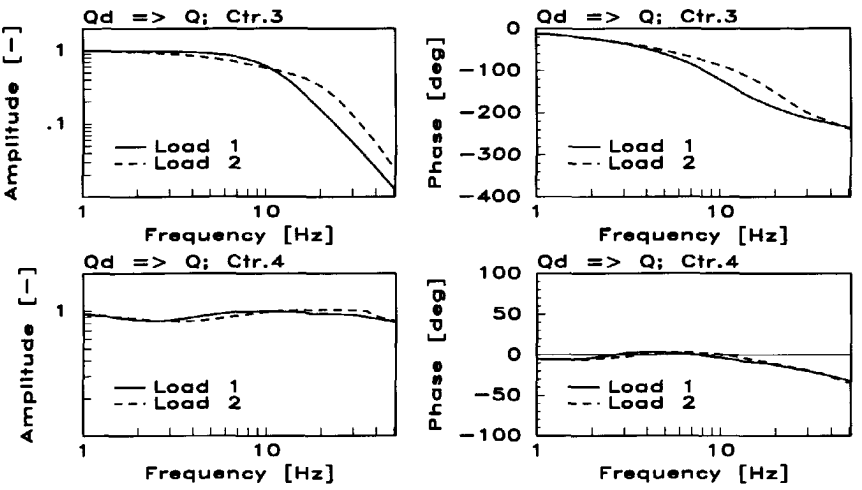


Fig. 4.9: Simulated closed loop frequency responses $\hat{H}_{qdq}^{0.01}(j\omega)$ for state feedback control Ctr.3 (upper) and Ctr.4 (lower); different load conditions Load 1 (solid) and Load 2 (dashed)

the practical upper limit, so that it may well be implementable in practice.

Applying the designed controllers to the non-linear actuator model of Fig. 4.5, with exactly the same settings for the reference generator as in the previous Subsection, closed loop frequency responses $\hat{H}_{qdq}^{0.01}(j\omega)$ have been simulated again for the different load conditions. The results are shown in Fig. 4.9.

Actually, the results are in some sense comparable to those of Fig. 4.7, although stronger conclusions can be drawn in the full state feedback case.

- A nice frequency response is obtained with Ctr.3, although the bandwidth is not too large; the feedback gains have not been maximized. Yet, the dependence on the load inertia M_p is clear in case no ΔP-reference is present. Note, that the phase lag (upper right) is smaller than for Ctr.1 (Fig. 4.7).
- Feedforward of ΔP-reference and emphasis on pressure control (Ctr.4) significantly improves input-output behaviour, both with respect to amplitude and phase lag. Note the y-scales of the lower plots of Fig. 4.9.
- With the velocity feedback loop included in the control, the feedforward of reference signals only slightly disturbs the low-frequency tracking behaviour; in fact, the velocity feedback loop provides 'damping' of the complex pair of zeros, that was seen

before in Fig. 4.7.

- Feedforward of inertial forces (`Ctr.4`) almost eliminates the load sensitivity of the input-output response over the whole frequency range.

In short, full state feedback considerably improves the closed loop performance, especially when the reference signals are fed forward. However, it should be noted here, that in the simulations, the actuator velocity is assumed to be measured directly. In practical situations, this is generally not possible, so that a velocity estimator will be required to obtain a velocity signal, as discussed in Subsection 4.5. This may lead to reduced performance of full state feedback control under experimental conditions, as the results of Section 4.6 show.

Although the input-output behaviour is reasonably independent of the load condition if full state references are supplied, the closed loop *poles* of the actuator feedback loop are principally dependent on the load. The control strategy to be discussed next, basically eliminates this load dependence, at least at the low actuator control level.

4.3.4 Cascade ΔP control

The strategy of cascade ΔP control of hydraulic actuators is relatively new, and was first presented by Sepheri et.al. [124]. The same idea is found in a paper by Matsui et.al. [93]. The method is worked out and formalized by Heintze et.al. [54]. In another reference Heintze et.al. show [53], how the cascade ΔP control strategy for hydraulic actuators fits in the two-level motion control structure for hydraulic motion systems, which was supposed to be recommendable for multiple DOF systems in the introduction of this Chapter, Section 4.1. Therefore, this method is considered here in more detail.

Basic control structure

Considering cascade ΔP control as a control strategy for a single actuator, a distinction is made between inner loop control and outer loop control, as depicted in Fig. 4.10. The inner loop control is the actual actuator control loop, and is aimed at controlling the actuator pressure difference $\overline{\Delta P}_p$, independent of the resulting motions of the load. In other words, it gives the actuator the character of a force generator. In a sort of cascaded structure, the outer loop control is concerned with the (stabilizing) control of the actuator load and the compensation of external forces $\bar{F}_{ext}$. As such, the outer loop control can be seen as the high-level control within the two level structure of Section 4.1.

Inner loop control

The inner loop control consists of two parts, namely a positive velocity feedback, and a high-gain pressure difference feedback.

Referring to the physical model of the hydraulic actuator (2.105) on page 100, the positive velocity feedback (mostly called velocity compensation) is meant to compensate for the contribution of the piston velocity to the mass balances of the actuator chambers. In other words, now referring to Fig. 4.5, positive velocity feedback eliminates the coupling between the actuator pressure dynamics at the one hand and the dynamics of the piston with load on the other hand, constituted by ζ_3. This directly indicates how the velocity compensation gain K_{vc} should be chosen; neglecting the input non-linearity of the valve

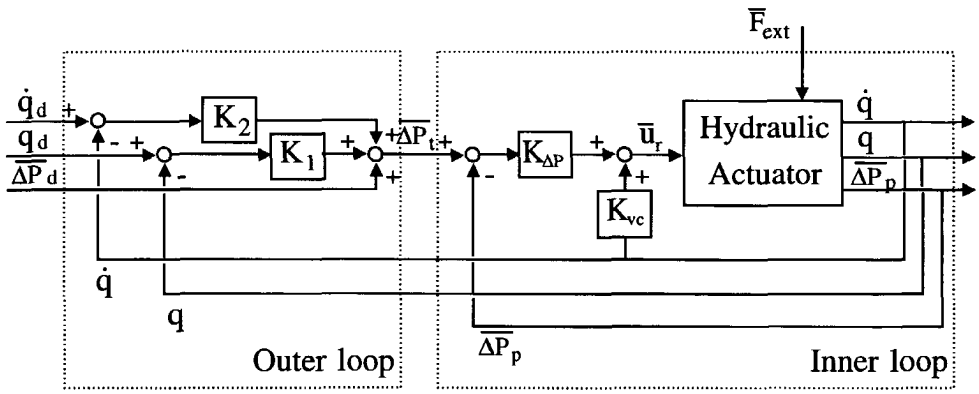


Fig. 4.10: Cascade ΔP control of hydraulic actuator, with inner loop control of actuator pressure difference and outer loop control of load motion

flow (see Subsection 4.3.6 how to include this non-linearity), K_{vc} should be chosen equal to ζ_3.

In case of perfect velocity compensation, a complete decoupling is achieved of the pressure dynamics and the load dynamics [54]. Subsequently, high-gain pressure difference feedback can be applied, in order to shape the pressure dynamics. For the simple model of Fig. 4.5, this pressure dynamics is of first order, where the bandwidth is determined by the proportional feedback gain $K_{\Delta P}$. Thus, according to Fig. 4.10, the inner loop cascade ΔP controller gives the actuator the character of a force generator, where the actuator pressure difference $\overline{\Delta P}_p$ follows the target pressure difference $\overline{\Delta P}_t$ with first order dynamics, independent of the piston motion.

With the piston motion decoupled from the controlled pressure dynamics by the velocity compensation in the inner loop, a marginally stable system is obtained. The target pressure difference is followed by the actuator pressure difference, which together with the external forces $\bar{F}_{ext}$ drives the load dynamics (the equation of motion of the piston) in an open loop manner. This requires a stabilizing feedback of the load dynamics, including a compensation for the external forces $\bar{F}_{ext}$. This part of the actuator control is taken care of by the outer loop.

Outer loop control

In fact, the outer loop design is just a standard mechanical motion control problem, where the actuator acts as force generator over a certain frequency range. In general motion control problems, this outer loop control will be the rather complex high-level control, mentioned in Section 4.1. For the single DOF case considered here, a rather general, though simple, structure for the outer loop control is given in Fig. 4.10. It consists of position and velocity feedback, including a feedforward term for the desired forces. Besides that, the reference generator of Fig. 4.4 is used again.

Considering the controlled actuator as force generator, and the load as slightly damped inertia, the shown outer loop feedback gives the system the character of a mass-spring-damper system. The poles of this system can be placed by the gains K_1 and K_2, represen-

ting a stiffness and a damping constant respectively. Thus, from an interaction point of view, the controlled actuator responds on external inputs as a physical system, of which the characteristics have been modified by control. This is generally referred to as impedance control [56]. For a more detailed discussion on this control strategy as outer loop control for hydraulic actuators, see the work of Heintze et.al. [54, 50] and Van der Linden [82].

Comparing the presented cascade ΔP control strategy, with outer loop control according to Fig. 4.10, to the state feedback strategy of Fig. 4.8, both strategies appear to be almost equivalent. This can be further elucidated by writing out the feedback law of the cascade ΔP controller with outer loop feedback:

$$\begin{aligned} \bar{u}_r &= K_{vc}\dot{q} + K_{\Delta P}\left[K_1(q_d - q) + K_2(\dot{q}_d - \dot{q}) + \left(\overline{\Delta P}_d - \overline{\Delta P}_p\right)\right] \\ &= K_q(q_d - q) + K_{\dot{q}}(\dot{q}_d - \dot{q}) + K_{\Delta P}\left(\overline{\Delta P}_d - \overline{\Delta P}_p\right) + K_{vc}\dot{q}_d \end{aligned} \tag{4.1}$$

where $K_q = K_{\Delta P}K_1$ and $K_{\dot{q}} = K_{\Delta P}K_2 - K_{vc}$. Apparently, the only difference is an additional velocity feedforward term $K_{vc}\dot{q}_d$, which is to be further discussed in Subsection 4.3.5.

Actually, the strength of the cascade ΔP control strategy is not the resulting feedback law or an improved performance for the one DOF case, but the method of designing complex controllers for hydraulic motion systems [53]. The inner loop control is easy to design, while the obtained decoupling of pressure dynamics and load dynamics reduces the outer loop control to a standard motion control problem. This implies, that not only simple state feedback schemes like in Fig. 4.10, but also more sophisticated control techniques can be utilized in the outer loop control design. For instance, Heintze et.al. successfully applied non-linear sliding mode control as outer loop control strategy [51, 50].

Application to simulation model

Like the earlier two control strategies, the cascade ΔP control is applied to the third order identified non-linear actuator model according to Fig. 4.5. The reference generator of Fig. 4.4 is used again, and the earlier given load conditions, denoted by `Load 1` and `Load 2` respectively, are considered.

In the basic control structure of Fig. 4.10, the input non-linearity of the actuator is not taken into account, i.e. the controller gains are designed on the basis of the linear actuator model. Thereby, $K_{vc} = \zeta_3$ is chosen to obtain decoupling. The pressure feedback gain was chosen high, in order to obtain fast tracking of the target pressure difference $\overline{\Delta P}_t$. For purposes of easy comparison with state feedback, $K_{\Delta P} = 2.5$ was chosen like for `Ctr.4` (see Table 4.2), placing the pole of the pressure difference feedback loop at about 500 [rad/s]. It might be noted here, that these control parameters are load independent; due to the decoupling, the resulting closed loop (pressure difference) dynamics of the actuator are independent of the load condition.

Contrary to the inner loop gains, the outer loop state feedback gains have been chosen dependent of the load condition[2], as indicated in Table 4.3. For `Load 1`, K_1 and K_2 have been chosen such that, according to (4.1), the same closed loop behaviour is obtained as with the state feedback controller `Ctr.4`. In order to obtain the same closed loop dynamics for `Load 2`, where the inertia M_p is half as large, the impedance gains K_1 and K_2 have

[2]In the philosophy of two-level control, this is reasonable: model knowledge is assumed to be available in the high-level controller, and can be used to adjust gains with respect to varying load conditions.

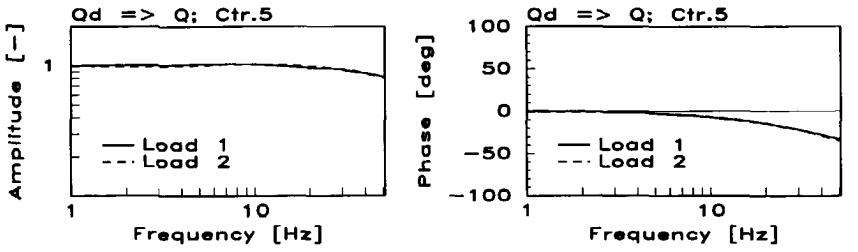


Fig. 4.11: Simulated closed loop frequency responses $\hat{H}_{q_d q}^{0.01}(j\omega)$ for cascade ΔP control `Ctr.5`; different load conditions `Load 1` (solid) and `Load 2` (dashed)

been reduced by the same factor, as shown in Table 4.3. Note once more, that the inner loop parameters remain unchanged.

`Ctr.5`	K_{vc} [s/m]	$K_{\Delta P}$ [-]	K_1 [1/m]	K_2 [s/m]	Closed loop poles
`Load 1`	0.831	2.5	20	1.93	$-499.92 \quad -12.51 \pm 10.38j$
`Load 2`	0.831	2.5	10	0.966	$-499.92 \quad -12.53 \pm 10.35j$

Table 4.3: Controller gains and closed loop poles cascade ΔP control for different load conditions

Under similar conditions as before, closed loop simulations of the non-linear actuator model Fig. 4.5 with the cascade ΔP controller have been performed. The results are shown in Fig. 4.11. As might be expected, there is hardly any load dependence. The inner loop of the cascade ΔP controller is basically independent of the load; different load conditions are accounted for by the high-level control, the outer loop.

Comparing the results of Fig. 4.11 to those of the lower plots of Fig. 4.9, a clear difference is seen in the low-frequency region. This difference between `Ctr.4` and `Ctr.5` lies in the fact that a kind of additional velocity feedforward term is present in the cascade ΔP control strategy, as (4.1) shows. Actually, it is this term, which realizes very good tracking behaviour in the frequency region from 1 to 10 [Hz], with gain 1 and very small phase lag. This motivates the investigation of the possible benifit of velocity feedforward as principal part of the hydraulic actuator control strategy.

4.3.5 Velocity feedforward

Considering the model structure of the hydraulic actuator, Fig. 4.5, in view of position servo control, it can be seen that the hydraulic servo-system is a so-called type-1 system. This means that under unity feedback, references with constant velocity can only be tracked with a constant tracking error. In terms of physics, a constant velocity motion requires a constant valve flow, implying a constant tracking error in case of feedback control. An obvious method to avoid this tracking error is the application of velocity feedforward, which is of course only possible if a velocity reference $\dot{q}_d$ is available.

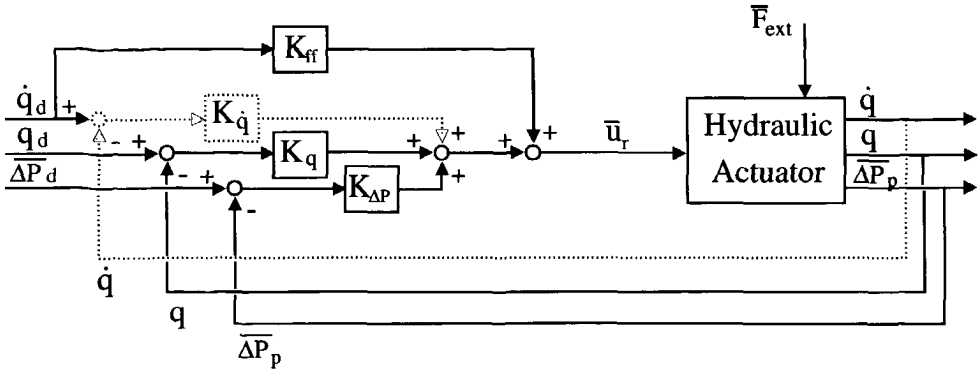


Fig. 4.12: Position control scheme and full state feedback scheme (dotted) including velocity feedforward for hydraulic actuator

Thus, for the position control schemes of Subsection 4.3.2 and 4.3.3, the structure of Fig. 4.12 is obtained. Still neglecting the input non-linearity of the actuator, which will be taken into account in the next Subsection, the design of the velocity feedforward gain K_{ff} is straightforward. Like the velocity compensation in the cascade ΔP controller, velocity feedforward should compensate for the effect of the piston velocity on the mass balance, so that $K_{ff} = \zeta_3$ should be chosen. It is noted once more, that velocity feedforward is inherently included in the cascade ΔP control, as (4.1) shows.

The effect of the velocity feedforward on the closed loop performance of the different position control schemes is illustrated in Fig. 4.13, where simulated frequency responses $\hat{H}^{0.01}_{q_d q}(j\omega)$ are shown. Because a velocity reference should be available, only the schemes including reference signals for all feedback loops are considered. The applied controllers are denoted as `Ctr.2a` and `Ctr.4a` respectively, with feedback settings according to Table 4.1 and 4.2 respectively, and $K_{ff} = 0.831$. For the load condition `Load 1`, it appears that for both strategies, the performance is improved considerably, especially in the low-frequency region. Actually, the zeros introduced by the feedforward of the pressure difference reference signal are cancelled again by applying the velocity feedforward, resulting in very good tracking behaviour for both position control schemes.

The conclusion is, that velocity feedforward should be applied whenever a velocity reference is available. This may be either as explicit velocity feedforward in a position control scheme, or implicitly by velocity compensation and outer loop feedback in a cascade ΔP control scheme.

4.3.6 Non-linear control

In the discussion so far, the input (flow) non-linearity of the actuator, given by (2.124) on page 114 and schematically depicted in Fig. 3.25 on page 175, has been left out of consideration. How this non-linearity affects the performance of the closed loop system, and how the modelled non-linearity can be used to design a non-linear controller, will be discussed below. Thereby, the two effects of load sensitivity and static non-linearity of the valve flow are distinguished again.

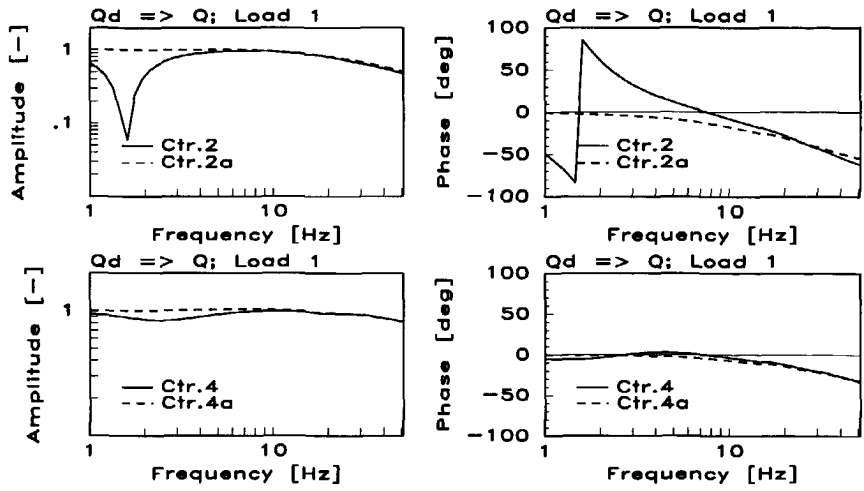


Fig. 4.13: Effect of velocity feedforward on simulated closed loop frequency responses $\hat{H}_{qdq}^{0.01}(j\omega)$ for position control schemes with Load 1; position servo control (upper) and state feedback control (lower); $K_{ff} = 0$ (solid) and $K_{ff} = 0.831$ (dashed)

Compensation for load sensitivity

The load sensitivity of the valve flow can be compensated for, by implanting an estimated inverse of the non-linearity in the control loop, just before the control signal enters the system. An early application of this technique is given by Ikebe et.al. [62], where the measured load sensitive flow characteristics (in which the square root expression is easily recognized) are approximated by a set of straight lines.

More recently, examples are available in literature, where the square root expression of (2.123) is inverted and used for control. Neumann et.al. show non-linear simulation results [104, 105], and conclude considerable performance improvement. They use an observed pressure difference for the compensation, because the actual pressure difference is not meausured. Heintze et.al. [54] show experimental results, in which the non-linear load compensation is included, where the measured pressure difference is used for compensation. In accordance to the latter reference, the following non-linearity is included in the control law, to compensate for the load sensitivity of the valve flow:

$$\bar{u}_r^c = \frac{\bar{u}_r^{uc}}{\sqrt{1 \pm \overline{\Delta P}_p}}$$

where the $\pm$-sign indicates the opposite sign of the uncompensated control signal $\bar{u}_r^{uc}$, and $\bar{u}_r^c$ is the compensated control signal.

Compensation for non-linear flow characteristic

Besides the load sensitivity of the flow, the static non-linearity f_2 indicated in Fig. 3.25 can be approximately compensated for. If an estimation $\hat{f}_2$ is available from identification,

as explained in Subsection 3.6.3, for instance as an interpolation table, then the inverse look-up table will approximately compensate for the actual non-linearity f_2. Combining this non-linear controller gain with the compensation for the load sensitivity, a non-linear control law is obtained, by applying the following non-linear operation to the output signal $\bar{u}_r^{uc}$ of the linear controller:

$$\bar{u}_r^c = \frac{\hat{f}_2^{-1}(\bar{u}_r^{uc})}{\sqrt{1 \pm \overline{\Delta P}_p}} \tag{4.2}$$

Application to simulation model

When applying the presented controller non-linearity (4.2) to the non-linear simulation model of the actuator of Fig. 4.5, two effects have to be investigated. First, the non-linear controller should eliminate non-linearity due to heavy loading of the actuator, for instance a large static load or large demanded acceleration forces. Second, the non-linear controller should reduce the amplitude dependence of the control performance due to the amplitude dependent gain of the static non-linearity.

In order to illustrate the effect of the controller non-linearity (4.2) on the load sensitivity, some time domain simulations have been performed, in exactly the same setting as other simulations in this Section. The well performing position control scheme with velocity feedforward `Ctr.2a` has been applied, while load condition corresponds to `Load 2`. For this load, with a large static component, the gain of the system is larger for upward motions than for downward motions, due to the load sensitivity of the flow. To illustrate this, a source input $\bar{r}$ has been applied, that consists of a positive and negative ramp successively, with a final amplitude of the triangle of 0.0625 [m].

The simulation results are shown in Fig. 4.14, with the left plot giving the resulting closed loop tracking error of the position q and the right plot giving the error in the pressure difference $\overline{\Delta P}_p$. The solid lines represent the simulated errors without the controller non-linearity (4.2), while the dashed lines give the results in case the compensation (4.2) is applied. The dotted lines give the reference signals (divided by 10) q_d and $\overline{\Delta P}_d$ respectively, that correspond to the given errors. The conclusion on this result is, that the proposed non-linear control law eliminates the position tracking errors due to the non-linear velocity gain and linearizes the closed loop response with respect to the load sensitivity.

The effect of the input non-linearity of the actuator on the closed loop performance is illustrated in Fig. 4.15, where a simulated closed loop amplitude response is given for sinusoidal source inputs of 5 [Hz] (solid line). The responses have been obtained under exactly the same conditions as the time responses of Fig. 4.14. Apparently, the closed loop performance is dependent on the amplitude of the source signal, and therewith on the amplitude of the reference signals for the actuator control loop.

The dashed line in Fig. 4.15 gives the same amplitude response in case that the non-linear controller is applied. The inclusion of the controller non-linearity (4.2) appears to be quite effective, at least if a good estimation of the input non-linearity is available. Whereas the latter is obviously the case for the shown simulation result, an experimental verification of the effectiveness of the method is necessary; it is given in Section 4.6.

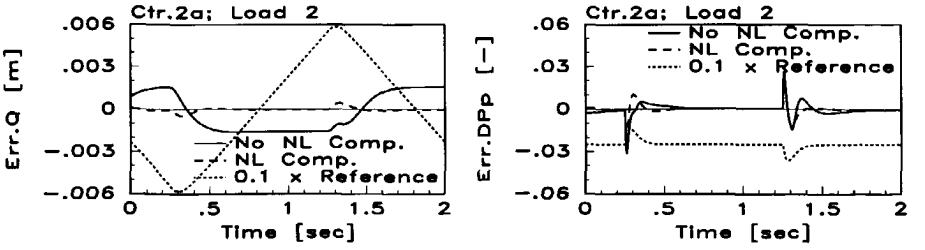


Fig. 4.14: Effect of non-linear control on simulated tracking errors for triangular reference input for position servo control including velocity feedforward (`Ctr.2a`) with `Load 2`; position responses (left) and pressure difference responses (right); errors without non-linear control (solid), errors with non-linear control (dashed) and scaled references (dotted)

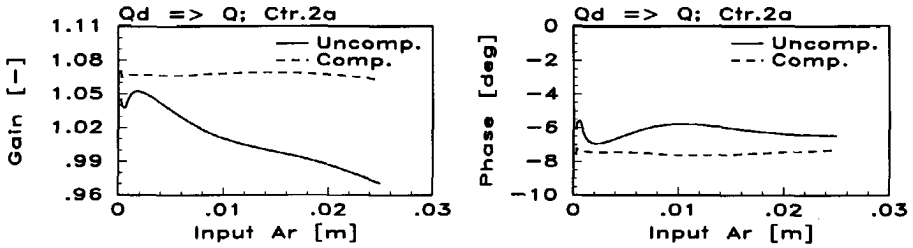


Fig. 4.15: Effect of non-linear control on simulated closed loop amplitude responses $\hat{N}^{5\,\mathrm{Hz}}_{q_d q}(A_{\bar{r}})$ for position servo control including velocity feedforward (`Ctr.2a`) with `Load 2`; linear control (solid) and non-linear control (dashed)

4.3.7 Effect of position dependence on control

Although less important than the input non-linearity of the hydraulic actuator, the position dependence of the actuator dynamics have to be considered briefly with respect to the closed loop performance of the servo-system. Without extensively showing simulation results, insight in the system dynamics, partly obtained from simulations, leads to the following remarks at this point:

- The position dependence of the parameter $\zeta_{56} = \frac{1}{2}(\zeta_5 + \zeta_6)$ makes the stiffness of the actuator, and therewith its natural frequency, position dependent. For instance, symmetric actuators have lowest stiffness in the middle position. The effect of this stiffness on the closed loop performance depends on the control strategy, i.e. on the feedback gain setting:
  - If position control is the primary aim, relatively high position feedback gains will be chosen. In this case, the position feedback gain is critical for stability; the feedback gain and the attainable performance is restricted by the actuator stiffness. A high stiffness allows high feedback gains. So a robust feedback design is based on the lowest stiffness, for instance the middle position for a symmetric actuator [139].

  - If pressure control is the primary objective, like in the cascade ΔP control strategy, the pressure difference gain is to be chosen as high as possible. For the 3rd order actuator model, this pressure difference gain is not principally restricted. The effect of the position dependence of the actuator is, that for certain pressure difference feedback setting, the bandwidth of the pressure difference control loop increases with increasing actuator stiffness. However, if this bandwidth is to be restricted for robustness reasons, as discussed in Section 4.4, the feedback design has to be based on the highest actuator stiffness occurring in the actuator stroke.
- The required velocity feedforward (Subsection 4.3.5) and non-linear control to linearize the input non-linearity (Subsection 4.3.6) are invariant under the position dependent actuator dynamics.

A slightly more extensive discussion of the role of position dependent actuator dynamics in the hydraulic actuator control design is given in Subsection 4.4.3. With the brief discussion here, the main issues concerning the control design for the basic actuator dynamics have been treated, and the Section can be ended with some conclusions.

4.3.8 Conclusion

Considering some basic control strategies for hydraulic actuators, it can be concluded that the solution to the control problem is related to the application, i.e. the setting of the control problem. If only a position reference is available, which is to be tracked, the control strategy necessarily focusses on position servo control. Besides a pressure difference feedback loop to provide damping, a velocity feedback loop can be added, resulting in full state feedback with improved performance.

In case additional reference signals are available, they should be used as feedforward signals for the different (state) feedback loops. Especially the use of a proper pressure difference reference, obtained from a feedforward model for the inertial and external forces acting on the piston, can improve the performance considerably. Thereby, the feedback design has to be directed towards pressure difference control, while position (and velocity) feedback is used to obtain tracking of the desired trajectory.

The emphasis on pressure difference control fits well in the two-level motion control scheme for multi DOF systems, where the high-level control generates the desired references for the low-level actuator control loops. Especially suited to this two-level control scheme is the cascade ΔP constrol strategy for hydraulic actuators. It inherently decouples the pressure dynamics of the actuator from the load dynamics. The low-level control gives the actuator the character of a force generator, while the high-level control can be used to stabilize and shape the mechanical dynamics of the load. In the one DOF case, the cascade ΔP control strategy is basically similar to full state feedback including velocity feedforward.

Whenever a reference for the velocity is available in the control setting, it should be fed forward to the servo-valve, to compensate for inherent velocity errors of the servo-system without feedforward. This velocity feedforward improves the low-frequency tracking behaviour considerably. The possible availability of a model of the input non-linearity of the hydraulic actuator should be utilized to linearize the controlled system. This concerns both the load sensitivity of the flow and the static non-linearity of the flow due to geometrical servo-valve properties. The non-linearity related to position dependence of the actuator

dynamics can be taken into account by designing controllers for the worst case actuator position.

A very principal restriction in the discussion of this Section is, that the actuator dynamics are assumed to be of 3rd order, while valve dynamics are neglected. As explained in the next Section, there are many applications, where these assumptions are not valid; in that case, serious implications for the control design are to be expected, especially in applications with high-gain pressure difference feedback.

4.4 Implications of servo-valve and transmission line dynamics

In the control design for a hydraulic actuator, the pressure difference feedback loop plays a dominant role, especially when a proper pressure difference reference is available from a higher-level control, as discussed in the previous Section. Basing the control design on a 3rd order actuator model, the pressure difference feedback gain is principally not restricted.

However, there are quite a number of applications, in which the assumption of a 3rd order actuator model is not valid. Rule A.1.4 on page 323 can serve as an indication, whether the assumption is valid for a specific application, or not. Especially when valve dynamics are are not fast enough, according to A.1.3, or when relatively long transmission lines are present between the servo-valve and the actuator, according to Rule A.1.2, it is dangerous to take the 3rd order actuator model as a basis for control design. Actually, serious implications for the control design are to be expected, in the sense that the allowable pressure feedback gain is seriously restricted for stability reasons. This is explained in this Section.

A direct restriction on the attainable performance of the pressure difference feedback loop is found, if valve dynamics are taken into account, as explained in Subsection 4.4.1. The situation is even far more serious, if transmission line dynamics play a role. In Subsection 4.4.2, it is shown how these dynamics easily destabilize the control loop; an example of dynamic pressure difference feedback design is given, as an ad-hoc solution for the arosen stability problems. A more fundamental approach to the given problems may be found in two directions.

First, a further utilization of the available model knowledge and current modern control design techniques would be necessary to achieve optimal control performance, given the characteristics of the system. This brings up a number of control design issues, which are to be investigated in further research. These issues are briefly adressed in Subsection 4.4.3.

Second, the obtained insight in the backgrounds of the arosen control problems should be utilized in the design of new hydraulic servo-systems. Thus, a number of system design issues may be put forward, which are directly related to closed loop control performance. This is done in Subsection 4.4.4.

4.4.1 Performance limitation due to valve dynamics

Root-locus analysis

The implication of valve dynamics on the feedback control of a hydraulic servo-system is best illustrated by a root locus plot. For the servo-valve model (2.104) and the actuator

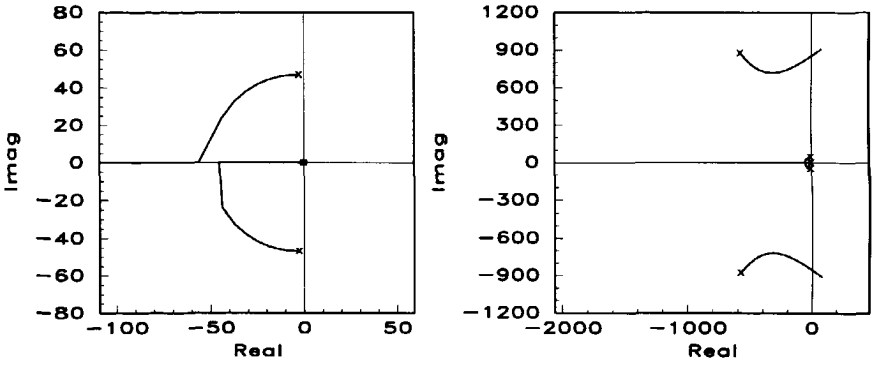


Fig. 4.16: Root locus $\bar{u}_r \rightarrow \overline{\Delta P_p}$ for $K_{\Delta P} = 0 \ldots 5$; dominant actuator poles (left) and dominant servo-valve poles (right)

model (2.108) on pages 98 and 101 respectively, with the pressure difference $\overline{\Delta P_p}$ the output to be controlled and $\bar{u}_r$ the control input, the root locus plot is shown in Fig. 4.16. Thereby, the identified parameters of Table 3.2 (`Model b`) are used for the servo-valve model, and those of Table 3.5 (middle position) for the actuator model.

In the left plot of Fig. 4.16, the shift of the dominant actuator poles is shown, under increasing pressure difference feedback gain $K_{\Delta P} = 0 \ldots 5$. Although difficult to see, a pole-zero cancellation takes place in the origin; this is the (unobservable) integrator, which is unaffected by pressure difference feedback. The pair of complex poles splits at the negative real axis; one tends to the zero close to the origin; the other is pushed away on the negative real axis. Actually, this pole is a measure for the bandwidth of the pressure difference control loop, and corresponds to the real pole in the case of the high-gain pressure difference feedback controllers `Ctr.2`, `Ctr.4` and `Ctr.5` of the previous Section.

Looking at the right plot of Fig. 4.16, which is a large scale view of the same root locus as in the left plot, the implication of the valve dynamics is clear. The strategy of high-gain pressure feedback pushes the dominant servo-valve poles into the right-half-plane (rhp). Actually, in order to keep the servo-valve poles reasonably damped, the pressure difference feedback gain should not be larger than $K_{\Delta P} = 2.5$. Roughly speaking, this means, that the bandwidth of the pressure difference feedback loop is restricted to about 1000 [rad/s] or about 160 [Hz]. Although this bandwidth will be sufficiently high for practical applications, it clearly indicates that there is a principal restriction in the performance in case servo-valve dynamics are present.

Robustness issues

The root-locus plots shown in Fig. 4.16 reflect the feedback behaviour of a single linear model of the hydraulic servo-system. However, due to the non-linearity of a real system, considerable variations in the dynamic behaviour of the system are present. At the one hand, the valve dynamics depend on the signal amplitude, as discussed in Section 3.5. On the other hand, the actuator dynamics depend on the actuator position, as discussed in Section 3.6. So, in order to come up with robust controller settings, the worst case behaviour of the system is to be considered.

Concerning the servo-valve, its dominant poles will be destabilized for smaller feedback

gains, if they are smaller. So, for robust controller settings, a servo-valve model should be used, which reflects the 'smallest bandwidth' of the non-linear servo-valve. For the valve considered in Section 3.5, this is the model obtained from a frequency response measurement with input amplitude filtering and a small input amplitude, which is just `Model b`.

Besides the location of the dominant servo-valve poles, the open loop gain of the servo-system is of importance for robust control design. Considering the open loop gain of the pressure difference dynamics, it can be seen from Fig. 4.5, that this gain is non-linear in two ways.

- It depends on the input non-linearity. As the worst case, the maximum gain of the input non-linearity should be considered, which is easily derived from a measured amplitude response, as shown in Fig. 3.26 on page 175.
- The loop gain also depends on the actuator position, due to the position dependence of ζ_{56}. Here again, the largest gain leads to the worst case. So in this respect, the middle position of the symmetric actuator is the best case, and for the example of Section 3.6 the lower offset position might be chosen as the worst case, according to Table 3.5.

Actually, it is the latter effect, which is also noted by Heintze et.al. [51]. They found in experiments that the feedback gain in the cascade ΔP loop is restricted in the sense that peaking of the closed loop frequency response occurs if the actuator is in a large offset position.

In conclusion, for robust pressure difference control by proportional feedback, valve dynamics have to be taken into account properly. Thereby, the worst case servo-valve model is the one with the 'smallest bandwidth' of the non-linear valve, and the worst case actuator model is the one with the largest loop gain.

4.4.2 Implication of transmission line dynamics

In practical applications with long transmission lines between valve and actuator, stability problems may occur with proportional pressure difference feedback, as earlier pointed out in [119]. Although these problems may be suppressed by simply adding a notch-filter in the control loop [51], a more fundamental solution is to take the transmission line dynamics into account explicitly in the feedback design. Yet, the closed loop performane is seriously restricted by the presence of transmission line dynamics.

Stability problems with transmission lines

The stability problems, possibly occurring in a hydraulic servo-system with transmission line dynamics, are clearly illustrated by a Nyquist plot of the open loop pressure difference transfer function. For the system of Chapter 3, this transfer function is plotted in Fig. 4.17, the left plot. Thereby, the identified parameters of Table 3.2 (`Model b`) are used for the servo-valve model (2.104), and those of Table 3.5 and 3.6 (middle position) for the actuator model (2.110). The right plot of Fig. 4.17 represents the open loop actuator dynamics without valve dynamics. For clarity, the different frequency ranges (resonance peaks) of the response have been indicated by different line styles.

It is obvious from Fig. 4.17, that the combination of phase lag due to servo-valve dynamics and gain amplification due to transmission line dynamics, both at about 200 [Hz]

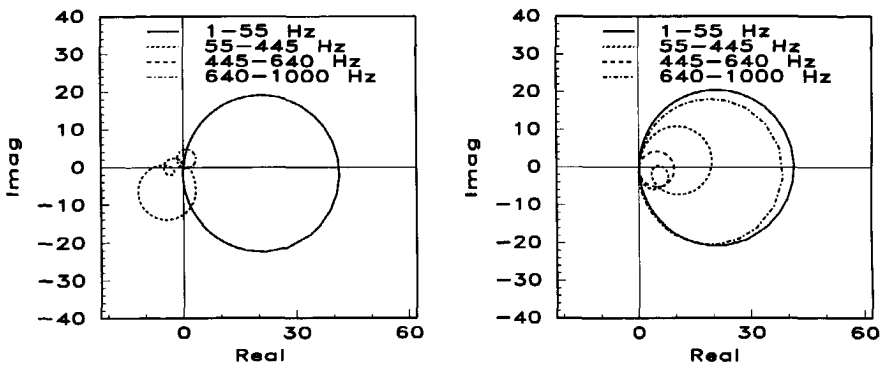


Fig. 4.17: Nyquist plot of open loop pressure difference transfer functions of the identified hydraulic actuator model, including transmission line dynamics; with valve dynamics $G_{\bar{u}_r\overline{\Delta P_i}}(j\omega)$ (left) and without valve dynamics $G_{\bar{x}_m\overline{\Delta P_i}}(j\omega)$ (right)

(compare Fig. 3.15 and 3.33), cause stability problems for proportional feedback. Actually, for a small pressure difference feedback gain of $K_{\Delta P} = 0.1$, the model already predicts unstable system behaviour. So with the given system, the proposed control strategies in Section 4.3 with proportional pressure difference feedback do not work properly.

In reality, the problem is even more serious than suggested by Fig. 4.17, because of the non-linearity of the system. Especially the non-linear dynamic behaviour of the servo-valve plays a role; as Fig. 3.16 on page 162 shows, the gain of the closed loop three-stage valve can vary with a factor 2 at 200 [Hz] due to non-linearity. Together with gain variations related to the input non-linearity of the actuator, as discussed in the previous Subsection, this means that a considerable robustness margin has to be taken into account, if the Nyquist criterion is to be applied to Fig. 4.17.

The serious stability problem sketched here, was actually observed with the experimental setup, by applying proportional pressure difference feedback. Increasing the feedback gain $K_{\Delta P}$ until 0.1 while the system was in a steady state equilibrium, the system remained stable. However, after excitation, a heavy self-sustaining oscillation of about 200 [Hz] occurred; apparently the excitation brought the servo-valve out of the small-gain region, so that the loop gain became to large, resulting in unstable behaviour. Saturation effects prevented the signals to grow further, leading to a kind of limit cycle behaviour.

The observed and explained stability problem for hydraulic servo-systems with long transmission lines between valve and actuator has a number of possible solutions [119]. Most of them lie in the area of constructive measures aimed at modifying the input-output transfer function, and will be discussed in Subsection 4.4.4. Another solution is the design of a dynamic pressure difference feedback loop, as discussed below.

Dynamic pressure difference feedback design

Considering the Nyquist plot of Fig. 4.17, it is clear that a dynamic feedback compensator is required, in order to obtain a reasonably high feedback gain in the low-frequency region of the basic actuator dynamics. From the point of view of classical frequency domain control design, three basic options can be thought of to avoid stability problems due to transmission line dynamics:

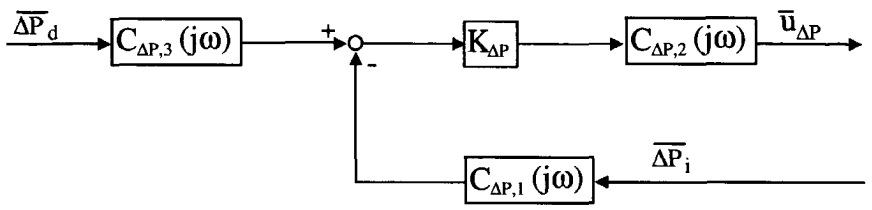


Fig. 4.18: Dynamic pressure difference controller structure

- Create phase lead in the critical frequency region around 200 [Hz]. A practical difficulty with this method is, that the computational delay due to digital implementation of the controller already gives some phase lag (even at 5 [kHz] sample rate). Moreover, phase lead goes along with gain amplification in the high-frequency region, which may well lead to stability problems with the higher harmonics of the transmission line dynamics.
- Create gain attenuation in the frequency region of the transmission line resonances. This might be done by a kind of notch-filter. The disadvantage is, that the filter should be sharp enough to obtain sufficient gain attenuation, while it should be broad enough to be robust against the considerable variations in the resonance frequencies due to the position dependence. This trade-off hardly leads to a feasible solution for the given system.
- Create phase lag in the loop, such that the resonance frequencies are turned away from the $(-1,0)$-point, while simultaneously attenuating the gain in the resonance frequency region. For the given system, this is the most suitable way to avoid stability problems due to the transmission lines.

Besides the design of the feedback loop, a prefilter can be applied, in order to shape the input-output behaviour. For instance, if the feedback loop is still rather sensitive in the frequency region of the transmission line resonances, a prefilter can be applied to avoid excitation in this sensitive region.

With these basic control design principles in mind, a dynamic pressure difference controller was designed intuitively, using the identified models of Chapter 3 to evaluate the expected performance in the frequency domain. With the controller structure depicted in Fig. 4.18, the resulting controller is characterized by the following transfer functions:

$$\begin{aligned} C_{\Delta P,1}(s) &= \frac{1}{\left(\frac{1}{(2\pi 75)^2}s^2+\frac{2\,0.3}{2\pi 75}s+1\right)} \\ C_{\Delta P,2}(s) &= \frac{1}{\left(\frac{1}{2\pi 100}s+1\right)} \\ C_{\Delta P,3}(s) &= \frac{\left(\frac{1}{(2\pi 200)^2}s^2+\frac{2\,0.2}{2\pi 200}s+1\right)}{\left(\frac{1}{(2\pi 400)^2}s^2+\frac{2\,0.2}{2\pi 400}s+1\right)} \frac{1}{\left(\frac{1}{(2\pi 150)^2}s^2+\frac{2\,0.6}{2\pi 150}s+1\right)} \end{aligned} \tag{4.3}$$

Because the controller has basically two degrees of freedom, two compensators would have been sufficient. Nevertheless, the controller has been split into three compensators for ease of implementation. Moreover, the structure of Fig. 4.18 is related to three steps in the intuitive design. From this point of view, the choice of compensators (4.3) can be motivated as follows:

- All compensators are given unity steady state gain, so that the interpretation of the pressure difference feedback gain $K_{\Delta P}$ for the low-frequency region is preserved.
- The compensator in the feedback path, $C_{\Delta P,1}(s)$, utilizes the presence of a pair of zeros in the open loop pressure difference transfer function, in order to create considerable attenuation of the transmission line resonances, combined with a phase lag, turning the transmission line resonances away from $(-1,0)$. Because the pair of poles of the compensator is lightly damped, the phase lag in the low-frequency region (< 50 [Hz]) is not too large. On the other hand, the damping of the compensator poles is chosen not too small, in order to avoid robustness problems due to the variations in the location of the pair of zeros of the system.
  The compensator is not placed in the forward path, i.e. at the location of $C_{\Delta P,2}(s)$, because that would cause heavy excitation of the (closed loop) system dynamics around 75 [Hz]. The reason is, that the pair of zeros is only present in the transfer function of the measured output $\overline{\Delta P}_i$ due to the transmission line dynamics, while it is not present in the transfer function of the pressure difference across the piston $\overline{\Delta P}_o$, compare Fig. 2.36 on page 89.
- The compensator in the forward path, $C_{\Delta P,2}(s)$, adds some phase lag and attenuation in the loop. Without this compensator, the closed loop response still tends to peak up around the resonance frequencies of the transmission lines, when increasing the feedback gain $K_{\Delta P}$. The cut-off frequency, 100 [Hz], is large enough to maintain a small phase lag in the low-frequency region.
- The prefilter, $C_{\Delta P,3}(s)$, is meant to further shape the input-output transfer function of the system. The major purpose of this compensator is to avoid excitation of the (lightly damped) high-frequency dynamics. This is done specifically for the transmission line resonances with the complex zero/pole-pair, and more generally with the second order low-pass filter with cut-off frequency 150 [Hz]. Actually, the prefilter appears to be very effective in avoiding noisy, nervous system behaviour. This is especially important if smooth motions are required, as in flight simulator motion systems.

Actually, the proposed controller according to Fig. 4.18 and (4.3) is just one solution to the arosen stability problems with standard proportional pressure difference control. As discussed in the next Subsection (4.4.3), a more fundamental approach would be the application of more sophisticated, modern control design techniques. This may well lead to better solutions, with better closed loop performance. Nevertheless, with the intuitively designed pressure difference controller proposed here, a reasonable indication of the attainable closed loop performance of the considered hydraulic servo-system can be given.

Implication for closed loop performance

In the given case that the combination of valve dynamics and transmission line dynamics cause stability problems with proportional feedback, the closed loop performance of the servo-system is seriously restricted, even if dynamic pressure control is applied. In order to provide an indication of the attainable closed loop performance, a number of simulations has been performed with the identified non-linear models of Chapter 3.

Thus, the setting for the closed loop simulations is as follows. The servo-valve model according to Fig. 2.40 is used with parameter settings from Table 3.2 (`Model b`) and identified non-linearity $\hat{f}_1$ as discussed in Subsection 3.5.3. For the hydraulic actuator, the

complete dynamic model (2.110) is used, including transmission line effects. The parameters are given in Table 3.5 and 3.6 respectively. Identified non-linearities are included in the actuator model, like described in Subsection 3.6.3. With respect to the reference generator of Fig. 4.4, exactly the same settings are used as in the simulations of Section 4.3, while the load condition corresponds to that denoted by `Load 1`, see page 210.

The controller applied in the simulations, denoted as `Ctr.6`, corresponds to Fig. 4.12, where the proportional pressure difference feedback loop is replaced by the dynamic pressure control scheme of Fig. 4.18, with compensators according to (4.3). For the controller gains, a reasonably robust setting has been chosen, given in Table 4.4. Herewith, the simulation results of Fig. 4.19 have been obtained.

	K_q [1/m]	$K_{\dot{q}}$ [s/m]	$K_{\Delta P}$ [-]	K_{ff} [s/m]
`Ctr.6`	7.5	0	0.75	0.831

Table 4.4: Controller gains position servo control with dynamic pressure control loop and velocity feedforward

The upper plot of Fig. 4.19 shows the simulated frequency response of the actuator position, with an input amplitude $A_{\bar{r}} = 6.25\ 10^{-4}$ [m], while the actuator is in the middle position $q_0^0 = 0$ [m]. Compared to the response of Fig. 4.13, the performance is worse, especially when considering the phase lag. Actually, this is the result of the slightly smaller pressure difference feedback gain $K_{\Delta P}$, combined with the dynamics in the pressure difference feedback loop. However, a higher performance could not be achieved, at least not by increasing $K_{\Delta P}$; $K_{\Delta P}$ was restricted to the chosen value to guarantee robustness against the modelled non-linearities. This is shown in the middle and the lower plots of Fig. 4.19, which give frequency responses $\hat{H}_{\overline{\Delta P}_d \overline{\Delta P}_i}(j\omega)$ of the pressure difference, including the frequency region where the dynamics of the servo-valve and the transmission lines play a role.

The middle plots show, how the performance depends on the input amplitude, with results for $A_{\bar{r}} = .313\ 10^{-3}$, $.625\ 10^{-3}$ and $1.25\ 10^{-3}$ [m] respectively. Especially in the frequency region from 100 to 400 [Hz], the effect is clear; the amplitude dependent dynamics of the servo-valve directly imply non-linearity in the closed loop frequency response. The lower plots show the effect of the position dependence of the actuator dynamics, with results for $q_0^+ = 0.47$ [m], $q_0^0 = 0$ [m] and $q_0^- = -0.47$ [m] respectively. This position dependence also appears to have serious implications for the closed loop performance, in the sense that different actuator positions lead to considerable differences in the closed loop dynamics of the pressure difference control loops. Although the differences shown here are acceptable (no excessive peaking), i.e. the proposed controller is sufficiently robust, these responses show clearly, that the robustness of the pressure difference control loop is an important issue in case non-linear valve dynamics and transmission line dynamics play a role.

The control design proposed in this Section, basically applies the standard control strategies of Section 4.3, while replacing the proportional pressure difference feedback loop by an intuitively designed dynamic pressure difference control loop. The controller gains are chosen conservatively, in order to obtain robustness against the modelled non-linearities of the servo-valve and the actuator. It is clear at this point, that a further utilization of the

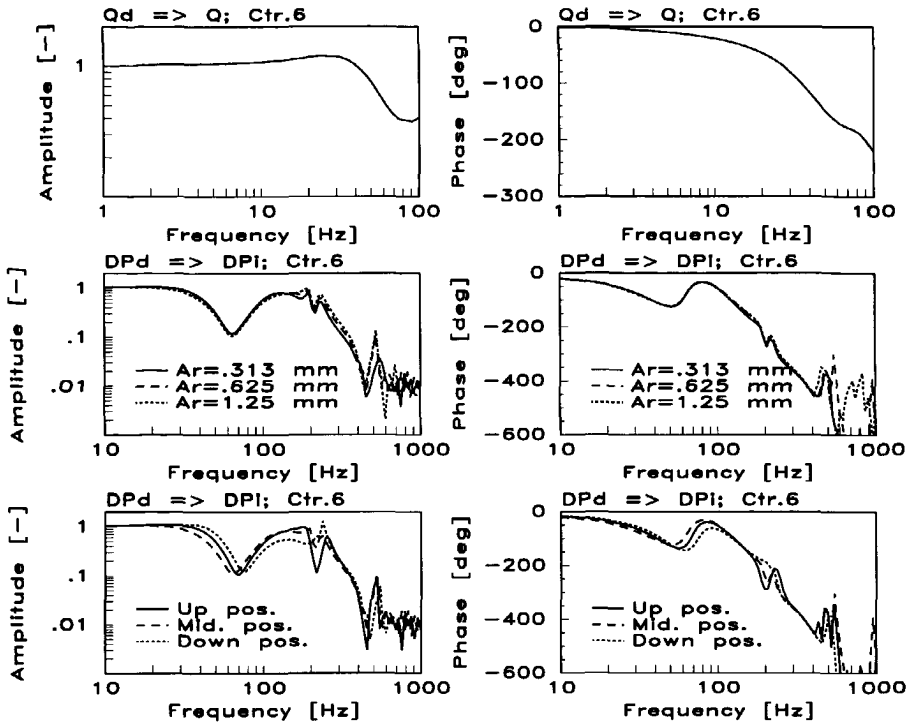


Fig. 4.19: Simulated closed loop frequency responses for position servo control with dynamic pressure control loop `Ctr.6`; position transfer $\hat{H}_{q_d q}^{6.25\ 10^{-4}}(j\omega)$ (upper); pressure difference transfer $\hat{H}_{\overline{\Delta P_d}\overline{\Delta P_l}}(j\omega)$ for different amplitudes (middle) and different actuator positions (lower)

available model knowledge might lead to better performing controllers, where some (still open) control design issues are to be tackled.

4.4.3 Open control design issues

Against the background of the available accurate model knowledge at the one side, and available modern control design techniques at the other side, a number of control design issues will be briefly adressed here. Whereas a thourough discussion of the techniques and application of them falls beyond the scope of this thesis, the discussion is to be seen as an indication of possible directions for further research.

Utilization of servo-valve non-linearity in control

In the process of identification of the servo-valve dynamics, much attention has been given to the non-linearity of the dynamics, where especially the static non-linearity of the pilot-valve spool flow appeared to play an important role. With the use of the non-linear identification techniques of Section 3.2, an experimental quantification of this non-linearity could be found in the form of an approximate non-linear function $\hat{f}_1$, Subsection 3.5.3.

Besides using this (validated) model knowledge for analysis as in the previous Subsection, it should actually be utilized for controller synthesis. This may be either in the form of robust control design or linearizing control.

Modern robust control design techniques like H_∞-control and μ-synthesis [87], can explicitly handle uncertainty in the system behaviour in the control design. A possible approach in handling the non-linearity of a system, is considering it as uncertainty. Especially the non-linearity of the servo-valve at hand, is easily interpreted as a structured uncertainty in the dynamics: the static non-linearity f_1 in Fig. 2.40 can be seen as an uncertain gain at the given location. The uncertainty interval is easily derived as the interval between the minimum and the maximum of the gain of the estimated amplitude responses $\hat{N}_{\bar{x}_s,\bar{\Phi}_m}(\hat{A}_{\bar{x}_s})$ in Fig. 3.17 on page 163. Thus, with the identification of a nominal model (the so-called linear dynamics of Section 3.5) and a hard specification of a structured uncertainty, the way is open to apply H_∞-control and even μ-synthesis. So, robust control design for hydraulic actuators, especially in cases where non-linear servo-valve dynamics are involved, is an open research issue.

A completely different approach of utilizing the servo-valve non-linearity in the control design, is trying to linearize the system by non-linear control techniques. In the case of a non-linear flapper-nozzle valve, Wang et.al. [144] propose the application of the feedback linearization technique. Although this might theoretically be possible, also in the case of the non-linear servo-valve model of Subsection 3.5.3, practical applicability is still questionable due to computational delay problems with digital control. With increasing computing power, this problem may be solved in the future, making model-based non-linear feedback control of electro-hydraulic servo-valves an intriguing research subject.

Utilization of position dependence in control

Besides the input non-linearity of the hydraulic actuator, which can be eliminated by including a non-linear modification (4.2) in the control, the dominant non-linearity in the identified actuator model is the position dependence. As well with respect to the basic actuator dynamics as with respect to the transmission line dynamics, this non-linearity could be experimentally identified and validated in a proper way, see Section 3.6 and Section 3.7 respectively. Again, this model knowledge should be utilized, not only for analysis, but also for controller synthesis.

Actually, the structure of the position dependence is quite suitable to use it explicitly in the control design. The system can just be considered as a linear system, where one or two parameters in the linear model are varying. This variation is parametrized by the actuator position q. In case of the basic actuator model (2.108), this parametrization concerns only one parameter ζ_{56}, and is given either by (3.27) or by (3.28). In case transmission line dynamics play a role, the actuator model (2.110) contains two position dependent parameters ζ_5 and ζ_6, which are parametrized by either (3.29) or (3.30). In both cases, control techniques for linear parametrically varying (LPV) [157] systems can be applied, such as gain scheduling methods [10, 55]. A more modern approach to the control of this type of systems is the application of robust control techniques, with solutions based on Linear Matrix Inequalities (LMI's) [109, 117]. This is again an open control design issue related to the given hydraulic servo-system.

Besides the suggested techniques of gain scheduling and LMI-based control, adaptive filtering techniques [32, 48] might be applicable. However, it is questionable whether

these techniques are really valuable in the given case, for two reasons. First, an explicit parametrization of the position dependence is available, while the position is measured, so model knowledge can be used instead of an on-line estimation of the resonance frequencies. Second, during fast motions of the actuator, the variations of the resonance frequencies may well be too fast to obtain a stable on-line estimation scheme. Therefore, the application of adaptive filtering techniques is not recommended for this system.

Robust control for different actuators

The third issue to be adressed here is related to the control design for multiple actuators, like for instance in a 6 degree-of-freedom flight simulator motion system. Obviously, it would be possible to dedicate a control design procedure to each individual actuator. However, for ease of implementation, it would be attractive to apply a general controller to all actuators. The requirement to this general controller is, that it performs robustly, despite the different dynamic properties of the different servo-systems. In fact, referring to Fig. 3.21 and Fig. 3.38 for the experimental characteristics of the servo-valves and the actuators respectively, it is clear that the general controller should especially be robust against variations in the dynamics of the servo-valves and in the open loop gains of the actuators.

The problem sketched here, can be solved by applying any robust control design method, which can deal with uncertain system behaviour. Thereby, the available knowledge on the individual actuators has to be translated into a structured or unstructured uncertainty description, which covers the variations in dynamic properties of the different servo-systems. Successively, robust control design methods like H_∞ and μ-synthesis can be applied to arrive at robust controllers.

A more direct approach to the stated problem is what is referred to as multi-model control [86]. This approach starts with a set of models, which are easily obtained by applying the identification procedure of Chapter 3, and tries to find a controller that provides satisfactory performance for all models within the set. One of the methods following this approach is the Quantitative Feedback Theory (QFT) [21, 58]. It starts with a set of (experimental) frequency responses, and finds a robust high-performance controller for all systems with frequency responses within the bounds specified by the given set of frequency responses. For the given hydraulic servo-systems, where sets of frequency response measurements are available, this method seems to be quite attractive. Further investigation of the applicability of QFT is therefore recommended.

All the open control design issues, which have been touched upon here, are stated against the background of a *given* hydraulic servo-system. However, in some cases, the control designer for a hydraulic servo-system may be involved in the actual system design in terms of hardware. In that case, problems should be avoided beforehand by proper system design.

4.4.4 System design issues for hydraulic servo-systems

Merrit [98], Viersma [139], and also Walters [143] have thourougly analysed and described the effect of system design parameters as supply pressure, piston area, stroke, etcetera, on the performance of a hydraulic servo-system. Thereby, they use basically the same physical actuator model as the one presented in Section 2.3, which was experimentally validated in

Section 3.6, and more specifically in terms of the reconstruction of physical parameters in Subsection 3.6.5. So, as far as the basic hydraulic servo-system design is concerned, the text-books [98, 139, 143] are very good references.

However, what is not so explicitly adressed in these references, is the implications of servo-valve dynamics and transmission line dynamics on closed loop control. Besides a model-based approach to control design, like described in the previous and the current Subsection, these implications require attention in system design, as described below.

Servo-valve requirements

In hydraulic servo technique, the servo-valve is too often seen as a static device. Because in reality, it is a dynamic device, which restricts the control performance, especially of high-gain pressure difference feedback loops, requirements on dynamic performance of the servo-valve should be taken into account in system design. In other words, the choice of servo-valve should not only be based on stationary characteristics, but also on dynamic characteristics. Thereby, preliminary model analysis should be performed, to judge whether a certain valve would allow to achieve the desired closed loop performance. In general this implies, that the servo-valve bandwidth should be considerably higher than the desired closed loop bandwidth of the pressure difference control loop.

Besides requirements on dynamics, the choice of a servo-valve in the system design stage should fulfil requirements on linearity. Although it is difficult to give hard specifications in this sense, the system designer should be aware of some aspects:

- Backlash and hysteresis of the servo-valve are hard non-linearities, which seriously deteriorate control performance. The use of servo-valves showing these properties should be avoided in high-performance applications.
- Especially when high-gain pressure difference feedback is applied, it is important that the no-load flow characteristic of the valve is linear, i.e. that the spool is of the critical-centre type. The reason is, that non-linearity implies uncertainty in the loop gain, which requires conservative feedback design for robustness reasons.
- The flow capacity of the servo-valve should be well-adjusted to the application, where parasitic resistances in manifolds should not be neglected. The nominal flow should be large enough to meet the velocity specifications without strong non-linearity due to saturation. On the other side, the valve should not be chosen too large, because it would then operate only in the null-region, where the non-linearity is most serious.

The servo-valve requirements mentioned here, hold generally for hydraulic servo-systems. However, in case transmission line dynamics play a role, the servo-valve behaviour is even more crucial, as is explained next.

Avoidance stability problems due to transmission lines

In Subsection 4.4.2 it has been argued, that the combination of servo-valve dynamics and transmission line dynamics may cause serious stability problems in case of proportional pressure difference feedback. In the system design stage, there are three different, complementary approaches to avoid these problems as much as possible, which are subsequently discussed here.

First, it is advisable to keep transmission lines between servo-valve and actuator chambers as short as possible, if the system design allows to do so. In this way, the resonance

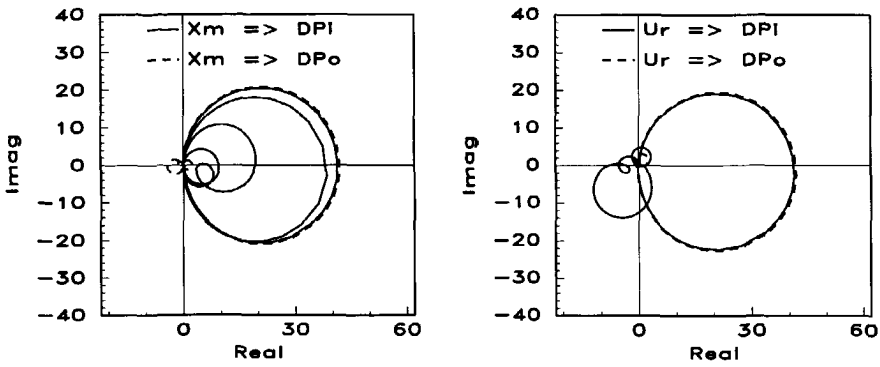


Fig. 4.20: Nyquist plot of open loop pressure difference transfer functions $G_{uy}(j\omega)$ of hydraulic actuator including transmission line dynamics; without valve dynamics, input $u = \bar{x}_m$ (left); with valve dynamics, input $u = \bar{u}_r$ (right); pressure difference measured at valve, output $y = \overline{\Delta P}_i$ (solid); and at actuator chambers, output $y = \overline{\Delta P}_o$ (dashed)

modes related to the transmission lines are kept in the (very) high-frequency range, far beyond the bandwidth of the servo-valve. Due to the high-frequency roll-off of the valve dynamics, sufficient attenuation of the transmission line resonances will be achieved, so that interference with the high-performance actuator control loop is avoided.

Second, if the system design inevitably requires long transmission lines, for instance in long-stroke actuators, stability problems may be avoided by a proper servo-valve choice. Thereby, a high-performance servo-valve does not automatically lead to wide stability margins, as the application in this thesis shows. If the application allows a valve with a small bandwidth related to the transmission line resonances, application of such a valve might be useful to yield wide stability margins under proportional pressure difference feedback. However, the performance of the pressure difference control loop will be definitely restricted by the servo-valve dynamics, as shown in Subsection 4.4.1.

Third, the placement of the pressure difference transducer is an important issue in case stability problems occur due to interference of valve dynamics and transmission line dynamics. In order to explain this, a number of open loop frequency responses is shown in two Nyquist plots in Fig. 4.20. The responses have been obtained with exactly the same model as in Subsection 4.4.2; actually the responses with $\overline{\Delta P}_i$ as output (solid) are identical to the ones shown in Fig. 4.17 on page 227. For the other (dashed) responses in Fig. 4.20, it is assumed that the pressure difference is measured as the difference of the two pressures in the actuator chambers, $\overline{\Delta P}_o$.

In order to illustrate the effect of servo-valve dynamics on desirable transducer placement, the left plot of Fig. 4.20 shows the open loop response without valve dynamics, representing the case that the servo-valve dynamics are *much faster* than the resonance frequencies of the transmission lines. It is clear from this plot, that in this situation, it would be better to measure the pressure difference at the valve side to avoid stability problems under proportional feedback; the Nyquist plot for $\overline{\Delta P}_i$ does not cross the negative real axis. However, the situation is different, if the transmission line resonance frequencies lie just in the region where the servo-valve still has a large gain, but already has conside-

rable phase lag, in the order of magnitude of -180 [deg]. This is shown in the right plot of Fig. 4.20; in this case, measuring the pressure difference for feedback at the actuator side would be advantageous.

So, from a control point of view, it depends on the valve dynamics, which pressure difference should be used for feedback. However, from a practical point of view, it is not always possible to measure the pressure difference at the desired location, especially not at the actuator side. For instance, with long-stroke actuators, the only solution is to use two absolute pressure transducers and subtract the two signals. Compared to the application of a standard pressure difference transducer, this solution has the disadvantage, that it is difficult to obtain a high accuracy both statically and dynamically. An alternative for measuring the pressure difference at the actuator side might be the measurement of the acceleration of the load; with known load inertia, this is a direct measure for the pressure difference. However, a serious disadvantage of this method is obviously, that varying loads and external forces should be taken into account in the actuator control.

Summarizing, stability problems with proportional pressure difference feedback may be avoided by proper system design. This starts with aiming at minimum length of the transmission lines and proceeds with the suitable choice of a servo-valve. It finally involves a proper choice and placement of transducers, to obtain the most suitable feedback signal for control.

4.4.5 Conclusion

In this Section, the implications of servo-valve dynamics and transmission line dynamics on the control of a hydraulic servo-system have been discussed. Especially for those control strategies described in Section 4.3, that make use of an available pressure difference reference signal by high-gain pressure difference feedback, these implications are serious.

If servo-valve dynamics are not negligible, the dominant servo-valve poles tend to shift into the right half plane under high-gain pressure feedback. Variations in the dynamic behaviour of the valve and in the static gain of the actuator, both due to non-linearity, make robustness of the control design a serious issue.

The combination of transmission line dynamics and servo-valve dynamics easily destabilizes a proportional pressure difference feedback loop. Dynamic pressure difference control may partly solve the problems, although the achievable performance is still seriously restricted due to the presence of badly damped resonance frequencies in the system. Again, robustness with respect to non-linearities of the system is an important issue.

Given the available model knowledge of the system, there are some open control design issues, setting the lines for further research. This research will have to focus especially on the application of modern robust control techniques as H_∞ and μ-synthesis and others. Thus, fundamental solutions may be found to the control problems, caused by servo-valve non-linearity, amplitude dependence of the actuator dynamics and variations in the dynamics for different actuators.

In case, that there is still freedom in the design of the hydraulic servo-system, this should be utilized to avoid problems with the control performance of the system. Important system design issues are the choice of the servo-valve, minimization of the transmission line length, and proper placement of the pressure difference transducer.

In the scope of this thesis, the focus is on basic control design issues related to hydraulic servo-systems. In this light, some control strategies have been adressed in Section 4.3, and

implications of higher order dynamics have been discussed in the current Section. Before this discussion can be extended to an experimental evaluation in Section 4.6, the problem of velocity estimation needs to be treated, because the velocity can not be measured directly in the experimental setup.

4.5 Velocity estimation

In some of the hydraulic actuator control strategies, discussed in Section 4.3, velocity feedback or velocity compensation is applied. However, the problem with the application considered in this thesis is, that velocity transducers are too expensive for the given flight simulator application. Actually, the application of a velocity transducer is often considered to be too expensive hydraulic servo technique, but due to the long stroke of the actuator the cost problem is even ore serious; long-stroke linear velocity transducers are relatively expensive. Therefore, in order to apply the proposed control strategies to the experimental setup, described in Section 3.3, a velocity estimation has to be performed.

For the given case of the long-stroke hydraulic actuator, some possibilities of velocity estimation are considered in Subsection 4.5.1 and 4.5.2, while an experimental evaluation of different velocity estimation techniques is given in Subsection 4.5.3. How the final choice for a specific velocity estimation method depends on the specific application at hand, is explained in Subsection 4.5.4.

4.5.1 Direct velocity estimation

The most direct way to obtain an estimated velocity is the application of a digital filter, with differentiating characteristics up to a certain frequency and high-frequency roll-off to avoid the generation of large amounts of noise [130]. The differentiating characteristics are basically obtained by applying some approximate (backward) difference method [8, 138]. Without additional filtering, this digital differentiator is extremely sensitive to (quantization) noise, especially for high sample rates, as the differentiation includes a division by the sample time.

Thus, a primary requirement for velocity estimation by differentiating the position signal is a good signal condition, i.e. a low noise level and high resolution sampling (quantization). Dependent on the experimental signal conditions, an additional digital filter can be designed, to cut the differentiator off at a certain frequency, in order to reduce noise effects. This obviously involves a trade-off between the noise level and the phase lag in the estimated velocity signal.

In the experimental setup, described in Section 3.3, it appeared to be difficult to achieve good signal conditions for the position signal. Even after application of an analog anti-aliasing filter with cut-off frequency 500 [Hz], and 16-bit AD-conversion (see Subsection 3.3.3) the signal was rather noisy. Therefore, strong low-pass filtering was required on the digitally differentiated position signal. Thus, the digital differentiating filter designed for this system consisted of a pure differentiator in series with two second order Butterworth filters, with cut-off frequencies of 20 and 50 [Hz] respectively. The filters were designed in the continuous time domain and then discretized and implemented at a sample rate of 5 [kHz]. An experimental evaluation of the resulting filter, denoted as `Est.1`, is given in Subsection 4.5.3, together with results for the other velocity estimators, that are

discussed next.

4.5.2 Standard estimator design

In state feedback control applications of hydraulic actuators, the use of a state estimator is common [36, 104, 105, 153]. Restricting attention to the basic dynamics of the hydraulic servo-system, while the pressure difference and the position are assumed to be measured, the state estimator basically serves as a velocity estimator.

Anderson et.al. [4] distinguish two types of state estimators: full order estimators and reduced order estimators. The advantage of full order estimators, utilizing the complete plant model, is that they have better noise reduction properties. This is due to the fact that there is no direct feedthrough of measured output signals to the estimated state signals [4]. The reduced order state estimator, usually of the order of the number of unmeasured states, may have such feedthrough terms and is therewith more sensitive to measurement noise. Considering the 3rd order model of the hydraulic actuator, both types of estimator design will be worked out below. Application results of the discussed designs will be given in Subsection 4.5.3.

Full order state estimator

The full order state estimator design is based on the (linear) 3rd order actuator model (2.108) given on page 101, with the state X constituted by the state varibables $\dot{q}$, q and $\overline{\Delta P}_p$. Because the system has multiple outputs, namely the position q and the pressure difference $\overline{\Delta P}_p$, the estimator feedback design is not easily performed by placing poles in a deterministic setting. Therefore, the full order estimator design is treated in a statistical setting, leading to the application of Kalman filter theory.

Adding white process and measurement noise terms to the system, the following system description is obtained for (2.108):

$$\begin{aligned} \dot{X} &= AX + BU + V \\ Y &= CX + W \end{aligned} \tag{4.4}$$

The Kalman filter that estimates the state of this system from the input U and the noisy output Y, reads as follows:

$$\begin{aligned} \dot{\hat{X}} &= \hat{A}\hat{X} + \hat{B}U - L[\hat{C}\hat{X} - Y] \\ \hat{X} &= I\hat{X} \end{aligned} \tag{4.5}$$

The Kalman filter design for the system (4.4) consists of the construction of the estimator feedback gain L, such that a proper state estimation is obtained, given noise levels on V and W respectively, by minimizing a certain criterion [4]. Actually, the covariance matrices Q and R, related to the process noise V and the measurement noise W respectively, serve as design parameters in this procedure. In order to keep the estimator design transparent, the covariance matrices are chosen diagonal, as follows:

$$Q = E\{VV'\} = \begin{bmatrix} Q_{11} & 0 & 0 \\ 0 & Q_{22} & 0 \\ 0 & 0 & Q_{33} \end{bmatrix} \qquad R = E\{WW'\} = \rho \begin{bmatrix} 1 & 0 \\ 0 & 1 \end{bmatrix} \tag{4.6}$$

Thus, the Kalman filter design is established by the choice of process noise variances Q_{11}, Q_{22} and Q_{33}, and the weighting factor ρ.

The weighting factor ρ can be interpreted as a measure for the reliability of the measured output signals, relative to the quality of the model used in the estimator. For small ρ, representing small measurement noise, the measured outputs are 'reliable', and high-gain feedback is allowed. In other words, by reducing ρ, the estimator poles can be made faster, resulting in fast decay of estimation errors with respect to the measured output signals. Obviously, the cost is an increased noise sensitivity.

The process noise variances Q_{11}, Q_{22} and Q_{33} can be interpreted as a measure for the reliability of the individual state equations of the system model. For instance, if the third state equation of the actuator model (2.108), which should describe the dynamic behaviour of the actuator pressure difference, is a bad approximation of the real pressure difference dynamics, Q_{33} can be made large. The effect on the Kalman filter design will be a high-gain feedback of the difference between the estimated and the measured pressure difference. In other words, the estimated pressure difference $\widehat{\Delta P}_p$ is based on the measured pressure difference rather than on the model describing the dynamic behaviour of the pressure difference as a result of the control input.

Against this background, two designs have been performed, from different points of view, although both are aimed at a proper estimation of the actuator velocity $\dot{q}$. The first viewpoint is, that the measured pressure difference signal contains significant information to derive an estimated velocity via the equation of motion, the first state equation of (2.108), because the acceleration is directly related to the pressure difference by ζ_2. The second viewpoint is just the contrary, namely that varying load conditions, i.e. varying ζ_2, make the equation of motion unfit to derive the velocity from the pressure difference.

The two Kalman filter designs, denoted as `Est.2` and `Est.3` respectively, have been obtained by choosing noise covariances as shown in Table 4.5. The resulting estimator feedback gains L are also given, as well as the closed loop poles of the estimator (4.5). With respect to these designs and preliminary simulations with these estimators, some remarks can be made:

- For the first design `Est.2`, Q_{11} is chosen small to allow velocity estimation based on the equation of motion. The result is, that there is only very weak feedback on the first state equation of the estimator, i.e. the first row of L contains small gains. The slow pole at -9.04 corresponds to this very weak feedback loop. The faster poles correspond to the loops for the position and the pressure difference respectively, which each have relatively large feedback gains in L.
- For the second design `Est.3`, Q_{11} is chosen large in order to reduce the sensitivity of the estimator to model errors concerning the load dynamics. The result is a large feedback of the pressure difference (the L_{12}-element) to the first state of the estimator. Actually, the estimator states related to the velocity and the pressure difference are strongly coupled in this design, with a complex pole pair related to their dynamics.
- The value for ρ was chosen similar for both designs. The rather small value reflects the expectedly good signal-to-noise ratio of the measured signals and results in reasonably fast estimator poles.
- Preliminary simulations with the first estimator design showed, that the velocity estimation is very good in case the model is correct. However, if the estimator is based on a wrong model for the load, i.e. $\hat{\zeta}_2 \neq \zeta_2$, considerable deviations occur

between estimated and actual velocity. So the velocity estimator `Est.2` is sensitive to load variations.

- Similar simulations with the second estimator design showed a good robustness of the velocity estimator `Est.3` against errors in the load model. However, the strong coupling between the estimated velocity and pressure difference also showed a serious drawback: high-frequency components (50-100 [Hz]) in the measured pressure difference are followed by the estimated velocity $\hat{q}$. If an actuator motion corresponds to a pressure difference signal with high-frequency contents, this signal is followed nicely by the estimated pressure difference, but the estimated velocity also contains these high-frequency components, while the actual velocity of the actuator does not. Thus, the velocity estimator `Est.3` may be sensitive to high-frequency components in the measured pressure difference.

	Q_{11}	Q_{22}	Q_{33}	ρ	L	Observer poles
`Est.2`	10^{-3}	1	1	10^{-5}	$\begin{bmatrix} 0.09 & -3.38 \\ 316 & -0.03 \\ -0.03 & 313 \end{bmatrix}$	$-9.04 \quad -309 \quad -316$
`Est.3`	10	1	1	10^{-5}	$\begin{bmatrix} 5.79 & -987 \\ 316 & -2.02 \\ -2.02 & 659 \end{bmatrix}$	$-316 \quad -232 \pm 250j$

Table 4.5: Noise covariances and resulting estimator feedback gains and poles for two Kalman filter designs `Est.2` and `Est.3`

For both designed Kalman filters, three orders are used to estimate the complete state of the hydraulic actuator. However, basically the estimation of the position and the pressure difference is not necessary, only the velocity needs to be estimated. This notion is reflected by the idea of the reduced order estimator, which is slightly simpler and allows easier physical interpretation of the estimator design.

Reduced order state estimator

According to Anderson et.al. [4], a multi-output system can be partioned such, that part of the state vector needs to be estimated, while the other part directly reflects the measured outputs. Actually, the model of the hydraulic actuator (2.108) is already in this form, with $\dot{q}$ to be estimated and q and $\overline{\Delta P_p}$ measurable. Or, in general state space form (compare (2.108)):

$$\begin{aligned} \begin{bmatrix} \dot{X}_1 \\ \dot{X}_2 \end{bmatrix} &= \begin{bmatrix} A_{11} & A_{12} \\ A_{21} & A_{22} \end{bmatrix} \begin{bmatrix} X_1 \\ X_2 \end{bmatrix} + \begin{bmatrix} B_1 \\ B_2 \end{bmatrix} U \\ Y &= \begin{bmatrix} 0 & I \end{bmatrix} \begin{bmatrix} X_1 \\ X_2 \end{bmatrix} \end{aligned} \tag{4.7}$$

The reduced order state estimator that estimates the unknown part of the state, X_1,

from the input U and the output Y, reads as follows, with $A_e = \hat{A}_{11} - L_e\hat{A}_{21}$ [4]:

$$\begin{aligned} \dot{X}_e &= A_e X_e + \left(\hat{B}_1 - L_e\hat{B}_2\right)U + \left(\hat{A}_{12} - L_e\hat{A}_{22} + A_e L_e\right)Y \\ \hat{X}_1 &= X_e + L_e Y \end{aligned} \tag{4.8}$$

The estimator feedback gain L_e can be used to locate the poles of the estimator, i.e. the eigenvalues of A_e. In fact, the given structure for the reduced order estimator is the implementable version of the underlying model-based estimator for X_1:

$$\begin{aligned} \dot{\hat{X}}_1 &= \left(\hat{A}_{11} - L_e\hat{A}_{21}\right)\hat{X}_1 + L_e\left(\dot{Y} - \hat{A}_{22}Y - \hat{B}_2U\right) + \hat{A}_{12}Y + \hat{B}_1U \\ \hat{X}_1 &= \hat{X}_1 \end{aligned} \tag{4.9}$$

where it might be noted from (4.7), that $\left(\dot{Y} - A_{22}Y - B_2U\right) = A_{21}X_1$.

In order to arrive at a proper estimator design by the choice of the estimator feedback gain L_e, it is useful to consider the physical interpretation of this estimator. For that purpose, (4.9) is rewritten in terms of the physical actuator model (2.108), writing the estimator feedback gain as $L_e = \begin{bmatrix} L_q & L_{\Delta P} \end{bmatrix}$:

$$\begin{aligned} \tfrac{d}{dt}(\hat{\dot{q}}) = & \left(-\hat{\zeta}_1 - \begin{bmatrix} L_q & L_{\Delta P} \end{bmatrix}\begin{bmatrix} 1 \\ -2\hat{\zeta}_3\hat{\zeta}_{56} \end{bmatrix}\right)\hat{\dot{q}} \\ & + \begin{bmatrix} L_q & L_{\Delta P} \end{bmatrix}\left(\begin{bmatrix} \dot{q} \\ \overline{\Delta P}_p \end{bmatrix} - \begin{bmatrix} 0 & 0 \\ 0 & -2\hat{\zeta}_4\hat{\zeta}_{56} \end{bmatrix}\begin{bmatrix} q \\ \overline{\Delta P}_p \end{bmatrix} - \begin{bmatrix} 0 \\ 2\hat{\zeta}_{56} \end{bmatrix}\bar{u}_r\right) \\ & + \begin{bmatrix} 0 & \hat{\zeta}_2 \end{bmatrix}\begin{bmatrix} q \\ \overline{\Delta P}_p \end{bmatrix} \\ \hat{q} = & \hat{\dot{q}} \end{aligned} \tag{4.10}$$

Note that, analoguous to (4.9), the expression between parenthesis (.) in the second row is equivalent to $\begin{bmatrix} 1 & -2\zeta_3\zeta_{56} \end{bmatrix}^T \dot{q}$, if the estimator model is correct.

From (4.10), it is clear that the velocity estimator in this form is a first order filter, of which the pole can be placed by the feedback gains L_q and $L_{\Delta P}$. The filter is basically fed by two terms, the second and the third row of (4.10).

As noted before, the first of these terms actually represents the velocity of the actuator, as it can be solved from the second and third state equation of the actuator model (2.108). In case of strong feedback of the filter, so with large gain L_e, this term is strongly emphasized, which means that the velocity estimation is strongly based on the second part of the actuator model. Because the load dynamics (ζ_2) are not involved in this part of the actuator model, high-gain feedback of the filter makes the velocity estimation robust against load variations.

In the form of (4.10), the measured outputs are differentiated and then fed into the first order filter. In the implementable form (4.8) however, differentiation and filtering are combined, so that a proper filter results. Yet, in the low-frequency region, the filter does differentiate the outputs. Thereby, the cut-off frequency for the differentiation is just the estimator pole, which equals $-\hat{\zeta}_1 - L_q + L_{\Delta P}2\hat{\zeta}_3\hat{\zeta}_{56}$. The freedom in locating this pole with the two gains L_q and $L_{\Delta P}$ can be utilized, to balance the contributions to the

velocity estimation from the measured position at the one hand and the measured pressure difference and the control signal at the other hand.

The second term which drives the velocity estimator (4.10) is given in the third row of the equation, and provides an estimation for the acceleration of the actuator, using the model knowledge $\hat{\zeta}_2$ concerning the load. Actually, it can be seen as a forward coupling of the measured pressure difference signal, which improves the velocity estimation in case the load model is correct. This term is especially important when the feedback gain L_e is small; in that case the estimator heavily relies on this open loop estimation of the velocity.

With the above discussion of the physical interpretation of the reduced order estimator, the actual design consisting of the choice of feedback gains L_q and $L_{\Delta P}$ is easily performed. In fact, the velocity estimator design involves a double trade-off:

- First, the location of the estimator pole is to be chosen. This involves a trade-off between reliance on the model knowledge concerning the load at the one hand and reliance on the actuator model including differentiation of measured signals on the other hand.
- Second, a trade-off has to be made between differentiating the position signal at the one hand and using the pressure difference and the control signal at the other hand. Thereby, differentiation of the position signal requires no model knowledge, but may produce lots of noise because the position signal may well be noisy. However, the use of the pressure difference and control signal heavily relies on model knowledge concerning the pressure dynamics of the actuator, while also a differentiation of the pressure difference signal is involved. Fortunately, the model knowledge used here is independent of the actuator load, so it may be obtained once for a given actuator, as described in Chapter 3. Moreover, the pressure difference signal is often well-conditioned, allowing differentiation over a reasonable bandwidth.

Like before in the full order case, two reduced order velocity estimators have been designed from different points of view, with feedback gains given in Table 4.6. The first, denoted as `Est.4`, is only based on differentiation of the position signal, choosing $L_{\Delta P} = 0$. Presuming rather bad signal conditions (compare Subsection 4.5.3), the estimator pole was chosen rather slow, meaning that the load model plays a significant role in the velocity estimation. The second design, denoted as `Est.5`, is just based on the model of the pressure dynamics by choosing a relatively large pressure difference feedback gain $L_{\Delta P}$, corresponding to a reasonably fast estimator pole, see Table 4.6. Preliminary simulations showed results comparable to those obtained with the two Kalman filter designs, discussed earlier.

Est.4	L_q	$L_{\Delta P}$	Observer pole	Est.5	L_q	$L_{\Delta P}$	Observer pole
	10	0	−10.0		0	−1	−173

Table 4.6: Observer feedback gains and poles for two reduced order estimator designs `Est.4` and `Est.5`

Conclusion

In this Subsection, the backgrounds of different model-based velocity estimators for hydraulic actuators have been discussed. Based on the theoretical background, it is expected that the full order state estimator is less sensitive to noise than the reduced order estimator. A disadvantage of the full order estimator or the Kalman filter is, that it does not allow a direct physical interpretation of the filter design. The reduced order estimator is easier to design in this sense.

In both the full order and the reduced order state estimator design, a sort of trade-off is involved between the use of the model-knowledge of the load and the use of the model-knowledge of the pressure dynamics of the actuator. When relying on the load model, smooth velocity estimations may be obtained. However, they are sensitive to load variations. Relying on the pressure dynamics model involves high-gain feedback of the measured pressure difference signal to the observer state(s). This results in robustness against load variations, but also in sensitivity to measurement noise and varying or unknown actuator properties.

The given conclusions are mainly based on preliminary simulations; a discussion of the experimental results, obtained with the setup of Section 3.3, is the topic of the next Subsection.

4.5.3 Experimental evaluation of velocity estimation

For the experimental evaluation of the different velocity estimation techniques, certain experimental conditions have been chosen to allow proper comparison of the results. After an evaluation of the different designs of Subsection 4.5.1 and 4.5.2 under these nominal conditions, the designs are compared to each other with regard to their sensitivity to variations in the load condition and in the actuator position.

Experimental conditions for evaluation

The experiments were performed with the experimental setup, described in Section 3.3. In order to obtain realistic results in the sense that the estimated velocity signal should be used for closed loop control, the measurements have been performed in a closed loop configuration, where *no* velocity feedback was used. Actually, the reference generator of Fig. 4.4 was used again, with $\omega_f = 2\pi 5$ [rad/s] and a reference input amplitude $A_{\bar{r}} = 0.625$ [mm]. The applied controller was the one depicted in Fig. 4.12, with $K_q = 7.5$, $K_{\dot{q}} = 0$, $K_{\Delta P} = 0.76$ and $K_{ff} = 0.831$, to be denoted by `E.Ctr.2a` later.

The nominal conditions for the evaluation of the velocity estimator correspond to those denoted by `Load 1` and by actuator position q_0^0. This means, that the load inertia $M_p = \hat{M}_p = 3140$ [kg], the static load $\bar{F}_{ext} = \hat{\bar{F}}_{ext} = -0.043$, while the actuator is in the middle position. In order to test the robustness of the velocity estimators, the performance has also been evaluated with `Load 2`, corresponding to a load inertia $M_p = \hat{M}_p = 1960$ [kg] and a static load $\bar{F}_{ext} = \hat{\bar{F}}_{ext} = -0.365$, and in actuator position $q_0^- = -0.47$ [m].

Under the described conditions the different estimators, designed in the continuous time domain, were implemented in the digital controller (after discretization) at a sample rate of 5 [kHz].

Evaluation criteria

After implementation of the designed velocity estimators, under specified experimental conditions, the performance has to be evaluated. An important criterion is, whether the estimated velocity represents the real velocity over a sufficiently large frequency range, with sufficiently small phase lag. An additional requirement is, that the noise level should be as small as possible.

The problem is hereby, that no true velocity measurement is available. It is even difficult to reconstruct the velocity (in the frequency domain) off-line. It might be obtained by multiplying the measured position frequency response with $j\omega$, but under closed loop control, the amplitude of the position is so small at higher frequencies, that the high-frequency part of the position frequency response is unfit to do so. Another possibility would be the multiplication of the measured acceleration frequency response by $\frac{1}{j\omega}$, but the problem here is, that this frequency response is seriously affected by parasitic dynamics of the test rig and its base.

For these reasons, the non-linear identified simulation model of Chapter 3 has been chosen as a reference, to evaluate the velocity estimation in the frequency domain. This choice is justified by the validation results of Section 3.6, which show good predictive quality with respect to the open loop behaviour of the actuator. In order to keep as close to this open loop behaviour as possible, the evaluation of the velocity estimators will take place by comparing the measured frequency response $H_{\bar{x}_m\dot{q}}(j\omega)$ to the simulated frequency response $\hat{H}_{\bar{x}_m\dot{q}}(j\omega)$. Thereby, the simulated response is obtained with the complete non-linear simulation model, under closed loop conditions as described above.

In order to obtain a clear view of the performance of the velocity estimators in the frequency domain, the errors in the measured responses will be considered rather than the measured responses themselves. Thereby, the relative amplitude error and the phase error are defined as follows:

$$\begin{aligned} E_{ampl}(j\omega) &= \frac{|H(j\omega)|-|\hat{H}(j\omega)|}{|H(j\omega)|} \\ E_{phase}(j\omega) &= \angle H(j\omega) - \angle \hat{H}(j\omega) \end{aligned} \tag{4.11}$$

Besides the frequency domain performance, the time domain performance has to be evaluated. This is done by specifying the following criterion for the noise level of the estimated velocity $\hat{q}$, given a time recording for zero reference input $\bar{r}$, containing N samples:

$$V_{\hat{\dot{q}}} = \frac{1}{N}\sum_{i=1}^{N}\left[\hat{\dot{q}}_i\right]^2 \tag{4.12}$$

Because the actuator will be at rest for zero reference input, this criterion would be zero in the case of a noise-free velocity estimation. In other words, $V_{\hat{\dot{q}}}$ is a direct measure for the generated noise on the estimated velocity, and should be as small as possible.

Evaluation of different techniques under nominal conditions

In order to get a first idea of the quality of the velocity estimation of two (arbitrarily chosen) estimators, namely `Est.1` and `Est.5`, the simulated and measured frequency responses are shown in Fig. 4.21. It is directly clear from this Figure, that `Est.5` performs better than `Est.1`; not only the amplitude is described very well by `Est.5` until frequencies of about

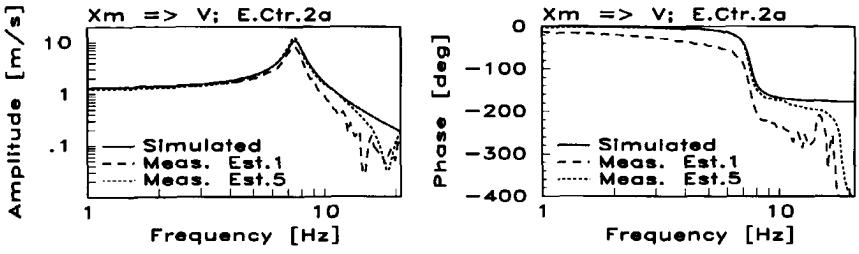


Fig. 4.21: Simulated frequency response $\hat{H}_{\bar{x}_m\dot{q}}(j\omega)$ (solid) and measured frequency responses $H_{\bar{x}_m\dot{q}}(j\omega)$ with velocity estimators `Est.1` (dashed) and `Est.5` (dotted), obtained under closed loop control `E.Ctr.2a` with `Load 1` in middle position q_0^0 and $A_{\bar{r}} = .625$ [mm]

13 [Hz], but also the phase, whereas `Est.1` shows considerable phase lag in the velocity estimation.

A complete picture of the performance of the different velocity estimators under nominal conditions is given in Fig. 4.22, where the errors between the measured and simulated frequency response are given according to the error definitions of (4.11). Based on the results, a number of conclusions can be drawn.

- The differentiating filter `Est.1` provides a correct steady state estimation (in gain at least) of the velocity. However, a serious drawback of this estimator is the large phase lag, even at low frequencies, which makes this filter less suitable for feedback control.
- The two estimators that are (mainly) based on the equation of motion, namely `Est.2` and `Est.4`, show very similar behaviour. More specifically:
  - Both estimators show bad performance in the low-frequency region. This is caused by the Coulomb friction; because the signal amplitude is small, Coulomb friction has a relatively large effect on the pressure difference signal. Because the estimator relies on the equation of motion of the system, in which this effect is not taken into account, the velocity estimation is biased by the presence of Coulomb friction. Additional experiments show, that this effect reduces with increasing signal amplitudes.
  - Both estimators show relatively small errors with respect to the simulated response in the high-frequency region. Due to the inertial load, the roll-off of the velocity in the high-frequency region is -20 [dB/dec] in the simulation. Because the velocity estimation of `Est.2` and `Est.4` is mainly based on the equation of motion of the inertial load, these estimators do reproduce this roll-off rather well.
- The two estimators that are (mainly) based on the mass balances of the actuator chambers, namely `Est.3` and `Est.5`, also show similar behaviour, when compared to each other. Some more specific remarks:
  - Both estimators show rather good performance in the low-frequency region. This can be ascribed to the fact that the (estimated) velocity gain of the model is used to predict the velocity at low frequencies. Thereby, the measured pressure difference (including friction effects) is not involved. So, with a good estimation

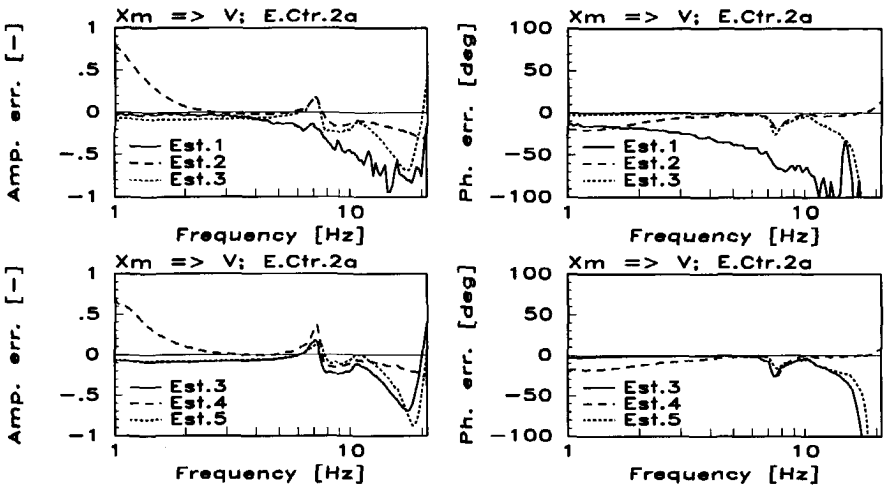


Fig. 4.22: Errors in frequency responses of different velocity estimators; relative amplitude errors $E_{ampl}(j\omega)$ (left) and phase errors $E_{phase}(j\omega)$ (right); obtained under closed loop control with `Load 1` in middle position q_0^0

of the open loop gain, a good velocity estimation is obtained, with a negligible phase error.

- In the high-frequency region, beginning from about 15 [Hz], the experimental results of `Est.3` and `Est.5` start to deviate from the simulated response, both with respect to amplitude and phase. The reason is, that these estimator designs are sensitive to high-frequency components in the measured pressure difference. Because of parasitic dynamics, both in the test rig and the base (see Subsection 3.3.1), the measured pressure difference in the frequency region beyond 15 [Hz] does not correspond to the accelerations of the inertial load, but includes other dynamic effects. Actually, this was observed earlier when discussing the cross-validation result of Fig. 3.30 on page 180, where the measured load acceleration shows a dip at about 20 [Hz]. It is just this dynamic effect, which is found back in the velocity estimation by `Est.3` and `Est.5`.

- In fact, the preceding discussion means that the simulated velocity response of Fig. 4.21 is not correct for the high-frequency region; it does not include the effect of parasitic dynamics, that are definitely present. For this reason, the judgement of the estimator performance is restricted to the frequency region 1-20 [Hz]. Although measurements have been performed beyond 20 [Hz], they do not allow hard performance conclusions; yet, it may be remarked, that the estimators `Est.3` and `Est.5` did not show a steady roll-off in the high-frequency region, like the other estimators `Est.2` and `Est.4`. This confirms the expected sensitivity to high-frequency components in the measured pressure difference signal (Subsection 4.5.2).
- Apart from the mentioned differences in performance, the different observers provide a good (on-line) estimation of the velocity under nominal conditions.

Besides the performance in the frequency domain, the noise levels of the different esti-

mators have been evaluated according to the criterion (4.12). The results are given in Table 4.7, where `Est.6` denotes the final estimator design, is to be discussed later. The presented noise levels can be provided with some remarks.

- The noise level of `Est.1` is not the largest, but it should be noted that heavy filtering was necessary to achieve this result.
- In good agreement with theory, the Kalman filter designs `Est.2` and `Est.3` (full order observers) appear to be less sensitive to noise than the reduced order observers `Est.4` and `Est.5`.
- The Kalman filter that is (mainly) based on the equation of motion, namely `Est.2`, is far less sensitive to measurement noise than the one based on the mass balance, `Est.3`, as expected. This is mainly due to high-frequency contents in the measured pressure difference signal.
- The noise level of `Est.4` is relatively large due to the noise on the measured position signal, which is amplified by the 'differentiating' character of the reduced order observer with pure position feedback.

	Est.1	Est.2	Est.3	Est.4	Est.5	Est.6
$V_{\dot{q}}$	$1.40\ 10^{-4}$	$1.74\ 10^{-7}$	$1.73\ 10^{-4}$	$4.27\ 10^{-4}$	$4.30\ 10^{-4}$	$1.29\ 10^{-6}$

Table 4.7: Experimental noise levels for different velocity estimator designs

Before concluding on the best performing velocity estimator, the sensitivity of the performance of the different estimators to different conditions (load inertia and actuator position) will be evaluated next. Thereby, only the results for the full order observers are given, as the results for the reduced order observers are completely comparable.

Sensitivity to load inertia

A comparison of the different velocity estimators with respect to different load conditions is given in Fig. 4.23. Before discussing the results, it may be noted that there are two major differences between the open loop velocity responses for `Load 1` and `Load 2` respectively (the responses themselves are not shown):

- Due to the smaller inertia of `Load 2`, the natural frequency is larger, namely 10 [Hz] instead of 7.8 [Hz]. Related to this difference is the fact, that there is a difference in the high-frequency gain of the velocity response: for the smaller inertia `Load 2`, the high-frequency gain is larger.
- Due to the load sensitivity of the servo-valve flow according to (2.124) (page 114), the static load of `Load 2` effectively reduces the low-frequency velocity gain for sinusoidal input signals. In the given case, the velocity gain has effectively reduced with a factor of about 0.9.

Keeping this in mind, the results of Fig. 4.23 give rise to the following conclusions:

- As might be expected, the differentiating filter `Est.1` is not at all sensitive to load variations (upper plots); only bad signal conditions cause errors in the higher frequencies.

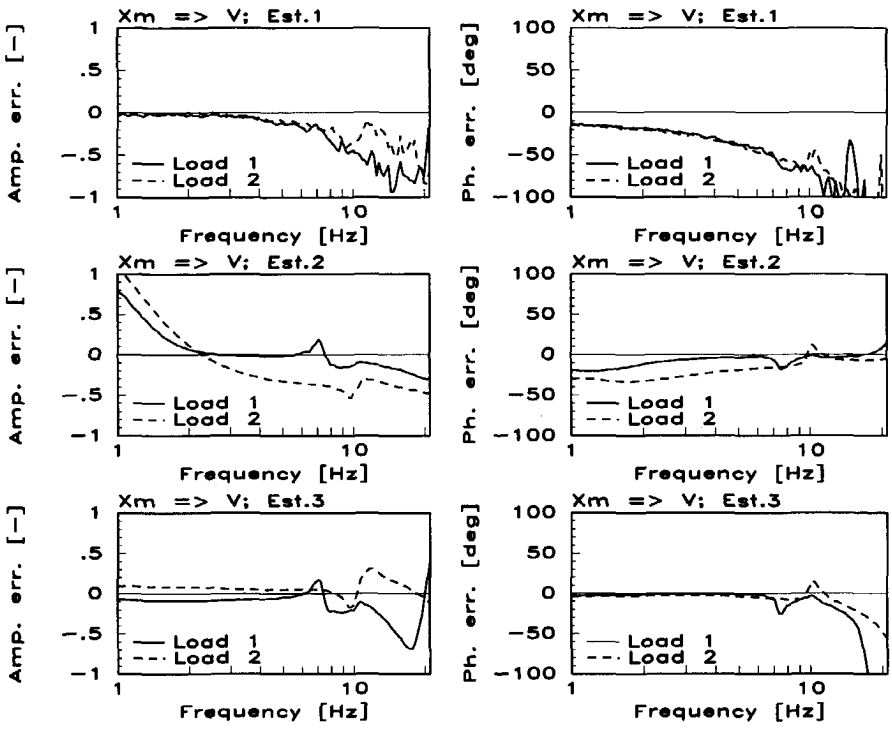


Fig. 4.23: Errors in frequency responses of different velocity estimators; relative amplitude errors $E_{ampl}(j\omega)$ (left) and phase errors $E_{phase}(j\omega)$ (right); obtained under closed loop control with different load conditions in middle position q_0^0

- Because the first Kalman filter design, `Est.2`, heavily relies on the open loop model of the actuator load, the equation of motion, considerable deviations are found for `Load 2`, even in the middle frequency range (middle plots). This is just because the load model is wrong; because $M_p < \hat{M}_p$, the required and measured pressure difference is smaller than for `Load 1`, so that the estimated accelerations are smaller, leading to an underestimation of the velocity (middle frequency region).
- Because the inertia for `Load 2` is smaller, the disturbing effect of the Coulomb friction in the low-frequency region (for `Est.2`) is larger.
- Because the low-frequency behaviour of the second Kalman filter design, `Est.3`, is based on the open loop velocity gain of the actuator model, an almost constant difference is found in the amplitude errors for the different load conditions, at least in the frequency region below the resonance frequency (lower left plot). Clearly, the linear estimator design does not take into account that the velocity gain is reduced by the static load. Actually, a non-linear compensation might be applied to avoid this load sensitivity of the given estimator design.
- Apart from the low-frequency behaviour, `Est.3` is quite robust against load variations, and performs better than the other estimator designs. Note especially the nice phase behaviour in the lower right plot.

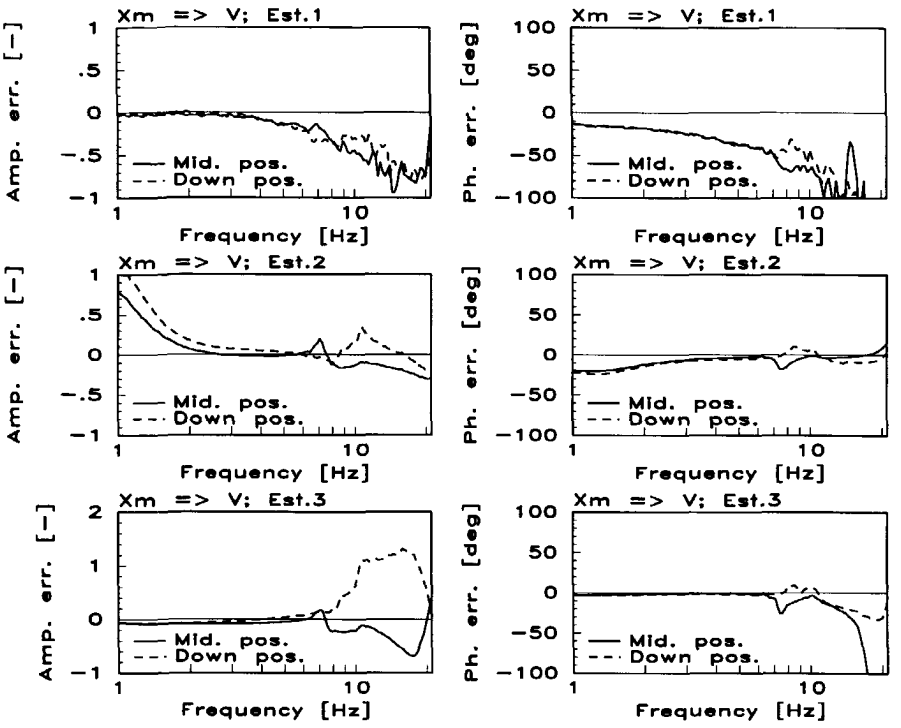


Fig. 4.24: Errors in frequency responses of different velocity estimators; relative amplitude errors $E_{ampl}(j\omega)$ (left) and phase errors $E_{phase}(j\omega)$ (right); obtained under closed loop control with `Load 1` in different positions q_0^0 and q_0^- respectively

Sensitivity to actuator stiffness

Whereas the state observers are based on a model of the actuator in the middle position, the performance of the different estimators is to be evaluated also in another position, corresponding to another actuator stiffness. In Fig. 4.24, a comparison of the performance of different velocity estimators is given for the middle position q_0^0 and the down position q_0^- respectively. The up position q_0^+ is not considered, because it provides no additional information in the low-frequency range considered here.

Again, it is noted beforehand, what the effect of the actuator stiffness on the open loop velocity responses themselves would be theoretically. Due to the increased actuator stiffness in the down position, the natural frequency of the actuator is increased from 7.7 to about 8.3 [Hz]. Related to this effect is an increased gain of the open loop system beyond the natural frequency.

In this light, the results of Fig. 4.24 can be interpreted as follows:

- As might be expected again, the differentiating filter `Est.1` is hardly sensitive to variations in the actuator stiffness (upper plots).
- According to preliminary simulations, the first Kalman filter design, `Est.2`, should not be sensitive to variations in the actuator stiffness. To some extent, this expectation is confirmed by the experiments (middle plots); there is no structural deviation

like in the case of the different loads of Fig. 4.23, especially not in the phase errors. Nevertheless, there are some deviations, which may partly be explained by the fact that the load properties are slightly different in the down position, due to the geometric non-linearity of the test rig, which have not been taken into account.

- Whereas the open loop velocity gain does not depend on the actuator positions, the second Kalman filter design, `Est.3`, performs equally well in both actuator position for frequencies below the natural frequency (lower plots).
- Beyond the natural frequency, `Est.3` is rather sensitive to the varying system properties due to varying actuator position. Although it may seem, that `Est.3` is sensitive to variations in the actuator stiffness, it should be noted that the considerable amplitude errors beyond 8 [Hz] (lower left plot) may also be caused by unmodelled variations in the load dynamics. Like mentioned before, this especially concerns parasitic dynamics in the test rig and the base, to which `Est.3` is particularly sensitive.

4.5.4 Conclusion

With different velocity estimation techniques explained in the previous Subsections, and an experimental evaluation at a real test rig provided in the preceding Subsection, a number of conclusions can be drawn. Moreover, for the given application, it can be argued how an optimal estimator should be designed.

The main conclusion should be, that the final choice for a velocity estimator for a hydraulic servo-system will depend on the application at hand. Thereby, the following issues have to be considered:

- It is highly dependent on the applied position transducer, whether (digital) differentiation is a good option to obtain an estimated velocity. In case of good signal to noise ratios and / or a digital transducer output, differentiation may be well-suited. An extra advantage of this method is its robustness, because it is not model-based; as long as a position signal is available, the velocity can be estimated. However, with bad signal conditions, the application of a model-based observer is recommendable.
- In the observer design for a hydraulic actuator, a principal trade-off is to be made between the use of the model-knowledge of the load at the one hand, and the use of the model-knowledge of the pressure dynamics of the actuator at the other hand. Both simulations and experiments show, that smooth velocity estimations can be obtained by relying on the open loop load model, although the velocity estimation is sensitive to load variations in that case. This can be avoided by high-gain feedback of the measured pressure difference, which means that the pressure dynamics model of the actuator is taken as the basis for observer design. The drawback of this method is, that it is more sensitive to variations in the actuator properties, and that it is rather sensitive to noise and high-frequency components in the measured pressure difference signal.
- The mentioned trade-off holds both for full order and for reduced order observer design for hydraulic actuators. Although the reduced order observer allows a more direct physical interpretation, the trade-off can be handled similarly by manipulating the (diagonal) state noise intensity matrix in the Kalman filter design.
- Experimental results confirm the theory that a full order observer (Kalman filter) is less sensitive to measurement noise than a reduced order observer.

With these conclusions, and given the experimental results for the different velocity

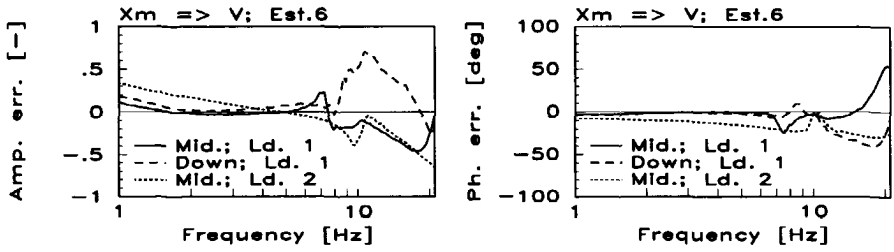


Fig. 4.25: Errors in frequency responses of final velocity estimator design `Est.6`; relative amplitude errors $E_{ampl}(j\omega)$ (left) and phase errors $E_{phase}(j\omega)$ (right); obtained under closed loop control with different loads and in different positions

estimators, a final estimator design has been performed. Because of the better noise properties, the full order observer has been chosen, where the final design, denoted as `Est.6`, can be seen as a compromise between `Est.2` and `Est.3`. The design was obtained by choosing Q_{11} in (4.6) equal to 0.1 (compare also Table 4.5). The experimental performance of the resulting estimator for different load conditions and actuator positions is given in Fig. 4.25; the experimental noise level was already given in Table 4.7.

Actually, this estimator performs quite well; a nice smooth estimated velocity is obtained, with very small phase lag, at least for nominal conditions. Whereas the principal trade-off in the observer design makes it impossible to obtain robustnes against both load variations and variations in (unmodelled) dynamics in the high-frequency region, the frequency domain performance for different loads and actuator positions, shown in Fig. 4.25 is quite acceptable. Therefore, `Est.6` is used when experimentally evaluating the performance of different control strategies, possibly including velocity feedback, in the next Section.

4.6 Experimental evaluation of control strategies

In this Section, the simulation results of Section 4.3 and 4.4 are experimentally verified, in order to provide an experimental evaluation of the different proposed control strategies for hydraulic servo-systems. Thereby, the evaluation takes place with respect to the task specification given in Subsection 4.2.3. This basically comprises the tracking of a desired position-velocity-acceleration trajectory from the reference generator, with robust performance with respect to varying load conditions.

After a description of the experimental conditions for the controller evaluation in Subsection 4.6.1, the evaluation starts in Subsection 4.6.2 with considering the robust performance of the dynamic pressure difference feedback loop, that was proposed in Subsection 4.4.2. Then, the performance of different actuator control strategies is evaluated in Subsection 4.6.3. The results given in Subsection 4.6.4 illustrate the performance improvement that can be achieved by applying velocity feedforward, while the sensitivity of the control performance to load variations is evaluated in Subsection 4.6.5. An experimental evaluation of the effect of non-linear control, as proposed in Subsection 4.3.6, can be found in Subsection 4.6.6. Finally, whereas the main part of this Section is concerned with frequency domain evaluation, Subsection 4.6.7 provides some experimental results evaluating the time domain performance.

4.6.1 Experimental conditions for controller evaluation

The experiments for the controller evaluation have been performed under exactly the same conditions as those for the experimental evaluation of velocity estimator design, and are described on page 243. In order to avoid stability problems (see Subsection 4.4.2), the proportional pressure feedback loop was replaced by the dynamic pressure control according to Fig. 4.18 and (4.3) during all measurements.

Because of the limitations of the performance of this control loop (see Section 4.4), especially under experimental conditions, the original designs for different actuator control strategies of Section 4.3 could not be implemented. Therefore, a set of new 'experimental' controllers has been designed, directly related to the different control strategies of Section 4.3. An overview of the resulting gains for the different controllers is given in Table 4.8.

Implemented controller	K_q [1/m]	$K_{\dot{q}}$ [s/m]	$K_{\Delta P}$ [-]	K_{vc} [s/m]	K_{ff} [s/m]	K_1 [1/m]	K_2 [s/m]
E.Ctr.1	15	-	0.2	-	-	-	-
E.Ctr.2	7.5	-	0.76	-	-	-	-
E.Ctr.2a	7.5	-	0.76	-	0.831	-	-
E.Ctr.3	80	2.5	0.76	-	-	-	-
E.Ctr.4	16	0.5	0.76	-	-	-	-
E.Ctr.4a	16	0.5	0.76	-	0.831	-	-
E.Ctr.5; Load 1	-	-	0.76	0.831	-	21	1.75
E.Ctr.5; Load 2	-	-	0.76	0.831	-	13.1	1.09

Table 4.8: Controller gains of different experimental controllers

In Section 4.3, the different actuator control strategies were evaluated with regard to the closed loop frequency responses $\hat{H}_{q_d q}(j\omega)$ from desired position to measured position. In fact, in the case of the noise-free simulations, with a single inertia M_p as actuator load in the simulation model, the acceleration frequency responses $\hat{H}_{\ddot{q}_d \ddot{q}}(j\omega)$, from desired acceleration to measured acceleration, were identical to the given ones for the position. In the experimental setting however, there is a difference between the measured position frequency response $H_{q_d q}(j\omega)$ and acceleration frequency response $H_{\ddot{q}_d \ddot{q}}(j\omega)$, for two reasons.

First, parasitic motions of the base cause a difference between the measured absolute acceleration of the load and the relative measurement of the piston displacement, as can be seen from the sketch of the experimental setup in Fig. 3.6 on page 147. Second, the reference generator excites the closed loop dynamics such, that the amplitude of the desired acceleration is constant for frequencies above 5 [Hz]. This means, that the amplitude of the position diminishes in that frequency region, resulting in bad signal to noise ratios, especially above 20 [Hz].

Given these differences, the acceleration frequency responses $H_{\ddot{q}_d \ddot{q}}(j\omega)$, obtained with a reference input amplitude $A_r = 0.625$ [mm], have been chosen to evaluate the performance of the different actuator control strategies. Hereby, the main reason is, that the signal to

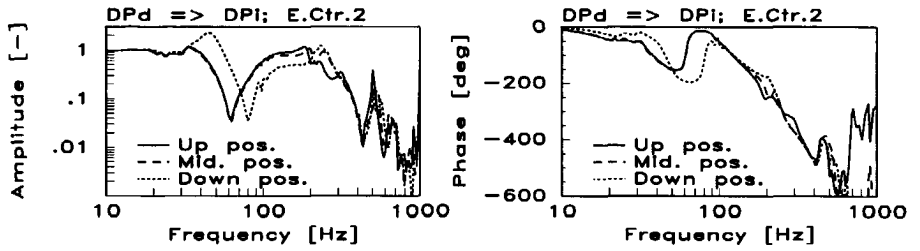


Fig. 4.26: Measured frequency responses $H_{\overline{\Delta P}_d \overline{\Delta P}_i}(j\omega)$ of pressure difference control loop in different actuator positions; $q_0^+ = 0.47$ [m] (solid), $q_0^0 = 0$ [m] (dashed) and $q_0^- = -0.47$ [m] (dotted); position feedback control `E.Ctr.2` with `Load 1`

noise ratio for the measurement of $H_{\ddot{q}_d \ddot{q}}(j\omega)$ is far better than that for $H_{q_d q}(j\omega)$. Moreover, it can be argued, that the motion control of the load is the prior control aim rather than piston displacement control, especially in applications like flight simulator motion systems.

Before evaluating the performance of the complete actuator control loop under different conditions, some experimental results will be given with respect to the dynamic pressure difference control loop.

4.6.2 Performance dynamic pressure difference control loop

In Subsection 4.4.2, a solution has been presented for the robust control of the actuator pressure difference by means of three dynamic compensators (4.3) according to Fig. 4.18. The actual robustness of this design has been experimentally verified, by performing closed loop frequency response measurements of the pressure difference control loop in the three actuator positions q_0^-, q_0^0, and q_0^+ respectively. A position feedback loop was added during the measurement to stabilize the system, i.e. `E.Ctr.2` from Table 4.8 was implemented. The results are shown in Fig. 4.26.

Comparing the experimental results of this Figure to the simulation results of Fig. 4.19, which were obtained under almost the same conditions, there is a remarkable qualitative agreement, especially for q_0^+ and q_0^0. For the lower position q_0^-, the experimental system performs not as good as the simulation model; especially in the region around 45 [Hz] there is high peaking. Actually, the system was close to the stability margin for the given pressure difference feedback gain $K_{\Delta P}$ in the given actuator position. Although it is not directly clear from the results of Fig. 4.19, it might be noted here, that the simulation model does predict stability problems at this frequency for the down position if $K_{\Delta P}$ is chosen to large. In fact, this can be seen as a good validation result concerning the quality of the dynamic models in view of closed loop control.

Another remark with respect to the closed loop response of Fig. 4.26 concerns the frequency region 20-35 [Hz]. In this region, slight irregularities are observed, which can be ascribed to parasitic motions and dynamics of test rig and base. Actually, they are hardly observable from the pressure difference transfer function, but they are definitely present in the system.

As a general conclusion on the performance of the dynamic pressure feedback loop, it can be stated that the implemented controller results in good low-frequency behaviour of the pressure difference, with a reasonable bandwidth of about 40 [Hz]. Moreover, the

controller is reasonably robust against variations in the actuator dynamics as a result of varying actuator position, so that the attention can be restricted to the middle position in the remainder. Note also, that especially the badly damped resonances of the transmission line dynamics around 200 [Hz] are robustly suppressed.

In fact, this result justifies the application of the dynamic pressure difference control loop, just instead of a proportional pressure difference feedback loop, as an effective means to avoid stability problems with transmission line dynamics. Because the performance of the pressure difference control loop appears to be hardly dependent on the remainder of the hydraulic actuator control strategy, the way is now open to compare the different actuator control strategies in the relevant frequency region up to 50 [Hz], without bothering about the high-frequency region including transmission line effects.

4.6.3 Experimental comparison of control strategies

In Fig. 4.27, a comparison of the different basic actuator control strategies is given, by showing the measured closed loop frequency responses $H_{\ddot{q}_d\ddot{q}}(j\omega)$, obtained under nominal conditions[3], i.e. the conditions on which the control designs were based. As far as the low-frequency region 1-15 [Hz] is concerned, the experimental results of Fig. 4.27 are in very good qualitative agreement with the simulation results of Section 4.3 (compare Fig. 4.7, 4.9 and 4.11). Note hereby, that quantitative differences were to be expected, as the controller gains are different. So, it can be stated, that the experiments validate the simulation results and corresponding conclusions on the different actuator control strategies.

A major difference between the simulation results of Section 4.3 and the measurements given in Fig. 4.27 lies in the frequency region 15-50 [Hz]. After an anti-resonance at about 18 [Hz], there is some additional dynamics in the region 20-40 [Hz], while beyond 40 [Hz] both gain and phase roll off again. As mentioned earlier, these effects can be ascribed to parasitic dynamics of the test rig and the base, which are not included in the simulations. For instance, the anti-resonance can be physically explained by the first bending mode of the horizontal lever of the test rig (refer to Fig. 3.6 on page 147); at that frequency the load at the actuator side does not move nor accelerate, while the pressure difference causes the actuator to counteract the oscillating motion of the load at the other side of the lever. This also explains, why the pressure difference transfer function of Fig. 4.26 does not show this anti-resonance.

Obviously, the observed high-frequency dynamics are not typical for the hydraulic actuator under consideration, but for the system that is driven by the actuator. In that sense, it is acceptable that the actuator control strategies that include a pressure difference reference cause high peaking in the acceleration transfer function $H_{\ddot{q}_d\ddot{q}}(j\omega)$ in the region 20-40 [Hz]. Acutally, it would be a matter of adjusting the feedforward model in the reference generator, rather than adjusting the actuator control strategy, to avoid this peaking. This is especially makes sense, because the pressure difference transfer function $H_{\overline{\Delta P}_d\overline{\Delta P}_i}(j\omega)$ in Fig. 4.26 shows desirable performance (no peaking).

As an overall evaluation of Fig. 4.27, it is easily seen, that the cascade-ΔP controller `E.Ctr.5` gives the best performance, in accordance with simulation results. As explained in Subsection 4.3.4, this can be ascribed to the implicit velocity feedforward that is present due to the velocity compensation term, see (4.1). This is further illustrated by showing

[3]In the remainder, all frequency responses have been obtained in the middle position q_0^0.

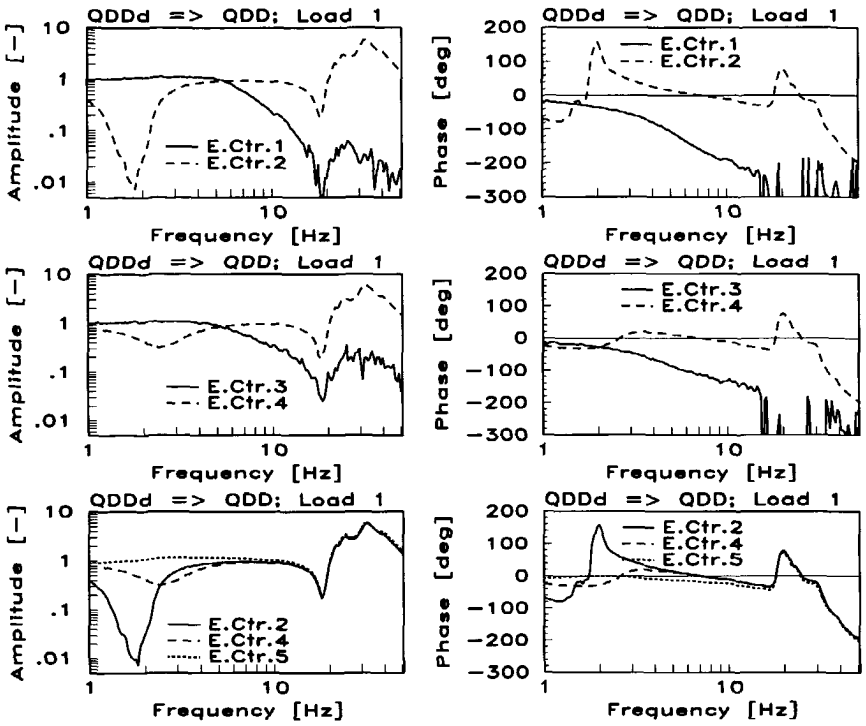


Fig. 4.27: Measured acceleration frequency responses $H_{\ddot{q}_d\ddot{q}}(j\omega)$ for different actuator control strategies, obtained with `Load 1`

the effect of velocity feedforward for the other control strategies in the next Subsection.

4.6.4 Improved performance by velocity feedforward

The addition of a velocity feedforward term considerably improves the performance, as Fig. 4.28 shows for the state feedback case. Though not shown, the position control strategy shows similar improvement by velocity feedforward, just like expected from the simulation results given in Fig. 4.13. What is also clearly confirmed by the result of Fig. 4.28, is the fact that in the one degree-of-freedom case, considered here, the cascade-ΔP control is essentially similar to state feedback with velocity feedforward. Actually, the performance obtained with this controller is quite satisfactory; there is only some slight variation in gain in the frequency region until about 15 [Hz], while the phase lag remains very small, at most $\approx$45 [deg] at 15 [Hz].

Besides the frequency domain results, the time domain results of Subsection 4.6.7 also show a clear performance improvement by velocity feedforward. Therefore, the application of velocity feedforward in a hydraulic servo-system, whenever a velocity reference is available, is strictly recommendable. For this reason, when considering the control strategies including reference signals in the remainder, velocity feedforward is always included, i.e. `E.Ctr.2a/4a` are considered and not `E.Ctr.2/4`.

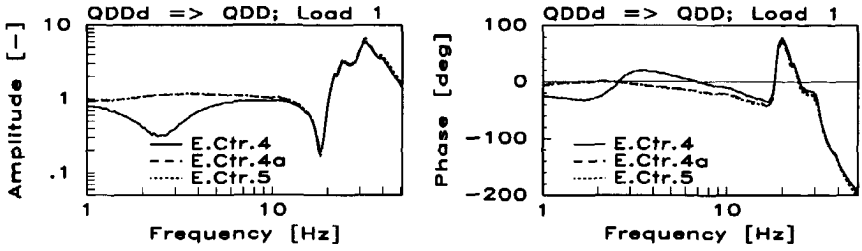


Fig. 4.28: Effect of velocity feedforward; measured acceleration frequency responses $H_{\ddot{q}_d\ddot{q}}(j\omega)$ obtained with Load 1; only state feedback E.Ctr.4 (solid), state feedback with velocity feedforward E.Ctr.4a (dashed) and cascade-ΔP control E.Ctr.5 (dotted)

4.6.5 Load sensitivity of actuator control performance

So far, the closed loop performance of the actuator control strategies was only evaluated for the nominal case, i.e. under load conditions where the controllers were designed for, namely Load 1. In order to test the sensitivity of the different control strategies to varying loads, a number of measurements has been performed under a different load condition, namely Load 2, as specified on page 243. Thereby, the settings of the (inner loop) actuator control were kept the same for both load conditions, while the reference generator was adapted to the load condition, and also the outer loop control settings in the case of the cascade-ΔP controller E.Ctr.5, see Table 4.8.

For the position control schemes E.Ctr.1 and E.Ctr.2a respectively, the effect of the different load conditions is shown in Fig. 4.29. It can be concluded from these results, that the sensitivity of the closed loop performance to varying loads is considerably reduced by the use of the pressure difference reference as expected from simulations, if the mid-frequency range 3-15 [Hz] is considered. Especially the phase lag shows considerable difference for E.Ctr.1 under different load conditions, while the phase lag of E.Ctr.2a is rather insensitive to the load variations in this frequency range. However, for the low- and the high-frequency ranges, E.Ctr.2a appears to be more sensitive to load variations. But, at this point, some relativation is justified.

The larger load sensitivity of E.Ctr.2a in the low-frequency region 1-3 [Hz] is actually caused by the input non-linearity (2.124) of the actuator. Because of the relatively large static load component in Load 2, this non-linearity causes an effective decrease in the low-frequency velocity gain of the system, as mentioned earlier on page 247. Unless a non-linear controller is applied to eliminate this non-linearity, as discussed in Subsection 4.6.6, this non-linearity will make the low-frequency performance sensitive to static load variations, especially for smaller position feedback gains. Thus, given the input non-linearity of the actuator, E.Ctr.2a is more sensitive to variations in the static load than E.Ctr.1.

Concerning the high-frequency region 15-50 [Hz], E.Ctr.2a seems to be more sensitive to load variations than E.Ctr.1. However, this is not really the case, in the sense that the performance of E.Ctr.1 is so bad in this region, that these differences can not be observed. In fact, the performance of the actuator control loop E.Ctr.2a is not sensitive to the different load conditions, but the excited load dynamics are different. Because the loads at the one side of the test rig (opposite the actuator, see Fig. 3.6) were removed in

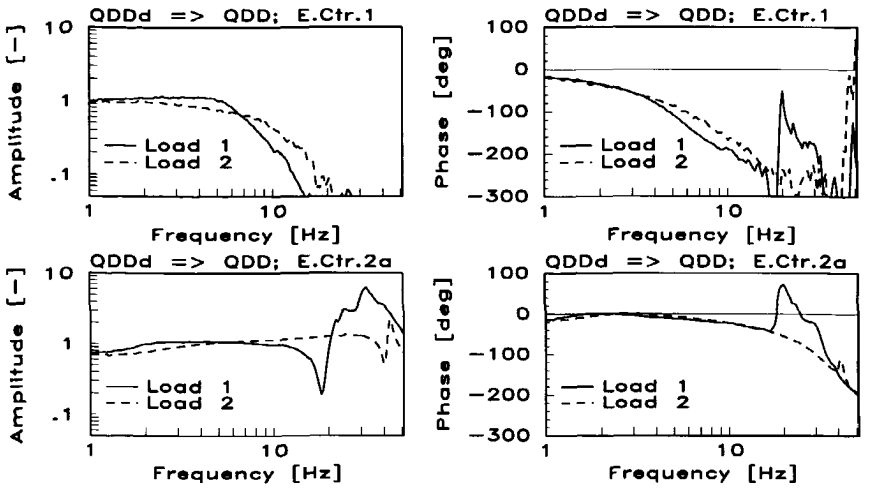


Fig. 4.29: Effect of different load conditions `Load 1` (solid) and `Load 2` (dashed); measured acceleration frequency responses $H_{\ddot{q}_d\ddot{q}}(j\omega)$; position servo control without pressure difference reference `E.Ctr.1` (upper) and with pressure difference reference plus velocity feedforward `E.Ctr.2a` (lower)

case of `Load 2`, the anti-resonance due to the first bending mode of the horizontal lever has shifted to a frequency of 40 [Hz]. This just makes the difference between the results of `Load 1` and `Load 2` in the high-frequency region beyond 15 [Hz]. Note that the phase lag at 50 [Hz] (so beyond the parasitic dynamics) is independent of the load condition, indicating that the actuator control loop itself is not sensitive to the load condition.

So, in conclusion on Fig. 4.29, the actuator control loop `E.Ctr.1` is principally dependent on the load condition in the control relevant mid-frequency range, while the actuator control strategy `E.Ctr.2a` is only sensitive to different loads due to parasitic effects in the low- and high-frequency region respectively. Although the results are not shown here, exactly the same conclusion holds for the measurements with the state feedback controllers `E.Ctr.3` and `E.Ctr.4a`, again confirming expectations from simulation results in Section 4.3.

Although the application of a good pressure difference reference signal in the control strategy almost eliminates the effect of the load inertia on the control performance, theoretically there is still some difference between the different load conditions, at least for position and state feedback control. The reason is, that the closed loop dynamics (poles) depend on the load inertia. The cascade-ΔP controller however, with adapted outer loop gains, should be insensitive to different load conditions. An experimental verification of this issue is given in Fig. 4.30. The upper plots show the load dependence of the state feedback controller `E.Ctr.4a` and the lower plots that of the cascade-ΔP controller `E.Ctr.5`, both with gains given in Table 4.8.

At first sight, there is no difference between the load sensitivity of the state feedback controller `E.Ctr.4a` and the cascade-ΔP controller `E.Ctr.5`. Only a very close look at the results shows minor differences; `E.Ctr.5` appears to be slightly more sensitive to (static) load variations in the region 1-2 [Hz]; `E.Ctr.4a` appears to show slightly more variation

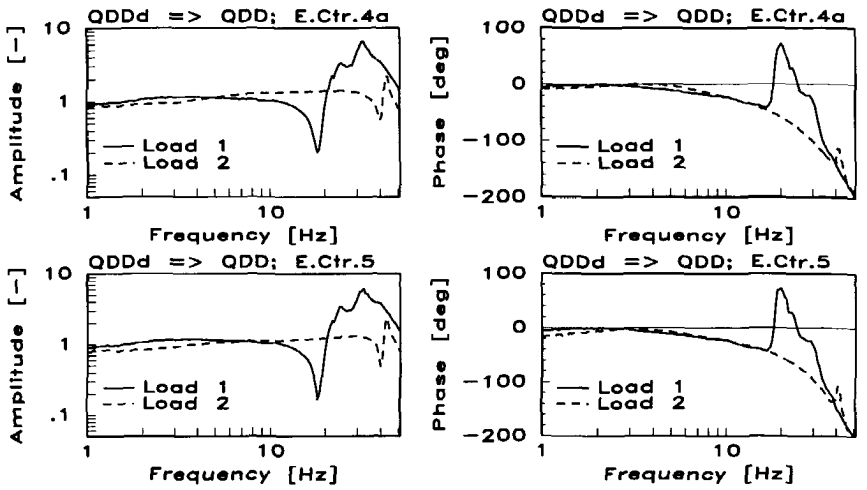


Fig. 4.30: Effect of different load conditions `Load 1` (solid) and `Load 2` (dashed); measured acceleration frequency responses $H_{\ddot{q}_d\ddot{q}}(j\omega)$; full state feedback control with velocity feedforward `E.Ctr.4a` (upper) and cascade-ΔP control `E.Ctr.5` (lower)

in phase in the mid-frequency region 3-9 [Hz]. This latter effect is the expected result of varying closed loop dynamics due to varying (inertial) load.

In practice, however, the discussed differences are not that relevant, and both control strategies perform equally well. Even when the results of `E.Ctr.4a` in Fig. 4.30 are compared with those of `E.Ctr.2a` in Fig. 4.29, it appears that there is hardly any difference in the load sensitivity of the control performance of the two. So, it can be concluded from these two Figures, that the load sensitivity is almost eliminated by proper feedforward of the desired signals, while the closed loop dynamics (determined by the feedback gains) play only a minor role in the load sensitivity of the performance.

Despite the fact that the effect of the closed loop dynamics on the load sensitivity is small, the load dependence itself is not negligible, especially not in the low-frequency region. It was already mentioned before, that the input non-linearity of the actuator plays an important role here. Therefore, the possible benefit of non-linear control to eliminate this non-linearity is discussed in the next Subsection.

4.6.6 Effect of non-linear control

In Subsection 4.3.6, on page 221, a non-linear control term (4.2) was proposed, which should eliminate the effect of the basic non-linearity of the hydraulic servo-system, namely the load dependent valve flow according to (2.124) (given on page 114). In order to verify this experimentally, the controller non-linearity (4.2) has been implemented in the digital controller, where the inverse static non-linearity $\hat{f}_2^{-1}$ has been implemented as a look-up table.

The effect of the application of this non-linear control on the measured frequency response is shown in Fig. 4.31, where the cascade-ΔP controller `E.Ctr.5` has been implemented. Clearly, there is hardly any load dependence left in the low-frequency region,

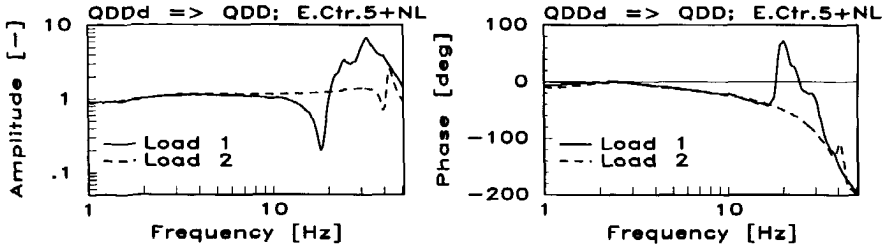


Fig. 4.31: Effect of different load conditions Load 1 (solid) and Load 2 (dashed) while applying non-linear control; measured acceleration frequency responses $H_{\ddot{q}_d\ddot{q}}(j\omega)$ obtained with cascade-ΔP control E.Ctr.5

contrary to the linear case, given in Fig. 4.31. So, the non-linear term in the controller is quite effective.

Although the results are not shown here, application of the non-linear term (4.2) in the other control strategies E.Ctr.2a and E.Ctr.4a also results in considerable reduction of the load sensitivity in the low-frequency region. However, a complete elimination of the load sensitivity in the low-frequency region is not achieved, like for E.Ctr.5. So, in the end, when non-linear control is applied, the cascade-ΔP controller E.Ctr.5 appears to be the least sensitive to load variations, as was expected from simulations.

Although the result of Fig. 4.31 shows a nice improvement by means of non-linear control, it does not show the benefits explicitly in terms of reduced sensitivity with respect to static loads and linearization of the amplitude dependent behaviour, like the simulation results of Subsection 4.3.6. Therefore, these simulation results have been experimentally verified; the results are discussed subsequently.

The first result concerns the tracking of a triangular reference signal with Load 2, in order to investigate the effect of non-linear control as a compensation for the load dependence of the servo-valve flow. The result is given in Fig. 4.32; it is actually an experimental verification of the simulation result of Fig. 4.14 on page 222. Obviously, a nice reduction of the position tracking error is achieved by the non-linear term in the controller, which corresponds to a compensation for the difference in velocity gain between upward and downward motion. Note also, that the control error in the pressure difference $\overline{\Delta P_i}$ is almost symmetric in case of non-linear control, contrary to the other case. Apparantly, the non-linear control term (4.2) does correctly compensate for the asymmetric behaviour due to the static load of Load 2.

The other result of the non-linear control term (4.2) concerns its effect on the amplitude dependence; this is shown in Fig. 4.33. The Figure gives measured amplitude responses at a frequency of 5 [Hz] for Load 2, corresponding to the simulations of Fig. 4.15 on page 222. Some remarks on the results:

- The non-linear control has slightly linearized the non-linear system behaviour due to the non-linear flow characteristic of the servo-valve: the amplitude response is reasonably flat for input amplitudes $A_r > 2$ [mm], contrary to the case of linear control. This corresponds to the simulation result.
- The non-linear control term causes a small gain increase to compensate for the gain reduction due to the static load. This also agrees with expectations from simulations.
- The behaviour for small amplitudes is strongly affected by Coulomb friction effects,

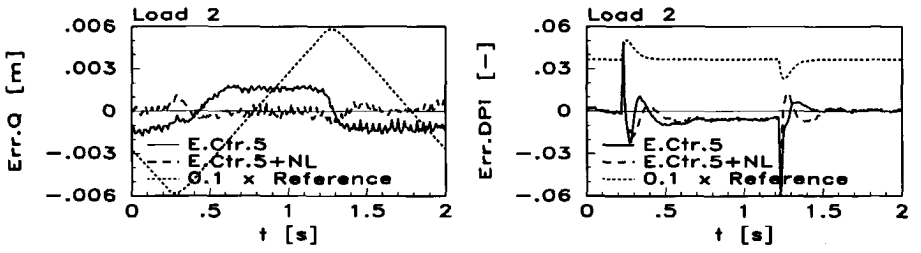


Fig. 4.32: Effect of non-linear control; measured closed loop time responses for cascade-ΔP control `E.Ctr.5` with `Load 2`; errors in position responses (left) and errors in pressure difference responses (right); linear control (solid), non-linear control (dashed); 0.1 x reference (dotted)

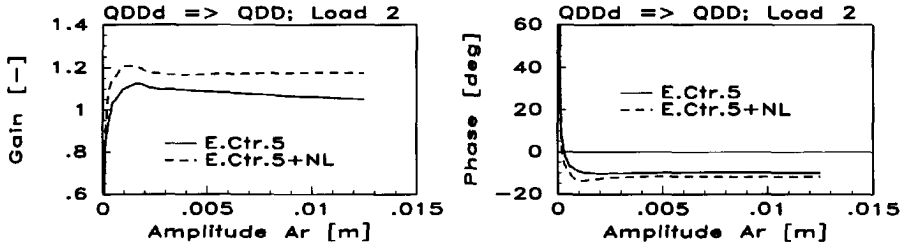


Fig. 4.33: Effect of non-linear control with `Load 2`; measured acceleration amplitude responses $N^{5\,\mathrm{Hz}}_{\ddot{q}_d\ddot{q}}(A_{\bar{r}})$ for cascade-ΔP control `E.Ctr.5` linear control (solid) and non-linear control (dashed)

which were neglected in the simulation. Obviously, the controller non-linearity does not compensate for these effects.

Summarizing the effect of non-linear control under experimental conditions, it may be stated that it allows a final performance improvement of the hydraulic actuator control. It effectively reduces the load sensitivity in the low-frequency region, especially the non-linear effect of a static load on the velocity gain of the actuator, and moreover it reduces the amplitude dependence of the closed loop dynamics as a result of the non-linear flow characteristic of the servo-valve.

In fact, with the discussion of the inclusion of the non-linear term (4.2) in the controller, the experimental evaluation of the performance of the different actuator control strategies is completed. Although this evaluation primarily has taken place in the frequency domain, the conclusions also hold for the time domain. This is shown in the next Subsection, where the experimental evaluation of control strategies is concluded, with some time domain results at hand.

4.6.7 Evaluation time domain performance and conclusions

In normal operation of a hydraulic servo-system, the basic requirement on the actuator control is to to perform well in the time domain, generally with unknown drive signals. Therefore, a number of measurements has been performed in the time domain, exciting

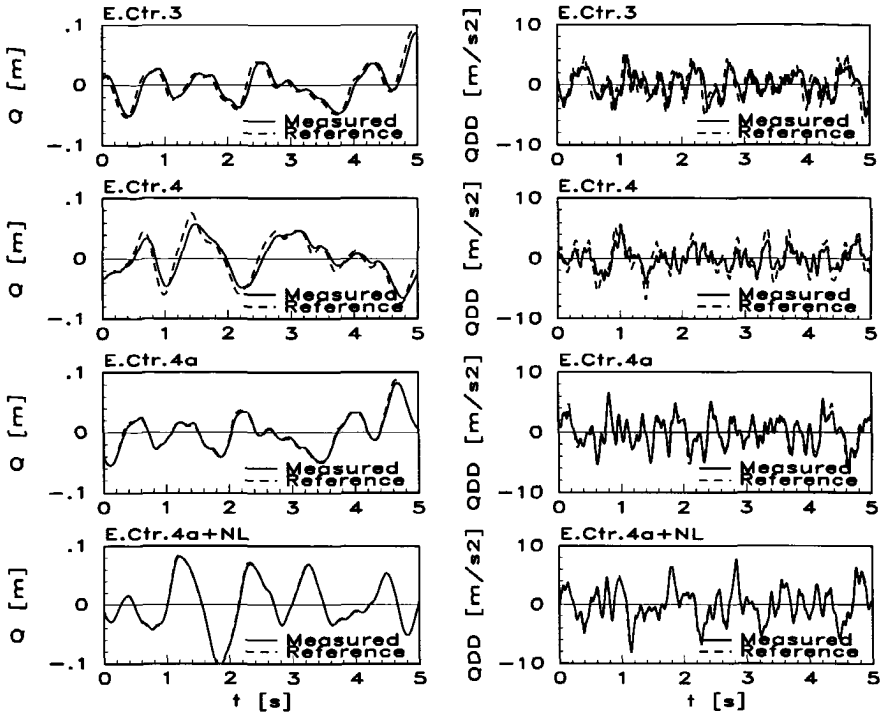


Fig. 4.34: Evaluation of actuator control performance in time domain with random source signal $\bar{r}$ and `Load 2`; measured position responses (solid,left), acceleration responses (solid,right) and references (dashed); state feedback `E.Ctr.3` (1st row), state feedback including references `E.Ctr.4` (2nd row), including velocity feedforward `E.Ctr.4a` (3rd row) and including non-linear term (4th row)

the system with a randomly varying source signal $\bar{r}$, which should support the frequency domain results of the preceding Subsections. The experimental conditions were just like described in Subsection 4.6.1.

In order to give a first impression of the achieved performance in the time domain for some control strategies, a number of time recordings is shown in Fig. 4.34, with measured position responses in the left plots, and accelerations in the right ones. The corresponding reference signals are given by a dashed line. It is directly clear from these results, which are obtained with `Load 2`, that the performance is successively improved by:

- using a pressure difference reference (`E.Ctr.4` shows considerably less phase lag than `E.Ctr.3`, especially in the acceleration, be it that the position tracking is worsened),
- adding velocity feedforward (tracking of both position and acceleration is much better for `E.Ctr.4a` than for `E.Ctr.4`),
- applying non-linear control (whereas `E.Ctr.4a` still shows some phase lag for fast upward motions, especially in the position response, this lag is almost eliminated by the non-linear action of `E.Ctr.4a+NL`).

Although Fig. 4.34 gives a nice indication of the achieved performance, it does not

provide a clear overview of the performance of the different control strategies under different load conditions. For that purpose, a much larger number of time domain recordings would have to be displayed. However, instead of doing that, the time domain performance is evaluated by means of two time domain error criteria V_q and $V_{\ddot{q}}$. These criteria serve as performance measures for the position tracking and the acceleration tracking respectively, and are defined as follows:

$$V_q = \frac{1}{N}\sum_{i=1}^{N}[q_{d,i} - q_i]^2 \qquad V_{\ddot{q}} = \frac{1}{N}\sum_{i=1}^{N}[\ddot{q}_{d,i} - \ddot{q}_i]^2 \tag{4.13}$$

These criteria are evaluated on time domain recordings, consisting of N samples, like given in Fig. 4.34. The results of this evaluation, for different basic actuator control strategies, both for `Load 1` and for `Load 2`, are shown in Table 4.9, where the applied controller settings are given in Table 4.8 on page 252. In a similar way, the effect of non-linear control on the time domain performance is evaluated, as well as the difference between state feedback control `E.Ctr.4a` and cascade-ΔP control `E.Ctr.5`. The results of this evaluation are given in Table 4.10.

	E.Ctr.1	E.Ctr.2	E.Ctr.2a	E.Ctr.3	E.Ctr.4	E.Ctr.4a
V_q; Load 1	$2.7\ 10^{-4}$	$5.4\ 10^{-4}$	$8.5\ 10^{-6}$	$1.2\ 10^{-4}$	$1.9\ 10^{-4}$	$6.0\ 10^{-6}$
V_q; Load 2	$2.1\ 10^{-4}$	$6.5\ 10^{-4}$	$2.3\ 10^{-5}$	$9.5\ 10^{-5}$	$1.3\ 10^{-4}$	$1.1\ 10^{-5}$
$V_{\ddot{q}}$; Load 1	$6.6\ 10^{-2}$	$2.6\ 10^{-2}$	$2.6\ 10^{-3}$	$3.9\ 10^{-2}$	$1.5\ 10^{-2}$	$2.9\ 10^{-3}$
$V_{\ddot{q}}$; Load 2	$4.7\ 10^{-2}$	$4.0\ 10^{-2}$	$3.9\ 10^{-3}$	$3.1\ 10^{-2}$	$1.4\ 10^{-2}$	$4.2\ 10^{-3}$

Table 4.9: Experimental tracking error levels for different control strategies

	E.Ctr.4a	E.Ctr.4a+NL	E.Ctr.5	E.Ctr.5+NL
V_q; Load 1	$6.0\ 10^{-6}$	$9.6\ 10^{-7}$	$6.2\ 10^{-6}$	$1.1\ 10^{-6}$
V_q; Load 2	$1.1\ 10^{-5}$	$3.3\ 10^{-6}$	$1.8\ 10^{-5}$	$4.7\ 10^{-7}$
$V_{\ddot{q}}$; Load 1	$2.9\ 10^{-3}$	$1.8\ 10^{-3}$	$2.6\ 10^{-3}$	$1.7\ 10^{-3}$
$V_{\ddot{q}}$; Load 2	$4.2\ 10^{-3}$	$1.9\ 10^{-3}$	$4.0\ 10^{-3}$	$2.6\ 10^{-3}$

Table 4.10: Effect of non-linear control on experimental tracking errors

The presented experimental tracking error levels give rise to a number of conclusions, which are in good agreement with the frequency domain results of this Section, so that they recapitulate the experimental evaluation of control strategies for hydraulic actuators:

- Inclusion of the pressure difference reference signal with increased pressure difference feedback gain improves the tracking of the desired acceleration, which mainly contains high-frequency components. However, the tracking of the desired position, with mainly low-frequency components, is worsened. (Compare `E.Ctr.1` to `E.Ctr.2` and

E.Ctr.3 to E.Ctr.4.) The reason is the introduction of a pair of zeros in the low-frequency region, see Fig. 4.27, as long as no velocity feedforward is applied.

- A major performance improvement is achieved by means of velocity feedforward (E.Ctr.2a and E.Ctr.4a). This holds for position control and for state feedback control; both for Load 1 and Load 2; as well with respect to position tracking as to acceleration tracking. Only with velocity feedforward included, the real benefit of high gain pressure difference feedback can be exploited.
- As the application of velocity feedback (full state feedback) allows higher feedback gains, a higher performance can be achieved than without velocity feedback. This mainly holds for the position tracking. However, the high feedback gains tend to introduce some acceleration noise, reducing the benefits for acceleration tracking (compare E.Ctr.2a to E.Ctr.4a).
- The position control strategies without feedforward of other reference signals (E.Ctr.1 and E.Ctr.3) perform better with Load 2 than with Load 1. This is caused by the load sensitivity: the closed loop dynamics are faster for Load 2.
- The control strategies including reference feedforward and velocity feedforward, but without a non-linear controller term, perform better with Load 1 than with Load 2. This is mainly the result of the fact that Load 2 contains a large static component, which causes tracking errors due to the input non-linearity of the actuator.
- Non-linear control provides a considerable improvement of the tracking performance in the time domain, see Table 4.10. It effectively compensates for the load sensitivity of servo-valve flow. This is especially important if the actuator is loaded heavily, like in the time domain experiments considered here.
- Considering the overall performance, E.Ctr.4a+NL and E.Ctr.5+NL are definitely the best control strategies. For the one degree-of-freedom motion system considered here, there is no relevant difference in experimental performance between the state feedback controller E.Ctr.4a+NL and the cascade-ΔP controller E.Ctr.5+NL.

With these conclusions ending the experimental evaluation of hydraulic actuator control strategies, the Chapter can be concluded.

4.7 Conclusions

Considering motion control problems in general, three main parts can be distinguished in the control strategy: trajectory generation, feedforward control and feedback control. Moreover, in the case of high-performance applications of hydraulic actuators in multi DOF motion systems, it is useful to distinguish two control levels. This distinction reflects the physical structure of the motion system, where the (common) mechanical load is driven by a number of individual hydraulic actuators. The high-level control then comprises a feedforward part and a feedback part, and takes care of the non-linear, multivariable load dynamics, which might affect the motion of the individual actuators. The outputs of the high-level control form the inputs (command signals) for the low-level feedback controllers, which have to follow the command signals as close as possible. These low-level feedback loops, for each individual actuator, give the actuators the character of force generators.

Considering the one DOF, as it is done in this Chapter, the distinction between high-level control and low-level control is not essential. What is quite important, is the number and type of references that are available for the feedback controller. This depends on the

application. In fact, it depends on the available trajectory generator and the feedforward controller, combined in the so-called reference generator, which type of feedback control strategy should be applied for a single hydraulic actuator.

If only a position reference is available, the possibilities are restricted to output feedback or state feedback including a state estimator. Simulations and experiments show, that the performance in terms of bandwidth is restricted to about the natural frequency of the actuator without velocity feedback. With velocity feedback, a larger bandwidth can be achieved, depending on the signal conditions. The closed loop system shows a large phase lag.

If the reference generator or the high-level control includes a model of the actuator load, the desired actuator pressure difference can be fed forward. Thereby, a trade-off can be made in the feedback design between position control and pressure difference control of the actuator. If the feedforward model is reliable, the pressure difference control can be emphasized and major improvements in the performance of the actuator control can be achieved, provided that velocity feedforward is included.

Whenever a desired velocity signal is available, it should be fed forward directly (with the correct velocity gain) to the valve control signal. This does not affect the stability or closed loop dynamics of the system, but it eliminates tracking errors due to the integrating character of the hydraulic servo-system. Combined with emphasis on pressure control and feedforward of a pressure difference reference, relatively high bandwidths from desired to actual motion signals can be achieved, with small phase lags. Thus, nice results have been obtained on simulation level, which have also been verified experimentally.

The dominant non-linearity of the hydraulic servo-system, namely the non-linear load dependent valve flow, can be (partly) compensated for by a including a non-linear term in the controller. This technique is quite effective, especially insimulations, but also under experimental conditions. A considerable performance improvement can be realized, for instance if a large static load is present.

The addition of velocity feedback to position and pressure difference feedback can improve the closed loop performance of the servo-system. As a velocity transducer is often not available, this will require a velocity estimator. Some possibilities in this respect are direct velocity estimation by filtering the position signal, the application of a Kalman filter or the use of a reduced order state estimator. Although the optimal solution will depend on the experimental conditions of a specific application, the design of a Kalman filter appears to be quite a suitable technique to obtain a high-quality estimated velocity.

If a good (estimated) velocity signal is available, the cascade-ΔP control strategy is quite valuable as actuator control strategy. The reason is, that it basically realizes a decoupling between the dynamics of the pressure difference control loop and the control of the load dynamics; the cascade ΔP controller gives the hydraulic actuator the character of a pure force generator. Thus, it allows a clear distinction between the (feedback) control of the hydraulic actuator, and the (possibly non-linear, multivariable) control of the load dynamics. So, the cascade-ΔP control strategy fits well in two-level control strategy, which is especially useful for multi DOF systems. It might be noted, however, that for the one DOF case, the cascade ΔP control strategy is principally equivalent to state feedback including velocity feedforward. This equivalence is confirmed by experimental results.

Besides the input non-linearity of the actuator, which can be compensated for by non-linear control, there are two important properties of a hydraulic servo-system, which do seriously restrict the attainable control performance for certain applications, namely valve

dynamics and transmission line dynamics. Both form a limitation for the attainable bandwidth of the pressure difference control loop. If the desired pressure difference control bandwidth approaches the magnitude of the dominant poles of the valve dynamics, stability problems are encountered. More serious is the case that the first resonance frequency related to transmission line dynamics lies around or below the bandwidth of the servo-valve. In that case, very small pressure difference feedback gains may already destabilize the control loop.

Not only do valve and transmission line dynamics restrict the attainable performance, modelled non-linearities in these dynamics, like for instance amplitude dependent gains and position dependent actuator dynamics, do pose the robustness issue in the control design. Actually, the model-based design of robust dynamic pressure difference control loops, utilizing modern control techniques, is still an open research issue.

Besides that model-based control design forms a proper approach to the control problem of an existing servo-system, it is also shown that it is recommendable to utilize a-priori knowledge of and insight in the behaviour of a hydraulic servo-system in the system design, if possible. Especially a proper servo-valve choice, proper pressure difference transducer placement and minimization of the transmission line lenght can avoid difficult control problems.

Chapter 5

Model-based cushioning design

5.1 Introduction

Whereas the previous Chapter was devoted to model-based control design, this Chapter will deal with the model-based design of two types of cushioning for hydraulic actuators. These buffers are meant to allow proper and safe operation of the actuator in case of control failure. Starting point thereby is the worst-case-scenario, that the servo-valve delivers a maximum flow to the actuator, such that the actuator moves towards the end of its stroke with full speed. In order to provide inherent safety, a hydraulic-mechanical cushioning is applied, which dissipates the kinetic energy of the inertia of the load and reduces the velocity smoothly to zero.

Obviously, such a cushioning feature is extremely important in applications, where human safety is involved in the proper operation of the servo-system. A good example is the SIMONA flight simulator motion system, discussed in Section 1.2. Actually, it has been this application, which has motivated the work on model-based cushioning design , described in this Chapter. The reason is, that the SIMONA flight simulator had to be provided with properly functioning cushionings. Although commercially available flight simulator motion systems do have such cushionings, the knowledge required to design these cushionings, is considered to be proprietary information by the manufacturers. Moreover, this knowledge is not available in literature.

Although it might have been possible to arrive at properly functioning cuhsionings by means of trial and error, it is clear that this would have been costly. Moreover, the cushioning design would have been highly dependent on the specific application, that was considered. However, with the knowledge of the dynamic behaviour of the hydraulic actuator, available from the physical modelling, identification and control design, as reported in this thesis, the way is open to a model-based approach. This not only leads to a direct solution for the specific cushioning design problem considered here, but actually leads to a design procedure, which is more generally applicable to a wide variety of hydraulic servo-systems, that can be represented by the developed models.

The specific cushioning design problem to be considered in this Chapter, is concerned with the hydraulic actuator, described in Section 3.3, which is to be applied in the SIMONA Research Simulator. This actuator is of the double-concentric type. Although this construction allows the realization of a symmetric actuator in the sense that both piston areas are equal, the construction itself is *not* symmetric. This is the reason, why two different types of cushioning have been applied in this actuator; the cushioning for downward

motion is of the peg-in-hole (PIH) principle, while the cushioning for upward motion is based on closing-drain-holes (CDH), as will be explained further in Subsection 5.2.1. The arguments that led to this choice, have been investigated and formulated in previous work by Mans [90], and are strongly related to the (im)possibilities of the constructive design and to costs of manufacturing.

In the discussion of the cushioning design in this Chapter, the physical models, as presented in Chapter 2, play an important role. In Section 5.2, the basic actuator model is adapted such as to include models of the two mentioned types of cushioning, respectively. After that, a model-based design procedure is presented in Section 5.3, which provides a structural approach to cushioning design, given specifications on the allowed accelerations during the cushioning stage. Finally, Section 5.4 gives an experimental evaluation, as well with respect to the validity of the used models as with respect to the realized performance of the designed cushionings.

5.2 Modelling of cushionings

After a description of the working principle of the safety buffers to be designed, given in Subsection 5.2.1, the modelling of these cushionings is treated in Subsection 5.2.2 and 5.2.3. These Subsections deal with the peg-in-hole (PIH) cushioning and with the closing-drain-holes (CDH) cushioning, respectively. So, each type of cushioning is separately modelled. Finally, the choice of parameters for the simulation models of the cushionings is discussed in Subsection 5.2.4, together with the intermediate validation of the models.

5.2.1 Description of the cushionings

Given the configuration of the double-concentric symmetric actuator to be considered here, the PIH cushioning has been chosen for the downward motion, and the CDH cushioning for the upward motion. The working principle of these cushioning types is illustrated in Fig. 5.1.

Both cushioning types are based on the principle, that the drain oil flow is restricted mechanically, if the piston approaches the end of its stroke. Due to this restriction, the pressure in the related actuator chamber increases rapidly, causing a braking force on the piston. This force reduces the piston velocity during the cushioning stage, so that the drain oil flow reduces again and the pressure in the actuator chamber releases again after the cushioning stage.

In the PIH cushioning, for the downward motion, the drain flow is restricted during the cushioning stage, because the peg enters the hole of the drain line in the middle of the actuator if the piston approaches the end of its stroke. With the drain line being a cylindrical hole with a sharp edge, the geometry of the peg determines the restriction of the oil flow in the course of the cushioning stage. This fact is exploited when designing the peg geometry in order to obtain a smooth cushioning behaviour.

The principle of the CDH cushioning is slightly different. At a certain distance from the end of the stroke, there is a row of regular drain holes. The number and diameter of these holes is large enough, to allow a drain flow at full actuator speed with negligible resistance. However, as soon as the piston head moves along these regular drain holes in the cylinder during the final part of the upward motion, they are (almost) closed. Only a very small

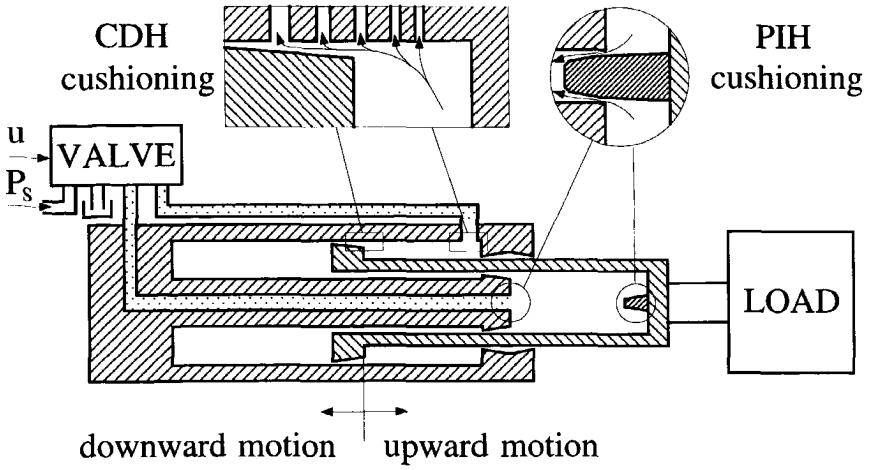


Fig. 5.1: Schematic drawing of double-concentric symmetric actuator with safety cushionings

drain flow is possible, due to the small clearance of the conical hydrostatic bearing of the piston head. If no additional drain holes were present, allowing a reasonable drain flow through a restriction with a large pressure drop, the sudden closure of the regular drain holes would cause the kinetic energy of the actuator to be accumulated by compression of the remaining oil volume. This would cause inadmissable high pressure peaks and a sudden badly damped stop of the actuator motion.

By adding extra drain holes, with sufficiently large resistance, which are closed subsequently during the course of the cushioning stage as the piston head moves along them, the drain flow during the cushioning stage can be controlled. Thereby, a reasonable increase of the chamber pressure will occur, necessary to brake the piston motion. Thus, like with the PIH cushioning, a smooth reduction of the piston velocity can be obtained.

After this description of the functionality of the cushionings, mathematical physical models are presented to describe the dynamic behaviour of the hydraulic actuator during the cushioning stage. Separate models for the PIH and the CDH cushioning are given subsequently in the following two Subsections.

5.2.2 Modelling of peg-in-hole (PIH) cushioning

After the definition of the geometry of the PIH cushioning, with corresponding geometrical variables and parameters, the modelling assumptions are given. With these assumptions, the mass and force balances of the actuator, previously given in Section 2.3, can be rewritten for the operational conditions during the cushioning stage. Finally, the crucial part in the modelling of the PIH cushioning is the modelling of the cushioning flow through the restriction, constituted by the narrow clearance of the peg entering the hole of the drain line.

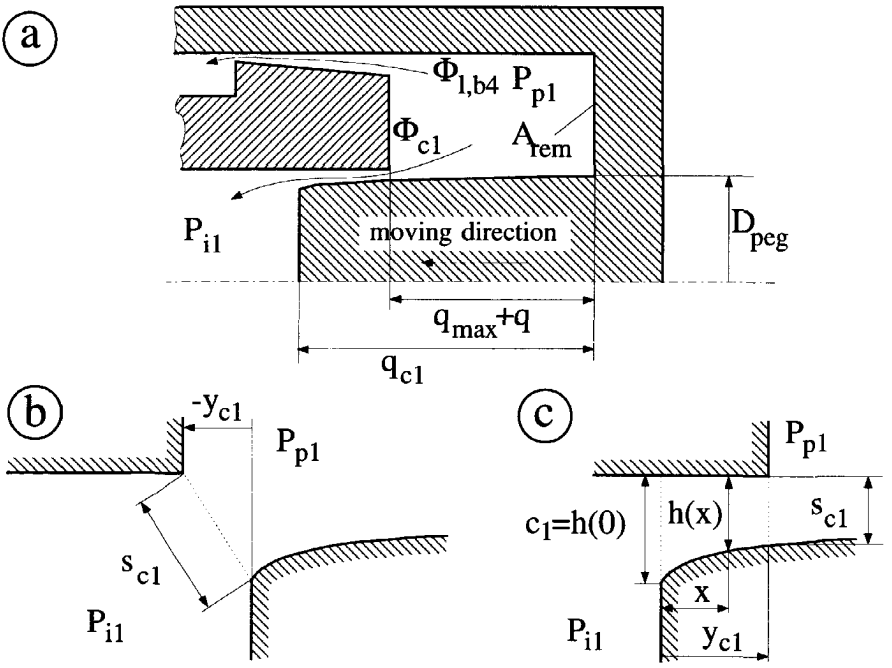


Fig. 5.2: Geometry and variable definition of PIH safety cushioning; overview (a); peg approaching hole (b); peg entering hole (c)

Definition of geometry

During the cushioning stage, the leftward moving peg enters the hole of the drain line as depicted in Fig. 5.2. The length of the cushioning is defined as q_{cl} and equals the length of the peg. The peg has a diameter D_{peg} and corresponding area $A_{peg} = \frac{\pi}{4} D_{peg}^2$. Therewith, the remaining circular area around the peg equals $A_{rem} = A_p - A_{peg}$. Finally, the distance over which the peg has entered the hole, is expressed as a function of the actuator position q as follows:

$$y_{cl} = -q_{max} + q_{cl} - q \tag{5.1}$$

Note, that this distance is negative, as long as the tip of the peg has not entered the hole, as indicated in subplot (b) in Fig. 5.2.

Modelling assumptions

For the modelling of the dynamic behaviour of the actuator during the cushioning stage, the following assumptions are made.

Assumption 5.2.1 *The actuator chamber and the drain line (transmission line) can be modelled as two separate compartments, each with uniform pressure distribution (see also Fig. 5.2):*

- *The cushioning compartment, with area A_{rem} and pressure P_{pl}.*

- *The drain compartment, with area A_{peg} and pressure P_{i1}*[1].

The walls of the compartments are assumed to be infinitely stiff.

Assumption 5.2.2 *The cushioning flow Φ_{c1} from the cushioning compartment into the drain compartment is:*

- *equal to the flow that is necessary to obtain identical pressure variations in both compartments, if the resistance of the PIH cushioning is negligibly small, i.e. if the peg is remote from the hole.*
- *equal to the flow corresponding to the pressure difference $P_{p1} - P_{i1}$ and the modelled resistance of the PIH cushioning, if this resistance is not negligible, i.e. if the peg is near or in the hole.*

Assumption 5.2.3 *The cushioning flow Φ_{c1} is assumed to be one-dimensional, i.e. rotational flow around the peg is neglected.*

Assumption 5.2.4 *The effect of frictional forces on the cushioning behaviour is neglected, i.e. $F_{vp} = F_{cp} = 0$.*

Assumption 5.2.3 is justified by the fact that the gap between peg and hole is very small. Comparable investigations for hydrostatic bearings [16, 139] have shown, that rotational flow effects are negligible.

Besides these basic assumptions, some weak assumptions are made concerning the servo-valve: valve dynamics are left out of consideration, while the servo-valve spool is assumed to be of the critical-centre type. These assumptions are justified by the fact that the cushioning analysis is restricted to steady state valve openings, where the actuator runs with constant (maximum) velocity towards the end of its stroke.

Mass and force balances

With the given assumptions, the mass and force balances of the actuator can be rewritten. Assumption 5.2.1 makes that the mass balance for the first actuator chamber is split into two mass balances; the mass balance for the second actuator chamber remains unchanged, see (2.34) and also Fig. 2.23 on page 56:

$$\begin{aligned} \dot{P}_{p1} &= \frac{E}{A_{rem}(q_{max}+q)}\left(-\Phi_{c1} - \Phi_{l1} - A_{rem}\dot{q}\right) \\ \dot{P}_{i1} &= \frac{E}{A_{peg}(q_{max}-q_{c1}+q)+V_{i1}}\left(\Phi_{p1} + \Phi_{c1} - A_{peg}\dot{q}\right) \\ \dot{P}_{p2} &= \frac{E}{A_p(q_{max}-q)+V_{l2}}\left(-\Phi_{p2} - \Phi_{l2} + A_p\dot{q}\right) \end{aligned} \tag{5.2}$$

In these equations, the leakage flows Φ_{l1} and Φ_{l2} are given by (2.35) and (2.36) respectively, given on page 57. The valve flows Φ_{p1} and Φ_{p2} are given by the valve flow equation (2.23) on page 37, or a simplified version of it.

With the different pressures defined by (5.2), the equation of motion or the force balance for the piston reads like (2.38), with frictional forces neglected according to Assumption 5.2.4:

$$M_p\ddot{q} = A_{rem}P_{p1} + A_{peg}P_{i1} - A_pP_{p2} + F_{ext} \tag{5.3}$$

[1]This is a slight abuse of notation: because the pressure distribution in the drain line is assumed to be uniform, the pressure at the end of the line equals the pressure at the valve side.

In this equation, F_{ext} is the external force acting upon the piston, e.g. a gravity force.

What still remains to be defined, and what is also the crucial part of the model, is the cushioning flow Φ_{c1}. First, the cushioning flow will be defined for the case that the peg is *not* in the hole. After that, the situation with the peg in the hole will be discussed.

PIH cushioning flow - peg not in hole

Based on Assumption 5.2.2, two cases are distinguished in the modelling of the cushioning flow, dependent on the occurring cushioning flow resistance, which is related to the distance between peg and hole. A condition for the determination which case applies, is given later in this Subsection, namely by (5.7) on page 273.

The first case to be considered, corresponds to normal operation of the actuator, with a large distance between peg and hole, i.e. with negligible cushioning flow resistance. If the cushioning flow were related to this very small resistance and the pressure difference $P_{p1} - P_{i1}$, the resulting (simulation) model would contain an extremely fast pole. This can be avoided, by combining the mass balances of the cushioning compartment and of the drain compartment, and solving the cushioning flow Φ_{c1}, such that the derivatives of the pressures, $\dot{P}_{p1}$ and $\dot{P}_{i1}$, are forced to be equal. This gives:

$$\frac{E}{A_{rem}(q_{max}+q)}\left(-\Phi_{c1}-\Phi_{l1}-A_{rem}\dot{q}\right)=\frac{E}{A_{peg}(q_{max}-q_{c1}+q)+V_{l1}}\left(\Phi_{p1}+\Phi_{c1}-A_{peg}\dot{q}\right)\Leftrightarrow$$

$$\Phi_{c1}=\frac{\left[-\Phi_{l1}-A_{rem}\dot{q}-\frac{A_{rem}(q_{max}+q)}{A_{peg}(q_{max}-q_{c1}+q)+V_{i1}}\left(\Phi_{p1}-A_{peg}\dot{q}\right)\right]}{\left[1+\frac{A_{rem}(q_{max}+q)}{A_{peg}(q_{max}-q_{c1}+q)+V_{i1}}\right]} \tag{5.4}$$

Using this expression for the cushioning flow Φ_{c1} in (5.2), the pressure variations of P_{p1} and P_{i1} are identical. Thus, starting with equal pressures as initial conditions, the actuator model according to (5.2) and (5.3), with cushioning flow according to (5.4) is equivalent with the original actuator model without cushioning. This just what is desirable if the peg-hole distance is large enough according to the condition (5.7).

The other case to be considered, corresponds to the situation that the peg approaches the hole. In that case, according to Assumption 5.2.2, the cushioning flow is determined by the flow resistance of the peg-hole configuration. With a sharp edge of the hole, it is reasonable to do the following assumption:

Assumption 5.2.5 *If the peg has not entered the hole, the cushioning flow is a turbulent flow through the opening between the tip of the peg and the edge of the hole.*

Referring to Fig. 5.2(b), the area of the opening between the tip of the peg and the edge of the hole, for negative y_{c1}, is determined by the shortest distance s_{c1}, with c_1 the clearance between peg and hole at the tip of the peg:

$$s_{c1}=\sqrt{c_1^2+y_{c1}^2} \qquad y_{c1}\leq 0 \tag{5.5}$$

Thus, with πD_{peg} the circumference of the peg, the cushioning flow according to Assumption 5.2.5 can be described, with well known expressions for turbulent flow, as:

$$\Phi_{c1}=C_{d1}\pi D_{peg}s_{c1}\sqrt{\frac{2|P_{p1}-P_{i1}|}{\rho}}\mathrm{sgn}(P_{p1}-P_{i1}) \qquad y_{c1}\leq 0 \tag{5.6}$$

In this expression, the discharge coefficient is denoted by C_{d1}, in order to indicate that it concerns the discharge coefficient related to the PIH cushioning, which will be chosen different from the one related to the turbulent servo-valve flow, C_d, as discussed in Subsection 5.2.4.

In fact, the expression (5.6) allows the definition of a condition, to decide whether the cushioning flow should be determined by (5.4) or by (5.6). The idea is, that the flow resistance is considered negligible, if the distance s_{c1} is so large, that a maximum actuator flow $\Phi_{p,nom}$ through the restriction would cause a pressure drop less than 0.01 P_s. Using (5.6), this means that the cushioning flow resistance is negligible and that (5.4) should be used, *if*:

$$s_{c1} > \frac{\Phi_{p,nom}}{C_{d1}\pi D_{peg}\sqrt{0.01\frac{2P_s}{\rho}}} \qquad y_{c1} \leq 0 \tag{5.7}$$

If this condition is not met, the cushioning flow is computed with (5.6), as long as the peg has not entered the hole.

PIH cushioning flow - peg in hole

As soon as the tip of the peg has passed the edge of the hole when entering the hole, (5.6) should again be replaced by another expression; the geometry of the peg will have to be taken into account. Thereby, as indicated in Fig. 5.2(c), the geometry of the peg is described by the distance $h(x)$ between peg and hole, perpendicular to the hole, with x the distance from the tip of the peg. At the tip of the peg, this distance is denoted as the clearance, which is $c_1 = h(0)$. At the edge of the hole, the shortest distance, s_{c1}, should theoretically be taken perpendicular to the peg. However, because the slope of the peg is very small for normal cushioning configurations, it is simply taken as the distance perpendicular to the hole, so:

$$s_{c1} = h(y_{c1}) \qquad y_{c1} > 0 \tag{5.8}$$

With these remarks concerning the peg geometry, the question arises, how the flow through the gap between peg and hole is to be modelled, i.e. as a laminar flow or as a turbulent flow. Although this principally depends on the Reynolds number, the complexity of the flow in this configuration, at least for the dynamic case, makes it difficult to define the type of flow properly. Therefore, a number of optional, very simple assumptions on the flow through the PIH cushioning is considered, with corresponding expressions for the cushioning flow. Further investigation of the implications of the different assumptions with regard to the simulated behaviour of the cushioning will have to make clear, which assumption is most suitable.

Assumption 5.2.6 *The flow resistance of the PIH cushioning is dermined by the turbulent flow loss at the inlet, i.e. at the edge of the hole.*

With this Assumption, the cushioning flow depends highly on the geometry of the peg, as s_{c1} given by (5.8) determines the flow loss:

$$\Phi_{c1} = C_{d1}\pi D_{peg} s_{c1}\sqrt{\frac{2|P_{p1} - P_{i1}|}{\rho}}\mathrm{sgn}(P_{p1} - P_{i1}) \qquad y_{c1} > 0 \tag{5.9}$$

Assumption 5.2.7 *The flow resistance of the PIH cushioning is dermined by the laminar flow through the gap between the peg and the hole, over a distance* y_{c1}.

With this Assumption, the cushioning flow not only depends on the geometry of the peg, but also on the distance y_{c1} over which the peg has entered the hole. Using Assumption 5.2.3, the following expression for the cushioning flow can be derived [90], with η the dynamic viscosity of the oil:

$$\Phi_{c1} = \frac{\pi D_{peg}(P_{p1} - P_{i1})}{12\eta \int_0^{y_{c1}} \frac{1}{h^3(x)} \mathrm{d}x} \qquad y_{c1} > 0 \tag{5.10}$$

Assumption 5.2.8 *The flow resistance of the PIH cushioning is dermined by the turbulent flow loss at the outlet, i.e. at the tip of the peg.*

With this Assumption, the cushioning flow is independent of the geometry of the peg, as c_1 determines the flow loss:

$$\Phi_{c1} = C_{d1}\pi D_{peg} c_1 \sqrt{\frac{2|P_{p1} - P_{i1}|}{\rho}} \mathrm{sgn}(P_{p1} - P_{i1}) \qquad y_{c1} > 0 \tag{5.11}$$

Actually, it can be stated a-priori, that Assumption 5.2.8 is not realistic. Nevertheless, it may be useful, when combined with the laminar flow assumption, Assumption 5.2.7, as follows.

Assumption 5.2.9 *The flow resistance of the PIH cushioning is dermined by the combination of a turbulent flow loss, either at the inlet or at the outlet of the peg-hole restriction, and the loss due to the laminar flow through the gap between the peg and the hole.*

This Assumption leads to a quadratic expression for the cushioning flow, which is easily solved for Φ_{c1}:

$$\frac{\rho \,\mathrm{sgn}(P_{p1} - P_{i1})}{2(C_{d1}\pi D_{peg} s_{c1})^2} \Phi_{c1}^2 + \frac{12\eta \int_0^{y_{c1}} \frac{1}{h^3(x)} \mathrm{d}x}{\pi D_{peg}} \Phi_{c1} = (P_{p1} - P_{i1}) \qquad y_{c1} > 0 \tag{5.12}$$

or, if the turbulent flow loss at the outlet is taken:

$$\frac{\rho \,\mathrm{sgn}(P_{p1} - P_{i1})}{2(C_{d1}\pi D_{peg} c_1)^2} \Phi_{c1}^2 + \frac{12\eta \int_0^{y_{c1}} \frac{1}{h^3(x)} \mathrm{d}x}{\pi D_{peg}} \Phi_{c1} = (P_{p1} - P_{i1}) \qquad y_{c1} > 0 \tag{5.13}$$

Hereby, the pressure loss due to the turbulent inflow or outflow, and the pressure loss due to the laminar resistance in the gap have been superponed.

Although it is not yet clear, which of the Assumptions 5.2.6 up to and including 5.2.9 is the most suitable for the modelling of the cushioning flow, a complete model of the hydraulic actuator including the PIH cushioning is now available. After an intermediate validation of the obtained model in Subsection 5.2.4, it can be used for the design of an optimal peg geometry, as discussed in Section 5.3. However, first the modelling of the other cushioning type, the CDH cushioning, is treated in the next Subsection.

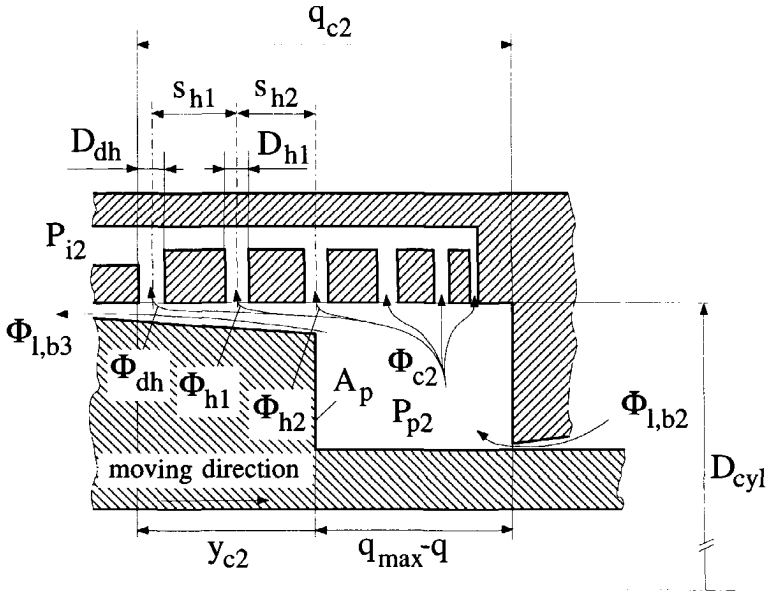


Fig. 5.3: Schematic view of CDH cushioning; definition of variables

5.2.3 Modelling of closing-drain-holes (CDH) cushioning

Like the for the PIH cushioning, the modelling of the CDH cushioning starts with a definition of the geometry, with corresponding geometrical variables and parameters. Using similar assumptions as for the PIH cushioning, the mass and force balances of the actuator, previously given in Section 2.3, can be rewritten again, now for the operational conditions during the cushioning stage of the CDH cushioning. After that, the most important part of the cushioning model, the cushioning flow, is described for the different stages of the cushioning process.

Definition of geometry

A schematic view of the CDH cushioning is given in Fig. 5.3, with some general definitions of the parameters that characterize the cushioning. During the cushioning stage, the piston head moves along the drain holes in the cylinder, which has inner diameter D_{cyl}. The cushioning stage starts at a distance q_{c2}, the cushioning length, from the end of the stroke, when the piston starts closing the first drain hole. In fact, this is not a single hole, but a row of n_{dh} drain holes, which are closed simultaneously. These n_{dh} drain holes with diameter D_{dh} form the regular drain port of the actuator chamber; if they are not closed by the piston head, n_{dh} and D_{dh} should be large enough to allow a free outflow Φ_{dh}.

After the piston has closed the regular drain holes during its motion rightward, the drain flow Φ_{dh} will be reduced considerably, and the cushioning flow Φ_{c2} will be forced to distribute over the closed regular drain holes and the remaining open drain holes, see Fig. 5.3.

These remaining drain holes constitute the actual CDH cushioning; during the cushioning stage the holes are closed subsequently by the piston head. So, the CDH cushioning is a series of n_h drain holes or cushioning holes, following the row of regular drain holes, placed at distances $s_{h1}, s_{h2}, \ldots, s_{hn_h}$ respectively from each other. Each cushioning hole has its own diameter $D_{h1}, D_{h2}, \ldots, D_{hn_h}$, and allows a flow $\Phi_{h1}, \Phi_{h2}, \ldots, \Phi_{hn_h}$ respectively, where the total cushioning flow is given as:

$$\Phi_{c2} = \Phi_{dh} + \Phi_{h1} + \ldots + \Phi_{hn_h} \tag{5.14}$$

Note finally from Fig. 5.3, that the closure of a certain drain hole is defined at the one hand by the distance:

$$y_{c2} = -q_{max} + q_{c2} + q \tag{5.15}$$

and at the other hand by the subsequent inter-hole distances and hole diameters.

Modelling assumptions

Concerning the modelling of the dynamic behaviour of the actuator including the CDH cushioning, similar assumptions are made as for the PIH cushioning on page 271.

Assumption 5.2.10 *The actuator chamber and the drain line (transmission line) can be modelled as two separate compartments, each with uniform pressure distribution (see also Fig. 5.3):*

- *The cushioning compartment, with area A_p and pressure P_{p2}.*
- *The drain compartment, with constant volume V_{l2} and pressure P_{i2}.*

The walls of the compartments are assumed to be infinitely stiff.

Assumption 5.2.11 *The cushioning flow Φ_{c2} from the cushioning compartment into the drain compartment is:*

- *equal to the flow that is necessary to obtain identical pressure variations in both compartments, if the resistance of the CDH cushioning is negligibly small, i.e. if the piston head has not (partially) closed the regular drain holes.*
- *equal to the flow corresponding to the pressure difference $P_{p2} - P_{i2}$ and the modelled resistance of the CDH cushioning, if this resistance is not negligible, i.e. if the piston head has (partially) closed the regular drain holes and possibly (some of) the cushioning holes.*

Assumption 5.2.12 *The cushioning flow Φ_{c2} is assumed to be one-dimensional, i.e. rotational flow around the (conical) piston head is neglected.*

Assumption 5.2.13 *The effect of frictional forces on the cushioning behaviour is neglected, i.e. $F_{vp} = F_{cp} = 0$.*

Theoretically, Assumption 5.2.12 is not justifiable; especially not for the cushioning holes, because there is only one single hole at a certain cross-section of the cylinder. This means that rotational flow must occur. However, for the intended use of the model, namely analysis of the dynamic actuator behaviour during the cushioning stage for certain configurations of a CDH cushioning, rigorous simplifying assumptions are desired and allowed.

From this point of view, some more rigorous assumptions will be made later on in this Subsection. Though not theoretically justifiable, assumptions like Assumption 5.2.12 can be justified by experiments, as shown in Subsection 5.4.3.

Concerning the servo-valve, similar (weak) assumptions are made as in the case of the PIH cushioning, see page 271.

Mass and force balances

Given the assumptions, the mass balances are easily obtained like in the previous Subsection, again referring to the theoretical model of Subsection 2.3.4:

$$\begin{aligned} \dot{P}_{p1} &= \tfrac{E}{A_p(q_{max}+q)+V_{l1}}\left(\Phi_{p1} - \Phi_{l1} - A_p\dot{q}\right) \\ \dot{P}_{i2} &= \tfrac{E}{V_{l2}}\left(-\Phi_{p2} + \Phi_{c2}\right) \\ \dot{P}_{p2} &= \tfrac{E}{A_p(q_{max}-q)}\left(-\Phi_{c2} - \Phi_{l2} + A_p\dot{q}\right) \end{aligned} \tag{5.16}$$

The equation of motion or the force balance for the piston can be taken from actually remains (2.38), while neglecting frictional forces according to Assumption 5.2.13:

$$M_p\ddot{q} = A_p(P_{p1} - P_{p2}) + F_{ext} \tag{5.17}$$

Obviously, the cushioning flow Φ_{c2} again plays the key role in the model of the actuator including the CDH cushioning. When the piston moves into the cushioning zone, different stages can be distinguished. For each of these stages, assumptions will be made and corresponding expressions for the cushioning flow derived subsequently.

CDH cushioning flow - negligible resistance

As long as the resistance of the (partially closed) drain holes is negligible, the cushioning flow Φ_{c2} is determined according to Assumption 5.2.11 by the requirement that the derivatives of the pressures, $\dot{P}_{p2}$ and $\dot{P}_{i2}$, are equal. With (5.16), it is easily derived that Φ_{c2} is then given by:

$$\begin{aligned} \tfrac{E}{V_{l2}}\left(-\Phi_{p2} + \Phi_{c2}\right) = \tfrac{E}{A_p(q_{max}-q)}\left(-\Phi_{c2} - \Phi_{l2} + A_p\dot{q}\right) \quad &\Leftrightarrow \\ \Phi_{c2} = \frac{\left[\Phi_{p2} + \frac{V_{l2}}{A_p(q_{max}-q)}\left(-\Phi_{l2} + A_p\dot{q}\right)\right]}{\left[1 + \frac{V_{l2}}{A_p(q_{max}-q)}\right]} \end{aligned} \tag{5.18}$$

The condition, which determines whether the resistance of the drain holes is negligible, is given later on, by (5.21) on page 279. Before giving this condition, a model for the resistance of the CDH cushioning flow is presented next.

CDH cushioning flow - partially closed drain hole

When modelling the flow through a cylindrical drain hole, partially closed by the piston head, the geometry sketched in Fig. 5.4 is to be considered. If there would be zero clearance between the piston head and the cylinder, the flow might simply be modelled as a turbulent flow, with a restriction of area A_c, as indicated in Fig. 5.4(b). However, due to the clearance

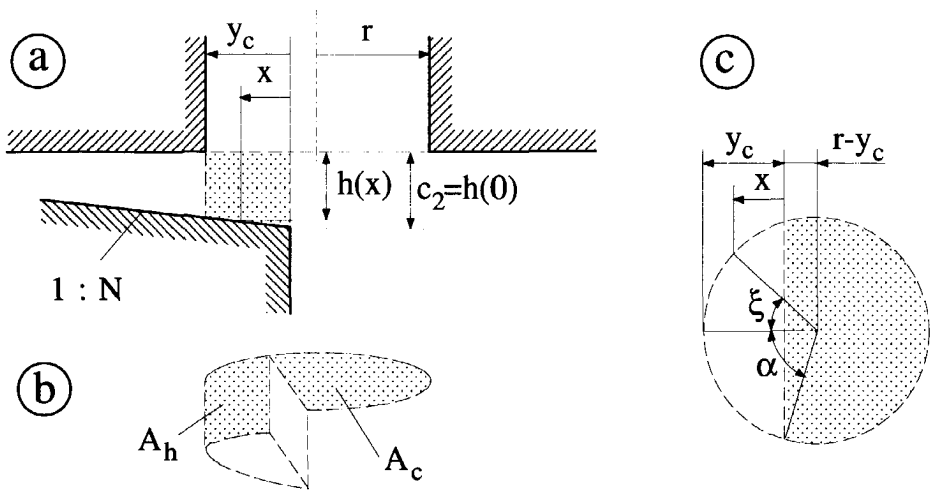


Fig. 5.4: Geometry and variable definition partially closed drain hole; side view control surfaces (a); 3-D representation of control surfaces (b); down view control surfaces (c)

c_2 at the tip of the conical bearing, the effective area will be larger than A_c. Thereby, the conicity of the bearing N also plays a role, especially when the drain hole is further closed.

Obviously, the flow occurring in this configuration is very complex. Yet, it is desirable to model it as a one-dimensional flow according to Assumption 5.2.12. Because of the narrow openings and the sharp edges, both of the hole and of the bearing, it is reasonable to assume turbulent flow. Thereby, some effective area has to be defined, which not only includes the opening area A_c of the cylindrical port, but also some additional area A_h, that takes the clearance and conicity of the piston head into account, as well as the distance over which the port has been closed, y_c. This leads to the following simplifying Assumption.

Assumption 5.2.14 *The flow resistance of a partially closed drain hole is determined by the flow loss, corresponding to a turbulent flow through a restriction with effective area $A_c + A_h$, where referring to Fig. 5.4:*

- *the area A_c is the open part of the circular drain hole, and:*
- *the area A_h is the curtain area between the (conical) piston head and the edge of the circular drain hole.*

With this Assumption, and denoting the discharge coefficient related to the CDH cushioning as C_{d2}, the cushioning flow Φ_{dh} through n_{dh} partially closed drain holes is given by:

$$\Phi_{dh} = C_{d2} n_{dh} (A_c + A_h) \sqrt{\frac{2|P_{p2} - P_{i2}|}{\rho}} \operatorname{sgn}(P_{p2} - P_{i2}) \qquad y_c \leq 2r \qquad (5.19)$$

where A_c and A_h are given as a function of the distance y_c (see Fig. 5.4) by:

$$\begin{aligned} A_c(y_c) &= \arcsin\left(\tfrac{r-y_c}{r}\right) r^2 + (r-y_c)\sqrt{r^2-(r-y_c)^2} + \tfrac{1}{2}\pi r^2 \\ A_h(y_c) &= \tfrac{2r}{N}\left[(Nc_2 + r - y_c)\arccos\left(\tfrac{r-y_c}{r}\right) - r\sin\left(\arccos\left(\tfrac{r-y_c}{r}\right)\right)\right] \end{aligned} \tag{5.20}$$

The derivation of these expressions is rather straightforward; the expression for A_c can be constructed directly. With regard to the computation of A_h, it is observed from Fig. 5.4(c), that $x = r\cos(\xi) + y_c - r$, so that:

$$h(x) = c_2 - \tfrac{x}{N} \quad \Leftrightarrow \quad h(\xi, y_c) = c_2 - \tfrac{r\cos(\xi)+y_c-r}{N}$$

Herewith, and using $\alpha(y_c) = \arccos\left(\frac{r-y_c}{r}\right)$, A_h is obtained as the solution of the following integral:

$$\begin{aligned} A_h(y_c) &= \int_{-\alpha(y_c)}^{\alpha(y_c)} h(\xi, y_c)\mathrm{d}(\xi r) \\ &= 2r\int_0^{\alpha(y_c)} \left[\tfrac{Nc_2-y_c+r}{N} - \tfrac{r\cos(\xi)}{N}\right]\mathrm{d}\xi \\ &= 2r\left[\tfrac{Nc_2+r-y_c}{N}\arccos\left(\tfrac{r-y_c}{r}\right) - \tfrac{r\sin\left(\arccos\left(\frac{r-y_c}{r}\right)\right)}{N}\right] \end{aligned}$$

So, Assumption 5.2.14 leads to an expression for the cushioning flow Φ_{dh} through n_{dh} partially closed drain holes, namely (5.19) with (5.20). In fact, the given expressions allow the definition of a condition, to decide whether the resistance for the cushioning flow is negligible or not, i.e. whether (5.18) or (5.19) should be used. The idea is again, that the flow resistance is considered negligible, if a maximum actuator flow $\Phi_{p,nom}$ through the partially closed drain holes would cause a pressure drop less than 0.01 P_s. Using (5.19), this means that the cushioning flow resistance is negligible and that (5.18) should be used, *if*:

$$n_{dh}(A_c + A_h) > \frac{\Phi_{p,nom}}{C_{d2}\sqrt{0.01\frac{2P_s}{\rho}}} \qquad y_c \leq 2r \tag{5.21}$$

This condition is easily checked by computing (5.20). If (5.21) is not met, the cushioning flow is computed with (5.19) and (5.20). However, these latter expressions are no longer valid, if the piston head has moved along the holes, such that they are 'closed', in the sense that the area A_c has become zero. This situation, corresponding to $y_c > 2r$, is considered next.

CDH *cushioning flow - 'closed' drain hole*

The configuration of a closed drain hole is sketched in Fig. 5.5. Again, the flow occurring in this configuration is extremely complex, but needs to be represented by a simple one-dimensional flow model according to Assumption 5.2.12. Therefore, a rigorously simplifying assumption is made again.

Assumption 5.2.15 *The flow through a closed drain hole is determined by a flow loss, which consists of three contributions (see also Fig. 5.5):*

- *a turbulent flow loss at the edge of the drain hole, with area A_h,*
- *a laminar flow loss in the conical gap between the piston head and the cylinder wall, over a distance $y_c - 2r$, and*

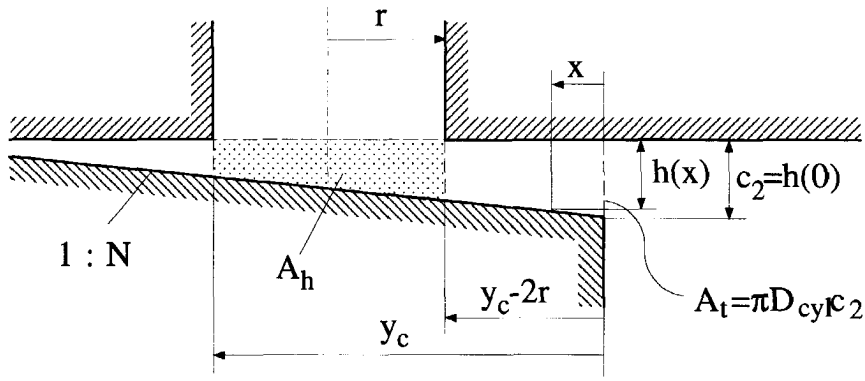


Fig. 5.5: Geometry and variable definition closed drain hole

- *a turbulent flow loss at the tip of the piston head, with area* A_t.

The idea behind this Assumption is as follows. If the drain hole is just closed, i.e. $y_c - 2r$ small, the loss due to turbulent flow at the edge of the drain hole will be important. However, a direct flow from the actuator chamber into the drain holes is not possible; the flow should first enter the gap between piston head and cylinder. Especially in case of the regular drain holes, the loss due to this inlet flow at the tip of the piston head is relevant; it is in the same order of magnitude as the loss at the edges of the drain holes, because A_t is in the same order of magnitude as $n_{dh}A_h$.

Although for very small $y_c - 2r$ the flow between the tip of the piston and the drain hole will hardly develop as a laminar flow, it is likely that the flow in the gap becomes laminar in the case that $y_c - 2r$ is large with respect to the gap clearance. Because the clearance at the tip c_2 is very small, this will readily occur when the piston head moves along the drain hole, for which reason a laminar flow loss is included in Assumption 5.2.15.

Thus, with Assumption 5.2.15, the total flow loss due to the flow Φ_{dh} through n_{dh} parallel closed drain holes can be written as:

$$\begin{aligned} &\tfrac{\rho\,\mathrm{sgn}(P_{p2}-P_{i2})}{2(C_{d2}n_{dh}A_h)^2}\,\Phi_{dh}^2 + \tfrac{12\eta\int_0^{y_c-2r}\frac{1}{h^3(x)}\mathrm{d}x}{\pi D_{cyl}}\,\Phi_{dh} + \tfrac{\rho\,\mathrm{sgn}(P_{p2}-P_{i2})}{2(C_{d2}A_t)^2}\,\Phi_{dh}^2 = (P_{p2}-P_{i2}) \Leftrightarrow \\ &\tfrac{\rho\,(A_h^2+A_t^2)\,\mathrm{sgn}(P_{p2}-P_{i2})}{2(C_{d2}n_{dh}A_hA_t)^2}\,\Phi_{dh}^2 + \tfrac{12\eta\int_0^{y_c-2r}\frac{1}{h^3(x)}\mathrm{d}x}{\pi D_{cyl}}\,\Phi_{dh} = (P_{p2}-P_{i2}), \quad y_c > 2r \end{aligned} \tag{5.22}$$

In this quadratic expression, from which Φ_{dh} can be solved explicitly, the areas A_t and A_h are given as (see also Fig. 5.5 and (5.20)):

$$\begin{aligned} A_t &= \pi D_{cyl}c_2 \\ A_h(y_c) &= \tfrac{2\pi r}{N}(Nc_2 + r - y_c) = 2\pi r c_2 - 2\pi r\tfrac{(y_c-r)}{N} \end{aligned} \tag{5.23}$$

while the integral expression in (5.22) can be written explicitly, using $h(x) = c_2 - \frac{x}{N}$:

$$\int_0^{y_c-2r}\frac{1}{h^3(x)}\mathrm{d}x = \frac{N(y_c-2r)^2 - 2N^2c_2(y_c-2r)}{2c_2^2(Nc_2^2-(y_c-2r))^2} \tag{5.24}$$

With the equations (5.18), (5.19) and (5.22), together with the condition (5.21), a model for the cushioning flow through a row of n_{dh} parallel drain holes is presented. Actually, the model presented so far, would describe the behaviour of the actuator in case the piston head moves along the regular drain holes, while there were no additional drain holes. However, for the design of the CDH safety cushioning, a model is required, that also takes into account the effect of n_h additional cushioning holes, as depicted in Fig. 5.3.

CDH cushioning flow - multiple drain holes in series

When discussing the geometry of the CDH safety cushioning at the beginning of this Section, the cushioning flow Φ_{c2} was already given as the sum of the flows through the separate cushioning holes by (5.14). Thereby, it is still to be determined, how these separate flows $\Phi_{h1}, \ldots, \Phi_{hn_h}$, as schematically depicted in Fig. 5.3, are to be modelled. As these flows are basically dependent of each other, it is not obvious to find an explicit expression for the total cushioning flow Φ_{c2} as a function of the pressure difference $P_{p2} - P_{i2}$ and the piston position y_{c2}, unless the following simplifying assumption is made.

Assumption 5.2.16 *The flow through a single cushioning hole of the CDH cushioning is not affected by the flow through other (regular) drain holes of the CDH cushioning, so that:*

- *Assumption 5.2.14 holds if the cushioning hole is partially closed as depicted in Fig. 5.4, and*
- *Assumption 5.2.15 holds if the cushioning hole is closed as depicted in Fig. 5.5.*

With this Assumption, the model for the CDH cushioning flow Φ_{c2} becomes modular, with independent contributions of the different cushioning holes according to (5.14). Thereby, the contribution of a single cushioning hole can be similarly modelled as the flow Φ_{dh} through the regular drain holes, using the equations (5.19) up to and including (5.24). For instance, the flow Φ_{h1} through the first cushioning hole is obtained as:

$$\Phi_{h1} = \begin{cases} C_{d2}(A_c + A_h)\sqrt{\frac{2|P_{p2}-P_{i2}|}{\rho}}\operatorname{sgn}(P_{p2} - P_{i2}), & y_{c2} \leq y_{h1} \\ \frac{\rho\,(A_h^2+A_t^2)\,\operatorname{sgn}(P_{p2}-P_{i2})}{2(C_{d2}A_hA_t)^2}\,\Phi_{h1}^2 + \frac{12\eta\int_0^{y_{c2}-y_{h1}}\frac{1}{h^3(x)}\mathrm{d}x}{\pi D_{cyl}}\,\Phi_{h1} = (P_{p2} - P_{i2}), & y_{c2} > y_{h1} \end{cases} \tag{5.25}$$

with:

$$\begin{aligned} y_{h1} &= \tfrac{1}{2}D_{dh} + s_{h1} + \tfrac{1}{2}D_{h1} \\ A_c(y_{c2}) &= \arcsin\left(\tfrac{(y_{h1}-r_{h1})-y_{c2}}{r_{h1}}\right) r_{h1}^2 + ((y_{h1} - r_{h1}) - y_{c2}) \cdots \\ &\qquad \cdots \sqrt{r_{h1}^2 - ((y_{h1} - r_{h1}) - y_{c2})^2} + \tfrac{1}{2}\pi(r_{h1})^2 \\ A_h(y_{2c}) &= \begin{cases} \frac{D_{h1}}{N}\left[(Nc_2 + (y_{h1} - r_{h1}) - y_{c2})\arccos\left(\frac{(y_{h1}-r_{h1})-y_{c2}}{r_{h1}}\right)\cdots\right. \\ \qquad \left.\cdots - r_{h1}\sin\left(\arccos\left(\frac{(y_{h1}-r_{h1})-y_{c2}}{r_{h1}}\right)\right)\right], & y_{c2} \leq y_{h1} \\ \frac{\pi D_{h1}}{N}\left(Nc_2 + (y_{h1} - r_{h1}) - y_{c2}\right), & y_{c2} > y_{h1} \end{cases} \\ A_t &= \pi D_{cyl} c_2 \\ \int_0^{y_{c2}-y_{h1}} \frac{1}{h^3(x)}\mathrm{d}x &= \frac{N(y_{c2}-y_{h1})^2 - 2N^2c_2(y_{c2}-y_{h1})}{2c_2^2(Nc_2^2-(y_{c2}-y_{h1}))^2} \end{aligned}$$

Obviously, the flows through the other cushioning holes can be modelled similarly.

Thus, a modular model for the flow through the CDH cushioning is obtained, based on a set of strong, and possibly unrealistic assumptions. Together with the flow and force balances of the actuator, given earlier in this Subsection, a complete model is obtained, which allows the simulation of the dynamic behaviour of the actuator during the cushioning stage. In order to prove the validity of the model, and therewith the validity of the model assumptions, both for the PIH and the CDH cushioning models, an intermediate model validation has been performed. The results of this validation, together with the choice of model parameters, are discussed briefly in the next Subsection.

5.2.4 Choice of model parameters and intermediate model validation

Before the safety cushioning models are used to optimize the design of the cushioning in Section 5.3, some intermediate validation results of the models are discussed. These validation results have been obtained with a parameterset, which has been chosen a-priori, based on physical knowledge of the system, as discussed below. The results allow some intermediate conclusions concerning the validity of the cushioning models, including a verification of the model assumptions, both for the PIH cushioning and for the CDH cushioning.

A-priori choice of model parameters

In fact, the models presented in the preceding two Subsections are just the theoretical, physical models of the hydraulic actuator of Subsection 2.3.4, slightly adapted to include detailed models of the safety cushionings. Because the parameters of the models of the actuator including the cushioning are just the same as those of the theoretical model of Subsection 2.3.4, the numerical values of the parameters have been chosen similar to those used to analyze the theoretical model in Subsection 2.3.5. They are given in Table F.2 and F.4, Appendix F.

However, a few parameters have been chosen different for the cushioning simulations; they are given in Table F.6, Appendix F. Also given in this Table are the parameter values, that are specific for the cushioning models, presented in Subsection 5.2.2 and 5.2.3. The background of the given parameter values may be clarified by the following comments:

- The supply pressure P_s has been 160 [bar] in the simulations of the cushioning models, just for practical reasons; the experimental evaluation Section 5.4 also took place with $P_s = 160$ [bar] in the scope of the flight simulator application of Chapter 1.
- The inertial load M_p is chosen to be 2000 [kg], being a representative value for the different load conditions that might occur during cushioning.
- For the static load force F_{ext}, a value of -10 [kN] is taken for the cushioning of the downward motion (PIH), and a value of 10 [kN] for the cushioning of the upward motion (CDH). This also represents realistic load conditions that might occur in the given application.
- As far as the PIH cushioning models are concerned, the discharge coefficient C_{d1} is chosen larger than for the turbulent flows of the servo-valve, namely $C_{d1} = 0.8$. The reason is, that the Reynolds number is not too large for the PIH cushioning flow, while it is more safe to overestimate the amount of flow through the cushioning by a large discharge coefficient, than to underestimate it.

- For the CDH cushioning models, the discharce coefficient C_{d2} is just given the standard value, namely $C_{d2} = 0.61$, as the flow through the narrow cushioning holes is expected to be really turbulent.
- The clearance at the tip of the peg of the PIH cushioning, c_1, corresponds to a conical peg with slope 1:350, as discussed below.
- The conicity N of the bearing of the piston head is obtained as l_{b3}/t_{b3}, with numerical values from Table F.3.
- The clearance at the edge of the piston head, c_2, is obtained as $c_{b3} + l_{b3}/N$.
- The remaining (geometrical) parameters, for instance the lengths of the safety cushioning zones, q_{c1} and q_{c2} respectively, were just given by the construction of the actuator.

With the parameter values of Table F.6, the simulation models of Subsection 5.2.2 and 5.2.3 were used to perform simulations, which were compared to preliminary experimental results. Although the experimental results and the corresponding simulations will not be presented here, because a more thorough experimental validation of the cushioning models is given in Section 5.4, some key issues concerning the intermediate validation of the cushioning models are adressed next, as well as some conclusions with respect to the validity of the models.

Intermediate validation of the PIH cushioning model

For the intermediate validation of the PIH cushioning model, an experimental actuator was available with a PIH cushioning, where the peg was conical, with conicity 1:350. Or, referring to Fig. 5.2, the peg geometry could be described by $h(x) = c_1 - \frac{x}{350}$. In fact, this geometry had been chosen rather arbitrarily, without real a-priori insight in the dynamic behaviour of a hydraulic actuator with a PIH cushioning. The result was a poor cushioning performance for the downward motion: in the experiments, a large acceleration peak was observed, just at the moment that the peg entered the hole.

Despite this poor performance, the preliminary experiments, mainly at low velocities, allowed an intermediate validation of the cushioning model, by comparing simulations to experiments. Thereby, special attention has been given to the model for the cushioning flow in the stage that the peg is in the hole, in order to determine which of the Assumptions 5.2.6 up to and including 5.2.9 is the most plausible. The conclusion of these investigations is, that the effect of the turbulent inflow at the edge of the hole is dominant, when describing the resistance of the cushioning flow in the dynamic experiments. Therefore, Assumption 5.2.6 is adopted, with corresponding cushioning flow model given by (5.9).

The remaining part of the PIH cushioning model, concerning the cushioning flow in the case that the peg is not (yet) in the hole, appeared to be reasonably good without adjustments. In fact, this indirectly justifies the basic model assumptions, given on page 271.

Intermediate validation of the CDH cushioning model

The same actuator used for the intermediate validation of the PIH cushioning model, was also used to validate the CDH cushioning model with preliminary experiments. In fact, a CDH cushioning was not present in this actuator, in the sense that no additional drain holes were present. So, the behaviour of the actuator when moving into the cushioning

zone was just determined by the closure of the regular drain holes, with the piston head moving along them. The result was again a poor cushioning performance, now for the upward motion: in the experiments, a large acceleration peak was observed, just at the moment that the piston head moved along the row of regular drain holes.

Obviously, not the complete CDH cushioning model could be validated with these preliminary elements, especially not Assumption 5.2.16. However, the crucial part of the model, concerning the flow through drain holes, (partially) closed by a conical bearing, could be validated. The conclusion of this intermediate validation is, that the modelling of the cushioning flow Φ_{dh} through n_{dh} drain holes with (5.19), (5.22) and related expressions is rather realistic. So, Assumption 5.2.14 and 5.2.15 are justified, as well as the basic model assumptions on page 276.

Thus, with some preliminary experiments, an intermediate validation of the simulation models of the safety cushionings was performed. The validated models could then be used for safety cushioning design, as discussed in the next Section.

5.3 Cushioning design

5.3.1 Introduction; design objective

With the description of the two types of safety buffers given in Subsection 5.2.1, and schematic representations in Fig. 5.2 and 5.3 respectively, it may be clear that the cushioning design comprises the definition of a number of geometrical parameters. Whereas some of the parameters are already determined by the actuator design, only a few characteristic parameters are still to be defined. Actually, it is a matter of optimizing the design, rather than performing the complete design.

In order to state the design objective properly, first an overview is given of the parameters that are given, and those that are still to be determined.

- For the PIH cushioning:
  - Given are the peg diameter D_{peg} and the cushioning length q_{c1}.
  - To be determined is the peg geometry $h(x)$, including the clearance at the tip c_1.
- For the CDH cushioning:
  - Given are the cylinder diameter D_{cyl}, the number of regular drain holes n_{dh}, the diameter of the regular drain holes D_{dh}, the conicity N and clearance c_2 of the piston head bearing, and the cushioning length q_{c2}.
  - To be determined are the number of additional drain holes n_h, their diameters $D_{h1}, D_{h2}, \ldots, D_{hn_h}$ and the respective distances $s_{h1}, s_{h2}, \ldots, s_{hn_h}$ between them.

Within the given setting, the objective of the cushioning design is to guarantee a safe and smooth stop of the actuator motion, under different load conditions, if the actuator moves with full speed into the cushioning zone. Within the scope of this objective, it may be required moreover, that the cushioning design is optimal for a certain well-defined load condition. Or, in a more concrete formulation, the design objective might be stated as:

Given a hydraulic actuator and a certain cushioning configuration, loaded with inertial load M_p and static load F_{ext}, having some maximum initial velocity $\dot{q}_0$. Optimize the cushioning design, such that:

- *the maximum cushioning pressure, occurring during the cushioning stage, is minimized (safety), and*
- *the maximum acceleration*[2]*, occurring during the cushioning stage, is minimized (smoothness).*

It might be noted here, that the maximum velocity $\dot{q}_0$ is determined by the servo-valve capacity (divided by the piston area) at maximum valve opening, and also by the static load F_{ext} (due to the load sensitivity of the servo-valve flow according to (2.124), page 114). In other words, a maximum servo-valve opening is assumed during the cushioning stage.

Given the design objective, it is possible to develope a desired motion profile for the cushioning stage, as discussed in Subsection 5.3.2. With respect to this desired motion profile, the cushioning design can be optimized, using earlier presented simulation models. Therefore, model-based design procedures have been developed, which are presented in Subsection 5.3.3 and 5.3.4 for the PIH cushioning and the CDH cushioning respectively.

5.3.2 Desired motion profile

Definition of the motion profile

The design objective, stated above, makes some strong demands on the dynamic behaviour of the hydraulic actuator in case it runs with full speed into the cushioning zone. These demands can be quantified by specifying some desired motion profile, which prescribes the desired actuator motion during the cushioning stage.

Suppose that the actuator moves into the cushioning zone with length q_c at time $t_0 = 0$. At that moment, the relative actuator position $y_c(0) = 0$. Then, the desired motion profile consists of a desired position trajectory $y_{des}(t)$ with corresponding higher derivatives $\dot{y}_{des}(t)$, $\ddot{y}_{des}(t)$ and $\dddot{y}_{des}(t)$, with $t \in [t_0, t_f]$. Hereby, t_f is the final time of the cushioning stage, i.e. the time at which the actuator has reached the end of the cushioning zone, so: $y_c(t_f) = q_c$. The optimal cushioning with respect to a certain motion profile would result in an actuator motion, such that $y_c(t) = y_{des}(t)$, $\forall t \in [t_0, t_f]$.

Besides that a motion profile can be defined in the time domain as above, it can also be defined in the displacement domain. Thereby, the desired trajectories are expressed as a function of the displacement variable x, which has the same dimension and scale as the relative actuator position y_c. Thus, the desired motion profile, expressed in the displacement domain, is given as $y_{des}(x) = x$ with corresponding higher time derivatives $\dot{y}_{des}(x)$, $\ddot{y}_{des}(x)$ and $\dddot{y}_{des}(x)$, with $x \in [0, q_c]$.

After discussing some general requirements on possible motion profiles, three different motion profiles will be defined in the following and considered in view of cushioning design.

General requirements on motion profiles

Primary requirement on a motion profile is, that the actuator motion during the cushioning stage is such, that the actuator velocity is (approximately) zero when the end of the actuator stroke is reached. Otherwise, an undesirable large acceleration peak would occur during the collision between the moving and the stationary part.

[2]In this Section, accelerations can be positive as well as negative. Speaking of maximum or minimum accelerations means maximum or minimum of the absolute acceleration, unless indicated otherwise.

Another requirement is, that the third derivative of the position trajectory, $\dddot{y}_{des}(t)$, also called the jerk, is finite. In other words, the second derivative, the acceleration profile $\ddot{y}_{des}(t)$, should be continuous. The reason is, that a discontinuous change of the acceleration would require a discontinuous change of the pressures. This would require infinite (cushioning) flows, as can be seen from the mass balances (5.2) and (5.16).

The third requirement is directly related to the design objective of page 284, namely that the maximum acceleration $\ddot{y}_{c,max}$ should be minimized.

Together with some trivial requirements, the general requirements on motion profiles can be summarized as follows:

- desired relative actuator position: $y_{des}(t_0) = 0$; $y_{des}(t_f) = q_c$.
- desired actuator velocity: $\dot{y}_{des}(t_0) = \dot{q}_0$; $\dot{y}_{des}(t_f) = 0$.
- desired actuator acceleration: $|\ddot{y}_{des}(t)| < \ddot{y}_{c,max}$, $\forall t \in [t_0, t_f]$, $\ddot{y}_{c,max}$ small.
- desired actuator jerk: $|\dddot{y}_{des}(t)| < c$, $\forall t \in [t_0, t_f]$, c finite.

Motion profile 1 (MP1) - constant acceleration

The motion profile that results in an absolute minimum of the maximum acceleration during the cushioning stage is a profile, that reduces the initial velocity $\dot{q}_0$ linearly, with a constant acceleration, to zero. However, in order to fulfil the requirement of finite jerk, a purely rectangular acceleration profile is not allowed. Therefore, it is approximated by a trapezoid acceleration profile, which is defined by the following expression for the jerk.

$$\dddot{y}_{des}(t) = \begin{cases} -c & t \in [t_0, t_1\rangle \\ 0 & t \in [t_1, t_2\rangle \\ c & t \in [t_2, t_f] \end{cases} \quad \text{with:} \quad \begin{aligned} t_1 &= t_0 + \ddot{y}_{c,max}/c \\ t_2 &= t_0 + \dot{q}_0/\ddot{y}_{c,max} \\ t_f &= t_0 + (t_1 - t_0) + (t_2 - t_0) \end{aligned} \tag{5.26}$$

Desired acceleration, velocity and position profiles can be obtained simply by integrating (5.26), either numerically or analytically.

Because the initial velocity is reduced approximately linearly to zero, the required cushioning distance $y_{des}(t_f)$ equals $\approx \frac{1}{2}(t_f - t_0)\dot{q}_0$. Obviously, this should be less than q_c. Presuming that c in (5.26) may be large, this means that $\ddot{y}_{c,max}$ should be large enough, as it primarily determines t_f and therewith $y_{des}(t_f)$.

For the PIH cushioning design example to be given in Subsection 5.3.3, a motion profile with constant acceleration has been determined, for a required cushioning length $q_c = 0.065$ [m], and an initial velocity $\dot{q}_0 = 1.13$ [m/s]. Thereby $c = 1000$ [m/s^3] was chosen, while $\ddot{y}_{c,max}$ could be chosen as small as 12.5 [m/s^2]. The resulting acceleration profile, denoted by MP1, is shown by the solid line in Fig. 5.6. The left plot shows the result in the time domain, and the right plot in the displacement domain. Not surprisingly, both profiles show approximately constant acceleration: if the acceleration is constant in the time domain, it is so in the displacement domain.

The advantage of the constant acceleration motion profile is, that the length of the cushioning zone is utilized to reduce the velocity with the maximum allowed acceleration. Especially in cases where high demands are made upon smooth cushioning behaviour, this is advantageous. However, the principle of constant acceleration also involves some disadvantages, namely the occurrence of large cushioning pressures and the risk of a non-zero final velocity.

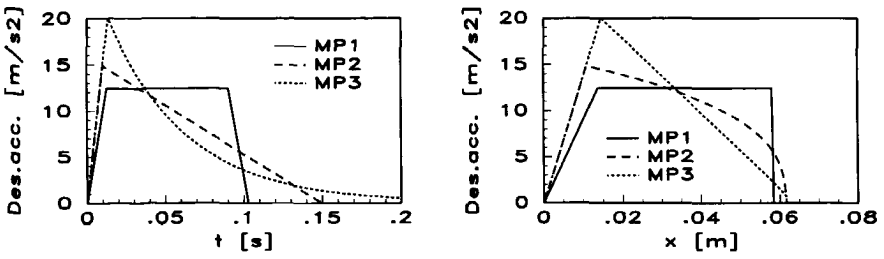


Fig. 5.6: Acceleration profiles in time domain (left) and displacement domain (right) for three different motion profiles; constant acceleration MP1 (solid); triangular acceleration time domain MP2 (dashed); triangular acceleration displacement domain MP3 (dotted)

For the realization of the desired acceleration of the inertial load, a constant actuator force is required during the cushioning stage. This force is to be delivered by the actuator pressure difference. Thereby, the opened servo-valve causes the pressure in the actuated actuator chamber to rise to the supply pressure P_s during the cushioning stage, as will be explained later, in Subsection 5.3.3. The result is, for constant acceleration, that the absolute pressure in the cushioning compartment may become extremely large in the final part of the cushioning stage, especially for large inertial loads. Thus, safe stress levels of the actuator construction may even be exceeded, making the proposed motion profile MP1 less suitable for large inertial loads.

The other disadvantage is related to the fact, that an actual cushioning will never perform perfectly, so that the desired acceleration will not be realized. Because the proposed motion profile MP1 requires a considerable reduction of the actuator velocity in the *final* part of the cushioning stage, the risk is relatively large, that the actuator has not reached zero velocity before the end of the cushioning zone. This is a serious disadvantage.

Motion profile 2 (MP2) - triangular acceleration in time domain

In order to overcome the disadvantages of the previous motion profile MP1, a triangular acceleration profile is proposed. After a short period of maximum jerk, the acceleration starts at some maximum value and then reduces linearly to zero. This motion profile, denoted as MP2, is defined by the following expressions for the jerk:

$$\dddot{y}_{des}(t) = \begin{cases} -c & t \in [t_0, t_1\rangle \\ \frac{\ddot{y}_{c,max}^2}{2\dot{q}_0 - \ddot{y}_{c,max}^2/c} & t \in [t_1, t_f] \end{cases} \quad \text{with:} \quad \begin{array}{l} t_1 = t_0 + \ddot{y}_{c,max}/c \\ t_f = t_0 + 2\dot{q}_0/\ddot{y}_{c,max} \end{array} \tag{5.27}$$

Desired acceleration, velocity and position profiles can be obtained by integrating (5.27), either numerically or analytically.

Again, the requirement that $y_{des}(t_f)$ should be less than q_c poses a lower bound on the maximum acceleration $\ddot{y}_{c,max}$. For the earlier mentioned design example, $\ddot{y}_{c,max}$ could now be chosen as small as 15 [m/s^2], i.e. slightly larger than for MP1. Thereby, $c = 1500$ [m/s^3] was taken. The resulting acceleration profiles in time domain and displacement domain are given by the dashed lines in Fig. 5.6. Note, that not only the maximum acceleration

is larger, but also the final time t_f. Note also, that in the displacement domain, the acceleration profile is still rather flat: only in the final part of the cushioning zone, the acceleration reduces (rapidly) to zero.

With this result, a sort of compromise has been found between the advantage and the disadvantages of MP1. The risk of a non-zero velocity at the end of the cushioning zone is considerable reduced, as a major velocity reduction takes place in the first part of the cushioning stage. The cost of this improvement is a slightly larger maximum acceleration, which may often be allowable. However, because the acceleration profile in the displacement domain is still rather flat, still rather high cushioning pressures are to be expected, especially in the middle part of the cushioning zone. For this reason, a third motion profile is considered.

Motion profile 3 (MP3) - triangular acceleration in displacement domain

The idea behind the third motion profile, denoted as MP3, is to concentrate the acceleration in the initial part of the cushioning stage. This is done by adopting a triangular acceleration profile again, but now in the displacement domain. After a short period of maximum jerk, the acceleration starts at some maximum value and than reduces linearly as a function of the relative actuator position y_c to zero. Expressed in the time domain, this means that the profile should satisfy $\ddot{y}_{des}(t) = C_1 y_{des}(t) + C_2$, with C_1, C_2 some real constants. Under the condition that the earlier given general requirements are met, the following solution is obtained:

$$\dddot{y}_{des}(t) = \begin{cases} -c & t \in [t_0, t_1\rangle \\ \ddot{y}_{c,max} a e^{-a(t-t_1)} & t \in [t_1, t_f\rangle \end{cases} \quad \text{with:} \quad \begin{array}{l} t_1 = t_0 + \ddot{y}_{c,max}/c \\ t_f = \infty \end{array} \tag{5.28}$$

where:

$$a = \left[\frac{\ddot{y}_{c,max}}{\dot{q}_0 - \ddot{y}_{c,max}^2/(2c)} \right]$$

Again, the corresponding desired acceleration, velocity and position profiles can be obtained by integrating the jerk, either numerically or analytically. Note, that the final time t_f is theoretically infinite; in practice however, the end of the cushioning zone will be reached within a reasonable time.

Applying the motion profile MP3 of (5.28) to the same design example again, the dotted lines of Fig. 5.6 are obtained. Thereby, the maximum acceleration had to be allowed to reach a value of 20 [m/s^2] in order to guarantee $y_{des}(t_f) < q_c$, with $c = 1500$ [m/s^3] again.

The result is clear: at the cost of a considerable increase of the maximum acceleration $\ddot{y}_{des}$, the velocity reduction is now concentrated in the inital part of the cushioning zone. Therewith, a more safe motion profile is obtained, in the sense that the maximum cushioning pressures will be lower, while the risk of a non-zero final velocity is small.

Thus, three alternative motion profiles have been defined and discussed in this Subsection, with their advantages and disadvantages. Against the background of these desired motion profiles, the design of the respective cushioning types will be discussed in the next two Subsections.

5.3.3 Design procedure for PIH cushioning

Basic idea and assumptions

In the PIH cushioning model, the cushioning flow is directly related to the peg geometry and the pressure difference $P_{p1} - P_{i1}$. Moreover, under Assumption 5.2.6, which was found to be valid by the intermediate validation results of Subsection 5.2.4, the reverse reasoning also makes sense: the peg geometry is directly related to some desired cushioning flow and pressure difference. This fact is utilized in the PIH cushioning design.

Thereby, the idea is to compute a desired profile for the pressure difference $P_{p1} - P_{i1}$, as well as for the cushioning flow Φ_{c1}, using the model of Subsection 5.2.2 and a desired motion profile from Subsection 5.3.2. Because the peg geometry is to be specified in the displacement domain, the desired profiles for the pressures and the cushioning flow are also to be computed in the displacement domain. As explained below, this is possible by transforming the dynamic equations from the time domain to the displacement domain, using the desired motion profile. After that, desired pressure and flow profiles can be computed and a peg geometry determined.

In order to simplify the design procedure slightly, only the basic properties of the model of the actuator including the cushioning are taken into account, by making the following assumption.

Assumption 5.3.1 *In the design procedure for the PIH cushioning, leakage effects are neglected, i.e.* $\Phi_{l1} = \Phi_{l2} = 0$.

Transformation from time domain to displacement domain

The transformation of the model of the actuator including the PIH cushioning, from time domain to displacement domain, involves two steps. First, all variables are expressed in the displacement domain, and second, the time derivatives are transformed into derivatives with respect to the displacement.

So, first the time variable t is replaced by the displacement variable x, meaning that the model states and related variables are expressed in x instead of t. Thereby, it is advantageous, to replace the actuator position q (and higher derivatives) by the relative actuator position y_{c1} (and higher derivatives), using (5.1), because $y_{c1}(x) = x$. Rewriting (5.2) this way, with Assumption 5.3.1, gives:

$$\dot{P}_{p1}(x) = \frac{E}{A_{rem}\,(q_{c1} - y_{c1}(x))}\,[-\Phi_{c1}(x) + A_{rem}\dot{y}_{c1}(x)] \tag{5.29}$$

$$\dot{P}_{i1}(x) = \frac{E}{V_{l1} - y_{c1}(x)A_{peg}}\,[\Phi_{p1}(x) + \Phi_{c1}(x) + A_{peg}\dot{y}_{c1}(x)] \tag{5.30}$$

$$\dot{P}_{p2}(x) = \frac{E}{A_p\,(2q_{max} - q_{c1} + y_{c1}(x)) + V_{l2}}\,[-\Phi_{p2}(x) - A_p\dot{y}_{c1}(x)] \tag{5.31}$$

The servo-valve flows in these expressions are just algebraically related to the pressures according to (2.124), whatever the domain may be.

Similarly, the force balance can be rewritten as:

$$M_p\ddot{y}_{c1}(x) = -A_{rem}P_{p1}(x) - A_{peg}P_{i1}(x) + A_pP_{p2}(x) - F_{ext} \tag{5.32}$$

In these expressions, the dot means the time derivative of the variable concerned. The second step is now, to transform the time derivatives into displacement derivatives, especially for the pressures. It is easily found, using $y_{c1}(x) = x$ again, that this corresponds to dividing by the velocity:

$$\frac{\mathrm{d}P(x)}{\mathrm{d}x} = \frac{\mathrm{d}P(x)}{\mathrm{d}t}\frac{\mathrm{d}t}{\mathrm{d}x} = \frac{\dot{P}(x)}{\dot{y}_{c1}(x)} \tag{5.33}$$

Thus, the model relations are rewritten in the displacement domain, and can be used to derive desired pressure and flow profiles.

Computation of desired pressure and flow profiles

The desired pressure profiles, describing the pressures as a function of the displacement x, that should occur during the cushioning stage, can be solved from the model equations, given a desired motion profile from Subsection 5.3.2. For that purpose, the desired position, velocity, etc. are substituted in the model, after which the differential equations for the pressures are solved in the displacement domain.

This method directly applies to the actuator pressure P_{p2}. Using the desired motion profile, and applying (5.33) to (5.31) results in:

$$\frac{\mathrm{d}P_{p2}(x)}{\mathrm{d}x} = \frac{E}{A_p\left(2q_{max} - q_{c1} + y_{des}(x)\right) + V_{l2}}\left[-\frac{\Phi_{p2}(x)}{\dot{y}_{des}(x)} - A_p\right] \tag{5.34}$$

This differential equation can be solved numerically for $P_{p2}(x)$. The initial condition is chosen as $P_{p2}(0) = \frac{1}{2}P_s + \frac{1}{2}\frac{F_{ext}}{A_p}$. This condition reflects the stationary equilibrium, occurring at zero acceleration (constant velocity), and can be obtained from (5.32).

For the computation of P_{i1} and P_{p1}, the pressures in the drain and the cushioning compartment respectively, the situation is more involved. First, the cushioning flow is eliminated from (5.30) and (5.29), by writing it explicitly as (using the desired motion profile again):

$$\Phi_{c1}(x) = -\frac{A_{rem}\left(q_{c1} - y_{des}(x)\right)}{E}\dot{P}_{p1}(x) + A_{rem}\dot{y}_{des}(x) \tag{5.35}$$

Substituting this in the mass balance for the drain compartment (5.30) gives, using $A_{peg} + A_{rem} = A_p$:

$$\dot{P}_{i1}(x) = \frac{E}{V_{l1} - y_{des}(x)A_{peg}}\left[\Phi_{p1}(x) + A_p\dot{y}_{des}(x)\right] - \frac{A_{rem}\left(q_{c1} - y_{des}(x)\right)}{V_{l1} - y_{des}(x)A_{peg}}\dot{P}_{p1}(x) \tag{5.36}$$

In order to solve this differential equation, another independent equation is required, relating the pressure derivatives $\dot{P}_{i1}(x)$ and $\dot{P}_{p1}(x)$ to each other. This independent equation is constituted by the (differentiated) force balance (5.32), which can be written as:

$$\dot{P}_{p1}(x) = -\frac{M_p}{A_{rem}}\,\ddot{y}_{des}\,(x) - \frac{A_{peg}}{A_{rem}}\dot{P}_{i1}(x) + \frac{A_p}{A_{rem}}\dot{P}_{p2}(x) \tag{5.37}$$

Substituting this in (5.36), and applying (5.33) after writing $\dot{P}_{i1}(x)$ explicitly again, results in (the variable x is omitted for reasons of readability):

$$\frac{\mathrm{d}P_{i1}}{\mathrm{d}x} = \frac{\frac{E}{V_{i1}-y_{des}A_{peg}}\left[\Phi_{p1} + A_p\dot{y}_{des}\right] - \frac{(q_{c1}-y_{des})}{V_{i1}-y_{des}A_{peg}}\left[-M_p\,\ddot{y}_{des} + A_p\dot{P}_{p2}\right]}{\dot{y}_{des}\left[1 - \frac{A_{peg}(q_{c1}-y_{des})}{V_{i1}-y_{des}A_{peg}}\right]} \tag{5.38}$$

This differential equation can be solved numerically for $P_{i1}(x)$. Similar as before, the initial condition is chosen as $P_{i1}(0) = \frac{1}{2}P_s - \frac{1}{2}\frac{F_{ext}}{A_p}$.

With the solution for $P_{i1}(x)$, all right hand terms in the differentiated force balance (5.37) are known, so an explicit expression for $\dot{P}_{p1}(x)$ is available. Clearly, this expression can be rewritten to a differential equation in the displacement domain, using (5.33), after which $P_{p1}(x)$ can be solved by numerical integration. The initial condition is equal to that for P_{i1}, namely $P_{p1}(0) = \frac{1}{2}P_s - \frac{1}{2}\frac{F_{ext}}{A_p}$.

Finally, with all three desired pressure profiles available, and using the desired motion profile, the desired cushioning flow $\Phi_{c1}(x)$ can be calculated with (5.35).

Determination of optimal (approximate) peg geometry

The determination of an optimal peg geometry is based on the application of Assumption 5.2.5 and 5.2.6. The corresponding cushioning flows are given by (5.6) and (5.9) respectively, which are actually identical. Reversing the simulation problem of Subsection 5.2.2 to the design problem considered here, the known desired cushioning flow and pressures can be used to compute the shortest distance $s_{c1}(x)$ explicitly as:

$$s_{c1}(x) = \frac{\Phi_{c1}(x)}{C_d\pi D_{peg}}\sqrt{\frac{\rho}{2|P_{p1}(x) - P_{i1}(x)|}}\mathrm{sgn}(P_{p1}(x) - P_{i1}(x)) \tag{5.39}$$

The problem is now, to find a geometry $h(x)$, such that the shortest distance s_{c1} according to (5.5) and (5.8) approximates the desired profile (5.39). Considering the case that the peg has not yet entered the hole, (5.5) holds. It is easily seen, that in this case, $-1 < \frac{\mathrm{d}s_{c1}(x)}{\mathrm{d}x} < 0$. Obviously, the same will hold for (5.8), as the gap between the peg and the hole is very small related to the length of the peg. The consequence is, that the desired shortest distance (5.39) makes no sense, as long as its derivative is smaller (negative) than one. This consideration, together with simulation results, suggests to neglect the first part of the desired profile (5.39), and use the remaining part to determine the peg geometry $h(x)$. This leads to the following rule.

Rule 5.3.2 *Suppose that:*

$$\frac{\mathrm{d}s_{c1}(x)}{\mathrm{d}x} < -1, \qquad x \in [0, x_0\rangle$$

where $s_{c1}(x)$ is the result of the PIH cushioning design procedure, given by (5.39). Then the peg geometry $h(x)$ should be chosen equal to the desired shortest distance, shifted over a distance x_0, so:

$$h(x) = s_{c1}(x + x_0), \qquad x \in [0, q_c] \tag{5.40}$$

Although the procedure proposed here provides a nice numerical result in the form of some curved optimal peg geometry, it is often desirable to have a more simple definition

of the peg geometry, e.g. for manufacturing purposes. In that case, the optimal geometry given by (5.40) may be approximated by, for instance, a piece-wise linear curve.

Before ending this Subsection on the PIH cushioning design, the developed procedure will be illustrated with design examples for two of the desired motion profiles of the previous Subsection. After that, some simulation results are discussed, providing a preliminary evaluation of the design.

Design examples: MP1 and MP3

As explained in Subsection 5.3.2, the desired motion profiles MP1 and MP3 are basically different in the sense that MP1 emphasizes constant acceleration, and MP3 minimal cushioning pressure peak. The profile MP2 lies in between. Therefore, the PIH cushioning design procedure is performed for MP1 and MP3, to illustrate some principal effects. In the design example, the actuator and cushioning parameters are similar as before; they are given in F.6, Appendix F.

Fig. 5.7 shows the results of the design procedure, with solid lines for MP1 and dashed ones for MP3[3]. In the upper left plot, the solutions of (5.34) are shown. It is clear from this plot, that the absolute pressure P_{p2} rises to the supply pressure P_s during the cushioning stage. This effect is caused by the compressibility of the oil in the actuator compartment, together with the non-linear servo-valve flow for maximum valve opening. Thereby, MP3 prescribes a faster pressure rise than MP1. The reason is, that MP3 prescribes a larger velocity reduction in the initial part of the cushioning; related to the lower velocity in the middle part of the cushioning zone, the pressure P_{p2} is larger for MP3.

The middle left plot gives the cushioning pressure $\bar{P}_{p1}$, that is desired for the given motion profiles, and has been obtained from (5.37), using (5.33). This plot illustrates, that MP1 requires a larger maximum cushioning pressure P_{p1} than MP3, due to the fact that a large acceleration is required in the final part of the cushioning stage, where P_{p2} has already approached P_s while it is acting in the 'wrong direction'.

The lower left plot gives the pressure in the drain line $\bar{P}_{i1}$ during the cushioning stage, which has been computed with (5.38). In fact, this plot is very much like the upper left plot; instead of a pressure rise to P_s, there is a pressure decay to zero, the return pressure.

In the right plots, the pressure difference $\bar{P}_{p1} - \bar{P}_{i1}$, the desired cushioning flow $\bar{\Phi}_{c1}$ and the desired distance s_{c1} are given respectively. Obviously, the latter two have been obtained directly from corresponding equations (5.35) and (5.39) respectively. Note hereby, that the discontinuity in the desired cushioning flow is caused by the sudden change in the slope of P_{p1} (middle left plot), due to the first term in (5.35). Note also, that the buffer flow in the final part of the cushioning zone is dominated by the desired velocity for the given motion profile, due to the second term in (5.35).

The desired distance s_{c1} in the lower right plot clearly reflects the difference between the two motion profiles: for MP3 the distance s_{c1} should be smaller in the beginning, while MP1 prescribes a fast decay of s_{c1} in the final part of the cushioning zone. Although it is difficult to see from the Figure, due to the scalings, the first part of the s_{c1} profiles in the lower right plot shows a large negative gradient. According to Rule 5.3.2, this part is to be neglected, in order to arrive at the desired geometries for the peg, $h(x)$.

[3]Like before, pressures are normalized with respect to the supply pressure P_s and flows with respect to the maximum valve flow $\Phi_{p,nom}$. Normalization is denoted with a bar.

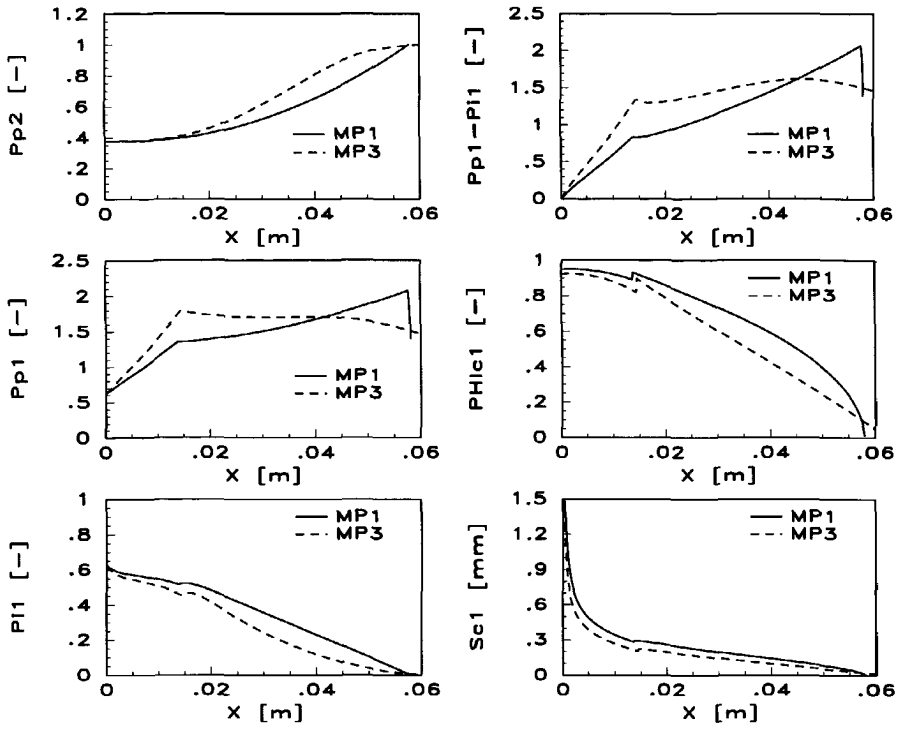


Fig. 5.7: PIH cushioning design example for two desired motion profiles MP1 (solid) and MP3 (dashed); desired profiles for pressure $\bar{P}_{p2}$ (upper left); $\bar{P}_{p1}$ (middle left); $\bar{P}_{i1}$ (lower left); pressure difference $\bar{P}_{p1} - \bar{P}_{i1}$ (upper right); cushioning flow $\bar{\Phi}_{c1}$ (middle right); distance s_{c1} (lower right)

The resulting respective peg geometries are shown in Fig. 5.8. Besides the optimal geometries $h(x)$ for the two motion profiles, approximated geometries $\hat{h}(x)$ are given, which have been used for manufacturing purposes[4]. The approximated geometries $\hat{h}(x)$ are defined as piece-wise-linear functions, as follows:

$$\hat{h}(x) = \max\left(\hat{h}_1(x), \hat{h}_2(x), \hat{h}_3(x), \hat{h}_4(x)\right); \begin{cases} \hat{h}_i(x) = -\frac{1}{a_i}(x - b_i), & i = 1,2,3 \\ \hat{h}_4(x) = 10\ 10^{-6}\ [\mathrm{m}], & i = 4 \end{cases} \tag{5.41}$$

The parameters of (5.41) that correspond to the approximations shown in Fig. 5.8, are given in Table 5.1.

In order to evaluate the obtained geometries with respect to the cushioning performance that may be expected, despite some approximations in the design procedure, some simulation results will be given next.

[4]The manufacturing of the optimal geometry would have required a transfer of the numerical data of the geometry to a NC-machine. The piece-wise-linear functions were easily defined in terms of four slopes, which could be used to adjust the grinding machine.

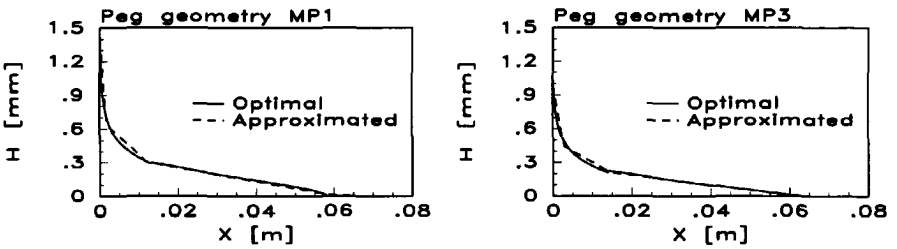


Fig. 5.8: Designed peg geometries for PIH cushioning; example for two desired motion profiles MP1 (left) and MP3 (right); optimal geometry $h(x)$ (solid) and approximated geometry $\hat{h}(x)$ (dashed)

	a_1 [-]	a_2 [-]	a_3 [-]	b_1 [m]	b_2 [m]	b_3 [m]
MP1	2.5	30	165	$3.5\ 10^{-3}$	$21.0\ 10^{-3}$	$61.5\ 10^{-3}$
MP3	5.0	50	225	$5.0\ 10^{-3}$	$25.0\ 10^{-3}$	$62.5\ 10^{-3}$

Table 5.1: Parameters piece-wise-linear approximations for peg geometries

Design evaluation by simulation

A preliminary evaluation of the proposed design procedure is given by the simulation results of Fig. 5.9. These results have been obtained with the simulation model of Subsection 5.2.2, with cushioning flow according to Assumption 5.2.6, and with the approximated geometries of Fig. 5.8. The solid line in Fig. 5.9 represents the cushioning behaviour of the PIH cushioning that was designed for MP1, while the dashed line corresponds to the design for MP3. The simulated state variables of the model are plotted in the displacement domain.

In the lower left plot of Fig. 5.9 the (normalized) cushioning pressure $\bar{P}_{p1}$ is given. It is actually this pressure, which should provide the required (negative) acceleration force to reduce the velocity to zero. Ideally, this cushioning pressure should follow the desired profile of the middle left plot of Fig. 5.7. Although the desired profile is not exactly reproduced by the simulation due to the approximations involved in the design procedure, the result is satisfactory. The simulated cushioning behaviour for the different peg geometries clearly reflects the underlying design specifications.

This can also be seen from the pressure difference $\overline{\Delta P}_i$, shown in the upper left plot. This pressure difference, which can be measured near the servo-valve (see Section 3.3), is defined as $\overline{\Delta P}_i = \bar{P}_{i1} - \bar{P}_{i2}$. Noting hereby, that $\bar{P}_{i2} = \bar{P}_{p2}$ in the PIH cushioning model, the simulated responses in the upper left plot of Fig. 5.9 should reflect the difference between the desired profiles for $\bar{P}_{i1}$ and $\bar{P}_{p2}$, given in the lower and upper left plots of Fig. 5.7 respectively. This is really the case.

Actually the most important part of the simulation result is found in the right plots of Fig. 5.9, showing the velocity and acceleration of the actuator respectively during the cushioning stage. Clearly, both peg geometries perform well in the sense that the considerable initial velocity $\dot{q}_0 \approx -1.1$ [m/s] is reduced to a reasonably small value, within the available cushioning zone, which ends at $q = -0.625$ [m]. Yet, there is a clear difference in the simulated acceleration profiles; they do clearly correspond to the motion profiles,

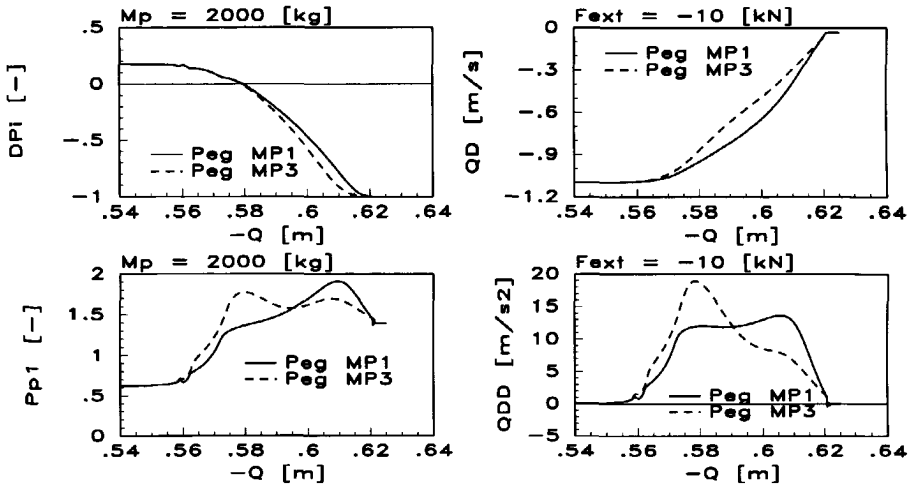


Fig. 5.9: Simulation results PIH cushioning design example for two desired motion profiles MP1 (solid) and MP3 (dashed); actuator pressure difference $\overline{\Delta P_i}$ (upper left); cushioning pressure $\bar{P}_{p1}$ (lower left); actuator velocity $\dot{q}$ (upper right); actuator acceleration $\ddot{q}$ (lower right)

which the peg geometries were based upon. Obviously, MP3 realizes a considerable velocity reduction in the first part of the cushioning zone, which is more safe, but at the cost of a considerably larger maximum acceleration.

With these simulation results, the idea behind the design procedure of the PIH cushioning, based on a prespecified motion profile, is validated. Therefore, the next step is an experimental evaluation of the performance of the resulting design. Before doing this in Subsection 5.4.2, the design of the other cushioning type, the CDH cushioning, is discussed in the next Subsection.

5.3.4 Design procedure for CDH cushioning

Basic idea

Contrary to the previous case of the PIH cushioning, a direct solution to the optimization problem with respect to the design objective of page 284 is not possible for the CDH cushioning. The reason is, that the CDH cushioning model is more complex, in the sense that the cushioning flow for certain relative actuator position is not directly related to a certain geometrical parameter, as a function of the relative actuator position. Instead of it, the cushioning flow is determined by the complete geometry of conical bearing and cushioning holes, together with the relative actuator position y_{c2} and the pressure difference $P_{p2} - P_{i2}$. Therefore, it is impossible to relate the cushioning geometry directly to some desired cushioning flow and pressure difference, both given as desired profiles in the displacement domain.

The consequence of the foregoing is, that the design has to be performed indirectly. This leads to a design strategy, in which simulations with the model of Subsection 5.2.3

plays a key role, as will be discussed next.

Design strategy

For reasons mentioned previously, the geometrical design of the CDH cushioning is not directly based on a desired motion profile like in the PIH cushioning design. Nevertheless, the optimization of the CDH cushioning can be performed with respect to a desired motion profile, in an indirect way. Because the principle of the CDH cushioning causes a relatively large velocity at the end of the cushioning zone, as explained later by simulation results, the most safe motion profile MP3 has been chosen. So, a triangular acceleration profile in the displacement domain is desired.

Because there is a discrete number of design parameters, as explained in Subsection 5.3.1, the design strategy consists of a number of 'nested' optimization steps. The procedure to go through these steps is as follows:

- Choose the number of additional drain holes n_h for the cushioning.
- Given n_h, optimize the cushioning geometry with respect to the desired motion profile and the design objective:
  - Choose a hole pattern, i.e. $s_{h1}, \ldots, s_{hn_h}$.
  - Given the hole pattern, optimize the diameters of the successive holes with respect to the desired motion profile and the design objective:
    * Choose the hole diameters $D_{h1}, \ldots, D_{hn_h}$.
    * *Perform simulation and judge the result with respect to the design objective.*
    * While the result can be improved, choose an other set of hole diameters.
  - If the result is not satisfactory, choose an other hole pattern, and optimize the hole diameters again.
- If the result is not satisfactory, choose an other number of holes n_h and optimize the cushioning geometry again.

As indicated by the emphasized text, the simulation and evaluation of the design with respect to the design objective plays a crucial role in this procedure. In fact, the simulation results provide the insight, that can be used to optimize the design, as will be discussed next.

Design evaluation by simulation

In order to provide some insight in the basic principles of the CDH cushioning design, a number of simulation results for different CDH cushioning geometries is given in Fig. 5.10. The cushioning pressures $\bar{P}_{o2}$ are given left, and the corresponding accelerations $\ddot{q}$ during the cushioning are given right. The geometry design has been optimized such, that the maximum cushioning pressure is minimal, while the acceleration approximates a triangular profile.

The shown results are some representative simulations, obtained during the design procedure, where the aim was to minimize the maximum cushioning pressure and to achieve a triangular acceleration profile in the displacement domain. The geometries corresponding to the shown results are characterized by the parameters given in Table 5.2. For all simulations, the number of regular drain holes is $n_{dh} = 16$, and their diameter is $D_{dh} = 5$ [mm]. The load conditions are similar to the case of the PIH cushioning design; only

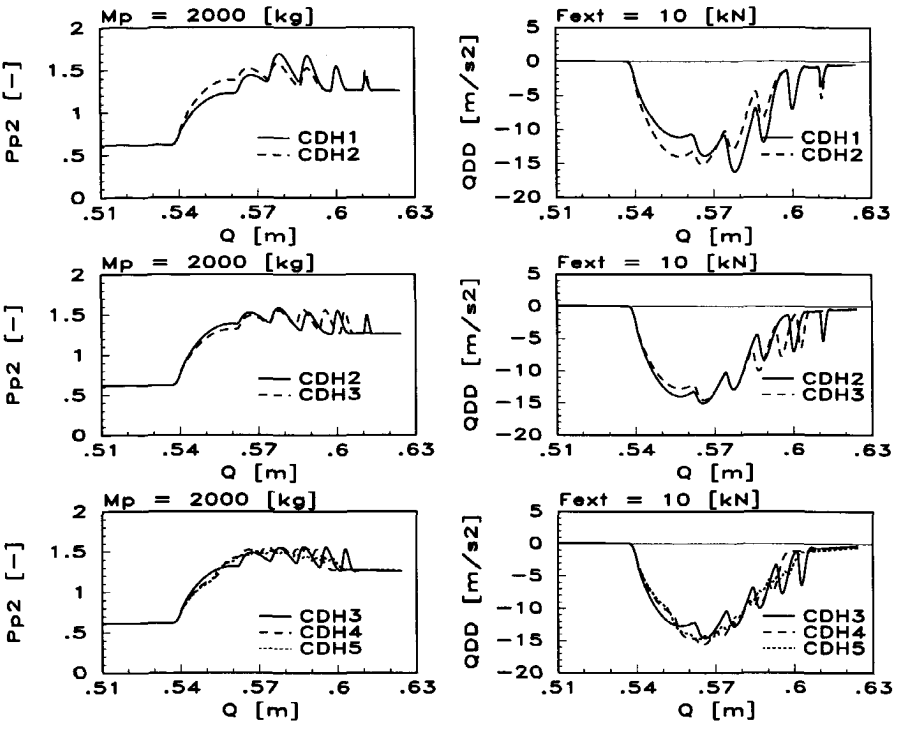


Fig. 5.10: Simulation results of CDH cushioning design examples for different geometries; cushioning pressure $\bar{P}_{p2}$ (left) and acceleration $\ddot{q}$ (right); different hole diameters (upper); different hole patterns (middle); different number of holes (lower)

the external force has been changed sign, in order to consider the more critical case. So, $M_p = 2.0\ 10^3$ [kg] and $F_{ext} = 10$ [kN]. The initial velocity for these simulations is $\dot{q}_0 \approx 1.1$ [m/s].

Besides a lot of other simulations, the simulation results of Fig. 5.10 have provided much insight in the effect of the design parameters on the simulated performance. The obtained insight and the observed phenomena can be summarized as follows:

- The first hole should be placed at a considerable distance s_{h1} from the regular drain holes. If this distance is too short, the resistance of this (still open) drain hole is large related to the resistance of the n_{dh} closed regular drain holes, mainly due the conicity of the bearing. Thus, the dynamic effect of the closure of the regular drain holes overrules the effect of the first drain hole if s_{h1} is too small.
- The sum of the areas $\frac{\pi}{4}D_{hi}^2$ of the unclosed drain holes is a rough measure for the actuator velocity during cushioning.
- The height of the acceleration peak due to the closure of a single hole is directly related to the diameter of the hole. A large diameter causes a large velocity reduction, and therewith a large acceleration peak, combined with a large peak in the cushioning pressure (see upper plots of Fig. 5.10).
- Related to the previous point is the fact, that a kind of 'waterbed'-effect is observed in the simulations. If a certain diameter is reduced, the corresponding acceleration

	CDH 1		CDH 2		CDH 3		CDH 4		CDH 5	
i	s_{hi}	D_{hi}	s_{hi}	D_{hi}	s_{hi}	D_{hi}	s_{hi}	D_{hi}	s_{hi}	D_{hi}
1	25.0	2.5	25.0	2.0	25.0	2.2	17.0	2.5	15	2.5
2	12.0	2.5	12.0	2.0	12.0	2.0	8.0	1.7	8.0	1.6
3	12.0	2.0	12.0	1.7	10.0	1.8	8.0	1.7	6.0	1.5
4	12.0	1.5	12.0	1.5	9.0	1.6	6.0	1.5	6.0	1.5
5	12.0	1.0	12.0	1.2	8.0	1.4	6.0	1.5	5.0	1.3
6	-	-	-	-	-	-	4.0	1.3	5.0	1.3
7	-	-	-	-	-	-	4.0	1.3	4.0	1.1
8	-	-	-	-	-	-	-	-	4.0	1.1
9	-	-	-	-	-	-	-	-	3.0	1.0
10	-	-	-	-	-	-	-	-	3.0	1.0

Table 5.2: Parameters for five CDH geometries (values in [mm]); $n_{dh} = 16$; $D_{dh} = 5$ [mm]

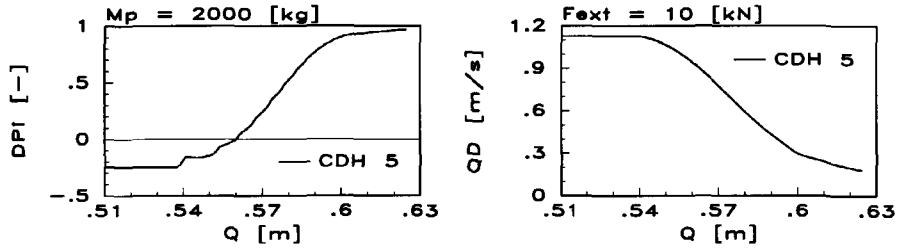


Fig. 5.11: Simulation results of CDH cushioning design example CDH 5; actuator pressure difference $\overline{\Delta P}_i = \bar{P}_{i1} - \bar{P}_{i2}$ (left) and actuator velocity $\dot{q}$ (right)

peak is reduced, but the peaks related to other holes become larger.

- In order to obtain an approximately triangular acceleration profile, the successive distances between the holes should decrease, as well as the successive diameters of the holes (see middle plots of Fig. 5.10).
- The approximation of the desired triangular acceleration profile is improved, if the number of holes is increased (lower plots of Fig. 5.10). The resulting cushioning pressure is smoothened as well.

In conclusion on the results of Fig. 5.10, it can be stated that the geometry denoted as CDH 5 in Table 5.2 is approximately optimal in the sense of the design objective. However, one aspect has not been considered here, namely the final velocity at the end of the cushioning stroke. Therefore, a more complete picture of the achieved performance is given by Fig. 5.11, showing the simulated pressure difference $\overline{\Delta P}_i = \bar{P}_{i1} - \bar{P}_{i2}$ and actuator velocity $\dot{q}$ for CDH 5.

Concerning the pressure difference, $\overline{\Delta P}_i$, similar behaviour is seen as for the PIH cushioning in Fig. 5.9, as might be expected. However, for the velocity $\dot{q}$, there is an important

difference with the simulation result of the PIH cushioning of Fig. 5.9: the simulation predicts a significant final velocity. Actually, this is an inherent property of the CDH cushioning, caused by the conicity of the bearing of the piston head. The clearance due to this conicity will still allow a significant cushioning flow, even if the piston head has closed the drain hole. This results in a non-zero velocity, while all drain holes are closed.

However, there is a way to reduce the final velocity, because the flow through a closed drain hole reduces if the piston head moves further along the hole. This is caused by the fact that A_h becomes smaller (see Fig. 5.5). Thus, the final velocity can be reduced by placing the final hole, indicated by hole number n_h, at a sufficiently large distance from the end of the cushioning zone. Note that this aspect is already taken into account in the proposed design `CDH 5`.

Although the presented simulation results provide reasonable insight in the behaviour of the CDH cushioning, as far as the presented model of Subsection 5.2.3 predicts this behaviour, an actual evalutation of the proposed design is impossible without an experimental validation of the model. Therefore, experimental results from an actual setup are presented in the next Section, not only for the CDH cushioning but also for the PIH cushioning.

5.4 Experimental evaluation of the cushioning design

The experimental evaluation of the proposed cushioning designs has been performed with the experimental setup, described in Section 3.3. Actually, the actuators that were used to obtain the experimental results of Chapter 3, and also those of Section 4.6, have been equipped with the cushionings according to the designs proposed in Subsection 5.3.3 and 5.3.4 respectively. These cushionings have been extensively tested under different load conditions and initial actuator velocities.

The large amount of available experimental data has not only been used to perform a final validation of the simulation models as will be discussed in Subsection 5.4.1, but also to evaluate the eventual experimental performance of the cushionings, as compared to the expected performance. In this scope, some representative results for the PIH and the CDH cushioning are shown in Subsection 5.4.2 and 5.4.3 respectively.

5.4.1 Final model validation

In Subsection 5.2.4, page 282, it was discussed how preliminary experiments allowed an intermediate validation of the cushioning models. However, with the final actuators equipped with the designed cushionings, it is possible to perform a final validation, which is more realistic than the intermediate validation. The reason is, that with the designed cushionings, the cushioning behaviour is close to the desired performance. That means, that the cushioning geometry is quite realistic, allowing a proper validation of the model and its underlying assumptions.

Whereas the intermediate validation results of Subsection 5.2.4 were obtained at relatively small velocities and loads for safety reasons, the final validation tests could be performed at maximum velocity and under different load conditions. As discussed in Subsection 3.3.1, the experimental test rig allowed to do so; using removable loads, different load conditions could be created. Four different load conditions have been considered in

the cushioning tests, with inertial loads M_p and static load F_{ext} given in Table 5.3. These load conditions reflect the various load conditions that might occur during cushioning in a flight simulator motion system, and can be described as follows.

- `Load a` represents a small inertial load with small static load, which may be critical with respect to the maximum acceleration that might occur during cushioning, both for the PIH and the CDH cushioning.
- `Load b` represents a medium inertial load with a large static load downward, which may be critical with respect to the maximum cushioning pressure $\bar{P}_{p1}$ that might occur during cushioning in downward direction, so for the PIH cushioning.
- `Load c` represents a large inertial load with a neglibible static load, which may be critical with respect to the overall cushioning behaviour, i.e. the smooth and safe dissipation of a large kinetic energy in a limited cushioning distance. This holds both for the PIH and the CDH cushioning.
- `Load d` represents a medium inertial load with a considerable static load upward, which may be critical with respect to the maximum cushioning pressure $\bar{P}_{p2}$ that might occur during cushioning in upward direction, so for the CDH cushioning.

	Load a	Load b	Load c	Load d
M_p [kg]	$0.78\ 10^3$	$1.96\ 10^3$	$3.14\ 10^3$	$1.96\ 10^3$
F_{ext} [kN]	-2.10	-14.40	-1.65	9.50

Table 5.3: Load conditions for experimental evaluation PIH and CDH cushionings

Comparing simulations with these load conditions to experiments, the final validation of the cushioning models has been performed. Without extensively showing intermediate results, some comments are given on the adjustments of the model, that were necessary to arrive at experimentally validated models.

- The value for the supply pressure P_s in the model has been chosen a bit smaller than the theoretical value, namely 155 instead of 160 [bar]. The reason is, that the power supply unit shows a slight decrease of the supply pressure if a large oil flow is demanded, which is the case for the full speed cushioning tests considered here.
- In order to simulate the absolute pressures in the actuator chambers correctly for the case that the actuator is moving with high velocity, manifold losses, as modelled by (2.85) on page 85, had to be taken into account, at least at the valve side of the transmission lines. The corresponding coefficients were chosen as follows: $A_{man,i1} = A_{man,i2} = 1.73\ 10^{-4}$ [m^2] and $A_{man,o1} = A_{man,o2} = \infty$, i.e. no manifold losses at actuator side.
- As far as the PIH cushioning is concerned, the dynamic effect of the compression of the oil in the cushioning compartment appeared to be much faster in simulations than in experiments. In the original simulation model, the cushioning compartment has a relatively small volume, so the dynamics of the pressure build-up are relatively fast. This effect was not found in the experimental results. Apparently, the actual stiffness of the (oil in the) cushioning compartment is considerably smaller than theoretically predicted. This may be caused by invalidity of the assumption that the walls of

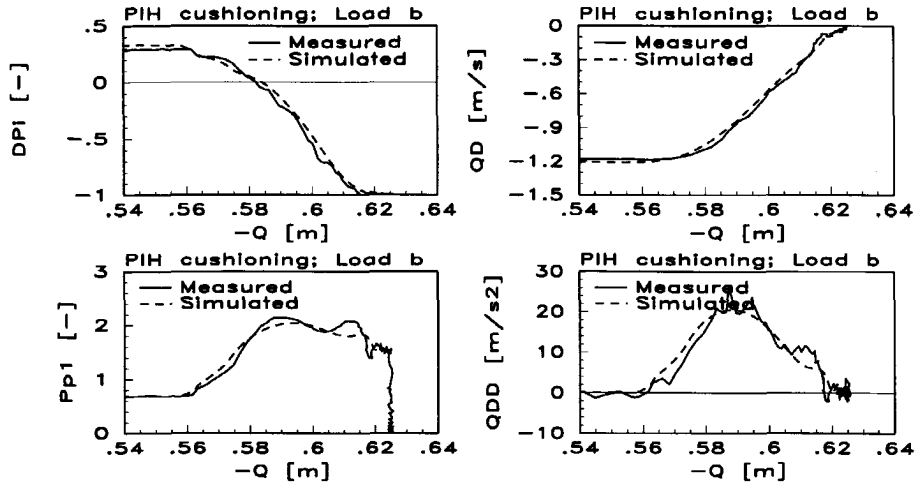


Fig. 5.12: Experimental validation results PIH cushioning design for load condition Load b; measurement (solid) and simulation (dashed); actuator pressure difference $\overline{\Delta P}_i = \bar{P}_{i1} - \bar{P}_{i2}$ (upper left); cushioning pressure $\bar{P}_{p1}$ (lower left); actuator velocity $\dot{q}$ (upper right); actuator acceleration $\ddot{q}$ (lower right)

the actuator are infinitely stiff, Assumption 5.2.1. In order to improve the predictive value of the models, the models were adjusted by lowering the effective stiffness of the cushioning compartment by means of adding an ineffective volume of 2.25 10^{-4} [m^3].

- A final adjustment concerns the discharge coefficient C_{d1} in the PIH cushioning model. The velocity reduction predicted by the original model appeared to be larger than observed in measurements, indicating that the resistance of the cushioning flow is smaller than expected. A more valid prediction of the velocity reduction has been obtained by adusting the discharge coefficient to a value of $C_{d1} = 0.9$ instead of 0.8.

After this discussion of the adjustments of the cushioning models, comprising the final validation of the models, the actual comparison of simulated and measured cushioning responses is given in the following Subsections.

5.4.2 Experimental evaluation of the PIH cushioning

Considering the experimental load conditions of Table 5.3, no one of them does exactly reflect the load condition, that the PIH cushioning was originally designed for. The best approximation is the condition denoted by Load b. For this condition, a comparison of simulation and experiment is given in Fig. 5.12.

Qualitatively, there is a very good agreement; quantitatively, there are some slight differences. The most important difference is, that the measured cushioning pressure peaks are larger than predicted. This may be due to unmodelled dynamic effects, or even non-linearity in the compressibility of the oil. Despite this difference in the cushioning pressure, the agreement in the acceleration is very good, and apart from a small peak at the top of the acceleration profile (which maybe caused by unmodelled dynamics too), the acceleration

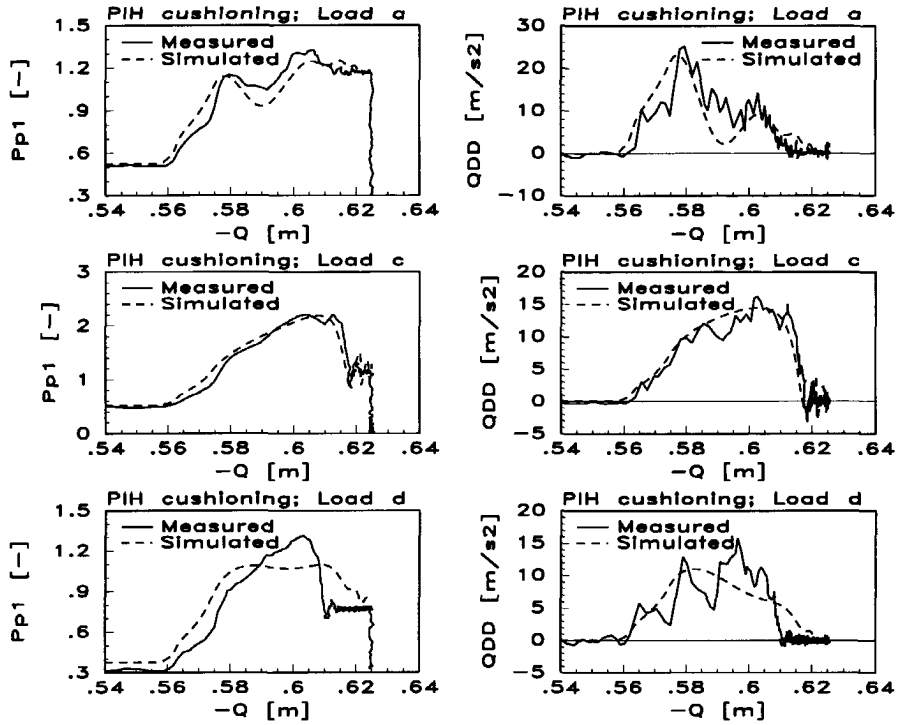


Fig. 5.13: Experimental validation results PIH cushioning design; measurement (solid) and simulation (dashed); cushioning pressure $\bar{P}_{p1}$ (left); actuator acceleration $\ddot{q}$ (right); different load conditions `Load a` (upper), `Load c` (middle) and `Load d` (lower)

is predicted very well. Moreover, it does not significantly exceed the maximum specified acceleration $\ddot{y}_{c,max} = 20$ [m/s^2], corresponding to the desired motion profile `MP3`, on which the applied cushioning design was based. Concerning the pressure difference ΔP_i and the velocity $\dot{q}$, the model performs well, both qualitatively and quantitatively.

Besides that the agreement between model and experiment is very good, the actual performance of the cushioning is also impressive. Note, that the energy of a large inertia, under a considerable static load, with a large initial velocity of ≈ 1.2 [m/s], is completely dissipated within a cushioning distance of about 60 [mm], without excessive accelerations. Actually, this result already allows the conclusion, that the model-based cushioning design is quite succesful.

A further evaluation of the performance of the same cushioning is given in Fig. 5.13, showing cushioning pressures and accelerations for different load conditions. Again, there are some quantitative differences between simulations and experiments, especially for the cushioning pressure, and also for the acceleration in case of `Load d` (lower right plot). This latter difference can be ascribed to parasitic motions of the base (see also Subsection 3.3.1); these motions were visually observable during the performed cushioning tests, especially for load condition `Load d`. However, in general, the qualitative agreement is satisfactory for all load conditions.

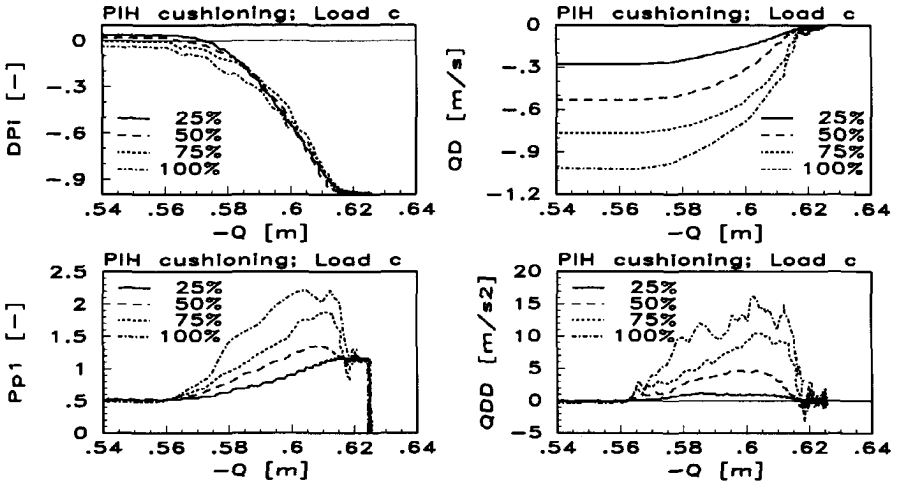


Fig. 5.14: Experimental results PIH cushioning for different initial velocities under load condition Load c; actuator pressure difference $\overline{\Delta P}_i = \bar{P}_{i1} - \bar{P}_{i2}$ (upper left); cushioning pressure $\bar{P}_{p1}$ (lower left); actuator velocity $\dot{q}$ (upper right); actuator acceleration $\ddot{q}$ (lower right)

Clearly the different resulting motion profiles for the acceleration of Fig. 5.13 deviate considerably from the desired (triangular) motion profile, as the load conditions are different from the condition for which the PIH cushioning was designed. In the sense of maximum acceleration, Load a appears to be critical indeed; for this load the specified maximum acceleration $\ddot{y}_{c,max} = 20$ [m/s^2] is exceeded, as already expected from simulations. For the other load conditions, the acceleration remains well beyond the specified maximum. So, in this sense, the designed and applied peg geometry results in a robustly performing PIH cushioning.

The results shown so far, have all been obtained at maximum velocity, i.e. at a maximum servo-valve opening. Although the sensitivity of the servo-valve flow with respect to the static load caused some differences in the initial velocities of Fig. 5.12 and 5.13, the effect of the initial velocity is not so clear. To illustrate this effect further, experimental results for four different initial velocities are shown in Fig. 5.14. Thereby, load condition Load c has been selected, as it can be seen as the worst case, in the sense that it relies most on the final part of the cushioning zone.

The conclusion from Fig. 5.14 is, that the PIH cushioning performs similar for all velocities. Thereby the occurring cushioning pressures and accelerations are almost proportionally related to the initial velocity. This implies, that it is highly important to have a realistic estimation of the maximum velocity that might occur in a system, when a cushioning is to be designed. In other words, experiments emphasize the role of the initial velocity $\dot{q}_0$ in the design objective of page 284.

As a final result concerning the experimental evaluation of the PIH cushioning design, the robustness of the design with respect to manufacturing tolerances is shown in Fig. 5.15. The Figure shows the measured accelerations at full speed cushioning under load condition Load c, for six different actuators. Apparently, the designed cushionings do all show a

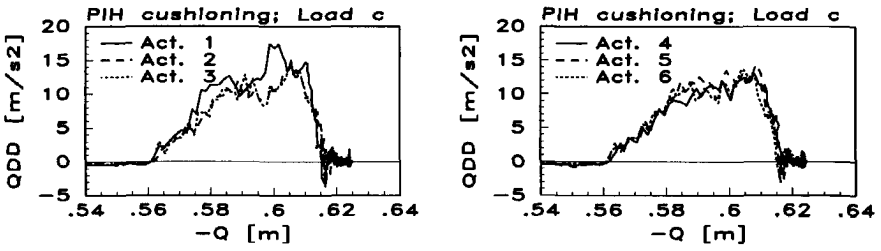


Fig. 5.15: Measured accelerations PIH cushioning for different actuators under load condition Load c; actuator 1, 2 and 3 (left); actuator 4, 5 and 6 (right)

good performance, with little differences between different actuators. Actually, the differences that are noticable from Fig. 5.15, can mainly be ascribed to differences in initial velocities, which in turn are caused by differences in maximum servo-valve flows according to Fig. 3.38. However, when concluding that manufacturing inaccuracies play a minor role in the experimental performance of the cushioning, it should be noted, that considerable attention has been paid to the manufacturing of the cushioning pegs; tolerances in the peg geometry were not allowed to exceed 5 [μm].

In conclusion on the experimental evaluation of the PIH cushioning, it can be stated, that the designed cushioning geometry performs well in practice, under different load conditions and initial velocities, and even for different tested actuators. Moreover, a good agreement between experiments and simulations with the validated PIH cushioning model is found. The next topic is now, to see whether similar results can be obtained with the CDH cushioning.

5.4.3 Experimental evaluation of the CDH cushioning

From the experimental load conditions of Table 5.3, the condition denoted by Load d forms the best approximation of the load condition, for which the CDH cushioning was originally designed. Therefore, it is used to compare simulations and experiments; the results are given in Fig. 5.16.

Compared to the results for the PIH cushioning in Fig. 5.12, the agreement between simulation and experiment is not so good. Like for load condition Load d with the PIH cushioning in Fig. 5.13, the measured cushioning pressure exceeds the simulated pressure $\bar{P}_{p2}$ considerably half-way the cushioning zone. And again, a significant difference is found in the initial part of the acceleration profile, and therewith in the velocity profile, for Load d. As mentioned before, this can be ascribed to parasitic motions of the base, which are especially induced by this load condition.

In the final part of the cushioning zone, however, there is a good qualitative agreement between model and experiment. Especially the final velocity of the actuator is well-predicted; the experimental result shows, that there is a considerable final velocity at the end of the cushioning zone, as expected. Apparently, the clearance of the conical bearing does really allow a considerable cushioning flow, even after all cushioning holes have been closed. Note hereby, that both simulation and experiment show a clear transition in the behaviour at the moment, that the last cushioning hole is closed.

With the result of Fig. 5.16, the inherent property of the CDH cushioning, the non-zero

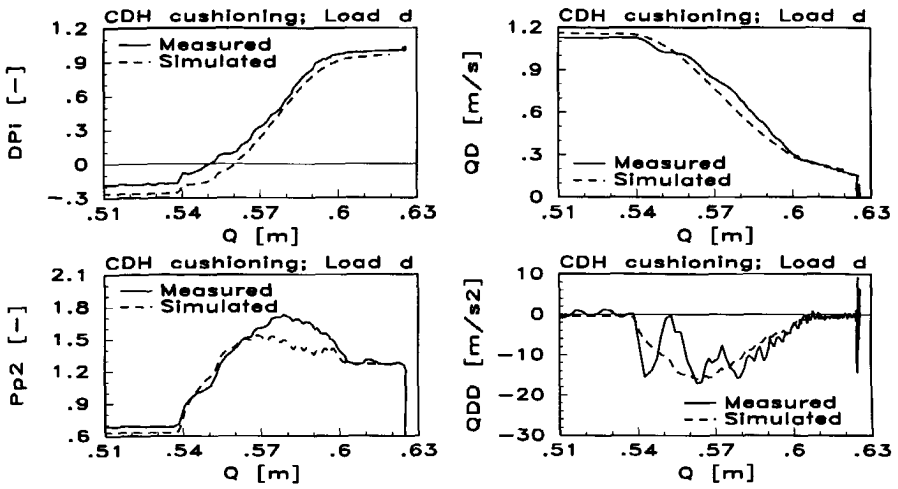


Fig. 5.16: Experimental validation results CDH cushioning design for load condition Load d; measurement (solid) and simulation (dashed); actuator pressure difference $\overline{\Delta P}_i = \bar{P}_{i1} - \bar{P}_{i2}$ (upper left); cushioning pressure $\bar{P}_{p2}$ (lower left); actuator velocity $\dot{q}$ (upper right); actuator acceleration $\ddot{q}$ (lower right)

final velocity, is experimentally verified. Actually, it can be seen as a disadvantage of this type of cushioning, because the final velocity suddenly drops to zero when the actuator reaches the end of its stroke. Thus a hard stop occurs, with rather high acceleration peaks, which may be almost as large as the maximum acceleration during the cushioning, as the lower right plot of Fig. 5.16 shows. Despite this final hard stop, it can be stated that the CDH cushioning performs well, as the overall maximum acceleration is yet smaller than 17 [m/s^2].

Not only for the load condition Load d, but also for the other load conditions, the model-based design of the CDH cushioning shows satisfactory performance. The experimental results of cushioning tests with maximum velocity, together with corresponding model simulations, are given in Fig. 5.17. The results give rise to a number of remarks:

- The model tends to underestimate the maximum cushioning pressure, especially halfway the cushioning zone.
- The acceleration profile during cushioning is well-predicted by the model for the various load conditions.
- Though the cushioning behaviour is slightly different for different load conditions, the performance is satisfactory in all cases. The initial velocity is reduced to an acceptable final value, without excessive acceleration peaks and cushioning pressures.

Summarizing, the results of Fig. 5.16 and 5.17 form a good qualitative validation of the adopted simulation model of the CDH cushioning, and provide an experimental justification of the use of this model for model-based design.

Comparing the results of the CDH cushioning to those of the PIH cushioning, given in Fig. 5.12 and 5.13, two differences are observed:

- The maximum cushioning pressure is considerably smaller for the CDH cushioning.

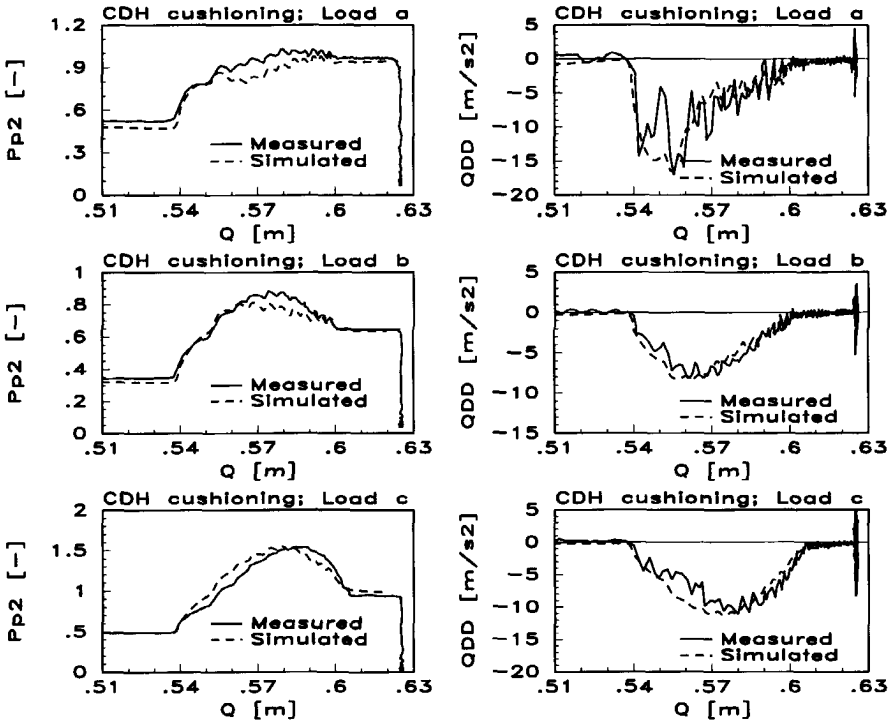


Fig. 5.17: Experimental validation results CDH cushioning design; measurement (solid) and simulation (dashed); cushioning pressure $\bar{P}_{p2}$ (left); actuator acceleration $\ddot{q}$ (right); different load conditions `Load a` (upper), `Load b` (middle) and `Load c` (lower)

The reason is twofold. First, the CDH cushioning utilizes the complete piston area A_p to decelerate the load, while in case of the PIH cushioning, the decelerating force is to be delivered by the cushioning pressure times the smaller area A_{rem}. Second, the cushioning takes place over a longer distance for the CDH cushioning, so that the acceleration and therewith the cushioning pressure can be smaller. In this sense, the CDH cushioning is more safe.

- The differences in acceleration profiles for the various load conditions are larger for the PIH cushioning than for the CDH cushioning. The CDH cushioning shows nice smooth profiles, especially for `Load b` and `Load c`, while the PIH cushioning shows more peaking of the acceleration either in the beginning (`Load a`), in the middle (`Load b`) or at the end (`Load c`) of the cushioning zone. So, the CDH cushioning is more robust against varying load conditions.

Like for the PIH cushioning, the initial velocity is an important factor, when considering the behaviour of the CDH cushioning, especially with respect to maximum cushioning pressures and accelerations. This is illustrated by Fig. 5.18, showing the experimental results for different initial velocities under load condition `Load c`. In general, the same conclusions concerning the effect of the initial velocity hold as for the case of the PIH cushioning. There is one difference, namely the behaviour in the final part of the cushioning

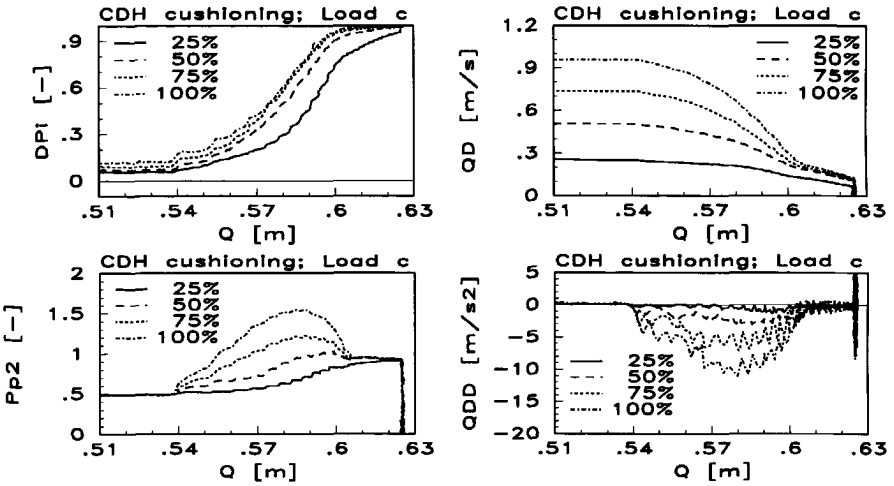


Fig. 5.18: Experimental results CDH cushioning for different initial velocities under load condition Load c; actuator pressure difference $\overline{\Delta P}_i = \bar{P}_{i1} - \bar{P}_{i2}$ (upper left); cushioning pressure $\bar{P}_{p2}$ (lower left); actuator velocity $\dot{q}$ (upper right); actuator acceleration $\ddot{q}$ (lower right)

zone.

Clearly, the upper right plot of Fig. 5.18 shows, that the velocity of the actuator during the final part of the cushioning, i.e. after the last cushioning hole is closed, does not significantly depend on the initial velocity $\dot{q}_0$, except for the smallest velocity (25 %). This is remarkable, and again illustrates the inherent property of the CDH cushioning, namely that the final velocity is determined by the clearance due to the conicity of the piston head, and not by the chosen geometry of the CDH cushioning. Actually, the observed effect makes that the CDH cushioning performs relatively better for higher velocities. Therewith, the design objective on page 284 is met by the CDH cushioning design, in the sense that a smooth and safe stop is guaranteed in the worst case, namely for large initial velocity.

The robustness of the CDH cushioning against manufacturing tolerances is shown in Fig. 5.19, with measured accelerations at full speed cushioning under load condition Load c, for six different actuators. Like for the PIH cushioning, little differences are observed, while the deviation for the first actuator can be ascribed to a larger initial velocity. Again, it can be conluded that manufacturing inaccuracies play a minor role in the experimental performance of the cushioning, provided that sufficient attention has been paid to the manufacturing, with allowable tolerances in the order of 5 [μm].

Thus, the experimental evaluation of the CDH cushioning can be concluded similarly as that of the PIH cushioning. The simulation model is experimentally validated, at least qualitatively, while the model-based CDH cushioning design leads to a satisfactory cushioning performance, under different conditions. Remarkable for the CDH cushioning is the significant but acceptable final velocity, which appears to be hardly dependent on load condition and initial velocity.

With the results of the experimental evaluation of the cushioning design in this Section, the discussion of the cushioning design is completed, and the Chapter can be concluded.

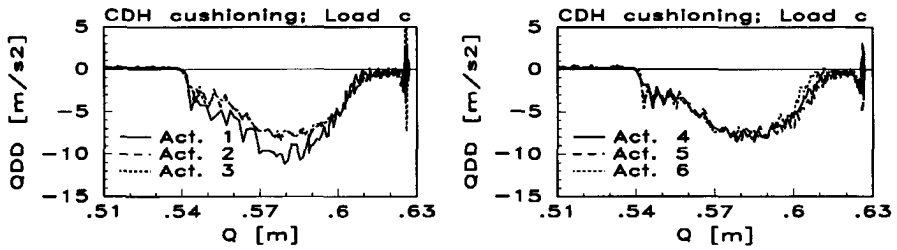


Fig. 5.19: Measured accelerations CDH cushioning for different actuators under load condition Load c; actuator 1, 2 and 3 (left); actuator 4, 5 and 6 (right)

5.5 Conclusions

Although the modelling of hydraulic servo-systems is mainly motivated by the desire for model-based control design, the obtained models are also quite useful for cushioning design. The model-based approach for the design of safety cushionings for hydraulic actuators, developed in this Chapter, leads to a satisfactory cushioning design, with a satisfying experimental performance. Where this approach is applied to a PIH cushioning and a CDH cushioning respectively, some typical similarities and differences have been found, which are summarized below.

The basic setup for the modelling of both types of cushioning is similar, and consists of extensions of the original theoretical model of the hydraulic actuator of Subsection 2.3.4 with models for the cushioning flow. These latter models have been based on some strong assumptions, where the PIH cushioning flow is assumed to be dominated by turbulent flow losses, while the CDH cushioning flow is assumed to involve laminar resistance as well.

In the design procedures for both types of cushioning, the design objective involves a kind of trade-off between maximum cushioning pressure and maximum acceleration during the cushioning. In order to avoid high cushioning pressures in the final stage of the cushioning, a larger acceleration should be allowed in the initial stage. This can be done by specifying the desired motion profile as a triangular acceleration profile in the displacement domain.

Given the actuator geometry and the desired motion profile, the cushioning models can be used to design an optimal cushioning geometry. For the PIH cushioning, the design procedure directly leads to an optimal peg geometry, which can be approximated with a finite number of slopes for manufacturing purposes. The design procedure for the CDH cushioning leads indirectly to an optimal geometry, in the form of required distances between and diameters of the cushioning holes, by means of simulation of the cushioning model.

Experimental evaluation of the designed cushionings shows the validity of the developed models, with good correspondence between measured and simulated responses, for different load conditions. This means, that the experimental performance of both types of cushioning is close to expectations from simulations, implying satisfactory experimental results with respect to the stated design objective.

Related to the principle of cushioning, there are some differences between the PIH cushioning and the CDH cushioning.

- The CDH cushioning typically shows a considerable final velocity, resulting in an ad-

ditional acceleration peak after the cushioning has taken place. In order to minimize this final velocity, a sufficiently large distance between the last cushioning hole and the end of the cushioning zone is required, resulting in a large cushioning distance, as compared to the PIH cushioning.

- Partly due to the shorter cushioning distance of the PIH cushioning, the maximum cushioning pressure and acceleration during cushioning are larger for the PIH cushioning than for the CDH cushioning.
- The PIH cushioning appears to be more sensitive to varying load conditions than the CDH cushioning; the latter generally shows more smooth acceleration profiles, even for small inertial load.

Finally, experimental results clearly show the effect of the initial velocity on the cushioning behaviour; maximum cushioning pressure and acceleration are almost proportionally related to the initial velocity. Actually, differences between the cushioning behaviour of different actuators can mainly be ascribed to differences in initial velocity due to differences in maximum servo-valve flows.

Chapter 6

Conclusions and recommendations

In the past decades, the hydraulic servo technique has developed to a high level of technology, among others due to the hydrostatic bearing technique for hydraulic actuators. Furthermore, recent developments in computer technology have created new possibilities in the digital control of this kind of servo-systems. Therewith, recent advances in the area of control theory, involving non-linear, multivariable and robust control techniques, can now be utilized and applied to real systems. Especially in applications where an improved performance of motion is required, such as in flight simulator motion systems, the application of sophisticated motion control strategies to multi degrees-of-freedom hydraulic servo-systems is expected to be beneficial.

The application of new motion control strategies in flight simulator motion systems poses high performance demands on the control of the hydraulic actuators. Because of these high demands, dynamic properties of the hydraulic servo-system become important, that were not important in conventional servo control designs, such as servo-valve dynamics and non-linearities and transmission line dynamics. Although transmission line dynamics may also be relevant in other applications, they are typical for flight simulator motion systems with long-stroke hydraulic actuators, where relatively long transmission lines between the servo-valve and the actuator chambers are present.

In the scope of the developments sketched here, the main contribution of this thesis is, that the extensive modelling of long-stroke hydraulic servo-systems has provided much insight in the behaviour of these systems, as well with respect to their dynamics as to their non-linearities. The developed models are shown to be quite useful, with experimental evidence, both for control design and for system design.

Related to the five main research topics of this thesis, mentioned in Subsection 1.3.2, the contribution of this thesis can be worked out in a number of conclusions, which is done in Section 6.1. Topics that fell beyond the scope of this thesis, but deserve further research, are discussed as recommendations for future work in Section 6.2.

6.1 Conclusions

After the conclusions concerning the modelling of the actuator, the servo-valve and the tranmission lines respectively, the results on control design and on system design are concluded, in the successive Subsections below.

6.1.1 Modelling of the hydraulic actuator

The given example of modelling a double-concentric symmetric hydraulic actuator shows, that theoretical modelling of hydraulic actuators forms a very good basis for the investigation of the behaviour of a hydraulic servo-system:

- Theoretical modelling provides insight in the basic dynamic behaviour of the actuator and in the most important non-linearities, possibly related to certain aspects of the construction design, e.g. the type of the applied bearings.
- The actuator model forms the kernel of any extensive model of the hydraulic servo-system. If a dynamic servo-valve model is taken into account, it is placed in series with the actuator model; if transmission line dynamics are taken into account via proper integration of the actuator model and the transmission line models, the dominant (low-frequency) dynamics are still determined by the actuator model.
- The theoretical model is easily simplified, and identified from experimental data. In this approach, an experimentally validated actuator model is obtained, which is shown to be useful for model-based control design, and also provides quantitative insight in certain physical aspects of the system behaviour, e.g. the friction level.
- The theoretical actuator model forms a starting point for successful model-based cushioning design.

So, the derivation of an application dependent theoretical model of the hydraulic actuator forms a key-stone for research in the hydraulic servo technique. Therefore, any serious attempt to consider (aspects of) the behaviour of a hydraulic servo-system should include this basic step of actuator modelling.

6.1.2 Modelling of the servo-valve

Because servo-valve dynamics may play an important role in high-performance control design for hydraulic servo-systems, it is important to have insight in the behaviour of the servo-valve. A general approach to the modelling of servo-valves, as presented in this thesis, provides this insight, as well as experimentally validated non-linear dynamic models, which can be used for control design and system design. This result can be further elucidated as follows:

- Much insight in the dynamics and non-linearities of two- and three-stage flapper-nozzle valves is obtained by theoretical modelling, although hard quantitative results can not be obtained due to a lack of information on parameter values in the theoretical model. Nevertheless, the derivation of a theoretical model is shown to be useful, because:
  - qualitative insight in the relevance of various non-linear effects is obtained from non-linear simulations; Coulomb friction and ball clearance should always be avoided while a critical-centre spool port geometry is highly recommendable to avoid non-linearity in the servo control loop.
  - realistic modelling assumptions allow simplifications of the model, that lead to low-order physically structured dynamic models, including dominant non-linearities, which are accessible for experimental identification.
- The technique of grey-box modelling, i.e. the identification of a physically structured servo-valve model including a dominant static non-linearity, appears to be

quite successful. Using the Sinusoidal Input Describing Function (SIDF) method, the dynamics and the static non-linearity of the servo-valve can be explicitly characterized. The linear dynamics are identified from measured frequency responses, obtained from properly designed experiments with well-defined signal amplitudes; the static non-linearity is identified from amplitude responses, characterizing the amplitude dependent behaviour of the valve at a certain frequency.
The result is an experimentally validated non-linear dynamic model of the servo-valve, which describes the real system behaviour with a high-accuracy, and which is especially well-suited for controller design and analysis of the closed loop behaviour of the hydraulic servo-system.

- Where the approach has been applied to the three-stage servo-valves of the hydraulic actuators of a flight simulator motion system, it is also applicable to other types of flapper-nozzle servo-valves. Given the extensive theoretical model of the servo-valve, there is some freedom in making assumptions, meaning that some alternative model structures, with possibly different model order, are available. A choice for a certain model structure, for a given application, should be made based on experimental (frequency response) data of the servo-valve under consideration.
- From a control design point of view, the hydraulic servo-system can be seen as a series connection of the servo-valve and the actuator. So, if servo-valve dynamics are relevant for a certain application, which is to be judged using Rule A.1.2 and A.1.3 on page 322, the servo-valve model should be included as additional dynamics in the control loop, in a series connection with the actuator model.

In the field of hydraulic servo control, it is usual to start the analysis and control design with neglecting servo-valve dynamics. Too often, servo-valve dynamics are only included in the investigations, after experimental results have shown that the desired performance can not be achieved with the designed controllers. Obviously, a servo-valve model should be included in an earlier stage, in order to investigate the possible implications of servo-valve dynamics on closed loop control at simulation level. This is especially important, if high performance levels are desired, where it can be expected a-priori, that servo-valve dynamics will play an important role.

In other words, high-performance applications of hydraulic servo control ask for a real model-based approach, including servo-valve dynamics in an early stage in the control design and even in the system design, so that costly iteration steps in the design process, due to unexpected unsatisfactory experimental results, may be avoided. In fact, this does not only hold with respect to servo-valve dynamics, but also with respect to transmission line dynamics.

6.1.3 Modelling of transmission line dynamics

Due to restrictions in the constructive design of hydraulic servo-systems, it may be inevitable that relatively long transmission lines are present between the servo-valve and the actuator chambers, e.g. in the case of the long-stroke actuators of a flight simulator motion system. These long transmission lines will introduce badly damped resonances in the dynamics of the hydraulic servo-system. By means of proper inclusion of these transmission line dynamics in the modelling of the hydraulic servo-system, crucial insight is obtained in the dynamic behaviour of the actuator with transmission lines. This insight can be

used to avoid stability problems due to the transmission line dynamics, either by means of model-based control design, or by means of proper system design.

The basic idea behind modelling transmission line dynamics in a hydraulic servo-system is the use of a suitable approximation of the theoretical model of a transmission line, in order to include transmission line models in a modular way in the model of the complete hydraulic servo-system. The modal approximation technique, presented by Yang and Tobler [160], was found to be well-suited for this purpose, for the following reasons:

- For a certain number of resonance modes, the modal approximation is an accurate, minimal-order approximation of the theoretical, physical (open loop) model of a *transmission line*.
- The modal approximation can be represented, among others, in state space form, allowing easy access to system theoretic analysis, both in the frequency domain and in the time domain. The parameters in this state space representation have a clear physical interpretation, so that the model is extremely useful for preliminary dynamic analysis of the hydraulic actuator including transmission lines in the system design stage.
- By means of proper definition of the inputs and the outputs of the four-port model, the approximations are causal / physically realizable, and can be integrated in a simple way with the basic actuator model by means of bilateral coupling. Thereby, the (approximate) transmission line model can be seen as a module, which is easily left out of the actuator model in case transmission line dynamics need not to be considered.
- The inclusion of modal approximations of the transmission line models in the actuator model provides a good basis for grey-box modelling. Good experimental results in the identification and validation of the actuator model including the transmission line models show the validity of the approach. The physical structure of the model even allows the inclusion of a relevant non-linear effect in the identification and validation: the position dependence of the actuator and transmission line dynamics has been successfully identified and validated on a real system.
- Besides that the inclusion of modal approximations of the transmission line dynamics in the actuator model provides insight in these dynamics, which can be used during control design, the identified and validated models also form a good basis for model-based control design, because they are of reasonably low order. It might be noted here, that the second harmonics of the transmission lines have also been included, and even could be validated experimentally, in this thesis. However, from a control design point of view, it will mostly be sufficient, to take only the first mode of the transmission line dynamics into account. This even allows for an 8^{th} (instead of 12^{th}) order model for a hydraulic actuator with two transmission lines.

Like servo-valve dynamics, transmission line dynamics are mostly neglected in the first instance. This is not necessarily unjustified, but for certain applications care should be taken in this respect. This especially holds for applications with relatively long transmission lines, where the resonance frequencies related to these transmission lines lie in a frequency range, in which servo-valve dynamics can not be neglected. Problems will also be encountered, when the desired control bandwidth, especially of a pressure difference control loop, is close to the (expected) transmission line resonance frequencies. In these cases, it is strongly recommendable to perform a preliminary analysis of the expected dynamic behaviour of

the system including transmission lines, in the system design stage already, by including modal approximations of the transmission line models in the actuator model.

In spite of preliminary analysis in the design stage, relevant transmission line dynamics might be unavoidable for a given application. In that case, the given approach of modelling of transmission line dynamics should be applied, in order to solve potential stability problems with proper model-based control design.

6.1.4 Control design for hydraulic servo-systems

In the field of high-performance applications of hydraulic servo-systems, especially in multi degree-of-freedom (DOF) motion systems, such as flight simulator motion systems, it is useful to adopt a two-level structure for control. The high-level control should typically account for geometric non-linearities of the system and for interaction between the different degrees of freedom. Actually, the high-level control is concerned with the control of the mechanics of the system, and computes the desired forces to be delivered by the actuators. These desired forces, in the form of a reference signal for the actuator pressure difference, are fed into the low-level actuator control loops, which give the hydraulic actuators the character of pure force generators.

In practice, there may be applications, in which the implementation of the advanced model-based two-level control strategy, sketched here, is not feasible for some reason. This may imply, for instance, that no reference signal for the actuator pressure difference is available, but only a position reference. The effects of the availability of proper reference signals for the actuator control loop on the achievable control performance can be investigated, by comparing a number of hydraulic actuator control strategies for a single DOF setup. Thereby, a rather general task specification is formulated, namely to follow the desired position-velocity-acceleration trajectory (generated by a trajectory generator) as close as possible, i.e. with minimum phase lag. In order to include the effects of load variations and coupling forces (playing a role in the multi DOF case) in the analysis, the sensitivity of the control strategies (in the single DOF case) to different load conditions is to be considered.

The conclusion on the analysis of different actuator control strategies is, that besides position and possibly velocity feedback, pressure difference feedback is very important to achieve a high-performance servo control. Especially when a good reference signal for the pressure difference is available from a feedforward controller, high-gain pressure difference feedback should be applied; it leads to a high control performance and a low sensitivity to different load conditions. Thereby, it is crucial for the low-frequency behaviour of the hydraulic servo-system, that either feedforward of the desired velocity or positive feedback of the real velocity is applied. The latter case, positive velocity feedback combined with high-gain pressure difference feedback, actually refers to the cascade ΔP control strategy. From the hydraulic actuator control strategies considered here, this strategy is the only one, that fits well in the two-level motion control structure, sketched in the beginning of this Subsection. Therefore, the cascade ΔP control strategy is recommended for multi DOF systems.

Initially, the comparison of hydraulic actuator control strategies has been based on the basic actuator model that is the result of the first main research topic, see Subsection 6.1.1. However, when a really high performance is to be obtained by applying a fast pressure difference control loop, it is extremely important to include all relevant dynamics in the

model-based design of this control loop. This means, that servo-valve dynamics and, if present, transmission line dynamics, should be explicitly taken into account (see also Subsection 6.1.2 and 6.1.3). Thereby, it is found that servo-valve dynamics basically restrict the achievable bandwidth of the pressure difference control loop, while relevant transmission line dynamics definitely require the design of a dynamic pressure difference feedback loop. Additionally, serious attention is required for the robustness of any designed controller, due to some dominant non-linearities of the servo-valve (non-linear flow characteristic) and the actuator (position dependence of the dynamics).

Provided that servo-valve and transmisison line dynamics are properly taken into account in the model-based control design, a very good agreement is found between experimental closed loop responses and simulated ones, at least if parasitic dynamics of the load and the actuator base are left out of consideration. Actually, this can be seen as a further validation of the obtained models of the hydraulic system, in a closed loop sense. Besides that, the good experimental results emphasize the real value of the approach of model-based control design and digital controller implementation, at least for the given application of a long-stroke actuator of a flight simulator motion system. This may be further elucidated as follows:

- With the model-based approach to control design, exploiting available model knowledge of the system, high performance levels have been achieved. With the standard approach to hydraulic servo control, consisting of the tuning of some proportional gains, this would not have been possible; stability problems due to transmission line dynamics would even have excluded the possibility to achieve a moderate performance.
- In good engineering practice with state-of-the-art hardware and software available, controller implementation issues do not form any limitation for the application of model-based control to hydraulic servo-systems. High performance levels are achieved under experimental conditions with a digital controller, comparable to those in continuous time simulations.
- Whereas velocity feedback can improve the closed loop performance, a practical problem arises in case of long-stroke actuators, as long-stroke velocity transducers are hardly available. However, again a model-based approach appears to be successful. For instance, the Kalman filter design technique leads to feasible solutions to estimate the velocity, with satisfactory performance under experimental conditions.

In short, utilizing the improved quality of the models of hydraulic servo-systems, as well as developments in motion control techniques, while exploiting recent advances in digital control technology, higher performance levels can be achieved in hydraulic servo control than before. Yet, it is important to note, that the achievable performance level is basically restricted by the inherent (dynamic) properties of the servo-system, i.e. by the system design.

6.1.5 System design and cushioning design

As pointed out earlier in Subsection 6.1.2 and 6.1.3, it is important to perform a preliminary analysis of the dynamic behaviour of the complete hydraulic servo-system, including servo-valve dynamics and transmission line dynamics, in the system design stage already. In this analysis, issues like servo-valve choice, geometrical design of transmission lines, and sensor

placement are to be considered. In this way, the undesirable situation may be avoided, that the desired performance is not at all attainable because of improper system design.

The idea of using model knowledge to avoid costly iterations in the system design process, including manufacturing of hardware prototypes, also applies to the design and optimization of safety cushionings. These cushionings are extremely important for the hydraulic actuators of a flight simulator motion system, because they have to provide a safe and smooth stop at the end of the actuator stroke in case of a control failure. Because no information on the design of these cushionings is available or accessible, a model-based approach for this cushioning design has been developed, and presented in this thesis. Because the actual constructive design of the actuator was already given, with a peg-in-hole (PIH) cushioning for the downward motion and a closing-drain-holes (CDH) cushioning for the upward motion, the model-based approach to cushioning design has been limited to the optimization of the geometry of both types of cushioning.

The basis for the developed cushioning design procedure lies in the basic actuator model (see Subsection 6.1.1), which is for this aim extended with models for the two types of cushioning respectively. By making some rather rigourous assumptions on flow effects during cushioning, physical models have been derived, which provide much insight in the cushioning behaviour of a hydraulic actuator. Utilizing this insight, and the models themselves, design procedures have been developed, which optimize the geometrical design of the cushionings with respect to some desired motion during cushioning. The specification of this desired motion, which is part of the design procedure, involves a trade-off between the maximum allowed acceleration (smoothness) and maximum allowed cushioning pressure (safety).

During experimental validation of the models, only qualitative validity could be proven. Quantitatively, there are some discrepancies between experiments and simulations. However, the primary objective was to achieve satisfactory experimental performance of the model-based cushioning designs, and not quantitative validity of the cushioning models. Actually, the experimental performance of the designed cushionings was found to be quite satisfactory, where both types of cushioning provide smooth and safe stops under different load conditions.

In this Section, a number of conclusions has been given, covering the scope of this research, with a division into five main research topics. Yet, there are some issues, directly related to this work, which fell beyond the scope of this thesis, but may be treated in future research. These issues are put forward in the next and final Section of this thesis.

6.2 Recommendations for future work

With the main emphasis of this thesis on the modelling of hydraulic servo-systems, the control design has been elaborated less thoroughly. Actually, the available model knowledge has not yet been fully exploited in control design. Moreover, recent advances in control theory in the field of robust control, such as H_∞-control, μ-synthesis, and Quantitative Feedback Theory (QFT), have not been utilized to optimize the hydraulic actuator control loops. Future work should therefore focus on this topic, where some open issues have already been adressed in Subsection 4.4.3. In other words, what requires further research efforts, is the design of robust hydraulic actuator control loops, taking into account non-linear servo-valve dynamics and transmission line effects.

Besides ongoing work on the low-level control of a single hydraulic servo-system, directly in line with the work of this thesis, application of the obtained insight and knowledge to the control design for multi DOF motion systems is an important future research topic. This mainly concerns the design of the high-level control, generating the reference signals for the robust actuator control loops at the low level, and the application of the complete two-level control structure to real applications. In this respect, the application of the results of this thesis to the control design for the motion system of the SIMONA Research Simulator (Section 1.2), as a continuation of this research, deserves high priority.

Finally, a thourough investigation of the implications of Coulomb friction on hydraulic servo control is recommended. Due to the fact that hydrostatic bearings were applied in the experimental setup described in this thesis, Coulomb friction has fallen beyond the scope of attention. However, in many (or even most) applications low-cost actuators are used, showing considerable amounts of Coulomb friction. In these applications, much would be gained, if sophisticated control design could cope with this friction.

Appendix A

Overview of properties of the model of a hydraulic servo-system

In Chapter 2, a thourough analysis has been given of the dynamics and non-linearities of a hydraulic servo-system, by means of an extensive analysis of the theoretical model of the system. In order to allow easy reference to the results of the given analysis, this Appendix provides an overview of modelling aspects of a hydraulic servo-system. Aspects of dynamic modelling are treated in Section A.1, while an overview of the non-linearities is given in Section A.2.

A.1 Overview of dynamics of a hydraulic servo-system

When considering the dynamics of a hydraulic servo-system, it is useful to distinguish a number of subsystems. They are the flapper-nozzle valve, the three-stage valve including the flapper-nozzle pilot-valve, the transmission lines and the hydraulic actuator. For each of these subsystems, this Section describes how the dynamic properties of the subsystem are modelled. Thereby, four aspects are highlighted:

1. *Theoretical model.*
   Which equations in the theoretical model constitute the dynamic behaviour.
2. *Linearization.*
   How the model is linearized to obtain a linear dynamic model.
3. *Possible simplifications.*
   When and how the dynamic model can be simplified.
4. *Resulting model.*
   Recommended linear model structure; physical interpretation and dynamic properties.

In the final part of this Section, some rules are given for the dynamic modelling of a complete hydraulic servo-system, dealing with the relevance of the subsystem models.

A.1.1 Dynamics of a flapper-nozzle valve

1. *Theoretical model.*
   - Second order equation of motion for the flapper, (2.4).

- Three mass balances for valve chambers, constituting first order equations for the nozzle pressures P_{n1}, P_{n2}, P_{n3} respectively, (2.11) and (2.6).
- Second order equation of motion for the spool, (2.12).
- Algebraic coupling (non-linear) between differential equations by means of flow equations (2.5), (2.10) and feedback spring equation, (2.13). If electrical spool position feedback is present, and no feedback spring, then the feedback spring equation (2.13) should be replaced by the electrical feedback law, for instance (2.15).

2. *Linearization.*
   - Linearization point for zero input i_{ca}, corresponding to zero flapper displacement and zero spool displacement; nozzle pressures have corresponding equilibrium values.
   - Hard non-linearities are neglected, Assumption 2.5.1.
   - Result: 7^{th} order linear model, with physical quantities as state variables, (2.86).
3. *Possible simplifications.*
   Depending on the servo-valve that is modelled, certain simplifications of the model are allowed, such as to reduce the model order. In most applications it is at least not necessary to use a 7^{th} order model; 5^{th} order or even lower is more appropriate. Possibilities of model reduction:
   - Due to uncontrollability of mean nozzle pressure level P_n and outlet pressure P_{n3}, only the dynamics of the nozzle pressure difference ΔP_n have to be taken into account. Result: 5^{th} order model.
   - Neglecting spool mass, Assumption 2.5.2.
   - Neglecting spool mass and viscous friction, Assumption 2.5.3.
   - Neglecting spool mass and oil compressibility, Assumption 2.5.4.
4. *Resulting model.*
   A linear dynamic model, with input current i_{ca} as input, and spool position x_s as output, and physical quantities as state variables. Depending on the assumptions during simplification, i.e. required model order:
   - Only uncontrollable pressures neglected $\Rightarrow$ 5^{th} order state space model with 12 parameters, (2.90), no transmission zeros. After scaling of state: 10 parameters.
   - Assumption 2.5.2 $\Rightarrow$ 4^{th} order state space model with 11 parameter combinations, (2.93), one transmission zero in rhp. After scaling of state: 9 parameters, (2.101).
   - Assumption 2.5.3 $\Rightarrow$ 3^{rd} order state space model with 7 parameter combinations, (2.96), one transmission zero in rhp. After scaling of state: 6 parameters.
   - Assumption 2.5.4 $\Rightarrow$ 3^{rd} order state space model with 6 parameter combinations, (2.100), no transmission zeros. After scaling of state: 5 parameters.

   For any of these models, the often badly damped second order dynamics of the flapper motion plays an important role. However, the dominant dynamics of the valve are consituted by the dynamics due to oil compressibility and/or spool friction.

A.1.2 Dynamics of a three-stage valve

1. *Theoretical model.*

- Static mass balances for main spool chambers, constituting one first order equation (integrator) for main spool position x_m, (2.20).
- Algebraic coupling (non-linear) with dynamics of pilot-valve, by means of pilot-valve flow equations (2.16), and electrical spool position feedback law, for instance (2.22).

2. *Linearization.*
   Given a linear model for the (flapper-nozzle) pilot-valve, the linear dynamic model of the three-stage valve is composed from the pilot-valve model, an integrator for the main spool and the (linear) spool position feedback law.
3. *Possible simplifications.*
   Apart from the possible simplifications for the pilot-valve model as described above, no simplifications are possible.
4. *Resulting model.*
   The linear dynamic model of a three-stage servo-valve basically depends on the pilot-valve model. For instance, adopting the 4^{th} order model (2.101) for the pilot-valve, results in a 5^{th} order state space model for the three-stage valve, with 10 parameters (excluding the electrical feedback gain), (2.104). The model has one transmission zero in the rhp, originating from the pilot-valve dynamics.

A.1.3 Dynamics of a hydraulic actuator

1. *Theoretical model.*
   - Second order equation of motion for the piston, (2.29).
   - Two mass balances for actuator chambers, constituting first order equations for the actuator pressures P_{p1}, P_{p2} respectively, (2.27).
   - Servo-valve flow Φ_p as control input related to actuator pressures by static valve flow equations, (2.23).
2. *Linearization.*
   - Linearization point for zero input flow Φ_p, and zero external force F_{ext}. This corresponds to zero pressure difference ΔP_p, and some actuator position q_0, not necessarily the middle position.
   - Hard non-linearities are neglected, Assumption 2.6.1.
   - Result: 4^{th} order linear model, with physical quantities as state variables, (2.105). After scaling of the state, 6 parameters are left in the state space model, (2.107).
3. *Possible simplifications.*
   Considering the low-frequency behaviour of a hydraulic actuator, the linear 4^{th} order model can generally be reduced to 3^{rd} order because of the uncontrollability of the mean pressure level P_p; only the dynamics of the actuator pressure difference ΔP_p have to be taken into account.
4. *Resulting model.*
   A third order state space model with 5 independent parameters, (2.108). Dominant dynamics are an integrator for the actuator position, and second order dynamics due to the coupling between the dynamics of the pressure difference and the piston motion.

A.1.4 Dynamics of a transmission line

1. *Theoretical model.*
   - Infinite order four port model, (2.67).
   - Model inputs: inlet flow Φ_i and outlet pressure P_o.
   - Model outputs: are outlet flow Φ_o and inlet pressure P_i.
   - Simplified to low order (two times the number of resonances taken into account) linear state space model, (2.68), by means of modal approximation.
2. *Linearization.*
   The theoretical model (modal approximation) is linear.
3. *Possible simplifications.*
   If necessary, fewer resonance modes can be taken into account by just truncating the state space representation of the modal approximation.
4. *Resulting model.*
   In case two resonance modes are taken into account for a single tranmission line, the 4^{th} order modal approximation is basically described by 6 independent parameters, (2.109). In case only one resonance mode is taken into account, the number of independent parameters reduces to 4.

A.1.5 Dynamics of complete hydraulic servo-system; rules for modelling

When composing a (linear) dynamic model for a complete hydraulic servo-system, a decision has to be made concerning the inclusion of the different subsystem models. Based on the insight obtained by model analysis as presented in Chapter 2, and by control design as described in Chapter 4, it can be argued which dynamic model structure is the most appropriate for some hydraulic servo-system. A sort of procedure to find this model structure is presented here as a set of rules for the dynamic modelling of a hydraulic servo-system.

Rule A.1.1 *The actuator chambers can be modelled by first order mass balances, and do not need to be seen as transmission lines.*

Rule A.1.2 *Dynamics due to transmission lines between valve and actuator chambers can be neglected, if the lines are so short, that the lowest corresponding resonance frequency according to (2.71) is both:*

1. *well beyond the bandwidth of the servo-valve, i.e. the servo-valve roll-off is large enough to attenuate the first transmission line resonance by at least 20 dB, and:*
2. *well beyond the desired closed loop bandwidth of the servo-system, i.e. larger than 10 times the desired control bandwidth.*

Rule A.1.3 *Servo-valve dynamics can be neglected, if both:*

1. *the bandwidth of actuator feedback control is small with respect to the servo-valve bandwidth, i.e. the servo-valve bandwidth is about 10 times larger than the desired closed loop bandwidth of the actuator, and:*

2. *the first resonance frequency due to transmission line dynamics is well beyond the bandwidth of the servo-valve, i.e. the servo-valve roll-off is large enough to attenuate the first transmission line resonance with at least 20 dB (compare Rule A.1.2).*

Rule A.1.4 *If transmission line dynamics and servo-valve dynamics can be neglected according to Rule A.1.2 and Rule A.1.3 respectively, then the dynamics of a hydraulic servo-system can be modelled by the third order actuator dynamics given by (2.108).*

Rule A.1.5 *If transmission line dynamics can not be neglected (Rule A.1.2), then:*

1. *the modal approximations of the transmission line models, (2.109), can be interconnected with the 4^{th} order actuator model, (2.107), resulting in a single dynamic model for the actuator including transmission lines, (2.110), and:*
2. *the 4^{th} order modal approximations of the transmission line models, (2.109), can generally be replaced by truncated (2^{nd} order) models, because only the first resonance of a transmission line is relevant for control, Section 4.4.*

Rule A.1.6 *If servo-valve dynamics can not be neglected (Rule A.1.3), then:*

1. *the dynamics of the hydraulic servo-system can be modelled as a series connection of the servo-valve model and the actuator model (possibly including transmission line dynamics according to Rule A.1.5), and:*
2. *it depends on the type of servo-valve, which dynamic model is most appropriate; some alternative models for a flapper-nozzle valve are available, and a three-stage valve model is composed of a pilot-valve model plus integrator and main spool position feedback law.*

A.2 Overview of non-linearities of a hydraulic servo-system

For each non-linearity that has been considered in Chapter 2, a brief evaluation is given concerning the following aspects:

1. *Theoretical model.*
   Which equations in the theoretical model describe the non-linearity.
2. *Effect on system behaviour.*
   How the presence of the non-linearity can be recognized in the system behaviour.
3. *Relevance and inclusion in simplified model.*
   whether the non-linearity is so relevant that it should be included in the linear dynamic models, and if so, how this should be done.

Most of the non-linearities considered here (Subsection A.2.1 up to and including A.2.7) are related to the flapper-nozzle valve, where the reader may refer to Fig. 2.5 on page 29 for an overview of the modelled effects. The remaining non-linearities, summarized in Subsections A.2.8, A.2.9 and A.2.10, are related to the hydraulic actuator.

A.2.1 Torque motor non-linearity

1. *Theoretical model.*
   The driving torque on the flapper T_t depends non-linearly on the input current i_{ca} and the flapper position x_f, (2.2).
2. *Effect on system behaviour.*
   Deviations of dynamic behaviour of the flapper-nozzle valve for large input amplitudes due to large flapper deflections during transients, Fig. 2.18.
3. *Relevance and inclusion in simplified model.*
   This non-linearity is important to describe amplitude dependent dynamics of the flapper-nozzle valve and should be taken into account for detailed modelling of this type of servo-valve. Rewriting the non-linear equation while preserving the structure of the non-linearity leads to a description with three tuning parameters, (2.111). After inclusion of the non-linearity in the linear dynamic model of the flapper-nozzle valve (2.101) while preserving the dynamic properties of the model, there are 2 tuning paramers left: k_2 for the measure of non-linearity in the input $\tilde{i}_{ca}$, and k_3 for the measure of non-linearity in the flapper-position $\tilde{x}_f$.

A.2.2 Flapper-nozzle non-linearity

1. *Theoretical model.*
   The flapper-nozzle non-linearity is mainly constituted by the turbulent flow equations (2.5) and (2.10), which are coupled to each other by the linear mass balances for the valve chambers, (2.11) and (2.6).
2. *Effect on system behaviour.*
   Unless the amplitude of the input is so large that the flapper hits the nozzles during transients, the non-linearity of the flapper-nozzle system does not affect the dynamic behaviour of the valve. The steady state behaviour is not influenced non-linearly either, because flapper-deflections in steady state are very small, Fig. 2.17.
3. *Relevance and inclusion in simplified model.*
   This non-linearity is not important and can in general be neglected. If it is to be inluded in the linear dynamic model, for instance to perform model analysis, the non-linear equations can be rewritten, (2.114). The scaling factors k_4, k_5, (2.115), are used to relate the non-linear equations to the linear model, (2.101). Requiring that the dynamic properties of the resulting non-linear model are the same as those of the linear model, only one tuning parameter k_4 remains, which determines the measure of non-linearity.

A.2.3 Non-linear flow forces on flapper

1. *Theoretical model.*
   The non-linear torque on the flapper due to non-linear flow forces on the flapper is given by (2.9). It is based on a momentum analysis for the fluid flow.
2. *Effect on system behaviour.*
   For the given theoretical model, the effect on the non-linearity of the dynamic behaviour is negligible, Fig. 2.18.

3. *Relevance and inclusion in simplified model.*
   Because there is no theoretical nor experimental evidence that these flow forces play an important role, they are not included in the dynamic model.

A.2.4 Coulomb friction on the spool

1. *Theoretical model.*
   A non-linear model for the Coulomb friction force including stiction is used, according to [131].
2. *Effect on system behaviour.*
   Coulomb friction causes a hysteresis loop in the steady state characteristic of the servo-valve, Fig. 2.12.
3. *Relevance and inclusion in simplified model.*
   The physical phenomenon as such is quite relevant for the operation of the servo-valve; the hysteresis loop can cause severe non-linearity of a controlled servo-system. However, the effect of Coulomb friction can effectively be minimized by applying a dither signal, which makes the inclusion of the phenomenon in the simplified linear model unnecessary.

A.2.5 Ball clearance of feedback spring

1. *Theoretical model.*
   Ball clearance is modelled by a zero feedback spring torque for flapper displacements corresponding to motion of the ball at the end of the spring within some clearance, (2.14).
2. *Effect on system behaviour.*
   Ball clearance results in a jump in the steady state characteristic of the servo-valve, Fig. 2.12.
3. *Relevance and inclusion in simplified model.*
   The inclusion of the ball clearance phenomenon in the simplified dynamic model is not relevant, because servo-valves showing this phenomenon are not suited for closed loop control of a hydraulic servo-system, and should not be used.

A.2.6 Non-linear flow through spool ports

1. *Theoretical model.*
   The non-linear flows through valve spool ports, depending on spool port geometry and the pressure at the spool ports is composed of turbulent port flows and laminar leakage flows. The equations for the spool flow of the flapper-nozzle valve and the main spool flows are similar, (2.16) and (2.23).
2. *Effect on system behaviour.*
   - The steady state flow characteristic for zero load pressure is non-linear for non-ideal port geometry, Fig. 2.14, 2.15 and 2.16:
     - Spool port underlaps cause an increased flow gain in the underlap region.
     - Spool port overlaps cause a zero flow gain in the overlap region.

  - Unequal spool port underlaps and/or overlaps generally cause a change in the equilibrium pressures of the controlled device for small spool displacements.
  - Radial clearance of the spool has a smoothing effect on the sharp transistions in the steady state characteristic due to underlaps and/or overlaps. Moreover it reduces the change in equilibrium pressures due to unequal underlaps and/or overlaps.
- The servo-valve flow depends non-linearly on the load pressure. The measure of this load dependence is linearly related to the magnitude of the spool port opening, Fig. 2.13.
- If the servo-valve is driving a device in closed loop configuration, the non-linearity of the steady state flow characteristic causes non-linearity in the closed loop dynamics, Fig. 2.20.

3. *Relevance and inclusion in simplified model.*
   Non-linear spool port flows constitute the basic and therewith most important non-linearity of a hydraulic servo-system. The non-linearity is included in the linear dynamic model by a non-parametric model for the flow characteristic at zero load pressure, like (2.120) or (2.122). The load dependence is included by adding a square root expression, (2.124).

A.2.7 Non-linear flow forces on spool

1. *Theoretical model.*
   The non-linear axial flow forces originate from the change of momentum of the fluid flow, (2.19).
2. *Effect on system behaviour.*
   Except for small spool displacements, the axial flow force varies linearly with the spool position; it tends to close the spool ports like a spring that trys to center the spool, Fig. 2.18.
3. *Relevance and inclusion in simplified model.*
   Because the effect of the axial flow force is almost linear, it is not explicitly taken into account in the linear model. The non-linear effects for small spool displacements are accounted for by the non-parametric model of the non-linear flow characteristic, (2.122).

A.2.8 Leakage of hydrostatic bearing

1. *Theoretical model.*
   The leak flows due to the presence of hydrostatic bearings mainly depend on the pressure difference across the bearing and on the bearing geometry, (2.36) and (2.37).
2. *Effect on system behaviour.*
   The effect of the leakage flows in a hydraulic actuator can be characterized by a modification of the steady state spool flow characteristic, depending on the load pressure and the spool displacement, Fig. 2.24. Besides that, the leakage flows slightly change the equilibruim pressures in the actuator compartments.

3. *Relevance and inclusion in simplified model.*
Besides the linear contribution of the leakage flows, which is already included in the linearized actuator model due to Assumption 2.6.1, the non-linear effects due to leakage, especially for small spool displacements, are taken into account by the non-parametric model of the non-linear flow characteristic, (2.122).

A.2.9 Coulomb friction in the actuator

1. *Theoretical model.*
A non-linear model for the Coulomb friction force including stiction is used, according to [131].
2. *Effect on system behaviour.*
Coulomb friction causes excitation of the (closed loop) actuator dynamics during change of moving direction, possibly resulting in an irregularity in the acceleration. Coulomb friction is easily recognized from the jump in the pressure difference across the piston during motion reversal, Fig. 2.28.
3. *Relevance and inclusion in simplified model.*
Depending on the magnitude of the Coulomb friction and the specific application, Coulomb friction may be quite relevant for the operation of the closed loop servo-system. For a fast preliminary analysis it is useful to include a simple Coulomb friction model in the dynamic actuator model, (2.126).

A.2.10 Position dependence of actuator dynamics

1. *Theoretical model.*
Because the volumes of the actuator chambers vary with the actuator position, the stiffnes of the actuator due to oil compressibility and therewith the actuator dynamics depend on the actuator position, (2.27).
2. *Effect on system behaviour.*
The resonance frequency related to the basic actuator dynamics, typical for a hydraulic servo-system, depends on the actuator position with variations of about 10 %. The same kind of variations is found for the resonance and anti-resonance frequencies related to transmission line dynamics, Fig. 2.37.
3. *Relevance and inclusion in simplified model.*
From the point of view of robustness of a high-performance actuator control loop, Chapter 4, the variation of actuator dynamics with actuator position is extremely important. The effect is taken into account by making two parameters (ζ_5 and ζ_6) in the linear actuator model position dependent. This holds both for the case that transmission line dynamics are neglected, (2.108), and for the case that they have to be included in the model, (2.110).

Appendix B

Algebraic loops in the simulation model

In the non-linear simulation model of the hydraulic servo-system, of which the model relations are presented in Chapter 2, algebraic loops are present. These loops require special attention, in case the model is to be simulated with standard simulation software. For this reason, the character of the algebraic loops is analyzed in this Appendix, while possible solutions to the problem are given. In Section B.1, the algebraic loops in the three-stage valve model of Subsection 2.2.4 are treated, while those due to the modelling of manifold losses in Subsection 2.4.4 are discussed in Section B.2.

B.1 Algebraic loops in three-stage valve model

The algebraic loops in the three-stage valve model are caused by the fact that the pilot-valve flows Φ_{m1} and Φ_{m2}, as well as the main spool pressures P_{m1} and P_{m2}, should simultaneously satisfy the algebraic model relations for the main spool (2.20) and (2.21), rewritten as:

$$\Phi_{m1} = \Phi_{m2}; \qquad P_{m1} = P_{m2} \tag{B.1}$$

and the algebraic expressions for the pilot-valve flows (2.16):

$$\begin{aligned} \Phi_{m1} &= C_d A_{s1}\sqrt{2\tfrac{P_s-P_{m1}}{\rho}} - C_d A_{s2}\sqrt{2\tfrac{P_{m1}-P_t}{\rho}} + \Phi_{l,s1} - \Phi_{l,s2} \\ \Phi_{m2} &= C_d A_{s3}\sqrt{2\tfrac{P_{m2}-P_t}{\rho}} - C_d A_{s4}\sqrt{2\tfrac{P_s-P_{m2}}{\rho}} + \Phi_{l,s1} - \Phi_{l,s4} \end{aligned} \tag{B.2}$$

Thereby, the main spool areas A_{si}, $i = 1,2,3,4$, are given as function of the pilot-valve spool position x_s by (2.17), and the leakage flows $\Phi_{l,si}$, $i = 1,2,3,4$, are to be obtained from (2.18), also as a function of the pilot-valve spool position x_s.

In the general case, for arbitrary spool port configurations, these equations are not analytically solvable for $\Phi_{m1}, \Phi_{m2}, P_{m1}$ and P_{m2}. Only in some special cases, for instance when the radial clearance c_{rs} is zero *and* all underlaps d_{si} are equal (to d_s), an analytic solution is available. Solving (B.1) and (B.2) for this case, noting that the leakage flows are zero, gives:

$$\begin{aligned} P_{m1} = P_{m2} &= \tfrac{P_s+P_t}{2} \\ \Phi_{m1} = \Phi_{m2} &= C_d(A_{s1}-A_{s2})\sqrt{\tfrac{P_s-P_t}{\rho}} = C_d(A_{s3}-A_{s4})\sqrt{\tfrac{P_s-P_t}{\rho}} \end{aligned} \tag{B.3}$$

with A_{si}, $i = 1,2,3,4$, given by (2.17).

However, in the general case, such a solution is not available. In that case, there are two ways to obtain valuable simulation results.

First, it is possible to introduce dynamic states for P_{m1} and P_{m2} by defining mass balances for the chambers of the main spool, while taking oil compressibility into account. Though physically justifiable, this method does not lead to a desirable solution, because fast poles are introduced again in the simulation model, which were avoided by modelling the main spool by (2.20) and (2.21). So, although it is an easy solution to obtain the desired non-linear simulation result, it is principally not justifiable, at least not from a modelling point of view. Therefore, the second method should be used.

The second way of solving the algebraic loops is the use of a stiff system solver, which iteratively solves the set of algebraic equations. Most simulation packages do have such a solver. The only problem is the implementation of the (algebraic) equations (B.1) and (B.2) in the simulation model. Obviously, (B.2) produces Φ_{m1} and Φ_{m2} as outputs, given P_{m1} and P_{m2} as inputs. Although it is straightforward to implement $P_{m1} = P_{m2} = P_m$ in the simulation model, the problem is to generate P_m, such that $\Phi_{m1} = \Phi_{m2}$ holds, when evaluating (B.2). This problem can be solved by implementing the following algebraic equation, which constitutes the coupling between (B.1) and (B.2):

$$P_m = P_m + \epsilon\,(\Phi_{m1} - \Phi_{m2}) \tag{B.4}$$

In this equation, ϵ is a real number, which affects the convergence of the stiff system solver to the desired solution (B.1). The numerical backgrounds are not treated here; in practice, it was found that a feasible solution was readily found, unless the absolute value of ϵ was too large, provided that a reasonable initial solution for P_m was used. An obvious choice is $P_m = \frac{1}{2}P_s$, which led to feasible solutions. Therewith, the second approach, using a stiff system solver, appears to be well-suited for the algebraic loops considered here.

B.2 Algebraic loops due to manifold losses

Referring to Fig. 2.34 on page 86 for the configuration of the hydraulic servo-system model including manifold losses, it is clear that the modelling of manifold losses at the valve side of the transmission lines leads to algebraic loops, because of the algebraic form of both the valve flow equations (2.76) and the manifold loss equations (2.85). However, at the actuator side, the modelling of manifold losses with (2.85) does not result in algebraic loops, because the D-matrix of the tranmission line models (2.68) is zero. This means, that there is no direct throughput from P'_{o1} and P'_{o2} to Φ_{o1} and Φ_{o2} respectively, so that no algebraic loops are involved.

So, only the manifold losses at the valve side need to be considered. Actually, the situation is quite similar to the one sketched in Section B.1. In this case, the valve flows Φ_{i1} and Φ_{i2}, as well as the valve port pressures P'_{i1} and P'_{i2}, should simultaneously satisfy the algebraic model relations for the manifold losses (2.85), rewritten as:

$$\begin{aligned} \Phi_{i1} &= C_d A_{man,i1}\,\mathrm{sign}(P'_{i1} - P_{i1})\sqrt{2\tfrac{|P'_{i1}-P_{i1}|}{\rho}} \\ \Phi_{i2} &= -C_d A_{man,i2}\,\mathrm{sign}(P'_{i2} - P_{i2})\sqrt{2\tfrac{|P'_{i2}-P_{i2}|}{\rho}} \end{aligned} \tag{B.5}$$

and the valve flow equations (2.76):

$$\begin{aligned}\Phi_{i1} &= C_d A_{m1}\sqrt{2\tfrac{P_s-P'_{i1}}{\rho}} - C_d A_{m2}\sqrt{2\tfrac{P'_{i1}-P_t}{\rho}} + \Phi_{l,m1} - \Phi_{l,m2}\\ \Phi_{i2} &= C_d A_{m3}\sqrt{2\tfrac{P'_{i2}-P_t}{\rho}} - C_d A_{m4}\sqrt{2\tfrac{P_s-P'_{i2}}{\rho}} + \Phi_{l,m1} - \Phi_{l,m4}\end{aligned} \tag{B.6}$$

Again, for a special case, namely when the radial clearance c_{rm} and the underlaps d_{mi} are zero, an analytic solution is available. Solving for the flows Φ_{i1} and Φ_{i2} by eliminating P'_{i1} and P'_{i2} from (B.5) and (B.6) for this case, noting that the leakage flows are zero, gives:

$$\begin{aligned}\Phi_{i1} &= \begin{cases} C_d\sqrt{\frac{A^2_{m1}A^2_{man,i1}}{A^2_{m1}+A^2_{man,i1}}}\sqrt{2\frac{P_s-P_{i1}}{\rho}} & x_m > 0\\ -C_d\sqrt{\frac{A^2_{m2}A^2_{man,i1}}{A^2_{m2}+A^2_{man,i1}}}\sqrt{2\frac{P_{i1}-P_t}{\rho}} & x_m \le 0\end{cases}\\ \Phi_{i2} &= \begin{cases} C_d\sqrt{\frac{A^2_{m3}A^2_{man,i2}}{A^2_{m3}+A^2_{man,i2}}}\sqrt{2\frac{P_{i2}-P_t}{\rho}} & x_m > 0\\ -C_d\sqrt{\frac{A^2_{m4}A^2_{man,i2}}{A^2_{m4}+A^2_{man,i2}}}\sqrt{2\frac{P_s-P_{i2}}{\rho}} & x_m \le 0\end{cases}\end{aligned} \tag{B.7}$$

In the general case, however, an analytical solution is not available, and a numerical solution is to be found. As before in Section B.1, the use of a stiff system solver is preferred here, instead of introducing new dynamic states for P'_{i1} and P'_{i2}. The problem is actually to generate P'_{i1} and P'_{i2}, such that Φ_{i1} and Φ_{i2} from (B.5) equal Φ_{i1} and Φ_{i2} from (B.6). This problem can be solved by implementing the following algebraic equations, which constitute the coupling between (B.5) and (B.6):

$$\begin{aligned}P'_{i1} &= P'_{i1} + \epsilon\,\Delta\Phi_{i1}\\ P'_{i2} &= P'_{i2} + \epsilon\,\Delta\Phi_{i2}\end{aligned} \tag{B.8}$$

In this equation, ϵ is a real number as before, while $\Delta\Phi$ represents the difference between the outcomes of (B.5) and (B.6). Thus, using a stiff system solver from the simulation package, and providing a feasible initial solution, for instance $P'_{i1} = P_{i1}$ and $P'_{i2} = P_{i2}$ at small flows, simulation problems due to the algebraic loops considered here, are effectively solved.

Appendix C

Leakage and axial forces of hydrostatic bearing

For the derivation of the leakage and friction model of a hydrostatic bearing, the configuration of Fig. C.1 is considered, according to [139]. The upper conical part of the bearing is stationary, and the lower cylindrical part moves to the right.

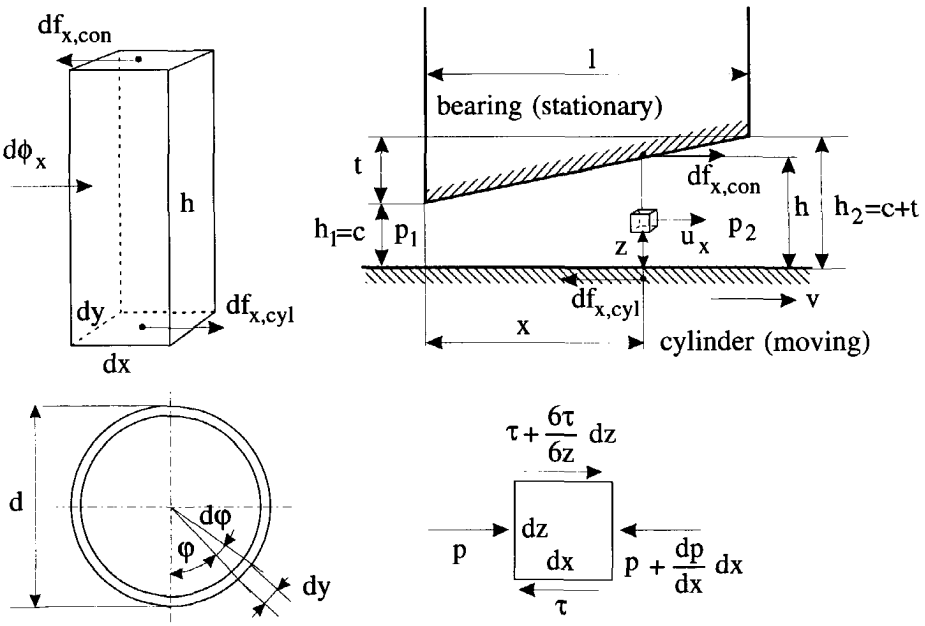


Fig. C.1: Schematic drawing of bearing – cylinder configuration

The flow in the gap between the bearing parts is assumed to be incompressible and laminar; moreover, only one-dimensional flow is considered, as this is a very good approximation of the more complex two-dimensional flow model [16], especially because zero excentricity is assumed, Subsection 2.3.3.

With these assumptions, first the leakage flows are derived according to Viersma [139] in Section C.1. Using the results of this Section, expressions for the axial bearing force are derived in Section C.2. For the notation of the variables in this Appendix, the reader is referred to Fig. C.1.

C.1 Leakage flow

Starting with a fluid particle in the gap, as shown in Fig. C.1, equilibrium of forces on this particle gives:

$$\frac{dp}{dx}\,dx\,dydz = -\frac{\partial\tau}{\partial z}\,dz\,dxdy$$

with p the local pressure and τ the local shear stress in the fluid. For the shear stress in a laminar fluid flow, with a dynamic viscosity of the fluid η, the following holds:

$$\tau = -\eta\frac{\partial u_x}{\partial z} \tag{C.1}$$

where u_x is the fluid velocity in x-direction. Combining this with the force equilibrium above, the Navier-Stokes equation for the flow is obtained:

$$\eta\frac{\partial^2 u_x}{\partial z^2} = \frac{dp}{dx}$$

Solving this differential equation by twice integrating, with boundary conditions $u_x = v$ at $z = 0$ and $u_x = 0$ at $z = h$ (see Fig. C.1), the parabolic velocity profile in the gap is found:

$$u_x = \frac{1}{2\eta}\frac{dp}{dx}\left(z^2 - zh\right) + v\left(1 - \frac{z}{h}\right) \tag{C.2}$$

Herewith, the axial flow $d\phi_x$ through a rectangle with height h and width dy is:

$$d\phi_x = \int_0^h u_x\,dzdy = dy\int_0^h u_x\,dz = \left[-\frac{h^3}{12\,\eta}\frac{dp}{dx} + \frac{vh}{2}\right]dy$$

Because only flow in x-direction is assumed, the continuity-equation for incompressible flow applied to the fluid particle of Fig. C.1 yields:

$$\frac{d\phi_x}{dy} = \text{constant} = -\frac{h^3}{12\,\eta}\frac{dp}{dx} + \frac{vh}{2} \tag{C.3}$$

This can be rewritten into the differential equation:

$$dp = -12\,\eta\frac{d\phi_x}{dy}\frac{dx}{h^3} + 6\,\eta v\frac{dx}{h^2}$$

For the conical bearing, the variable x can be substituted, by observing from Fig. C.1 that:

$$h = h_1 + \frac{x}{l}t, \qquad \text{so:} \qquad dx = \frac{l}{t}\,dh \tag{C.4}$$

This substitution results in:

$$dp = -\frac{12\,\eta l}{t}\frac{d\phi_x}{dy}\frac{dh}{h^3} + \frac{6\,\eta v l}{t}\frac{dh}{h^2}$$

Solving this differential equation with boundary conditions $p = p_1$ at $h = h_1$ and $p = p_2$ at $h = h_2$ leads to:

$$p_2 - p_1 = \frac{6\,\eta l}{t}\,\frac{d\phi_x}{dy}\left[\frac{1}{h_2^2} - \frac{1}{h_1^2}\right] - \frac{6\,\eta l v}{t}\left[\frac{1}{h_2} - \frac{1}{h_1}\right]$$

This finally results in an expression for the flow in x-direction per unit length in y-direction, as given by Viersma [139]:

$$\frac{d\phi_x}{dy} = \frac{p_2 - p_1 + \frac{6\,\eta l v}{t}\left[\frac{1}{h_2} - \frac{1}{h_1}\right]}{\frac{6\,\eta l}{t}\left[\frac{1}{h_2^2} - \frac{1}{h_1^2}\right]} = \frac{p_2 - p_1}{\frac{6\,\eta l}{t}\left[\frac{1}{h_2^2} - \frac{1}{h_1^2}\right]} + v\frac{\left[\frac{1}{h_2} - \frac{1}{h_1}\right]}{\left[\frac{1}{h_2^2} - \frac{1}{h_1^2}\right]} \tag{C.5}$$

Note here, that there are basically two terms contributing to this flow: one originating from the pressure difference across the bearing, $p_2 - p_1$ and one caused by the velocity of the moving part, v. Viersma states, that the effect of the velocity can be neglected here, because the leakage flow is small in comparison with the displacement flow [139]. In order to verify this, both contributions in (C.5) are taken into account when deriving the leakage flow by integrating (C.5).

Before performing this integration, (C.5) is rewritten once more:

$$\begin{aligned} d\phi_x &= \left[\frac{t(p_2-p_1)}{6\,\eta l\left[\frac{1}{h_2^2}-\frac{1}{h_1^2}\right]} + v\frac{\left[\frac{1}{h_2}-\frac{1}{h_1}\right]}{\left[\frac{1}{h_2^2}-\frac{1}{h_1^2}\right]}\right] dy \\ &= \left[\frac{t(p_2-p_1)}{6\,\eta l}\,\frac{h_1^2h_2^2}{(h_1-h_2)(h_1+h_2)} + v\frac{\left[\frac{h_1^2h_2}{(h_1h_2)^2}-\frac{h_2^2h_1}{(h_1h_2)^2}\right]}{\left[\frac{h_1^2}{(h_1h_2)^2}-\frac{h_2^2}{(h_1h_2)^2}\right]}\right] dy \\ &= \left[\frac{t(p_2-p_1)}{6\,\eta l}\,\frac{h_1^2h_2^2}{(h_1-h_2)(h_1+h_2)} + v\,\frac{h_1h_2(h_1-h_2)}{(h_1-h_2)(h_1+h_2)}\right] dy \end{aligned}$$

The total leakage flow through the gap between the bearing and the cylindrical part, is now obtained by integrating this expression around the circumference of the bearing, which has diameter d. Thereby, some substitutions are applied, with c the clearance between bearing and cylinder, t the tapering of the bearing and φ an angular coordinate, according to Fig. C.1:

$$dy = \frac{d}{2}d\varphi; \quad h_1 = c; \quad h_2 = c + t \tag{C.6}$$

Thus, for the case of zero excentricity, the leakage flow is obtained as:

$$\begin{aligned} \phi_x &= \frac{d}{2}\int_0^{2\pi}\left[\frac{t\,(p_2-p_1)}{6\,\eta l}\,\frac{c^2(c^2+2ct+t^2)}{-t(2c+t)} + v\,\frac{c^2+ct}{2c+t}\right] d\varphi \\ &= \frac{\pi dc^3}{6\,\eta l}\,\frac{\left(1+\frac{t}{c}\right)^2}{\left(2+\frac{t}{c}\right)}\,(p_1-p_2) + \pi dc\,\frac{\left(1+\frac{t}{c}\right)}{\left(2+\frac{t}{c}\right)}\,v \end{aligned} \tag{C.7}$$

It might be noted here, that (C.7) holds as well for the case that the cylindrical part is moving, as for the case that the bearing is the moving part.

C.2 Axial bearing force

Whereas the radial bearing force is found by integrating the pressure-distribution along the bearing area [16, 139], the axial bearing force is found by integrating the shear-stress distribution in the fluid along the same area. Therefore, the expression for the shear-stress (C.1) is elaborated using the velocity profile according to (C.2):

$$\tau = -\eta \frac{\partial u_x}{\partial z} = -\eta \left[\frac{1}{2\eta} \frac{dp}{dx} (2z - h) - \frac{v}{h} \right] = -z \frac{dp}{dx} + \frac{1}{2} \frac{dp}{dx} h + \eta \frac{v}{h}$$

The shear-stress at the cylindrical surface and at the conical surface are found by substituting $z = 0$ and $z = h$ respectively, using the continuity-equation (C.3) again:

$$\tau_{z=0} = \frac{1}{2} h \frac{dp}{dx} + \eta \frac{v}{h} = -6\eta \frac{d\phi_x}{dy} \frac{1}{h^2} + 3\eta v \frac{1}{h} + \eta \frac{v}{h} = -\frac{6\eta}{h^2} \frac{d\phi_x}{dy} + \frac{4\eta v}{h}$$

$$\tau_{z=h} = -\frac{1}{2} h \frac{dp}{dx} + \eta \frac{v}{h} = 6\eta \frac{d\phi_x}{dy} \frac{1}{h^2} - 3\eta v \frac{1}{h} + \eta \frac{v}{h} = \frac{6\eta}{h^2} \frac{d\phi_x}{dy} - \frac{2\eta v}{h}$$

Integrating the expression for $z = 0$ along the length of the bearing l, the axial force on a strip of the cylindrical part with length l and width dy is obtained, using (C.4):

$$df_{x,cyl} = \int_0^l \tau_{z=0}\, dx dy = \frac{l}{t} dy \int_{h_1}^{h_2} \tau_{z=0}\, dh = \frac{l}{t} dy \int_{h_1}^{h_2} \left[-\frac{6\eta}{h^2} \frac{d\phi_x}{dy} + \frac{4\eta v}{h} \right] dh$$

$$= \frac{l}{t} dy \left[\frac{6\eta}{h} \frac{d\phi_x}{dy} + 4\eta v \ln(h) \right]_{h_1}^{h_2} = \frac{l}{t} dy \left[\left(\frac{1}{h_2} - \frac{1}{h_1} \right) 6\eta \frac{d\phi_x}{dy} + 4\eta v \ln\left(\frac{h_2}{h_1} \right) \right]$$

Substituting (C.5) in this expression results in:

$$df_{x,cyl} = \frac{l}{t} dy \left[6\eta \left(\frac{1}{h_2} - \frac{1}{h_1} \right) \left[\frac{p_2 - p_1}{\frac{6\eta l}{t} \left[\frac{1}{h_2^2} - \frac{1}{h_1^2} \right]} + v \frac{\left[\frac{1}{h_2} - \frac{1}{h_1} \right]}{\left[\frac{1}{h_2^2} - \frac{1}{h_1^2} \right]} \right] + 4\eta v \ln\left(\frac{h_2}{h_1} \right) \right]$$

$$= dy \left[\frac{(h_1 - h_2)}{h_1 h_2} \frac{h_1^2 h_2^2}{(h_1^2 - h_2^2)} \left[(p_2 - p_1) + \frac{6\eta l v}{t} \frac{(h_1 - h_2)}{h_1 h_2} \right] + \frac{4\eta l v}{t} \ln\left(\frac{h_2}{h_1} \right) \right]$$

$$= dy \left[\frac{h_1 h_2}{(h_1 + h_2)} (p_2 - p_1) + \frac{6\eta l v}{t} \frac{(h_1 - h_2)}{(h_1 + h_2)} + \frac{4\eta l v}{t} \ln\left(\frac{h_2}{h_1} \right) \right]$$

Like for the leakage flow, the total axial force is obtained by integrating this expression around the circumference of the bearing, having diameter d. Thereby, the same substitutions according to (C.6) are applied again. The axial force on the cylindrical part then becomes:

$$f_{x,cyl} = \frac{d}{2} \int_0^{2\pi} \left[\frac{(c^2 + ct)}{(2c + t)} (p_2 - p_1) - \frac{6\eta l v}{t} \frac{t}{(2c + t)} + \frac{4\eta l v}{t} \ln\left(\frac{(c + t)}{c} \right) \right] dy$$

$$= \pi dc \frac{\left(1 + \frac{t}{c}\right)}{\left(2 + \frac{t}{c}\right)} (p_2 - p_1) + \left[-\frac{\pi d}{c} \frac{6\eta l}{\left(2 + \frac{t}{c}\right)} + \frac{\pi d}{t} 4\eta l \ln\left(1 + \frac{t}{c}\right) \right] v \qquad \text{(C.8)}$$

In a similar way, the axial force on the conical part of the bearing can be derived from the expression for the shear-stress at $z = h$, which gives:

$$\begin{aligned} f_{x,con} &= \frac{d}{2}\int_0^{2\pi}\left[-\frac{(c^2+ct)}{(2c+t)}(p_2-p_1)+\frac{6\,\eta l v}{t}\frac{t}{(2c+t)}-\frac{2\,\eta l v}{t}\ln\left(\frac{(c+t)}{c}\right)\right]dy \\ &= -\pi dc\frac{\left(1+\frac{t}{c}\right)}{\left(2+\frac{t}{c}\right)}(p_2-p_1)+\left[\frac{\pi d}{c}\frac{6\,\eta l}{\left(2+\frac{t}{c}\right)}-\frac{\pi d}{t}2\,\eta l\ln\left(1+\frac{t}{c}\right)\right]v \end{aligned} \tag{C.9}$$

Appendix D

Modal approximation of pressure dynamics in actuator chamber

For the inclusion of a distributed pressure dynamics model for the actuator chambers in the servo-system model, a modal approximation of the following theoretical model has to be derived (see Subsection 2.4.2, equation (2.66)), where $\bar{s}$ is the normalized Laplace operator defined as $r_0^2 s/\mu$:

$$\begin{bmatrix} P_i(\bar{s}) \\ P_o(\bar{s}) \end{bmatrix} = \begin{bmatrix} \frac{Z_c(\bar{s})\cosh\Gamma(\bar{s})}{\sinh\Gamma(\bar{s})} & -\frac{Z_c(\bar{s})}{\sinh\Gamma(\bar{s})} \\ \frac{Z_c(\bar{s})}{\sinh\Gamma(\bar{s})} & -\frac{Z_c(\bar{s})\cosh\Gamma(\bar{s})}{\sinh\Gamma(\bar{s})} \end{bmatrix} \begin{bmatrix} \Phi_i(\bar{s}) \\ \Phi_o(\bar{s}) \end{bmatrix} \tag{D.1}$$

Using the frequency dependent factors α, β introduced by Yang and Tobler, and D_n and Z_0 from (2.70), the propagation operator $\Gamma(\bar{s})$ and the line characteristic impedance $Z_c(\bar{s})$ can be written as [160] (compare (2.57) and (2.59)):

$$\begin{aligned} \Gamma(\bar{s}) &= D_n \bar{s}\sqrt{\alpha^2 + \tfrac{8\alpha\beta}{\bar{s}}} \\ Z_c(\bar{s}) &= Z_0\sqrt{\alpha^2 + \tfrac{8\alpha\beta}{\bar{s}}} \end{aligned} \tag{D.2}$$

In order to obtain a modal approximation of (D.1), first the modal representations of the transfer functions in (D.1) are derived in Section D.1. After that, the low-order modal approximation is given, both as transfer function matrix and as state space model, in Section D.2.

D.1 Modal representations of the terms $Z_c\cosh(\Gamma)/\sinh(\Gamma)$ and $Z_c/\sinh(\Gamma)$

A modal approximation of (D.1) is easily found, if the modal representations are available of the transfer functions:

$$\frac{Z_c(\bar{s})\cosh\Gamma(\bar{s})}{\sinh\Gamma(\bar{s})} \qquad \text{and} \qquad \frac{Z_c(\bar{s})}{\sinh\Gamma(\bar{s})} \tag{D.3}$$

The problem of finding these modal representations is very similar to the derivation of the modal representations of the transfer functions of (2.67), which is given by Yang and

Tobler in the Appendix of their paper [160]. So, the derivation given below is obtained by adopting their procedure.

The procedure starts with finding the poles of (D.1), i.e. the zeros of $\sinh\Gamma(\bar{s})$, which are then used to obtain the corresponding residues and quadratic modal expressions for the transfer functions (D.3).

The zeros of $\sinh\Gamma(\bar{s})$ can be determined using the infinite product series representation as given by Goodson and Leonard [42], and setting it equal to zero:

$$\sinh\Gamma(\bar{s}) = \Gamma(\bar{s}) \prod_{i=1}^{\infty} \left[1 + \frac{\Gamma^2(\bar{s})}{D_n^2 \lambda_{si}^2}\right] = 0 \tag{D.4}$$

with λ_{si} given by (2.72). Contrary to the case described by Yang and Tobler [160], there are basically two types of solutions to this equation, which can be solved for the system poles $\bar{s}$ using $\Gamma(\bar{s})$ from (D.2):

1. **Low-frequency poles.** These poles describe the low-frequency behaviour, and are found by solving:

$$\begin{aligned} &\Gamma(\bar{s}) = 0 && \Leftrightarrow \\ &\bar{s} = 0 \ \vee \ \bar{s} = -8\tfrac{\beta}{\alpha} \end{aligned} \tag{D.5}$$

2. **High-frequency poles.** These poles describe the resonant high-frequency behaviour, and are found by solving:

$$\begin{aligned} &\Gamma(\bar{s}) = \pm j D_n \lambda_{si}, && i = 1, 2, 3, \ldots \ \Leftrightarrow \\ &\bar{s}_i = -4\tfrac{\beta}{\alpha} \pm \tfrac{1}{\alpha}\sqrt{16\beta^2 - \lambda_{si}^2}, && i = 1, 2, 3, \ldots \end{aligned} \tag{D.6}$$

For later use, it is noted here, that for these solutions of $\Gamma(\bar{s})$, the cosine hyperbolic functions in the transfer functions (D.3) have values:

$$\begin{aligned} &[\cosh\Gamma(\bar{s})]_{\Gamma=0} = 1 \\ &[\cosh\Gamma(\bar{s})]_{\Gamma=\pm j D_n \lambda_{si}} = (-1)^i, \quad i = 1, 2, 3, \ldots \end{aligned} \tag{D.7}$$

because $jD_n\lambda_{si} = j\pi i$, $i = 1, 2, 3, \ldots$ according to (2.72), and $\cosh jy = \cos y$.

The idea behind the modal representation of the transfer functions (D.3) is now, that each transfer function is represented as an infinite sum of modes, where each mode corresponds to a solution of (D.5) or (D.6). Each term in this sum consists a denominator, which is the characteristic equation for the corresponding mode, and a numerator, which is constructed from the residues of the original transfer function corresponding to the considered poles.

Because of the different character of the low-frequency behaviour and the high-frequency behaviour, the infinite sum of modes is split into the low-frequency mode and another infinite sum describing the high-frequency modes. First, the terms corresponding to the low-frequency mode of the transfer functions (D.3) will be derived, and later the terms corresponding to the high-frequency modes.

The low-frequency mode of the transfer functions (D.3), characterized by (D.5), can be found by substituting $\Gamma(\bar{s}) = 0$ in the respective transfer functions, while using (D.2) and (D.7):

$$\left[\frac{Z_c(\bar{s})\cosh\Gamma(\bar{s})}{\sinh\Gamma(\bar{s})}\right]_{\Gamma=0} = \left[\frac{Z_c(\bar{s})}{\sinh\Gamma(\bar{s})}\right]_{\Gamma=0} = \frac{Z_0\sqrt{\alpha^2+\frac{8\alpha\beta}{\bar{s}}}}{D_n\bar{s}\sqrt{\alpha^2+\frac{8\alpha\beta}{\bar{s}}}} = \frac{Z_0}{D_n\bar{s}} \tag{D.8}$$

For each of the high-frequency poles (D.6) of the transfer functions (D.3), the corresponding residues can be calculated by using L'Hopital's rule and taking first derivatives of the denominators and setting $\bar{s}$ equal to the pole in the remaining expressions [160], i.e.:

$$\begin{aligned}\text{Residue}\left[\frac{Z_c(\bar{s})\cosh\Gamma(\bar{s})}{\sinh\Gamma(\bar{s})}\right]_{\bar{s}=pole} &= \left[\frac{Z_c(\bar{s})\cosh\Gamma(\bar{s})}{\Gamma'(\bar{s})\cosh\Gamma(\bar{s})}\right]_{\bar{s}=pole} = \left[\frac{Z_c(\bar{s})}{\Gamma'(\bar{s})}\right]_{\bar{s}=pole}\\ \text{Residue}\left[\frac{Z_c(\bar{s})}{\sinh\Gamma(\bar{s})}\right]_{\bar{s}=pole} &= \left[\frac{Z_c(\bar{s})}{\Gamma'(\bar{s})\cosh\Gamma(\bar{s})}\right]_{\bar{s}=pole}\end{aligned} \tag{D.9}$$

With $\Gamma(\bar{s})$ given by (D.2), its derivative is:

$$\Gamma'(\bar{s}) = \frac{1}{\Gamma(\bar{s})}D_n^2\left(\alpha^2\bar{s}+4\alpha\beta\right) \tag{D.10}$$

Substituting now equations (D.2), (D.7) and (D.10) in the residue equations (D.9), the following is obtained:

$$\begin{aligned}\text{Residue}\left[\frac{Z_c(\bar{s})\cosh\Gamma(\bar{s})}{\sinh\Gamma(\bar{s})}\right]_{\bar{s}=pole} &= \left[\frac{Z_0\left(\alpha^2\bar{s}_i+8\alpha\beta\right)}{D_n(\alpha^2\bar{s}_i+4\alpha\beta)}\right]_{\bar{s}_i=pole}\\ \text{Residue}\left[\frac{Z_c(\bar{s})}{\sinh\Gamma(\bar{s})}\right]_{\bar{s}=pole} &= \left[\frac{D_n\bar{s}_i\sqrt{\alpha^2+\frac{8\alpha\beta}{\bar{s}_i}}}{D_n^2(\alpha^2\bar{s}_i+4\alpha\beta)}\frac{Z_0\sqrt{\alpha^2+\frac{8\alpha\beta}{\bar{s}_i}}}{(-1)^i}\right]_{\bar{s}_i=pole} = \left[\frac{(-1)^i Z_0\left(\alpha^2\bar{s}_i+8\alpha\beta\right)}{D_n(\alpha^2\bar{s}_i+4\alpha\beta)}\right]_{\bar{s}_i=pole}\end{aligned} \tag{D.11}$$

For a pair of poles $-x_i \pm y_i$ related to mode i, $i = 1, 2, 3, \ldots$, with

$$x_i = 4\frac{\beta}{\alpha} \qquad y_i = \frac{1}{\alpha}\sqrt{16\beta^2-\lambda_{si}^2}, \qquad i = 1, 2, 3, \ldots \tag{D.12}$$

corresponding residues $R^{\pm}$ can be calculated for each transfer function with (D.11). Using these residues $R^{\pm}$, and the corresponding poles (D.12), the corresponding term in the infinite sum of modes is found by calculating the combined real valued quadratic function [160]:

$$\frac{\left(R^+ + R^-\right)\left(\bar{s}+x_i\right) + \left(R^+ - R^-\right)y_i}{\left(\bar{s}+x_i\right)^2 - y_i^2} \tag{D.13}$$

After some elaborous calculations, this results in the following terms for the high-frequency modes of the transfer functions of (D.3):

$$\frac{\frac{2Z_0}{D_n}\left(\bar{s}+8\frac{\beta}{\alpha}\right)}{\bar{s}^2+8\frac{\beta}{\alpha}\bar{s}+\frac{\lambda_{si}^2}{\alpha^2}} \quad \text{and} \quad \frac{(-1)^i\frac{2Z_0}{D_n}\left(\bar{s}+8\frac{\beta}{\alpha}\right)}{\bar{s}^2+8\frac{\beta}{\alpha}\bar{s}+\frac{\lambda_{si}^2}{\alpha^2}}, \qquad i = 1, 2, 3, \ldots \tag{D.14}$$

Combining these high-frequency terms with the low-frequency mode described by (D.8), the modal representations of (D.3) are finally obtained as:

$$\frac{Z_c(\bar{s})\cosh\Gamma(\bar{s})}{\sinh\Gamma(\bar{s})} = \frac{Z_0}{D_n\bar{s}} + \sum_{i=1}^{\infty}\frac{\frac{2Z_0}{D_n}\left(\bar{s}+8\frac{\beta}{\alpha}\right)}{\bar{s}^2+8\frac{\beta}{\alpha}\bar{s}+\frac{\lambda_{si}^2}{\alpha^2}}$$

(D.15)

$$\frac{Z_c(\bar{s})}{\sinh\Gamma(\bar{s})} = \frac{Z_0}{D_n\bar{s}} + \sum_{i=1}^{\infty} \frac{(-1)^i \frac{2Z_0}{D_n}\left(\bar{s} + 8\frac{\beta}{\alpha}\right)}{\bar{s}^2 + 8\frac{\beta}{\alpha}\bar{s} + \frac{\lambda_{ai}^2}{\alpha^2}}$$

Given these modal representations, it is easy to find low-order approximations of (D.1) in the frequency domain, and to construct state space representations of these approximations.

D.2 Modal approximation and state space form

Concerning the modal approximation of the transfer function matrix (D.1), it is clear from (D.15) that any low-order approximation should contain the low-frequency mode plus some desired number of high-frequency resonance modes. For the case that n resonance modes are taken into account, the modal approximation in the frequency domain is given as[1]:

$$\begin{bmatrix} P_i(\bar{s}) \\ P_o(\bar{s}) \end{bmatrix} = \sum_{i=0}^{n} \begin{bmatrix} P_{i_i}(\bar{s}) \\ P_{o_i}(\bar{s}) \end{bmatrix}, \text{with:}$$

$$\begin{bmatrix} P_{i_0}(\bar{s}) \\ P_{o_0}(\bar{s}) \end{bmatrix} = \begin{bmatrix} \frac{Z_0}{D_n\bar{s}} & -\frac{Z_0}{D_n\bar{s}} \\ \frac{Z_0}{D_n\bar{s}} & -\frac{Z_0}{D_n\bar{s}} \end{bmatrix} \begin{bmatrix} \Phi_i(\bar{s}) \\ \Phi_o(\bar{s}) \end{bmatrix} \tag{D.16}$$

$$\begin{bmatrix} P_{i_i}(\bar{s}) \\ P_{o_i}(\bar{s}) \end{bmatrix} = \frac{1}{\bar{s}^2 + 8\frac{\beta}{\alpha}\bar{s} + \frac{\lambda_{ai}^2}{\alpha^2}} \begin{bmatrix} \frac{2Z_0}{D_n}\left(\bar{s} + 8\frac{\beta}{\alpha}\right) & -\frac{(-1)^i 2Z_0}{D_n}\left(\bar{s} + 8\frac{\beta}{\alpha}\right) \\ \frac{(-1)^i 2Z_0}{D_n}\left(\bar{s} + 8\frac{\beta}{\alpha}\right) & -\frac{2Z_0}{D_n}\left(\bar{s} + 8\frac{\beta}{\alpha}\right) \end{bmatrix} \begin{bmatrix} \Phi_i(\bar{s}) \\ \Phi_o(\bar{s}) \end{bmatrix}$$

For the purpose of time domain simulations, a state space realization of this model is required. Again, the low-frequency mode and the high-frequency modes are distinguished. In fact, the low-frequency mode is a simple integrator, with the "mean pressure" $P_{i_0} = P_{o_0}$ as integrator state, resulting in the following state space model:

$$\begin{aligned} \frac{1}{\omega_c}\dot{x}_0 &= [0]\,x_0 + \begin{bmatrix} \frac{Z_0}{D_n} & -\frac{Z_0}{D_n} \end{bmatrix} \begin{bmatrix} \Phi_i \\ \Phi_o \end{bmatrix} \\ \begin{bmatrix} P_{i_0} \\ P_{o_0} \end{bmatrix} &= \begin{bmatrix} 1 \\ 1 \end{bmatrix} x_0 \end{aligned} \tag{D.17}$$

Hereby, the factor ω_c originates from the scaling of the Laplace operator: $\bar{s} = r_0^2 s/\mu = s/\omega_c$.

For the high-frequency modes, different state space realizations are possible. In order to allow physical interpretation of the model, an observable canonical form has been chosen, so that the states consist of scaled (derivatives) of the output. Thereby, care has to be taken of the signs of the transfer functions in (D.16), depending on the mode. This can be done by observing that the transfer function matrix of the high-frequency modes in (D.16) can be replaced by a mode-independent transfer function matrix, if both the second input and the second output are multiplied by the mode-dependent sign $(-1)^i$. For the state space

[1]For the pressures, the subscript i indicates the pressure at the inlet side, while subsubscript i denotes the mode number of the modal approximation.

realization this means, that this mode-dependent sign $(-1)^i$ is placed in both the input and the output matrix. Thus, the following state space realization for the high-frequency modes is obtained:

$$\begin{aligned}
\frac{1}{\omega_c}\begin{bmatrix}\dot{x}_{1_i}\\ \dot{x}_{2_i}\end{bmatrix} &= \begin{bmatrix}0 & -\frac{\lambda_{si}^2}{\alpha_{si}^2}\\ 1 & -\frac{8\beta_{si}}{\alpha_{si}}\end{bmatrix}\begin{bmatrix}x_{1_i}\\ x_{2_i}\end{bmatrix} + \begin{bmatrix}\frac{2Z_0}{D_n}\frac{8\beta}{\alpha} & (-1)^{i+1}\frac{2Z_0}{D_n}\frac{8\beta}{\alpha}\\ \frac{2Z_0}{D_n} & (-1)^{i+1}\frac{2Z_0}{D_n}\end{bmatrix}\begin{bmatrix}\Phi_i\\ \Phi_o\end{bmatrix} \qquad i=1,\ldots,n\\
\begin{bmatrix}P_{i_i}\\ P_{o_i}\end{bmatrix} &= \begin{bmatrix}0 & 1\\ 0 & (-1)^i\end{bmatrix}\begin{bmatrix}x_{1_i}\\ x_{2_i}\end{bmatrix}
\end{aligned} \tag{D.18}$$

Denoting the state, input and output matrices of (D.17) with $A_{ac_0}, B_{ac_0}, C_{ac_0}$ respectively, and those of (D.18) by $A_{ac_i}, B_{ac_i}, C_{ac_i}$, $i = 1,\ldots,n$ respectively, the complete state space realization of (D.16) is easily constructed:

$$\begin{aligned}
\frac{1}{\omega_c}\dot{X}_{ac} &= A_{ac}X_{ac} + B_{ac}U_{ac}\\
Y_{ac} &= C_{ac}X_{ac}
\end{aligned} \tag{D.19}$$

with:

$$\begin{aligned}
X_{ac} &= \begin{bmatrix} x_0 & x_{1_1} & x_{2_1} & \ldots & x_{1_n} & x_{2_n}\end{bmatrix}^T\\
U_{ac} &= \begin{bmatrix}\Phi_i & \Phi_o\end{bmatrix}^T\\
Y_{ac} &= \begin{bmatrix}P_i & P_o\end{bmatrix}^T\\
A_{ac} &= \operatorname{diag}\begin{bmatrix}A_{ac_0} & A_{ac_1} & \ldots & A_{ac_n}\end{bmatrix}\\
B_{ac} &= \begin{bmatrix}B_{ac_0}^T & B_{ac_1}^T & \ldots & B_{ac_n}^T\end{bmatrix}^T\\
C_{ac} &= \begin{bmatrix}C_{ac_0} & C_{ac_1} & \ldots & C_{ac_n}\end{bmatrix}
\end{aligned}$$

It might be noted here, that the steady state behaviour of this approximate model is not exactly equal to that of the theoretical model (D.1), although the model describes the transient behaviour of the pressures correctly in a certain frequency range, and also gives an exact description of the low-frequency mode (integrator gain). The reason is, that the approximation of the infinite sums in (D.15) by a small number of terms as in (D.16) introduces a steady state error. A more detailed discussion of this topic can be found in Appendix E.

Appendix E

Steady state behaviour of modal approximations

The modal approximations of the theoretical transmission line models, considered in Subsection 2.4.3, were obtained by taking only a finite number of modes into account, while neglecting the infinite number of higher order modes. Although this method leads to nice low-order, strictly proper and accurate approximations of the dynamic input-output behaviour of the theoretical four-port models, at least for the resonance modes that are taken into account, the steady state gain of these approximate four-port models is not correct. This can be explained as follows.

As described by Yang and Tobler [160], the transfer functions of the theoretical transmission line model (2.67) can be represented by infinite sum series of second order systems; the same is done in Appendix D for the other theoretical transmission line model (2.66). Using these infinite series representations, the exact steady state gains of the theoretical transmission line models can be calculated. For (2.67), corresponding to `Config.2` from Table 2.1, the exact steady state gain is [160]:

$$\begin{bmatrix} P_i(0) \\ \Phi_o(0) \end{bmatrix} = \begin{bmatrix} 1 & 8Z_0D_n \\ 0 & 1 \end{bmatrix} \begin{bmatrix} P_o(0) \\ \Phi_i(0) \end{bmatrix} \tag{E.1}$$

For (2.66), corresponding to `Config.1` from Table 2.1, the situation is different. As the infinite sum representations (D.15) show, the transfer functions for this configuration include a pure integrator. Because the gain of this integrator is exact, and remains unchanged by the modal approximation, it can be left out of consideration here. Thus only the steady state gains of the infinite sums of (D.15) need to be considered. They can be calculated to be:

$$\begin{aligned} \left[\sum_{i=1}^{\infty} \frac{\frac{2Z_0}{D_n}\left(\bar{s}+8\frac{\beta}{\alpha}\right)}{\bar{s}^2+8\frac{\beta}{\alpha}\bar{s}+\frac{\lambda_{si}^2}{\alpha^2}}\right]_{\bar{s}=0} &= \frac{2Z_0}{D_n}8\alpha\beta\sum_{i=1}^{\infty}\frac{1}{\lambda_{si}^2} = \frac{2Z_0}{D_n}8\alpha\beta\sum_{i=1}^{\infty}\frac{D_n^2}{\pi^2 i^2} = \frac{8}{3}\alpha\beta Z_0 D_n \\ \left[\sum_{i=1}^{\infty} \frac{(-1)^i\frac{2Z_0}{D_n}\left(\bar{s}+8\frac{\beta}{\alpha}\right)}{\bar{s}^2+8\frac{\beta}{\alpha}\bar{s}+\frac{\lambda_{si}^2}{\alpha^2}}\right]_{\bar{s}=0} &= \frac{2Z_0}{D_n}8\alpha\beta\sum_{i=1}^{\infty}\frac{(-1)^i}{\lambda_{si}^2} = \frac{2Z_0}{D_n}8\alpha\beta\sum_{i=1}^{\infty}\frac{(-1)^i D_n^2}{\pi^2 i^2} = -\frac{4}{3}\alpha\beta Z_0 D_n \end{aligned} \tag{E.2}$$

where the following analytical solutions to the infinite series, occurring in the expressions

above, are used:

$$\sum_{i=1}^{\infty} \frac{1}{i^2} = \frac{\pi^2}{6}; \qquad \sum_{i=1}^{\infty} (-1)^{i-1} \frac{1}{i^2} = \frac{\pi^2}{12}$$

So, with the relations (E.2), the exact steady state gain of the theoretical transmission line model for `Config.1` can be written as (see also (D.16)):

$$\begin{bmatrix} P_i(0) \\ P_o(0) \end{bmatrix} = \left[\begin{bmatrix} \frac{Z_0}{D_n \bar{s}} & -\frac{Z_0}{D_n \bar{s}} \\ \frac{Z_0}{D_n \bar{s}} & -\frac{Z_0}{D_n \bar{s}} \end{bmatrix}_{\bar{s}=0} + \begin{bmatrix} \frac{8}{3} Z_0 D_n \alpha\beta & \frac{4}{3} Z_0 D_n \alpha\beta \\ -\frac{4}{3} Z_0 D_n \alpha\beta & -\frac{8}{3} Z_0 D_n \alpha\beta \end{bmatrix} \right] \begin{bmatrix} \Phi_i(0) \\ \Phi_o(0) \end{bmatrix} \tag{E.3}$$

The fact that steady state gains of the modal approximations (2.68) and (2.69), given in Subsection 2.4.3, do not agree with (E.1) and (E.3) respectively, is now easily explained. The point is, that the part of the infinite sums that is truncated in the modal approximation, delivers a small but non-zero contribution to the steady state gain (compare (E.2)) of the theoretical model. Actually, this directly indicates, how the steady state accuracy might be recovered; the steady state gains of the truncated parts of the transfer functions of the theoretical models should be added, as constant gains, to the modal approximations. In this way, the steady state gain of the modal approximation, including the additive gain, equals the exact steady state gain of the transmission line model again.

In the state space representation of the modal approximations, the foregoing means, that a direct throughput from input to output is added, i.e. a D-matrix is added. For the modal approximations (2.68) and (2.69), the required D-matrices are easily found, by noting that the steady state gains of these modal approximations, H_{tl} and H_{ac} respectively, are given by:

$$\begin{aligned} H_{tl} &= -\left(A_{tl_1}^{-1} B_{tl_1} + A_{tl_2}^{-1} B_{tl_2} \right) \\ H_{ac} &= -\left(C_{ac_1} A_{ac_1}^{-1} B_{ac_1} + C_{ac_2} A_{ac_2}^{-1} B_{ac_2} \right) \end{aligned} \tag{E.4}$$

Using these gain matrices, the exact steady state gains are simply recovered by adding throughput terms $D_{tl}U_{tl}$ and $D_{ac}U_{ac}$ to the output equations of the modal approximations (2.68) and (2.69) respectively, with:

$$\begin{aligned} D_{tl} &= \begin{bmatrix} 1 & 8Z_0 D_n \\ 0 & 1 \end{bmatrix} - H_{tl} \\ D_{ac} &= \begin{bmatrix} \frac{8}{3} Z_0 D_n \alpha_{si}\beta_{si} & \frac{4}{3} Z_0 D_n \alpha_{si}\beta_{si} \\ -\frac{4}{3} Z_0 D_n \alpha_{si}\beta_{si} & -\frac{8}{3} Z_0 D_n \alpha_{si}\beta_{si} \end{bmatrix} - H_{ac} \end{aligned} \tag{E.5}$$

A slight disadvantage of the method of steady state gain recovery, given here, is the fact that the model is no longer *strictly* proper. This may lead to practical problems, when modal approximations of different transmission line elements are to be coupled to each other in a simulation model. The D-matrices of the coupled models then constitute a set of linear algebraic relations, which have to be solved analytically first, in order to be able to simulate the coupled model.

Woods et.al. [155] and Yang and Tobler [160] have avoided these problems, by performing a multiplicative modification of the modal approximation, instead of the additive modification described here. For instance, the input modification method modifies the input matrix B, by means of a postmultiplication, such that the steady state gain of

the resulting model exactly matches the steady state gain of the theoretical model [160]. Thus, the model remains strictly proper and is easily coupled to other transmission line elements. Note however, that the multiplicative modification methods are principally not correct, because not only the *static* input-output behaviour is modified, but also the *dynamic* input-output behaviour.

Appendix F

Parameter values for simulation theoretical model

c_{rm}	$= 1.60\ 10^{-6}$	[m]	B_a	$= 2.5\ 10^{-2}$	[N.m.s/m]
c_{rs}	$= 1.95\ 10^{-6}$	[m]	C_d	$= 0.6$	[−]
d_{m1}	$= 8.0\ 10^{-6}$	[m]	D_n	$= 6.0\ 10^{-4}$	[m]
d_{m2}	$= 8.0\ 10^{-6}$	[m]	E	$= 1.0\ 10^{9}$	[N/m^2]
d_{m3}	$= 8.0\ 10^{-6}$	[m]	J_a	$= 1.0\ 10^{-7}$	[kg.m^2]
d_{m4}	$= 8.0\ 10^{-6}$	[m]	K_a	$= 3.34\ 10^{3}$	[N.m/m]
d_{s1}	$= 3.9\ 10^{-6}$	[m]	K_b	$= 3.26\ 10^{3}$	[N.m/m]
d_{s2}	$= 3.9\ 10^{-6}$	[m]	K_{fbs}	$= 120$	[N.m/m]
d_{s3}	$= 3.9\ 10^{-6}$	[m]	K_t	$= 0.783$	[N.m/A]
d_{s4}	$= 3.9\ 10^{-6}$	[m]	K_{ca}	$= 6.0\ 10^{-3}$	[A/V]
g	$= 4.0\ 10^{-4}$	[m]	K_{ms}	$= 6.25\ 10^{-3}$	[V/m]
h_m	$= 2.0\ 10^{-2}$	[m]	K_{pm}	$= 2.5$	[−]
h_s	$= 4.0\ 10^{-3}$	[m]	M_0	$= 1.0\ 10^{3}$	[A]
l_a	$= 1.0\ 10^{-2}$	[m]	M_s	$= 1.4\ 10^{-2}$	[kg]
l_f	$= 1.0\ 10^{-2}$	[m]	N	$= 600$	[−]
l_{fbs}	$= 2.0\ 10^{-2}$	[m]	P_s	$= 1.4\ 10^{7}$	[N/m^2]
w_s	$= 20$	[N.s/m]	P_t	$= 0.0$	[N/m^2]
x_{f0}	$= 6.29\ 10^{-5}$	[m]	V_{n1}	$= 4.1\ 10^{-7}$	[m^3]
A_0	$= 1.26\ 10^{-7}$	[m^2]	V_{n2}	$= 4.1\ 10^{-7}$	[m^3]
A_g	$= 1.66\ 10^{-5}$	[m^2]	V_{n3}	$= 2.5\ 10^{-7}$	[m^3]
A_m	$= 3.14\ 10^{-2}$	[m^2]	η	$= 2.5\ 10^{-2}$	[kg/m.s]
A_{n3}	$= 4.10\ 10^{-7}$	[m^2]	μ_0	$= 4\pi\ 10^{-7}$	[V.s/A.m]
A_s	$= 4.95\ 10^{-5}$	[m^2]	ρ	$= 850$	[kg/m^3]

Table F.1: Parameterset for simulation of servo-valve model

i_{max}	$= 60\ 10^{-3}$	[A]	$F_{s,max}$	$= 6.93\ 10^{2}$	[N]
x_{f0}	$= 6.29\ 10^{-5}$	[m]	$F_{m,max}$	$= 4.40\ 10^{3}$	[N]
$x_{s,max}$	$= 3.9\ 10^{-4}$	[m]	$F_{p,max}$	$= 3.50\ 10^{4}$	[N]
$x_{m,max}$	$= 1.6\ 10^{-3}$	[m]	P_s	$= 1.4\ 10^{7}$	[N/m^2]
q_{max}	$= 0.625$	[m]	T_{max}	$= 4.7\ 10^{-2}$	[N.m]
$\dot{q}_{max}$	$= 0.986$	[m/s]	$\Phi_{n,nom}$	$= 9.1\ 10^{-6}$	[m^3/s]
$\ddot{q}_{max}$	$= 23.3$	[m/s^2]	$\Phi_{m,nom}$	$= 1.2\ 10^{-4}$	[m^3/s]
			$\Phi_{p,nom}$	$= 2.5\ 10^{-3}$	[m^3/s]

Table F.2: Scaling constants for variables in simulations

c_{b1}	$= 25\ 10^{-6}$	[m]	l_{b1}	$= 65\ 10^{-3}$	[m]
c_{b2}	$= 25\ 10^{-6}$	[m]	l_{b2}	$= 65\ 10^{-3}$	[m]
c_{b3}	$= 25\ 10^{-6}$	[m]	l_{b3}	$= 97\ 10^{-3}$	[m]
c_{b4}	$= 25\ 10^{-6}$	[m]	l_{b4}	$= 48\ 10^{-3}$	[m]
d_{b1}	$= 80\ 10^{-3}$	[m]	t_{b1}	$= 72\ 10^{-6}$	[m]
d_{b2}	$= 80\ 10^{-3}$	[m]	t_{b2}	$= 72\ 10^{-6}$	[m]
d_{b3}	$= 98\ 10^{-3}$	[m]	t_{b3}	$= 92\ 10^{-6}$	[m]
d_{b4}	$= 56\ 10^{-3}$	[m]	t_{b4}	$= 1.4\ 10^{-4}$	[m]

Table F.3: Design parameters of hydrostatic bearings

c_{rm}	$= 1.6\ 10^{-6}$	[m]	C_d	$= 0.6$	[−]
d_{m1}	$= 8.0\ 10^{-6}$	[m]	E	$= 1.0\ 10^{9}$	[N/m^2]
d_{m2}	$= 8.0\ 10^{-6}$	[m]	$F_{cp,s}$	$= 1.75\ 10^{3}$	[N]
d_{m3}	$= 8.0\ 10^{-6}$	[m]	$F_{cp,d}$	$= 1.75\ 10^{3}$	[N]
d_{m4}	$= 8.0\ 10^{-6}$	[m]	LP_{b1}	$= 7.8\ 10^{-13}$	[m^5/Ns]
h_m	$= 2.0\ 10^{-2}$	[m]	LP_{b2}	$= 7.8\ 10^{-13}$	[m^5/Ns]
$w_{p,b1}$	$= 17.2$	[N.s/m]	LP_{b3}	$= 8.0\ 10^{-13}$	[m^5/Ns]
$w_{p,b2}$	$= 17.2$	[N.s/m]	LP_{b4}	$= 13.5\ 10^{-13}$	[m^5/Ns]
$w_{p,b3}$	$= 10.2$	[N.s/m]	M_p	$= 1.5\ 10^{3}$	[kg]
$w_{p,b4}$	$= 7.7$	[N.s/m]	P_s	$= 1.4\ 10^{7}$	[N/m^2]
q_{max}	$= 0.625$	[m]	P_t	$= 0.0$	[N/m^2]
A_p	$= 25\ 10^{-4}$	[m^2]	V_{l1}	$= 4.1\ 10^{-4}$	[m^3]
$A_{p,b1}$	$= 5.0\ 10^{-6}$	[m^2]	V_{l2}	$= 2.1\ 10^{-4}$	[m^3]
$A_{p,b2}$	$= 5.0\ 10^{-6}$	[m^2]	η	$= 2.5\ 10^{-2}$	[kg/m.s]
$A_{p,b3}$	$= 6.3\ 10^{-6}$	[m^2]	ρ	$= 850$	[kg/m^3]
$A_{p,b4}$	$= 3.8\ 10^{-6}$	[m^2]			

Table F.4: Parameterset for simulation of actuator model

$r_{h,ac1}$	$= 2.82\ 10^{-2}$	[m]	$\alpha_{s1,ac1}$	$= 1.01$	[–]
$r_{h,ac2}$	$= 8.95\ 10^{-3}$	[m]	$\alpha_{s2,ac1}$	$= 1.01$	[–]
r_{tl1}	$= 1.0\ 10^{-2}$	[m]	$\alpha_{s1,ac2}$	$= 1.01$	[–]
r_{tl2}	$= 1.0\ 10^{-2}$	[m]	$\alpha_{s2,ac2}$	$= 1.01$	[–]
E	$= 1.0\ 10^{9}$	[N/m^2]	$\beta_{c1,tl1}$	$= 7.0$	[–]
L_{ac1}	$= 0.625 + q$	[m]	$\beta_{c2,tl1}$	$= 8.0$	[–]
L_{ac2}	$= 0.625 - q$	[m]	$\beta_{c1,tl2}$	$= 6.5$	[–]
L_{tl1}	$= 1.40$	[m]	$\beta_{c2,tl2}$	$= 8.0$	[–]
L_{tl2}	$= 1.20$	[m]	$\beta_{s1,ac1}$	$= 8.0$	[–]
$\alpha_{c1,tl1}$	$= 1.03$	[–]	$\beta_{s2,ac1}$	$= 8.0$	[–]
$\alpha_{c2,tl1}$	$= 1.02$	[–]	$2\beta_{s1,ac2}$	$= 8.0$	[–]
$\alpha_{c1,tl2}$	$= 1.03$	[–]	$\beta_{s2,ac2}$	$= 8.0$	[–]
$\alpha_{c2,tl2}$	$= 1.02$	[–]	η	$= 2.5\ 10^{-2}$	[kg/m.s]
			ρ	$= 850$	[kg/m^3]

Table F.5: Parameterset for simulation of transmission line effects

A_{peg}	$= 2.54\ 10^{-4}$	[m^2]	F_{ext}	$= \pm 10\ 10^{3}$	[N]
A_{rem}	$= 2.25\ 10^{-3}$	[m^2]	M_p	$= 2.0\ 10^{3}$	[kg]
C_{d1}	$= 0.8$	[–]	P_s	$= 1.6\ 10^{7}$	[N/m^2]
C_{d2}	$= 0.61$	[–]	c_1	$= 1.86\ 10^{-4}$	[m]
D_{cyl}	$= 9.8\ 10^{-2}$	[m]	c_2	$= 1.17\ 10^{-4}$	[m]
D_{dh}	$= 5.0\ 10^{-3}$	[m]	n_{dh}	$= 16$	[–]
D_{peg}	$= 1.8\ 10^{-2}$	[m]	q_{c1}	$= 65\ 10^{-3}$	[m]
N	$= 1050$	[–]	q_{c2}	$= 90\ 10^{-3}$	[m]

Table F.6: Additional parameterset for simulation of cushioning models

Appendix G

Technical specifications of transducers

In the list below, an overview is given of the different transducers, that were available in the experimental setup, described in Section 3.3, where the reader is referred to Fig. 3.7 on page 148 for a schematic view of the experimental setup. In the list of transducers, the purpose of the transducer is given first, followed by the transducer type, the measurement range and the gain of the sensor.

Position transducer (q)

Purpose:	Identification, Validation & Feedback control
Sensor type:	Santest Co., Ltd.; GYcRP-1400
Measurement range:	-0.625 - 0.625 [m]; 0 - 100 [Hz]
Sensor gain:	10/0.625 [V/m]

Pressure difference transducer (ΔP)

Purpose:	Identification, Validation & Feedback control
Sensor type:	Paine Co.; 210-60-090-06
Measurement range:	-210 - 210 [bar]; 0 - 2000 [Hz]
Sensor gain:	10/210 [V/bar]

Absolute pressure transducer (P_1 & P_2), Type 1

Purpose:	Validation cushioning models
Sensor type:	Hottinger Baldwin Messtechnik; P3M
Measurement range:	0 - 500 [bar]; 0 - 500 [Hz]
Sensor gain:	10/500 [V/bar]

Absolute pressure transducer (P_1 & P_2), Type 2

Purpose:	Validation transmission line models (note sensor location, Fig. 3.7)
Sensor type:	Kistler; 701 G; (Piëzo)
Measurement range:	0 - 210 [bar]; 1 - 2000 [Hz]
Sensor gain:	10/140 [V/bar]

Acceleration transducer ($\ddot{q}$)

Purpose:	Validation frequency responses & cushioning models; Evaluation of feedback control
Sensor type:	Schaevitz; (Mechanical)
Measurement range:	−10 - 10 [g]; 0 - 500 [Hz]
Sensor gain:	0.48 [V/g]

Main spool position transducer (x_m)

Purpose:	Identification & Validation servo-valve models
Sensor type:	LVDT
Measurement range:	−1.6 - 1.6 [mm]; 0 - 2000 [Hz]
Sensor gain:	10/1.6 [V/mm]

Bibliography

[1] A. Abo-Ismail and F.M. Wassef. Dynamics of a speed control servo system with some nonlinearities. *The Journal of Fluid Control, Vol 19, Iss. 3*, 1988.

[2] S.K. Advani. The development of simona: A simulator facility for advanced research into simulation techniques, motion system control and navigation systems tech. In *AAIA-93-3574-CP*, 1993.

[3] C.H. An, C.G. Atkeson, and J.M. Hollerbach. *Model-Based Control of a Robot Manipulator.* The MIT Press, 1988.

[4] B.D.O. Anderson and J.B. Moore. *Optimal Control, linear quadratic methods.* Prentice-Hall International Inc., 1989.

[5] H.A. Arafa and M. Rizk. Spool hydraulic stiffness and flow force effects in electro-hydraulic servovalves. In *Proc. Inst. Mech. Engrs., vol. 201, no. C3, Egypt*, 1987.

[6] B. Armstrong-Helouvry, P. Dupont, and Wit C. De. A survey of models, analysis tools and compensation methods for the control of machines with friction. *Automatica, Vol. 30, No. 7, 1994*, 1994.

[7] H. Asada and J.J.E. Slotine. *Robot Analysis and Control.* John Wiley and Sons, Inc., 1986.

[8] K.J. Astrom and B. Wittenmark. *Computer controlled systems. Theory and design.* Prentice-Hall, Englewood Cliffs, 1984.

[9] D.P. Atherton. *Nonlinear Control Engineering.* van Nostrand Reinhold Co., London, 1975.

[10] M. Athans and J.S. Shamma. Gain-scheduling: potential hazards and possible remedies. *IEEE Control Systems Magazine, vol. 12*, 1992.

[11] M. Baarspul. Lecture notes on flight simulation techniques. Technical report, Delft University of Technology, 1989.

[12] L. Bergeron. *Water Hammer in Hydraulics and Wave Surges in Electricity.* Wiley, New York, 1961.

[13] S.A. Billings. Identification of nonlinear systems - a survey. *IEE Proceedings, vol. 127, Pt.D, no. 6*, 1980.

[14] S.A. Billings and S.Y. Fakhouri. Identification of systems containing linear dynamic and static nonlinear elements. *Automatica, vol. 18, no. 1*, 1982.

[15] J.F. Blackburn, G. Reethof, and J.L. Shearer. *Fluid Power Control.* Technology Press of M.I.T. and Wiley, New York, 1960.

[16] P. Blok. *The hydrostatic conical bearing.* PhD thesis, Laboratory for Measurement and Control, Delft University of Technology, 1976. (In German), Published: Delft.

[17] J.E. Bobrow and K. Lum. Adaptive, High Bandwidth Control of a Hydraulic Actuator. *Trans. ASME, Journal of Dynamic Systems, Measurement and Control, vol. 118, (december)*, 1996.

[18] H.W. Bode. *Network Analysis and Feedback Amplifier Design.* Holt, Rinehart and Winston, New York, 1945.

[19] F.G. de Boer. *Multivariable servo control of a hydraulic RRR-robot.* PhD thesis, Mechanical Engineering Systems and Control Group, Delft University of Technology, 1992. Published: Delft.

[20] B. Bona, L. Giacomello, C. Greco, and A. Malandra. Position control of a plastic injection moulding machine via feedback linearization. In *Proceedings of the 31st Conference on Decision and Control, Tucson, Arizona*, 1992.

[21] C. Borghesani, Y. Chait, and O. Yaniv. *The Quantitative Feedback Theory MATLAB Toolbox, User's Guide and Software.* The MathWorks, Inc., Massachusetts, March 1995.

[22] F.T. Brown. The transient response of fluid lines. *Trans. ASME, Journal of Basic Engineering, vol. 84-D, no. 4 (dec)*, 1962.

[23] F.T. Brown. A quasie method of characteristics with application to fluid lines with frequency dependent wall shear and heat transfer. *Trans. ASME, Journal of Basic Engineering, vol. 91*, 1969.

[24] R.T. Burton, C.M. Sargent, and G.J. Schoenau. Using an aritficial neural network to direct a hydraulic circuit. In *Proceedings of 43rd Int. Conf. on Fluid Power, Chicago, USA*, 1992.

[25] M.J. Chapman and K.R. Godfrey. On structural equivalence and identiability constraint ordering. In *Identifiability of Parametric models, E. Walter (Ed.), Pergamon Press, Oxford, England*, 1987.

[26] C-T. Chen. *Linear System Theory and Design.* Holt-Saunders International Editions, New York, 1984.

[27] T.-L. Chern and Y.-C. Wu. Design of integral variable structure controller and application to electrohydraulic servosystems. In *IEE Proceedings D, Vol. 138, no. 5 (september)*, 1991.

[28] Q.P. Chu, J.A. Mulder, and P.T.L.M. van Woerkom. Modified Recursive Maximum Likelihood Adaptive Filter for Nonlinear Aircraft Flight-Path Reconstruction. *AIAA Journal of Guidance, Control, and Dynamics, vol. 19, no. 6*, 1996.

[29] C.S. Cox and I.G. French. Limit cycle prediction conditions for a class of hydraulic control system. *Trans. ASME, Journal of Dynamic Systems, Measurement and Control, vol. 108, (march)*, 1986.

[30] J. Delforge, L. d'Angio, and S. Audoly. Results and conjectures on the identifiability of linear systems. In *Identifiability of Parametric models, E. Walter (Ed.), Pergamon Press, Oxford, England*, 1987.

[31] V.N. Dmitriyev and A.G. Shashkov. Force of the jet action on the baffle in pneumatic and hydraulic control units. *Pneumatic and Hydraulic Control Systems, London, Pergamon Press*, 1968.

[32] H.G.M. Dötsch, H.T. Smakman, P.M.J. Van den Hof, and M. Steinbuch. Adaptive repetitive control of a compact disc mechanism. In *Proc. 34th IEEE Conf. Decision and Control, dec. 13-15, 1995, New Orleans, Louisiana, USA*, 1995.

[33] A.F. d'Souza and R. Oldenburger. Dynamic response of fluid lines. *Trans. ASME, Journal of Basic Engineering, vol. 86-D, no. 3 (sep)*, 1964.

[34] F.D. Ezekiel and H.M. Paynter. Computer representations of engineering systems involving fluid transients. In *Trans. ASME, vol. 79 (november)*, 1957.

[35] M. Fanhua and G. Fengyang. A simulation method for modeling of electro-hydraulic servo system. In *Proceedings of the Beijing International Conference on System Simulation and Scientific Computing, Vol. 2*, 1989.

[36] A. von Feuser. Design of state controllers in the time and frequency domain for position control of valve-controlled servo-hydraulic linear drive. *Regelungstechnik, vol. 32, iss. 9*, 1984. (In German).

[37] J.M. Finney, A. de Pennington, M.S. Bloor, and G.S. Gill. A pole-assignment controller for an electrohydraulic cylinder drive. *Transactions ASME, Journal of Dynamic Systems, Measurement, and Control, vol. 107, (june)*, 1985.

[38] O. Föllinger. *Nonlinear Control I.* R.Oldenbourg Verlag, Muenchen, BRD, 1993. (In German).

[39] J.M. Gasiorek and W.G. Carter. *Mechanics of Fluids for Mechanical Engineers.* Blackie and Son, London, 1967.

[40] K.R. Godfrey and J.J. DiStefano. Identifiability of model parameters. In *Identifiability of Parametric models, E.Walter (Ed.), Pergamon Press, Oxford, England*, 1987.

[41] S.G. Goodhart, K.J. Burnham, and D.J.G. James. A retrospective self-tuning controller. *International Journal of Adaptive Control and Signal Processing, Vol. 5*, 1991.

[42] R.E. Goodson and R.G. Leonard. A survey of modeling techniques for fluid line transients. *Trans. ASME, Journal of Basic Engineering, vol. 94, june*, 1972.

[43] W. Greblicki and M. Pawlak. Hammerstein system identification by non-parametric regression estimation. *International Journal of Control, vol. 45, no. 1*, 1987.

[44] R.D. Grose. Orifice flow at low reynolds number. *Journal of Pipelines, 3, Elsevier Science Publishers B.V., Amsterdam*, 1983.

[45] L. Guo and H. Schwarz. A control scheme for bilinear systems and application to a secondary controlled hydraulic rotary drive. In *Proceedings of the 28th IEEE Conference on Decision and Control*, 1989.

[46] R.G. Hakvoort. *System Identification for Robust Process Control.* PhD thesis, Mechanical Engineering Systems and Control Group, Delft University of Technology, 1994. Published: Delft.

[47] A.A. Ham. *On the dynamics of hydraulic lines supplying servosystems.* PhD thesis, Laboratory for Measurement and Control, Delft University of Technology, 1982. Published: Delft.

[48] P. Händel and A. Nehorai. Tracking analysis of an adaptive notch filter with constrained poles and zeros. *IEEE Transactions on Signal Processing, SP-42*, 1994.

[49] H.M. Handroos and M.J. Vilenius. Flexible semi-empirical models for hydraulic flow control valves. *Transactions of the ASME, vol. 113*, 1991.

[50] J. Heintze. *Design and control of a hydraulically actuated industrial Brick Laying Robot.* PhD thesis, Mechanical Engineering Systems and Control Group, Delft University of Technology, 1997. Published: Delft.

[51] J. Heintze, R.M. Peters, and A.J.J. van der Weiden. Cascade delta p and sliding mode for hydraulic actuators. In *Proceedings of the 1995 European Control Conference, sept. 5-8, Roma, Italy*, 1995.

[52] J. Heintze, G. van Schothorst, A.J.J. van der Weiden, and P.C. Teerhuis. Modelling and control of an industrial hydraulic rotary vane actuator. In *Proc. 32nd IEEE Conf. Decision and Control, dec. 15-17, 1993, San Antonio, TX, USA*, 1993.

[53] J. Heintze, P.C. Teerhuis, and A.J.J. van der Weiden. Controlled hydraulics for a direct drive brick laying robot. In *Proc. 12th Int. Symp. Automation and Robotics in Construction, Warsaw, Poland*, 1995.

[54] J. Heintze and A.J.J. van der Weiden. Inner loop design and analysis for hydraulic actuator, with application to impedance control. *Control Engineering Practice, 3*, 1995.

[55] A. Helmersson. *Methods for Robust Gain-Scheduling.* PhD thesis, Linköping University, 1995. Published: Linköping, Sweden.

[56] N. Hogan. Impedance control: An approach to manipulate; part 1 - theory, part 2 - implementation, part 3 - applications. *Trans. ASME, Journal of Dynamic Systems, Measurement, and Control, vol. 107*, 1985.

[57] N. Hori, P.R. Ukrainetz, P.N. Nikiforuk, and D.V. Bitner. Robust discrete-time adaptive control of an electrohydrualic servo actuator. In *Fluid Power 8*, 1988.

[58] I.M. Horowitz. *Quantitative Feedback Design Theory (QFT).* QFT Publications, Boulder, Colorado, USA, 1993.

[59] D.A. Hullender and A.J. Healy. Rational polynomial approximations for fluid transmission line models. *Fluid Transmission Line Dynamics, ASME Special Publication, New York*, 1981.

[60] D.A. Hullender and C.Y. Hsue. Modal approximations for the fluid transmission line dynamics. *Fluid Transmission Line Dynamics, ASME Special Publication, New York*, 1983.

[61] A.S. Iberall. Attenuation of oscillatory pressures in instrument lines. *Journal of Research, National Bureau of Standards, vol. 45, R.P. 2115*, 1950.

[62] Y. Ikebe, T. Nakada, S. Yokata, and al. et. Load insensitive electrohydraulic servosystem. *Jounal of Fluid Control, vol. 13, no. 4*, 1982.

[63] ISI. *Matrixx / System-Build Users Guide.* Santa Clara, 1991.

[64] Y. Jen and C. Lee. Robust speed control of a pump-controlled motor system. *IEE Proceedings-D, vol. 139, no. 6 (march)*, 1992.

[65] S.S. Karar and E. Rose. Adaptive control of a two-actuator hydraulic system with load interaction. In *Proc. 12th IFAC World Congress, Sydney, Australia, 18-23 july 1993*, 1993.

[66] A. Koeckemann, J. Konertz, and H. Lausch. Control algorithms for electro-hydraulic servo drives based on industrial marginal conditions. *Automatisierungstechnik, Vol. 39, no. 6*, 1991. (In German).

[67] P.F.M. Kok. Validation techniques for nonlinear systems. application to electro-hydraulic servo-valve. Master's thesis, Delft University of Technology, Mechanical Engineering Systems and Control Group, 1995. (In Dutch).

[68] P. Kraniauskas. *Transforms in Signals and Systems.* Beccles, Addison-Wesley Publishers Ltd., 1992.

[69] P. Krus, K. Weddfelt, and J.O. Palmberg. Fast pipeline models for simulation of

hydraulic systems. *Journal of Dynamic Systems, Measurement,and Control, Vol. 116, march 1994*, 1994.

[70] P.F. Lambrechts. *The Application of Robust Control Theory Concepts to Mechanical Servo Systems.* PhD thesis, Mechanical Engineering Systems and Control Group, Delft University of Technology, 1994. Published: Delft.

[71] Z.Q. Lang. Controller design oriented model identification method for hammerstein system. *Automatica, vol. 29, no. 3*, 1993.

[72] M. Lebrun. A model for a four-way spool valve applied to a pressure control system. *The Journal of Fluid Control, vol. 17, no. 4*, 1987.

[73] M. Lebrun and S. Scavarda. Simulation of the nonlinear behaviour of an electro-hydraulic exciter. *Simulation Councils*, 1979.

[74] M. Lebrun, S. Scavarda, and A. Jutard. Simulation sur ordinateur d'une servovalve a deux etages. *Automatisme, vol. 23, no. 3-4*, 1978. (In French).

[75] Y. Lecourtier and A. Raksanyi. The testing of structural properties through symbolic computation. In *Identifiability of Parametric models, E.Walter (Ed.), Pergamon Press, Oxford, England*, 1987.

[76] I.J. Leontaritis and S.A. Billings. Experimental design and identifiability for non-linear systems. *International Journal of Science, vol. 18, no. 1*, 1987.

[77] I.J. Leontaritis and S.A. Billings. Model selection and validation methods for non-linear systems. *International Journal of Control, vol. 45, no. 1*, 1987.

[78] F.L. Lewis. *Optimal Estimation.* John Wiley and Sons, New York, 1986.

[79] A. Lichtarowicz. Flow and force characteristics of flapper valves. In *3rd International Fluid Power Symposium, held at Turin, Italy. B.H.R.A. Fluid Engineering, paper B1*, 1973.

[80] S.J. Lin and A. Akers. A dynamic model of the flapper-nozzle component of an electrohydraulic servovalve. *Journal of Dynamic Systems, Measurement, and Control, vol. 111, no. 1*, 1989.

[81] S.J. Lin and A. Akers. Dynamic analysis of a flapper-nozzle valve. *Journal of Dynamic Systems, Measurement, and Control, Vol. 113*, 1991.

[82] G.W. van der Linden *High Performance Robust Manipulator Motion Control. Theory, Tools, and Experimental Implementation.* PhD thesis, Mechanical Engineering Systems and Control Group, Delft University of Technology, 1997. Published: Delft.

[83] G.W. van der Linden. Comparison of four control schemes for an experimental hydraulic robot. In *Proc. IFAC Workshop "Motion Control", oct. 9-11, Munich, Germany*, 1995.

[84] G.W. van der Linden. Design and implementation of a model based nonlinear controller for an experimental hydraulic robot. In *Proc. 3rd Mechatronics and Robotics Conference, Paderborn, Germany*, 1995.

[85] L. Ljung. *System Identification. Theory for the user.* Prentice-Hall Information and System Science Series, 1987.

[86] D.P. Looze. A dual optimization procedure for linear quadratic robust control problems. *Automatic, Vol. 10, no. 3*, 1983.

[87] J.M. Maciejowski. *Multivariable feedback design.* Electronic systems engineering

series, Addison-Wesley Publishing Company, 1989.

[88] R.E. Maine and K.W. Iliff. Identification of Dynamic Systems. *AGARD Flight Test Techniques Series, AGARDograph 300, Vol. 2*, 1994.

[89] Mannesmann-Rexroth. Proportional, control- and servo-valves; electronic components and systems. Technical report, Mannesmann-Rexroth GmbH, Lohr am Main, Germany, 1993. (In German).

[90] A. Mans. Modelling of safety buffers for linear hydraulic actuators. Master's thesis, Delft University of Technology, Mechanical Engineering Systems and Control Group, 1993. (In Dutch).

[91] D. Mao and P.I. Chen. Mathematical models of sawmill carriage hydraulic drive systems. In *Flucome 91, ASME*, 1991.

[92] D.L. Margolis and W.C. Yang. Bond graph models for fluid networks using modal approximation. *Journal of Dynamic Systems, Measurement, and Control, vol. 107, september*, 1985.

[93] T. Matsui and Y. Mochizuki. Effect of positive angular velocity feedback on torque control of hydraulic actuator. *JSME Int. Journal, Series III, vol. 35, no. 3, 1992*, 1992.

[94] T.W. McClain, E.K. Iverson, C.C. Davis, and S.C. Jacobsen. Development, simulation and validation of a highly nonlinear hydraulic servosystem model. In *Proceedings of the American Control Conference, vol. 1 (of 3)*, 1989.

[95] N.H. McClamroch. Displacement control of flexible structures using electrohydraulic servo-actuators. *Transactions ASME, Journal of Dynamic Systems, Measurement, and Control, vol. 107, (march)*, 1985.

[96] D. McCloy. Discharge characteristics of servovalve orifices. In *Proceedings of the 1968 Fluid Power International Conference, London*, 1968.

[97] D. McCloy and H.R. Martin. *Control of Fluid Power, Analysis and Design.* Chicester U.K., Halsted Press, 1980.

[98] H.E. Merrit. *Hydraulic control systems.* John Wiley and Sons, Inc., New York, 1967.

[99] R. von Mises. Berechnung von ausflusz- und ueberfallzahlen. *Zeitschrift des Vereines deutscher Ingenieure, vol. 61, no. 21*, 1917. (In German).

[100] MOOG. Type 30 flow control servovalves. Technical report.

[101] J.A. Mulder, J.K. Sridhar, and J.H. Breeman. Identification of Dynamic Systems - Applications to Aircraft. Part 2: Nonlinear Analysis and Manouevre Design. *AGARD Flight Test Techniques Series, AGARDograph 300, Vol. 3, Pt. 2*, 1994.

[102] A. Nassirharand, J.H. Taylor, and K.N. Reid. Controller design for nonlinear systems based on simultaneous stabilization theory and describing function models. *Trans. ASME, Journal of Dynamic Systems, Measurement and Control, vol. 110, (june)*, 1988.

[103] Th. Naujoks and Chr. Wurmthaler. Bilinear controller and observer design for nonlinear systems with application to a hydraulic rotary drive. *Automatisierungstechnik, vol. 36, no. 1*, 1988. (In German).

[104] R. Neumann, A. Engelke, and W. Moritz. Digital trajectorycontrol of a hydraulic portalrobot. *Ölhydraulik und Pneumatik, Vol. 35, no. 3*, 1991. (In German).

[105] R. Neumann, A. Engelke, and W. Moritz. Robust simultaneous controller-observer design by parameter optimization for a hydraulic portal robot. *Automatisierungstechnik, Vol. 39, no. 5*, 1991. (In German).

[106] N.B. Nichols. The linear properties of pneumatic transmission lines. *Transactions of the Instrument Society of America, vol. 1*, 1962.

[107] H. Nijmeijer and A.J. van der Schaft. *Nonlinear Dynamical Control Systems.* Springer-Verlag, New York, 1990.

[108] R. Oldenburger and R.E. Goodson. Simplification of hyudraulic line dynamics by use of infinite products. *Trans. ASME, Journal of Basic Engineering, vol. 86*, 1964.

[109] A. Packard. Gain-scheduling via linear fractional transformations. *Systems Control Letters, 22*, 1994.

[110] A.S. Pannala, P. Dransfield, M. Palaniswami, and J.H. Anderson. Controller design for a multichannel electrohydraulic system. *Journal of Dynamic Systems, Measurement, and Control, Vol. 111, no. 2*, 1989.

[111] H.J. Park, H.S. Cho, and B.S. Hyun. An adaptive control of non-linear time-varying hydraulic servosystems. In *Proceedings of the American Control Conference, 1989*, 1989.

[112] H.J. Park, H.S. Cho, and C.O. Lee. An iterative learning control algorithm for the position tracking control of hydraulic servo systems. In *Flucome 91, ASME*, 1991.

[113] R. Parkkinen, M. Jaerviluoma, and K. Nevala. An intelligent hydraulic actuator for varying loads. In *Fluid Power 8*, 1988.

[114] J.C. Peyton-Jones and S.A. Billings. Interpretation of non-linear frequency response functions. *International Journal of Control, vol. 52, no. 2 (aug.)*, 1990.

[115] S. Ramachandran and P. Dransfield. Interaction between the actuators in loaded multi-channel electrohydraulic drives. *Journal of Dynamic Systems, Measurement, and Control, Vol. 115, no. 2A*, 1993.

[116] P. Saffe and H.-J. Feigel. Nonlinear control concepts for servohydraulic drives. In *Fluid Power 8*, 1988.

[117] C.W. Scherer. Mixed H_2/H_∞ control. *Trends in Control, A European Perspective. Springer-Verlag Berlin.*, 1995.

[118] G. van Schothorst. Independent hydraulic actuator control loops: The basis of flight simulator motion control. In *Proc. CEAS Symposium on Simulation Technology "Making it REAL", oct. 30 - nov. 1, Delft, The Netherlands*, 1995.

[119] G. van Schothorst, P.C. Teerhuis, and A.J.J. van der Weiden. Stability analysis of a hydraulic servo-system including transmission-line effects. In *Proc. Third International Conference on Automation, Robotics and Computer Vision, nov. 9-11, Singapore*, 1994.

[120] G. van Schothorst, P.C. Teerhuis, and A.J.J. van der Weiden. Dynamic modelling of a hydraulic servo-valve on behalf of flight simulator motion control. In *Proc. IFAC Workshop "Motion Control", oct. 9-11, Munich, Germany*, 1995.

[121] G. van Schothorst, P.C. Teerhuis, and A.J.J. van der Weiden. Non-linear dynamic modelling and identification of an electro-hydraulic servo-valve. In *Proc. Third IASTED International Conference on Robotics and Manufacturing, jun. 14-17, Cancun, Mexico*, 1995.

[122] R.J.P. Schrama. *Approximate Identification and Control Design - with application to a mechanical system.* PhD thesis, Mechanical Engineering Systems and Control Group, Delft University of Technology, 1992. Published: Delft.

[123] H. Schwarz and R. Ingenbleek. Observing the state of hydraulic drives via bilinear approximated models. *Control Engineering Practice, vol. 2, no. 1*, 1994.

[124] N. Sepehri, G.A.M. Dumont, and P.D. Lawrence. Cascade control of hydraulically actuated manipulators. *Robotica, vol. 8, no. 3 (jul/sept)*, 1990.

[125] J.L. Shearer. Digital simulation of a coulomb-damped hydraulic servosystem. *Trans. ASME, Journal of Dynamic Systems, Measurement and Control, vol. 105, december*, 1983.

[126] M.-C. Shih and S.-N. Ho. Hydraulic variable piston motor position control by using model reference adaptive control method. In *Flucome 91, ASME*, 1991.

[127] N.P. Shumskii. The results of experimental and theoretical investigations of control devices of the nozzle-baffle type. *Pneumatic and Hydraulic Control Systems, London, Pergamon Press*, 1968.

[128] R.S. Sidell and D.N. Wormley. An efficient simulation method for distributed lumped fluid networks. *Journal of Dynamic Systems, Measurement, and Control, march 1977*, 1977.

[129] M. Simon and G.R. Tomlinson. Use of the hilbert transform in modal analysus of linear and nonlinear structures. *Journal of Sound and Vibration*, 1984.

[130] J.J.E. Slotine and W. Li. *Applied nonlinear control.* Prentice-Hall International Inc., 1987.

[131] S.C. Southward, C.J. Radcliffe, and C.R. MacCluer. Robust nonlinear stick-slip friction compensation. *Journal of Dynamic Systems, Measurement, and Control, Vol. 113*, 1991.

[132] M.W. Spong and M. Vidyasagar. *Robot Dynamics and Control.* John Wiley and Sons, Inc., 1989.

[133] P. Stoica and T. Söderström. Instrumental-variable methods for identification of hammerstein systems. *International Journal of Control, vol. 35, no. 3*, 1982.

[134] W.J. Thayer. Specification standards for electro-hydraulic flow control servovalves. *Moog Technical Bulletin, 117, New York*, 1962.

[135] W.J. Thayer. Transfer function for moog servovalves. *Moog Technical Bulletin, 103, New York*, 1965.

[136] G.R. Tomlinson. Development in the use of the hilbert transform for detecting and qualifying non-linearity associated with frequency response functions. *Mechanical Systems and Signal Processing (vol. 2)*, 1987.

[137] D.R. Towill. *Transfer Function Techniques for Control Engineers.* Lliffe Books Ltd., London, 1970.

[138] N.D. Vaughan. A digital position controller for an integrated hydraulic actuator system. In *Proceedings of the Institution of Mechanical Engineers International Conference Mechatronics: Designing Intelligent Machines*, 1990.

[139] T.J. Viersma. *Analysis, Synthesis and Design of Hydraulic Servosystems and Pipelines.* 2nd edition, Delft, 1990.

[140] M.J. Vilenius and T.K. Vivaldo. The effect of nonlinearities on the dynamic characteristics of an electrohydraulic servovalve. *Hydraulic and Pneumatic, Mechanical Power, vol. 22, no. 263 (november)*, 1976.

[141] D.K. de Vries. *Identification of Model Uncertainty for Control Design.* PhD thesis, Mechanical Engineering Systems and Control Group, Delft University of Technology, 1994. Published: Delft.

[142] E. Walter (Ed.). *Identifiability of Parametric Models.* Pergamon Press, Oxford, England, 1987.

[143] R.B. Walters. *Hydraulic and electro-hydraulic control systems.* Elseviers applied science, London, 1991.

[144] D. Wang, R. Dolid, M. Donath, and J. Albright. Development and verification of a two-stage flow control servovalve model. In *Proc. ASME 1995 IMECE, nov. 11-17, San Francisco, CA, FPS and T-Vol. 2*, 1995.

[145] J. Watton. The stability of electrohydraulic servomotor systems with transmission lines and nonlinear motor friction effects. part a: System modeling. *The Journal of Fluid Control, vol. 16, no.2-3*, 1986.

[146] J. Watton. The dynamic performance of an electrohydraulic servovalve/motor system with transmission line effects. *Trans. ASME, Journal of Dynamic Systems, Measurement and Control, vol. 109, (march)*, 1987.

[147] J. Watton. A digital compensator design for electrohydraulic servomotor systems using reduced-order observers. *The Journal of Fluid Control, Vol 19, Iss. 3*, 1988.

[148] J. Watton. The effect of servovalve underlap on the accuracy and dynamic response of single-rod actuator position control systems. *The Journal of Fluid Control, Vol. 20*, 1989.

[149] J. Watton. A digital compensator design for elechtrohydraulic single-rod cylinder position control systems. *Transactions ASME, Journal of Dynamic Systems, Measurement, and Control, Vol. 112 (september)*, 1990.

[150] J. Watton and M.J. Tadmori. Damping characteristics of transmission lines with sudden closure of underlapped electrohydraulic servovalves. In *Dynamic Systems: Modelling and Control, presented at ASME Winter Annual Meeting, Miami Beach, FL, USA, nov. 17-22*, 1985.

[151] J. Watton and M.J. Tadmori. A comparison of techniques for the analysis of transmission line dynamics in electrohydraulic control systems. *Appl. Math. Modelling, vol. 12, october*, 1988.

[152] O.P. van Wel. The modelling of an electrohydraulic servovalve. Master's thesis, Delft University of Technology, Mechanical Engineering Systems and Control Group, 1992.

[153] T. von Wierschem. Position control of weakly-damped drives by state feedback. *Regelungstechnik, vol. 29, iss. 1*, 1981. (In German).

[154] T. Wigren. *Recursive Identification based on the Nonlinear Wiener Model.* PhD thesis, Automatic Control and Systems Analysis Group, Department of Technology, Uppsala University, 1990. Published: Uppsala, Sweden.

[155] R. Woods, D.A. Hullender, and C.H. Hsu. Time domain simulation of fluid transmission lines using minimum order state variables models. *Fluid Transmission Line Dynamics, vol. 2, ASME Special Publication, New York*, 1983.

[156] P.M.R. Wortelboer. *Frequency-Weighted Balanced Reduction of Closed-Loop Mechanical Servo Systems: Theory and Tools.* PhD thesis, Mechanical Engineering Systems and Control Group, Delft University of Technology, 1994. Published: Delft.

[157] F. Wu. *Control of Linear Parameter Varying Systems.* PhD thesis, University of California at Berkeley, 1995. Published: Berkeley, USA.

[158] E.B. Wylie and V.L. Streeter. *Fluid Transients.* McGraw-Hill International Book Company, 1978.

[159] M. Yamashita, K. Fujimori, C. Uhlik, R. Kawatani, and H. Kimura. H-inf control of an automotive active suspension. In *Proceedings of the 29th Conference on Decision and Control*, 1990.

[160] W.C. Yang and W.E. Tobler. Dissipative modal approximation of fluid transmission lines using linear friction model. *Trans. ASME, Journal of Dynamic Systems, Measurement and Control, vol. 113, no. 1*, 1991.

[161] J.S. Yun and H.S. Cho. Application of an adaptive model following control technique to a hydraulic servo system subjected to unknown disturbances. *Journal of Dynamic Systems, Measurement,and Control, Vol. 113, sept. 1991*, 1991.

[162] T. Zhao and T. Virvalo. Fuzzy control of a hydraulic position servo with unknown load. In *Proceedings IEEE Conference on Fuzzy Systems, San Francisco, CA, USA*, 1993.

[163] W. Zielke. Frequency-dependent friction in transient pipe flow. *Trans. ASME, Journal of Basic Engineering, vol. 90-D, no. 1 (march)*, 1968.

Index

absolute pressure, 152, 188, 287, 292, 300
acceleration, 61
  constant, 286
  control, 6, 207
  desired, 204, 205
  measured frequency response, 244, 252
  minimization, 285
  noise, 207, 263
  peak, 9, 64, 283–285, 305
  transfer function, 177
actuator
  dynamics, 52, 54, 61, 83, 101, 103, 147, 169, 185, 204, 254, 323
  non-linearity, 52, 58, 111, 173, 174, 226, 236, 256
algebraic loop, 37, 85, 329
amplitude
  dependence, 26, 124, 131, 169, 196, 221, 230, 259
  filter, 133, 153, 170, 185
    design, 134, 160
  response, 133, 140, 153, 162, 175, 259
asymmetric
  actuator, 3
  port configuration, 46

badly damped, 8, 21, 79, 87, 170, 229, 254, 313
ball clearance, 30, 43, 325
Bessel characteristic, 212
Bessel function, 75
bilinear, 114, 208
black-box modelling, 11, 121
Bode plot, 86
buffer, *see* cushioning
bulk modulus, 32, 52
Butterworth characteristic, 212

causality, 69, 72
characteristic impedance, 74, 81, 102
clearance
  ball, *see* ball clearance
  of hydrostatic bearing, 54, 269, 277, 304, 335
  of PIH cushioning, 269, 273
  radial, *see* radial clearance
computational delay, 228
control
  design, 7, 13, 120, 201, 207
    aim, 207
    open issues, 231
    software, 151
  digital, *see* digital control
  hardware, 5
  high-level, 202
  low-level, 202
  motion, *see* motion control
  multivariable, *see* multivariable control
  non-linear, *see* non-linear control
  strategy, 13, 201, 207
    cascade ΔP, 13
    experimental evaluation, 254
  two-level, 202
controllability, 108
  of pressures, 93, 101
controllable inputs, 171
Coulomb friction, 10, 24, 33, 42, 53, 63, 115, 150, 177, 245, 318
criterion
  $M = 1.3$, 209
  cost, 139, 186
  least squares, 132
  mean squares, 132
  noise level, 244
  Nyquist, 227
  quadratic, 192
critical-centre, 3, 44, 111, 114, 149, 234, 312
cross-validation, 126, 144, 156, 164, 177, 188
cushioning, 9, 267
  closing-drain-holes, 268
  design, 14, 267, 284
    experimental evaluation, 299
    objective, 284
  distance, 286, 300, 309

geometry, 14, 296, 299
peg-in-hole, 268

damping, 5, 62, 101, 181
amplitude dependent, 62, 114
bad / low, *see* badly damped
by pressure feedback, 5, 209
coefficient, 102
in impedance control, 217
modification factor, 81
viscous, 28, 60, 70
delay operator, *see* propagation operator
Describing Function, 15, 123, 128
Random Input, *see* Random Input Describing Function
Sinusoidal Input, *see* Sinusoidal Input Describing Function
design procedure
cushioning, 308
closing-drain-holes (CDH), 295
model-based, 16, 285
peg-in-hole (PIH), 289
differentiation, 175, 237, 241
digital control, 5, 150, 232, 258
digital filter, 151, 160, 185
differentiating, 237
direct drive, 2
discharge coefficient, 31, 273, 278, 282, 301
constant, 34, 35, 110
uncertain, 110
dither, 43, 107, 150, 153
double-concentric actuator, 4, 6, 56, 65, 66, 146, 268, 312
drain
compartment, 271
flow, 268
hole
additional, 269, 276, 281
closed, 279
partially closed, 277
regular, 268, 275
line, 268
DSP, 5, 151
dynamics
(non)-linear, *see* (non)-linear dynamics
actuator, *see* actuator dynamics
parasitic, *see* parasitic dynamics
servo-valve, *see* servo-valve dynamics
transmission line, *see* transmission line dynamics

electrical drive, 2, 202
electrical feedback, 28, 37, 152, 320
excitation signal, 125, 165
random, 125, 260
sinusoidal, 125

feedback
electrical, *see* electrical feedback
mechanical, *see* mechanical feedback
feedback linearization, 202, 232
feedback spring, 28, 33, 48, 95, 320
flapper dynamics, 29, 31, 96
flapper hitting nozzles, 49, 156, 163, 324
flapper-nozzle
non-linearity, 40, 108, 324
servo-valve, 3, 23, 27, 33, 91, 94, 106, 152, 198, 313, 319
system, 30, 33, 40, 153
flight simulator, 1, 5
motion control, 6
motion system, 6, 145, 201, 267
flow control, 1, 26, 41, 43
flow force, 27
on flapper, 11, 29, 32, 41, 106, 324
on spool (axial), 30, 35, 46, 326
flow non-linearity, 50, 111, 158, 174, 211, 219
fluid power, 1
four-way valve, 3
frequency
modification factor, 81, 102
response, 120, 123, 129, 133, 207
actuator, 171
actuator & transmission lines, 186
flapper-nozzle valve, 153
three-stage valve, 160
frequency dependent friction, 76, 78, 82
full order estimator, *see* Kalman filter

grey-box modelling, 11, 312
grey-box modelling/identification, 120

Hammerstein model, 122, 141

hard non-linearity, 92, 116, 124, 129, 234
harmonic
  analyzer, 133
  base, 102, 129, 131
  first, 103
  higher, 129, 228
Hilbert Transform, 134
hydrostatic bearing, 4, 54, 58, 60, 170, 181, 318

identifiability, 96, 125, 137
identification approach, 121, 126
impedance
  characteristic, *see* characteristic impedance
  constant (Z_0), 80
  control, 217
input amplitude filter, *see* amplitude filter
input non-linearity, 114, 122, 136, 170, 221, 226, 256
inter-kernel interference, 124, 134
intra-kernel interference, 124, 133

jet angle, 36

Kalman filter, 238
  extended, 121

laminar, 34, 38, 52, 70, 273, 308, 333
leakage, 52, 101, 112, 181, 271
  across piston, 52
  causing damping, 62, 209
  in spool, 34, 45
  of hydrostatic bearing, 54, 55, 58, 326, 333
  of nozzle flows, 31
linear dynamics, 120, 123, 124, 131, 137, 232, 313
  actuator, 116, 170
  pilot-valve, 153
linearization, 15, 23
  by control, 259
  by feedback, *see* feedback linearization
  of actuator model, 99
  of servo-valve model, 91
  quasi, *see* quasi-linearization
load
  compensation, 176, 205, 220, 248, 259
  dependence, 44, 113, 178, 218, 264
  sensitivity, 212, 219, 256, 285
long-stroke actuator, 2, 8, 65, 145, 235

main spool, 36, 50, 91, 136, 162
  pressures, 36
manifold loss, 85, 234, 300, 330
Matrix_X, 139, 151
Maximum Likelihood, 121
mechanical feedback, 5, 31, 43
modal approximation, 12, 79, 102, 314, 339
  steady state behaviour, 81, 345
model reduction, 15, 25, 93, 100
model-based
  control design, 7, 208, 265
  cushioning design, 9, 267, 285
  estimator, 241
  system design, 234
modelling approach, 13, 22, 68, 124
motion
  control, 1, 5, 201, 311
    strategy, 201
  profile, 285, 289, 302
  system, *see* flight simulator
    electric, 202
    hydraulic, 6, 201, 215
multivariable control, 7, 13, 202

noise, 125, 237, 243
  level of velocity estimation, 244
  measurement, 166, 172, 238
  random, 144
  reduction, 238
  white, 165
non-linear
  control, 219, 258
  dynamics, 86, 109, 131
    flapper-nozzle valve, 33, 157
  frequency response, 124, 133
  friction, *see* Coulomb friction
  identification, 11, 120, 121
non-linearity
  dominant, 15, 105, 130, 209, 232, 264, 316
  flow, *see* flow non-linearity
  hard, *see* hard non-linearity
  input, *see* input non-linearity

main, 105, 113
output, *see* output non-linearity
servo-valve, *see* servo-valve non-linearity
static, *see* static non-linearity
torque motor, *see* torque motor non-linearity
nozzle flow, 29, 31, 40
Nyquist plot, 226, 235

observer, *see* velocity estimation
oil compressibility, 21, 52, 61, 65, 95, 292, 301
outlet restriction, 31, 41
output non-linearity, 110, 122, 136, 153
overlap, 34, 35, 45, 110, 149, 163, 325

parasitic
dynamics, 147, 180, 187, 244
motions, 21, 147, 252, 302
peg geometry, 268, 289, 291, 304
physical parameters, 22, 58, 78, 82
reconstruction of, 127, 144, 157, 168, 180, 191
physical realizability, 72
pilot-valve, 28, 36, 50, 120, 149, 152, 321
dynamics, 91, 153, 158
non-linearity, 106, 111, 153, 162, 231
pole(s), 94
closed loop, 211
dominant, 225, 236
estimator, 239
fast, 272, 330
number of, 138
of transmission line model, 340
pole-placement, 212
pole/zero cancellation, 140
poles
dominant, 265
position
control, 5, 13, 204, 210, 256, 263
dependence, 63, 101, 170, 182, 192
implications for control, 222, 232
of actuator dynamics, 63, 81, 88, 173, 327
of actuator stiffness, 63
feedback, 31, 149, 209, 222
transducer, 5, 250
pressure (absolute), *see* absolute pressure
pressure difference, 19
across bearing, 54
actuator, 21, 61, 100
at actuator, 88, 188
at valve, 88, 104, 191
feedback, 8, 224, 314, 315
at actuator, 236
at valve, 235
dynamic, 227, 253
for damping, 209
high-gain, 13, 216, 234
proportional, 209, 234
stability problems with, 226
nozzle, 41, 93
reference, 205, 210, 315
transducer, 5
placement, 235
propagation operator ($\Gamma(s)$), 73, 81, 339

quasi-linearization, 129

radial clearance, 34, 44, 45, 177, 326
Random Input Describing Function, 125
reduced order estimator, 238, 240
return pressure, 19, 31, 41, 60
robot, 7, 201
robust control, 7, 131, 208, 232, 317
robustness, 144, 223, 225, 327
analysis, 11
experimental verification, 253
of cushioning, 303, 307
of velocity estimator, 240
problems, 202
rotary actuator, 3, 66, 208

safety, 9, 14, 151, 267, 285, 317
saturation, 2, 132, 149, 160, 163, 213, 227, 234
sensor, *see* transducer
servo-valve, 3, 312
dynamics, 8, 11, 23, 28, 91, 159, 188, 224, 234, 312, 319, 320
implications for control, 224
flapper-nozzle, *see* flapper-nozzle
non-linearity, 11, 23, 28, 106, 162, 196, 225, 231, 234, 247, 312, 323
three-stage, 3, 28, 36, 91, 120, 148, 149, 158, 227, 320

two-stage, 27, 33, 91
signal analyzer, 151
simulation problems, *see* algebraic loop
Sinusoidal Input Describing Function, 125, 128, 175, 313
spool, 5, 27, 234
dynamics, 29, 33, 111
mass, 33, 94
port configuration, 30, 34, 45, 110, 149, 312
port flow, 30, 34, 43, 110, 112, 231
third stage, *see* main spool
valve, 3
stability, 120, 252, 264
analysis, 128
problems, 7, 12, 226, 234, 314, 316
static non-linearity, 119, 124, 140, 153, 162, 175, 220, 231
steady state
characteristic
flapper-nozzle system, 40
servo-valve, 43, 106
gain, 101, 102, 172
positioning, 207
test facility, 152
velocity, 58, 99, 178
step response
actuator, 61
flapper-nozzle valve, 47
three-stage valve, 50
stiffness
in impedance control, 217
magnetic, 39
of actuator, 3, 63, 88, 182, 222, 249
of oil, 181, 300
parameter, 186
supply pressure, 60, 233, 282, 287, 300
constant, 3, 19, 21, 148
supply unit, 2, 19, 21, 66, 300
symmetric
actuator, 3, 56, 147, 222, 312
non-linearity, 142
port configuration, 45, 59
pressure dynamics, 101
system design, 4, 9, 14, 144, 182

test rig, 146, 178, 244, 253, 299
torque motor, 27, 28, 30, 107
non-linearity, 28, 39, 48, 107, 154, 324
trajectory, 201, 251, 285
transducer, 5, 20, 150, 353
transmission line, 21, 65
between valve and actuator, 8, 148
dynamics, 12, 102, 313, 322
identification, 184
implications for control, 65, 224
stability problem, 12, 234
modelling, 24, 102
resonance, 8, 88, 103, 185, 194, 254
supply line dynamics, 12
turbulent, 10, 31, 34, 38, 85, 273, 283, 308

uncontrollable, 88, 93, 101, 108, 114
undamped natural frequency, 70, 81
underlap, 34, 44, 64, 110, 149, 177, 325
unobservable, 101

validation approach, 126
velocity
compensation, 215, 237, 254
estimation, 14, 237
feedback, 212, 216, 263
feedforward, 217, 218, 255
reduction, 267
reduction (cushioning), 288, 297, 301
transducer, 5, 237
viscous damping, *see* damping
viscous friction, 53, 57, 60, 101
coefficient (flapper), 31
coefficient (piston), 53, 112, 182
coefficient (spool), 33
in transmission line, 71
Volterra kernel, 121

weighting, 172, 186
factor, 239
frequency-dependent, 120, 139
white-box modelling, 11
Wiener kernel, 121
Wiener model, 122, 141

zero(s), 96, 182, 320
number of, 138
pair of, 212, 229, 263
right-half-plane, 94, 95, 153, 160

Glossary of symbols

Arabic symbols (small)

a_i	Fourier coefficient of i^{th} cosine term, $i = 0, \ldots, \infty$
b_i	Fourier coefficient of i^{th} sine term, $i = 1, \ldots, \infty$
$b_{56,i}, b_{5,i}, b_{6,i}$	i^{th} coefficient of polinomial fit for position dependent parameters ζ_{56}, ζ_5 and ζ_6 respectively, $i = 0, 1, 2$
c	1. clearance of single hydrostatic bearing, [m] 2. maximum allowable jerk during cushioning, [m/s^3]
c_0	sound velocity in oil, [m/s]
c_1	clearance at the tip of the peg in PIH cushioning, [m]
c_2	clearance at the tip of the conical bearing in CDH cushioning, [m]
$c_1, \ldots, c_{10}$	parameters in simplified/reduced linear servo-valve model
c_{11}, c_{12}, c_{13}	parameters in simplified non-linear servo-valve model
c_b	ball clearance flapper-nozzle valve, [m]
c_{b_i}	clearance of hydrostatic bearing i, $i = 1, 2, 3, 4$, [m]
c_{rm}	radial clearance of main spool in bushing, [m]
c_{rs}	radial clearance of spool in bushing, [m]
d	diameter of single hydrostatic bearing, [m]
d_{b_i}	diameter of hydrostatic bearing i, $i = 1, 2, 3, 4$, [m]
d_{m_i}	underlap of main spool port i, $i = 1, 2, 3, 4$, [m]
d_{s_i}	underlap of spool port i, $i = 1, 2, 3, 4$, [m]
$f(.)$	static non-linear function mapping u into x in non-linear system of Fig. 3.1
$f_1(.)$	static non-linear function representing non-linear flow characteristic of pilot-valve, [-]
$f_2(.)$	static non-linear function representing non-linear flow characteristic of servo-valve, [-]
$f_{cp}(.)$	general non-linear function representing friction in simplified non-linear actuator model, [-]
$f_{x,cyl}$	axial force of single hydrostatic bearing on cylindrical part, [N]
$f_{x,con}$	axial force of single hydrostatic bearing on conical part, [N]
g	gap distance at neutral position armature, [m]
$h(x)$	1. peg geometry of PIH cushioning; distance between peg and hole, perpendicular to hole, [m] 2. distance between piston head and cylinder, perpendicular to cylinder (CDH cushioning), [m]
$\hat{h}(x)$	approximate piece-wise-linear peg geometry in PIH cushioning design; built up with linear functions $\hat{h}_1, \hat{h}_2, \hat{h}_3, \hat{h}_4$, [m]
h_m	1. width of main spool port openings, [m] 2. quantization step at the m^{th} point of a quantized non-linearity according to Fig. 3.4 (b), [-]
h_s	width of spool port openings , [m]
i_{ca}	flapper-nozzle valve steering current from current amplifier, [A]
i_{max}	maximum steering current flapper-nozzle valve, [A]

j	imaginary number; $j = \sqrt{-1}$
$k_1, \ldots, k_6$	tuning parameters for non-linearities in simplified non-linear models of servo-valve and actuator
l	length of single hydrostatic bearing, [m]
l_a	armature length, [m]
l_{b_i}	length of hydrostatic bearing i, $i = 1, 2, 3, 4$, [m]
l_f	flapper length, [m]
l_{fbs}	feedback spring length, [m]
m	dimension of parameter vector θ
n	number of identifiable parameters / coefficients in transfer function
n_{dh}	number of normal drain holes in CDH cushioning (closed simultaneously at start of cushioning), [-]
n_h	number of cushioning holes in CDH cushioning (closed subsequently during cushioning), [-]
p	number of poles in transfer function
p_1, p_2	local pressures at low pressure side and high pressure side respectively of hydrostatic bearing, [N/m^2]
$q, \dot{q}, \ddot{q}$	actuator position, [m], velocity, [m/s], and acceleration, [m/s^2]
$q_d, \dot{q}_d, \ddot{q}_d$	desired trajectory for actuator position, [m], velocity, [m/s], and acceleration, [m/s^2]
q_0	initial actuator position (for linearization), [m]
q_0^+, q_0^0, q_0^-	upper, middle and down position respectively of the actuator, [m] (upper and down positions at +75 % and −75 % of q_{max} respectively)
$\dot{q}_0$	maximum initial actuator velocity in cushioning desing, [m/s]
q_c	cushioning length, [m]
q_{c1}	length of PIH cushioning; equals length of the peg, [m]
q_{c2}	length of CDH cushioning, [m]
q_{max}	half the actuator stroke, [m]
$\dot{q}_{max}$	maximum actuator velocity at nominal valve flow, [m/s]
$\ddot{q}_{max}$	maximum actuator acceleration at maximum actuator force, [m/s^2]
r	1. radial coordinate in PDE of single transmission line, [m] 2. reference input of non-linear system according to Fig. 3.1 3. radius of single drain hole in CDH cushioning, [m]
$\bar{r}$	source signal for reference generator in two-level control setting of Fig. 4.3
r_0	radius of a single transmission line, [m]
r_{tl1}, r_{tl2}	radius of transmission line 1, 2 respectively, [m]
r_h	hydraulic radius of a single transmission line, [m]
$r_{h,ac1}$, $r_{h,ac2}$	hydraulic radius of actuator chamber 1, 2 respectively, [m]
s	1. Laplace variable, [1/s] 2. source input of non-linear system with input amplitude filtering according to Fig. 3.3
s_{c1}	shortest distance between the tip of the peg and the edge of the hole in PIH cushioning, [m]
$s_{h1}, \ldots, s_{hn_h}$	distances between n_h cushioning holes in CDH cushioning, [m]
t	1. tapering of single hydrostatic bearing, [m] 2. time variable, [s]
t_0	start time of cushioning stage, [s]

t_{b_i}	tapering of hydrostatic bearing i, $i = 1, 2, 3, 4$, [m]
t_f	final time of cushioning stage, [s]
u	1. valve control signal, [V] 2. axial fluid velocity in PDE of single transmission line, [m/s] 3. input of static non-linearity in non-linear system of Fig. 3.1
u_r	three-stage valve (reference) control signal, [V]
$\bar{u}_r^{uc}, \bar{u}_r^{c}$	uncompensated and compensated (normalized) valve control signal respectively, in case of non-linear control, [-]
$u_{cos,N}$	discrete time series of cosine function in (3.5)
$u_{sin,N}$	discrete time series of sine function in (3.5)
v	1. relative velocity of cylinder with respect to hydrostatic bearing, [m/s] 2. radial fluid velocity in PDE of single transmission line, [m/s]
w_p	viscous friction coefficient of actuator piston, [N.s/m]
w_{p,b_i}	viscous coefficient actuator bearing i, $i = 1, 2, 3, 4$, [N.s/m]
w_s	viscous friction coefficient of valve spool, [N.s/m]
x	1. spatial variable in PDE of single transmission line, [m] 2. output of static non-linearity in non-linear system of Fig. 3.1 3. distance from tip of the peg in PIH cushioning, [m] 4. distance from tip of piston head in CDH cushioning, [m] 5. displacement variable for definition of motion profile for cushioning in displacement domain, [m]
x_g	displacement of the armature tip, [m]
$x_f, \dot{x}_f, \ddot{x}_f$	flapper deflection / displacement between the nozzles, [m], velocity, [m/s], and acceleration, [m/s^2]
x_{f0}	flapper-nozzle distance in neutral position, [m]
x_{fb}	internal feedback signal in non-linear system of Fig. 3.1
$x_m, \dot{x}_m$	main spool position, [m], and velocity, [m/s]
$x_{m,max}$	maximum main spool displacement, [m]
$x_s, \dot{x}_s, \ddot{x}_s$	flapper-nozzle valve spool displacement, [m], velocity, [m/s], and acceleration, [m/s^2]
$x_{s,max}$	maximum flapper-nozzle valve spool displacement, [m]
y	output of non-linear system of Fig. 3.1
y_c	1. distance of piston head along single drain hole in CDH cushioning, [m] 2. relative actuator position, related to start of cushioning, [m]
y_{c1}	distance of peg in hole in PIH cushioning, [m]
y_{c2}	distance of piston head along cushioning holes in CDH cushioning, [m]
$\ddot{y}_{c,max}$	maximum acceleration during cushioning, [m/s^2]
$y_{des}, \dot{y}_{des}, \ddot{y}_{des}, \dddot{y}_{des}$	desired motion profile for cushioning; position in [m], velocity in [m/s], acceleration in [m/s^2] and jerk in [m/s^3] respectively
y_{hi}	distance of piston head along cushioning holes in CDH cushioning such that hole i is just closed, $i = 1, \ldots, n_h$, [m]
z	number of zeros in transfer function
z_1, z_2	transformed variables in transmission line model, describing forward and backward propagation effects respectively, as function of x and s

Arabic symbols (large)

A	1. surface area of transmission line, [m^2] 2. state matrix (of hydraulic actuator model)
A_0	orifice area of inlet restrictions, [m^2]
A_{ac}	state matrix of modal approximation of actuator chamber
A_c	(part of) circular area of drain hole in CDH cushioning, [m^2]
A_e	state matrix of reduced order estimator
A_g	area of gap in torque motor, [m^2]
A_h	curtain area between (conical) piston head and the edge of the circular drain hole in CDH cushioning, [m^2]
$A_{\bar{i}}$	amplitude of sinusoidal input signal for flapper-nozzle valve $\bar{i}_{ca}$, [-]
A_{n3}	orifice area of outlet restriction, [m^2]
A_m	main spool side area, [m^2]
A_{m_i}	opening area main spool port i, $i = 1, 2, 3, 4$, [m^2]
A_{man}	representative area of turbulent restriction in manifold [m^2]
A_p	piston area, [m^2]
A_{p1}	piston area 1 in case of asymmetric actuator, [m^2]
A_{p2}	piston area 2 in case of asymmetric actuator, [m^2]
A_{p,b_i}	virtual piston area related to bearing i, $i = 1, 2, 3, 4$, [m^2]
A_{peg}	area of the peg of PIH cushioning, [m^2]
A_r	amplitude of sinusoidal input signal $r(t)$
$A_{\bar{r}}$	amplitude of sinusoidal input signal $\bar{r}(t)$ of reference generator, [m]
A_{rem}	remaining area around peg of PIH cushioning, [m^2]
A_s	1. valve spool side area, [m^2] 2. amplitude of sinusoidal source input signal $s(t)$
A_{s_i}	opening area spool port i, $i = 1, 2, 3, 4$, [m^2]
A_t	circular area between edge of the piston head and cylinder in CDH cushioning, [m^2]
A_{tl}	state matrix of modal approximation of single transmission line
A_u	amplitude of periodic input signal of the non-linearity $u(t)$
$A_{u,max}$	maximum of input amplitude range for $u(t)$
$A_{\bar{u}_r}$	amplitude of sinusoidal input signal $\bar{u}_r(t)$ of three-stage valve
$A_{\bar{u}_r,tt}$	top-top amplitude range of random noise input signal $\bar{u}_r(t)$
$A_{\bar{u}_s}$	amplitude of sinusoidal input signal $\bar{u}_s(t)$ of input amplitude filter
$A_{\bar{x}_m}$	amplitude of sinusoidal input signal $\bar{x}_m(t)$ for actuator measurements
$A_{\overline{\Delta P}_p}$	amplitude of periodic signal $\overline{\Delta P}_p(t)$ for actuator measurements
B	input matrix (of hydraulic actuator model)
B_a	viscous friction coefficient of the flapper, [N.m.s/m]
B_{ac}	input matrix of modal approximation of actuator chamber
B_{tl}	input matrix of modal approximation of transmission line
C	output matrix (of hydraulic actuator model)
C_{ac}	output matrix of modal approximation of actuator chamber
C_d	*discharge coefficient*, [-]
C_{d1}	discharge coefficient in PIH cushioning model, [-]
C_{d2}	discharge coefficient in CDH cushioning model, [-]
C_{tl}	output matrix of modal approximation of single transmission line

$C_{\Delta P,1}(s)$	dynamic compensator in pressure difference feedback path
$C_{\Delta P,2}(s)$	dynamic compensator in pressure difference forward path
$C_{\Delta P,3}(s)$	dynamic precompensator for pressure difference feedback loop
D_{ac}	direct feedthrough matrix of modal approximation of actuator chamber
D_{cyl}	inner diameter of cylinder containing drain holes of CDH cushioning, [m]
D_{dh}	diameter of normal drain holes in CDH cushioning (closed simultaneously at start of cushioning), [m]
D_{hi}	diameter of cushioning holes i, $i = 1, \ldots, n_h$, in CDH cushioning, [m]
D_n	1. nozzle diameter, [m] 2. transmission line dissipation number, [-]
D_{peg}	diameter of the peg of PIH cushioning, [m]
D_{tl}	direct feedthrough matrix of modal approximation of transmission line
E	bulk modulus of oil / oil stiffness, [N/m^2]
E_{ampl}	relative amplitude error according to (4.11)
E_{phase}	phase error according to (4.11)
$F(j\omega)$	transfer function / frequency response of input amplitude filter
F_{ax}	axial flow force on valve spool, [N]
F_{cp}	Coulomb friction force on piston, [N]
F_{cs}	Coulomb friction force on valve spool, [N]
F_{ext}	external load force on actuator, [N]
F_{f1}, F_{f2}	forces of nozzle flows 1, 2 respectively on flapper, [N]
$F_{p,max}$	maximum actuator force (excerted when $\Delta P_p = P_s$), [N]
$F_{s,max}$	maximum force on spool of flapper-nozzle valve, [N]
F_{v,b_i}	viscous friction force on piston due to bearing i, $i = 1, 2, 3, 4$, [N]
F_{vp}	viscous friction force on piston, [N]
FR_1, FR_2	(flow) force ratio for nozzle flow 1, 2 respectively, [-]
$G(j\omega)$	transfer function / frequency response of linear system
G_1, G_2, G_3	transfer functions of linear blocks in non-linear system of Fig. 3.1
$G_{pv}(j\omega)$	transfer function of linear dynamics of pilot-valve
$H_{ry}^{A_r}(j\omega)$	frequency response of non-linear system, from input r to output y, obtained at input amplitude A_r
H_{ac}	steady state gain matrix of modal approximation of actuator chamber
H_{tl}	steady state gain matrix of modal approximation of transmission line
I	unity matrix
J_0, J_1	Bessel functions of the first kind, of order zero and one respectively
J_a	inertia of flapper armature, [kg.m^2]
K	number of frequency responses in frequency domain identification
K_1	actuator position feedback gain (stiffness) in cascade ΔP control, [1/m]
K_2	actuator velocity feedback gain (damping) in cascade ΔP control, [s/m]
K_a	spring constant of armature flexure tube, [N.m/m]
K_b	magnetic stiffnes of the torque motor, [N.m/m]
K_{ca}	current amplifier gain, [A/V]
$\bar{K}_{dm}$	scaled differential main spool position feedback gain, [-]
K_{fbs}	feedback spring constant, [N.m/m]
K_{ff}	velocity feedforward gain in actuator control loop, [s/m]
K_{ms}	main spool position sensor gain, [V/m]
$K_{pm}(\bar{K}_{pm})$	(scaled) proportional main spool position feedback gain, [V/m] ([-])

K_q	proportional actuator position feedback gain, [1/m]
$K_{\dot{q}}$	proportional actuator velocity feedback gain, [s/m]
K_{sp}	spool position feedback gain, [V/m]
K_t	torque motor gain, [N.m/A]
K_{vc}	velocity compensation gain in cascade ΔP control, [s/m]
$K_{\Delta P}$	proportional actuator pressure difference feedback gain, [-]
L	1. length of a single transmission line, [m] 2. estimator feedback gain matrix
L_e	feedback gain matrix of reduced order estimator
L_{ac1}, L_{ac2}	length of actuator chamber 1, 2 respectively, [m]
L_q	position feedback gain of reduced order estimator
L_{tl1}, L_{tl2}	length of transmission line 1, 2 respectively, [m]
$L_{\Delta P}$	pressure difference feedback gain of reduced order estimator
LP_{b_i}	laminar leakage coefficient for bearing i, $i = 1, 2, 3, 4$, [m^5/N.s]
LP_p	laminar leakage coefficient for leakage across piston, [m^5/N.s]
LP_1, LP_2	laminar leakage coefficient for leakage out of actuator chamber 1, 2 respectively, [m^5/N.s]
M	1. amplitude of approximate output signal in SIDF definition 2. number of intervals for quantization of static non-linearity
$M(\theta)$	model structure / structured state space model, parametrized by θ
M_0	magnetomotive force of permanent magnets, [A]
M_p	actuator load inertia, [kg]
M_s	valve spool inertia, [kg]
N	1. number of coil windings, [-] 2. number of data points 3. conicity of the piston head bearing in CDH cushioning, [-]
$N(A_r, \omega)$	complex valued Sinusoidal Input Describing Function at input amplitude A_r and frequency ω
$N^{\omega}_{ry}(A_r)$	amplitude response of non-linear system, from input r to output y, obtained at input frequency ω
O	circumference of transmission line, [m]
P_i	pressure at inlet of a single transmission line, [N/m^2]
P_{i1}, P_{i2}	pressure at inlet or valve-side of transmission line 1, 2 respectively, [N/m^2]
P_m	pressure level (mean pressure) at pilot-valve spool ports, [N/m^2]
P_{m1}, P_{m2}	main spool pressures at spool port 1, 2 respectively of flapper-nozzle valve, [N/m^2]
P_n	mean nozzle pressure, [N/m^2]
P_{n1}, P_{n2}	nozzle pressure for nozzle 1, 2 respectively, [N/m^2]
P_{n3}	common nozzle outlet pressure, [N/m^2]
P_o	pressure at outlet of a single transmission line, [N/m^2]
P_{o1}, P_{o2}	pressure at outlet or actuator-side of transmission line 1, 2 respectively, [N/m^2]
P_p	pressure level (mean pressure) in actuator chambers, [N/m^2]
P_{p1}, P_{p2}	pressure in actuator chamber 1, 2 respectively, [N/m^2]
P_s	oil supply pressure, [N/m^2]
P_t	return pressure, [N/m^2]
Q	covariance matrix related to process noise V (Kalman filter design)

R	covariance matrix related to measurement noise W (Kalman filter design)
T_{fbs}	feedback spring torque on flapper, [N.m]
T_{ff}	torque on flapper due to flow forces, [N.m]
T_{max}	maximum torque delivered by torque motor, [N.m]
T_t	torque delivered by torque motor, [N.m]
$T_{t,lin}$	linearized torque delivered by torque motor, [N.m]
U	input vector (of hydraulic actuator model)
U_{ac}	input vector of modal approximation of actuator chamber
U_{tl}	input vector of modal approximation of single transmission line
V	process noise input vector
V_{ac1}, V_{ac2}	volumes of actuator chamber 1, 2 respectively, [m^3]
V_{cv}	error function according to (3.25) for time domain cross validation of three-stage valve model
V_{l1}, V_{l2}	ineffective volumes of actuator chamber 1, 2 respectively, [m^3]
V_{n1}, V_{n2}	oil volumes of valve chamber 1, 2 respectively, [m^3]
V_{n3}	oil volume between nozzles and outlet restriction, [m^3]
$V_N(\theta)$	least squares cost criterion
V_q	time domain error criterion for position tracking according to (4.13)
$V_{\dot{q}}$	criterion for noise level of velocity estimation according to (4.12)
$V_{\ddot{q}}$	time domain error criterion for acceleration tracking according to (4.13)
W	measurement noise input vector
W_{uy}, W_k	real positive frequency weighting vectors frequency domain identification
X	state vector (of hydraulic actuator model)
X_1, X_2	unknown part and known part, respectively, of the state vector (for reduced order estimator design)
X_e	state vector of reduced order estimator
X_{ac}	state vector of modal approximation of actuator chamber
X_{tl}	state vector of modal approximation of single transmission line
Y	output vector (of hydraulic actuator model)
Y_{ac}	output vector of modal approximation of actuator chamber
Y_{tl}	output vector of modal approximation of single transmission line
Z_0	transmission line impedance constant, [N.s/m^2.m^3]
$Z_c(s)$	characteristic impedance of single transmission line, [N.s/m^2.m^3]

Greek symbols (small)

α_{ci}	frequency modification factor of blocked line for mode i, $i = 1, 2$, [-]
α_{si}	frequency modification factor of open line for mode i, $i = 1, 2$, [-]
α_s	constant source input amplitude of $s(t)$ when applying input amplitude filter
α_u	constant input amplitude of $u(t)$ when applying input amplitude filter
β	real gain of static non-linearity when applying input amplitude filter
β_{ci}	damping modification factor of blocked line for mode i, $i = 1, 2$, [-]
β_{si}	damping modification factor of open line for mode i, $i = 1, 2$, [-]
η	dynamic viscosity of oil, [kg/m.s]
θ	1. jet angle of spool port flows, [deg] 2. parameter vector

θ_0	initial estimate for parameter vector θ
$\theta_1, \ldots, \theta_{19}$	parameters of linearized servo-valve model
$\zeta_1, \ldots, \zeta_6$	parameters of linearized actuator model
ζ_{56}	position dependent parameter combination in linearized actuator model; $\zeta_{56} = \frac{1}{2}(\zeta_5 + \zeta_6)$
$\zeta_{56}^-, \zeta_{56}^0, \zeta_{56}^+$	ζ_{56} in positions q_0^-, q_0^0, q_0^+ respectively (similar notation applied to ζ_5 and ζ_6)
$\xi_1, \ldots, \xi_{12}$	parameters of transmission line models in linearized actuator model
λ_{ci}	normalized natural frequency of blocked line for mode i, $i = 1, 2$, [-]
λ_{si}	normalized natural frequency of open line for mode i, $i = 1, 2$, [-]
μ	kinematic viscosity of oil, [m^2/s]
μ_0	magnetic permeability of air, [V.s/A.m]
ρ	1. oil density, [kg/m^3] 2. weighting factor for diagonal measurement noise convariance matrix
ϕ_x	leakage flow through single hydrostatic bearing (zero excentricity), [m^3/s]
ϕ	phase of approximate output signal in SIDF definition
ω	frequency, [rad/s] (or [Hz] if indicated so)
ω_c	viscosity frequency μ/r_0^2, [1/s]
ω_f	cut-off frequency of reference generator for actuator control, [rad/s]

Greek symbols (large)

$\Gamma(s)$	wave propagation operator of single transmission line, [-]
$\Delta\dot{q}$	deviation in steady state velocity due to leakage, [m/s]
$\overline{\Delta P}_d$	normalized desired trajectory for actuator pressure difference, [-]
ΔP_i	actuator pressure difference at valve side of transmission lines, [N/m^2]
ΔP_m	pressure difference at flapper-nozzle valve spool ports, [N/m^2]
ΔP_n	nozzle pressure difference, [N/m^2]
ΔP_o	actuator pressure difference at actuator side of transmission lines, [N/m^2]
ΔP_p	actuator pressure difference, across piston, [N/m^2]
$\overline{\Delta P}_t$	normalized target pressure difference for cascade ΔP control, [-]
Φ_{01}, Φ_{02}	flows through inlet restriction 1, 2 respectively, [m^3/s]
Φ_{c1}	cushioning flow of PIH cushioning, [m^3/s]
Φ_{c2}	cushioning flow of CDH cushioning, [m^3/s]
Φ_{dh}	outflow through normal drain holes in CDH cushioning, [m^3/s]
Φ_{hi}	flow through cushioning holes i, $i = 1, \ldots, n_h$, in CDH cushioning, [m^3/s]
Φ_i	oil flow at inlet of a single transmission line, [m^3/s]
Φ_{i1}, Φ_{i2}	oil flow at inlet (valve-side) of transmission lines, into and from actuator chamber 1, 2 respectively, [m^3/s]
Φ_{l1}, Φ_{l2}	leakage flow out of actuator chamber 1, 2 respectively, [m^3/s]
Φ_l	leakage flow through single hydrostatic bearing, [m^3/s]
Φ_{l,b_i}	leakage flow through hydrostatic bearing i, $i = 1, 2, 3, 4$, [m^3/s]
Φ_{lp}	leakage flow across the piston, [m^3/s]
Φ_{l,m_i}	leakage flow overlapped main spool port i, $i = 1, 2, 3, 4$, [m^3/s]
Φ_{l,s_i}	leakage flow overlapped spool port i, $i = 1, 2, 3, 4$, [m^3/s]
Φ_m	oil flow driving the main spool, [m^3/s]
Φ_{m1}, Φ_{m2}	oil flow (through flapper-nozzle valve spool ports) into and from main

	spool chamber 1, 2 respectively, [m^3/s]
$\Phi_{m,nom}$	nominal (maximum) spool flow flapper-nozzle valve, [m^3/s]
Φ_{n1}, Φ_{n2}	nozzle flows through nozzle 1, 2 respectively, [m^3/s]
$\Phi_{n,nom}$	nominal nozzle flow (neutral flapper position), [m^3/s]
Φ_N	regression vector
Φ_o	oil flow at outlet of a single transmission line, [m^3/s]
Φ_{o1}, Φ_{o2}	oil flow at outlet (actuator-side) of transmission lines, into and from actuator chamber 1, 2 respectively, [m^3/s]
Φ_p	oil flow driving the actuator piston, [m^3/s]
Φ_{p1}, Φ_{p2}	oil flow into and from actuator chamber 1, 2 respectively, [m^3/s]
$\Phi_{p,nom}$	nominal (maximum) spool flow (three-stage) servo-valve, [m^3/s]

Normalizations

Reference:	Normalized variable(s) and parameter(s):
i_{max}	$\bar{i}_{ca}$
q_{max}	$\bar{q}$
$\dot{q}_{max}$	$\bar{\dot{q}}$, $\overline{\Delta\dot{q}}$
$\ddot{q}_{max}$	$\bar{\ddot{q}}$
x_{f0}	$\bar{x}_f$
$x_{s,max}$	$\bar{x}_s$, $\bar{c}_{rs}$, $\bar{d}_{s1}$, $\bar{d}_{s2}$, $\bar{d}_{s3}$, $\bar{d}_{s4}$,
$x_{m,max}$	$\bar{x}_m$, $\bar{c}_{rm}$, $\bar{d}_{m1}$, $\bar{d}_{m2}$, $\bar{d}_{m3}$, $\bar{d}_{m4}$
$F_{p,max}$	$\bar{F}_{cp}$, $\bar{F}_{ext}$
$F_{s,max}$	$\bar{F}_{cs}$
$K_{ms}x_{m,max}$	$\bar{u}_r$
P_s	$\bar{P}_i$, $\bar{P}_{i1}$, $\bar{P}_{i2}$, $\bar{P}_m$, $\bar{P}_{m1}$, $\bar{P}_{m2}$, $\bar{P}_n$, $\bar{P}_{n1}$, $\bar{P}_{n2}$, $\bar{P}_{n3}$, $\bar{P}_o$, $\bar{P}_{o1}$, $\bar{P}_{o2}$, $\bar{P}_p$, $\bar{P}_{p1}$, $\bar{P}_{p2}$, $\overline{\Delta P}_i$, $\overline{\Delta P}_m$, $\overline{\Delta P}_n$, $\overline{\Delta P}_o$, $\overline{\Delta P}_p$
T_{max}	$\bar{T}_t$, $\bar{T}_{ff}$
ω_c	$\bar{s}$
$\Phi_{m,nom}$	$\bar{\Phi}_m$, $\bar{\Phi}_{m1}$, $\bar{\Phi}_{m2}$
$\Phi_{n,nom}$	$\bar{\Phi}_{01}$, $\bar{\Phi}_{02}$, $\bar{\Phi}_{n1}$, $\bar{\Phi}_{n2}$
$\Phi_{p,nom}$	$\bar{\Phi}_p$, $\bar{\Phi}_{p1}$, $\bar{\Phi}_{p2}$

Abbreviations

rhp	right half plane
AD	Analog to Digital
CDH	Closing-Drain-Holes (cushioning)
DF	Describing Function
DOF	Degrees-Of-Freedom
LMI	Linear Matrix Inequality
LPV	Linear Parametrically Varying
LVDT	Linear Variable Differential Transformer
MISO	Multiple Input Single Output
MIMO	Multiple Input Multiple Output
NL	Non-Linear
NL-ΔP_n	Non-Linearity due to the Flapper-Nozzle system
NL-TM	Non-Linearity due to the Torque Motor

PDE	Partial Differential Equation
PIH	Peg-In-Hole (cushioning)
QFT	Qualitative Feedback Theory
RIDF	Random Input Describing Function
SIDF	Sinusoidal Input Describing Function
SIMONA	International Research Centre for Simulation, Motion and Navigation Technologies
SISO	Single Input Single Output
SIMO	Single Input Multiple Output
TFID	Transfer Function IDentification (Matrix_X-command)

Accents

$\dot{}$	time derivative
$\hat{}$	estimated or simulated
$\tilde{}$	1. scaled (state) 2. obtained with input amplitude filter (frequency response) 3. obtained by interpolation between equidistant input amplitudes (open loop amplitude response)
$\bar{}$	normalized
$'$	(pressure) including manifold loss

Samenvatting

Modelvorming van lange-slag hydraulische servo-systemen voor de regeling van de bewegingen van een vluchtsimulator en voor servo-systeemontwerp

G. van Schothorst

In veel toepassingen zijn hydraulische aandrijvingen nog steeds beter geschikt dan andere aandrijftechnieken. Zo worden hydraulische actuatoren bijvoorbeeld nog steeds veelvuldig toegepast in de bewegingssystemen van vluchtsimulatoren. Dit omdat de technologie van lineaire electrische aandrijvingen (nog) niet zo ver is ontwikkeld, dat zij dezelfde prestaties kunnen leveren als hydraulische actuatoren; dit betreft met name het leveren van hoge vermogens over een lange slag. Echter, met de toenemende eisen aan de prestaties van complexe bewegingssystemen komen ook de grenzen van de hydraulische servo-techniek in beeld. De toepassing van lange slag hydraulische actuatoren in een bewegingssysteem voor een vluchtsimulator, beschouwd in dit proefschrift, maakt duidelijk dat de dynamica en niet-lineariteiten van de servoklep enerzijds, en van de leidingen tussen de servoklep en de actuatorcompartimenten anderzijds, de principiële grenzen vormen voor de haalbare prestaties van het geregelde servosysteem. Vooral bij de traditionele, proportionele terugkoppelstrategieën blijkt, dat de combinatie van klepdynamica en leidingdynamica de drukregelkring gemakkelijk kan destabiliseren.

Teneinde structureel inzicht te verkrijgen in de manier waarop de eigenschappen van de (subsystemen van) het hydraulische servo-systeem de mogelijke prestaties beperken, is de modelvorming van dit systeem uitgebreid uiteengezet in dit proefschrift. Enerzijds heeft dit de weg geopend naar modelgebaseerd regelaarontwerp, zodat de theoretische grenzen aan de prestaties dicht kunnen worden benaderd. Anderzijds blijkt het verkregen inzicht nuttig voor systeemontwerp, zodat potentiële regelproblemen reeds in de systeemontwerpfase kunnen worden vermeden.

Vanwege het tweevoudige doel van de modelvorming, waarbij regelaarontwerp kwantitatief nauwkeurige modellen vereist, en systeemontwerp kwalitatief inzicht in het systeemgedrag, is de zogenaamde 'grey-box' aanpak voor modelvorming gevolgd. Deze aanpak begint met de fysische modelvorming van het systeem, waarbij het model geanalyseerd wordt door middel van simulaties; daarna worden de verkregen (fysisch gestructureerde) modellen geïdentificeerd en gevalideerd aan de hand van experimentele data.

Bij de fysische modelvorming zijn uitgebreide niet-lineaire dynamische modellen afgeleid voor de drie subsystemen van het hydraulische servo-systeem: de electro-hydraulische servoklep (van het vaan-tuit type), de hydraulische actuator (van het dubbel-concentrische type), en de leidingen tussen de klep en de actuator. Met behulp van linearisaties van de verkregen theoretische modellen zijn de dynamische eigenschappen van de verschillende subsystemen geanalyseerd. De beschouwde drietrapsklep vertoont een 5^e orde laagdoorlaatkarakteristiek, waarbij de hoofdschuif zich gedraagt als een pure integrator, terwijl de twee-

traps voorstuurklep 4^e orde dynamica vertoont. De actuator zelf wordt goed beschreven door de welbekende 3^e orde dynamica van een hydraulisch servo-systeem: een pure integrator in serie met een slecht gedempt tweede orde systeem. Het gedrag van de leidingen in het hydraulische servo-systeem, tenslotte, laat zich goed beschrijven door een serie van slecht gedempte resonanties in het hoogfrequente deel van de overdrachtsfunctie, gemeten van klepsturing naar actuatordrukverschil. De eerste modes van deze leidingdynamica kunnen binnen de bandbreedte van de servoklep liggen.

Naast de dynamische eigenschappen, zijn ook de niet-lineariteiten onderzocht, en wel door middel van simulaties met het fysische model. Dit heeft geleid tot het inzicht, dat slechts enkele van de gemodelleerde niet-lineariteiten werkelijk relevant zijn. Dit zijn met name de niet-lineaire karakteristiek van de oliestroom door de servoklep ten gevolge van niet-ideale poortgeometrieën en ten gevolge van grote belastingdrukken, en de positieafhankelijkheid van de dynamica van de actuator.

Het uiteindelijke resultaat van de fysische modelvorming is een aantal fysisch gestructureerde niet-lineaire dynamische modellen, die de relevante dynamica en niet-lineariteiten van de verschillende subsystemen van het hydraulische servo-systeem beschrijven, en wel in een kwalitatieve zin. Kwantitatieve nauwkeurigheid van de modellen is verkregen door middel van experimentele indentificatie van de modelparameters en van de niet-lineariteiten van het systeem. Deze identificatiestap is uitgevoerd in het frequentiedomein, waarbij de Beschrijvende Functie Methode voor sinusvormige ingangssignalen is gebruikt om de niet-lineariteiten van het systeem expliciet te karakteriseren. Naast impliciete modelvalidatie door middel van bevredigende identificatieresultaten, is de geldigheid van de modellen verder aangetoond door middel van enkele kruisvalidatieresultaten.

Bij experimenten met een proefopstelling van een hydraulische actuator met één graad van vrijheid is gebleken, dat de verkregen modellen geschikt zijn voor een modelgebaseerde aanpak van het regelaarontwerp. De analyse van een aantal regelstrategieën voor de experimentele opstelling leidde tot de conclusie, dat goede prestaties bereikt kunnen worden met een drukverschilregeling met een hoge terugkoppelversterking, mits een goed referentiesignaal voor het drukverschil beschikbaar is. Daarbij bleek overigens wel, dat het noodzakelijk (maar tevens voldoende) was een modelgebaseerd ontwerp van een robuuste dynamische drukregeling uit te voeren, teneinde instabiliteit als gevolg van de combinatie van klepdynamica en leidingdynamica te voorkomen. Overigens bleek het voor goede regelprestaties in het laagfrequente gebied van essentieel belang te zijn, de gewenste snelheid voorwaarts te koppelen. Als alternatief kan positieve terugkoppeling van de werkelijke of van de geschatte snelheid worden toegepast. Omdat de snelheid in de gebruikte proefopstelling niet gemeten kon worden, moest deze geschat worden; een aantal methoden hiervoor zijn experimenteel geëvalueerd.

De combinatie van drukverschilterugkoppeling (met een hoge versterking) en positieve snelheidsterugkoppeling wordt ook wel de cascade ΔP regeling genoemd; deze regelstrategie zorgt voor een ontkoppeling van de regeling van de drukdynamica van het hydraulische servo-systeem en van de regeling van de mechanica van de last. Daarom is deze regelstrategie voor hydraulische actuatoren goed geschikt voor de regeling van bewegingssytemen met meerdere graden van vrijheid; de cascade ΔP regeling past goed in een regelstrategie van twee niveau's, waarin de regeling op het hoge niveau de niet-lineaire multivariabele regeling van de dynamica van de last omvat, terwijl de regeling op het lage niveau de drukdynamica van de hydraulische actuatoren regelt.

Indien mogelijk, moet in de systeemontwerpfase een modelanalyse uitgevoerd worden, om te voorkomen dat de prestaties van het systeem ernstig beperkt worden door slecht systeemontwerp. Deze modelanalyse kan helpen bij de keuze van de servoklep, de plaatsing van de drukverschil opnemers, en bij het ontwerp van de leidingen.

Bij bewegingssystemen voor vluchtsimulatoren vormt het ontwerp van een veiligheidsbuffer aan het einde van de actuatorslag een bijzonder belangrijk aspect van het totale systeemontwerp. Daarom is in dit onderzoek een modelgebaseerde ontwerpprocedure ontwikkeld en in de praktijk getest; de veiligheidsbuffers, die met deze procedure zijn ontworpen, leveren goede prestaties. Met behulp van de ontwikkelde procedure kunnen kostbare iteraties in het ontwerpproces (vanwege herhaalde experimentele verificatie) vermeden worden.

Curriculum Vitae

7 april 1969	Geboren te Ede
1981 – 1987	VWO, Van Lodenstein scholengemeenschap te Amersfoort
1987 – 1992	Studie Werktuigbouwkunde aan de Technische Universiteit Delft; afstudeerwerk bij de vakgroep Meet- en Regeltechniek: modelvorming en regeling van een hydraulische roterende vaanactuator
1992 – 1996	Assistent in Opleiding in de vakgroep Meet- en Regeltechniek, Faculteit der Werktuigbouwkunde en Maritieme Techniek, Technische Universiteit Delft; promotie-onderzoek in het kader van SIMONA, het *International Centre for Research in Simulation, Motion and Navigation Technologies* van de Technische Universteit Delft
1996 –	Werkzaam bij Philips Research (Group Mechanics) te Eindhoven